HEAT FLOW THROUGH EARTH DAMS

A DAM PERFORMANCE MONITORING TOOL

by

Fiona Colleen Esford

B.A.Sc., The University of Waterloo, 1995

A thesis submitted in partial fulfillment of the requirements
for the degree of Master of Applied Science

in

The Faculty of Graduate Studies
Department of Civil Engineering

We accept this thesis as conforming to the required standard

THE UNIVERSITY OF BRITISH COLUMBIA

June 2002

In presenting this thesis in partial fulfilment of the requirements for an advanced degree at the University of British Columbia, I agree that the Library shall make it freely available for reference and study. I further agree that permission for extensive copying of this thesis for scholarly purposes may be granted by the head of my department or by his or her representatives. It is understood that copying or publication of this thesis for financial gain shall not be allowed without my written permission.

Department of Civil Engineering

The University of British Columbia
Vancouver, Canada

Date June 24, 2002

ABSTRACT

Reservoirs located in temperate climates undergo seasonal temperature fluctuations, warm in the summer and cold in the winter. As a result, the temperature of the water seeping through embankment varies with the season. Heat from the reservoir propagates through dams by two main processes: convection and conduction. The variation in seepage water temperature can be used as a tracer to detect and monitor seepage flow through dams. Temperature measurements from the saturated zone of dams have been collected and qualitative and simplified quantitative methods of data analysis have been used to detect relative changes in the seepage regime.

This thesis used two dimensional, uncoupled (fluid and heat flows) numerical models to simulate heat flow through dams and determine seepage velocities. The numerical programs used in this thesis were SEEP/W and a modification of CTRAN/W, produced by GEO SLOPE International Inc. of Calgary. The programs were run in succession, beginning with SEEP/W. The analytical method was first tested by comparing results to a closed form solution simulating one dimensional flow (heat and water) through a homogenous material. Secondly the numerical method was applied to analyse heat flow through a field scale model dam in Germany, followed by an analysis of BC Hydro's Coquitlam Dam.

The numerical method was successful in simulating one dimensional flow. The method was also capable of simulating fluid and heat flow through the field scale dam, which had a simple stratigraphy. However, the hydraulic conditions at Coquitlam Dam are more complex and a two dimensional model was not able to account for the flow variations at this dam. A three dimensional model appears necessary to accurately simulate the fluid and heat flow conditions of Coquitlam Dam. Temperature data collected from Coquitlam Dam was qualitatively assessed. No obvious signs of preferential seepage paths were detected.

Although the numerical models used in this thesis were shown to effectively model fluid and heat flow, the three step process required to use these modelling programs became cumbersome for more complicated flow conditions. It is recommended that an integrated program be utilized to analyse complex systems, such as Coquitlam Dam.

Key words: heat transfer, embankment dams, dam monitoring, seepage monitoring, numerical modelling

TABLE OF CONTENTS

ABSTRACT ii
LIST OF TABLES vii
LIST OF FIGURES viii
ACKNOWLEDGEMENTS xii

CHAPTER 1: INTRODUCTION 1
1.1 THESIS OBJECTIVES 2
1.2 SCOPE OF THESIS 2
1.3 ORGANIZATION 3
1.4 SPONSORSHIP 3
CHAPTER 2: BACKGROUND AND THEORY 4
2.1 INTRODUCTION 4
2.2 HISTORICAL PERSPECTIVE 4
2.3 APPLICATION OF METHOD TO EMBANKMENT DAMS 5
2.4 HEAT FLOW THEORY 5
2.4.1 Conduction 6
2.4.2 Convection 7
2.4.3 Radiation 8
2.4.4 Dispersion 8
2.5 HEAT FLOW EQUATIONS 10
2.5.1 Coupled Heat and Fluid Flow Equations 10
2.5.2 Uncoupled Heat and Fluid Flow Equations 11
2.5.3 Assumptions for Uncoupled Heat and Fluid 13
2.6 HEAT TRANSPORT AND CONTAMINANT TRANSPORT EQUATIONS 13
2.7 TEMPERATURE VARIATION IN BODIES OF WATER 14
2.8 TEMPERATURE VARIATION WITHIN DAMS 15
2.9 DAMS 17
2.10 DAM FAILURES 17
2.11 MONITORING DAM PERFORMANCE 18
2.12 POTENTIAL BENEFITS OF INCORPORATING TEMPERATURE MONITORING INTO A DAM MONITORING PROGRAM 19
2.13 GENERAL REQUIREMENTS FOR THE IMPLEMENTATION OF A TEMPERATURE MONITORING PROGRAM 20
2.14 SUMMARY AND CONCLUSIONS 20
CHAPTER 3: NUMERICAL MODELLING 26
3.1 INTRODUCTION 26
3.2 SEEP/W 26

3.3 CTRAN/W 27
3.4 GENERAL MODELLING PROCEDURE 30
3.5 MODEL VERIFICATION 31
3.5.1 Analytical Solution using a Step Temperature Change Boundary 31
3.5.2 Analytical Solution using a Sinusoidal Temperature Boundary 32
3.5.3 Model Parameters 32
3.5.4 Setup and Analysis of SEEP/W and CTRAN/W Models 32
3.5.5 Results 34
3.6 SUMMARY AND CONCLUSIONS 34
CHAPTER 4: NUMERICAL MODELLING OF KARLSRUHE GERMANY FIELD SCALE MODEL DAM 41
4.1 INTRODUCTION 41
4.2 MODELLING OF FIELD SCALE MODEL DAM, KARLSRUHE, GERMANY 41
4.3 TRANSIENT SEEPAGE ANALYSIS 42
4.4 INITIAL THERMAL CONDITIONS 44
4.5 TRANSIENT SEEPAGE ANALYSIS AND THERMAL DISTRIBUTION 46
4.5.1 Results from the 48 Hour Test 47
4.5.2 Results from the 14 Day Test 48
4.5.3 Summary of Transient Analysis 49
4.6 SUMMARY AND CONCLUSIONS 49
CHAPTER 5: FIELD PROGRAM 69
5.1 INTRODUCTION 69
5.2 COQUITLAM DAM 69
5.3 REGIONAL GEOLOGY 70
5.3.1 Bedrock Geology 70
5.3.2 Surficial Geology 70
5.4 SITE GEOLOGY 71
5.4.1 Foundation Bedrock 71
5.4.2 Foundation Soils 71
5.4.3 Dam Fill Soils 73
5.5 COQUITLAM DAM, HYDRAULIC CONDITIONS 74
5.5.1 Reservoir 75
5.5.2 Piezometer Performance 75
5.5.3 Piezometer Measurements Through Section B-B of Coquitlam Dam 75
5.5.4 Weirs at Coquitlam Dam 76
5.6 COQUITLAM DAM, TEMPERATURE MONITORING PROGRAM 77
5.6.1 Instrumentation 77
5.6.2 Monitoring Locations 77
5.6.3 Procedures 78

5.7 COQUITLAM DAM, TEMPERATURE MONITORING PROGRAM 78
5.7.1 Reservoir *79*
5.7.2 Upstream Shell *79*
5.7.3 Hydraulic Fill Core and Foundation Units *80*
5.7.4 Downstream Toe *82*
5.7.5 Abutment Piezometers *82*
5.7.6 Overall Comparison of Temperature Monitoring Results *83*
5.8 IMPLICATIONS TO MODELLING OF COQUITLAM DAM 84
5.9 SUMMARY OF FIELD PROGRAM 85
CHAPTER 6: NUMERICAL MODELLING OF COQUITLAM DAM 124
6.1 INTRODUCTION 124
6.2 SEEP/W MODELLING OF COQUITLAM DAM 124
6.2.1 Grid and Stratigraphic Units *124*
6.2.2 Properties of Stratigraphic Units *124*
6.2.3 Hydraulic Boundary Conditions *125*
6.2.4 Time Steps *125*
6.2.5 Initial Conditions *125*
6.3 SEEP/W RESULTS 126
6.4 PROBLEMS WITH THE SEEPAGE MODELLING 127
6.5 CTRAN/W MODELLING OF COQUITLAM DAM 128
6.5.1 Grid and Stratigraphic Units *128*
6.5.2 Properties of Stratigraphic Units *128*
6.5.3 Thermal Boundary Conditions *128*
6.5.4 Time Steps *128*
6.5.5 Initial Conditions *129*
6.6 CTRAN/W RESULTS 129
6.7 PROBLEMS WITH THE HEAT TRANSPORT MODELLING 130
6.8 SUMMARY AND CONCLUSIONS 131
CHAPTER 7: CONCLUSIONS AND RECOMMENDATIONS 162
7.1 CONCLUSIONS 162
7.2 RECOMMENDATIONS 164

REFERENCES 166

APPENDIX A MODEL VERIFICATION USING CLOSED FORM SOLUTIONS 176
A-1 CLOSED FORM SOLUTIONS – VISUAL BASIC FUNCTIONS AND SPREADSHEETS..... 177
A-2 CALCULATIONS FOR MODEL VERIFICATION INPUT PARAMETERS 184

APPENDIX B CALCULATIONS FOR KARLSRUHE, GERMANY FIELD DAM..... 186
B-1 CALCULATIONS FOR MODEL THERMAL INPUT PARAMETERS SECTION 5.4 187
B-2 CALCULATIONS FOR MODEL THERMAL INPUT PARAMETERS SECTION 5.5.....190

APPENDIX C INDIVIDUAL TEMPERATURE PLOTS FOR EACH MONITORING LOCATION AT COQUITLAM DAM.....193

List of Tables

Table 3.1:	Model Verification Input Parameters	35
Table 4.1	SEEP/W Input Parameters and Their Source	50
Table 4.2:	Hydraulic Properties Used in Transient SEEP/W Simulation	51
Table 4.3:	Thermal Soil Properties Used in CTRAN/W Simulation – With Basal Heat Flux	52
Table 4.4:	Summary of Thermal Properties for CTRAN/W Models (Conduction Only)	52
Table 4.5:	Hydraulic and Thermal Properties Used in SEEP/W and CTRAN/W for Simulation Results Presented in Figure 4.13	52
Table 4.6:	Summary of Volumetric Water Content Function Substitutions for CTRAN/W Models	53
Table 4.7:	Summary of Thermal Properties for CTRAN/W Models (Convection and Conduction)	53
Table 5.1:	Coquitlam Dam Foundation Soils	86
Table 5.2:	Summary of Dam Fill Materials and Hydraulic Properties	86
Table 5.3:	Coquitlam Dam Piezometers, Construction Details and Performance Summary	87
Table 5.4:	Temperature Monitoring Piezometers and Installation Details	89
Table 5.5:	Temperature Monitoring Locations Within Coquitlam Dam	90
Table 5.6:	Summary of Annual Temperature Variation Data	91
Table 6.1:	Range of Hydraulic Conductivity Values Used in SEEP/W Simulations	132
Table 6.2:	Material Parameters for Computer Simulations	133
Table 6.3:	Material Parameters for Computer Simulations (for Figures 6.11 and 6.12)	135
Table 6.4:	Material Thermal Properties Used in the Modelling of Coquitlam Dam	136

List of Figures

Figure 2.1:	Velocity Variation Due to Pore Systems and Resulting Temperature Variation Schematic of Thermal Dispersion.....	21
Figure 2.2:	Temperature Density Relation of Water at 1 Atmosphere.....	21
Figure 2.3:	Schematic Temperature Profile – Shallow Water Body.....	22
Figure 2.4:	Schematic Temperature Profile - Deep Water Body.....	22
Figure 2.5:	Schematic View of a Heat Waves Propagation Through a Homogeneous Dam.....	23
Figure 2.6:	Comparison of a Heat Wave Propagated Through a Lower Conductivity Dam and a Higher Conductivity Dam.....	23
Figure 2.7:	Temperature Profiles Within a Dam's Saturated Zone.....	24
Figure 2.8:	Sample Temperature Distribution Within a Piezometer – With a Zone of High Conductivity.....	25
Figure 3.1:	Volumetric Water Content as a Function of Pore Water Pressure.....	36
Figure 3.2:	Volumetric Water Content Functions for Fine Sand, Silt and Clay....	36
Figure 3.3:	SEEP/W Grid and Hydraulic Head Distribution Results for the One - Dimensional Seepage Analysis.....	37
Figure 3.4:	Modified SEEP/W Grid and Hydraulic Head Distribution Using Infinite Elements for the One – Dimensional Seepage Analysis.....	38
Figure 3.5:	Sample CTRAN/W Output with Numerical Dispersion.....	39
Figure 3.6:	Comparison of Closed Form Solution and Numerical Model Results - Step Change in Boundary Temperature.....	40
Figure 3.7:	Comparison of Closed Form Solution and Numerical Model Results – Sinusoidal Variation in Boundary Temperature.....	40
Figure 4.1:	Cross Section of the Field Scale Dam, Karlsruhe, Germany.....	54
Figure 4.2:	SEEP/W Grid Used to Analyze Field Scale Dam.....	55
Figure 4.3:	Seepage Front Development as a Function of Time Field Scale Dam, Karlsruhe, Germany.....	56
Figure 4.4:	Steady State Seepage Results Obtained Using SEEP/W to Match Initial Conditions Measured in Field Dam.....	57
Figure 4.5:	Hydraulic Properties Assigned to SEEP/W Model of Field Dam.....	58
Figure 4.6:	Comparison of Measured Seepage Front Development to SEEP/W Model Results of Field Dam.....	59
Figure 4.7:	Comparison of Measured Discharge Rates to SEEP/W Model Results.....	60
Figure 4.8:	Initial Thermal Conditions Measured in the Field Scale Dam, Karlsruhe, Germany (Dry Reservoir).....	61
Figure 4.9:	CTRAN/W Model Simulation Results Using a Geothermal Gradient to Match Measured Data.....	61
Figure 4.10:	Predicted Thermal Distribution as a Result of Cooling (9 days).....	62
Figure 4.11:	Measured Thermal Distribution - 18 Days After Reservoir Impoundment.....	63
Figure 4.12:	Predicted Thermal Distributions Within The Field Dam - 18 Days After Reservoir Impoundment.....	63
Figure 4.13:	Sample Output Showing the Predicted Thermal Distribution With Leakage at the Base - 18 Days After Reservoir Impoundment.....	64

Figure 4.14: Measured Thermal Distribution as a Result of Seepage Through an Upper Leakage Zone 65
Figure 4.15: Predicted Seepage Front Progression during the First 48 Hours After Upper Leakage Zone Was Opened 66
Figure 4.16: Predicted Seepage Front Progression during the First 14 Days After Upper Leakage Zone Was Opened 66
Figure 4.17: Measured and Predicted Thermal Distributions Within the Field Dam - 48 Hours After Upper Leakage Zone Was Opened 67
Figure 4.18: Measured and Predicted Thermal Distributions Within the Field Dam - 14 Days After Upper Leakage Zone Was Opened 68

Figure 5.1: Coquitlam Dam - Site Location 92
Figure 5.2: Hydraulic Filling of Coquitlam Dam 93
Figure 5.3: Construction Photographs of Coquitlam Dam 94
Figure 5.4: 1915 As Built Cross Section of Coquitlam Dam 95
Figure 5.5: Plan View of Coquitlam Dam, 2001 96
Figure 5.6: Typical Cross Section of Coquitlam Dam, 2001 97
Figure 5.7: Recent Photographs of Coquitlam Dam 98
Figure 5.8: Regional Bedrock Geology 99
Figure 5.9: Buried Valleys Near Coquitlam Dam 99
Figure 5.10 Interpreted Distribution of Foundation Soils 100
Figure 5.11: Geological Cross Section A-A and B-B of Coquitlam Dam 101
Figure 5.12: Geological Cross Section C-C and D-D of Coquitlam Dam 102
Figure 5.13: Geological Cross Section E-E of Coquitlam Dam 103
Figure 5.14: Grain Size Distribution Curves for Unit 1B, Coquitlam Dam 104
Figure 5.15: Grain Size Distribution Curves for Unit 2A, Coquitlam Dam 104
Figure 5.16: Grain Size Distribution Curves for Unit 3, Coquitlam Dam 105
Figure 5.17: Grain Size Distribution Curves for Unit 4, Coquitlam Dam 105
Figure 5.18: Grain Size Distribution Curves for Unit 5, Coquitlam Dam 106
Figure 5.19: Grain Size Distribution Curves for Unit 6A, Coquitlam Dam 106
Figure 5.20: Grain Size Distribution Curves for the Shell of Coquitlam Dam 107
Figure 5.21: Grain Size Distribution Curves for the Core of Coquitlam Dam 107
Figure 5.22: Piezometeric Elevations Through Section A-A 108
Figure 5.23: Piezometeric Elevations Through Section B-B 109
Figure 5.24: Piezometeric Elevations Through Section C-C 110
Figure 5.25: Piezometeric Elevations on the West Abutment 111
Figure 5.26: Piezometeric Elevations on the East Abutment 112
Figure 5.27: Temperature Monitoring Locations 113
Figure 5.28: Weir Flow Measurements Correlated with Precipitation at Coquitlam Dam 114
Figure 5.29: Temperature Monitoring Equipment – Prototype Probe 115
Figure 5.30: Temperature Monitoring Equipment - BC Hydro Probe 115
Figure 5.31: Reservoir Temperature Profiling 116
Figure 5.32: Reservoir Annual Temperature Monitoring at Selected Elevations 116
Figure 5.33: Supplemental Reservoir Temperature Profiling 117
Figure 5.34: Sample Temperature Profile Graph from Upstream Shell Piezometers 118
Figure 5.35: Annual Temperature Variation at Selected Elevations in the Upstream Shell 118
Figure 5.36: Sample Temperature Profile Graph from Upstream Core Piezometers 119

Figure 5.37:	Temperature Profile Graph of SP99-2	119
Figure 5.38:	Annual Temperature Readings in Upstream Core Piezometers at Selected Elevations	120
Figure 5.39:	Annual Temperature Readings in Downstream Core Piezometers at Selected Elevations	120
Figure 5.40:	Sample Temperature Profile Graph from Downstream Core Piezometers	121
Figure 5.41:	Temperature Profile Graph from SP99-10	121
Figure 5.42:	Annual Temperature Readings in Abutment and Downstream Toe Piezometers at Selected Elevations	122
Figure 5.43:	Sample Temperature Profile Graph from Abutment Piezometers	122
Figure 5.44:	Annual Temperature Readings at Selected Elevations Through Section B-B	123
Figure 6.1	Initial SEEP/W Model of Coquitlam Dam	138
Figure 6.2	Modified SEEP/W Grid of Coquitlam Dam	139
Figure 6.3	Measured Reservoir Elevations from Coquitlam Dam	140
Figure 6.4	Measured Piezometric Elevations from Coquitlam Dam	141
Figure 6.5	Comparison of Predicted versus Measured Piezometeric Elevations from Coquitlam Dam, with a High Reservoir Level	142
Figure 6.6	Comparison of Predicted versus Measured Piezometeric Elevations from Coquitlam Dam, with a Low Reservoir Level	143
Figure 6.7	Comparison of Predicted versus Measured Piezometeric Elevations from Coquitlam Dam, with a High Reservoir Level	144
Figure 6.8	Comparison of Predicted versus Measured Piezometeric Elevations from Coquitlam Dam, with a Low Reservoir Level	145
Figure 6.9	Comparison of Predicted versus Measured Piezometeric Elevations from Coquitlam Dam, with a High Reservoir Level	146
Figure 6.10	Comparison of Predicted versus Measured Piezometeric Elevations from Coquitlam Dam, with a Low Reservoir Level	147
Figure 6.11	Predicted versus Measured Piezometric Elevations from Coquitlam Dam Using Constant Head Values - High Reservoir Level	148
Figure 6.12	Predicted versus Measured Piezometric Elevations from Coquitlam Dam Using Constant Head Values - Low Reservoir Level	149
Figure 6.13	Reservoir Temperature Data Inputted Into CTRAN/W	150
Figure 6.14	Average Daily And Average Weekly Air Temperature Data	150
Figure 6.15	Predicted Temperature Distribution within Coquitlam Dam, Model Simulation XB-mix2	151
Figure 6.16	Predicted Temperature Distribution within Coquitlam Dam, Model Simulation XB-mix2	152
Figure 6.17	Comparison of Measured versus Predicted Temperature Distribution within Coquitlam Dam	153
Figure 6.18	Coquitlam Dam Heat Transport Model Results for Model Simulation "XB-mix2"	154
Figure 6.19	Coquitlam Dam Heat Transport Model Results for Model Simulation "XB-tr2"	155
Figure 6.20	Coquitlam Dam Heat Transport Model Results for Model Simulation "XB-tr-mix"	156
Figure 6.21	Coquitlam Dam Heat Transport Model Results for Model Simulation "XB-tr6-mix"	157

Figure 6.22 Coquitlam Dam Heat Transport Model Results for Model Simulation "nXB-tr-mix"..... 158
Figure 6.23 Coquitlam Dam Heat Transport Model Results for Model Simulation "re-XB-tr-mix"..... 159
Figure 6.24 Coquitlam Dam Heat Transport Model Results for Model Simulation "XB-tr2-PB-2h"..... 160
Figure 6.25 Coquitlam Dam Heat Transport Model Results for Model Simulation "XB-tr2-PB-5h"..... 161

ACKNOWLDEGEMENTS

There are many people to whom I owe my thanks for help conducting my research and preparing this thesis.

I would like to thank Professor Peter Byrne for acting as my supervisor, and for providing valuable input and suggestions during my research. Secondly, I would like to thank Professor Jonathan Fannin for his assistance in reviewing my thesis and for the recommendations he provided.

I am also grateful for the support and funding that BC Hydro provided for this research, without which this research would not have been conducted. There are many people from BC Hydro to whom I wish to extend my thanks and to express my gratitude for their assistance and advise over this period, including Dr. Michael Lee, Mr. Ken Lum, Mr. Peter Buchanan, and the rest of the Geotechnical department.

I would also like to thank my fellow colleges, with whom I have had the pleasure of attending classes and sharing experiences during the pursuit of our Masters of Applied Science degrees. While I consider all of them my friends, special thanks are extended to Megan Sheffer.

Lastly, I would like to thank my family and friends for their undaunted support and encouragement over the last few years.

CHAPTER 1: INTRODUCTION

Dams are used for water supply, flood management, navigation, irrigation, mining, other industries, power generation, and recreation. There are tens of thousands of dams currently in operation, of all sizes and types (Yong, 2000). Dams and their associated reservoirs create many benefits for societies, but also have detrimental effects. Many dams have the potential to severely impact the natural environment and downstream communities if they were to fail. As a result, dam owners and operators are required to demonstrate that their dam is effectively managed and maintained to:

- protect the public,
- protect the dam owners' investment;
- ensure the integrity of the dam and that the benefits it was designed to provide are achieved; and
- prevent catastrophic failure.

This requires dam operators and owners to utilize best management practices during design, construction and operation, including long term monitoring. In 1995, the International Commission on Large Dams (ICOLD) published Bulletin 99, on Dam Failures – Statistical Analysis. Based on their findings 15% of embankment dam failures were attributed to internal erosion in the dam's body and 12% were attributed to erosion in the foundation. These statistics emphasize the need to monitor and detect changes in seepage through dams, in order to identify problems prior to dam failure. Seepage through dams has been monitored for many years using various types of piezometers and weirs. Due to the significance of seepage measurements and their implications on monitoring dam performance and integrity, new and/or improved methods for monitoring seepage through dams are continually sought.

One method of obtaining additional information about the seepage regime through dams is through the collection and analysis of temperature data from within the saturated zone of the dam and from the reservoir. This method is applicable for dams located in temperate climates in which the accompanying reservoir undergoes annual temperature fluctuations. Since the reservoir temperature varies throughout the year, the temperature of seepage water entering the dam at any given point also varies. The temperature (heat) of the reservoir propagates through the dam by two primary processes: convection, and conduction. Convection refers to the transfer of heat by flowing fluid. Conduction is the transfer of heat through the fluid and the solid phase of elements in contact with one another as a result of temperature gradients (i.e. flow of heat from warm to cold region). Essentially, the temperature (heat) of the seepage water acts as a tracer of the seepage water as it moves through the dam, in a similar manner as chemicals can be used as tracers. The heat of seepage water can then be measured and used in conjunction with traditional piezometric data to infer seepage water velocities and to detect variations in seepage velocities.

Temperature measurements can be collected from existing dams or within newly constructed dams. Temperature measurements within a dam can be collected through dedicated temperature monitoring installations such as thermisters or fibre optic cables. Alternatively, measurements can be taken within existing piezometers using a temperature probe that can be slowly lowered through the piezometer into the water column. Regardless of which measuring system is utilized, data are typically collected at one metre intervals throughout the water column. The collection and analysis of these data primary benefit is achieved due to the significant increase in the array of seepage velocity monitoring locations beyond what is otherwise monitored using piezometers, thus enhancing overall dam performance monitoring capabilities.

1.1 THESIS OBJECTIVES

The objectives of this thesis are to:

1. Develop an understanding for seepage and heat flow through porous media. Develop and apply a numerical modelling procedure to simulate heat and seepage flow in one dimension through porous media. Compare simulated results to results obtained from a closed form solution.
2. Utilize a two dimensional, numerical model to characterize the temperature distribution and seepage regime measured within the homogeneous, field scale model dam constructed in Karlsruhe, Germany.
3. Collect temperature measurements from Coquitlam Dam and reservoir. Evaluate and monitor the performance of Coquitlam Dam by qualitatively analysing heat flow through the dam.
4. Apply the numerical model and procedure used to evaluate seepage and heat flow through the field scale model dam built in Karlsruhe to Coquitlam Dam.
5. Use piezometric and temperature data to assess and monitor the seepage regime within an embankment dam. Assess if temperature data would be a useful tool for dam performance monitoring.

1.2 SCOPE OF THESIS

The theoretical equations relating heat transport and fluid flow through porous media have been studied to develop an understanding of their applications and limitations to analysing heat flow through dams. The inter-relation of these equations when used to examine seepage flow through dams was examined to develop an understanding of how temperature measurements in dams can be used as an indicator of seepage velocity.

This thesis used the uncoupled solution of water flow and heat flow equations to numerically study the application of heat flow through dams as a potential method for monitoring and detecting changes in seepage through dams. The computer programs SEEP/W and CTRAN/W were utilized in the numerical analysis. A comparison was performed to test the procedure for using these two programs to model water and heat flow through porous media. The results obtained from the numerical programs were compared to two closed form solution results for the one dimensional heat flow and water flow through porous media. Then, the numerical programs and method of analysis were applied to model seepage water flow and heat flow through a field scale model dam, constructed in Karlsruhe, Germany.

Concurrently with the numerical modelling, temperature data from the saturated zone of BC Hydro's Coquitlam Dam and the reservoir was collected over a one and a half year period. The numerical modelling programs and procedure used to evaluated the Karlsruhe Germany dam were then applied to analyse the measured temperature data collected from Coquitlam dam and to determine the applicability of the programs and procedure to simulate seepage and heat flow through this dam.

1.3 ORGANIZATION

The concept of using temperature measurement data to infer groundwater and seepage flow is introduced and discussed in Chapter 2. Chapter 2 also presents the theoretical equations used to evaluate heat and water flow through porous media, and describes their application to dams. The importance and potential benefits that this type of monitoring system could provide for dam owners and operators is also discussed. Chapter 3 describes the numerical modelling programs, modelling procedures, and the results of the model verification performed.

Chapter 4 presents the results of the numerical analysis performed on the field scale model dam, constructed in Karlsruhe Germany. Chapter 5 describes the field work component of this thesis and a description of Coquitlam Dam. Temperature and hydraulic monitoring results from Coquitlam Dam are also presented in this chapter. The numerical modelling results for Coquitlam Dam are presented in Chapter 6.

Chapter 7, the final chapter, contains concluding remarks regarding the potential to use temperature measurement data and heat flow modelling as a method of monitoring seepage through dams.

Figures and Tables referenced in the text are presented at the conclusion of each chapter.

This thesis has been written at a level to enable easy understanding of the concept of using temperature measurement data to monitor the seepage condition of an embankment dam. This includes the understanding of heat flows through a dam, of how heat flow is related to seepage, and for what engineering applications it can be used.

1.4 SPONSORSHIP

This thesis was conducted as part of the BC Hydro/UBC Professional Partnership Program. The thesis topic was selected through discussions with BC Hydro. UBC and BC Hydro staff provided technical assistance, support and guidance for this research project and thesis preparation. BC Hydro provided the financial support for the thesis and provided access and information about Coquitlam Dam that has been used and presented in this thesis.

CHAPTER 2: BACKGROUND AND THEORY

2.1 INTRODUCTION

The concept of using temperature data to infer seepage velocities is introduced and discussed in this Chapter. Section 2.2 provides a brief historic perspective on the use and applications of temperature measurement data. Section 2.3 describes the extension of temperature measurement data for the assessment of groundwater velocity to seepage monitoring of embankment dams. The basic theory of heat flow, and groundwater flow are described in Section 2.4. The uncoupled solution of these equations and the required assumptions are presented in Section 2.5. Section 2.5 also describes and presents the coupled solution for heat and fluid transport. Section 2.6 describes the similarity between the heat and contaminant transport equations. Sections 2.7 and 2.8 explain temperature variations that occur in bodies of water and within dams, respectively. Section 2.9 and Section 2.10 discuss the benefits and drawbacks of dams and the principal causes for dam failures. Section 2.11 introduces the concepts of dam performance monitoring and briefly discusses techniques used to monitor dam performance. The benefits of incorporating temperature measurements as one component of dam performance monitoring are outlined in Section 2.12. Section 2.13 outlines the general requirement for the implementation of a dam temperature monitoring program, and a summary is provided in Section 2.14.

2.2 HISTORICAL PERSPECTIVE

Temperature logging of boreholes in the United States began in the 1890's by W.B. Hallock in 1897. Downhole temperature data was plotted and anomalous readings were used to identify zones of escaping gas and flowing water (Keys and MacCary, 1971). Thermal logging of boreholes continues to be used in geophysics along with an array of other logging techniques.

More recently, the idea to utilize temperature data and heat transmission as an indicator of groundwater flow velocity and direction began in the 1960's. In 1960, Taylor and Cary published a paper describing laboratory experiments involving the analysis of water and heat flow through soil columns. Kunii and others (1961, 1962) published a series of papers describing other laboratory experiments conducted to analyse heat transfer through porous media and to obtain measurements of thermal conductivity (Stevens, Ficke and Smoot, 1975).

Between 1960 and 1965, Stallman, in association with others, presented some of the first quantitative estimates of groundwater velocities using temperature measurement data (Stallman, 1965). He presented differential equations for the one dimensional, coupled flow of water and heat through porous media. In 1965, Bredehoeft and Papadopulos used these equations to generate type curves of temperature versus depth below ground surface that could be compared to measured data. Matching measured data to the type curves provided estimates of vertical groundwater flow. Stallman in 1967 and Sorey in 1971 also applied the equations to estimate flow rates through semiconfined aquifers. Cartwright also used Stallman's equations in 1970 to estimate the quantity and rate of water discharged from an aquifer (Stevens, Ficke and Smoot, 1975). Since the late 1960's numerous studies have applied the equations to evaluate flow rates, and quantities, hydraulic conductivity, and the hydraulic transmissivity.

Other studies were conducted to show the effect of recharge and discharge zones on groundwater such as those by Flynn, Silliman, and Simpson, in 1985, and Ingebritsen, Sherrod and Mariner, in 1992.

Another application of groundwater and temperature measurements is to monitor man-induced changes in the groundwater environment, for example through the injection of waste materials that produce heat (i.e. radioactive) or the injection of steam to enhance oil recovery (Stevens, Ficke, and Smoot, 1975; and Domenico and Schwartz, 1998).

Studies of groundwater and temperature have also been conducted in relation to geothermal exploration. However, due to the high temperature gradients that may occur in geothermally active areas, the equations used in these analyses are much more complex. Density driven flow (caused by variations in fluid temperature) may significantly influence overall fluid movement and the potential for water to exist as steam as well as in a liquid state (Ingerbritsen and Sanford, 1998).

2.3 APPLICATION OF METHOD TO EMBANKMENT DAMS

In more recent years, the application of temperature measurement data has expanded to include the assessment of seepage through embankment dams. The application of temperature measurement data for the evaluation of seepage through dams began in the 1980's with the studies of Sam Johansson in Sweden, and others in Germany. Initially, temperature data measured within a dam was compared to reservoir temperature data on a qualitative basis. Then gradually, numerical procedures were adopted based on:

- lag time of peak temperatures in the reservoir to those measured within the dam; and
- annual temperature variations (minimum and maximum variation within the reservoir and within the dam).

Research has continued in this field to improve methods of data collection and analysis. Today temperature measurements are being collected from dams in Sweden, Germany, the United States, Canada (British Columbia and Quebec), at least.

BC Hydro has been involved in this research, through the support of Sam Johansson's work and Martin Artéus and Thomas Johansson. Temperature data have been collected on a number of dams including Coquitlam Dam.

2.4 HEAT FLOW THEORY

Heat is transferred through porous media by:

- conduction through the solid and liquid phase;
- convection through the liquid phase;
- radiation through the solid phase at the material boundary; and
- thermal dispersion through the liquid phase.

Although each of these modes of heat transfer is described by separate equations, they do not act independently from one another. The following subsections will describe each mode of heat transfer.

2.4.1 Conduction

Conduction is the transfer of heat from a warmer region to a cooler region, as a result of a temperature gradient. Fourier's Law describes this process. The general form of the equation is:

$$q_h = -\lambda \frac{dT}{dl} \tag{2-1}$$

where: q_h = conductive heat flux per unit area [E/L^2t]
λ = thermal conductivity of the medium (or K_m) [E/LT]
$\frac{dT}{dl}$ = temperature gradient [T/L]

Thermal conductivity (λ) is a property of materials that expresses the heat flux that will flow through the material if a certain temperature gradient exists across the material. Thermal conductivity varies for different substances. For example the thermal conductivity of water is about 0.6 J/ms°K (at 25°C), of granite is about 3 J/ms°K, and of air is 0.026 J/ms°K (at 25°C) (Ingebritsen and Sanford, 1998). For these three substances heat is transferred best through granite, followed by water and then air.

The following assumptions apply to Equation 2-1:

- media is homogeneous and isotropic;
- flow is steady state; and
- porous media is incompressible.

In porous media where there are solid grains and fluid, heat can be transferred by conduction in any of the following ways:

- from fluid to fluid;
- from solid to fluid;
- from fluid to solid; and
- from solid to solid.

As a result of the complex interaction of heat transfer between the solid and fluid, for analytical purposes when the problems are analyzed on a macroscopic scale, the assumption that the solid and fluid are in thermal equilibrium (i.e. same temperature), for a localized zone is frequently used. This assumption is made for this thesis. Consequently, an effective thermal conductivity value (i.e. average) for the solid and fluid will be used in place of individual thermal conductivity values. The effective conductivity is calculated by:

$$\lambda_{effective} = n\lambda_w + (1-n)\lambda_s \tag{2-2}$$

where: n = porosity [L^3/L^3]
λ_w = thermal conductivity of fluid (i.e. water) [E/LT]
λ_s = thermal conductivity of the solid (i.e. soil) [E/LT]
$\lambda_{effective}$ = effective thermal conductivity [E/LT]

For this thesis the effective thermal conductivity was calculated using Equation 2-2, assuming parallel heat conduction through the solid and liquid phase (Bear 1988; Domenico and Schwartz, 1998; Jumikis, 1977).

2.4.2 Convection

Convection is the transfer of heat by moving fluid (liquid or air). Convection can be subdivided into forced convection and free convection. Forced convection is when external forces such as a hydraulic gradient cause the fluid flow in groundwater systems. In this case Darcy's Law applies. Free convection occurs when the motion of fluid is a result of density variations caused by temperature gradients. In this case, Darcy's Law does not describe the fluid motion: the equations for determining free convection are therefore based on buoyancy.

In analysing heat flow through a dam, the driving force causing water movement is dominated by external forces the hydraulic gradient thus Darcy's Law applies.

Darcy's Law was published in 1856 (Freeze and Cherry, 1979). The general form of this equation is:

$$Q = -K\frac{dh}{dl}A \tag{2-3}$$

where: Q = hydraulic flow rate [L^3/t]
K = hydraulic conductivity [L/t]
$\frac{dh}{dl}$ = hydraulic gradient (change in head/change in length) [L/L]
A = discharge area [L^2]

The following assumptions apply to Equation 2-3:

- porous media is homogeneous and isotropic;
- steady state, saturated flow;
- fluid is single phase and Newtonian;
- fluid is incompressible and homogeneous;
- porous media is incompressible; and
- flow is laminar.

Darcy's Law can be expanded to two and three dimensions. These equations have been studied and applied to numerous problems analysing the flow of groundwater through porous media, including dams and used as the basis for the analysis and solution of seepage problems in this thesis.

The forced convective flow of heat through a saturated porous media is calculated by (Bear, 1988):

$$\frac{\partial T}{\partial t} = \frac{\partial}{\partial x}\left(v_x \frac{\rho_w c_w n T}{\rho c}\right) \tag{2-4}$$

where: T = temperature [T]
x = distance [L]
v_x = seepage velocity [L/t]
ρ = effective density of soil [M/L^3]
ρ_w = density of pore fluid/water [M/L^3]
n = porosity [dimensionless]
c = effective specific heat of the soil [E/MT]
c_w = specific heat of water [E/MT]
t = time [t]

The terms identified as effective density, and specific heat are calculated by the following:

$$\rho = n\rho_w + (1-n)\rho_s \tag{2-5}$$

$$c = \frac{n\rho_w c_w + (1-n)\rho_s c_s}{\rho} \tag{2-6}$$

The calculation of effective specific heat (Equation 2-6) uses a volumetric average of specific heat for the soil and water (Bear, 1988). Specific heat is a measure of the quantity of heat (energy) required to raise 1.0 grams of a substance by 1.0 degrees Celsius or Kelvin. Not all substances warm and cool at the same rate. The specific heat of a substance describes how efficient the substance heats and cools. For example, the specific heat of air is lower than that of soil. As a result air heats and cools faster than soil.

2.4.3 Radiation

Radiation is the emission of electromagnetic waves from a body that allows energy (heat) to be transported with the speed of light through regions of space or other gases (i.e. air) to another body, without altering the temperature of the intervening air. The earth radiates heat to the atmosphere and the sun radiates energy (heat) to the earth. Radiant energy or heat is only transmitted through the solid grains in a porous media. The effective of thermal radiation is relatively shallow and typically does not exceed 10 meters below the ground surface (Domenico and Schwartz, 1998). The effect of heat transport by radiation was neglected in this thesis.

2.4.4 Dispersion

Heat is also transported through porous media by thermal dispersion in the flowing fluid. This form of heat transfer is analogous to the transfer of contaminants by hydrodynamic dispersion. Thermal dispersion is due to distribution of local velocities around soil particles and interconnected pore systems and the subsequent variation in heat within the pore fluid and conduction of heat to the solid (Bear, 1988). Figure 2.1 schematically illustrates the velocity distribution between soil grains, and the variation in heat transported by the fluid. Thermal dispersion tends to promote further spreading of the heat carried by the fluid both in the longitudinal and transverse direction. In a similar manner to hydrodynamic dispersion, longitudinal dispersion is greater than transverse dispersion. Thermal dispersion results in the apparent increase in the thermal conductivity of a porous media (Kuznetsov, 2001). In the absence of fluid motion there is no thermal dispersion.

Numerous experiments and numerical simulations have been conducted to understand the physics of thermal dispersion and to enable this effect to be incorporated into equations used to solve for the heat transport through porous media (Amiri and Vafai, 1994; Wang, and Du, 1993; Hsu and Cheng, 1990; Yuan, Somerton, and Udell, 1991). As described in Moyne et.al. (2000), methods of incorporating the effects of thermal dispersion include: method of moments (Brenner, 1980), volume average method (Hsu and Cheng, 1990), homogenization method (Auriault and Adler, 1995), and ensamble average method (Koch and Brady, 1995). Many of these methods use model constants determined on the basis of comparisons to experimental data. Although numerous methods exist for estimating or incorporating the effects of thermal dispersion into heat transport analyses, inputs parameters are highly idealized (i.e. particle diameter) and may be difficult to apply to more variable porous media, that occur in nature. Another method of calculating thermal dispersion was presented by Bear (1988) as follows (Golder Associates, 2001):

$$E_{long} = \alpha_{long} \frac{n\rho_w c_w}{\rho c} v_i$$

$$E_{trans} = \alpha_{trans} \frac{n\rho_w c_w}{\rho c} v_i \qquad (2\text{-}7)$$

where: v_i = seepage velocity (k_i * i/n) [L/t]
α_{long} = longitudinal thermal diffusivity [L]
α_{trans} = transverse thermal diffusivity [L]

Equation 2-7 was used to estimate thermal dispersion in this thesis.

In general, thermal dispersion is less significant in the overall heat transport equation for flow through porous media, at low Reynolds numbers (<10) (Kuwahara, Nakayama, and Koyama, 1996) than hydrodynamic dispersion is for the solution of the contaminant transport equation. In heat transport thermal conduction plays a more significant role than molecular diffusion in the contaminant transport equation (Bear, 1988). Dispersion is also small in comparison to the convective component of the heat transport equation at low Reynolds numbers.

As flow rates increase through porous media, and turbulent flow results, then the effect of thermal dispersion may play a significant role in the overall transfer of heat (Kuznetsov, 2001; Wang and Du, 1993). In turbulent flow some have suggested that longitudinal thermal dispersion can be neglected, as it is relatively insignificant in comparison to the convective heat transport component of the equation (Kuznetsov, 2001).

Thermal dispersion is neglected in many solutions of the heat transport equation for natural systems or geologic materials, such as in the heat transport program HYDROTHERM (Hayba and Ingebritsen, 1994). However, other programs such as FEFLOW allow the user to include thermal dispersion in the solution of the heat transport equation. Thermal dispersion was included as a very small component in the overall heat transport equation used in this thesis.

2.5 HEAT FLOW EQUATIONS

To determine the overall quantity of heat flowing through a system all components of heat transfer discussed in Section 2.4 must be considered. This can be described in simple terms by:

(energy inflow rate) – (energy outflow rate) = (change in energy storage with respect to time) (2-8)

The heat flow equation (Equation 2-8) can be coupled with the fluid flow equation (Equation 2-3) or uncoupled. The following sections will describe the circumstances and provide examples when each type of equation is appropriate for solving the heat flow equation.

2.5.1 Coupled Heat and Fluid Flow Equations

The flow of water can be induced by hydraulic gradients, as described in Equation 2-3. In addition, temperature gradients, electrical gradients, and chemical concentrations can also induce water flow. In general, heat can be transferred as a result of temperature gradients and also by flowing water (hydraulic gradients in forced convection). It is apparent that these two processes are linked, or coupled and very complex.

One dimensional forms of the coupled heat and water flow equations are (Ingebritsen and Sanford, 1998):

$$\frac{\partial(n\rho_f)}{\partial t} - \frac{\partial\left[\frac{\rho_s k_{rs} k}{\mu_s}\frac{\partial(P+\rho_s gz)}{\partial z}\right]}{\partial z} - \frac{\partial\left[\frac{\rho_w k_{rw} k}{\mu_w}\frac{\partial(P+\rho_w gz)}{\partial z}\right]}{\partial z} = 0 \quad (2\text{-}9)$$

$$\frac{\partial\left[n\rho_f H_f + (1-n)\rho_r H_r\right]}{\partial t} - \frac{\partial\left[\frac{H_s\rho_s k_{rs} k}{\mu_s}\frac{\partial(P+\rho_s gz)}{\partial z}\right]}{\partial z} - \frac{\partial\left[\frac{H_w\rho_w k_{rw} k}{\mu_w}\frac{\partial(P+\rho_w gz)}{\partial z}\right]}{\partial z} - \frac{\partial\left[K_m\left(\frac{\partial T}{\partial z}\right)\right]}{\partial z} = 0 \quad (2\text{-}10)$$

where:
- n = porosity [L^3/L^3]
- ρ_f, ρ_s, ρ_w, ρ_r = density of: fluid (single or two phases), steam, liquid water, and, rock, respectively [M/L^3]
- k_{rs}, k_{rw} = relative permeability of: steam, and liquid water, respectively [dimensionless]
- k = intrinsic permeability [L^2]
- P = pressure [M/Lt^2]
- g = gravitational acceleration [L/t^2]
- z = elevation head [L]
- H_f, H_s, H_w = enthalpy of: fluid (single or two phase), stream, and liquid water, respectively [E]. Enthalpy is a property of the substance and is equal to the internal energy plus the product of the pressure and volume (E + PV)
- K_m = thermal conductivity of porous media [E/LT]
- T = temperature [T]
- t = time [t]
- μ_s, μ_w = dynamic viscosity of: stream, and liquid water, respectively [M/Lt]

These equations can be extended to two and three dimensions as well.

The use of these coupled equations is necessary for the solution of geothermal problems and other problems involving water at high temperatures and relatively low hydraulic head differences. In these types of problems, the two driving forces, water density changes caused by temperature differences, and hydraulic gradients, both play a significant role in determining the overall groundwater velocity. Specific computer modelling programs exist which compute coupled heat and fluid transport, such as HYDROTHERM (Hayba and Ingebritsen, 1994), SUTRA (Voss, 1984) and CFEST (Gupta et.al., 1987). HYDROTHERM is a finite-difference program for modelling three-dimensional, multiphase flow of pure water and heat over a temperature range from 0 °C to 1,200 °C and a pressure range of 0.5 to 10,000 bars. The program was written by the U.S. Geological Survey for modelling magmatic and hydrothermal systems. SUTRA is also available from the U.S. Geological Survey. It is a finite-element program for modelling saturated and unsaturated, fluid-density-dependent groundwater flow with energy transport or chemically reactive single species solute transport. The energy transport component of SUTRA may be used to model thermal regimes in aquifers, subsurface heat conduction, aquifer thermal energy storage systems, geothermal reservoirs, thermal pollution of aquifers, and natural hydrogeologic convection systems. CFEST is a coupled fluid, energy, and solute transport code for the study of multi layered, nonisothermal, groundwater systems. It was written by Pacific Northwest Laboratory, Battelle Division, for the nuclear waste industry.

2.5.2 Uncoupled Heat and Fluid Flow Equations

The density of water is affected by temperature. Figure 2.2 plots water density versus temperature. The maximum density of water is 1.0 g/ml (grams per millilitre) at 3.94°C, below this temperature density decreases slightly to 0.9998679 g/ml at 0°C. At temperatures above 3.94°C, density also decreases as temperature increases. The water density, temperature relation shown on Figure 2.2, is nonlinear. The change in density between water at 5°C and 15°C is less than between water at 15°C and 25°C (Stevens, Ficke, and Smoot, 1975).

In many geotechnical groundwater flow problems and some natural circumstances, the two driving forces (pressure gradient and density gradient) that can cause water flow do not play an equal role in determining the overall groundwater velocity. For example, the seepage of water through embankment dams (Golder Associates, 2000). In these cases the hydraulic (pressure) gradient is the primary driver of water flow (Domenico and Schwartz, 1998).

The temperature variation within Canadian reservoirs typically ranges between 0°C and 20°C. However, the temperature variation within the main body of embankment dams in Canada is usually less, approximately between 4°C and 15°C, with many dams experiencing less temperature variation. Based on this observation and work conducted by Golder Associates (2000), the density driven component of seepage flow through embankment dams is minor in comparison to the hydraulic gradient component. The density driven flow component caused by differences in water density (caused by temperature variations) is negligible. The groundwater flow component of the problem can be solved independently from the heat transport problem. In other words, uncoupled equations can be used to solve the problems. This means a simplified form of Equation 2-9 can be used to solve the groundwater seepage problem. The velocity values obtained from the solution of the seepage flow equation can then be used to solve the following heat transport equation (Bear, 1988).

$$\frac{\partial T}{\partial t} = \frac{\partial}{\partial z}\left(E_{ij}\frac{\partial T}{\partial z}\right) - \frac{\partial}{\partial z}\left(v\frac{\rho_w c_w n T}{\rho c}\right) \qquad (2\text{-}11)$$

where: T = temperature [T]
x_i = distance [L]
v_i = seepage velocity [L/t]
E_{ij} = thermal conductivity and dispersion tensor
ρ = effective density of soil [M/L^3]
ρ_w = density of pore fluid/water [M/L^3]
ρ_s = density of solid [M/L^3]
n = porosity [dimensionless]
c_s = effective specific heat of the soil [E/MT]
c_w = specific heat of water [E/MT]
λ, ρ, c = effective values
λ_s, ρ_s, c_s = values for soil/solid
λ_w, ρ_w, c_w = values for water

The thermal conductivity and dispersion tensor (E_{ij}) combines the terms from the conduction component of the heat transport equation with the dispersion component as they are both second order terms in the overall heat transport equation. This tensor is calculated using:

$$E_i = \alpha_{long}\frac{n\rho_w c_w}{\rho c}v_i + E^* = E_{long} + E^*$$

$$E_j = \alpha_{trans}\frac{n\rho_w c_w}{\rho c}v_i + E^* = E_{trans} + E^*$$

$$E^* = \frac{\lambda}{\rho c} \qquad (2\text{-}12)$$

where: E^* = is commonly referred to as the materials thermal diffusivity [L^2/t] (Kreith and Bohn, 1993)

Equation 2-11 calculates the rate of temperature change with respect to time, at each point. The first term on the right hand side of the equation represents the diffusion of heat. Two mechanisms cause heat diffusion:

- thermal conduction through solid and liquid filled pores; and
- dispersion due to microscopic variations in pore fluid velocity.

The second term on the right side of the equation represents the convective component, or heat transported by the moving fluid.

When temperature and/or density gradients do not play an important role in fluid flow:

- Equation 2-9 becomes the standard consolidation (or transient seepage flow) equation (Equation 2-3); and
- Equation 2-10 simplifies to equation 2-11.

In this case, the fluid/heat flow equations are not fully coupled but a 'weak' coupling exists. That is, the velocity field, v, calculated using the transient flow equation 2-3 is used in equation 2-11 to calculate the temperature field.

2.5.3 Assumptions for Uncoupled Heat and Fluid

At this point, it is important that we review the assumptions and limitations of the uncoupled heat and fluid flow modelling approach, discussed above. The following assumptions apply:

- the seepage regime is independent of temperature;
- on the microscopic scale, the soil and water are considered to be in thermal equilibrium, or in other words have the same temperature;
- the fluid must be single phase and Newtonian;
- the flow is laminar, the fluid is incompressible, and homogeneous;
- the solid is non deformable and chemically inert with respect to the fluid;
- for each material there is a constant coefficient of thermal dispersion; and
- no heat sources or sinks must exist within the fluid.

This section has outlined the basic heat flow equations that will be used in this thesis for modelling. The basic heat flow Equation 2-11 is very similar to the equation for contaminant transport. The similarities between these two equations will be discussed in the next section.

2.6 HEAT TRANSPORT AND CONTAMINANT TRANSPORT EQUATIONS

The standard equation used for the solution of contaminant transport problems is presented below.

$$\frac{\partial C}{\partial t} = \frac{\partial}{\partial x_i}\left(D_{ij} \frac{\partial C}{\partial x_j} \right) - \frac{\partial}{\partial x_i}(v_i C) \qquad (2\text{-}13)$$

where: C = concentration of dissolved contaminants [M/L^3]
D = coefficient of molecular diffusion [L^2/t]
v = seepage velocity [L/t]
t = time [t]
x = distance [L]

The solution of the contaminant transport equation can be solved as a coupled equation with the groundwater flow equation or solved sequentially (i.e. uncoupled). If solved sequentially, the groundwater flow equation is solved first, then the velocity values from this solution are used in the solution of the contaminant transport equation. For most applications, an uncoupled solution is adequate, as the concentration gradients have limited effect on the overall groundwater flow system.

Equation 2-13 is very similar to Equation 2-11. The only difference between the two is the constant term that is multiplied with the seepage velocity term. The one dimensional forms of Equation 2-11 and Equation 2-13 are:

$$\frac{\partial T}{\partial t} = E\frac{\partial^2 T}{\partial x^2} - \left(\frac{\rho_w c_w n}{\rho c}\right)\left(\frac{u}{n}\right)\frac{\partial T}{\partial x} \tag{2-14}$$

$$\frac{\partial C}{\partial t} = D\frac{\partial^2 C}{\partial x^2} - \left(\frac{u}{n}\right)\frac{\partial C}{\partial x} \tag{2-15}$$

where: u = Darcian velocity

Equation 2-15 can be converted into Equation 2-14 if the following substitution for porosity is applied to Equation 2-14.

$$n = \frac{\rho c}{\rho_w c_w} \tag{2-16}$$

This means that contaminant transport programs could be used to solve the uncoupled, heat transport problem, by utilizing the porosity substitution described by Equation 2-16, and providing the appropriate thermal dispersion values were used.

2.7 TEMPERATURE VARIATION IN BODIES OF WATER

In temperate climates, such as Canada experiences, there are annual cycles of cold and warm weather. The changes in climate throughout the year result in water bodies being warmer for a portion of the year, summer, and then cooler for another portion of the year, winter. Bodies of water go through a transition phase, between these two temperature extremes, in the spring and fall. The actual temperature of any given body of water depends on various climatic factors as well as particular details about the body of water and its surroundings. However, the general shape of the temperature profile, or temperature variation with depth, for each season has been observed to be predictable. The temperature profile for shallow bodies of water and deep bodies of water are significantly different, as shown schematically in Figure 2.3 and Figure 2.4, respectively.

For shallow bodies of water, generally less than 10 metres, during the summer months, the surface temperature is warmest and the temperature gradually decreases as depth of water increases (Stevens, Ficke, and Smoot, 1975). Then in the fall, as air temperatures moderate, the surface temperature along with the rest of the water body gradually decreases. In the winter, ice may form on the water surface, in this case, the surface will be cooler and the water temperature will gradually increase as depth increases, to about 4°C. If ice does not form on the water surface, the temperature will either be constant with depth, or show a slight increase with depth in the top one to two metres, below which the temperature will be constant. Then as temperatures in the spring increase, the surface temperature of the water increases first, and this heat is gradually transmitted to greater depths within the body of water.

For deep bodies of water, thermal stratification occurs, as shown on Figure 2.4. Thermal stratification occurs when temperature differences within the water body, causes density differences, that effectively isolates the warmer and cooler water zones. For example, in the summer the upper portion of the water is warmer, and the water has a lower density. Below a certain depth the water is significantly cooler and has a higher density than the warm surface water. Between the two zones is a zone of rapid temperature change. As surface temperatures

decrease in the autumn, the upper warm water zone gradually cools, and moves deeper into the water column. Complete mixing occurs when the surface water temperature is approximately equal to the temperature at the base. The temperature of the water body will be constant or nearly constant with depth during the winter, if ice does not form on the surface. If ice does form on the water's surface, then thermal stratification may again result. In this case, the frozen water has a lower density, and therefore floats above the warmer water which has a higher density. Figure 2.4 schematically demonstrates a winter profile, when ice forms on the water's surface. Then in spring, surface temperatures again increase and this heat is transmitted gradually through the water column, until the density differences become significant enough. At this point, thermal stratification will again result and minimize any further mixing of warm surface water and cool base water.

These seasonal changes in water temperature described above also occur in reservoirs. As a result, the temperature of seepage water entering a dam varies throughout the year. This temperature variation can be used as a tracer to indicate groundwater velocity.

2.8 TEMPERATURE VARIATION WITHIN DAMS

The actual temperature measured within a dam can be influenced by many factors including:

- reservoir temperature and annual fluctuation;
- reservoir depth;
- hydraulic flow rate through the dam;
- air temperature and climatic region;
- groundwater flow, especially near the foundation, abutments and dam toe;
- geothermal gradient;
- sun's radiation; and
- vegetative cover.

As discussed in section 2.4.1 the reservoir temperature varies throughout the year and varies with depth. Since the majority of the seepage water within the dam originates from the reservoir, the reservoir's temperature naturally has a significant influence on the water temperature within the dam. Similarly, the source of seepage water's depth is also significant. Seepage water that originates near the reservoir's surface will have a larger annual fluctuation in temperature, in comparison to seepage water that originates from the base of the reservoir.

Seepage through a soil unit with higher hydraulic conductivity will respond faster to changes in reservoir elevations. Similarly, the temperature of a higher conductivity layer will responded faster to changes in the reservoir temperature, and will have a greater annual fluctuation, than a lower conductivity unit, located at the same distance from the reservoir.

The climatic region plays an important role in the temperature measured within the dam, as it significantly affects the reservoir temperature and annual variation. In addition, changes in air temperature also affect the temperature of soil near the surface. This heat or cool temperature then propagates down by conduction to other soil grains. Typically air temperature will affect temperatures measured within the top ten metres for soil, below ground surface (Stevens, Ficke, and Smoot, 1975; Domenico, 1972).

Groundwater temperatures are typically very constant throughout the year. Shallow groundwater is influenced by heat conduction from the ground surface, but this attenuates with depth.

Groundwater located more than ten metres below ground surface generally will show less than 0.5 °C fluctuation annually (Stevens, Ficke, and Smoot, 1975). Groundwater located ten to twenty metres below the ground surface generally exceeds the local mean annual air temperature by 1°C to 2°C (Stevens, Ficke, and Smoot, 1975). Typically, the temperature of groundwater located 20 metres or more below the ground surface increases with depth due to the geothermal gradient. The magnitude of the geothermal gradient can vary depending on geographic location, type of rock, presence of thermal sources, volcanic activity, and other factors (Bear, 1988). Stevens, Ficke, and Smoot (1975) reported a typical temperature increase, caused by the geothermal gradient, of 2°C to 3°C for a 100 metre increase in depth. Bear (1998) reported an increase of 1°C for a 20 to 40 metre increase in depth. Jakosky (1957) reported a geothermal gradient of 1°C for a 60 metre increase in depth. In areas of the dam where groundwater and reservoir seepage water mix, the recorded temperature will be influenced by both the reservoir temperature and groundwater temperature.

Geothermal gradients influence groundwater temperatures as depth below the ground surface increases. The geothermal heat source may increase the temperature of the soil, and seepage water through conduction in high dams or dams located in regions with high geothermal activity.

The sun's radiation adds energy in the form of heat to the surface soil particles and to the water's surface in the reservoir. The depth of influence of the sun's radiation attenuates rapidly. Vegetation on the dam's surface reflects the sun's radiation, therefore decreasing the surface soil's temperature, during the daytime. However, vegetation can act as an insulating blanket to keep the surface of the dam warmer during the night. Both of these factors are less significant, except in very small dams.

As part of the modelling process, it is important to conceptually understand the movement of heat from the reservoir into a dam. This is important in any modelling procedure in order to verify the output generated from a computer model. If we consider the annual temperature variation in a reservoir as a wave of heat, then we can look at how the heat wave is propagated through a section of the dam. If we consider a homogeneous dam, constructed of low conductivity, then heat from the reservoir will be carried by the seepage water (convection) and also through conduction of heat through the soil and water. The amplitude of the heat wave (annual temperature variation) will decrease along the flow path. In addition, as distance from the reservoir increases the response time to changes in reservoir temperature will increase. Figure 2.5 schematically shows the propagation of the maximum and minimum annual temperatures and how the heat from these two seasons moves through the dam. Now if we consider the heat propagation through a section of a homogeneous dam with a higher hydraulic conductivity, we would see a similar pattern as depicted in Figure 2.5. However, the annual temperature variation at any given distance from the reservoir would be larger. Figure 2.6 schematically compares the temperature variations for a low conductivity dam to that of higher conductivity dam.

A second way to look at the measured temperature data in the dam is by considering the annual temperature profile measurements made in a piezometer. Figure 2.7 shows typical temperature profile data measured within a dam's piezometer. The annual temperature variation depicted in Figure 2.7a is for a piezometer with minimal air temperature effects. In contrast, the temperature distribution shown in Figure 2.7b is for a piezometer that is significantly influenced by changes in air temperature. No high conductivity layers are apparent from the temperature data shown in Figure 2.7. If a higher conductivity layer did exist, we would expect that there would be a change in the temperature profile data. Figure 2.8a schematically compares the profile for a constant hydraulic conductivity zone to one with a higher conductivity zone between two low conductivity

zones. There is a change in the slope of the profile data that corresponds to the higher conductivity layer. In addition, the annual temperature variation is greater in the high conductivity layer. Figure 2.8b shows real data with a higher conductivity layer at the 125 metre elevation. In this case a lower temperature occurs at the 125 metre elevation and there is a general change in slope of the profile data, but the maximum temperature does not occur at this elevation.

2.9 DAMS

Throughout the world, there are tens of thousands of dams of all sizes and types currently in operation (Yong, 2000). Approximately 45,000 of these dams are higher than 15 metres (Williams, 2000). The number of dams continues to increase each year. Harry Blohm, Chairman of the International Commission on Large Dams (ICOLD) stated the major driving force for dams throughout the world will be the need for reliable safe water supply, and in particular in the developing world (Blohm, 2000).

Dams are used for water supply, flood management, navigation, irrigation, mining or other industries, power generation, and recreation. Dams and their associated reservoirs create many benefits, but also have negative impacts.

Recently, the negative impacts of dams have received greater attention in the North American media and general public. The public and media's focus has primarily related to dams impacts on salmon and their aquatic habitat, due to the declining populations of many salmon species (i.e. McClure, 2000; Paulson, 1999; Cantrell and Helm, 2001). This concern has lead to the removal of some dams including; Rat Lake Dam on Whitestone Creek (Washington), Marine Dorian Dam on the Walla Walla River (Oregon), Lewiston Dam on the Clearwater River (Idaho), and Goldsborough Dam on the Goldsborough Creek (Washington) (Cantrell and Helm, 2001). The increased awareness and concerns regarding dams led ICOLD to include this as one of their four topics at the 20th Congress of the ICOLD, September 2000, held in Beijing, China.

With increased public focus on dams and their potential impacts, there is a need for dam owners and operators to demonstrate that each dam is effectively managed and maintained. This management provides protection for the public, protection of the owner's investment, insurance that objectives of the dam are obtained, and prevention of a catastrophic failure. This requires dam operators and owners to utilize best management practices during design, construction and operation, including long term monitoring.

2.10 DAM FAILURES

As is customary with most engineering disciplines, the analysis of failures or problems is key to improving, and preventing future failures. Since the early 1900's, engineers have been compiling information on dam failures and incidents to improve their knowledge and the safety of these structures (ICOLD, 1995). In 1995, ICOLD published Bulletin 99, on Dam Failures – Statistical Analysis. Based on this study the following conclusions were reached regarding dam failures.

- Prior to 1950, 5,268 dams were constructed. Between 1951 and 1986, 12,138 dams were constructed. These numbers exclude dams constructed in China.
- Of the dams constructed prior to 1950, 117 failures were reported (2.2%). Only 0.5% (51) of the dams constructed between 1951 and 1986 have failed.

- The largest number of dam failures has occurred in dams less than 30 metres in height. However, this is because more dams in this height category have been constructed. When the data is normalized, to the number of dams built in each height category, then there is no appreciable difference in number of dam failures, for each height category (less than 30 metres, 30 to 60 metres, and greater than 60 metres).
- Most dams that have failed were embankment dams constructed of soil and/or rock. When the dam failure data is normalized according to the number of dams constructed in each category, then there are just slightly more failures in the embankment dam category than the other dam type categories.
- Seventy percent of dam failures occur in the first ten years of operation, with sixty one percent of failures occurring during the first year of operation.
- Most concrete dam failures have been attributed to problems with the foundation. Internal erosion and insufficient shear strength of the foundation were reported as the primary causes of the foundation failures.
- Forty-three percent of masonry dams failed due to overtopping and twenty-nine percent failed as a result of internal erosion in the foundation units.
- The primary cause of embankment dam failure was overtopping (31%). Subsequently rated failure causes were attributed to internal erosion in the dam's body (15%) and erosion in the foundation (12%).

With the relatively high incidences of failures due to internal erosion, methods of assessing abnormal seepage flow, such as temperature measurements, which is likely to accompany erosion is very important.

2.11 MONITORING DAM PERFORMANCE

Catastrophic failure of dams, such as the Malpasset Dam in France, 1959, has served to emphasize the potential risk associated with dams and the importance of monitoring dam performance (Yong, 2000). Monitoring the status and performance of dams is important for all dam operators and owners, however, it is particularly important for large dams or dams classified as high risk. Dam performance monitoring is a standard of practice. It is conducted to ensure the integrity of the dam is maintained, to detect potential problems, and to protect the safety of surrounding populations. The ICOLD recognized the importance of establishing standards and procedures for the monitoring of dams in 1965. ICOLD released their first publication "Dam Monitoring" in 1969 (Bulletin 21). Since that time, revised versions dealing with this subject have been published by ICOLD including:

- Dam Monitoring, Bulletin 60, 1988;
- Monitoring of Dams and Their Foundations, Bulletin 68, 1989; and
- Improvement of Existing Dam Monitoring, Bulletin 87, 1992.

These publications along with numerous others have introduced and discussed methods, and applications for various dam monitoring techniques, that are applicable during dam construction, reservoir filling, and for post construction monitoring. Post-construction monitoring techniques for embankment dams may include the measurement of:

- pore pressures using piezometers;
- seepage rates using weirs or other flow measuring devices;
- settlement using settlement gauges, plates, or other survey instruments;

- turbidity in seepage water discharges;
- vertical movements using inclinometers;
- horizontal movements using survey measurements, or other geodetic measurements;
- differential displacements using extensometers;
- strain measurements using strain gauges;
- seismic movements using ground motion detectors and recorders;
- seepage measurements using streaming potential, temperature measurements within the saturated zone of the dam;
- surface temperature measurements using thermography; and
- visual inspections.

Through the use and effective implementation of dam monitoring techniques the safety performance of dams can be increased, the potential risk of dam failure can be decreased, the performance of dams can be improved and the security for surrounding communities can be improved (Yong, 2000).

As stated previously, the focus of this thesis is the use of temperature measurements at points within dams, as an indicator of seepage through a dam.

2.12 POTENTIAL BENEFITS OF INCORPORATING TEMPERATURE MONITORING INTO A DAM MONITORING PROGRAM

Temperature measurement data collected from the saturated zone within a dam when compared to the temperature variation within the reservoir can be used as an indicator of seepage through a dam. The annual warm and cool cycles of a reservoir can act as a tracer of the seepage water and seepage velocity through the dam. Since the early 1990's temperature measurements have been collected from within selected dams, and analysed in a qualitative manner, as section 2.4.6 described, to evaluate seepage. Gradually more quantitative and numerical methods are developing for the analysis of heat flow through dams, such as the work conducted by Konrad et.al. (2000), Johansson (2001), this thesis, and others.

The incorporation of temperature monitoring into a dam monitoring program may provide the following benefits to monitor seepage flow in addition to more traditional piezometric monitoring:

- there is flexibility in implementation, as temperature data can be collected from within existing piezometers or specifically designed installations;
- temperature data can be collected manually or using automated systems; and
- temperature readings can provide a far denser array of readings that can be used to monitor seepage.

2.13 General Requirements for the Implementation of a Temperature Monitoring Program

To implement a program to collect temperature data from a new dam or an existing dam, temperature readings need to be collected from the reservoir and from within the dam's saturated zone. Temperature readings can be collected manually using a temperature probe or a multi-probe that includes temperature as one component array of monitoring parameters. Alternatively, temperature data may be collected using thermisters, vibrating wire sensors, or fibre optic cables. If any of these devices are used it is possible that readings could be automatically collected, stored and remotely assessed using data loggers or other data acquisition systems. If manual devices, such as a temperature probe are utilized, then they can be used in the reservoir (fixed location) in existing piezometers, or specifically installed tubes filled with water. The piezometers should not have vertical flow (i.e. not within leaky piezometers) and should be less than 7 centimetres in diameter. The diameter restriction comes from research conducted by Sammel (1968) who found that the potential for thermal disturbance in a piezometer caused by buoyancy effects is minimized if readings are collected from small diameter piezometers. Regardless of which type of instrument is used to measure the temperature, a minimum accuracy of 0.1°C is required in order to accurately detect the small fluctuations that may be necessary to indicate changes in seepage. Temperature readings are typically collected at one metre intervals throughout the water column and within the reservoir, and generally should be collected on a monthly basis in order to provide sufficient information on annual temperature variations (Johansson and Hellström, 2001).

More specific information about the temperature monitoring program implemented at Coquitlam Dam is presented in Chapter 5.

2.14 Summary and Conclusions

The initial concepts of using temperature measurements to indicate zones of groundwater flow, flow direction and velocity have existed since the late 1890's. Applications and implementation of these ideas became more widespread in the 1960's and 1970's and has continued to expand. In the 1980's these concepts were expanded to include the assessment of seepage through dams. Research has been conducted to evaluate the potential benefit of using temperature measurement data to detect concentrated zones of seepage that may indicate problems within a dam. Dam owner's and operators are cognizant of the need to protect public safety and the environment from potential dam failures, as well as to protect the large capital investment required to build and maintain dams. The inclusion of a temperature monitoring program and the associated heat flow analysis for dams which are classified as high risk or could cause severe consequences if failure occurred, could be beneficial.

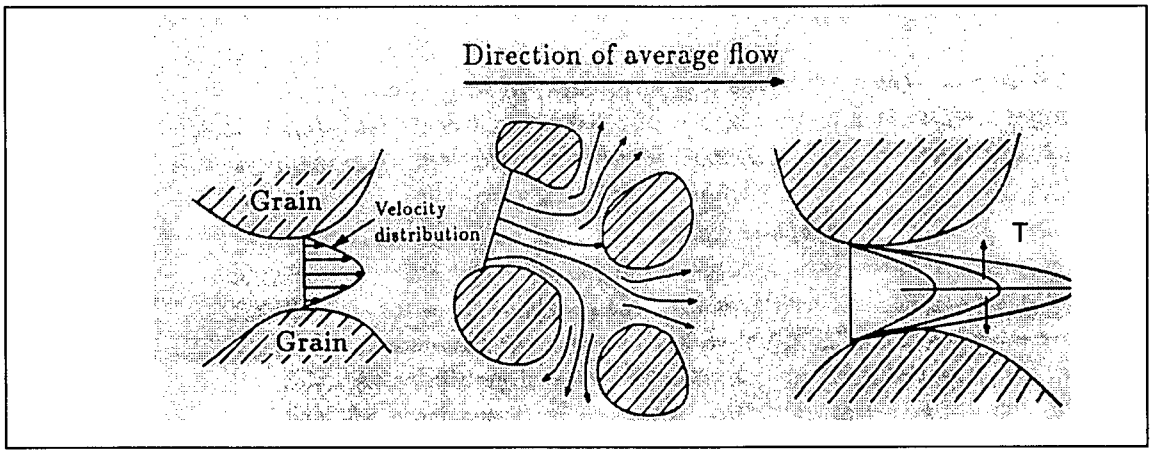

Figure 2.1: Velocity Variation Due to Pore Systems and Resulting Temperature Variation Schematic of Thermal Dispersion (Bear and Bachmat, 1990)

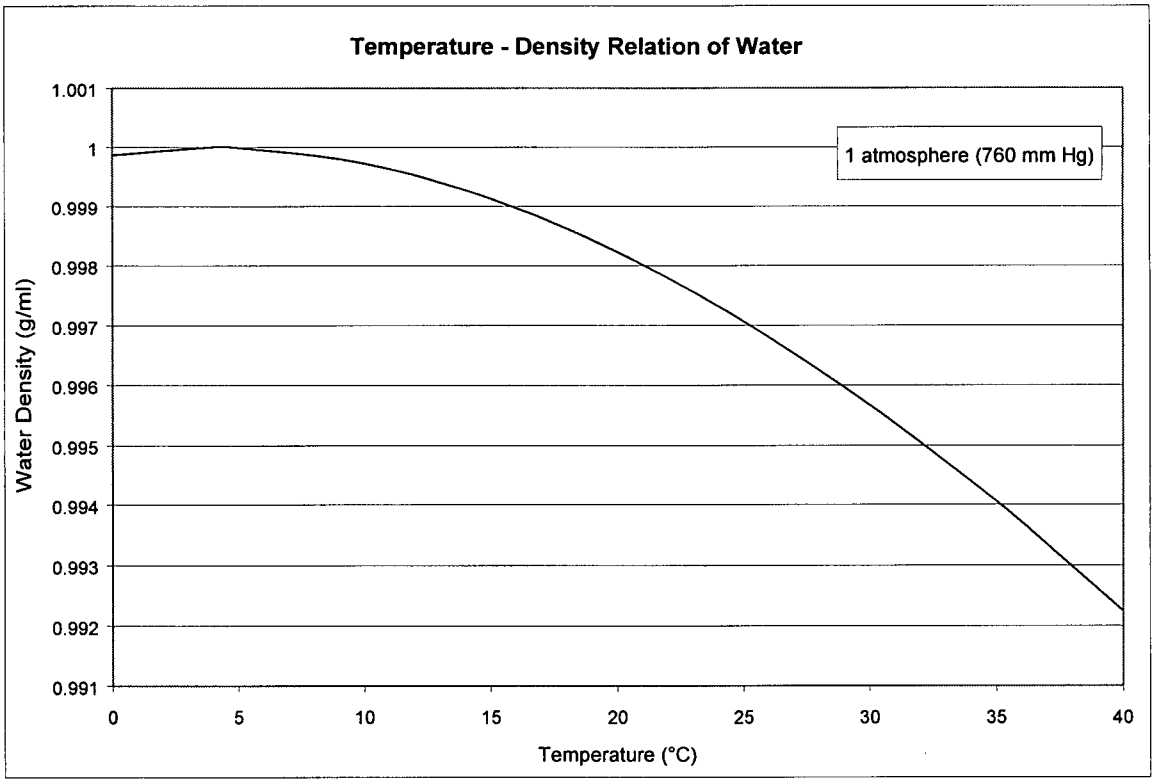

Figure 2.2: Temperature Density Relation of Water at 1 Atmosphere (Stevens, Ficke, and Smoot, 1975)

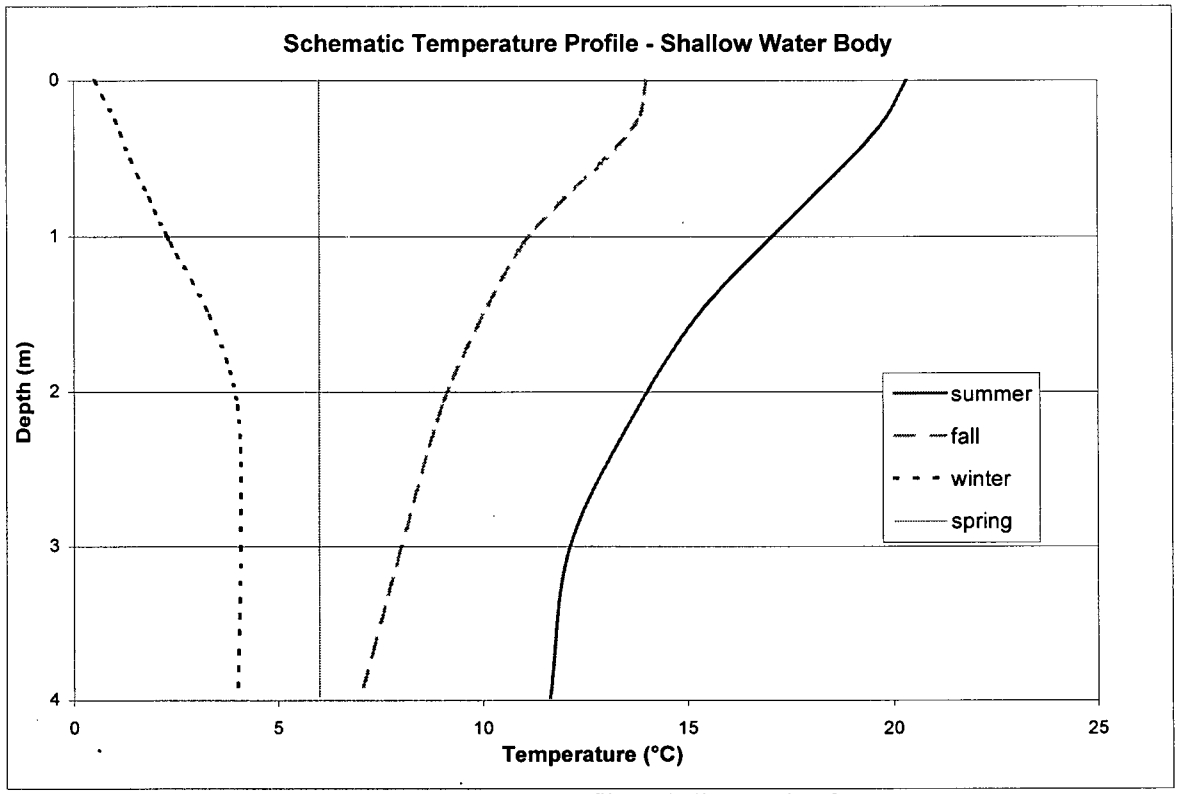

Figure 2.3: Schematic Temperature Profile – Shallow Body of Water

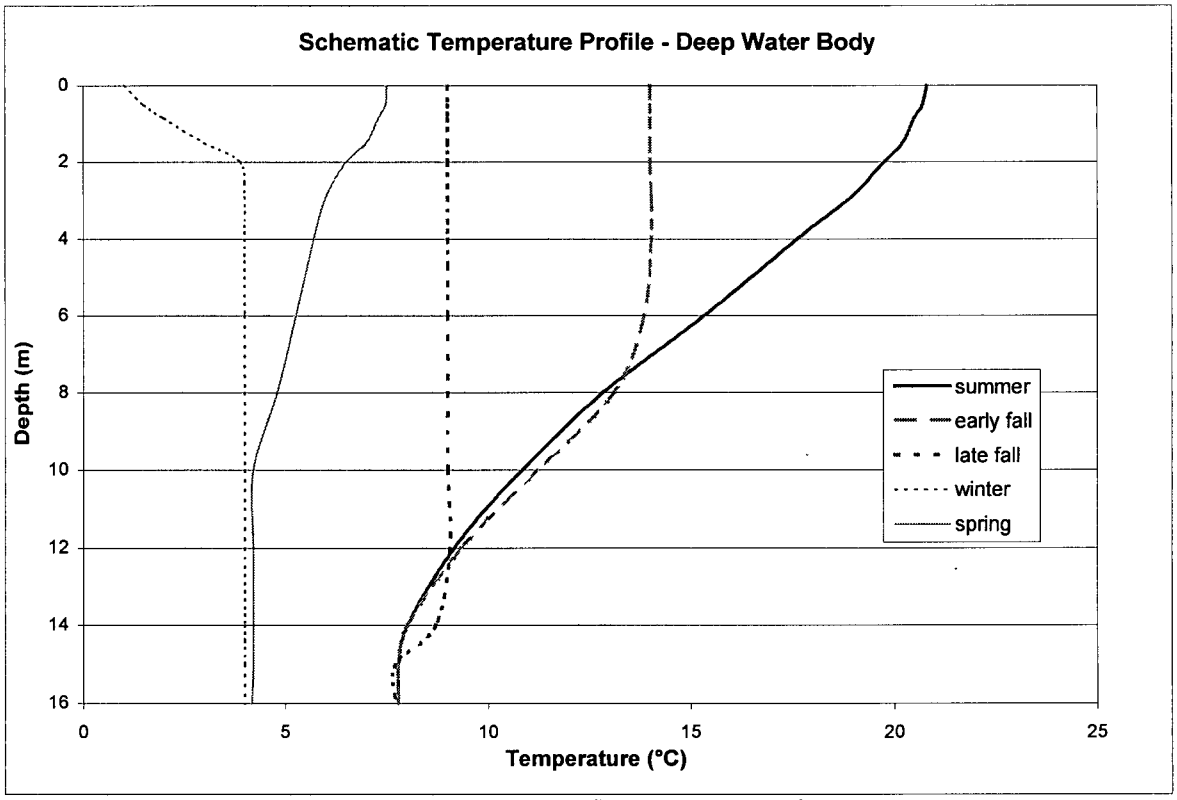

Figure 2.4: Schematic Temperature Profile – Deep Body of Water

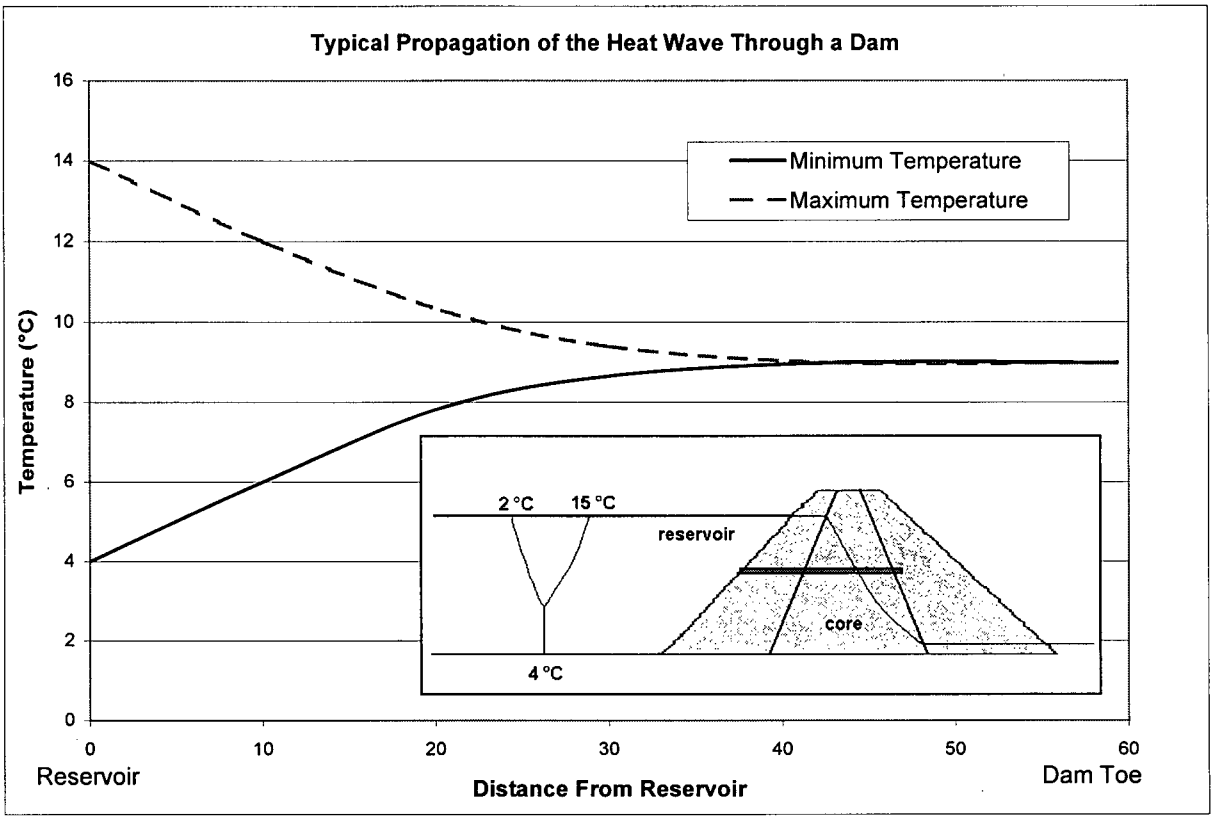

Figure 2.5: Schematic View of a Heat Waves Propagation Through a Homogenous Dam

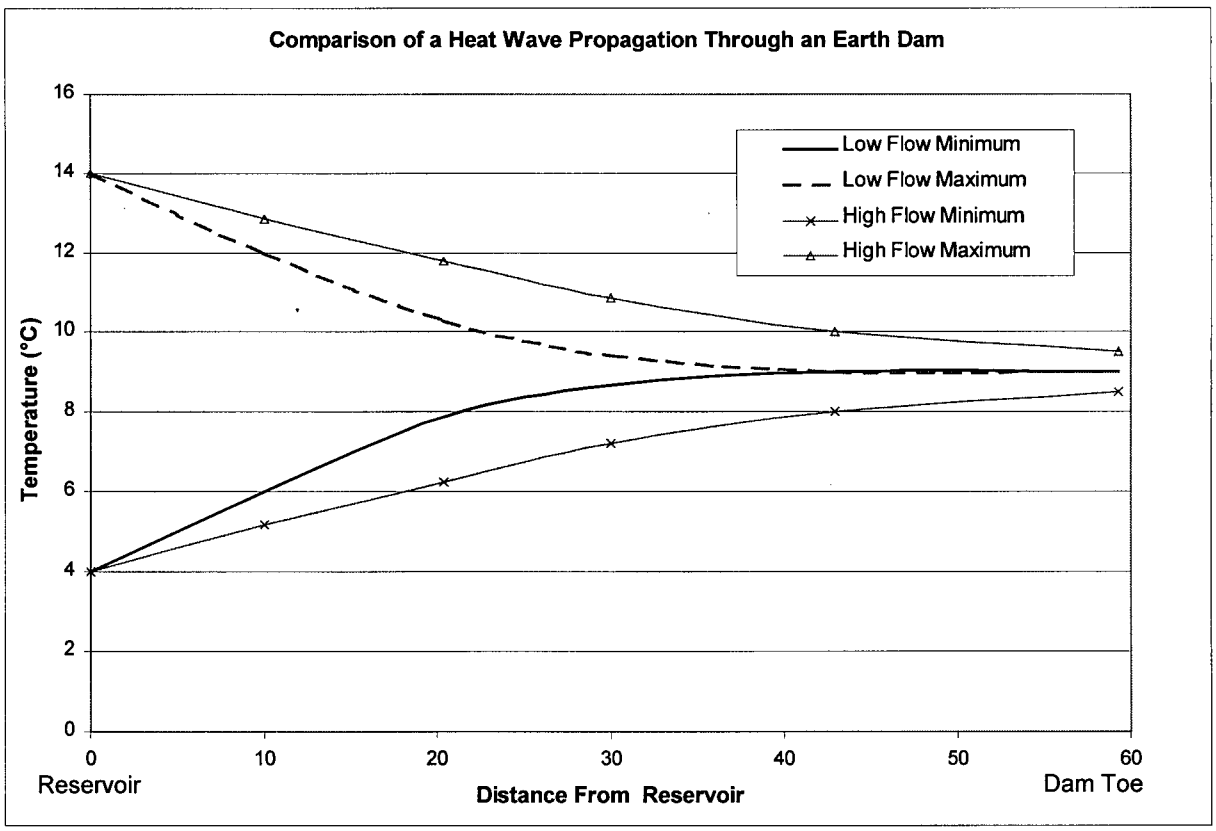

Figure 2.6: Comparison of a Heat Wave Propagated Through a Lower Conductivity Dam and a Higher Conductivity Dam

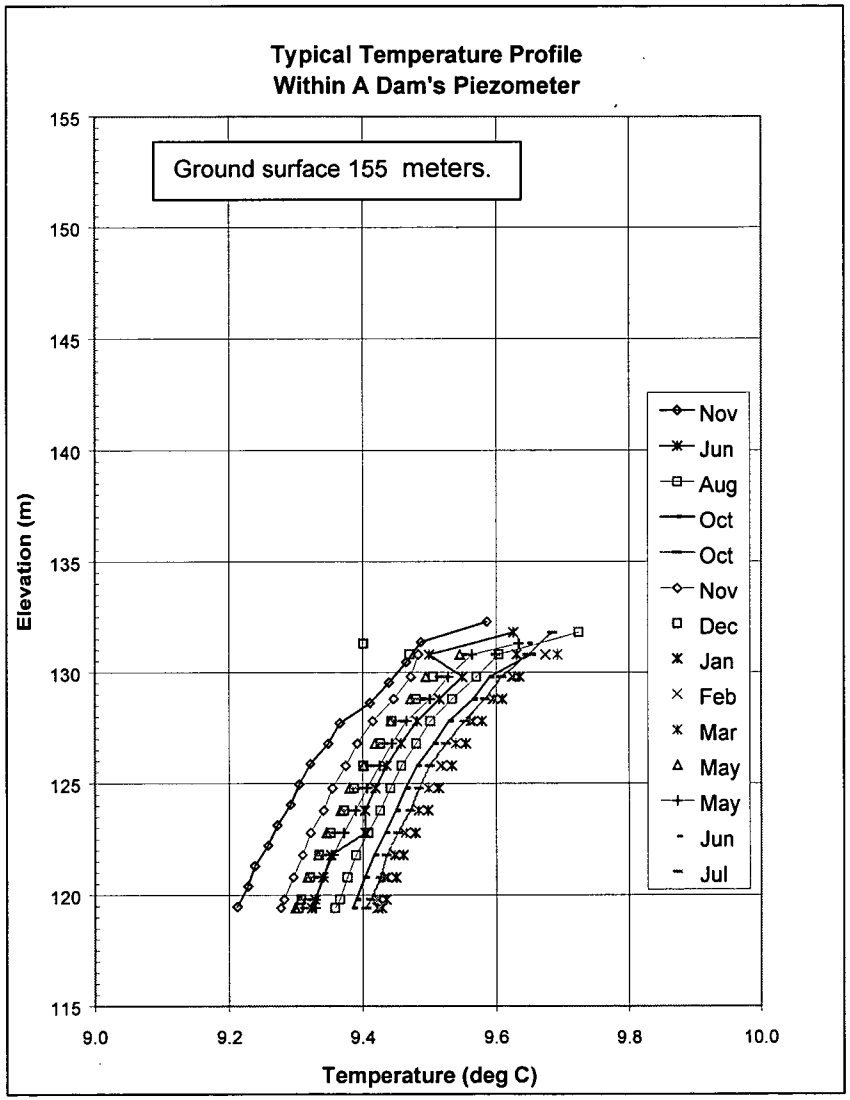

a: Typical Temperature Distribution Within A Dam's Piezometer Without Air Temperature Effects

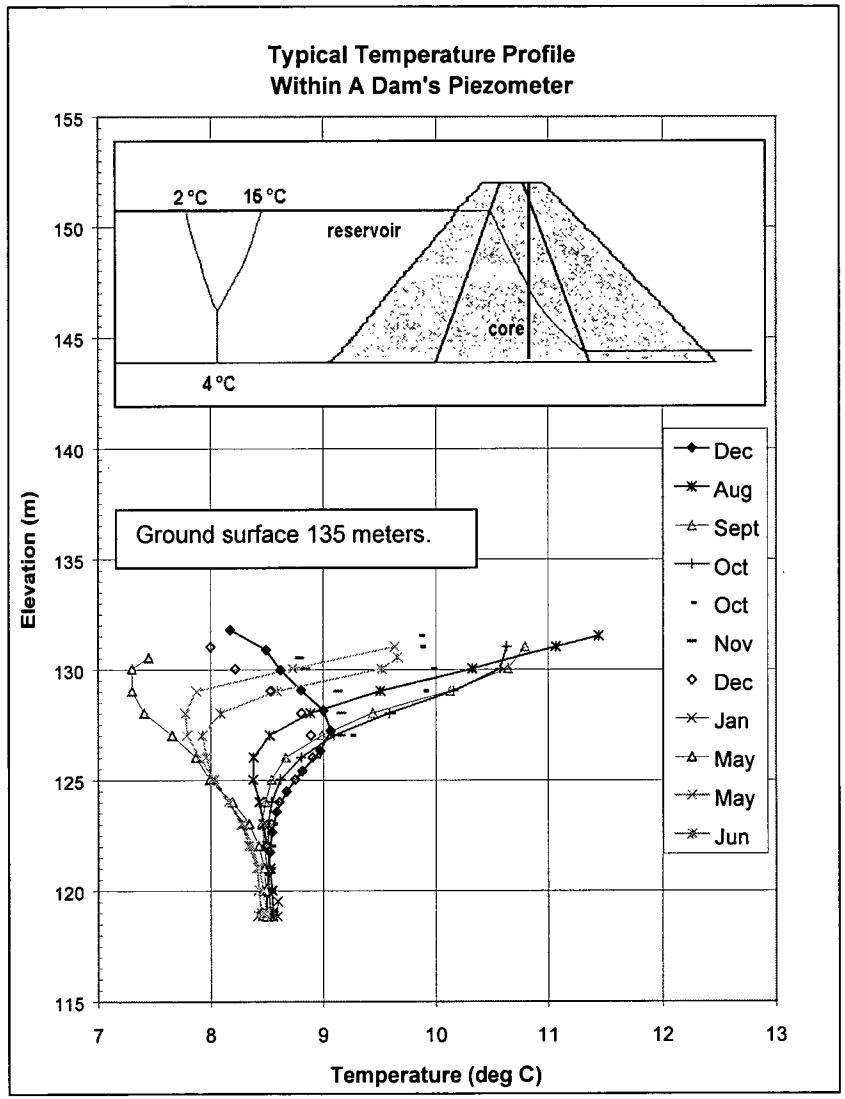

b: Typical Temperature Distribution Within A Dam's Piezometer With Air Temperature Effects

Figure 2.7: Temperature Profiles Within A Dam's Saturated Zone

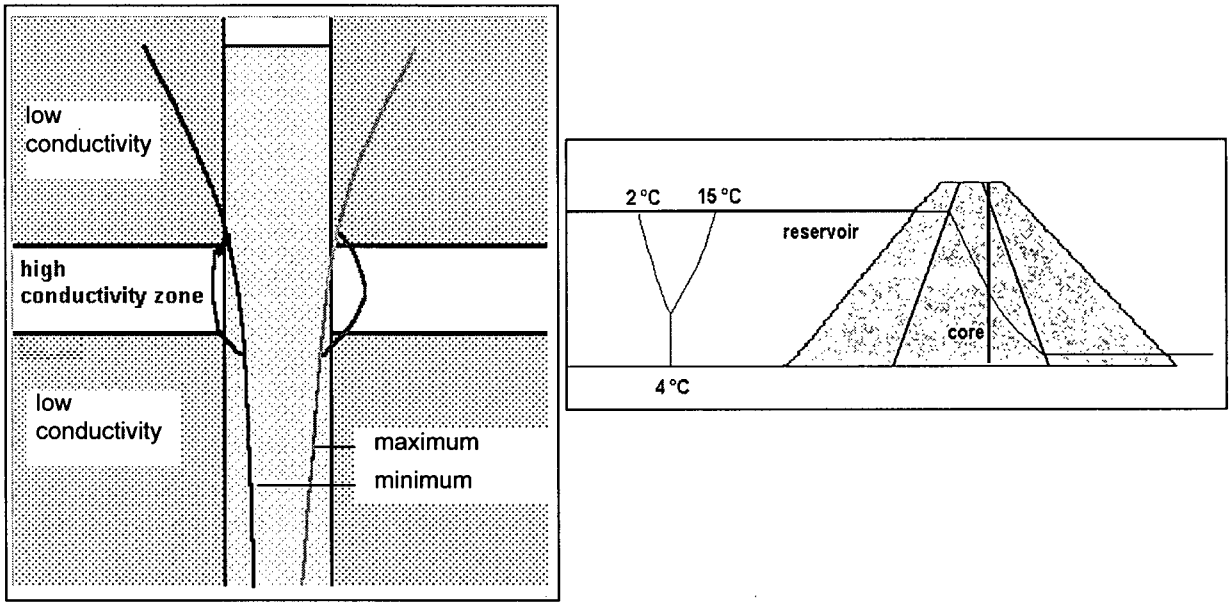

a: Schematic Comparison of a Normal Temperature Distribution To One With a Higher Conductivity Zone

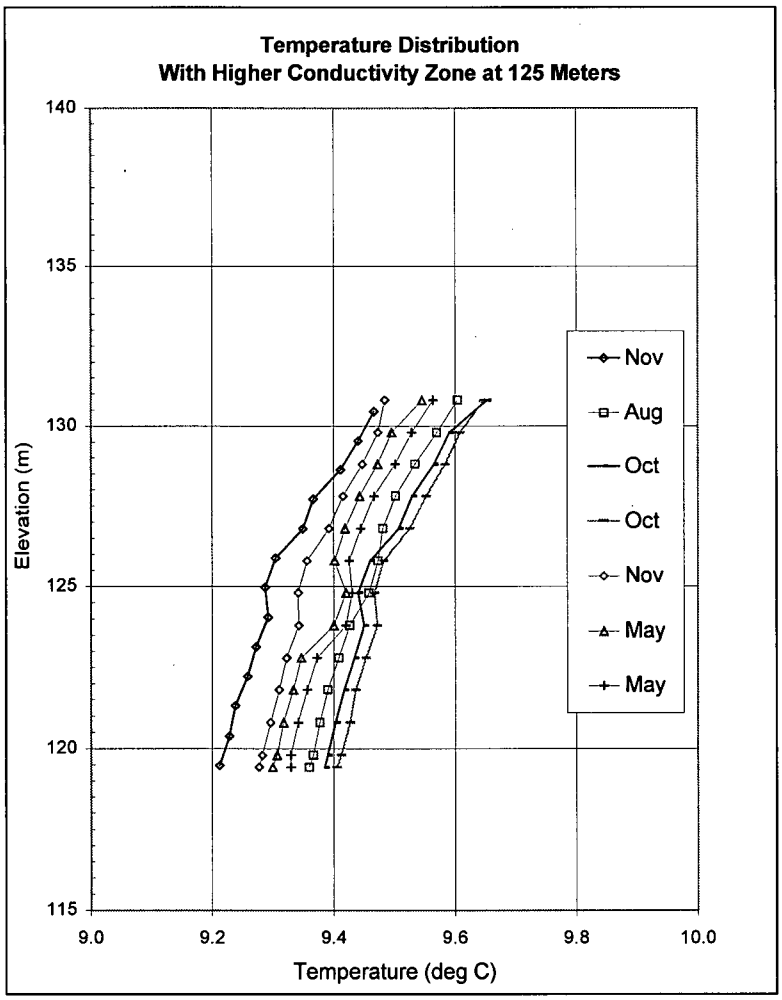

b: Temperature Distribution In A Piezometer With A Higher Conductivity Zone At 125 Meters

Figure 2.8: Sample Temperature Distribution Within A Piezometer – With A Zone of High Conductivity

CHAPTER 3: NUMERICAL MODELLING

3.1 INTRODUCTION

The numerical models used to simulate groundwater flow and heat propagation through embankment dams are described in this Chapter. Section 3.2 describes SEEP/W, the finite element, groundwater modelling program utilized to determine seepage rates through dams. Section 3.3 describes CTRAN/W, the finite element, contaminant transport program that was modified to model heat propagation through dams. SEEP/W and CTRAN/W are integrated, software programs produced and distributed by GEO-SLOPE International Inc. of Calgary. Section 3.4 summarizes the modelling procedures. Section 3.5 presents the results of the model verification, comparing the closed form solution for one dimensional heat transport through a semi-infinite, homogeneous media, with the results from SEEP/W and CTRAN/W. Section 3.6 contains summary remarks and conclusions for Chapter 3.

3.2 SEEP/W

SEEP/W is a two-dimensional, finite element program used to model groundwater movement and calculate pore water pressure distributions in porous media. SEEP/W can perform steady state and transient seepage analysis, in confined and unconfined aquifers. It models both saturated and unsaturated flow. SEEP/W is integrated with GEO-SLOPE International Inc.'s other software programs that perform slope stability analysis (SLOPE/W), contaminant transport analysis (CTRAN/W), and stress and deformation analysis (SIGMA/W).

SEEP/W is formulated using Darcy's Law for both saturated and unsaturated flow. The governing differential equation used in SEEP/W is:

$$\frac{\partial}{\partial x}\left(k_x \frac{\partial H}{\partial x}\right) + \frac{\partial}{\partial y}\left(k_y \frac{\partial H}{\partial y}\right) + Q = \frac{\partial \Theta}{\partial t} \qquad (3\text{-}1)$$

where:

H = total head
k_x = hydraulic conductivity in the x-direction
k_y = hydraulic conductivity in the y-direction
Q = applied boundary flux
Θ = volumetric water content
t = time

For unsaturated flow conditions, the hydraulic conductivity is not constant, but varies as a function of the pore water pressure. To conduct a saturated-unsaturated seepage analysis, a conductivity function for each soil type is required.

SEEP/W permits a variety of boundary conditions to be applied, total head, nodal seepage flux, and area seepage flux. In addition, boundary conditions may be specified as:

- transient such that the user may define a boundary function that varies with time;
- zero pressure boundaries may be used to create a free surface, by setting the total head equal to the nodal elevation;

- head as a function of volume groundwater flow into or out of the system, for boundaries that fluctuate between discharge and recharge zones; and
- review boundaries, which allow water to exit the system where pore water pressures exceed atmospheric pressure (i.e. on a seepage face). SEEP/W uses an iterative procedure to determine the correct boundary condition on seepage face.

SEEP/W also permits the use of infinite elements at the boundaries of a problem for situations where the domain is unbounded. This enables the model domain size to be reduced. In addition, SEEP/W also allows anisotriopic soil properties to be specified as a hydraulic conductivity ratio (k_y/k_x) with or without a rotation of the principal axes from the x and y directions (GEO-SLOPE International Inc, 1998). Version 4.22 of SEEP/W was used in this thesis.

3.3 CTRAN/W

CTRAN/W is a two-dimensional, finite element program used to model contaminant migration through porous media. CTRAN/W must be used in conjunction with SEEP/W. CTRAN/W utilizes the Darcian velocities calculated in SEEP/W to compute the movement of dissolved constituents in the pore water. The same grid is required for both the SEEP/W and CTRAN/W analysis. CTRAN/W allows problems to be analysed in a simplified manner, through particle tracking or in a more complete approach by utilizing the advection dispersion equation. In addition, problems including diffusion, adsorption, radioactive decay, and density dependent flow may be analysed.

The one dimensional formulation of the advection dispersion equation for contaminant transport, including adsorption, and radioactive decay, solved by CTRAN/W is:

$$\Theta\frac{\partial C}{\partial t}+\rho_d\frac{\partial S}{\partial C}\frac{\partial C}{\partial t}=\Theta D\frac{\partial^2 C}{\partial x^2}-U\frac{\partial C}{\partial x}-\lambda\Theta C-\lambda S\rho_d \qquad (3\text{-}2)$$

where:

advection = $-U\frac{\partial C}{\partial x}$

dispersion = $\Theta D\frac{\partial^2 C}{\partial x^2}$

adsorption = $-\rho_d\frac{\partial S}{\partial C}\frac{\partial C}{\partial t}$

radioactive decay = $-\lambda\Theta C-\lambda S\rho_d$

v = average linear velocity = U/Θ S = U/n
Θ = volumetric water content
C = concentration
D = hydrodynamic dispersion coefficient
U = Darcian velocity (specific discharge)
S = adsorption = (mass of solute attached to the solids) / (mass of the solids)
ρ_d = mass of solids
λ = decay coefficient
t = time

Only the advective (convection) and dispersive (conduction and thermal dispersion) terms of Equation 3-2 are used in the heat transport analysis. As previously discussed in section 2.4.5, due to the similarity in the heat and contaminant transport equations, the contaminant transport equation can be converted into the heat transport equation if the value for the porosity (n) is replaced by:

$$n_{sub} = \frac{\rho c}{\rho_w c_w} \tag{3-3}$$

This substitution is correct assuming that the groundwater velocity is independent of temperature (uncoupled solution of the groundwater flow and heat transport equations). For further discussion regarding this assumption and its applicability to modelling heat transport through dams, see section 2.4.4.

Porosity is not directly specified as an input parameter for the CTRAN/W analysis. Since CTRAN/W uses the pore water velocities calculated in SEEP/W for further computations, it is actually in SEEP/W where the porosity substitution is required. As seen in section 3.2 and in Equation 3-2, SEEP/W and CTRAN/W equations are written and solved in terms of the volumetric water content function, Θ, defined by:

$$\Theta = nS = V_w / V \tag{3-4}$$

where: n = porosity
S = degree of saturation
V_w = volume of water
V = total volume

In SEEP/W the volumetric water content is entered into the program as a function of pore water pressure. When the degree of saturation is 100%, the volumetric water content is equivalent to the soil porosity. Figure 3.1 presents the relation between volumetric water content and pore water pressure. This relation is also known as the soil water characteristic function (Fredlund, D.G. and Rahardjo, H., 1993). The shape of the curves will vary due to the characteristics of the soil structure and their ability to retain water, as shown in Figure 3.2. The curves presented in Figure 3.2 are values obtained by Ho, 1979 for fine sand, silt and clay. The slope (m_w) of the volumetric water content function (Figure 3.1) is required in transient seepage analysis.

Contaminant dispersion (D), in Equation 3-2, for one dimensional flow is defined as:

$$D = \alpha v + D^* \tag{3-5}$$

where: α = dispersivity (material property)
v = Darcian velocity divided by volumetric water content (U/Θ)
D^* = coefficient of molecular diffusion

The dispersion coefficient is defined in matrix form, for two dimensional flow:

$$\begin{bmatrix} D_{11} & D_{12} \\ D_{21} & D_{22} \end{bmatrix}$$

$$D_{11} = \alpha_L \frac{v_x^2}{v} + \alpha_T \frac{v_y^2}{v} + D^*$$

$$D_{22} = \alpha_T \frac{v_x^2}{v} + \alpha_L \frac{v_y^2}{v} + D^* \qquad (3\text{-}6)$$

$$D_{12} = D_{21} = (\alpha_L - \alpha_T) \frac{|v_x v_y|}{v}$$

$$v = \sqrt{v_x^2 + v_y^2}$$

where: α_L = longitudinal dispersivity
α_T = transverse dispersivity

As seen in Equation 3-6, the dispersion coefficient entered into CTRAN/W consists of the two components: the dispersivity terms (α_L and α_T) and the coefficient of diffusion (D*). CTRAN/W permits the coefficient of diffusion to be defined as a function of volumetric water content. This relationship is important for unsaturated flow conditions.

It is important to note the similarity between Equation 3-6 and the thermal conduction and dispersion tensor (Equation 2-12) used in the heat transport equation.

In addition the longitudinal and transverse dispersivity terms can be specified for each material in CTRAN/W. Transverse dispersivity is typically less than the longitudinal dispersivity. The dispersivity terms (α_L and α_T) for solving the heat transport equation (using CTRAN/W), are calculated by:

$$\alpha_L = \alpha_{long} \frac{n \rho_w c_w}{\rho\, c} \qquad \alpha_T = \alpha_{trans} \frac{n \rho_w c_w}{\rho\, c} \qquad (3\text{-}7)$$

where: α_{long} and α_{trans} = the longitudinal and transverse thermal diffusivity of the soil.

Thermal boundary conditions must be specified in order to conduct the heat transport modelling. Options for boundary types are:

- constant temperature (degrees);
- total nodal heat flux (degrees/time unit);
- unit heat flux (degrees/length^2*time unit);
- boundary functions for the three types listed above; and
- exit review boundaries.

The constant temperature boundary is applied to a boundary of a problem when a known, fixed temperature occurs at that surface over the length of the analysis period. CTRAN/W then calculates a flux across the boundary based on the flow of water across that boundary (as determined by the SEEP/W analysis).

The total nodal heat flux boundary condition can be used when the flux of heat across a point (i.e. node) is known.

The unit heat flux across the boundary condition can be specified for problems when the heat flux along the entire edge of the problem is constant and known.

The boundary function option allows the constant temperature, total nodal heat flux, and unit heat flux boundary conditions to be specified as a function of time, or in other words varying with time. For example, if the boundary temperature varies throughout the year, such as the air temperature may in a problem, then the temperature versus time function could be selected. Allowing the user to define the change in temperature through out the analysis period.

If an exit review boundary is specified, then at each time step, the program checks whether the water flux is negative, and if so, applies an exit boundary condition. If not, then no boundary condition is applied. An exit review boundary should be applied when neither the heat flux nor the temperature is known, or where the nodal water flux may reverse directions. If CTRAN/W applies an exit boundary to a node that was specified as an exit review node, two options exist. The first option assumes that heat leaves the boundary by advection only and the dispersive flux is set to zero (Q_d=0). The second and more realistic option allows heat to leave the system by advection and dispersion (Q_d>0). This is called a free exit boundary (Frind, 1988). If no boundary is specified, then CTRAN/W assumes that there is no heat flux across the boundary (neither gain or loss of heat). Initial thermal conditions may be specified directly in CTRAN/W or from a previous model simulation (i.e. separate file).

CTRAN/W requires the user to specify the time steps to be used for the analysis and at what intervals data is to be saved. If a transient seepage analysis was performed, the same time steps should be selected for the heat transport analysis (GEO-SLOPE International Inc, 1998a). Version 4.23 of CTRAN/W was used in this thesis.

3.4 GENERAL MODELLING PROCEDURE

In order to use SEEP/W and CTRAN/W to analyse the heat transport equation and resulting temperature distribution in a dam, the following steps are required. Initially, SEEP/W is used to model the phreatic surface measured in the dam and, if available, the discharge volume, or discharge rate measured in the field. Either a steady state or transient seepage analysis is selected, to best simulate field conditions. The SEEP/W analysis is performed using the best estimate of parameters (geometry, soil stratigraphy, boundary conditions, and for each soil type: hydraulic conductivity ratio (k_y/k_x), volumetric water content function, and hydraulic conductivity function). Depending on the quality and quantity of data available to determine values for the input parameters, a range of values for each soil type may exist. In this case, several SEEP/W runs may be performed until the best fit to the measured hydraulic data is achieved, using the range of parameter values. Once a satisfactory hydraulic model is achieved, the SEEP/W analysis is re-analysed with the modified volumetric water content function for each soil unit in place ($\Theta_{sub} = S\rho c/\rho_w c_w$). The average linear velocities (U/Θ which is the Darcian velocity divided by the volumetric water content) generated from this SEEP/W analysis are then utilized in the CTRAN/W analysis.

The grid used for the SEEP/W analysis is imported into CTRAN/W. To perform the heat transport analysis using CTRAN/W, the analysis type must be set to advection dispersion. Then, the appropriate thermal boundaries and initial thermal conditions must be assigned to the model domain. Under the heading material properties, the dispersion (D*), and dispersivity (α_L and α_T) values for each soil type should be assigned. Lastly, the time step size, and increments for saving the analysis must be specified. If a transient seepage analysis was performed in SEEP/W, then it

is better if the same time step increments are selected in CTRAN/W. If the time step selected in CTRAN/W is smaller than that used in SEEP/W, then CTRAN/W will interpolate a velocity for use in the CTRAN/W analysis.

Next SOLVE command in CTRAN/W was run. The resulting solution can be viewed under the CONTOUR portion of the program. The solution can be viewed graphically, as data points, or as a contour plot. The graphical plots display results as concentration, instead of temperature, but the data can easily be exported to another spreadsheet and a graph created with the appropriate labeling.

3.5 MODEL VERIFICATION

In order to verify the combined use of SEEP/W and CTRAN/W as an appropriate method for modelling heat transport through porous media, a comparison was conducted between the results obtained from these programs and the closed form analytical solution for the one dimensional advective dispersion equation (Equation 2-5 and Equation 2-11, described in Chapter 2).

Numerous analytical solutions exist for the advective dispersion equation; each solution is distinct for a particular set of initial conditions and boundary conditions. Two particular boundary condition scenarios, and hence analytical solutions, were selected for the model verification. Each is discussed in the following subsections.

3.5.1 Analytical Solution using a Step Temperature Change Boundary

The first analytical solution used for the comparison was a semi-infinite, one dimensional, homogeneous medium, with a step change in the finite boundary temperature. The analytical solution for this scenario, was derived by Ogata, A. and Banks R.B. (1961), as presented herein:

$$T = \frac{\Delta T}{2}\left[erfc\left(\frac{x-Ut}{2\sqrt{Dt}}\right) - \exp\left(\frac{Ux}{D}\right) erfc\left(\frac{x+Ut}{2\sqrt{Dt}}\right)\right] + T_0 \qquad (3\text{-}8)$$

where: T = temperature
T_o = initial temperature
ΔT = change in temperature at the finite boundary (new temperature – initial temperature)
t = time
x = distance from the finite/upstream boundary
D = dispersion coefficient
U = transformed seepage velocity, $U = n\rho_w c_w / \rho c v$
v = seepage velocity

The analytical solution was implemented using as a visual basic function in an excel spreadsheet, prepared by Golder Associates (Golder Associates, 2000). Table 3.1 lists the values entered into the closed form solution spreadsheet used for the model verification. The visual basic function and spreadsheets for this comparison are included in Appendix A-1.

3.5.2 *Analytical Solution using a Sinusoidal Temperature Boundary*

The second analytical solution used for the model verification simulated a semi-infinite, one dimensional, homogeneous medium, with a sinusoidal variation in temperature at the finite boundary. The analytical solution for this scenario was derived by Ogata, A. and Banks R.B. (1961), as presented herein:

$$T = \Delta T \exp\left(\frac{Ux}{2D} - xa^{1/2}\cos(\phi/2)\right)\cos(\omega t - xa^{1/2}\sin(\phi/2) + \theta) + T_0 \qquad (3\text{-}9)$$

where:

$$a = \left(\frac{U^4}{16D^4} + \frac{\omega^2}{D^2}\right)^{1/2}$$

$$\phi = \arctan\left(\frac{\omega}{D}\frac{4D^2}{U^2}\right)$$

θ = phase shift

The analytical solution was implemented using as a visual basic function in an excel spreadsheet, prepared by Golder Associates (Golder Associates, 2000). Table 3.1 lists the values entered into the closed form solution spreadsheet used for the model verification. The visual basic function and spreadsheets for this comparison are included in Appendix A-1.

3.5.3 *Model Parameters*

Table 3.1 presents the input parameters utilized for model verification. Appendix A-2 presents detailed calculations for the values presented in Table 3.1.

3.5.4 *Setup and Analysis of SEEP/W and CTRAN/W Models*

To compare the results of the closed form solution presented in section 3.5.1 and 3.5.2, to the results obtained from the combined, SEEP/W and CTRAN/W analysis, a grid was generated in SEEP/W. The selected grid had dimensions 100 metres in length, 10 metres high, and one metre wide, to simulate groundwater flow and heat propagation through a one dimensional zone, of homogeneous porous media. The domain was subdivided into 40 grid cells in the x-direction and 6 grid cells in the y-direction, for a total of 240 cells. Six grid cells were used in the y-direction to confirm that the analysis method works with more than just one row, and to evaluate some two dimensional aspects. A head of 110 metres was specified on the upstream boundary (left), and a head of 10 metres on the downstream boundary (right), such that the hydraulic gradient was equal to one. The top and bottom boundaries were specified as no flow, so that water could neither enter nor leave the system. The material properties listed in Table 3.1 were then entered into the program. A flux section was placed at approximately 98 metres so that SEEP/W would calculate the flow out of the section. The steady-state velocities and head distribution were obtained from SEEP/W. A diagram showing the SEEP/W grid, and results of the one dimensional seepage analysis are presented on Figure 3.3.

A second SEEP/W grid was generated by adding infinite elements on the downstream boundary to the grid presented in Figure 3.3. A diagram of the new grid, and the results from this seepage analysis, are shown in Figure 3.4. In place of the downstream head, a boundary flux (flow out of the cells) was utilized for this analysis, to create the same groundwater velocities and head distribution that was generated from the first seepage analysis.

The SEEP/W models presented in Figure 3.3 and Figure 3.4 were then reanalysed using the substituted volumetric water content function, Θ_{sub} of 1.39.

The second grid (Figure 3.4), with the infinite elements was imported into CTRAN/W, and used to solve the heat transfer component of the equation described in subsection 3.5.1. A step temperature change on the upstream boundary, from 3°C to 12°C was selected for the simulation. To create the step change boundary condition in CTRAN/W, a boundary function was utilized. The function started with an initial temperature of 3°C and was instantly increased and then held constant at 12°C for the length of analysis. On the downstream boundary, a constant temperature of 3°C was specified. An initial temperature of 3°C was specified for all nodes. The top and bottom boundaries were specified as no flow meaning heat could not enter or leave the system through the sides. A time step of 10 days (864,000 seconds) was used for the analysis. Table 3.1 list the additional input parameters used for the CTRAN/W analysis. The SOLVE command in CTRAN/W was then used. A solution for the temperature distribution along the flow path was generated. The advective component of the heat transfer equation was calculated in CTRAN/W, using the groundwater velocities obtained from the SEEP/W analysis, with Θ_{sub} of 1.39.

The equation described in subsection 3.5.2 can be used to solve the temperature distribution along a flow path (one dimensional flow) with a sinusoidal temperature variation on the upstream boundary. This problem was initially analysed using the same SEEP/W grid and velocities presented in Figure 3.4, and Θ_{sub} of 1.39. The CTRAN/W model was set up with a boundary function on the upstream boundary. The annual variation was specified, as a sine wave with a minimum temperature of 3°C on January 1st and a maximum temperature of 12°C on July 1st. The initial temperature at all nodes was specified as 3°C and the downstream temperature was specified as 7.5°C, which is the mean temperature of the sine wave. The top and bottom boundary conditions were set as no heat flow. Table 3.1 list the additional input parameters used for the CTRAN/W analysis. The SOLVE command in CTRAN/W was then utilized to determine the temperature variation along the flow path for the particular boundary conditions. As shown in Figure 3.5, numerical dispersion occurred near the downstream boundary. This is caused by the use of infinite elements on the downstream boundary. The results of this model simulation can be used to verify the assumption that the downstream boundary temperature approaches the mean temperature of the sine wave.

The problem was then reanalysed using the grid created without the infinite elements (Figure 3.3) and the velocities obtained from this SEEP/W analysis using Θ_{sub} of 1.39. The downstream boundary temperature, at 100 metres, was set at a constant value of 7.5°C. The setup for the remainder of the CTRAN/W analysis remained the same.

3.5.5 Results

Figure 3.6 presents a graph of the temperature distribution versus distance along the flow path, at intervals of one, three, six and nine years, resulting from a step change in the upstream boundary temperature from 3 to 12°C. This plot compares the results from the SEEP/W and CTRAN/W analysis with those obtained from the one dimensional closed form solution analysis. The solutions from the two analyses agree. The step in boundary temperature effects does not reach the downstream boundary within the 9 year analysis period.

Figure 3.7 presents a graph of the temperature distribution along the flow path as a result of a sinusoidal temperature variation at the upstream boundary. Figure 3.7 presents the temperature distributions that occur along the flow path when the upstream temperature is at the minimum and maximum. The results from the closed form solution are compared to the results obtained from the SEEP/W and CTRAN/W analysis. There is good agreement between the two analyses. The downstream boundary temperature is affected in this analysis by the changes in the upstream boundary temperatures.

Based on these two comparisons, the method of obtaining the seepage velocities for the problem using SEEP/W and the substituted porosity value, and then using CTRAN/W to solve the heat transport equation, appears reasonable and valid.

3.6 SUMMARY AND CONCLUSIONS

Chapter 3 described the methodology and computer programs, SEEP/W and CTRAN/W, utilized to analyse problems involving heat transport through a porous media. The methodology was then successfully tested by comparing the results obtained from the computer model with the solution to two closed form, one dimensional, analytical solutions for heat transport.

Table 3.1: Model Verification Input Parameters

Property	Value Entered into Each Program		
	Analytical Solution	SEEP/W	CTRAN/W
Length of Flow Path	100 m	Grid 100 m by 10 m each cell 2 m by 1.67 m	Grid 100 m by 10 m each cell 2 m by 1.67 m
Density of water (ρ_w)	1000 kg/m^3	9.807 kN/m^3	- -
Specific heat of water (c_w)	4180 J/kg ° K	- -	Used in the calculation of E
Saturated density of soil (ρ)	2320 kg/m^3	- -	Used in the calculation of E
Specific heat of saturated soil (c)	2500 J/kg °K (1)	- -	Used in the calculation of E
Hydraulic conductivity (k)	1E-7 m/s	1E-7 m/s , k_{ratio} = 1, k_{dir} = 0	- -
Hydraulic gradient	1	Head on upstream boundary 110 m, Head on downstream boundary 10 m	- -
Porosity (n)	0.3	Θsub = 1.39 (2)	- -
Thermal dispersion and dispersivity (E)	1.1E-6 m^2/s (3) E*= 6.9E-7 m^2/s E_{long} = 4.1E-7 m^2/s	- -	E*= 6.9E-7 m^2/s α_L = 5.699 m (4) α_T = 0.599 m
Initial temperature (5)	3 °C	- -	3 °C
Instantaneous temperature change on upstream boundary (6)	12 °C	- -	12 °C
Constant temperature on downstream boundary (6)	- -	- -	3 °C
Maximum temperature of sine wave (7)	12 °C	- -	12 °C
Minimum temperature of sine wave (7)	3 °C	- -	3 °C
Period of sine wave (7)	1 year	- -	1 year
Lag of sine wave (7)	0.5 (8)	- -	Minimum temperature at time = 0 Maximum temperature at time = 15768000 s
Constant temperature on downstream boundary (7)	7.5 °C	- -	7.5 °C
Time step	- -	Steady state analysis	8.64E5 s

Notes:

(1) Specific heat of saturated soil calculated using: $c = (n\rho_w c_w + (1-n)\rho_s c_s)(1/\rho)$ for more detail see 2.4.2 (Equation 2-6).

(2) Θsub, is the modified volumetric water content function, calculated using, $\Theta = S\rho c/\rho_w c_w$

(3) E is calculated using Equation 2-12, described in section 2.4.4 and 2.5.4. The value of thermal conductivity used in the calculation of E, was calculated using Equation 2-2, described in section 2.4.1.

(4) α_L and α_T values entered into CTRAN/W were calculated using: $\alpha_L = E_{long}/(k_x i / \Theta)$ and $\alpha_L = E_{long}/(k_y i / \Theta)$

(5) Initial temperature in media and on the upstream temperature boundary.

(6) For the solution to Equation (3-8).

(7) For the solution to Equation (3-9).

(8) A lag of 0.5 was assigned so that peak temperature would correspond with July 1 and the minimum temperature would correspond with January 1.

(9) All temperature values entered into CTRAN/W are actually treated as concentrations.

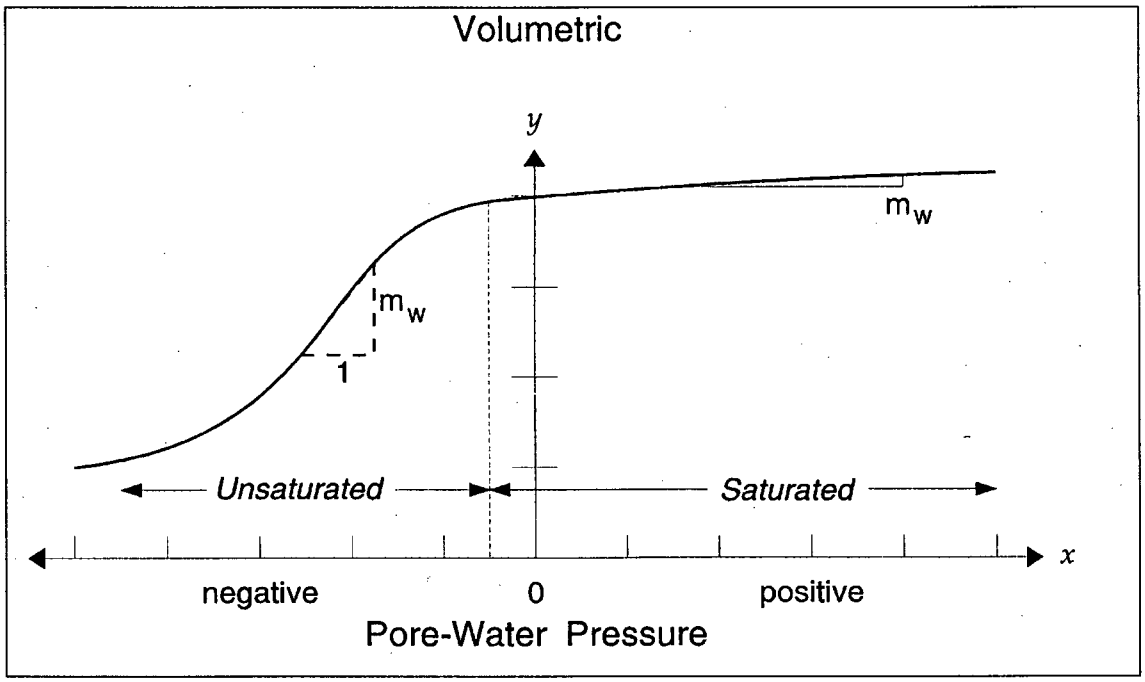

Figure 3.1: Volumetric Water Content as a Function of Pore Water Pressure (as presented in GEO-SLOPE International Inc., 1998)

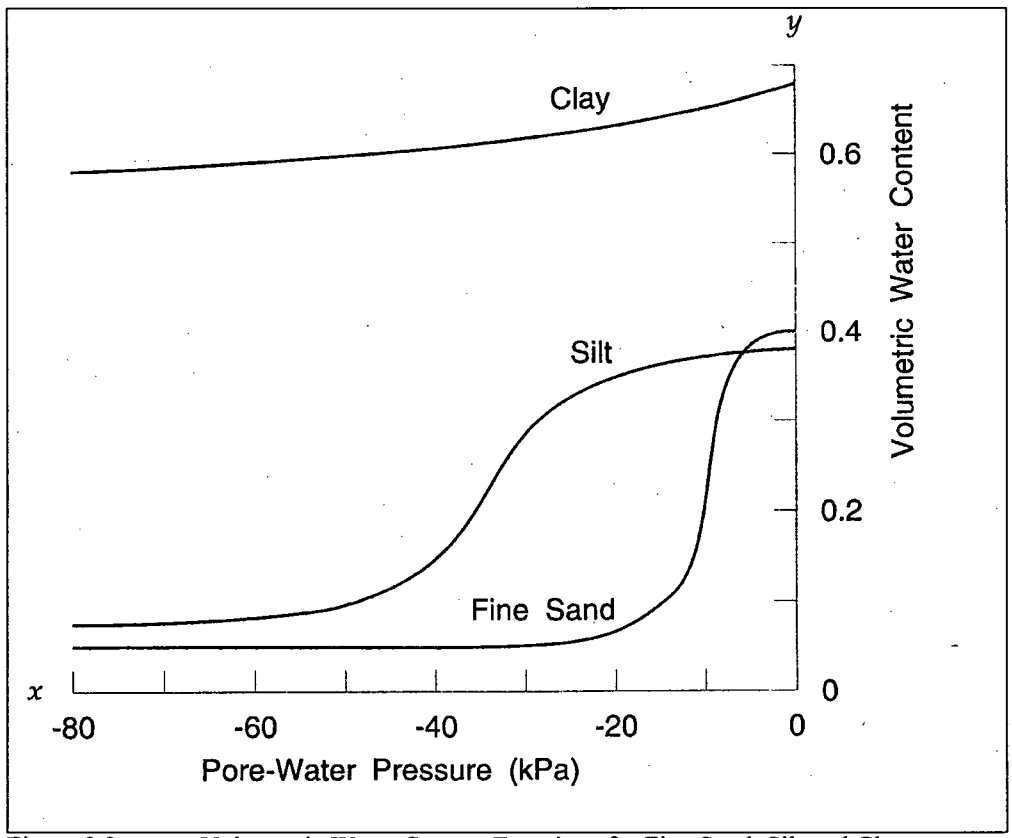

Figure 3.2: Volumetric Water Content Functions for Fine Sand, Silt and Clay (from Ho, 1979, as provided in GEO-SLOPE International Inc., 1998)

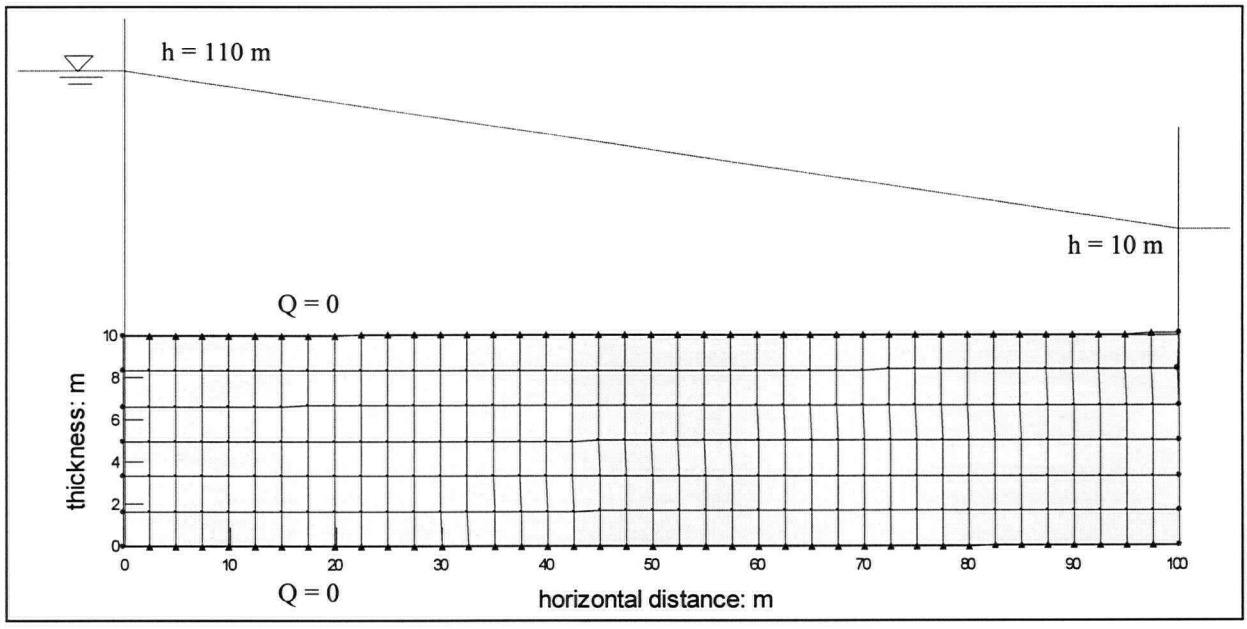

a: One – Dimensional Grid Used For SEEP/W Model Verification

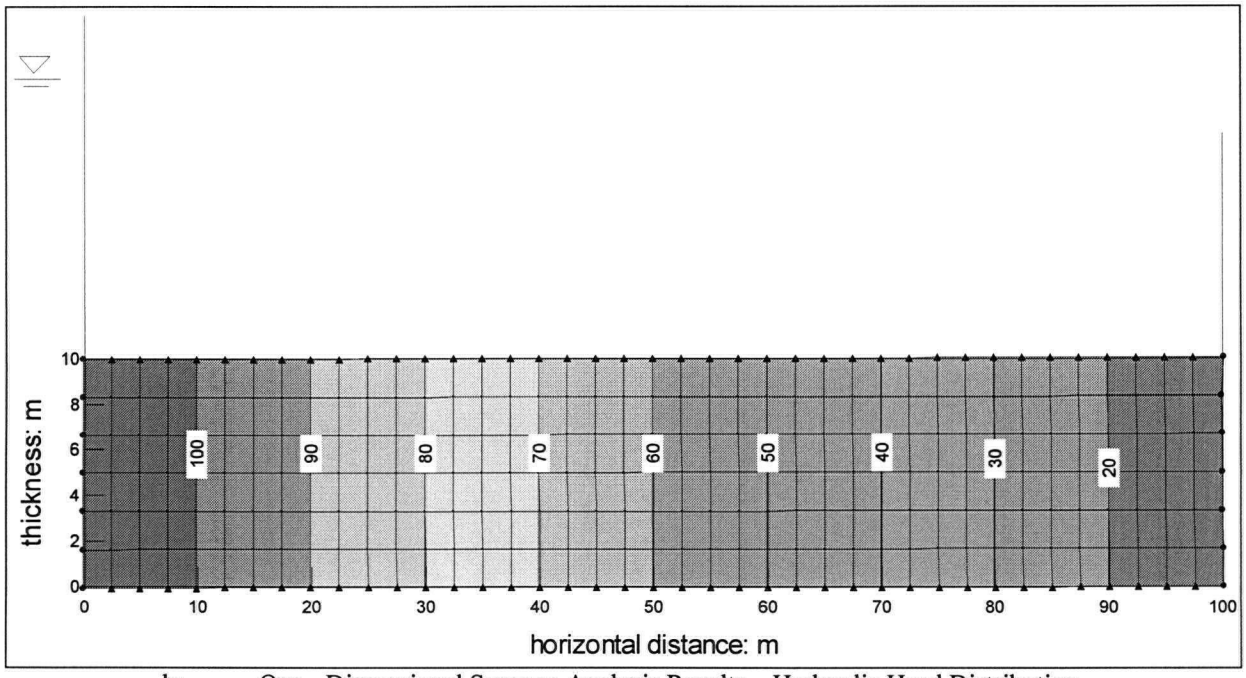

b: One - Dimensional Seepage Analysis Results – Hydraulic Head Distribution

Figure 3.3: SEEP/W Grid and Hydraulic Head Distribution Results For The One - Dimensional Seepage Analysis

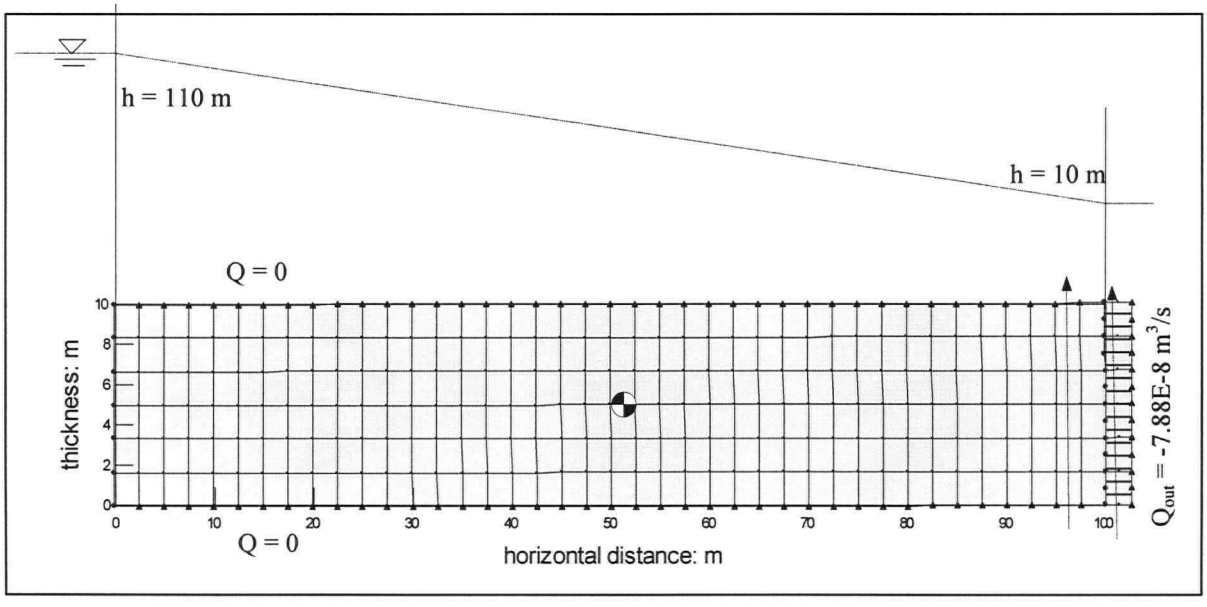

a: Modified SEEP/W Grid Using Infinite Elements

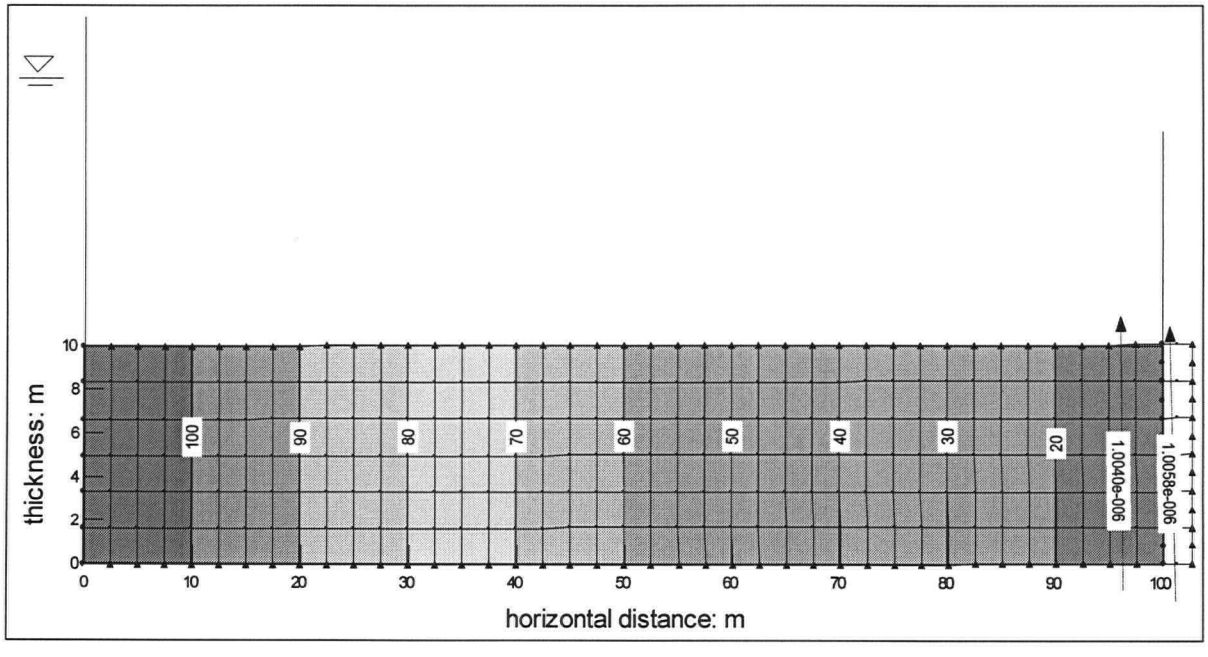

b: Hydraulic Head Distribution Obtained Using Modified SEEP/W Grid

Figure 3.4: Modified SEEP/W Grid and Hydraulic Head Distribution Using Infinite Elements For The One - Dimensional Seepage Analysis

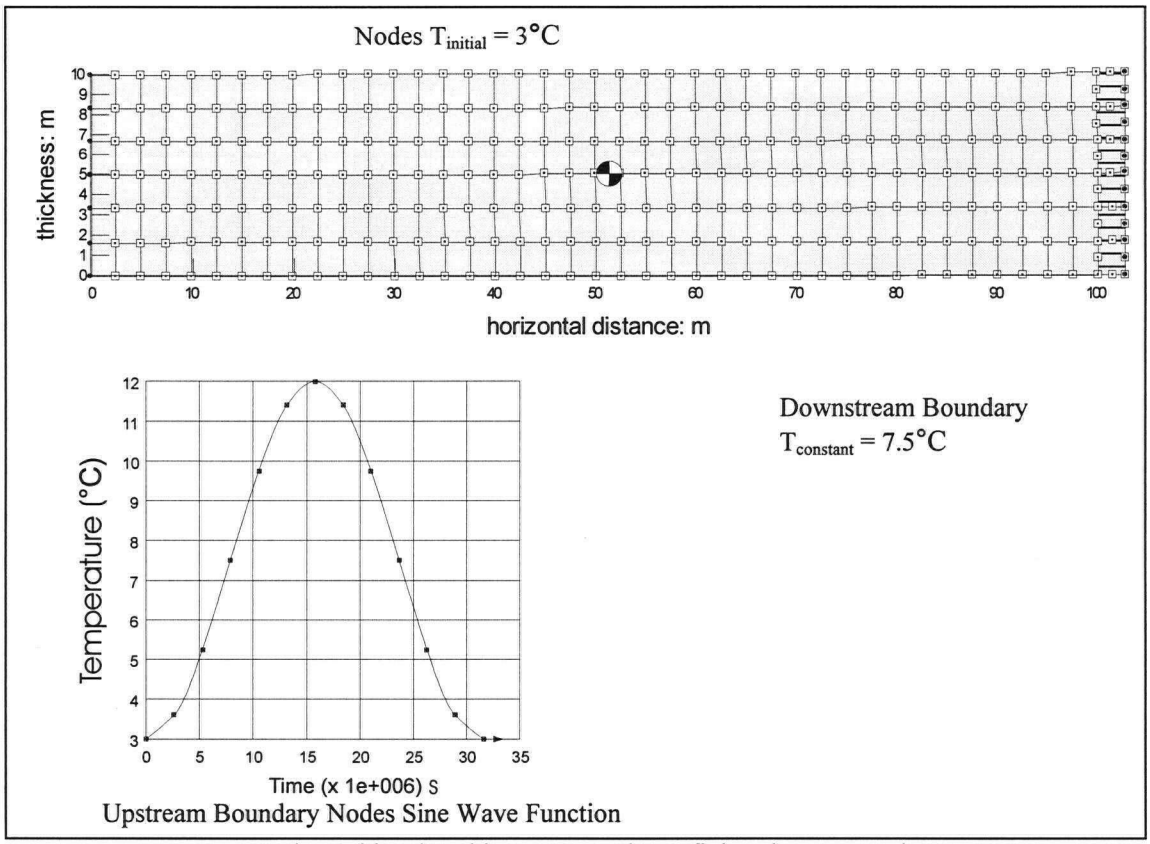

a: CTRAN/W Grid and Problem Setup Using Infinite Elements on the Downstream Boundary

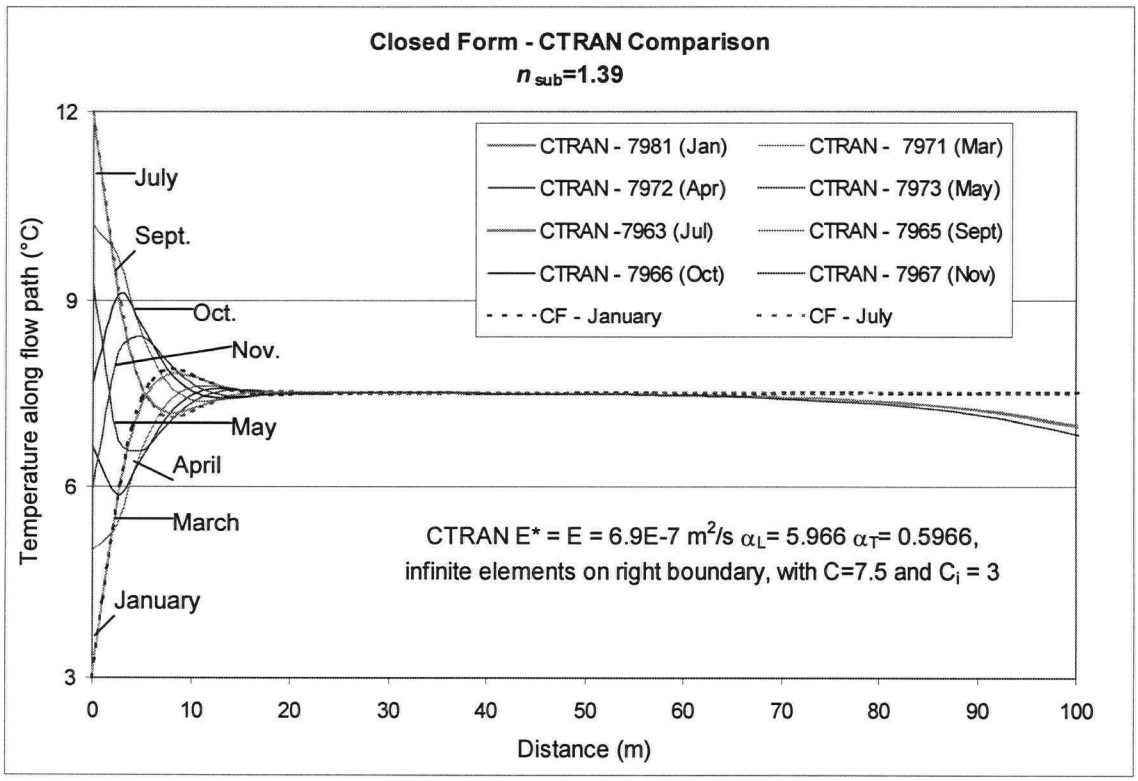

b: Numerical Dispersion Near Downstream Boundary

Figure 3.5: Sample CTRAN/W Output With Numerical Dispersion

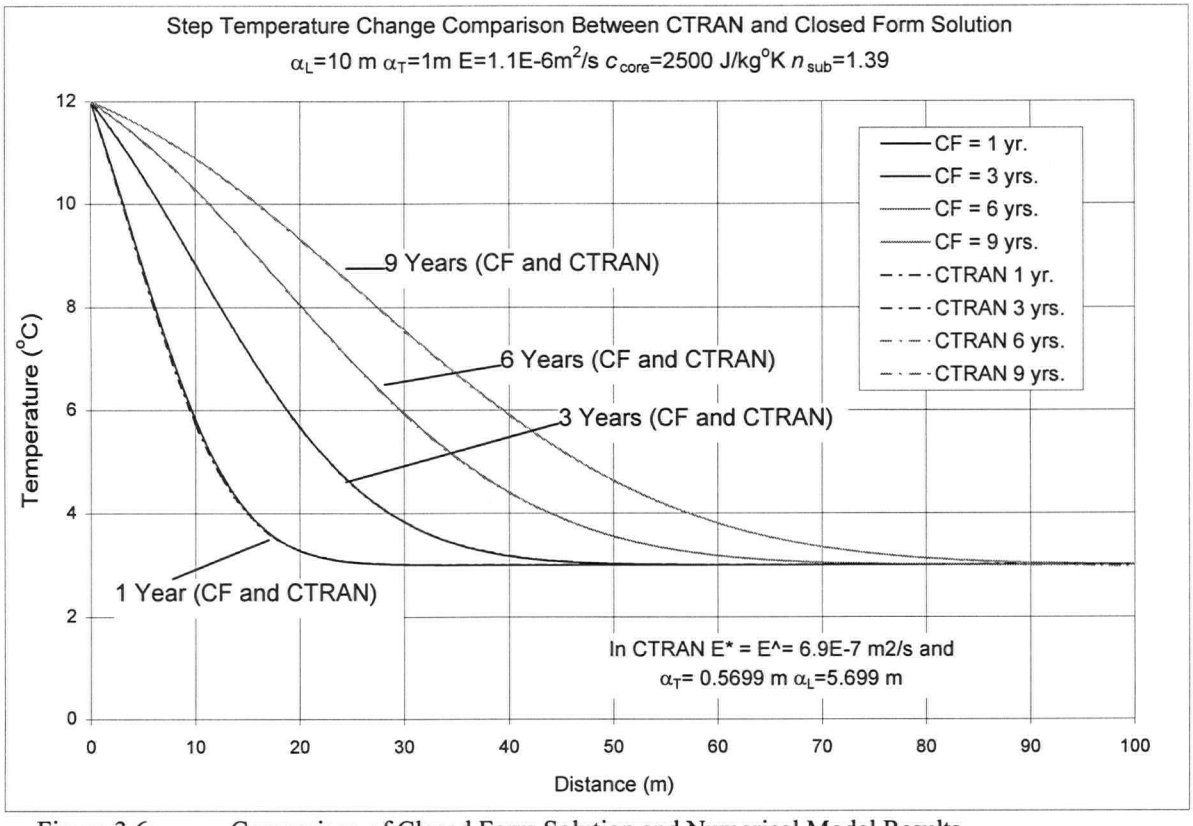

Figure 3.6: Comparison of Closed Form Solution and Numerical Model Results – Step Change in Boundary Temperature

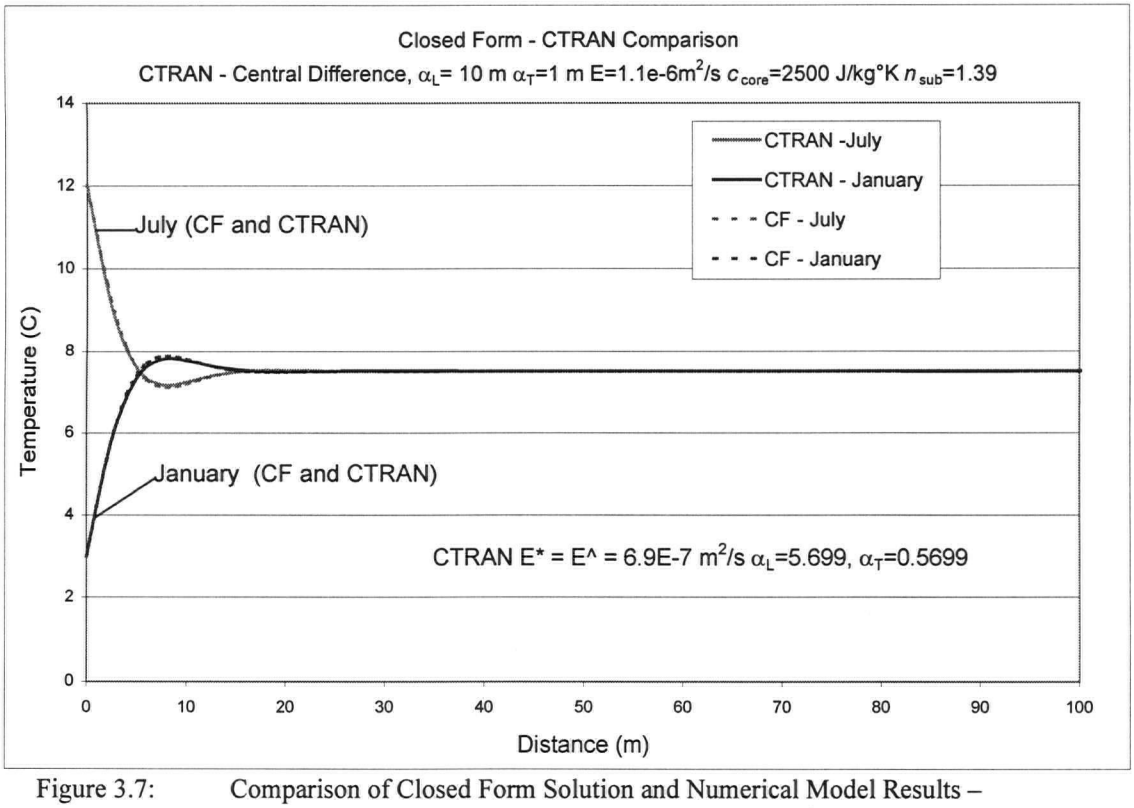

Figure 3.7: Comparison of Closed Form Solution and Numerical Model Results – Sinusoidal Variation in Boundary Temperature (3 -12°C)

CHAPTER 4: NUMERICAL MODELLING OF KARLSRUHE GERMANY FIELD SCALE MODEL DAM

4.1 INTRODUCTION

The programs and modelling procedure described in Section 3, and used in the model verification process, were then applied to analyse the seepage and heat transport through a test dam built in Karlsruhe Germany. Section 4.2 describes the construction details, instrumentation, and test set up at the field scale model dam. Section 4.2 also describes the SEEP/W and CTRAN/W grid used for the numerical analysis of the test dam. Section 4.3 through Section 4.5 present specific details of the field scale model dam scenarios simulated using SEEP/W and CTRAN/W. In each section, the modelled results are compared to the observed data. Section 4.6 contains summary remarks and conclusions for Chapter 4.

4.2 MODELLING OF FIELD SCALE MODEL DAM, KARLSRUHE, GERMANY

In 1984, the University of Karlsruhe and the Federal Waterways Engineering and Research Institute constructed a large scale model dam, to investigate leakage in sealing elements of dams and test methods for detecting resulting seepage zones in dams (Armbruster et. al., 1989). Testing on the model dam was conducted over three and a half years. The dam was constructed of uniform medium to coarse sand, (grains 0.2 to 2 millimetres in diameter) with a conductivity of 2E-4 metres per second. The dam measured 3.5 metres high, 22.5 metres in length at the top, 13.4 metres in length at the base, 1.1 metres wide at the crest, and 17.2 metres wide at the base, and had a total volume of 600 cubic metres.

The reservoir and impermeable base were sealed with a 2.5 millimetre thick, high density polyethylene (HDPE) liner. The upstream face of the dam was also sealed with a membrane. Thirty-five prefabricated concrete modules were installed at 3 levels (high, medium, and low) in the membrane, to act as designated leakage zones each measuring 3 centimetres by 80 centimetres. The concrete modules contained moveable plates to permit leakage zones to be opened and closed at full reservoir height. This allowed investigators to control in inflow of water into the test dam, both the number of leakage zones were controllable and the location of each leakage zone could be controlled. In cross section the location of the leakage zones (high, medium and low) are shown on Figure 4.1. A toe drain was constructed at the downstream side of the dam using gravel (grain size 2 to 16 millimetres). Figure 4.1 presents a cross section of the model dam showing construction materials and dimensions, leakage zones, and monitoring locations.

The dam was instrumented with piezometers and temperature cells at various elevations through the dam and along different profile lines as. Figure 4.1 indicates, in profile, the locations of the hydraulic and temperature monitoring locations. In addition to the collecting temperature data and piezometric data, the following instruments were also used to collect data:

- electrodes for self-potential measurements were installed on the downstream face of the dam;
- an infrared camera was used to measure surface temperatures of the dam;
- a weir was used to measure seepage volumes at the toe of the dam; and
- a weather station was used to record weather conditions precipitation, air temperature and water temperature.

Initially, a test was conducted on the model dam, without the sealing, to provide a reference hydraulic condition, at reservoir levels of one third, two thirds, and full impoundment. Seepage rates measured at the weir were 0.14, 0.61, and 1.55 litres per second, for the three reservoir conditions. Based on this data seepage through the dam appears to be primarily laminar. Then, the sealing face with designated leakage zones was installed. Between 1985 and 1987, over thirty tests were conducted with various leak positions, leak sizes, and reservoir levels. For each scenario tested, hydraulic and thermal conditions were measured throughout the dam and at various times throughout the testing phase. Selected results from these tests were presented in a paper by Armbruster et.al., 1989. It is these results that have been used as a second stage to verify the stepwise modelling procedure, described in Chapter 3 of this thesis.

In order to model groundwater flow and heat transport through the field scale model dam, a grid was created in SEEP/W, as shown in Figure 4.2. Each grid cell was assigned a thickness of 16 metres, with the exception of the designated leakage grid cell. A thickness of 16 metres was selected as an average thickness for the computer model of the dam, making it quasi-three dimensional. A thickness of 0.22 metres (area 0.048 square metres) was selected for the leakage cell, such that the opening was equivalent in area to the opening size of two leakage zones, in the field scale dam.

The following three sections, Section 4.3, through Section 4.5, will present specific details of the field scale dam scenarios simulated using SEEP/W and CTRAN/W. The modelled results will be compared to the observed data. Section 4.5 presents and compares the results of the transient seepage analysis using SEEP/W to the seepage zone developed in the field scale dam. Section 4.4 presents the results of heat transport analysis obtained using CTRAN/W for two cases:

- dry reservoir and an air temperature of 1°C; and
- a full reservoir with a water temperature of 19°C, and an air temperature of 6°C.

The results are compared to those recorded at the field scale dam. Section 4.5 presents the results from the seepage modelling and heat transport modelling for the development of a leakage front with time and the resulting change in the thermal distribution within the dam. The modelled results are compared to the data recorded at the field scale dam.

4.3 TRANSIENT SEEPAGE ANALYSIS

Two low elevation leaks in the centre of the field scale model dam were opened with the reservoir at full height. The development of a seepage front with time through the dam was recorded and the results are presented on Figure 4.3. Figure 4.3a shows the progression of the piezometric surface with time, after the leakage zones were opened. The location of the piezometric surface approached steady-state conditions after 81 hours. Figure 4.3b graphically shows the quantity of water flowing out of the dam with time measured in the weir. Figure 4.3c shows the progression of the saturated area with time.

As shown in Figure 4.3, a small amount of water (0.017 litres per second) was seeping through the dam, prior to opening the leakage zones. In order to simulate this initial seepage condition, the bottom facing grid cell, shown in purple on Figure 4.2, was assigned an increased hydraulic conductivity value to produce a flow rate out of the dam equal to that measured in the field scale dam. By trial and error, the hydraulic conductivity value for this cell was determined to be 2.2E-7 metres per second. Figure 4.4 presents the steady state seepage results obtained using the increased hydraulic conductivity for that grid cell. Figure 4.5 presents the hydraulic properties

(hydraulic conductivity, hydraulic conductivity ratio, and volumetric water content function) assigned to each material for the model simulation. Test data for the soil material utilized in the construction of the field scale dam, was not available to specifically identify the shapes and values of the hydraulic conductivity functions, and volumetric water content functions for the SEEP/W model. As a result, the hydraulic conductivity functions and volumetric water functions utilized in the SEEP/W model were selected based on the soil descriptions provided in the Armbruster et.al. (1989) paper. Typical hydraulic conductivity functions were constructed in SEEP/W for each soil material. Table 4.1 lists input parameters used in SEEP/W and identifies which values were measured, deduced or assumed for the model simulation.

The hydraulic head values obtained for the initial seepage scenario (Figure 4.4) were then used as the initial condition input for the transient analysis. A transient analysis in SEEP/W was then conducted to predict the seepage pattern that developed once the two low elevation holes in the centre of the dam were opened. Table 4.2 outlines the hydraulic properties assigned to each soil type. A hydraulic head of 3.2 metres (total head of 8.2 metres, elevation head of 5 metres) was assigned to the nodes along the upstream face of the dam. No flow boundary conditions were specified along the base of the dam, crest of the dam, and along the downstream face. A unit seepage flux, to be reviewed based on elevation was specified for nodes along the toe drain. This makes use of the exit review boundary type available in SEEP/W (see Section 3.2) and CTRAN/W (see Section 3.3) (Frind, 1988).

Time steps for the transient analysis were specified with small time increments that gradually increased. Solutions were obtained for the following times: 0, 60, 180, 420, 900, and 1500 seconds, after the leakage holes were opened. Then, the time step increment increased at a constant rate of 600 seconds up to 12 hours. At this point the time step increment was increased again. Solutions were then obtained for the following times: 19, 27, 41, 54, 68, and 81 hours after the leakage holes were opened.

Figure 4.6 presents the piezometric surfaces, as a function of time that developed in the dam, as a result of the leakage and compares the predicted surfaces with that measured in the field scale dam. Figure 4.7 graphically presents the predicted flow data versus time and compares it to the field data. The predicted steady state phreatic surface is lower than the measured phreatic surface. The differences in the predicted and measured transient seepage results are likely due to three dimensional effects in the field scale dam and the use of a two dimensional numerical modeling program, SEEP/W. Since the concrete modules were points rather than a continuous slot across the entire length of the dam, that permitted leakage into the dam. As a result, the measured data has a three dimensional aspect, that cannot be entirely simulated using the two dimensional program SEEP/W.

This modelling process also assumes laminar flow. Although flow through the designated leakage zones and the soil immediately adjacent to these zones is likely not laminar, the assumption is valid for the majority of the seepage regime.

However, reasonable agreement is achieved between the SEEP/W model results and the observed field data. It is important to note that the results of the seepage analysis depicted in Figure 4.6 and Figure 4.7 do not represent a unique solution. Similar results could be achieved by slight changes in the model material properties. The hydraulic properties used in this simulation will be used as a basis for all further thermal analyses of the field scale dam.

4.4 INITIAL THERMAL CONDITIONS

Figure 4.8 presents the initial thermal conditions measured within the dam, when the reservoir was dry and the surrounding air temperature was 1°C. This was the measured initial thermal condition in the dam prior to the start of a leakage test.

This condition was first simulated using CTRAN/W with a surface air temperature of 1°C, and a basal heat flux, to simulate a geothermal gradient. The grid presented in Figure 4.2 was modified by adding additional grid cells below the base of the dam, such that a uniform heat flux could be applied across the base of the CTRAN/W model dam. The basal heat flux was increased until the predicted steady state thermal distribution matched the measured thermal condition in the field scale dam. Figure 4.9 presents the results of this model simulation and Table 4.3 presents the soil thermal conditions utilized for this model simulation.

To evaluate the appropriateness of the CTRAN/W results, it is important to know what typical geothermal gradients are and at what depth air temperature effects are dominant over geothermal effects. Stevens, Ficke, and Smoot (1975), Artéus and Johanson (1998), and Keys and Brown (1978) all report typical geothermal gradients. The overall range reported by these authors is from 0.01°C to 0.03°C per metre depth. Stevens, Ficke and Smoot (1975) and Domenico (1972) have reported that air temperatures typically affect the thermal profile of the soil up to a depth of 10 metres. Below this depth, minimal, if any, air temperature effects are observed. The basal heat flux used in CTRAN/W to achieve the measured thermal distribution in the dam (Figure 4.8) is significantly larger than the average geothermal gradient. The temperature gradient in the CTRAN/W model is approximately 2°C per metre depth. Based on this analysis it is apparent that the thermal distribution presented in Figure 4.8 is not a result of a geothermal gradient, rather it is a result of a cooling process. The initial temperature of soil within the dam must have been higher and then must have decreased as a result of the cool air temperature.

To test this hypothesis, another simulation was done using CTRAN/W. For this simulation, the grid presented in Figure 4.2 was utilized. Each node within the dam was assigned an initial temperature of 7°C, and a boundary temperature of 1°C to represent the air temperature. No heat flow was permitted across the base of the model. Figure 4.10 presents the thermal distribution within the dam after 9 days of cooling. This is not a steady state temperature distribution, but the thermal distribution is similar to that recorded in the field. Based on the field data available it appears that the thermal distribution presented in Figure 4.8 is a result of cooling, rather than geothermal heat flow. The results presented in Figure 4.10 have been utilized as the initial thermal condition input for the next phase of the CTRAN/W analysis.

The next step in the leakage test involved filling the reservoir. The reservoir was filled to a height of 3.2 metres, with 19°C water. After 18 days, the thermal distribution within the dam was recorded and the results are presented on Figure 4.11. During the 18 days the air temperature increased from 1°C to 6°C. The thermal distribution presented in Figure 4.11 is a result of conduction only as there was no water flowing through the dam.

This scenario was modelled in CTRAN/W. The following thermal boundary conditions were assigned to the model:

- an instantaneous change in temperature for nodes along the upstream dam face from 1°C to 19°C;
- a linear change in air temperature from 1°C to 6°C for nodes along the downstream dam face;
- heat flow was permitted out of the top of the dam; and
- no heat flow was permitted across the base of the dam (either in or out of the system).

A range of values for each thermal property of the sand was calculated for use in the CTRAN/W model. From these calculations three combinations were selected for use. Table 4.4 summarizes the thermal properties assigned to each soil layer, for the three model simulations. Calculations for the values presented in Table 4.4 are included in Appendix B-1, along with a table showing how the range of parameters were selected. For these simulations it is important to remember that there is no water flowing through the reservoir, hence the porosity, volumetric water content functions, and longitudinal and transverse thermal diffusivity terms are inconsequential. For all three simulations a time step of 4 hours (14,400 seconds) was selected. A total of 108 steps were used, for the 18 day simulation period, to match the field data. Since CTRAN/W requires seepage velocities from SEEP/W, a SEEP/W model with no flow through the dam was used to provide the seepage velocities ($v = 0$) for the CTRAN/W analyses, therefore simulating conduction of heat only (no convection). The thermal conditions presented in Figure 4.10 were selected as the initial conditions for the start of each simulation. Results from the three model simulations are presented in Figure 4.12 and compared to the results measured in the field scale dam.

The results of the three simulations are similar to those obtained from the field scale dam. However, they do not match exactly. The temperature distribution in the dam, resulting from Simulation 1 has isotherms that run parallel to the upstream dam face and decrease with distance from the reservoir. The temperature of these isotherms decreases from 19°C along the upstream face of the dam to 6°C in the middle of the dam. The downstream portion of the dam ranges in temperature between 5°C and 6°C. The 5°C isothermal appears at the base of the dam, in an elliptical shape. The thermal distribution that is predicted in Simulation 1 correlates well with the thermal pattern recorded in the upstream portion of the field scale dam. Despite these similarities, the temperatures predicted in the central and downstream portion of the dam are cooler in Simulation 1 than those recorded in the field scale dam.

Results from Simulation 2 and Simulation 3 are very similar to one another hence they will simultaneously be described and compared to the field scale dam results. The isotherms in the upstream portion of the dam, resulting from these two simulations, are also parallel to the upstream face. However, these isotherms are spread out more than the isotherms in Simulation 1 and they curve slightly inward towards the base of the dam and do not extend out to the upstream dam toe. In comparison to the field scale dam thermal profile, the predicted temperature in the upstream portion of the dam is slightly warmer in these model simulations. The temperature in the central portion of the field scale dam measured between 8°C and 9°C, while the temperature in the simulated models was slightly warmer, and ranged between 8°C and 11°C. The predicted and measured temperature in the downstream portion of the dam was the same, between 6°C and 7°C. However, the temperature profile is not the same. The 6°C and 7°C isotherms in the model simulations are approximately vertical through the downstream portion of the dam. In contrast, the 6°C isotherm from the field scale dam is parallel to the downstream face of the dam, and the 7°C isotherm is drawn vertically through the dam and then sweeps out along the base in a thin finger like shape towards the toe drain.

The downstream temperature distribution in the field scale dam appears to be a result of seepage flow along the base. However, the upstream temperature distribution does not appear to be influenced by seepage. The SEEP/W and CTRAN/W models were used to explore the potential thermal distribution within the dam, when a small quantity of water seeps through the base of the dam. A base flow of 0.017 litres per second was selected to test this scenario. This seepage rate was selected as it is equivalent to the initial seepage condition measured in the field scale dam at the beginning of the transient seepage analysis, presented in Figure 4.3. Several model simulations were run with various thermal and volumetric water content functions selected. In all cases, the computer simulation results are less similar to the measured field data, than the computer simulations conducted with no flow through the dam. Figure 4.13 shows the predicted thermal distribution within the dam, from one of these simulations. Table 4.5 lists the thermal and hydraulic conditions used for the results presented in Figure 4.13. As Figure 4.13 portrays, the seepage water influences the isotherms in both the upstream and downstream portion of the dam.

4.5 TRANSIENT SEEPAGE ANALYSIS AND THERMAL DISTRIBUTION

This section presents and compares the results from the combined transient seepage and heat transport computer analysis, with the results recorded in the field scale dam. Two upper elevation leakage zones in the central portion of the field scale dam were opened. The resulting change in thermal distribution within the dam was recorded after 48 hours and again after 14 days of seepage through the dam. The measured thermal distributions in the dam are shown on Figure 4.14. A constant reservoir temperature of 19°C was used during the test period. The air temperature recorded in the field scale dam increased from 6°C to 7°C in the first 48 hours and then to 10°C after 14 days.

For the transient computer simulations the grid presented in Figure 4.2 was utilized. The hydraulic properties assigned to the transient seepage analysis (Table 4.2) and described in Section 4.3 were once again assigned to each soil layer. A hydraulic head of 3.2 metres was assigned to the nodes on the upstream dam face. No flow boundary conditions were specified along the base of the dam, crest of the dam, and along the downstream face. A unit flux, to be reviewed based on elevation, was specified for nodes along the toe drain.

Using the general model setup described above, two hydraulic model simulations were conducted, one for the first 48 hours, and then one for the next 12 days. One hundred times steps were used for the 48 hour analysis. The time steps were defined starting with a time of zero seconds. The first time step was set at 60 seconds, with subsequent time steps increasing incrementally by a factor of 2 up to a maximum increment of 1800 seconds. Time step number 100 had a time of 48 hours (1.7286E5 seconds). The hydraulic head values obtained for the initial seepage scenario (Figure 4.4) were used as the initial condition input for 48 hour transient analysis. The hydraulic head values from the 48 hour transient seepage analysis were subsequently used as the initial condition input for the 12 day analysis. The time step for the12 day analysis was set at a constant increment of 1,800 seconds. Time step number 576 (1.0368E6 seconds) represents 14 days since the leak was first opened.

The seepage front progression through the dam during the first 48 hours of leakage, obtained from the SEEP/W analysis, is presented on Figure 4.15. Similarly, the seepage front progression during the first 14 days of leakage is presented on Figure 4.16. The Armbruster et.al., 1989 paper which describes and presents selected results from the field scale dam site, does not include piezometric information for this model scenario. As a result, the computer results cannot be compared to the field results.

The two analyses were then rerun using the substituted volumetric water content function for each soil layer. Table 4.6 lists the volumetric water content functions for each soil layer. The velocities obtained from each analysis were then used by CTRAN/W to calculate the advective (convection) heat transport component through the dam, for the 48 hour and 12 day analysis.

Two model simulations were also run for the heat transport analysis, one for the first 48 hours and one for the following 12 days. The thermal boundary conditions for each model were identical, only the time steps varied, as was the case in the SEEP/W analyses. The time steps selected for the CTRAN/W analyses correspond with those selected for the SEEP/W analyses, for the 48 hour and 12 day periods.

The following thermal boundary conditions were assigned to each model:

- a constant temperature of 19°C for nodes along the upstream dam face;
- a linear change in air temperature from 6°C to 7°C for nodes along the downstream dam face, for the 48 hour period, and a linear change in temperature from 7°C to 10°C for the 12 day period;
- no heat flow was permitted out of the top of the dam; and
- no heat flow was permitted across the base of the dam.

As described in Section 4.4, a range of values for the thermal properties of the materials was calculated for use in the CTRAN/W model, since actual values for the field scale dam soils was unknown. From these calculations three combinations were selected for use. Table 4.7 summarizes the thermal properties assigned to each soil layer for the three model simulations. Calculations for the values presented in Table 4.7 are included in Appendix B-2 along with a table showing how the ranges of parameters were selected.

The thermal conditions presented in Figure 4.12 were selected as the initial conditions for the start of each 48 hour simulation. The results from each 48 hour simulation (Simulation 1 through 3) were in turn used as the initial thermal conditions for the subsequent 12 day test period.

4.5.1 Results from the 48 Hour Test

Results from the three model simulations, for the 48 hour test period, are presented and compared to the results measured in the field scale dam in Figure 4.17. The results of the three simulations are very close to those obtained from the field scale dam; however, they do not match exactly.

The temperature distribution in the dam resulting from Simulation 1 has isotherms that form a bulb shape into the core of the dam, originating from the leakage zones at the top of the dam, and spreading towards the downstream toe. A cooler zone (16°C) remains near the upstream base of the dam. Isotherms in the downstream portion of the dam extend vertically down from the crest, and then run approximately parallel to the downstream face of the dam. In Simulation 1, the temperature distribution in the upstream portion of the dam resembles more closely the field data than does the temperature distributions obtained from Simulations 2 and 3. However, the central and downstream portion of the core is cooler in Simulation 1 than that observed in the field scale dam. In addition, the isotherms near the base of the dam in Simulation 1 tend to turn sharply towards the base to intersect at right angles in contrast to the more gradual pattern seen in the field scale dam and in Simulations 2 and 3.

The isotherms resulting from Simulation 2, 48 hours after the leakage zones were opened, show a bulb shape, originating from the leakage area. The isotherms spread out in a slightly distorted fashion towards the downstream toe. Similarly to the temperature distribution in Simulation 1, a cooler region exists near the upstream base of the dam. However, this region has moved slightly downstream, and is approximately 1°C warmer in Simulation 2. The isotherm contours in the central and downstream portion of the dam extend vertically from the crest into the dam, and then flare outwards towards the toe of the dam, nearly parallel to the downstream slope. Then, the contours curve inward towards the base of the dam. The results from Simulation 2 resemble closely the field data in the central and downstream portions of the dam. However, the upstream toe portion of the core in this simulation is slightly warmer than the field results, and the region immediately below the leak is slightly cooler in the simulation than was measured in the field scale dam. The contour shape in the downstream portion of the core is more similar to the field scale dam results than the contours produced from Simulation 1.

The isotherms from Simulation 3 extend down from the leakage zone and then curve outwards towards the downstream toe of the dam, parallel to the downstream slope. Then, they curve slightly down to intersect the base of the dam. As was seen in Simulations 1 and 2 and in the field results, a slightly cooler region near the upstream toe continues to exist. In Simulation 3 however, this region is approximately 2°C warmer than that measured in the field scale dam, and occurs further downstream. Simulation 3's temperature distribution directly below the leakage zone, in the central and downstream portion of the dam matches well with the temperature data recorded in the field scale dam.

In general, the temperature distribution in the upstream portion of the dam is best predicted by Simulation 1. However, the temperature distribution in the rest of the dam is best predicted by Simulation 3 for the 48 hour leakage period.

4.5.2 Results from the 14 Day Test

Results from the three model simulations, for the 14 day test (48 hour test period plus 12 additional day), are presented and compared to the results measured in the field scale dam in Figure 4.18. The results of the three simulations are similar to those obtained from the field scale dam; however, they do not match exactly.

The isotherm contours from Simulation 1 are approximately parallel to the downstream slope, for the top two thirds of the dam, then they curve sharply downward (approximately 90° bend) to the base. In comparison to measured field results, the temperatures in the central portion of the dam are slightly cooler. The 17.5°C contour interval in Simulation 1 occurs at approximately the same 18.5°C contour interval in the field scale dam. The cooler zone (18.5°C) measured near the upstream toe of the field dam is not apparent in Simulation 1 results. The temperatures in the downstream portion of both dams is similar; however the sharp bend in the contours near the base of the dam is not apparent in the field data. As a result, the temperature along the base of the dam in Simulation 1 is also slightly cooler than the measured temperature.

Results from Simulation 2 and Simulation 3 are virtually identical to one another hence they will simultaneously be described and compared to the field scale dam results. The isotherm contours are approximately parallel to the downstream slope, through the entire dam. No sharp bend in the contour shape occurs near the base of the dam, as was apparent in Simulation 1. The temperatures predicted by Simulations 2 and 3 in the centre and downstream portion of the dam

are essentially identical to the temperature data recorded in the field scale dam. The temperatures measured in the upstream portion of the field scale dam do not match the values in Simulations 2 and 3. The cooler zone near the upstream toe (18.5°C) and the 19.5°C zone below the leakage zone, are not predicted by the CTRAN/W models.

In general, the temperature distribution in the upstream portion of the dam is not predicted by any of the three simulations. It is interesting to note in the field data, that the area along the lower portion of the upstream face, showed minimal warming between the end of the 48 hour period and after 14 days. Thermal convection would dominate in this area, since the leak is above and further downstream. One would expect that this area should increase in temperature, although at a slower rate than in the portion of the dam influenced by both thermal convection and conduction. There is a second irregularity in the field data, from the 14 day period. A 19.5°C contour is shown. This temperature exceeds both the reservoir temperature (19°C) and air temperature (10°C). Based on these observations, and without any further information from the test dam site, it appears that the reservoir temperature may not have been held at a constant temperature. The bottom of the reservoir could have been slightly cooler and the top of the reservoir may have been slightly warmer, than the reported 19°C reservoir temperature. The temperature distribution in the downstream portion of the dam is best predicted by Simulation 2 and Simulation 3, for the 14 day test period.

4.5.3 Summary of Transient Analysis

The transient hydraulic and thermal modelling of the field scale dam, for the 48 hour leakage period and for the 14 day test period, was successful, although an exact match between the predicted and measured values was not achieved, there is a reasonable agreement. As was discussed in Section 4.3 with the transient seepage analysis, no unique solution to the seepage problem has been presented. The solution for the heat transport problem presented in this thesis is also not unique. The thermal values used in Simulation 3 provide the best overall match for the two time intervals.

4.6 SUMMARY AND CONCLUSIONS

Chapter 3 described the methodology and computer programs, SEEP/W and CTRAN/W, utilized to calculate the heat transport through a porous media. The methodology was then successfully tested by comparing the results obtained from the computer model with the solution to two one dimensional analytical solutions for heat transport. The programs and analysis procedure was then applied to the solution of seepage and heat transport through a test dam built in Karlsruhe Germany. Although the computer solutions did not exactly match the measured field data, there was generally good agreement between the simulated results and the measured data. The methodology was shown to be effective as an analysis tool for modelling seepage and heat transport through dams.

Table 4.1: SEEP/W Input Parameters and Their Source

SEEP/W Input Parameters	Data Source
Saturated Hydraulic Conductivity	Measured
Hydraulic Conductivity Function	Deduced
Hydraulic Conductivity Ratio (k_y/k_x)	Deduced
Volumetric Water Content Function	Assumed/Deduced
Saturated Volumetric Water Content	Assumed
Hydraulic Head	Measured

Table 4.2: Hydraulic Properties Used In Transient SEEP/W Simulation

Material	Hydraulic Conductivity Function or Value (m/s)	Hydraulic Conductivity Ratio	Volumetric Water Content Function Or Value
Impermeable facing	1E-9	1.0	0.3
toe drain	1E-1	1.0	0.4
Sand/ Partially Saturated Sand Base	function (see below)	1.0	function (see below)
hole	function max. = 8E-4	1.0	function max. = 0.53
Leak at base	2.1E-7	1.0	0.3

Sand

Pt. #	Pressure	Conductivity
1	-1.8673e+001	9.0220e-008
2	-1.5079e+001	8.9894e-008
3	-1.2157e+001	9.4067e-008
4	-9.5503e+000	1.0799e-007
5	-8.4110e+000	2.4492e-007
6	-7.2808e+000	2.4002e-006
7	-6.5416e+000	1.4413e-005
8	-5.5414e+000	7.4691e-005
9	-3.7596e+000	1.4645e-004
10	-1.5000e+000	2.0000e-004
11	1.4913e+000	2.0000e-004
12	6.3505e+000	2.0000e-004
13	1.0000e+001	2.0000e-004

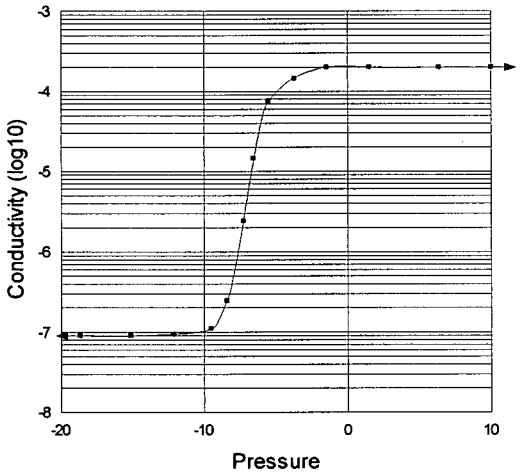

Sand

Pt. #	Pressure	Vol. Water Content
1	-1.0000e+002	1.9000e-001
2	-5.6320e+001	2.0000e-001
3	-2.5213e+001	2.1254e-001
4	-1.7755e+001	2.4401e-001
5	-1.3000e+001	2.9000e-001
6	-7.3298e+000	3.4297e-001
7	0.0000e+000	3.8000e-001
8	2.0000e+001	3.8000e-001

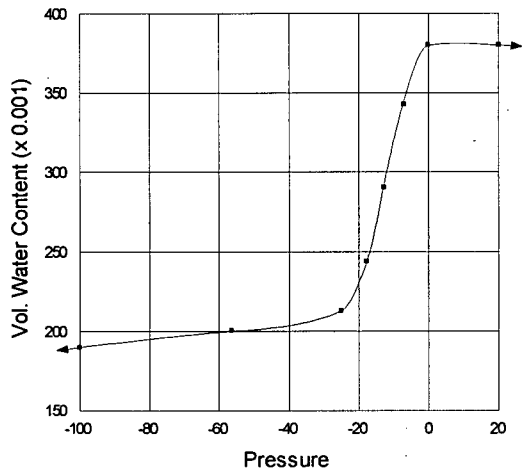

Table 4.3: Thermal Soil Properties Used In CTRAN/W Simulation - With Basal Heat Flux

Thermal Property	Value
E^* (m^2/s)	1.75E-6
α_L (m)	0.1
α_T (m)	0.001

Table 4.4: Summary of Thermal Properties for CTRAN/W Models Thermal Conduction through Field Dam

	Simulation 1	*Simulation 2*	*Simulation 3*
Soil Layer	E^* (m^2/s)	E^* (m^2/s)	E^* (m^2/s)
Impermeable Face	7.0E-7	1.75E-6	2.5E-6
Sand	7.0E-7	1.75E-6	2.5E-6
Gravel Toe Drain	7.0E-7	1.75E-6	2.5E-6

Table 4.5: Hydraulic and Thermal Properties Used In SEEP/W and CTRAN/W For Simulation Results Presented in Figure 4.13

Soil Layer	Saturated Hydraulic Conductivity (m/s)	Θ_{sub}	E^* (m^2/s)	α_L and α_T (m)
Impermeable Face	1E-9	0.50	6.7E-7	9, 0.9
Sand	2E-4	0.60	9.6E-7	10, 1
Gravel Toe Drain	1E-1	0.57	7.5E-7	10, 1

Table 4.6: Summary of Volumetric Water Content Function Substitutions for CTRAN/W Models Thermal Convection and Conduction through Field

	Simulation 1	*Simulation 2*	*Simulation 3*
Soil Layer	Θ_{sub}	Θ_{sub}	Θ_{sub}
Impermeable Face	0.57	0.3	0.3
Sand	0.60	0.6	0.6
Gravel Toe Drain	0.57	0.6	0.6

Table 4.7: Summary of Thermal Properties for CTRAN/W Models Thermal Convection and Conduction through Field Dam

	Simulation 1	*Simulation 2*	*Simulation 3*
Soil Layer	E^* (m²/s)	E^* (m²/s)	E^* (m²/s)
Impermeable Face	7.0E-7	1.75E-6	2.5E-6
Sand	7.0E-7	1.75E-6	2.5E-6
Gravel Toe Drain	7.0E-7	1.75E-6	2.5E-6
	α_L (m)	α_L (m)	α_L (m)
Impermeable Face	2	0.1	0.1
Sand	2	0.1	0.1
Gravel Toe Drain	2	0.1	0.1
	α_T (m)	α_T (m)	α_T (m)
Impermeable Face	0.2	0.01	0.01
Sand	0.2	0.01	0.01
Gravel Toe Drain	0.2	0.01	0.01

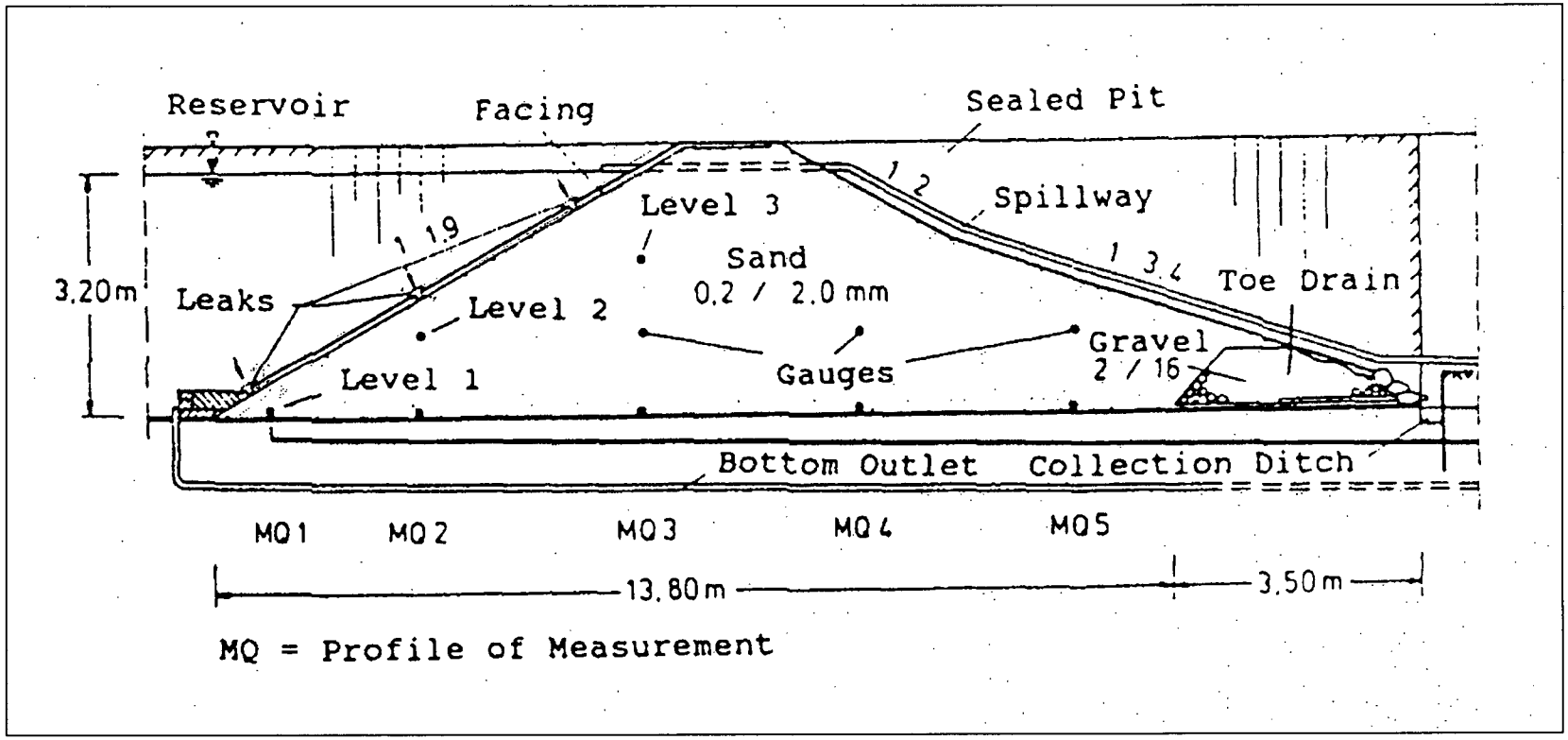

Figure 4.1: Cross Section of Field Scale Dam, Karlsruhe, Germany (as presented in Armbruster, Brauns, Mazur, and Merkler, 1989)

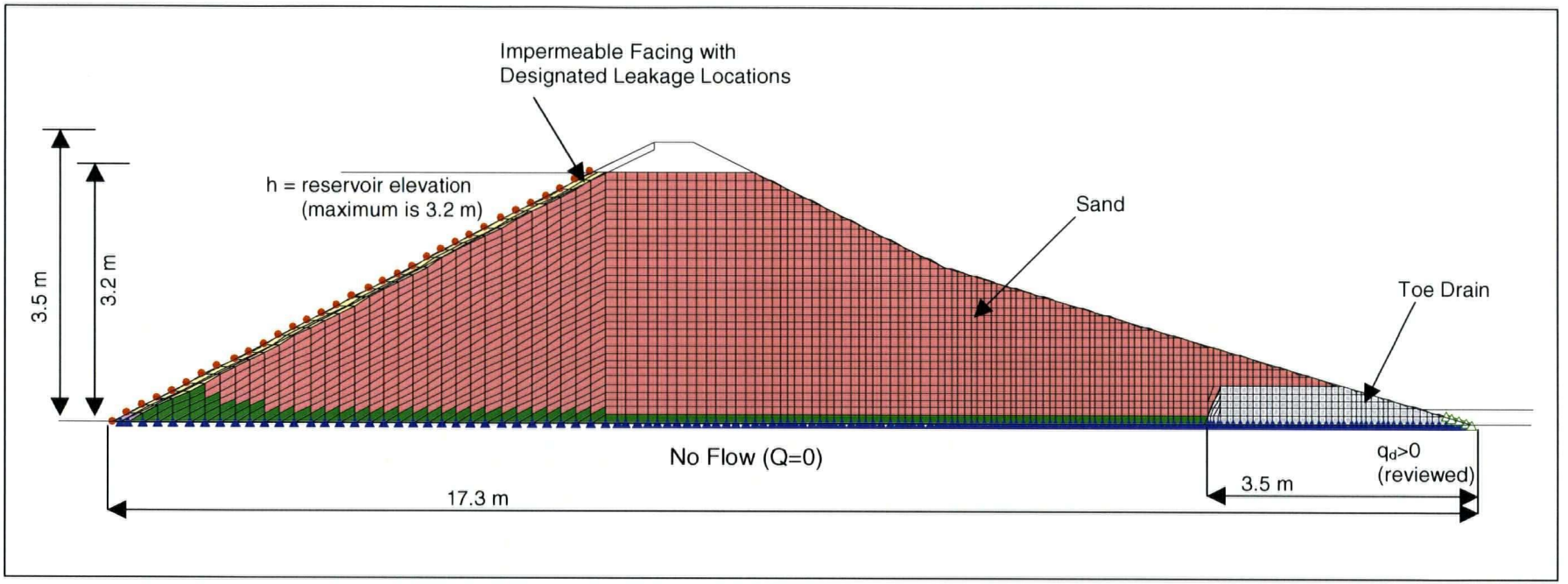

Figure 4.2: SEEP/W Grid Used to Analyze Field Scale Dam

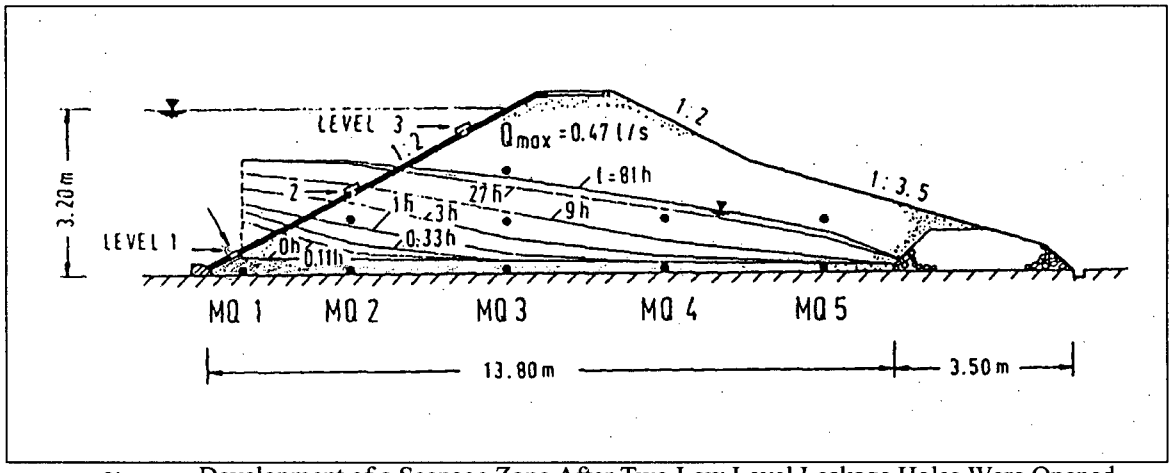

a: Development of a Seepage Zone After Two Low Level Leakage Holes Were Opened

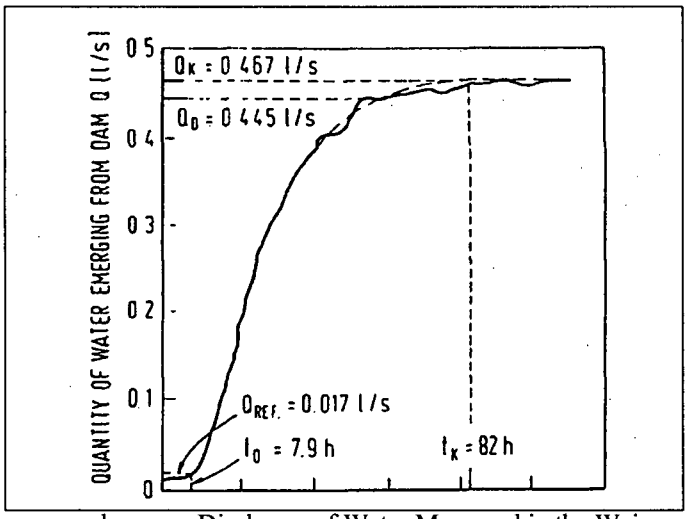

b: Discharge of Water Measured in the Weir as a Function of Time, Since Leakage Holes Were Opened

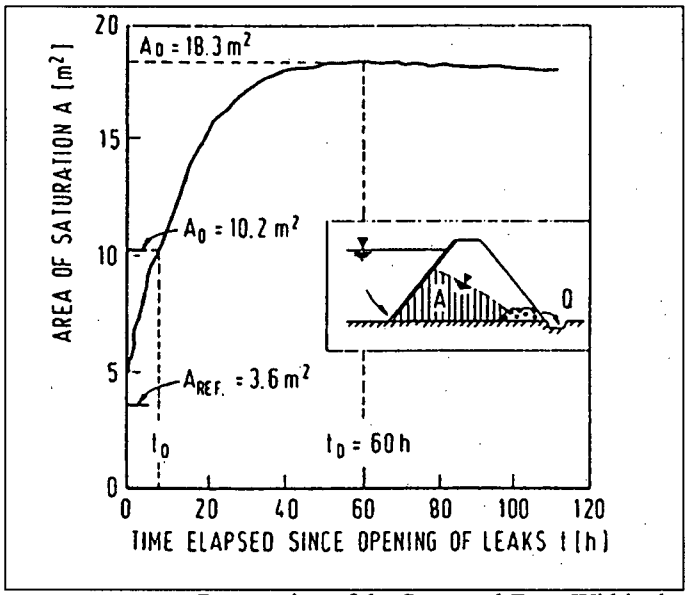

c: Progression of the Saturated Zone Within the Dam as a Function of Time, Since Leakage Holes Were Opened

Figure 4.3: Seepage Front Development as a Function of Time Field Scale Dam, Karlsruhe, Germany (as presented in Armbruster, Brauns, Mazur, and Merkler, 1989)

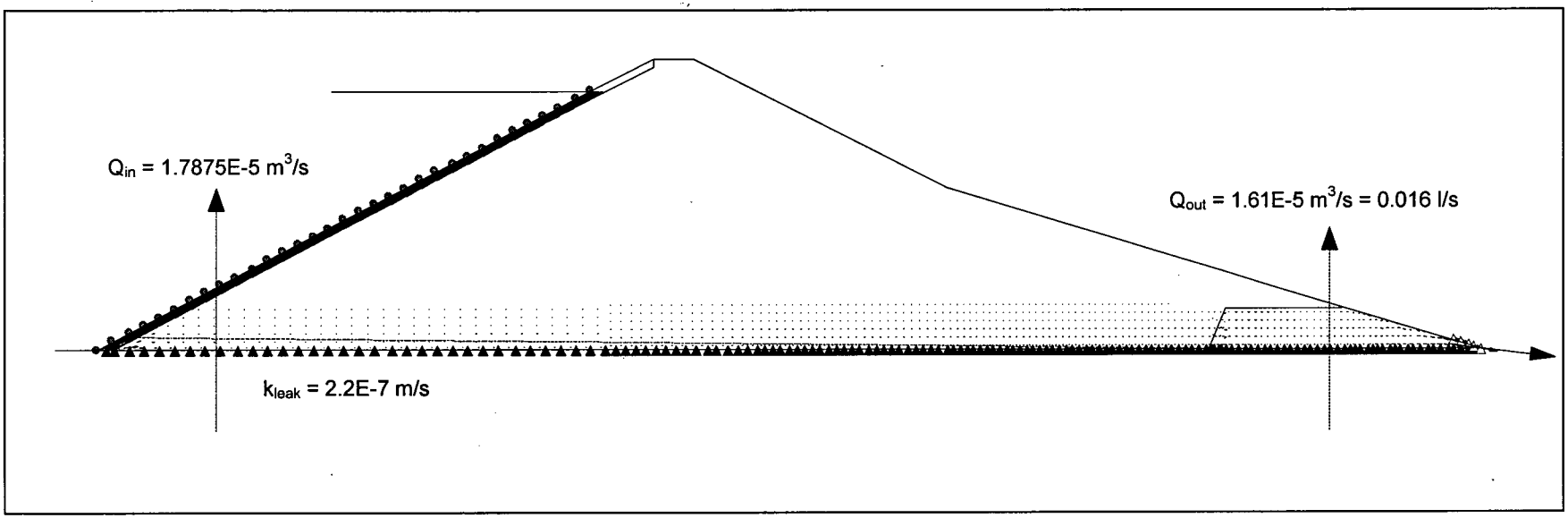

Figure 4.4: Steady State Seepage Results Obtained Using SEEP/W To Match Initial Conditions Measured in Field Dam

Material	Hydraulic Conductivity Function or Value (m/s)	Hydraulic Conductivity Ratio	Volumetric Water Content Function Or Value
impermeable facing	1E-9	1.0	0.3
toe drain	1E-1	1.0	0.4
Sand/ Partially Saturated Sand Base	function K-Fn No. 3	1.0	function W.C. Fn No. 6
hole	function K-Fn No. 5	1.0	function W.C. Fn No. 4
leak at base	2.2E-7	1.0	0.3

K-Fn No. 3 (sand and partially saturated sand base)

Pt. #	Pressure	Conductivity
1	-1.8673e+001	9.0220e-008
2	-1.5079e+001	8.9894e-008
3	-1.2157e+001	9.4067e-008
4	-7.2882e+000	1.0799e-007
5	-4.4733e+000	2.4492e-007
6	-3.9295e+000	2.4006e-006
7	-3.5676e+000	1.1453e-005
8	-3.2028e+000	4.9409e-005
9	-2.6706e+000	1.3987e-004
10	-1.5000e+000	2.0000e-004
11	1.4913e+000	2.0000e-004
12	6.3505e+000	2.0000e-004
13	1.0000e+001	2.0000e-004

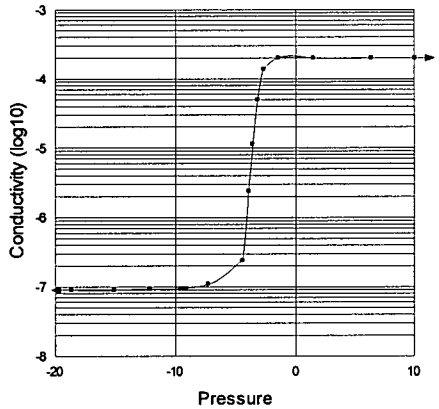

K-Fn No. 5 (hole)

Pt. #	Pressure	Conductivity
1	-1.0000e+002	1.0000e-006
2	-7.8994e+001	1.0608e-006
3	-4.0706e+001	1.2432e-006
4	-2.5255e+001	2.1862e-006
5	-1.8723e+001	9.4019e-006
6	-1.6318e+001	4.5152e-005
7	-1.3338e+001	1.8518e-004
8	-1.0562e+001	4.5139e-004
9	-7.0960e+000	7.8470e-004
10	5.8084e+000	8.0000e-004
11	1.6425e+001	8.0000e-004

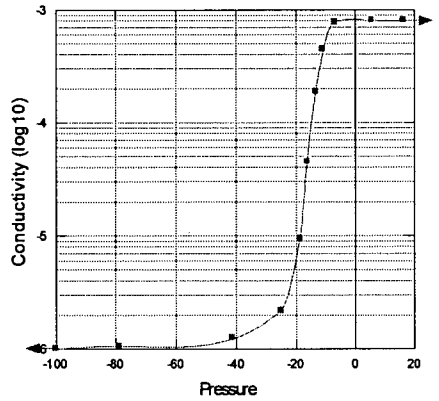

W.C. Fn No. 6 (sand and partially saturated sand base)

Pt. #	Pressure	Vol. Water Content
1	-1.0000e+002	1.9000e-001
2	-5.6320e+001	2.0000e-001
3	-2.5213e+001	2.1254e-001
4	-1.7755e+001	2.4401e-001
5	-1.3000e+001	2.9000e-001
6	-7.3298e+000	3.4297e-001
7	0.0000e+000	3.8000e-001
8	2.0000e+001	3.8000e-001

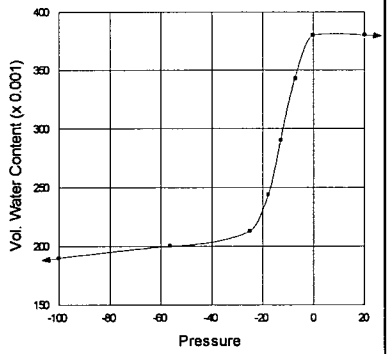

W.C. Fn No. 4 (hole)

Pt. #	Pressure	Vol. Water Content
1	-1.0000e+002	6.0000e-002
2	-8.0000e+001	7.8449e-002
3	-5.9949e+001	1.1595e-001
4	-4.8883e+001	1.5690e-001
5	-3.0000e+001	3.0000e-001
6	-1.0000e+001	5.0000e-001
7	-3.0000e+000	5.2000e-001
8	1.0000e+001	5.3000e-001

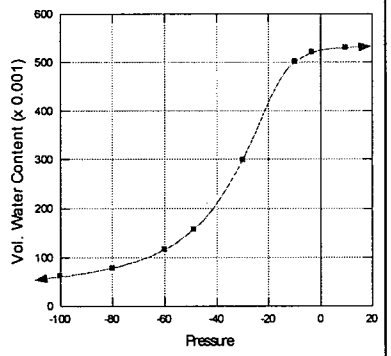

Figure 4.5: Hydraulic Properties Assigned To SEEP/W Model Of Field Dam

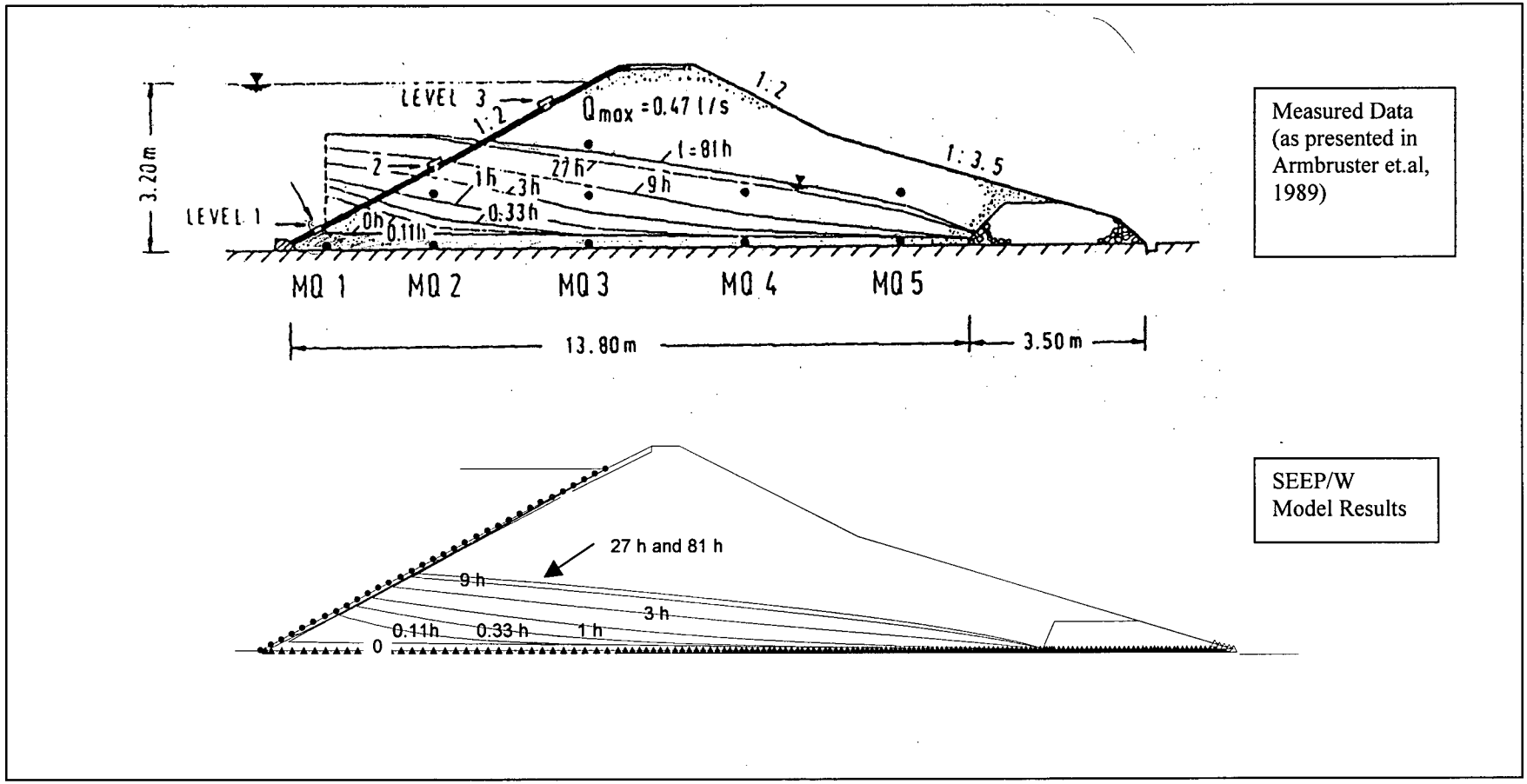

Figure 4.6: Comparison of Measured Seepage Front Development to SEEP/W Model Results of Field Dam

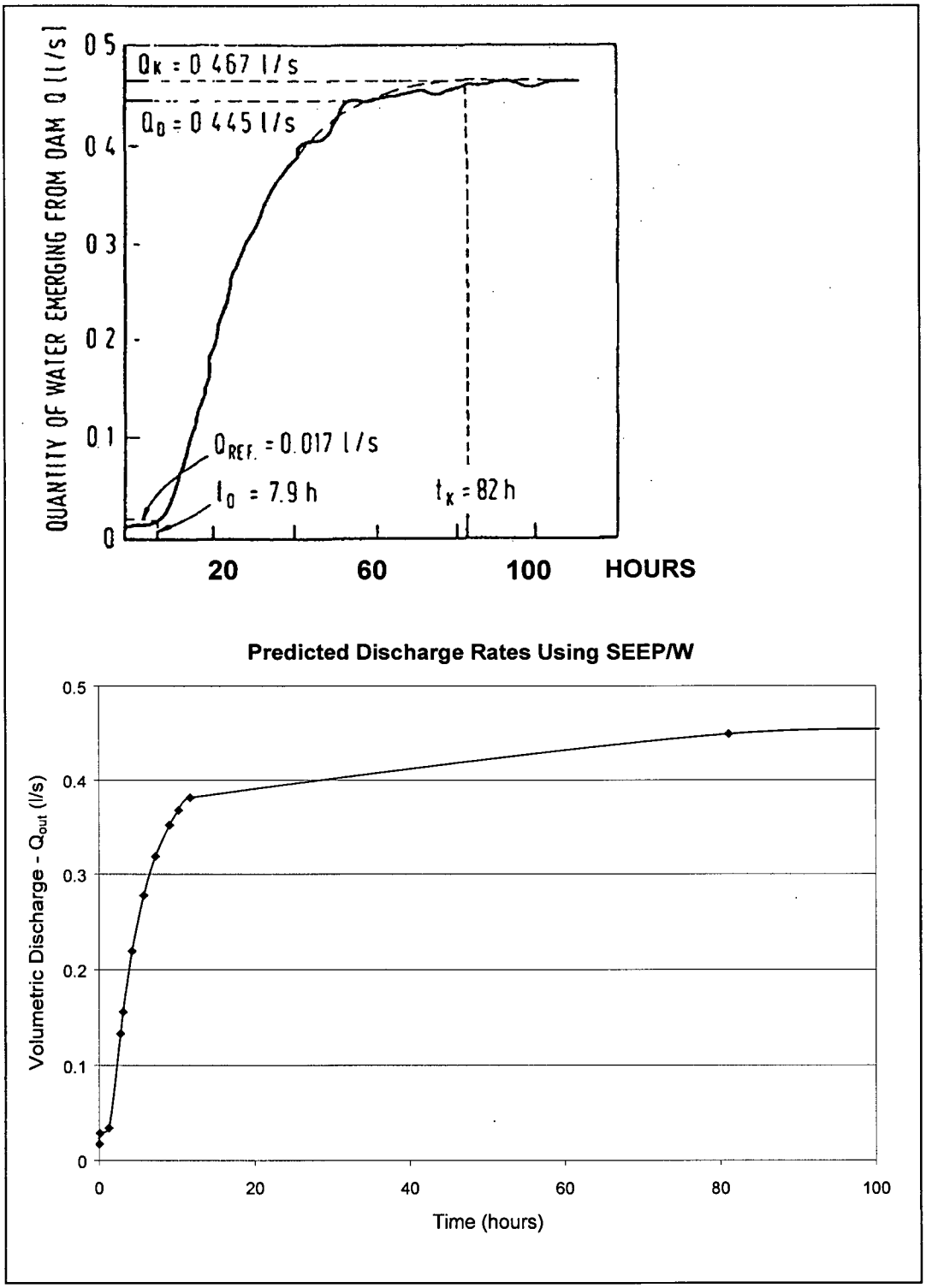

Figure 4.7: Comparison of Measured Discharge Rates to SEEP/W Model Results

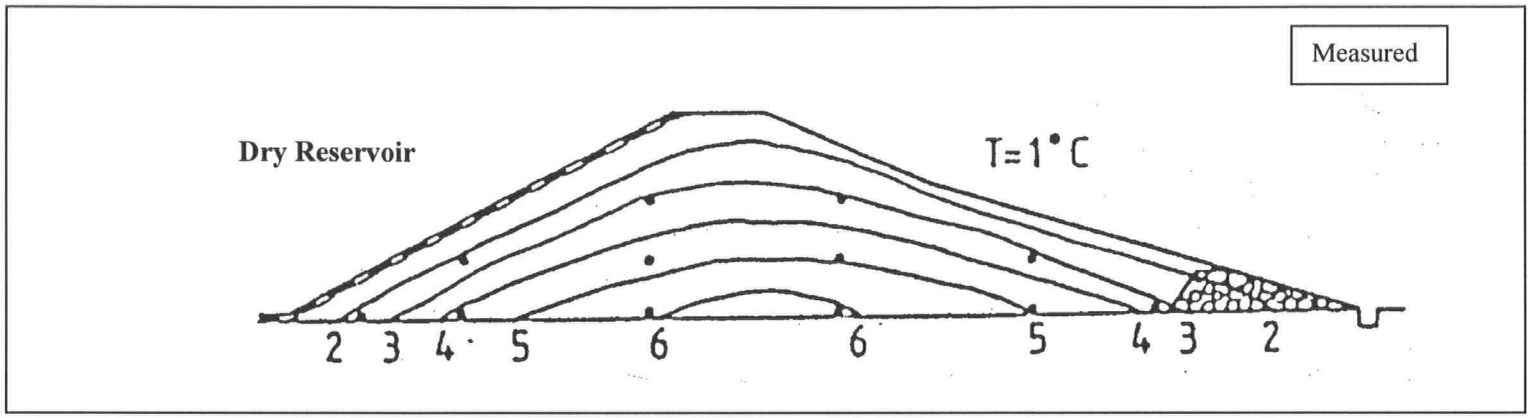

Figure 4.8: Initial Thermal Conditions Measured in the Field Scale Dam, Karlsruhe, Germany (as presented in Armbruster et.al., 1989)

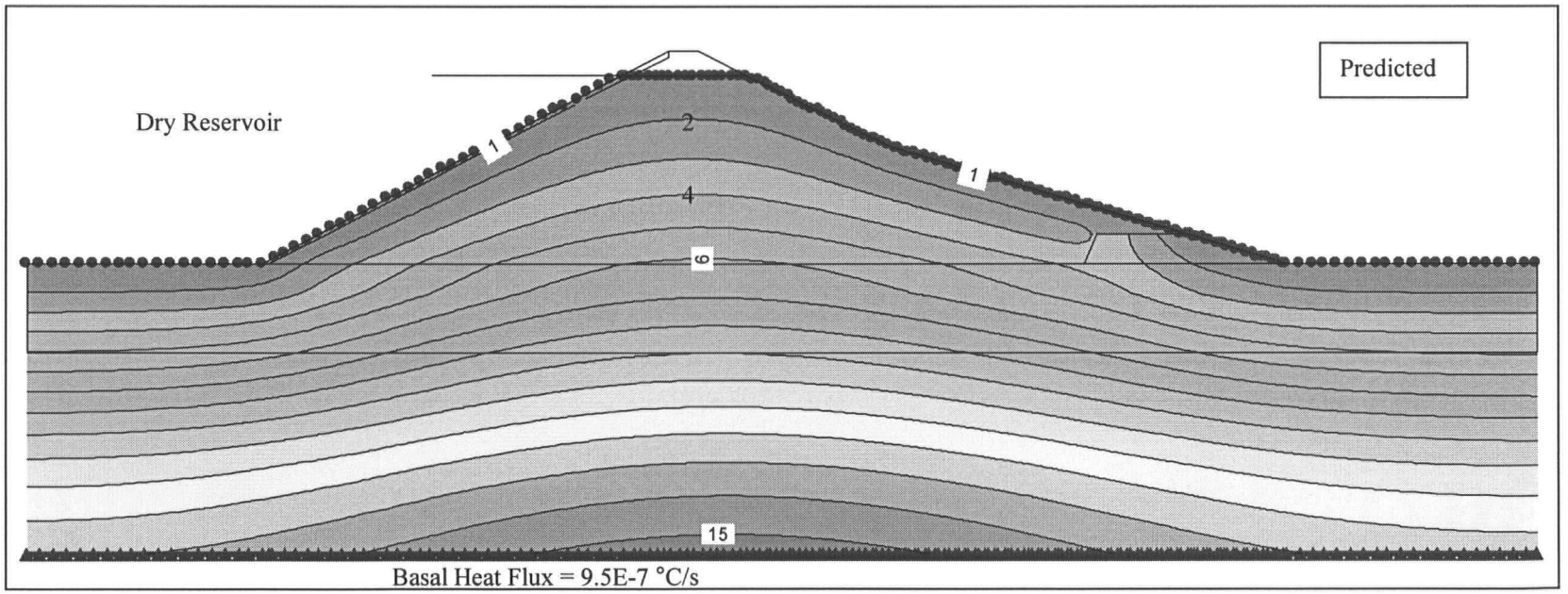

Figure 4.9: CTRAN/W Model Simulation Results Using A Geothermal Gradient To Match Measured Data

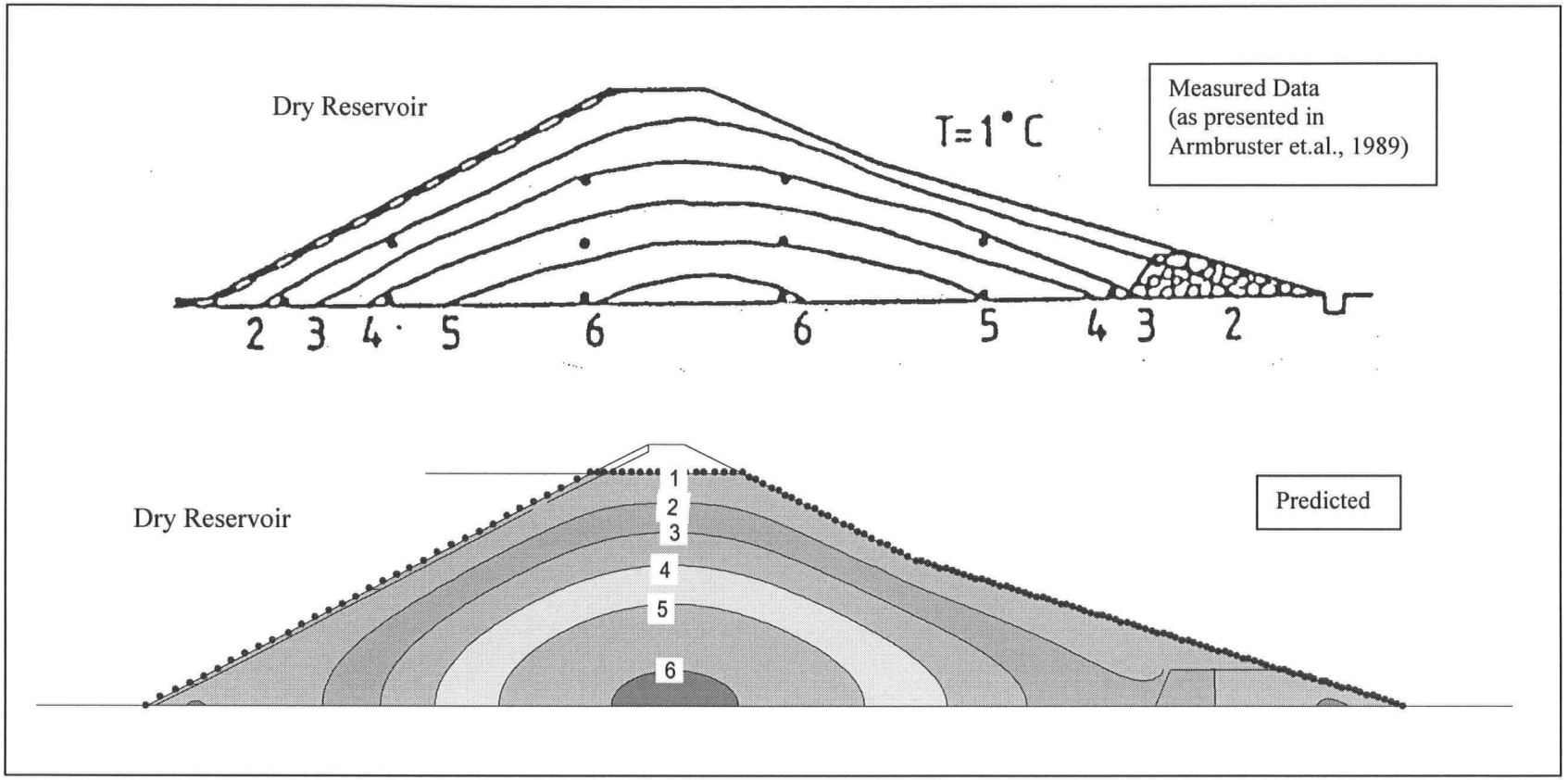

Figure 4.10: Predicted Thermal Distribution As A Result of Cooling (9 days) Compared to the Measured Thermal Distribution in Field Dam

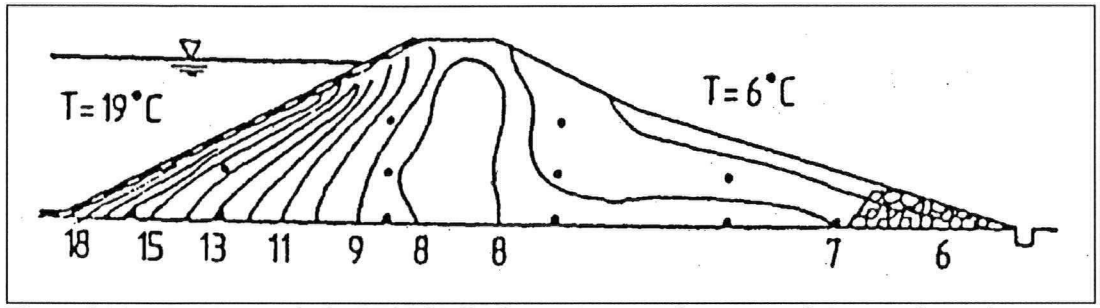

Figure 4.11: Measured Thermal Distribution - 18 Days After Reservoir Impoundment (as presented in Armbruster et.al., 1989)

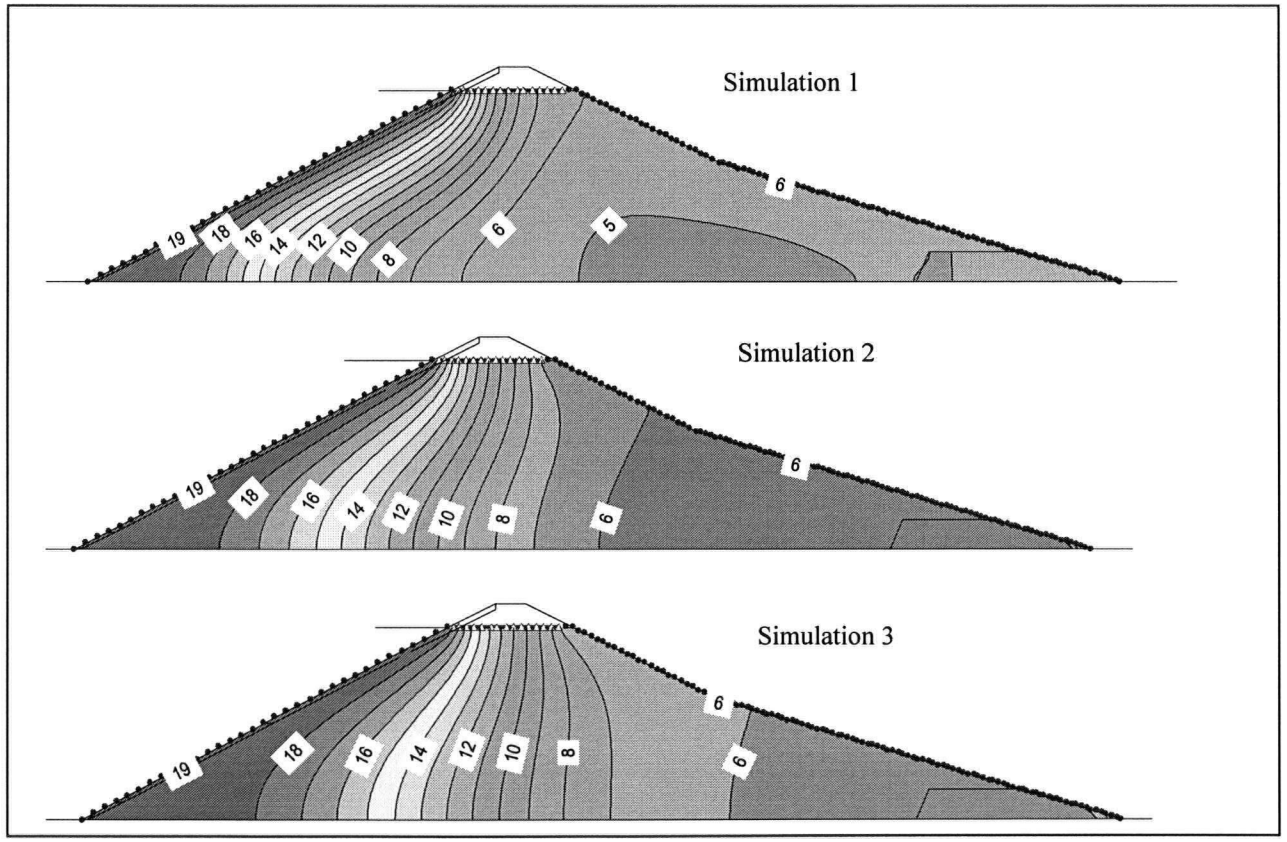

Figure 4.12: Predicted Thermal Distributions Within The Field Dam - 18 Days After Reservoir Impoundment

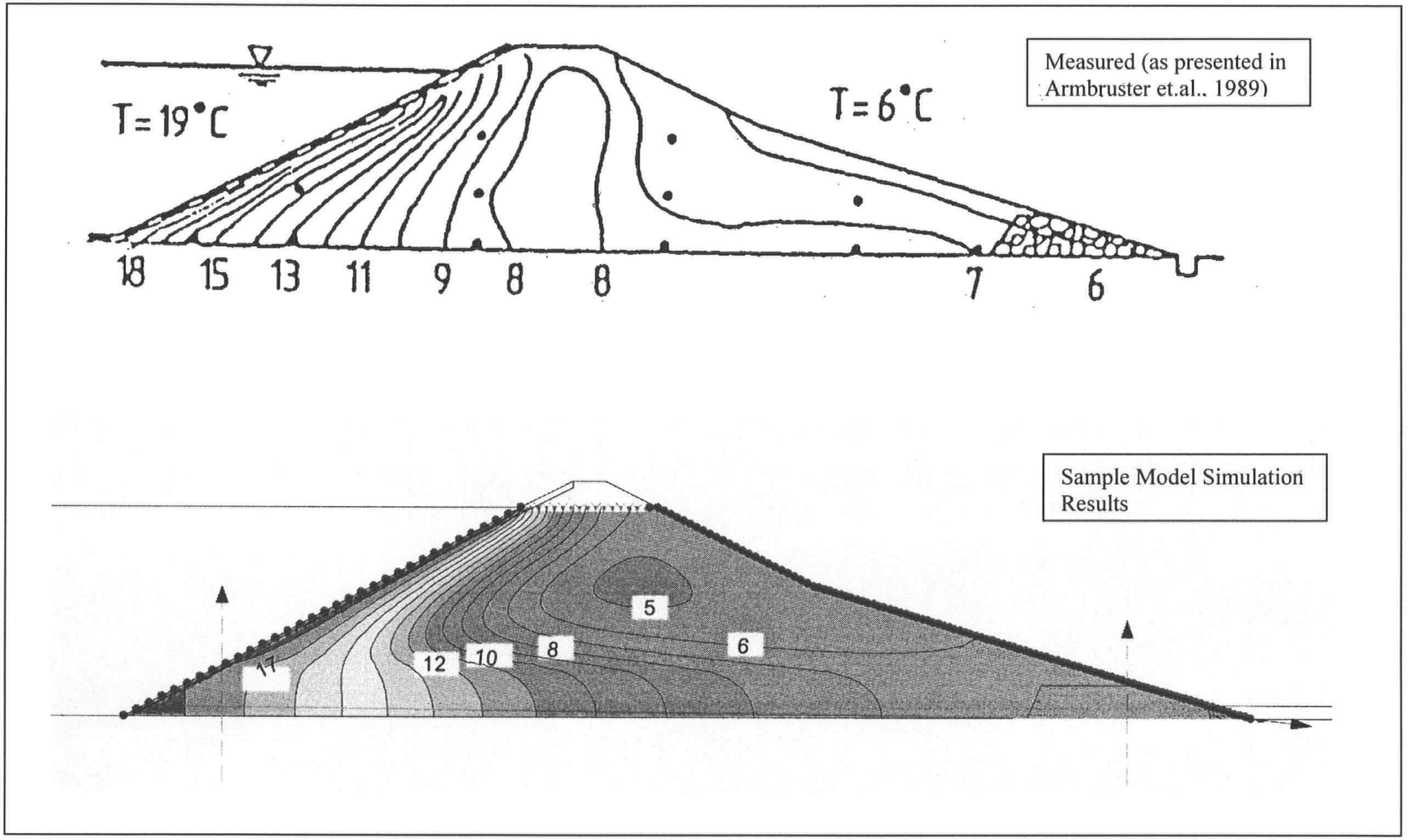

Figure 4.13: Sample Output Showing the Predicted Thermal Distribution With Leakage at the Base - 18 Days After Reservoir Impoundment Compared to Measured Results

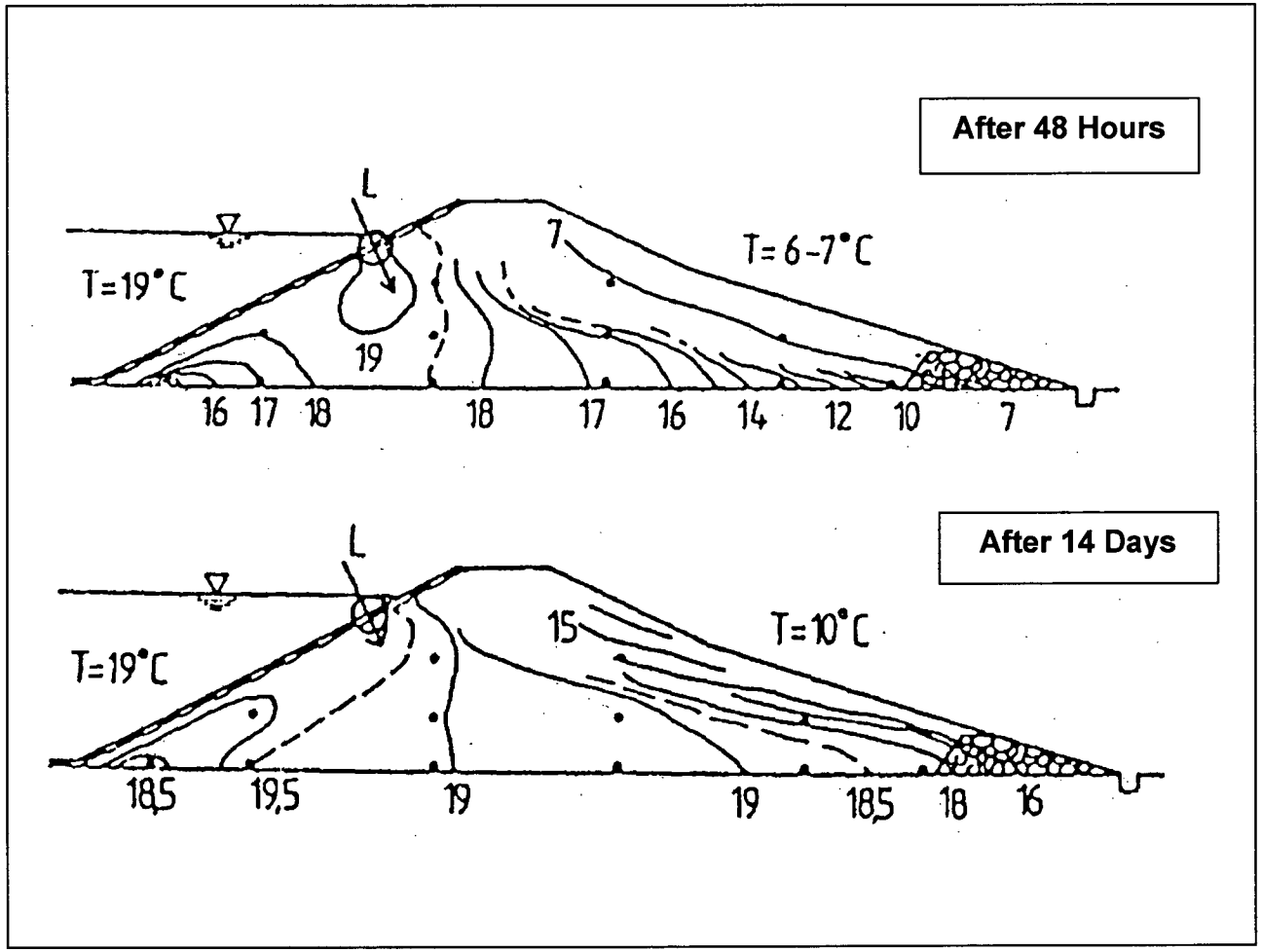

Figure 4.14: Measured Thermal Distribution as a Result of Seepage through an Upper Leakage Zone

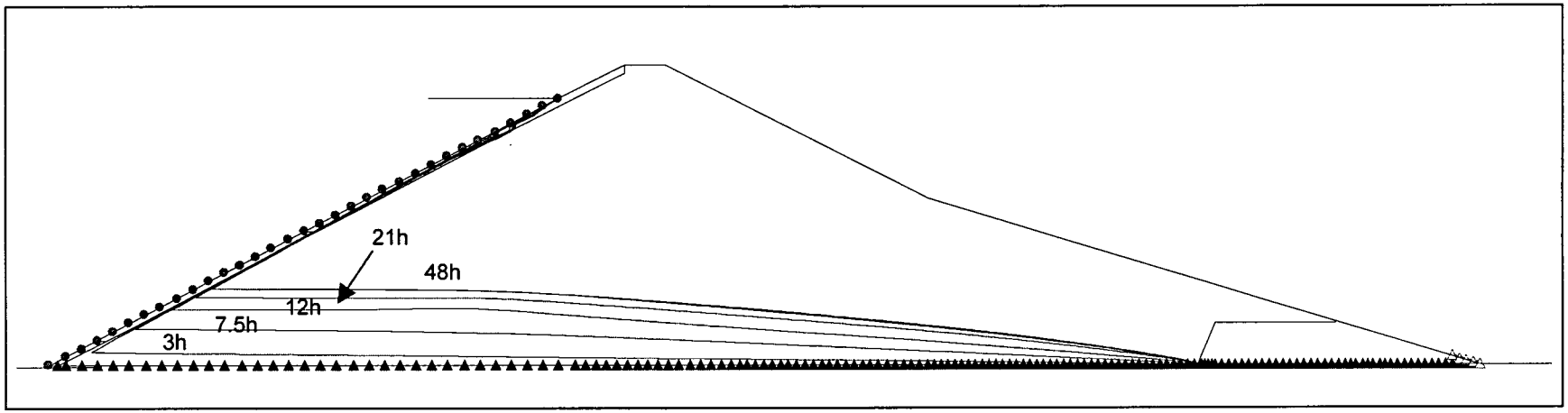

Figure 4.15: Predicted Seepage Front Progression during the First 48 Hours after Upper Leakage Zone Was Opened

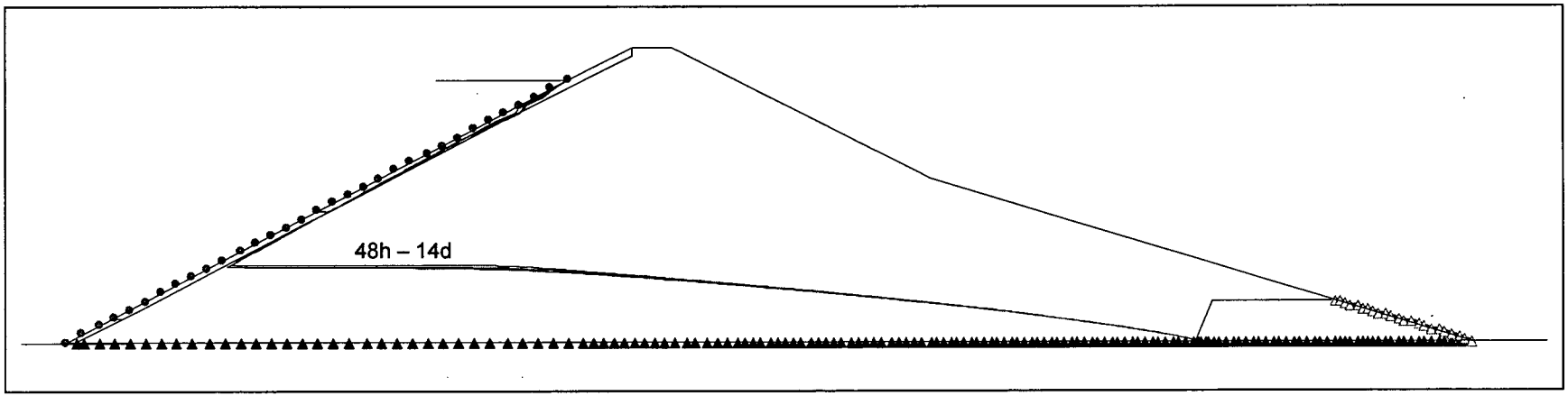

Figure 4.16: Predicted Seepage Front Progression during the First 14 Days after Upper Leakage Zone Was Opened

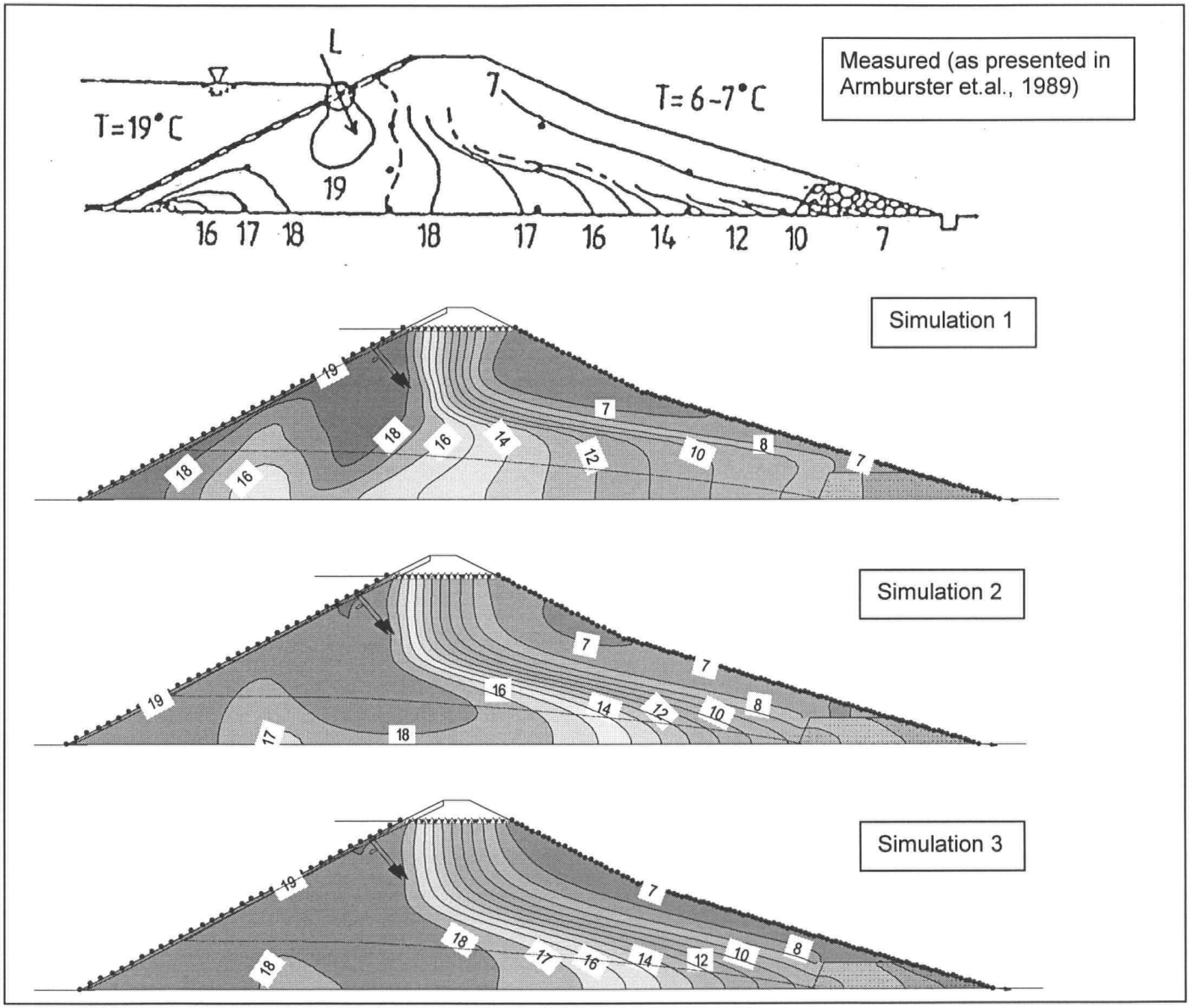

Figure 4.17: Measured and Predicted Thermal Distributions within the Field Dam - 48 Hours After Upper Leakage Zone Was Opened

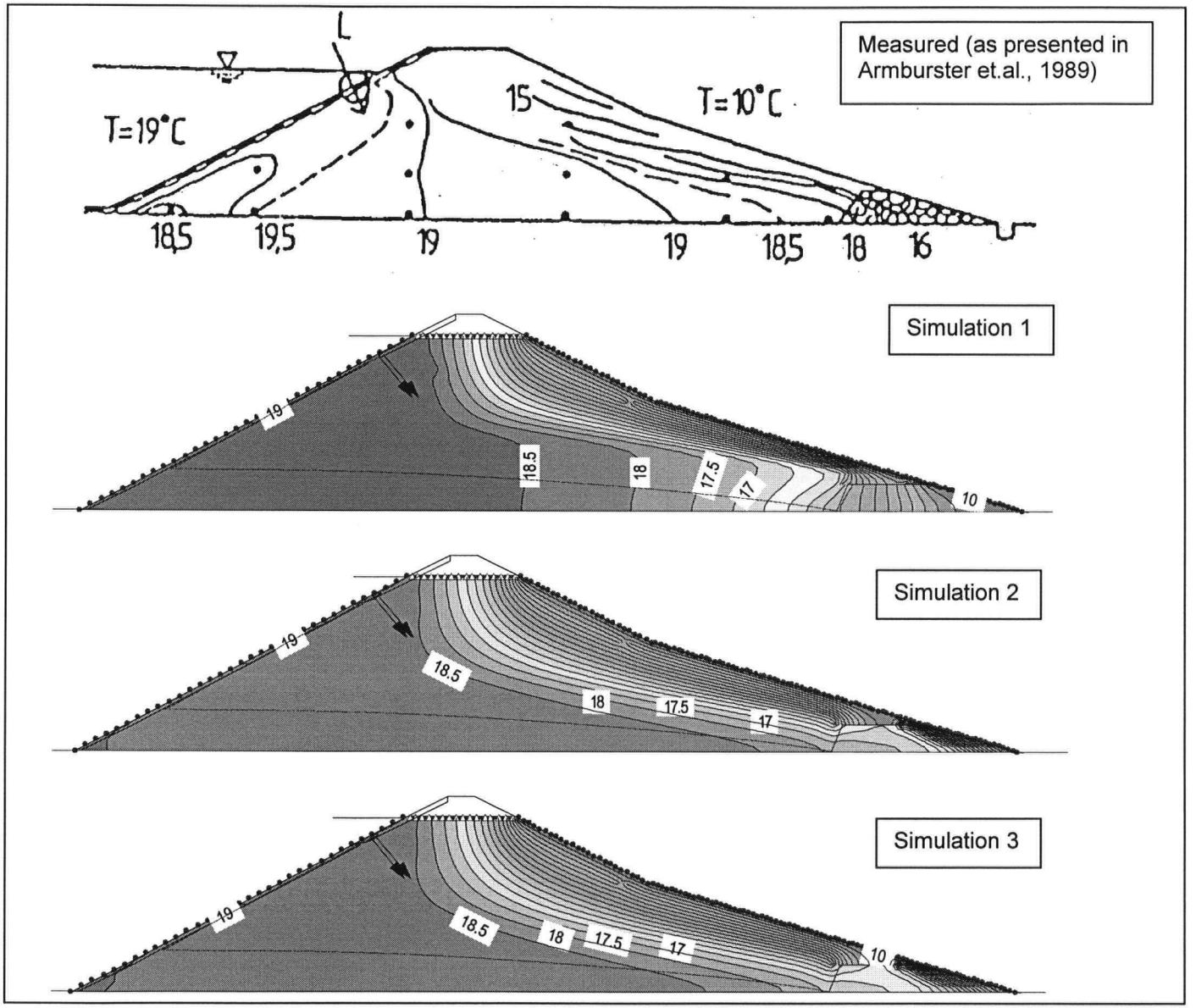

Figure 4.18: Measured and Predicted Thermal Distributions within the Field Dam - 14 Days After Upper Leakage Zone Was Opened

CHAPTER 5: FIELD PROGRAM

5.1 INTRODUCTION

Chapter 5 describes the field component of this thesis, specifically the temperature monitoring conducted within the piezometers and reservoir at BC Hydro's Coquitlam Dam. Section 5.2 presents information on the general location and construction of Coquitlam Dam. Section 5.3 describes the regional geology. Section 5.4 describes the site geology, with specific emphasis on the stratigraphic units that form the dam foundation, and the fill materials that comprise the dam itself. Section 5.5 describes the hydraulic conditions of Coquitlam Dam. This is followed by a description of the temperature monitoring program implemented at Coquitlam Dam, in Section 5.6. Section 5.7 presents the temperature monitoring data and general observations about the data. Section 5.8 discusses the results of the temperature monitoring program implication on the heat transport numerical modelling of Coquitlam Dam. Section 5.9 contains summary remarks and conclusions about the field program.

5.2 COQUITLAM DAM

The Coquitlam Dam is located on the Coquitlam River, approximately fifteen kilometres upstream of its confluence with the Fraser River, as shown on Figure 5.1. The cities of Port Coquiltam and Coquitlam are located downstream of the dam.

The reservoir impounded by the dam provides water storage for power generation, and is a source of potable water for the Greater Vancouver Water District (GVWD). In addition the dam regulates discharge water to maintain river flows for fish habitat and migration, and provides some flood control for Port Coquitlam, and Coquitlam. Water from the reservoir is piped through a tunnel to Buntzen Lake where power is generated at Buntzen (LB1) and Lake Buntzen 2 (LB2) generating stations. Water from the Coquitlam reservoir supplies a portion of the drinking water for the Greater Vancouver area of 2 million people. The reservoir is 13 kilometres long and has a maximum capacity of 202 million cubic metres. The normal operating elevation is between 142 and 154.9 metres.

The Vancouver Power Railway Company Limited constructed the Coquitlam Dam between 1908 and 1913. The dam is a zoned embankment dam with a hydraulic fill core and shell, upstream and downstream rockfill toes, and a spillway. The dam is about 30 metres high, is 3.8 metres wide at the crest, 200 metres wide at the base, and has a crest length of 290 metres. The original upstream slope was 5H:1V and the downstream slope varied from 2H:1V at the top to 4H:1V at the base. Additional rockfill was placed on the upstream and downstream slopes in 1980, and in 1984/85 to improve stability.

Prior to constructing the dam, a rockfill crib overflow dam was built in 1903, raising the original water level of the lake by 3.4 metres. During construction of the dam, the height of this structure was increased twice, by sluicing silt upstream of the crib dam. The crib dam was eventually buried in the upper toe of the current dam.

The dam was built by first constructing the upstream and downstream rockfill toes, using rock from the spillway and diversion tunnel excavations. The sand and gravel shells materials were hydraulically placed against the rockfill. Flumes were constructed parallel to the dam crest, as shown in Figure 5.2a, to sluice fill the core of the dam (Figure 5.2b). Two borrow pits, one on either side of the dam, were excavated and high pressure water was used to transport the fill materials through the flumes to the dam. Construction of the shell and core was sequenced in such a manner that the elevations were similar. As construction progressed the flumes were raised and moved towards the centre line of the dam. Water used in sluicing the shell materials would run off quickly. Conversely, drainage from the core materials was much slower, as a result, a large sedimentation pond formed during placement of the core materials. Figure 5.3 shows the pool of water in the centre portion of the dam and the completed dam prior to reservoir filling. Recent drilling has revealed thin layers of sand and gravel amongst the primarily silt core. This is consistent with staged sluicing. The timber trestles that were used to support the flumes during hydraulic filling were buried amongst the dam fill materials. The spillway channel was cut in the bedrock at the left abutment, on the east side of the dam. The spillway is about 60 metres wide, 50 metres long, and the invert elevation is approximately 154 metres. Figure 5.4 shows an as-built cross section of the dam from 1915 (Conway, 1915; BC Hydro, 1984; and BC Hydro, 1986).

In 1980 and 1984/85, additional rockfill was placed on the upstream and downstream slopes to improve the dam's stability during an earthquake. In 1985, the dam crest elevation was raised by two metres, and the logging road was moved from the crest to the top of the upstream berm. Figure 5.5 shows a current plan view of the dam. Figure 5.6 shows a typical cross section of the dam with the additional rockfill. The photographs presented on Figure 5.7 show current conditions of the dam (BC Hydro).

5.3 REGIONAL GEOLOGY

5.3.1 Bedrock Geology

The Canadian Cordillera is divided into five general morphogeological belts. The Coast Belt includes the Coast Mountains to the north, and the Cascade Mountains to the south, separated by the Fraser Lowland. Coquitlam Dam is located at the southern end of the Coast Mountains. Bedrock in the area is plutonic in origin from the Cretaceous to late Tertiary, 20 to 135 million years old (Geological Survey of Canada, 1965). Figure 5.8 shows the bedrock geology in the area. Granodiorite is the dominant rock type. It is typically fine to medium grained, very strong and massive. Locally the rock quality may be variable with jointing and shearing.

5.3.2 Surficial Geology

The mountains along the edge of the Fraser Lowland are rugged with peak elevation between 1,500 and 2,100 metres. Between these mountains are deep U-shaped valleys, oriented in a north-south direction, with floor elevations ranging from near sea level to 100 metres. The physiographic setting of the area is a reflection of repetitive glacial cycles, with scoured bedrock, deposited, eroded and re-deposited sediments from glacial and interglacial periods, followed by post-glacial deposition. In the vicinity of Coquitlam Dam, the most significant features of these glacial cycles is the presence of two buried channels or valleys, as shown on Figure 5.9. Coquitlam Dam is actually built over top of the buried valley labelled as one on Figure 5.9 (Armstrong, 1984).

5.4 SITE GEOLOGY

In comparison to more recently constructed dams, Coquitlam Dam has limited geotechnical information or construction quality control information. As a result, BC Hydro has conducted numerous investigations between 1979 and 2001. The investigations were used to obtain information, including:

- dam stratigraphy;
- description of soil materials, and their properties (density, shear strength, friction angle, cohesion, hydraulic conductivity);
- insitu moisture contents; and
- installation of instruments to monitor the dam (settlement gauges, pneumatic and standpipe piezometers, inclinometer, weirs, and strong motion detectors).

The following summary of the bedrock, foundation soils, and dam fill materials is based on information compiled from the aforementioned investigations. BC Hydro continues to gain additional information through studies and investigations. As a result, interpretations of the subsurface geology and dam fill materials presented in this report may be subject to change.

5.4.1 Foundation Bedrock

Bedrock at the Coquitlam Dam is composed of medium grained granodiortie with mafic inclusions, andesitic dykes and basaltic dykes. Outcrop mapping has indicated that the bedrock is strong and widely jointed with minimal groundwater flow. Bedrock outcrops on the east (left) abutment of the dam and then plunges west and southward. The GVWD has installed two drill holes (BH97-1 and BH97-2) to bedrock in the vicinity of the dam. In these holes, bedrock was encountered at an elevation of 48 metres, 80 metres west to the dam crest, and at an elevation of 28 metres, 800 metres south of the dam. The maximum thickness of sediments in the buried valley exceeds 120 metres (GVWD, 1997, and information provided by BC Hydro).

5.4.2 Foundation Soils

Coquitlam Dam foundation soils have been classified into ten units (Table 5.1), based on the glacial events, depositional environments, soil textures, and densities observed during field investigations. The deposits have been labelled numerically from oldest to youngest, based on interpreted ages. Figure 5.10 presents the interpreted, distribution of foundation soils. Figure 5.11 and Figure 5.12 present geologic cross sections A-A to D-D through the dam, from west to east. Figure 5.13 presents a longitudinal section E-E through the dam crest. These cross sections are a compilation of information obtained from various drilling programs, soil testing and analysis, and pre and post construction geologic mapping prepared by BC Hydro staff (information provided by BC Hydro). Stratigraphic variation in both the dam foundation soils and dam fill materials is apparent from comparisons between sections A-A through E-E.

The basal foundation soil layer, identified in Table 5.1 as Unit 1A, consists of glaciofluvial sand. The unit is identified as SP (poorly graded sand, containing less than 5% fines) using the Unified Soil Classification System (USCS), and described as; dense, grey, fine to coarse sand, trace to some gravel, trace to some silt. This unit fills most of the buried valley. Hydraulic conductivity estimates for this unit, are based on limited borehole data, and range from 5E-5 to 1E-6 metres per second.

Unit 1A is overlaid by Unit 1B. Unit 1B is approximately 8 metres thick and consists of glaciofluvial gravel and sand. The top of the unit dips gently from east to west (Figure 5.13) and appears to be locally elevated over the bedrock outcrop on the east abutment. The unit is described as dense, sandy gravel to gravel and sand, trace fines (GP, GP-GM using the USCS). The gravel is typically subrounded to subangular. Figure 5.14 shows soil sample gradation curves for this unit. Hydraulic conductivity estimates for this unit range from 1E-2 to 1E-5 metres per second, based on the grain size curve data.

Unit 2A is a glaciolacustrine silt, that forms the low permeability unit for the dam foundation. This unit is up to 30 metres thick on the west abutment and tapers to less than 5 metres on the east abutment, as seen in Figure 5.13. Unit 2A is described as a stiff to hard, grey, inorganic silt with trace to some sand and clay. Liquid limits range from 20 to 30 percent and plasticity indices range from 0 to 10. Unit 2A is classified as a ML/CL using the USC system. Varves ranging from 75 to 150 millimetres thick were observed during excavation of the GVWD tunnel on the east abutment. Figure 5.15 presents grain size distribution curves for samples collected from this unit. Hydraulic conductivity estimates for Unit 2A range from 5E-6 to 1E-7 metres per second, based on the grain size curve data.

Unit 2B is interbedded within Unit 2A, as shown on section E-E (Figure 5.13). Unit 2B is described as very dense, sand and gravel, trace silt, cobbles and boulders. It is classified as a GW - SW, using the USC system.

Unit 3 is a glacial till deposit from the Vashon period. This unit overlies Unit 2A, Unit 1B and the granodiorite bedrock on the east abutment. The thickness varies from 2 to 8 metres. Unit 3 is not present in the river channel or on the west abutment. Typically the till consists of dense, silty sand with some gravel, to gravelly sand with trace to some silt (SP-SM, SM using the USCS). Figure 5.16 shows the grain size distribution curves for samples collected from this unit. Hydraulic conductivity estimates for this unit range from 1E-6 to 1E-7 metres per second, based on grain size curve data collected from 16 samples.

Unit 4 is a granular glaciofluvial soil deposited in front of the retreating valley glaciers. Unit 4 is present on the east abutment. The thickness ranges from 5 to 9 metres on the west side and then tapers out towards the east. Grain size distribution curves for Unit 4 are presented on Figure 5.17. Soil descriptions for this unit vary from; a poorly graded fine to medium sand, with some silt (SM), sandy silt (ML), to gravelly fine to coarse sand (SP-SM). The fines content for this unit varies from 5 to 70 percent. This unit varies from loose to medium dense. Hydraulic conductivity estimates range from 1E-4 to 1E-5 metres per second, based on grain size curve data.

Unit 5 is a glaciolacustrine silt, also deposited in front of the retreating valley glaciers. Unit 5 forms a thick blanket over Unit 3 and Unit 4 on the east abutment. Natural thickness of this unit ranges from approximately 6 metres over the bedrock mound to greater than 10 metres downstream. Grain size distribution curves for Unit 5 are presented on Figure 5.18. Unit 5 is described as a poorly graded, silt with trace to some sand and clay. The unit is varved silt and clay. The silt is an inorganic, low plasticity (liquid limit 20 to 30 percent, and plasticity index between 0 and 10) and is classified as ML. The clay is a medium plasticity, with liquid limits between 40 to 50 percent, plasticity indices of 25 to 30, and is classified as CL. Hydraulic conductivity estimates for Unit 5, are also based on the grain size curve data and, range from 1E-6 to 1E-7 metres per second.

Unit 6A and Unit 6B are post glacial, alluvial sediments deposited along the Coquitlam River channel. Unit 6A appears to be a high energy, channel deposit. Unit 6B appears to be a point bar deposit, deposited on the inside of a river bend, in a slightly lower energy environment. Both units range from 3 to 5 metres in thickness and occur along the Coquitlam River channel prior to dam construction, as shown on Figure 5.10. Gradation curves for Unit 6A are presented in Figure 5.19. This unit consists of boulders, cobbles, gravel, and sand, with 5 to 10 percent fines (GP-GM). The coarse material is typically rounded to subrounded. The unit is considered to be dense. Unit 6B is a dense, sand and gravel with some silt (SM). Hydraulic conductivity estimates for Unit 6A range from 5E-3 to 1E-4 metres per second, and for Unit 6B 1E-4 to 1E-5 metres per second. Construction photographs indicate that the alluvium material was reworked during foundation preparations, as a result the distribution of Unit 6A and 6B material may not be uniform or continuous.

Unit 7 consists of granodiorite rock that has spalled off adjacent rock outcrops. It consists of a thin sporadic layer of angular, loose rubble at the base of small cliffs.

5.4.3 Dam Fill Soils

Figure 5.4 presents an as-built cross section of the dam in 1915. Figure 5.6 presents a typical cross section of the dam, in 2001. Table 5.2 presents a summary of dam fill materials and their hydraulic properties.

The upstream and downstream rockfill toes consist of hard durable, angular, granodiorite rock. The maximum rock size is about 0.6 metres. The hydraulic conductivity of the rockfill is estimated to be 1E-1 to 1E-2 metres per second (BC Hydro, 1984).

The design specified the upstream shell should consist of cobbles, gravel, and coarse sand, that was to be placed by hydraulically sluicing. Grain size distribution curves obtained from soil samples of the shell material are presented on Figure 5.20. There is considerable variation in the grain size distribution of samples collected from the shell as is apparent in Figure 5.20. In general, the grain size decreases closer to the core, and the density decreases. Fines content is approximately 5% at some distance from the core and increases to about 15% near the core. The hydraulic conductivity of the upstream shell is estimated to be between 1E-4 and 1E-5 m/s, based on grain size curves (BC Hydro, 1984).

Drilling records show that there is no distinct line between the upstream shell and core material, which is not surprising since these units were built simultaneously.

The downstream shell was constructed in a similar manner to the upstream shell. Soil samples from the downstream shell indicate that this unit is slightly coarser than the upstream shell.

The hydraulic fill core was placed in a similar manner to the upstream and downstream shells, however, finer materials were used for core construction. During construction the degree of fines could be controlled in two manners, at the burrow pit source and to some degree by the depth of the settling pool. As is customary with hydraulic filled dams, it is anticipated that the core materials were in a semi-liquid state, during and immediately after construction, due to the length of time required for these materials to drain. Over time as these materials drained and consolidated the strength of the material would increase (Terzaghi and Peck, 1948). The core of Coquitlam Dam, consists of soft silts and sandy silts, with thin layers of sand and occasionally gravel, randomly present. Figure 5.21 presents the grain size distribution curves for samples

collected from the core. There is also considerable variation in the grain size distribution curves of samples collected from the core. However, in comparison to the upstream shell samples, the core is finer. The hydraulic conductivity values for the core are based on triaxial tests conducted on shelby tube samples collected from the core and grain size curve data. The estimated values are:

- horizontal permeability (k_h) 1E-4 to 1E-6 m/s
- vertical permeability (k_v) 1E-6 to 1E-8 m/s (BC Hydro, 1984).

Modifications were made to the dam in 1980 and 1984/85. In 1980, rockfill berms were placed on the upstream and downstream slope, to add reinforcement to the dam, for earthquakes. A further upgrade to the upstream and downstream berms was made in 1984. A portion of the previously placed rockfill on the upstream face was excavated and placed on the downstream berm. The rockfill from the upstream berm was excavated and replaced by compacted sand and gravel. A one metre thick layer of rockfill was placed over the sand and gravel. Figure 5.6 shows a typical cross section of the dam, and indicates changes made in 1980, and 1984/85.

5.5 COQUITLAM DAM, HYDRAULIC CONDITIONS

Prior to 1979, BC Hydro does not have any record of instrumentation or data from Coquitlam Dam that would monitor the hydraulic conditions within the dam. Between 1979 and June 2001, 14 pneumatic and 33 standpipe piezometers have been installed at the dam. Three of the standpipe piezometers have been damaged or destroyed and are no longer in use.

For an idealized dam with similar material properties as Coquitlam Dam, the following flow conditions would be expected:

- water in the upstream shell would be at a similar elevation as the water in the reservoir, and the water level would respond quickly to changes in the reservoir level;
- the water elevation in the core would decrease, as distance from the reservoir increased. The response time to changes in the reservoir elevation would increase, and the magnitude of the fluctuation in the water level would be less. The water elevation on the downstream side of the core would equal that of the tailwater;
- piezometers installed in the downstream toe would be minimally influenced by changes in the reservoir level. The water elevation in these piezometers would be influenced by changes in the tailwater level and by precipitation and infiltration.

Figure 5.22 through 5.24 present plots of the piezometric elevation data and the measured reservoir elevation, through Section A-A, B-B, and C-C, respectively. Similarly, Figure 5.25 and Figure 5.25 present plots of the piezometric and reservoir elevation data for the west and east abutments, respectively. As seen in Figure 5.22 through 5.24, piezometric levels recorded along each section are similar, and do not deviate significantly from the general pattern, described above. However, the seepage regime at Coquitlam Dam is fairly complex due to the presence of the higher permeable sand and gravel deposits (Units 1A and 1B) that underlay the thin, low permeability silt layer (Unit 2). The regional aquifer flows in Unit 1A and 1B, may influence the seepage regime of the dam (information provided by BC Hydro).

Based on BC Hydro's geologic interpretation, and the soils encountered during the various drilling investigations, the silt layer beneath the former Coquitlam River channel is very thin, and in some places may have been eroded entirely, exposing the underlaying sand and gravel units.

The former river channel extends under a portion of the dam, as indicated on Figure 5.5. It is believed that a portion of the silt layer does not exist beneath the dam. However, the exact size and location of the sand and gravel layer exposure is not currently known. Depending on the size and location of this permeable window, the interaction between the seepage flows through the dam and the regional aquifer could be strong (information provided by BC Hydro).

5.5.1 Reservoir

Figure 5.22 through Figure 5.26 compare the reservoir elevation to the piezometric elevation of the various piezometer located in and near Coquitlam Dam. The water level in the reservoir fluctuates normally between elevation 137.5 and 154.9 metres. This is a change of 16 metres, which is greater than 50% of the dam height. During the study period for this thesis (August 1999 to July 2001) the variation in the reservoir elevation has been less. It varied between an elevation of 142.3 metres and 151.7 metres, which represents a change of approximately 30% of the dam's total height. Since 1998, typical reservoir operation has resulted in two elevation peaks each year. Although the timing of reservoir peak elevations vary by up to two months, the first peak typically occurs between June and August, and the second peak between October and December.

5.5.2 Piezometer Performance

As part of BC Hydro's 2001 Coquitlam Dam Deficiency Investigation, the performance of each piezometer was evaluated. Table 5.3 lists the piezometers, selected construction details, and provides comments on the accuracy and reliability of the data obtained from each piezometer.

SP-6 and SP-7 were installed near the spillway, on the left abutment. Approximately 80% of their readings are above the reservoir elevation. It is believed that these piezometers are measuring water other than that directly associated with seepage from the reservoir.

The following pneumatic piezometers were installed with their tips near the phreatic surface; PP-2, PP-6, PP-7, PP-12, and PP-14. Questionable readings occasionally occur in these piezometers due to the fluctuation in the phreatic surface, as noted in Table 5.3. Frequently PP-5 records low readings that cannot be explained. It is likely that PP-5 malfunctions intermittently. Piezometric elevation plots for these piezometers are included in Figure 5.23 and Figure 5.24.

Following installation of each new piezometer in 1999, and 2001, falling head tests were conducted. SP99-2 showed no response after 10 litres of water were added. Since that time, the water level in SP99-2 has been artificially elevated, and piezometric elevations recorded at this location do not respond to changes in the reservoir level.

5.5.3 Piezometer Measurements Through Section B-B of Coquitlam Dam

Section B-B, shown on Figure 5.5, contains the most piezometric data. The following piezometers are installed along this plane: SP99-12, SP-2, PP-8, PP-9, PP-10, SP99-2, SP-1, PP-5, PP-6, PP-7, SP99-7A, SP99-7B, PP-13, PP-14, SP-4, PP-11, PP-12, and SP99-10. Time history plots of piezometric elevations for these piezometers and the reservoir are presented on Figure 5.24 (standpipe and pneumatic piezometers). The following paragraphs briefly comment on the trends observed in this data, and the implications to the overall seepage regime of the dam.

SP99-12 is installed in the upstream shell, with a tip elevation of 135.4 metres. The piezometric elevation recorded at this location responds rapidly to changes in the reservoir water level with virtually no time lag and the amplitude of the signal is large and similar to that of the reservoir.

Piezometers SP-2, PP-8, PP-9, and PP-10 were installed in the upstream portion of the core at different elevations within the same drill hole (DH84-4). Their tip elevations are 127.4, 132.0, 145.0, and 149.5 metres, respectively. These piezometers respond to the changes in the reservoir water level with minimal time lag. The amplitude of the responses is relatively large, and similar to that of the reservoir. The tip elevation of PP-10 is high, and reads a constant value when the reservoir elevation is below 149.5 metres. The piezometric elevations show a downward hydraulic gradient, likely caused by seepage into the foundation.

Piezometers SP-1, PP-5, PP-6, and PP-7 were installed in the central portion of the core at different elevations within the same drill hole (DH84-3). Their tip elevations are 126.0, 131.5, 140.0, and 144.0 metres, respectively. SP99-2 is also installed in this area, however, it is not responding to reservoir fluctuations. Piezometric elevation data recorded at PP-6 and PP-7 correlate well with the reservoir level. As discussed previously, PP-5 appears to malfunction periodically. Some of the piezometric elevations recorded at PP-5 can be correlated to the reservoir level. Time for these piezometers to respond to change in the reservoir level is longer than that in the upstream portion of the core, and the magnitude of the water level fluctuations in these locations is less. A downward component of the hydraulic gradient is also evident in this portion of the core. The downward gradient is approximately 0.47 (m/m) in both the core and foundation unit, using the July 14, 1998 data.

Piezometers PP-13 and PP-14 were installed in the downstream portion of the core in the same drill hole (DH85-1). The tip elevations are 134.2, and 140.2 metres, respectively. Piezometers SP-4, PP-11, and PP-12 were installed in the same drill hole (DH84-7) in the downstream portion of the core. Tip elevations for these piezometers are 133.8, 137.9, and 142.3 metres, respectively. A nested pair of piezometers was also installed in 1999 in the downstream core, SP99-7A and SP99-7B. Their tip elevations are 124.7, and 133.7 metres, respectively. Responses of these piezometers to changes in the reservoir level are smaller in amplitude, lag significantly, and in some cases cannot be distinctly correlated. It is likely that the tailwater level, percolating water, and groundwater also influence the piezometric levels in the downstream core.

SP99-10 is installed at the toe of the dam, near the fish pond. The piezometric levels at this location cannot be correlated with the reservoir level. The tailwater, percolating water, and groundwater primarily influence the piezometric level of SP99-10.

5.5.4 Weirs at Coquitlam Dam

Two weirs exist on the downstream side of Coquitlam Dam. The locations are shown on Figure 5.27. Manual readings of the weirs were taken between 1991 and 1998, when a data logger was installed to take hourly readings. In 2000 an Automatic Data Acquisition System (ADAS) was installed to collect readings on a continuous basis. In addition, an automatic rain gauge was installed as part of the ADAS system. Hourly rainfall is measured and is recorded by the ADAS to enable weir flow volumes to be correlated to rainfall. Since 1991 periodically high flows, for short durations have been recorded in the weirs. As shown in Figure 5.28, peak flows recorded in the weirs correspond to precipitation and subsequent runoff events. The peak flows are not a result of increased seepage through the dam.

5.6 COQUITLAM DAM, TEMPERATURE MONITORING PROGRAM

The temperature monitoring program at Coquitlam Dam was implemented in August 1999. Monthly temperature measurements have been recorded in the reservoir and water column of each piezometer to develop a database of seasonal temperature fluctuations in the reservoir and within the dam. The data is being collected and analysed as an additional dam performance monitoring tool, to detect and evaluate potential variations in hydraulic conductivity. The first two years of temperature monitoring data is included in this thesis. However, data collected between February and May, 2000 have not been reported as there was a technical problem with the probe on these dates, and as a result the temperature readings are not accurate. Monthly temperature measurements continue to be taken at Coquitlam Dam. Temperature monitoring locations are presented on Figure 5.27.

5.6.1 Instrumentation

Two different thermal probes designed by Bo Chandra & Associates, have been used to collect temperature data from Coquitlam Dam. A pilot thermal probe was initially used, between August 1999 and August 2000. Beginning in September 2000 BC Hydro purchased a thermal probe from Bo Chandra & Associates, for exclusive use at Coquitlam Dam.

The pilot probe temperature monitoring system consisted of a probe and cable, 1000 foot, (300 metre) thin line kevlar reinforced cable, mounted on a portable reel, a small battery, and a lap-top computer. The laptop computer provided the digital readout for the probe and enabled the data to be logged and saved electronically. The thermal probe was mounted in a stainless steel housing unit, approximately 1.25 centimetres in diameter and 20 centimetres in length. A 500 Ω platinum resistance element was used in the probe tip to measure the temperature. Downhole digitizing of the resistance measurement was used to avoid problems with noise transmission of an analog signal over the long cable length. The probe is accurate to 0.02°C and its resolution is 0.001°C. Figure 5.29 shows the probe and monitoring system.

BC Hydro's temperature monitoring system consists of a probe and cable (250 metre flat, 1.3 centimetre wide, polyethylene with counter twisted stainless steel stranded wire). The cable and probe are mounted on a portable reel, which includes a digital display of the temperature reading, and an interface cable for connection to a computer, to allow data to be logged and saved electronically. A 9-volt battery provides power for the probe and readout. Figure 5.30 shows the new probe and reel with the digital display. The probe is accurate to 0.02°C and its resolution is 0.001°C.

5.6.2 Monitoring Locations

Temperature profiling was initially conducted in eight piezometers (standpipes): SP-1, SP-2, SP-4, SP-6, SP-8, SP-9, SP97-1A, SP97-1B, one inclinometer, and in the reservoir.

During the fall of 1999, as part of a dam investigation project, 16 additional piezometers were installed within the dam. Temperature readings have been collected within these piezometers since the end of November 1999. Figure 5.27 shows the location of the piezometers, inclinometer, and the reservoir monitoring station. Early in 2001, six additional piezometers were installed in the downstream shell and on the east abutment of the dam. Temperature readings have been collected within these piezometers since March/April 2001. Table 5.4 presents a list of

the temperature monitoring piezometers and installation details including; depths, screen intervals, diameters, and construction materials.

Temperature profiling of the reservoir was conducted from the floating dock, east of the GVWD boathouses. Additional temperature data from the reservoir was collected on July 13, 2000. The approximate location of each of the profiling sites is shown on Figure 5.27.

5.6.3 Procedures

In each piezometer, the depth of water was first established using a thin line water level indicator. Care was taken not to lower the water level probe below the top of the water surface, so that there would be minimal disturbance to the water column. Then the temperature probe was slowly lowered down the piezometer casing, to minimize mixing of the water within the riser while temperature measurements were recorded. Initially, temperature measurements were recorded at 0.9 metre (3 foot) intervals from the groundwater surface to the bottom of each piezometer. Then a procedural change was implemented (May 2000) so that temperature readings would be taken at the same elevation during each monitoring period. Temperature data in each piezometer is now collected at constant elevations in each piezometer below the groundwater surface. The readings are taken at one metre intervals. At each monitoring interval the temperature reading was allowed to stabilize to two decimal places and then was recorded.

5.7 COQUITLAM DAM, TEMPERATURE MONITORING PROGRAM

The temperature monitoring results for Coquitlam Dam, collected between August 1999 and July 2001, will be presented and discussed in the following subsections. The results have been divided into five areas:

- reservoir,
- upstream shell,
- core and foundation soils,
- downstream toe, and
- abutments.

Table 5.5 lists the temperature monitoring stations and groups them according to the material through which they were installed.

Temperature data collected between February 2000 and May 2000 has not been included in this thesis as there was a malfunction with the probe, or a calibration problem during this period. The first round of temperature data collected in August 1999, appears abnormally higher than all other readings. This data has been included in the graphical plots as the temperature profiles within each piezometer are similar; however, the actual temperatures have not been included in the general discussion. Appendix C contains plots for each piezometer showing the temperature profiles, and the annual temperature variation at selected elevations.

The graphical plots of the temperature data collected from the six new piezometers installed in 2001 have been included in Appendix C. However, minimal discussion is provided for these piezometers, due to the limited amount of temperature data that exists for these locations.

5.7.1 Reservoir

Figure 5.31 graphically presents the reservoir profiling data collected from the floating dock. Figure 5.32 presents the annual temperature data at selected elevations in the reservoir. The temperature in the reservoir varied from 20°C at the surface in July or August a low of 4°C throughout the reservoir in January or February. Two distinct patterns can be seen in Figure 5.31. Typically, between November and March the temperature in the reservoir is almost constant irrespective of depth. During the remainder of the year the temperature varies significantly with depth.

The water at the base (Elevation 134 metres) of the reservoir varied between a high of 14°C in October to a low of 4°C in January/February. However, the water at the base of the reservoir is only warm for a very short period of time. The typical range in water temperature at the base is between 4°C and 8°C.

Temperature measurements collected within the reservoir show a significant variation between 1999 and 2001. Changes in reservoir elevation and to some extent climatic conditions (air temperature) are likely the cause.

Temperature profiling at four additional locations within the reservoir was conducted on July 13, 2000 to determine if there was any significant difference in reservoir temperatures along the face of the dam in comparison to the temperatures measured from the floating dock. Each location was approximately 25 to 30 metres upstream of the dam face. Temperature data was collected with two instruments, the pilot thermal probe, and a multi probe produced by Yellow Springs Instruments, YSI 600XL. The YSI probe only had a 20 metre cable. As a result temperature readings made with this probe did not reach the bottom of the reservoir. The accuracy of this probe is reported to be ±0.5°C. Figure 5.33 presents the additional reservoir monitoring data. Good correlation exists between the temperatures recorded by each probe at each location. Slight differences are attributed to the different accuracy of each probe, and drifting of the boat while measurements were being recorded. All of the additional monitoring locations were shallower than the floating dock monitoring location. As a result, cooler temperatures are recorded at the dock location due to the deeper water conditions. There is good correlation between the temperatures recorded at the floating dock and those closer to the dam face, at similar elevations. Based on this data, the floating dock location appears to be an acceptable location for profiling reservoir temperatures.

5.7.2 Upstream Shell

Three piezometers are installed in the upstream shell; SP99-11, SP99-12, and SP99-13. Individual plots of temperature profiling data with depth, along with plots of annual temperature variation at selected elevations for each piezometer, are included in Appendix C. Figure 5.34 presents a sample temperature profile graph from upstream shell piezometers. Figure 5.35 presents a plot of the annual temperature variation at selected elevations for the upstream shell piezometers. The temperature data recorded in all three of these piezometers is very uniform. It is interesting to note that the temperatures recorded in SP99-11 are slightly cooler than those obtained from SP99-12 and SP99-13 at the same elevation. Temperatures recorded in SP99-12 and SP99-13 are more similar, although generally SP99-12 is slightly cooler than SP99-13, at the same elevation.

Surface temperature effects, caused by the surrounding air temperature and conduction, can be seen in all piezometers above an elevation of 142 metres. When initial surface temperature effects are ignored, all the piezometers show a decrease in temperature with depth. The average temperature, when surface effects are eliminated, ranges between 9.7°C and 10.7°C. At any given elevation in these piezometers, the average annual change in recorded temperature is between 0.2°C and 0.3°C. The average annual temperature change within each piezometer, irrespective of depth is between 0.5°C and 0.7°C.

Piezometric levels in the upstream shell material respond quickly to changes in reservoir level. So one would anticipate that the temperature profiles in these piezometers would show similar oscillations as observed in the reservoir. However, no distinct minimum or maximum temperature is apparent in these piezometers, as is the case in the reservoir. In addition, the range of temperatures recorded in the upstream shell throughout the year is significantly less than that recorded in the reservoir (both bottom and surface).

5.7.3 Hydraulic Fill Core and Foundation Units

Piezometers installed in the hydraulic core material or foundation materials are identified in Table 5.5. For this discussion the piezometers have been divided into two categories, those that are located in the upstream portion of the dam, and those located in the downstream portion of the dam, as indicated on Table 5.5. In general, the temperature profiling data collected from these piezometers show slight surface temperature effects in the top one to two metres.

Figure 5.36 presents a sample temperature profile graph, representative of temperature data collected from piezometers in the upstream portion of the core. Although many of the piezometers in the upstream portion of the dam penetrate both the core and the foundation units, only slight changes (i.e. SP99-1 and SP-2) in either the slope of the temperature profile data, or in the actual readings are apparent at the interface between the two units. All piezometers in the upstream portion of the core show a decrease in temperature with depth, similar to that observed in the upstream shell piezometers, with the exception of SP99-3B. This piezometer shows an increase in temperature with depth.

Following installation of each new piezometer in 1999, and 2001, falling head tests were conducted. SP99-2 showed no response after 10 litres of water was added. As a result, the water level in SP99-2 is artificially elevated. Temperature readings in this piezometer have been collected in both the unsaturated and saturated zones. Air temperature effects are more predominant in this piezometer, than in the other piezometers. The temperature profile plot for SP99-2 is presented in Figure 5.37.

Figure 5.38 presents a graph of the annual temperature variation, at selected elevations, for the piezometers in the upstream portion of the core. The annual temperature data recorded in all of these piezometers shows a very uniform pattern. It is interesting to note that the temperatures recorded in SP-2 are warmer, and the temperatures recorded in the Inclinometer are cooler than those obtained from the remaining piezometers, at the same elevation. This could be due to SP-2 being located closer to the reservoir and the Inclinometer being farther from the reservoir. SP99-3A/3B, SP99-2, SP-1, and SP99-1A/1B are located at approximately the same distance from the reservoir, although spatially located along the linear axes of the dam. Temperature readings from SP99-2 are warmer than the other piezometers in this alignment. Temperature readings obtained from elevation 140 and 130 metres in piezometers SP99-3A/3B, SP-1, and SP99-1A/1B are approximately the same, throughout the year.

The average temperature, when surface effects are eliminated for the upstream core piezometers, ranges between 9.2°C and 10.9°C. At any given elevation in these piezometers, the average annual change in recorded temperature is between 0.14°C and 0.3°C. The average annual temperature change within each piezometer, irrespective of depth, is between 0.3°C and 1.15°C.

Piezometric levels in the upstream core and foundation silt material are slower to respond to changes in the reservoir elevation. However, they show a greater response than piezometers located in the downstream core and foundation silt. Although there are small fluctuations in recorded temperature in these piezometers, no distinct minimum or maximum temperature is apparent in these piezometers, as is the case in the reservoir. In addition, the range of temperatures recorded in the upstream core and foundation material throughout the year is significantly less than that recorded in the reservoir (both bottom and surface). The average temperature in these piezometers is slightly less than that recorded in the upstream shell.

The downstream core and foundation unit piezometers, identified in Table 5.5 are all located on the downstream berm of Coquitlam Dam. The piezometric surface in these piezometers is at an elevation between 131 and 140 meters, depending on location and piezometer screen interval. This elevation is approximately 5 metres lower than that measured in the upstream core piezometers. The water column length in these piezometers is smaller than in the upstream piezometers. As a result, there are fewer temperature readings at each monitoring station.

Figure 5.39 presents a graph of the annual temperature variation, at selected elevations, for piezometers in the downstream portion of the core and foundation. The annual temperature data recorded in all of these piezometers shows a very uniform pattern. The recorded temperature in SP99-5 is consistently warmer than that recorded in the other piezometers.

Figure 5.40 presents a sample temperature profile graph, representative of temperature data collected from piezometers in the downstream portion of the core. Temperature profile data collected from SP-4, SP99-7B, and SP99-8 is approximately constant with depth, once the air temperature effects are ignored. The temperature profile plots from SP99-7A and SP99-5 show a small decrease in temperature with depth. The temperature profile plot from SP99-9 shows a slight increase in temperature with depth, and is slightly cooler than temperatures in the other piezometers. SP99-9 is screened at a lower elevation in the stiff silt, and lower sand and gravel unit.

Although many of the piezometers penetrate both the core and the foundation units, only slight changes can be seen in SP99-7B at the interface between the two units. Due to the short water column length in SP99-7B, it is difficult to determine if these changes are due to changes in the hydraulic conductivity of the materials, or due to air temperature effects.

The average temperature, when surface effects are eliminated for the downstream core piezometers ranges between 9.0°C and 9.5°C. At any given elevation in these piezometers, the average annual change in recorded temperature is between 0.12°C and 0.3°C. The average annual change in temperature within each piezometer, irrespective of depth, is between 0.17°C and 0.37°C. No annual minimum or maximum temperature is apparent in these piezometers. The average recorded temperature in these piezometers is slightly cooler than those from the upstream portion of the core and foundation.

5.7.4 Downstream Toe

One piezometer, SP99-10 is installed at the downstream toe of the dam, near the fish pond. The temperature profile plot for this piezometer is significantly different than the other piezometers within the dam, as shown on Figure 5.41. The water piezometric surface in this piezometer is located only one to two metres below the ground surface. As a result, air temperature effects are more predominant in this piezometer and extend further into the water column, to an elevation of 121 metres. Heat conduction creates a symmetric profile around the mean temperature. The profile of SP99-10 is approximately symmetric about 8.5°C. The annual temperature variation below 121 metres is between 8.45°C and 8.56°C.

Figure 5.42 presents a graph of the annual temperature variation, at selected elevations, for the downstream toe piezometer, SP99-10 and abutment piezometer. The annual temperature data recorded in all of these piezometers shows a very uniform pattern, and all temperatures are approximately constant throughout the year. The recorded temperature in SP99-10 is consistently warmer than that recorded in the abutment piezometers, but the average temperature appears closer to the abutment piezometers, than the downstream core piezometers. This indicates that water in SP99-10 is more closely connected with the regional groundwater flow, rather than with seepage from the reservoir.

5.7.5 Abutment Piezometers

A nested pair of piezometers exists on the west abutment of the dam, SP97-1A and SP97-1B. Four piezometers on the east abutment existed, until 2001 when four additional piezometers were installed. In addition, two piezometers on the eastern side of the downstream berm (SP99-4 and SP01-3) temperatures are more reflective of the temperatures recorded in the abutment piezometers, than the downstream core piezometers, so they have been included with this group of piezometers. Although SP-6 is installed in the spillway on the east abutment, this piezometer is very shallow and has a very short water column typically, one metre or less. As a result, there are a limited number of temperature readings to establish a temperature profile, which makes discerning the actual temperature in the soil unit versus air temperature effects impossible. Therefore, temperature readings from SP-6 have not been included in the discussion of the abutment piezometers.

Figure 5.43 presents a sample temperature profile graph from abutment piezometers. Temperature profile data collected from SP97-1A and SP97-1B shows a slight decrease in temperature with depth. Temperature profile data from SP97-1A (Figure 5.43) actually shows a change in slope and also abrupt changes in the temperature at the interface between the different stratigraphic units. This pattern is indicative at the interface between units with different hydraulic conductivity.

Figure 5.42 presents the annual temperature variation graph at selected elevations for the abutment piezometers, and SP99-10. The annual temperature pattern recorded in these piezometers is very uniform. The temperatures recorded in SP99-10 and SP99-4 are warmer than those obtained from the abutment piezometers, yet they are cooler than the downstream core piezometers. In addition, SP99-4 is screened at a shallower elevation than the other piezometers. This indicates that the water in these piezometers is connected with the regional groundwater as well as seepage water from the dam. The temperatures recorded in SP99-7A/7B, and SP-8 are virtually identical. The recorded temperature in SP-9 is slightly warmer, but this could in part be due to the shallower screen interval in this piezometer.

The average temperature, when surface effects are eliminated for the abutment piezometers, ranges between 7.9°C and 8.9°C. At any given elevation in these piezometers, the average annual change in recorded temperature is between 0.15°C and 0.27°C. The average annual change in temperature within each piezometer, irrespective of depth, is between 0.15°C and 0.4°C. No annual minimum or maximum temperature is apparent in these piezometers. The average recorded temperature in these piezometers is slightly cooler than those from the other piezometers installed within the dam.

5.7.6 Overall Comparison of Temperature Monitoring Results

In general, the temperature within Coquitlam reservoir shows significant seasonal fluctuation (4°C to 20°C) and thermal stratification within the reservoir occurs between May and mid November.

Figure 5.44 presents two (upper and lower elevation) plots of annual temperature variation, at selected elevations, through section B-B (reservoir, SP99-12, SP-2, SP-1, SP99-7A/SP-4, and SP99-10). From these plots it is evident that as distance from the reservoir increases, temperature decreases. The average measured temperature was 10.2°C, 10°C, 9.25°C, and 8.5°C in the upstream shell, upstream core/foundation, downstream core/foundation, and at the base of the dam, respectively. The average temperature in the abutments was 8.2°C. Table 5.6 presents a summary of the annual temperature variation data, according to piezometric location. The average decrease in temperature along the seepage path is a symbol of heat loss occurring along the flow path. There are two potential processes that could explain the heat loss seen at Coquitlam Dam:

- the mean temperature of the seepage water is higher than the annual mean air temperature, and the seepage rate is small; and/or
- seepage in the foundation is occurring with inflow of the colder regional groundwater in the downstream part of the dam.

It is likely that the seepage temperature pattern observed in Coquitlam Dam is a result of a combined influence of the two processes listed above. The mean annual air temperature between April 1999 and April 2001 was 9.5°C, which is just slightly cooler than the mean seepage water temperature measured in the upstream shell piezometers of 10.2°C. Likely there is some heat loss to the atmosphere. In addition, the cooler temperatures recorded in SP99-10, and SP99-4 are likely due to seepage water mixing with the cooler regional groundwater, which supports the second process.

It is also apparent from Figure 5.44 that significant annual temperature fluctuations occur in the reservoir in contrast to the almost constant temperatures recorded within each piezometer, at a constant elevation.

The seepage water temperatures measured in Coquitlam Dam are caused by normal seepage through the dam. Although small differences in seepage velocity can be seen (i.e. SP-1, S-2, SP99-1A, and SP97-1A) no significant or concentrated seepage zones have been detected.

At this time, no clear seasonal variation in temperature is apparent. As a result, it has not been possible to verify seepage velocity differences using a lag time analysis.

5.8 IMPLICATIONS TO MODELLING OF COQUITLAM DAM

As discussed in Chapter 2 and Chapter 3, the heat transport modelling used in this thesis uses a two step process. First the seepage analysis is performed using SEEP/W, then CTRAN/W uses the seepage velocities obtained from the SEEP/W analysis to analyse the heat transport analysis. The field investigation data and temperature monitoring program have revealed several factors about Coquitlam Dam that are important to the numerical modelling.

The following factors are important to remember about Coquitlam Dam when performing a seepage analysis:

- the geology and hence the seepage pattern within the Coquitlam Dam is complex due to the buried valley, varied stratigraphy and hence hydraulic conductivity of the core, the presence of higher permeability sand and gravel beneath the stiff foundation silt, the partially eroded stiff silt layer in a portion of the former Coquitlam River channel, and the potential for preferential seepage paths exist due to the decay of the timber trestles used to support the flumes left in place, during hydraulic fill construction;
- variation in stratigraphy through the different dam sections;
- there is significant annual fluctuation in reservoir elevation (20 to 50% of dam height), which causes changes in head and therefore gradient and the resulting seepage velocity through the dam (i.e. transient seepage analysis is required);
- since 1998, typical reservoir operation has resulted in two elevation peaks each year. However, the actual peak reservoir elevation, time of year when the peaks occur, and duration of each peak varies from year to year due to changes in the reservoir operation; and
- complicated boundary conditions, due to seepage flow interaction with the regional groundwater flow near the dam abutments and at the base of the dam, the potential for seepage flow out of the base of the dam into the lower sand and gravel units, and the inability to monitor and hence determine the actual seepage volume/rate through the dam. Weirs only catch a very small portion of the seepage.

A transient seepage analysis is definitely required to account for the reservoir variability, and it is important that actual measured reservoir elevation data be used for the study period of interest, rather than average values. A two dimensional seepage analysis is definitely required to account for the variability. It may be necessary to use a three dimensional seepage model to adequately account for the complex conditions at Coquitlam Dam.

The following factors are important to remember about Coquitlam Dam when performing the heat transport analysis:

- to date, limited temperature data exists to use as input and to compare results;
- temperature stratification is significant in the reservoir, and varies throughout the year. Therefore it is important that different temperature values (curves) be assigned to various elevations along the dam face;
- combined effect (interaction) of reservoir level on temperature stratification within reservoir and temperature change from year to year;
- annual air temperature variations from one year to the next effect heat conduction and reservoir temperature;
- during the late fall and early winter reservoir peak (mid October to mid January) there is increased seepage flow caused by the increased gradient. The temperature of this water varies from year to year due to the timing of the reservoir peak, peak duration, and ambient

weather conditions. Based on reservoir temperature data collected between August 1999 and July 2001, the seepage water temperature could be between 4 and 7°C;

- water level fluctuations will significantly affect the temperature in the upper part of the standpipes in the upstream shell and core piezometers;
- coarse shell allows a quick response to water level fluctuations, allowing for both inflow and outflow of water. Therefore temperature in the upstream core will be influenced by the change in flow direction of the water. The upper part of this water column may be more disturbed than the lower portion;
- the seepage water and groundwater have different temperatures. Water from these two sources mix in the dam abutments, foundation units and dam toe areas creating a complex temperature pattern;
- heat losses as water seeps through the dam, evident from the decreasing average temperature along the seepage path; and
- complicated boundary conditions due to annual changes.

5.9 SUMMARY OF FIELD PROGRAM

This chapter has portrayed the complex nature of the geology and structure of Coquitlam Dam, and the implications on the hydrogeology and seepage pattern at the dam. A detailed description of the temperature monitoring program was provided along with a qualitative analysis of the temperature monitoring data collected between August 1999 and July 2001. Although small differences in seepage velocity can be seen in the temperature profile data, no significant or concentrated seepage zones have been detected. Based on the temperature monitoring experiences at Coquitlam Dam, and from reported results from other temperature monitoring programs, collection and analysis of temperature data from within dam structures provides supplemental data on which to evaluate dam performance and to monitor seepage within a dam. Temperature monitoring should continue at Coquitlam Dam in order to enhance the data base established to date, and to verify annual changes observed in the reservoir and piezometers temperatures. Only small variations in the temperature data within the piezometers atCoquitlam Dam have been detected to date. Due to the small temperature variations it is imperative that the probe is accurately calibrated and frequently checked. To maximize the potential benefits from the temperature monitoring program for evaluating dam performance and monitoring the seepage regime, the data must be reviewed on a regular basis.

Table 5.1: Coquitlam Dam Foundation Soils (provided by BC Hydro)

Unit No.	Soil Description	Depositional Environment
7	Rubble	Colluvial (rockfall)
6B	Sand	Alluvial
6A	Sandy Gravel, Gravel and Sand, Cobbles and Boulders	Alluvial
5	Silt, Clay	Glaciolacustrine
4	Sand, Silt and Sand, Gravelly Sand	Glaciofluvial
3	Sand and Gravelly Sand	Subglacial
2B	Sand and Gravel, Sand	Glaciofluvial
2A	Silt, Clay	Glaciolacustrine
1B	Sandy Gravel, Gravel and Sand, Cobbles and Boulders	Glaciofluvial
1A	Sand	Glaciofluvial

Table 5.2: Summary of Dam Fill Materials and Hydraulic Properties (provided by BC Hydro)

Fill Material	Soil Description	Est. k (m/s)
Rockfill Toe	Rockfill	1E-2 to 1E-1
Shell	Sand and Sand and Gravel; coarser away from core	1E-3 to 1E-5
Core	Silt, Sandy Silt with interlayered sand	1E-5 to 1E-7
Rockfill berm	Rockfill	1E-2 to 1E-1
Compacted Sand and Gravel	Sand and Gravel	1E-3 to 1E-2

Table 5.3: Coquitlam Dam Piezometers, Construction Details and Performance Summary (provided by BC Hydro)

Piezometer	Drill Hole	Installation Date	Tip Elevation (m)	Soil Material at Tip	Location	Comments	Performance
PP1	DH79-3	1979	125.90	2A and 1B	Centre		S
PP2	DH79-3	1979	141.10	Core	Centre	Almost 1/3 of all readings above reservoir water level.	*
PP3	DH79-1B	1979	130.20	Core	Centre	Scattered. 5 readings appears too low.	S
PP4	DH79-2	1979	129.50	Core and 6A	US	Readings generally correlate with reservoir water level. About 10 readings appears unreasonable.	S
PP5	DH84-3	1984	131.50	Core	US	1/3 to 1/2 of all readings are at tip elevaiton.	?
PP6	DH84-3	1984	140.40	Core	US	1/6 to 1/5 of all readings are above reservoir water level.	*
PP7	DH84-3	1984	144.00	Core	US	1/3 to 1/2 of all readings are above reservoir water level.	*
PP8	DH84-4	1984	132.00	Core	US	Good correlation with reservoir.	S
PP9	DH84-4	1984	145.00	Core	US	Similar to PP8. Reservoir water level drops below tip elevation.	S
PP10	DH84-4	1984	149.50	Core	US	Similar to PP9. Reservoir water level drops below tip elevation.	S
PP11	DH84-7	1984	137.90	Core	DS	Readings do not correlate with reservoir water level.	S
PP12	DH84-7	1984	142.30	Core and Shell	DS	1/4 to 1/3 of all readings above reservoir water level.	*
PP13	DH85-1	1985	134.20	Core	DS	Similar to PP11.	S
PP14	DH85-1	1985	140.20	Core	DS	Similar to PP12.	*
SP1	DH84-3	1984	126.20	6B and 1B	US	Good correlation with reservoir water level.	S
SP2	DH84-4	1984	127.40	6B and 1B	US	Similar to or better performance then SP1.	S
SP3	DH84-6	1984	123.50	---		Destroyed.	X
SP4	DH84-7	1984	133.80	Core	DS	Scattered response.	S
SP5	DH85-2	1985	143.00	---		Destroyed.	X
SP6	DH85-3	1985	145.20	5 and 3	E - Abutment	Readings generally respond to reservoir water level. 80 to 90 % of all readings are above reservoir water level.	?
SP7	DH85-4	1985	138.40	---	US	Destroyed.	X
SP8	PDH83-1	1983	128.60	2A	E - Abutment	Weak but finite response to reservoir water level.	S
SP9	PDH83-2	1983	133.70	3 and 2A	E - Abutment	Scattered, poor correlation with reservoir water level.	?

Notes:

US - Upstream of dam centre line.
DS - Downstream of dam centre line.
Centre - Located near dam centre line.
S - Satisfactory performance.
* - Some readings are above the reservoir water level.
? - Performance is questionable.
X - Destroyed

Table 5.3: Coquitlam Dam Piezometers, Construction Details and Performance Summary (provided by BC Hydro)

Piezometer	Drill Hole	Installation Date	Tip Elevation (m)	Soil Material at Tip	Location	Comments	Performance
SP97-1A	DH97-1	1997	115.03	1B and 2A	W - Abutment	Short response history. Appears reasonable. Behaviour similar to that of PP1.	S
SP97-1B	DH97-1	1997	127.43	1B	W - Abutment	Measured heads between 1A and 1B are less than 1 m apart.	S
SP99-1A	DH99-1	1999	123.35	6A	US	Good correlation with reservoir water level.	S
SP99-1B	DH99-1	1999	134.55	Core	US	Good correlation with reservoir water level.	S
SP99-2	DH99-2	1999	132.12	6B	US	No correlation with reservoir water level.	?
SP99-3A	DH99-3	1999	119.48	1B	US	Generally good correlation with reservoir water level.	S
SP99-3B	DH99-3	1999	140.74	Core	US	Generally good correlation with reservoir water level.	S
SP99-4	DH99-4	1999	137.91	4 and 3	E - Abutment	Poor correlation with reservoir water level.	S
SP99-5	DH99-5	1999	129.77	Core and 6A	DS	Slight correlation with reservoir water level.	S
SP99-6	DH99-6	1999	133.11	Core and 6A	DS	Slight correlation with reservoir water level.	S
SP99-7A	DH99-7	1999	124.73	1B and 2A	DS	Generally good correlation with reservoir water level.	S
SP99-7B	DH99-7	1999	133.65	Core	DS	Generally good correlation with reservoir water level.	S
SP99-8	DH99-8	1999	136.61	Core and 2A	DS	Generally good correlation with reservoir water level.	S
SP99-9	DH99-9	1999	124.58	1B and 2A	DS	Generally good correlation with reservoir water level.	S
SP99-10	DH99-10	1999	119.54	1B	Toe	Generally good correlation with reservoir water level.	S
SP99-11	BPT99-1	1999	136.60	Core	US	Good correlation with reservoir water level.	S
SP99-12	BPT99-2	1999	135.42	Core	US	Good correlation with reservoir water level.	S
SP99-13	BPT99-3	1999	136.91	Core and 4	US	Good correlation with reservoir water level.	S
SP01-1A	DH01-1A	2001	149.91	3	E - Abutment		S
SP01-1B	DH01-1B	2001	154.87	5	E - Abutment		S
SP01-2A	DH01-2A	2001	137.30	5 and 4	E - Abutment		S
SP01-2B	DH01-2B	2001	143.99	3 and 2A	E - Abutment		S
SP01-3	DH01-3	2001	147.97	Core and 5	E - Abutment		S
SP01-10	BOC01-10	2001	133.59	Core	DS		S

Notes:

US - Upstream of dam centre line.
DS - Downstream of dam centre line.
Centre - Located near dam centre line.
S - Satisfactory performance.
* - Some readings are above the reservoir water level.
? - Performance is questionable.
X - Destroyed

Table 5.4: Temperature Monitoring Piezometers and Installation Details (information provided by BC Hydro)

Monitoring Point	Northing	Easting	Ground Surface Elevation (m)	Top of Riser Elevation (m)	Screen Elevation (m)	Screen Length (m)	Diameter (cm)	Construction Material
SP-1	10004.91	9868.06	--	160.00	126.20 - 129.20	3.0	2.54	PVC
SP-2	10027.80	9870.14	156	156.70	127.40 - 130.40	3.0	2.54	PVC
SP-4	9974.34	9864.20	151.2	154.70	133.80 - 136.80	3.0	2.54	PVC
SP-6	10026.42	9981.57	154.2	154.21	145.20 - 148.20	3.0	2.54	PVC
SP-8	9906.65	9977.95	--	148.87	128.60 - 131.60	3.0	2.54	PVC
SP-9	9942.76	9974.98	--	152.34	133.70 - 136.70	3.0	2.54	PVC
SP97-1A	9970.64	9748.74	160.5	161.06	113.40 - 114.90	1.5	3.175	PVC
SP97-1B	9970.64	9748.74	160.5	161.03	125.60 - 127.10	1.5	3.175	PVC
Inclinometer	--	--	--	161.28	-- --	--	6.033	
SP99-1A	10008.11	9905.90	158.17	158.95	123.12 - 123.58	0.46	5.08	PVC
SP99-1B	10008.11	9905.90	158.17	158.92	133.79 - 135.31	1.52	3.175	PVC
SP99-2	10009.58	9855.93	157.88	158.74	131.36 - 132.88	1.52	3.175	PVC
SP99-3A	10008.73	9823.24	157.96	158.80	119.25 - 119.71	0.46	3.175	PVC
SP99-3B	10008.73	9823.24	157.96	158.78	139.98 - 141.50	1.52	3.175	PVC
SP99-4	9975.45	9939.44	154.22	154.80	137.15 - 138.67	1.52	3.175	PVC
SP99-5	9980.52	9908.46	154.31	154.86	129.01 - 130.53	1.52	3.175	PVC
SP99-6	9975.28	9908.11	154.29	155.14	132.34 - 133.86	1.52	3.175	PVC
SP99-7A	9975.35	9871.09	154.22	155.00	124.50 - 124.96	0.46	3.175	PVC
SP99-7B	9975.35	9871.09	154.22	155.05	132.88 - 134.40	1.52	3.175	PVC
SP99-8	9980.57	9828.14	154.29	155.22	135.85 - 137.37	1.52	3.175	PVC
SP99-9	9975.25	9828.50	154.37	155.16	124.35 - 124.81	0.46	3.175	PVC
SP99-10	9886.08	9876.99	133.10	133.04	118.77 - 120.29	1.52	3.175	PVC
SP99-11	10042.56	9825.40	155.90	156.62	135.84 - 137.36	1.52	5.08	PVC
SP99-12	10042.28	9871.88	156.05	156.92	134.66 - 136.18	1.52	5.08	PVC
SP99-13	10041.88	9904.75	156.21	156.87	136.15 - 137.67	1.52	5.08	PVC
SP01-1A	--	--	160.1	160.8	149.91 - 151.43	1.52	--	PVC
SP01-1B	--	--	160.1	160.9	154.87 156.39	1.52	--	PVC
SP01-2A	--	--	153.2	144.65	137.3 138.82	1.52	--	PVC
SP01-2B	--	--	153.2	154.01	143.99 145.514	1.52	--	PVC
SP01-3	--	--	154.4	155.13	147.97 149.494	1.52	--	PVC
SP01-10	--	--	154.3	155.06	133.59 135.114	1.52	--	PVC

Notes:

1. Screen elevation data from borehole logs.
2. Ground surface elevation data from borehole logs.
3. Top of riser elevation data, and northing and easting data from surveillance.
4. PVC - polyvinyl chloride

Table 5.5: Temperature Monitoring Locations within Coquitlam Dam

Upstream Shell Monitoring Locations	*Distance From Dam Centerline (metres)*	*Material Surrounding Screen*
SP99-11	42.56 u/s	upstream sand and gravel shell
SP99-12	42.28 u/s	upstream sand and gravel shell
SP99-13	41.88 u/s	upstream sand and gravel shell
Core and Foundation Monitoring Locations		
SP-2	27.8 u/s	foundation sand and gravel
SP-1	4.91 u/s	foundation sand and gravel
SP99-1A	8.11 u/s	foundation sand and gravel
SP99-1B	8.11 u/s	core silt
SP99-2	9.58 u/s	core silt
SP99-3A	8.73 u/s	foundation sand and gravel
SP99-3B	8.73 u/s	core silt
inclinometer	1.5 d/s	- -
Downstream Shell and Sand/Gravel Monitoring Locations		
SP-4	25.66 d/s	sand and gravel shell
SP99-5	19.48 d/s	sand and silt
SP99-6	24.72 d/s	sand and gravel
SP99-7A	24.65 d/s	silt, sand and gravel
SP99-7B	24.65 d/s	silt and sand
SP99-8	19.43 d/s	foundation silt
SP99-9	24.75 d/s	foundation sand and gravel
SP99-10	113.74 d/s	sand and gravel
East Abutment		
SP-8		
SP-9		
SP-6		
SP99-4		
West Abutment		
SP97-1A		
SP97-1B		

Notes:
u/s - upstream of dam centerline
d/s - downstream of dam centerline

Table 5.6: Summary of Annual Temperature Variation Data

Location	Annual Temperature			
	Range (°C)	Average (°C)	Change at a Specific Elevation (°C)	Change within a Piezometer (°C)
Upstream Shell	9.7 - 10.7	10.2	0.2 - 0.3	0.5 - 0.7
Upstream Core and Foundation	9.2 - 10.9	10.0	0.14 - 0.2	0.3 - 1.15
Downstream Core and Foundation	9.0 - 9.5	9.25	0.12 - 0.3	0.17 - 0.37
Toe	8.5	8.5	0.11	0.11
Abutments				
- including SP99-4	7.9 - 8.9	8.4	0.15 - 0.27	0.15 - 0.4
- excluding SP99-4	7.9 - 8.4	8.15	0.15 - 0.27	0.15 - 0.4

Note: These values are based on temperatures recorded at Coquitlam Dam, at depths below where air temperature and conduction effects are apparent.

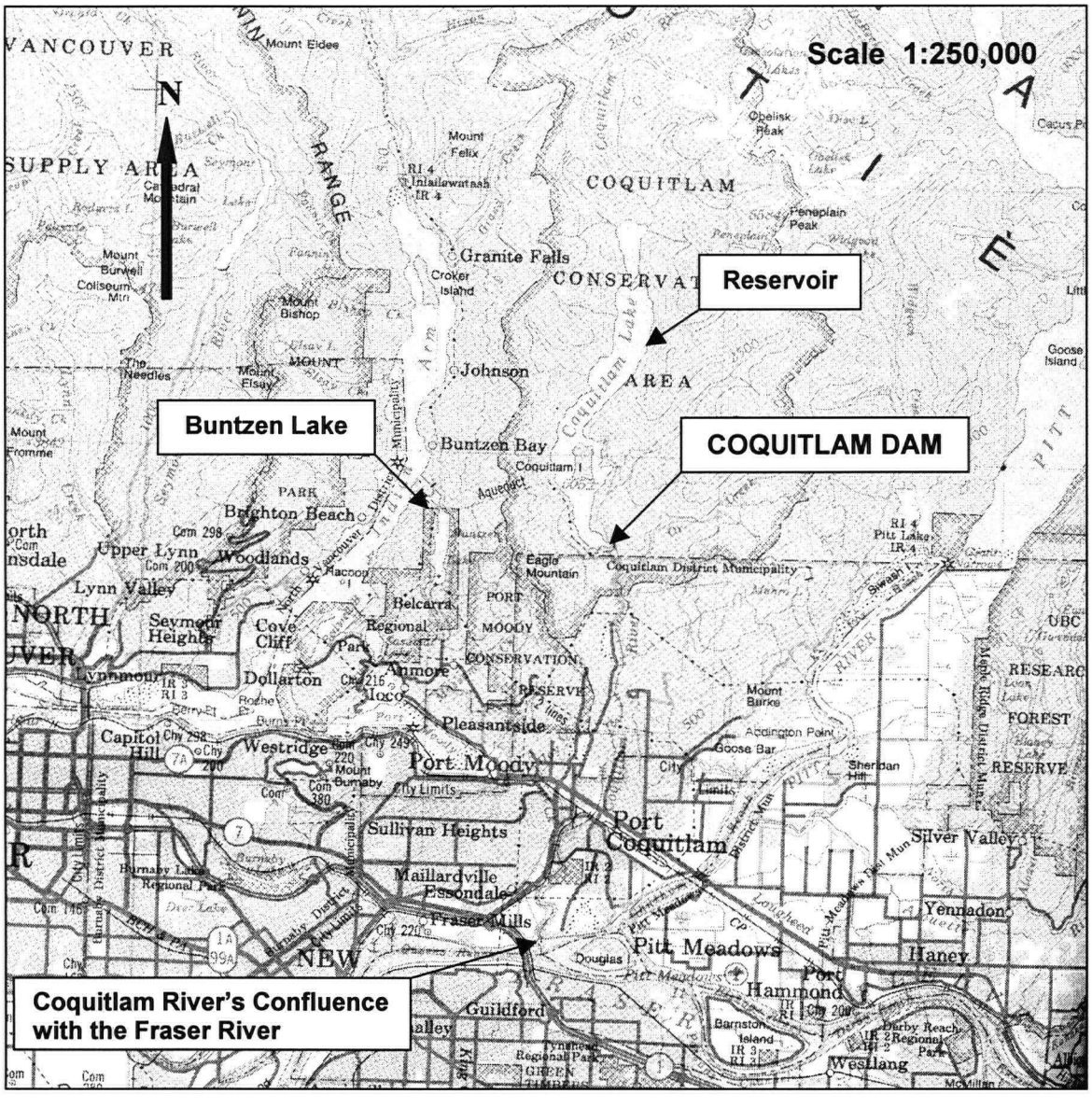

Figure 5.1: Coquitlam Dam - Site Location
(Energy, Mines and Resources Canada, Surveys and Mapping Branch, 1986)

a: Looking downstream, at both rockfill toes, trestles and flumes for sluice filling and hydraulic puddle in the centre.

b: Hydraulic filling.

Figure 5.2: Hydraulic Filling of Coquitlam Dam (photographs provide by BC Hydro).

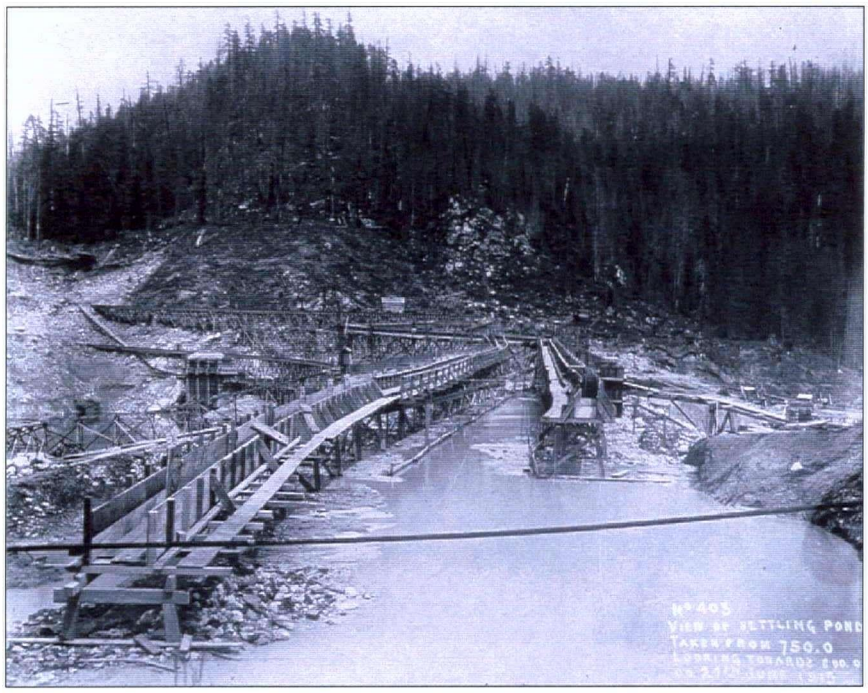

a: Looking west, hydraulic filling nearly complete. Small hydraulic puddle in centre of dam.

b: Looking west, completed view of Coquitlam Dam, prior to reservoir impoundment.

Figure 5.3: Construction Photographs of Coquitlam Dam (photographs provided by BC Hydro).

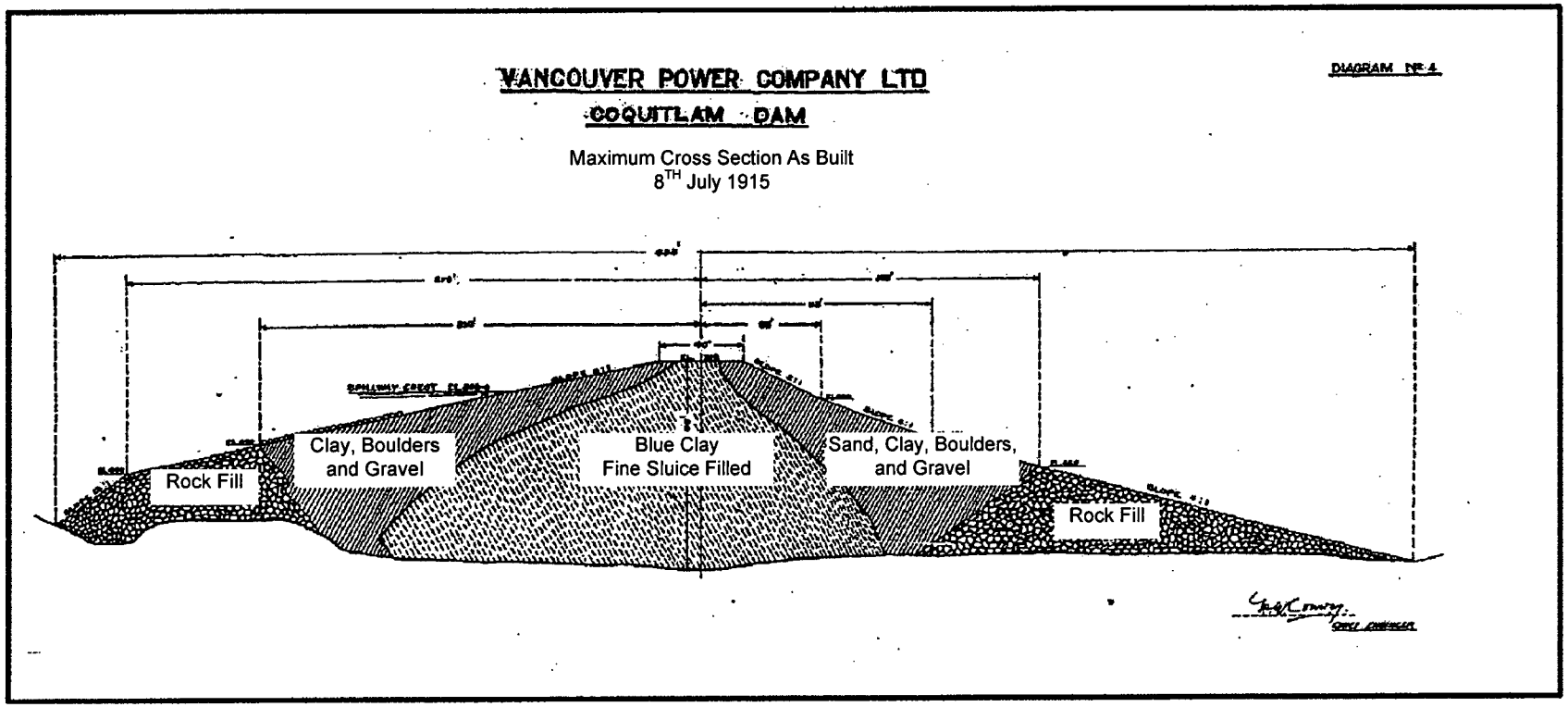

Figure 5.4: 1915 As Built Cross Section of Coquitlam Dam (provided by BC Hydro)

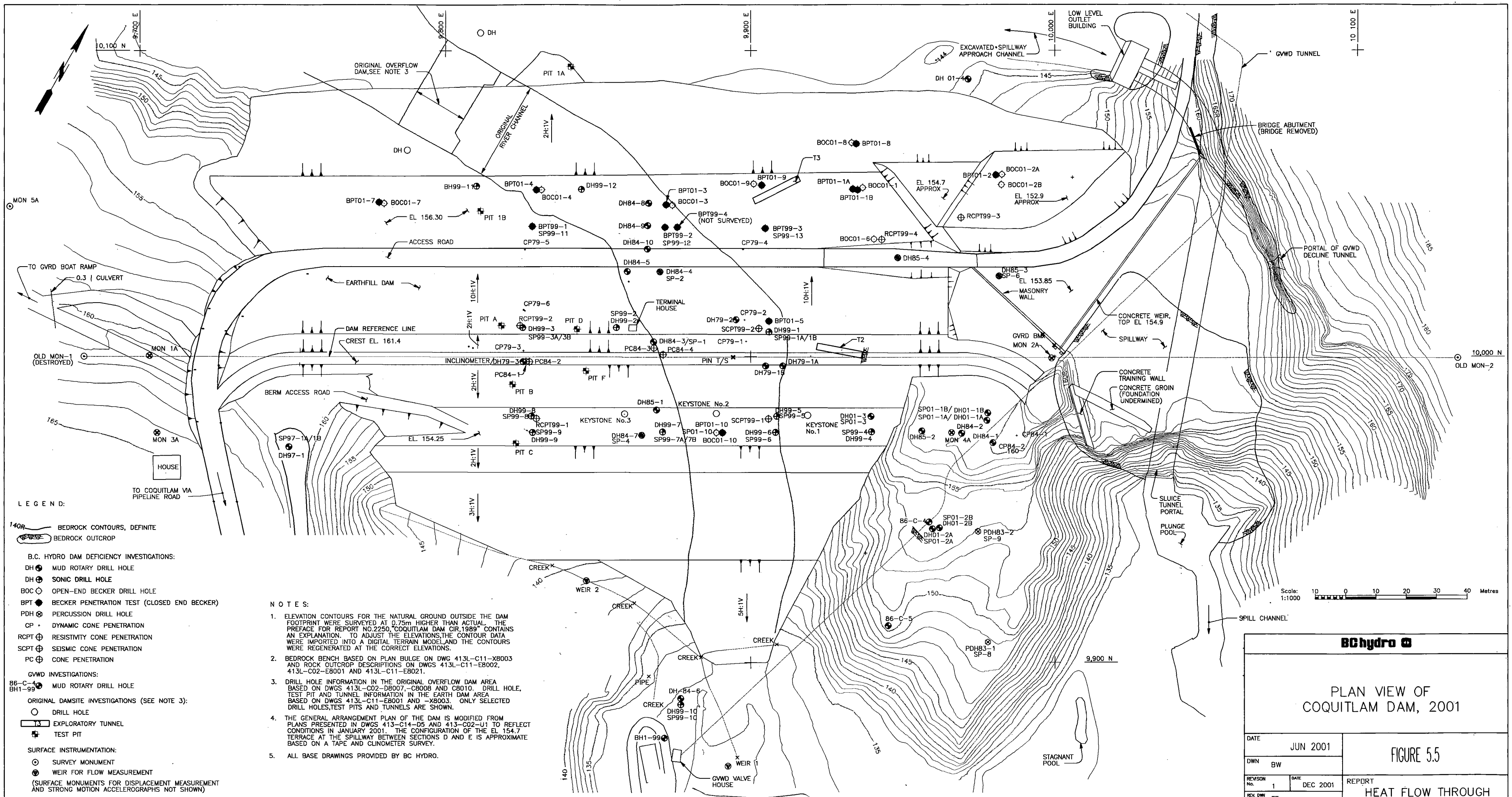

L E G E N D:

- 140R — BEDROCK CONTOURS, DEFINITE
- REVISE — BEDROCK OUTCROP

B.C. HYDRO DAM DEFICIENCY INVESTIGATIONS:

- DH — MUD ROTARY DRILL HOLE
- DH — SONIC DRILL HOLE
- BOC — OPEN-END BECKER DRILL HOLE
- BPT — BECKER PENETRATION TEST (CLOSED END BECKER)
- PDH — PERCUSSION DRILL HOLE
- CP — DYNAMIC CONE PENETRATION
- RCPT — RESISTIVITY CONE PENETRATION
- SCPT — SEISMIC CONE PENETRATION
- PC — CONE PENETRATION

GVWD INVESTIGATIONS:

- 86-C-4 / BH1-99 — MUD ROTARY DRILL HOLE

ORIGINAL DAMSITE INVESTIGATIONS (SEE NOTE 3):

- DRILL HOLE
- T3 — EXPLORATORY TUNNEL
- TEST PIT

SURFACE INSTRUMENTATION:

- SURVEY MONUMENT
- WEIR FOR FLOW MEASUREMENT

(SURFACE MONUMENTS FOR DISPLACEMENT MEASUREMENT AND STRONG MOTION ACCELEROGRAPHS NOT SHOWN)

N O T E S:

1. ELEVATION CONTOURS FOR THE NATURAL GROUND OUTSIDE THE DAM FOOTPRINT WERE SURVEYED AT 0.75m HIGHER THAN ACTUAL. THE PREFACE FOR REPORT NO.2250,"COQUITLAM DAM CIR,1989" CONTAINS AN EXPLANATION. TO ADJUST THE ELEVATIONS,THE CONTOUR DATA WERE IMPORTED INTO A DIGITAL TERRAIN MODEL,AND THE CONTOURS WERE REGENERATED AT THE CORRECT ELEVATIONS.
2. BEDROCK BENCH BASED ON PLAN BULGE ON DWG 413L-C11-X8003 AND ROCK OUTCROP DESCRIPTIONS ON DWGS 413L-C11-E8002, 413L-C02-E8001 AND 413L-C11-E8021.
3. DRILL HOLE INFORMATION IN THE ORIGINAL OVERFLOW DAM AREA BASED ON DWGS 413L-C02-D8007, -C8008 AND C8010. DRILL HOLE, TEST PIT AND TUNNEL INFORMATION IN THE EARTH DAM AREA BASED ON DWGS 413L-C11-E8001 AND -X8003. ONLY SELECTED DRILL HOLES,TEST PITS AND TUNNELS ARE SHOWN.
4. THE GENERAL ARRANGEMENT PLAN OF THE DAM IS MODIFIED FROM PLANS PRESENTED IN DWGS 413-C14-D5 AND 413-C02-U1 TO REFLECT CONDITIONS IN JANUARY 2001. THE CONFIGURATION OF THE EL 154.7 TERRACE AT THE SPILLWAY BETWEEN SECTIONS D AND E IS APPROXIMATE BASED ON A TAPE AND CLINOMETER SURVEY.
5. ALL BASE DRAWINGS PROVIDED BY BC HYDRO.

BC hydro

PLAN VIEW OF COQUITLAM DAM, 2001

DATE	JUN 2001		FIGURE 5.5
DWN	BW		
REVISON No.	1	DATE	DEC 2001
REV. DWN	FE		REPORT HEAT FLOW THROUGH EARTH DAMS
REVISON No.		DATE	96

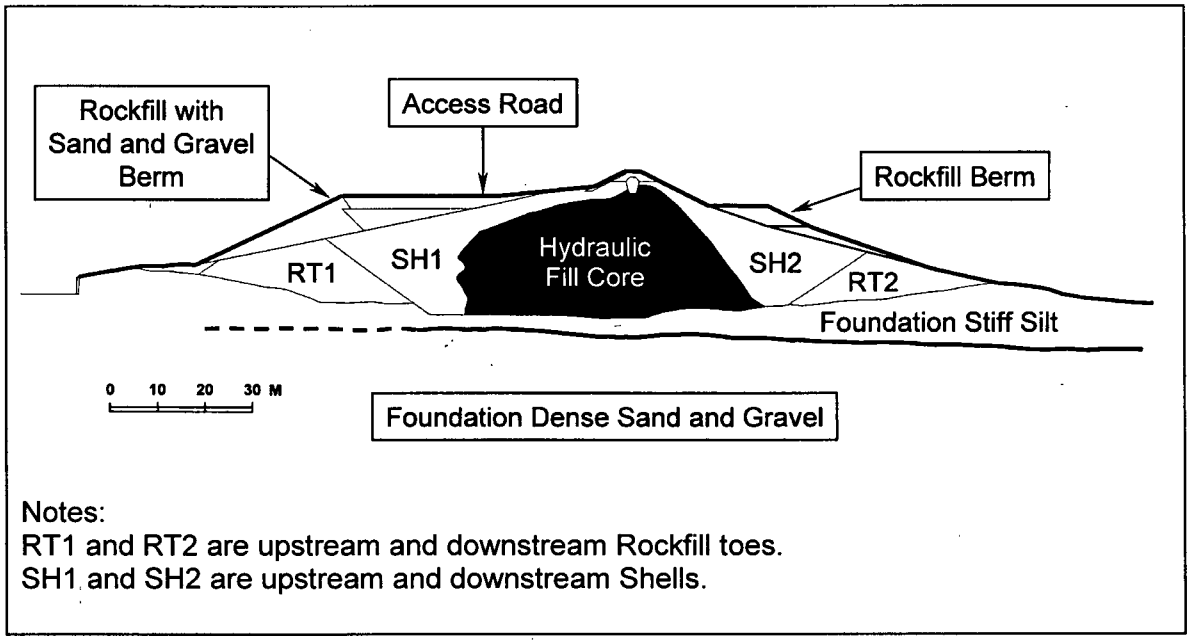

Figure 5.6: Typical Cross Section of Coquitlam Dam, 2001 (provided by BC Hydro)

a. Aerial view of Coquitlam Dam.

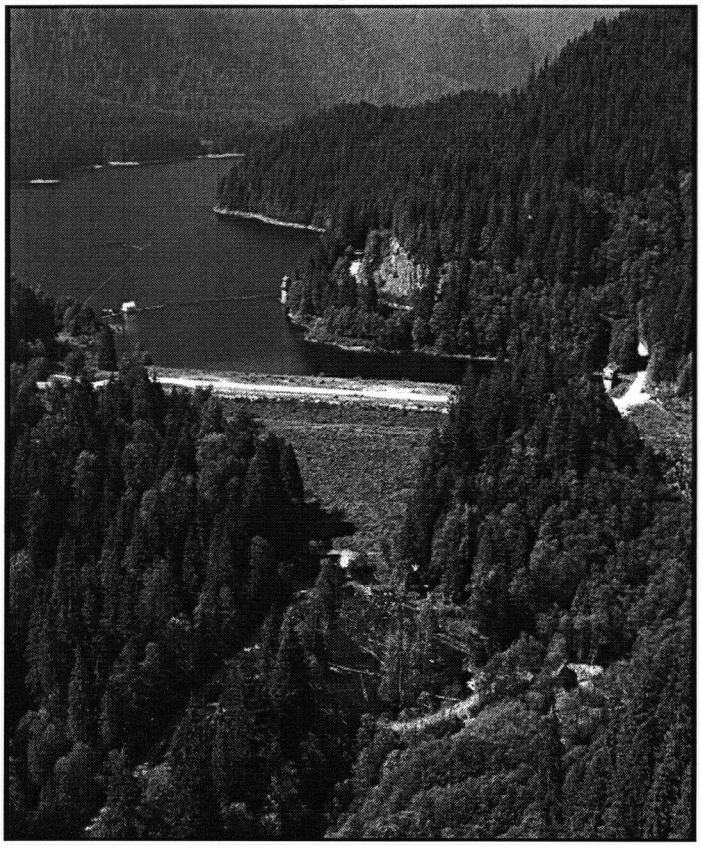

b. Downstream slope of Coquitlam Dam.

Figure 5.7: Recent Photographs of Coquitlam Dam. (provided by BC Hydro)

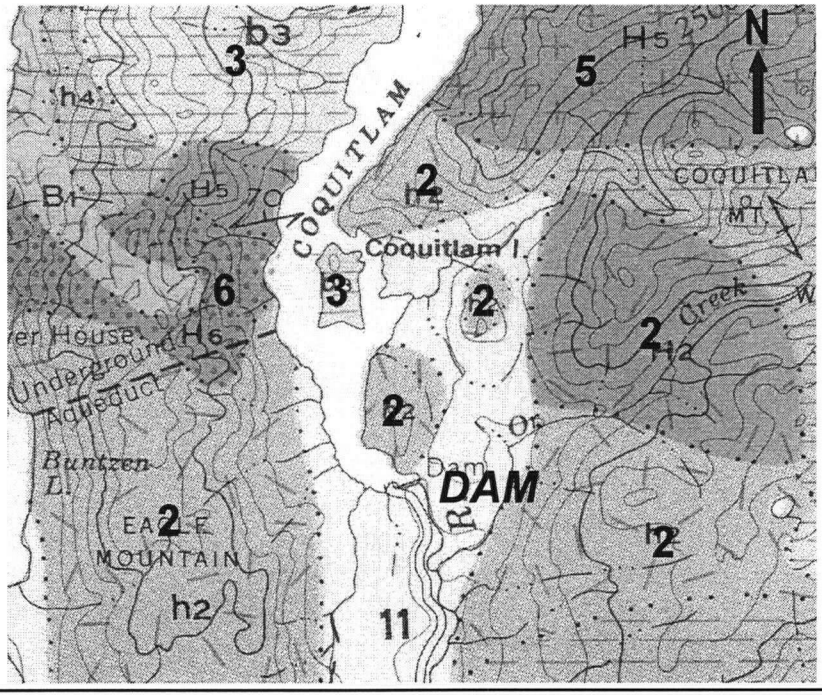

Figure 5.8: Regional Bedrock Geology (provided by BC Hydro)

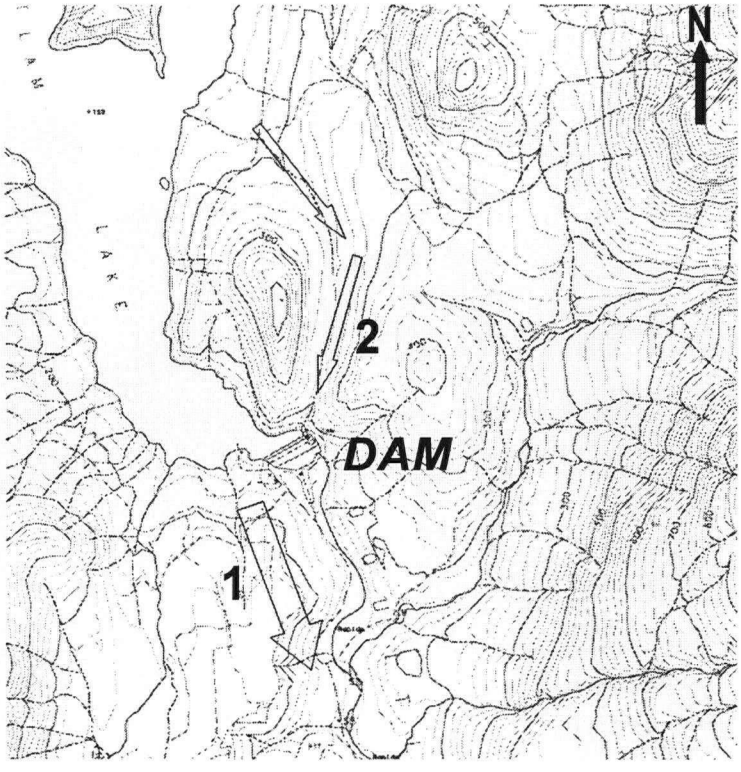

Figure 5.9: Buried Valleys Near Coquitlam Dam (provided by BC Hydro)

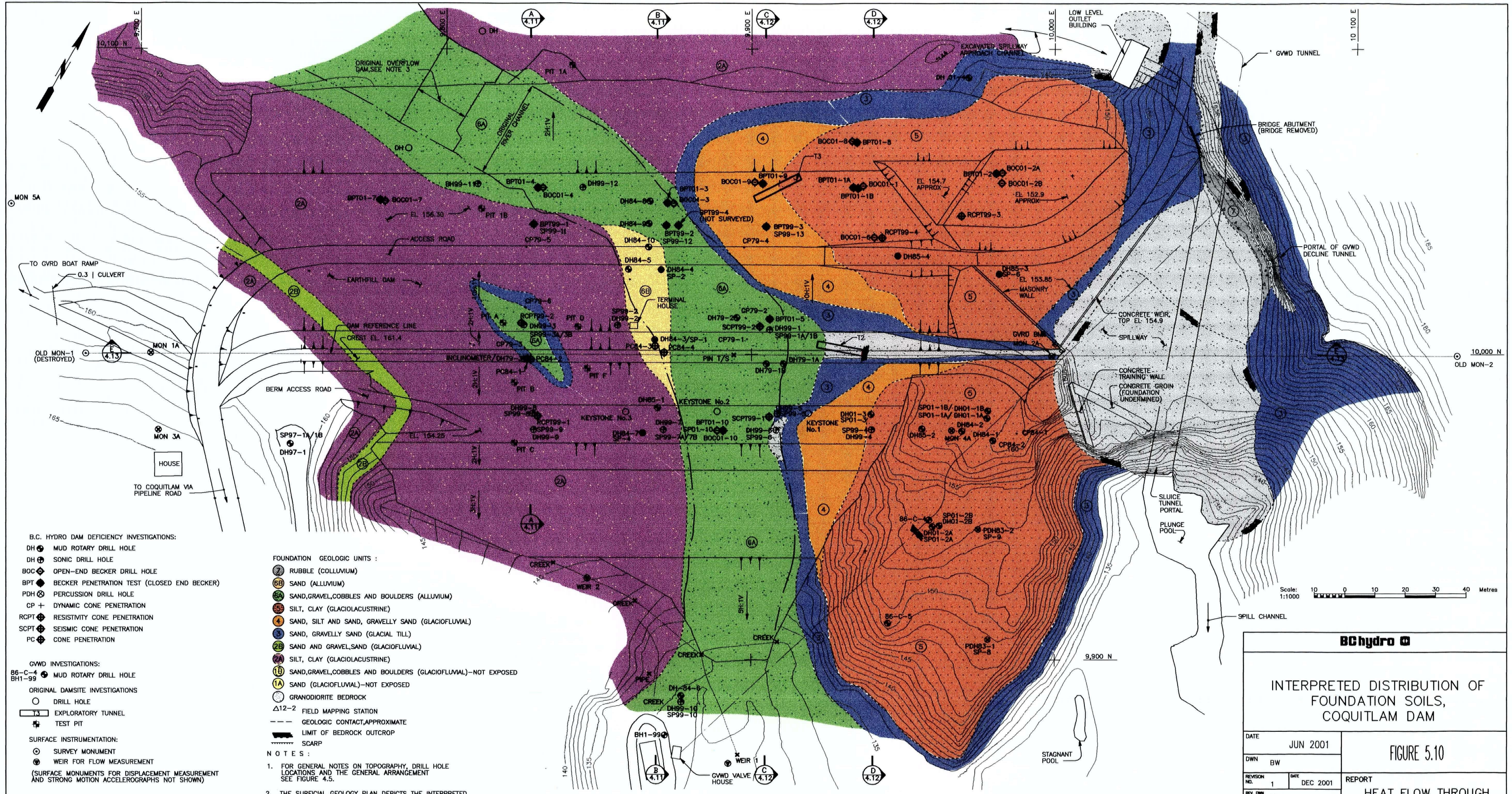
B.C. HYDRO DAM DEFICIENCY INVESTIGATIONS:
DH MUD ROTARY DRILL HOLE
DH SONIC DRILL HOLE
BOC OPEN-END BECKER DRILL HOLE
BPT BECKER PENETRATION TEST (CLOSED END BECKER)
PDH PERCUSSION DRILL HOLE
CP DYNAMIC CONE PENETRATION
RCPT RESISTIVITY CONE PENETRATION
SCPT SEISMIC CONE PENETRATION
PC CONE PENETRATION
GVWD INVESTIGATIONS:
86-C-4 BH1-99 MUD ROTARY DRILL HOLE
ORIGINAL DAMSITE INVESTIGATIONS
DRILL HOLE
T3 EXPLORATORY TUNNEL
TEST PIT
SURFACE INSTRUMENTATION:
SURVEY MONUMENT
WEIR FOR FLOW MEASUREMENT
(SURFACE MONUMENTS FOR DISPLACEMENT MEASUREMENT AND STRONG MOTION ACCELEROGRAPHS NOT SHOWN)
FOUNDATION GEOLOGIC UNITS :
Z RUBBLE (COLLUVIUM)
6B SAND (ALLUVIUM)
6A SAND,GRAVEL,COBBLES AND BOULDERS (ALLUVIUM)
5B SILT, CLAY (GLACIOLACUSTRINE)
4 SAND, SILT AND SAND, GRAVELLY SAND (GLACIOFLUVIAL)
3 SAND, GRAVELLY SAND (GLACIAL TILL)
2B SAND AND GRAVEL,SAND (GLACIOFLUVIAL)
2A SILT, CLAY (GLACIOLACUSTRINE)
1B SAND,GRAVEL,COBBLES AND BOULDERS (GLACIOFLUVIAL)–NOT EXPOSED
1A SAND (GLACIOFLUVIAL)–NOT EXPOSED
GRANODIORITE BEDROCK
△12–2 FIELD MAPPING STATION
GEOLOGIC CONTACT,APPROXIMATE
LIMIT OF BEDROCK OUTCROP
SCARP
NOTES :
1. FOR GENERAL NOTES ON TOPOGRAPHY, DRILL HOLE LOCATIONS AND THE GENERAL ARRANGEMENT SEE FIGURE 4.5.
2. THE SURFICIAL GEOLOGY PLAN DEPICTS THE INTERPRETED FOUNDATION CONDITIONS BENEATH THE EARTH DAM AND OTHER FILL AT THE TIME OF CONSTRUCTION.
ORIGINAL OVERFLOW DAM,SEE NOTE 3
ORIGINAL RIVER CHANNEL
EXCAVATED SPILLWAY APPROACH CHANNEL
LOW LEVEL OUTLET BUILDING
GVWD TUNNEL
BRIDGE ABUTMENT (BRIDGE REMOVED)
PORTAL OF GVWD DECLINE TUNNEL
CONCRETE WEIR, TOP EL 154.9
SPILLWAY
CONCRETE TRAINING WALL
CONCRETE GROIN (FOUNDATION UNDERMINED)
SLUICE TUNNEL PORTAL
PLUNGE POOL
SPILL CHANNEL
STAGNANT POOL
GVWD VALVE HOUSE
WEIR 1
WEIR 2
TERMINAL HOUSE
KEYSTONE No.1
KEYSTONE No.2
KEYSTONE No.3
EARTHFILL DAM
ACCESS ROAD
BERM ACCESS ROAD
DAM REFERENCE LINE
CREST EL. 161.4
TO GVRD BOAT RAMP
0.3 I CULVERT
TO COQUITLAM VIA PIPELINE ROAD
HOUSE
MASONRY WALL
EL. 153.85
EL. 154.7 APPROX
EL. 152.9 APPROX
EL. 156.30
EL. 154.25
MON 5A
MON 1A
MON 3A
OLD MON–1 (DESTROYED)
OLD MON–2
10,000 N
9,900 N
10,100 N
9,700 E
9,800 E
10,000 E
10,100 E
Scale: 1:1000
10 0 10 20 30 40 Metres
BC hydro
INTERPRETED DISTRIBUTION OF FOUNDATION SOILS, COQUITLAM DAM
DATE JUN 2001
DWN BW
REVISION NO. 1
DATE DEC 2001
REV. DWN FE
REVISION NO.
DATE
FIGURE 5.10
REPORT
HEAT FLOW THROUGH EARTH DAMS
100

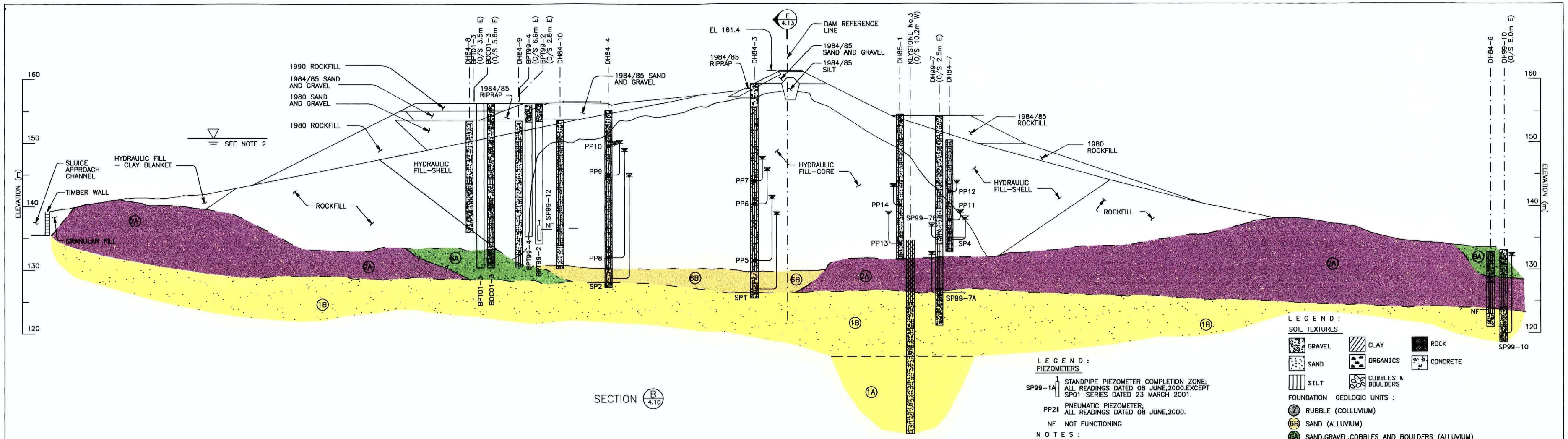

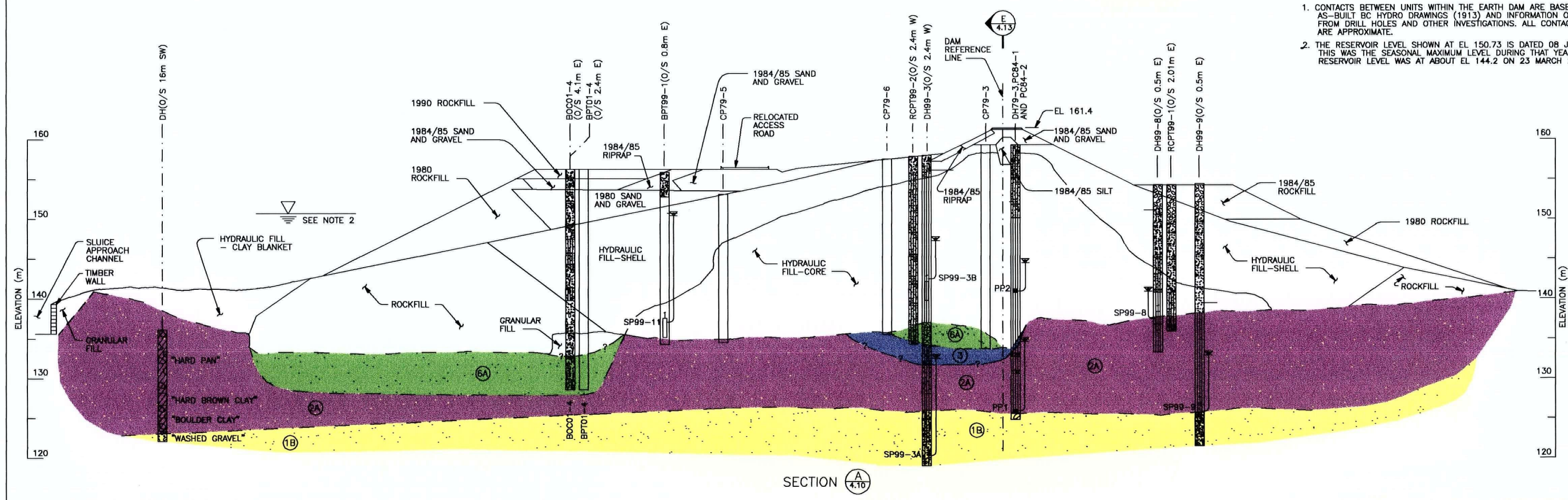

LEGEND:
PIEZOMETERS

SP99-1A — STANDPIPE PIEZOMETER COMPLETION ZONE; ALL READINGS DATED 08 JUNE,2000.EXCEPT SP01-SERIES DATED 23 MARCH 2001.

PP21 — PNEUMATIC PIEZOMETER; ALL READINGS DATED 08 JUNE,2000.

NF NOT FUNCTIONING

NOTES:

1. CONTACTS BETWEEN UNITS WITHIN THE EARTH DAM ARE BASED ON AS-BUILT BC HYDRO DRAWINGS (1913) AND INFORMATION OBTAINED FROM DRILL HOLES AND OTHER INVESTIGATIONS. ALL CONTACTS ARE APPROXIMATE.
2. THE RESERVOIR LEVEL SHOWN AT EL 150.73 IS DATED 08 JUNE,2000. THIS WAS THE SEASONAL MAXIMUM LEVEL DURING THAT YEAR. THE RESERVOIR LEVEL WAS AT ABOUT EL 144.2 ON 23 MARCH 2001.

LEGEND:
SOIL TEXTURES

GRAVEL, CLAY, ROCK, SAND, ORGANICS, CONCRETE, SILT, COBBLES & BOULDERS

FOUNDATION GEOLOGIC UNITS :

- 7 RUBBLE (COLLUVIUM)
- 6B SAND (ALLUVIUM)
- 6A SAND,GRAVEL,COBBLES AND BOULDERS (ALLUVIUM)
- 5 SILT, CLAY (GLACIOLACUSTRINE)
- 4 SAND, SILT AND SAND, GRAVELLY SAND (GLACIOFLUVIAL)
- 3 SAND, GRAVELLY SAND (GLACIAL TILL)
- 2B SAND AND GRAVEL,SAND (GLACIOFLUVIAL)
- 2A SILT, CLAY (GLACIOLACUSTRINE)
- 1B SAND,GRAVEL,COBBLES AND BOULDERS (GLACIOFLUVIAL)–NOT EXPOSED
- 1A SAND (GLACIOFLUVIAL)–NOT EXPOSED
- GRANODIORITE BEDROCK

1:500
SCALE: 5 0 5 10 15 20 METRES

BC hydro

SECTION A AND B INTERPRETED DISTRIBUTION OF FOUNDATION SOILS COQUITLAM DAM

DATE JUN 2001	FIGURE 5.11
DWN STL	
REVISON No. 1 / DATE DEC 2001	REPORT HEAT FLOW THROUGH EARTH DAMS
REV. DWN FE	
REVISON No. / DATE	101

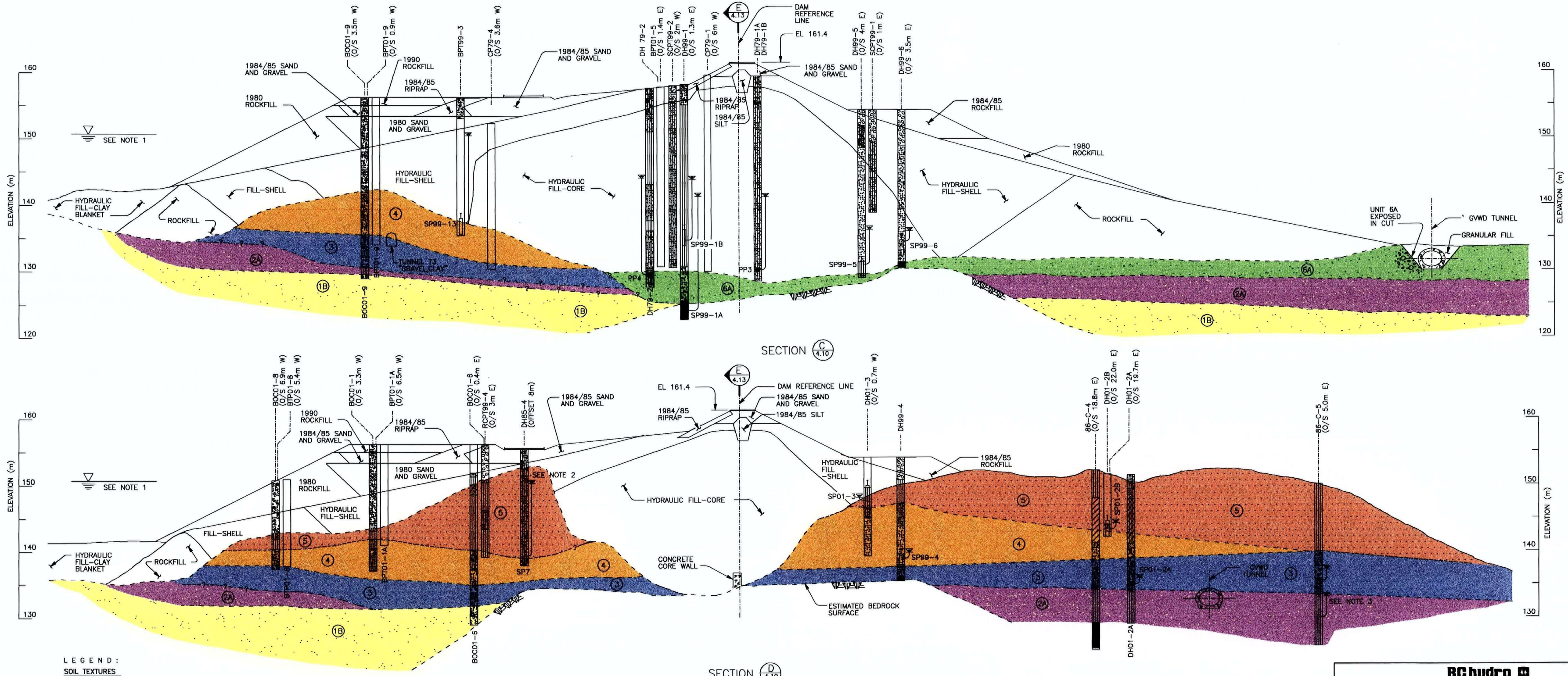

LEGEND:

SOIL TEXTURES

GRAVEL, SAND, SILT, CLAY, ORGANICS, COBBLES & BOULDERS, ROCK, CONCRETE

PIEZOMETERS

SP99-1A | STANDPIPE PIEZOMETER COMPLETION ZONE; ALL READINGS DATED 08 JUNE,2000.EXCEPT SP01-SERIES DATED 23 MARCH 2001.

PP2 | PNEUMATIC PIEZOMETER; ALL READINGS DATED 08 JUNE,2000.

NF NOT FUNCTIONING

FOUNDATION GEOLOGIC UNITS :

7 RUBBLE (COLLUVIUM)
6B SAND (ALLUVIUM)
6A SAND,GRAVEL,COBBLES AND BOULDERS (ALLUVIUM)
5 SILT, CLAY (GLACIOLACUSTRINE)
4 SAND, SILT AND SAND, GRAVELLY SAND (GLACIOFLUVIAL)
3 SAND, GRAVELLY SAND (GLACIAL TILL)
2B SAND AND GRAVEL,SAND (GLACIOFLUVIAL)
2A SILT, CLAY (GLACIOLACUSTRINE)
1B SAND,GRAVEL,COBBLES AND BOULDERS (GLACIOFLUVIAL)–NOT EXPOSED
1A SAND (GLACIOFLUVIAL)–NOT EXPOSED
GRANODIORITE BEDROCK

SCALE: 1:500 — 5 0 5 10 15 20 METRES

NOTES:

1. CONTACTS BETWEEN UNITS WITHIN THE EARTH DAM ARE BASED ON AS-BUILT BC HYDRO DRAWINGS (1913) AND INFORMATION OBTAINED FROM DRILL HOLES AND OTHER INVESTIGATIONS. ALL CONTACTS ARE APPROXIMATE.
2. STANDPIPE PIEZOMETER SP7 WAS DESTROYED IN 1999. THE PIEZOMETRIC LEVEL SHOWN DATES FROM 29 JUNE,1998, WHEN THE RESERVOIR LEVEL WAS AT EL 150.76m.
3. DRILLHOLE 86-C-5 BY GVWD CONTAINS PIEZOMETRIC DATA DATING FROM INSTALLATION IN 1986. SUBSEQUENT PIEZOMETRIC LEVEL DATA ARE NOT AVAILABLE.
4. THE RESERVOIR LEVEL SHOWN AT EL 150.73 IS DATED 08 JUNE,2000. THIS WAS THE SEASONAL MAXIMUM LEVEL DURING THAT YEAR. THE RESERVOIR LEVEL WAS AT ABOUT EL 144.2 ON 23 MARCH 2001.

BC hydro

SECTION C AND D INTERPRETED DISTRIBUTION OF FOUNDATION SOILS COQUITLAM DAM

DATE JUN 2001	FIGURE 5.12
DWN STL	
REVISON No. 1 DATE DEC 2001	REPORT HEAT FLOW THROUGH EARTH DAMS
REV. DWN FE	102
REVISON No. DATE	

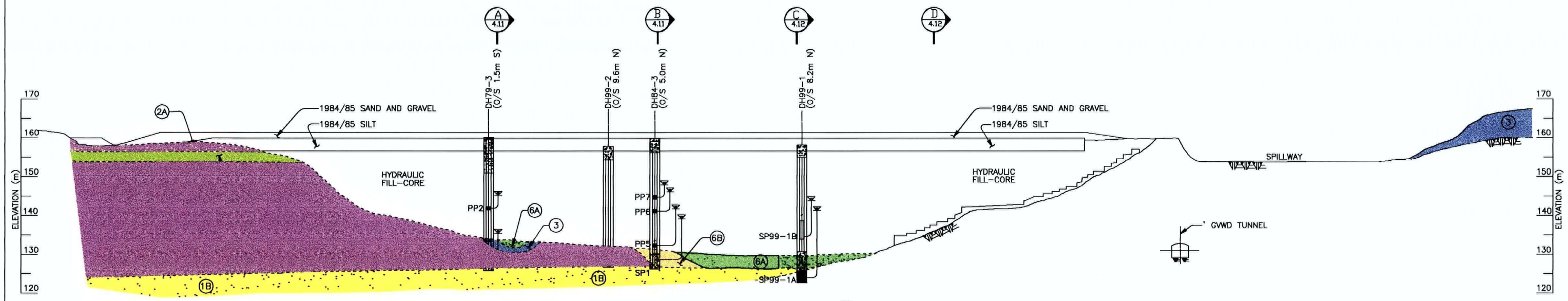

L E G E N D :

SOIL TEXTURES

GRAVEL · CLAY · ROCK
SAND · ORGANICS · CONCRETE
SILT · COBBLES & BOULDERS

FOUNDATION GEOLOGIC UNITS

- 6B SAND (ALLUVIUM)
- 6A SAND AND GRAVEL (ALLUVIUM)
- 3 SILT,SAND AND GRAVEL (GLACIAL TILL)
- 2B SAND AND GRAVEL, SAND (GLACIOFLUVIAL)
- 2A SILT (GLACIOLACUSTRINE)
- 1B SAND,GRAVEL,COBBLES AND BOULDERS (GLACIOFLUVIAL)

PIEZOMETERS

SP99-1A — STANDPIPE PIEZOMETER COMPLETION ZONE; ALL READINGS DATED 08 JUNE,2000.

PP2 — PNEUMATIC PIEZOMETER; ALL READINGS DATED 08 JUNE,2000.

NF NOT FUNCTIONING

N O T E S:

1. CONTACT UNITS SHOWN ARE BASED ON PREVIOUS RECORDS, DRILL HOLE DATA AND RESULTS FROM OTHER INVESTIGATIVE WORK. ALL CONTACTS ARE APPROXIMATE.
2. THE CROSS SECTION DEPICTS THE INTERPRETED SURFICIAL GEOLOGY FOUNDATION BENEATH THE EARTH DAM AT THE TIME OF COSNTRUCTION

1:1000 Scale: 10 0 10 20 30 40 Metres

BC hydro

SECTION E
INTERPRETED DISTRIBUTION OF FOUNDATION SOILS
COQUITLAM DAM

DATE JUN 2001	FIGURE 5.13
DWN GCB	
REVISON No. 1 DATE DEC 2001	REPORT HEAT FLOW THROUGH EARTH DAMS 103
REV. DWN FE	
REVISON No. DATE	

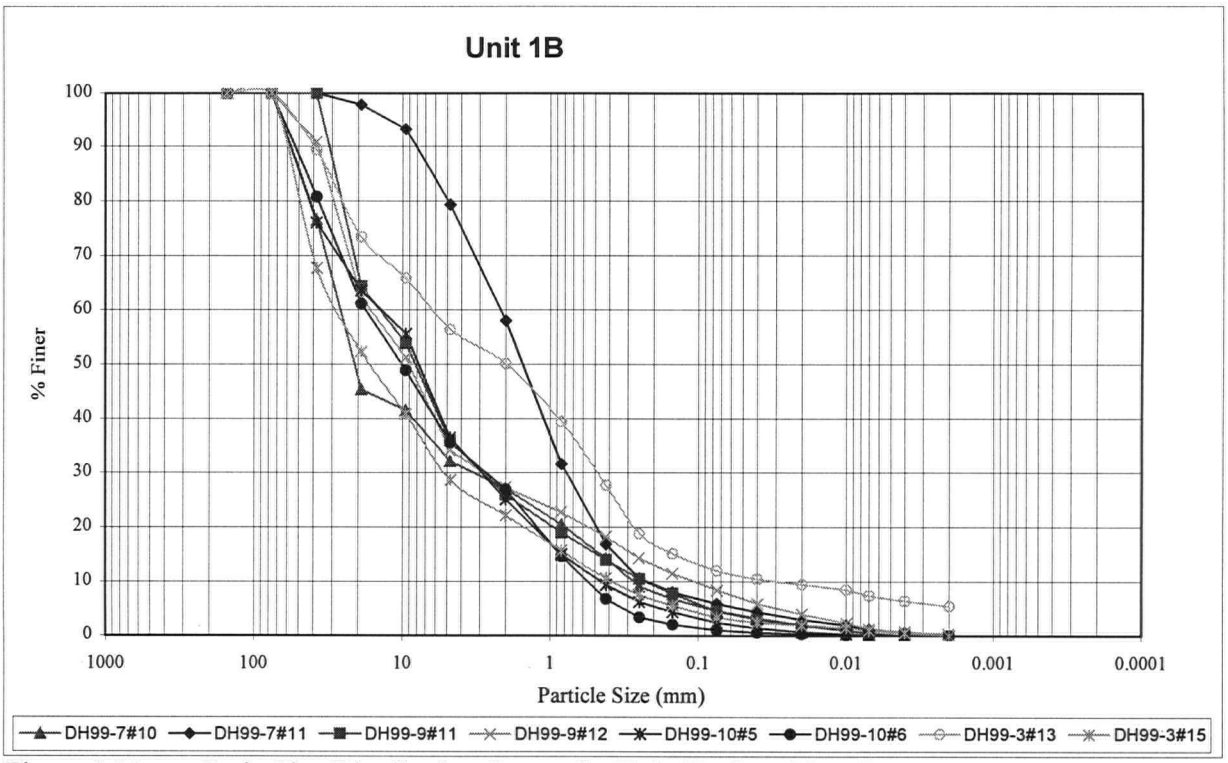

Figure 5.14 : Grain Size Distribution Curves for Unit 1B, Coquitlam Dam (provided by BC Hydro)

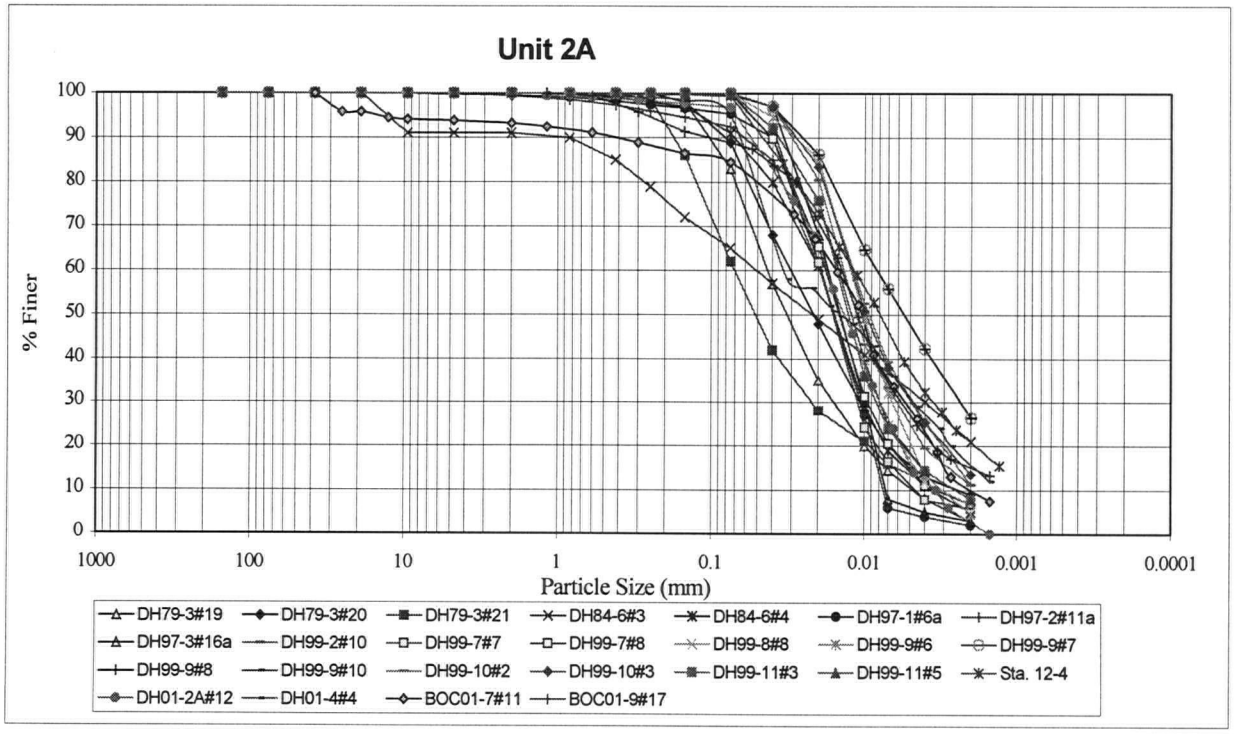

Figure 5.15: Grain Size Distribution Curves for Unit 2A, Coquitlam Dam (provided by BC Hydro)

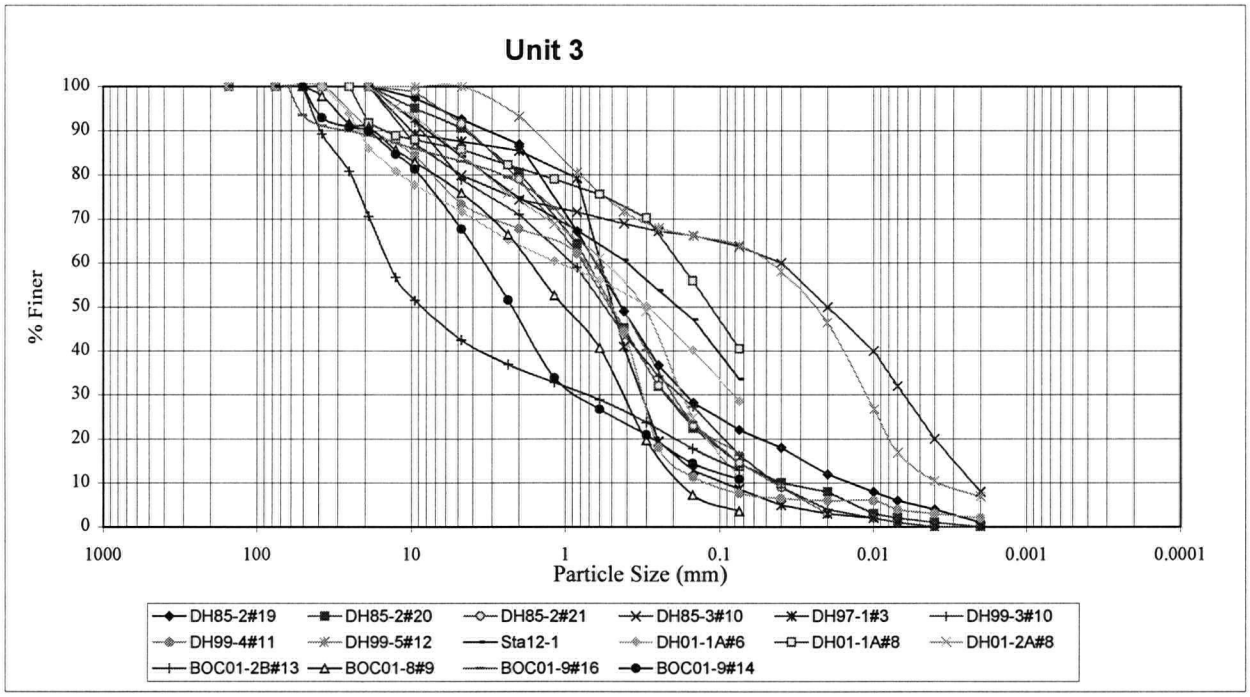

Figure 5.16: Grain Size Distribution Curves for Unit 3, Coquitlam Dam (provided by BC Hydro)

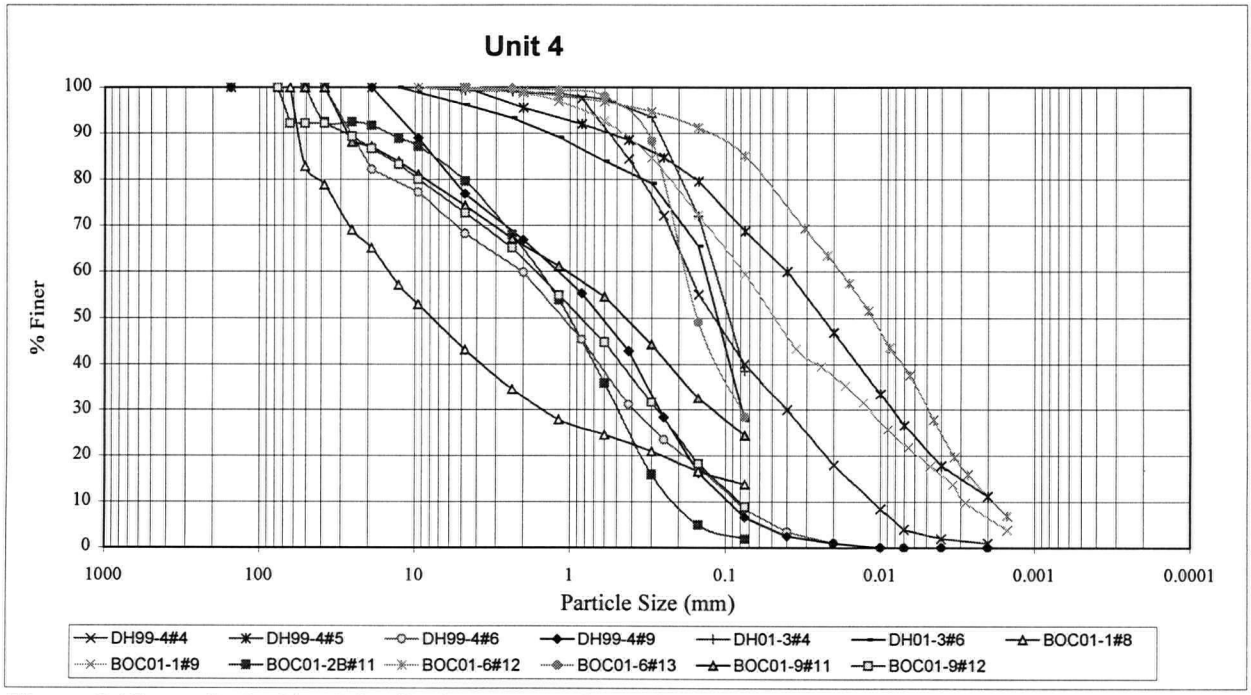

Figure 5.17: Grain Size Distribution Curves for Unit 4, Coquitlam Dam (provided by BC Hydro)

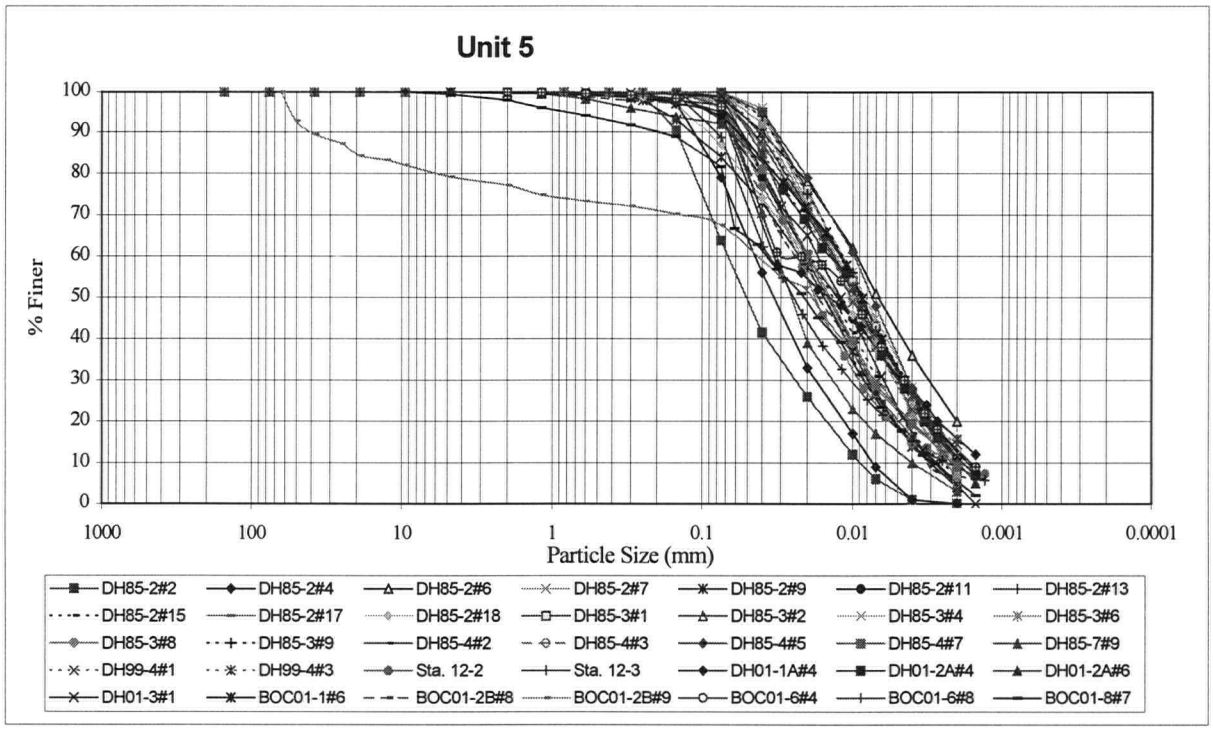

Figure 5.18: Grain Size Distribution Curves for Unit 5, Coquitlam Dam (provided by BC Hydro)

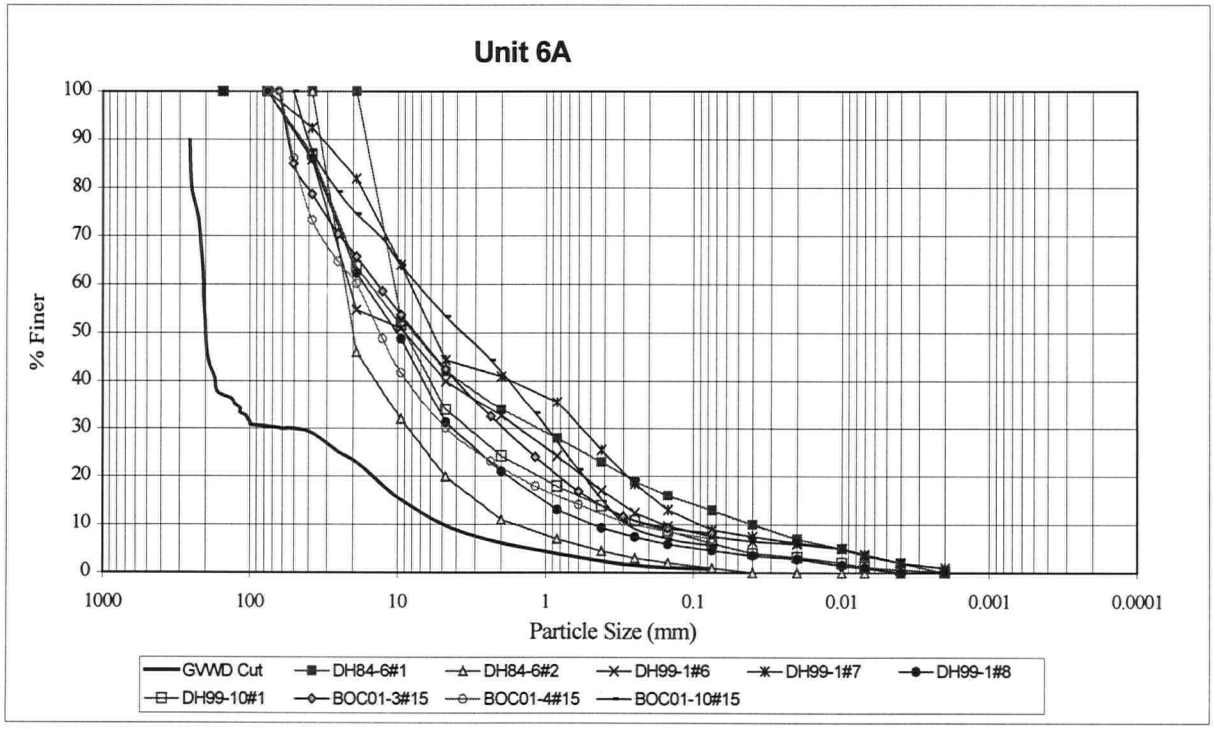

Figure 5.19: Grain Size Distribution Curves for Unit 6A, Coquitlam Dam (provided by BC Hydro)

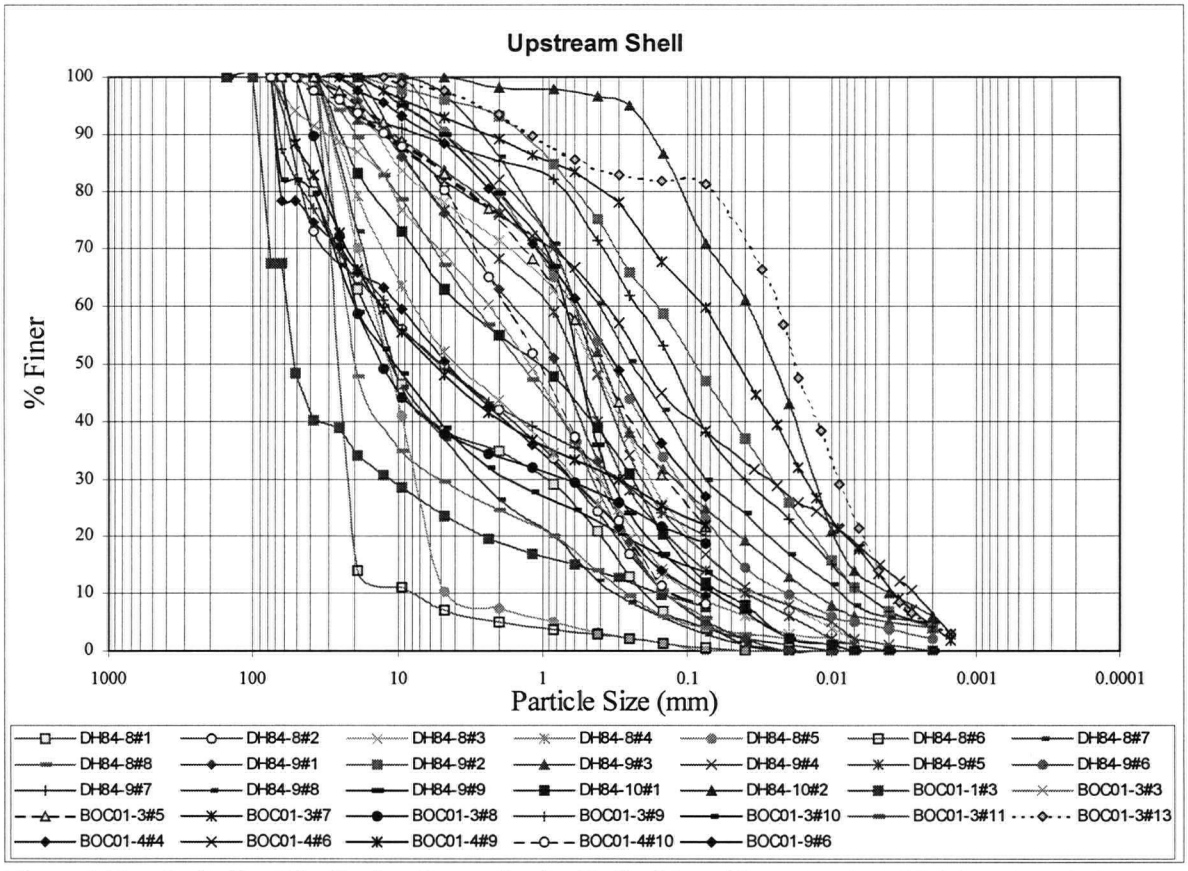

Figure 5.20: Grain Size Distribution Curves for the Shell of Coquitlam Dam (provided by BC Hydro)

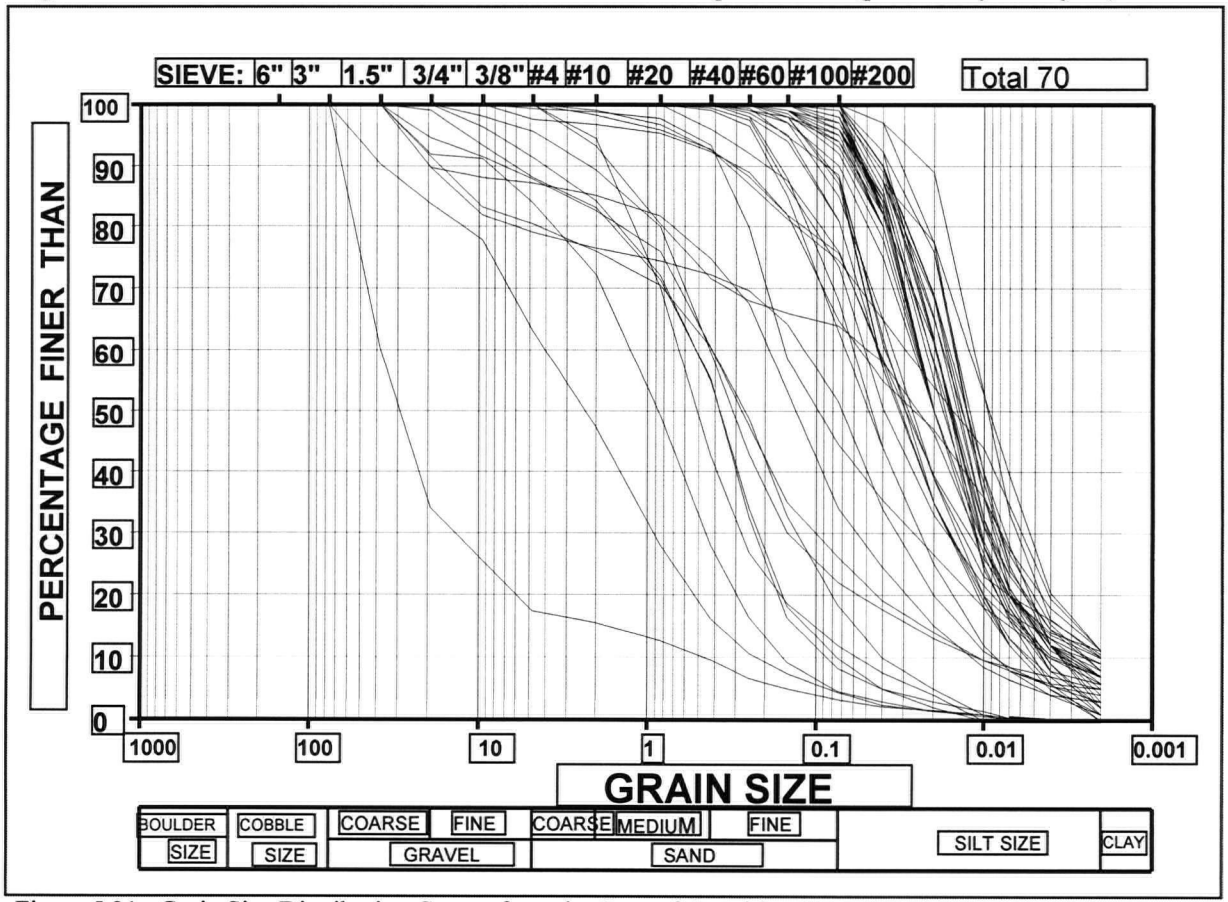

Figure 5.21: Grain Size Distribution Curves from the Core of Coquitlam Dam (provided by BC Hydro)

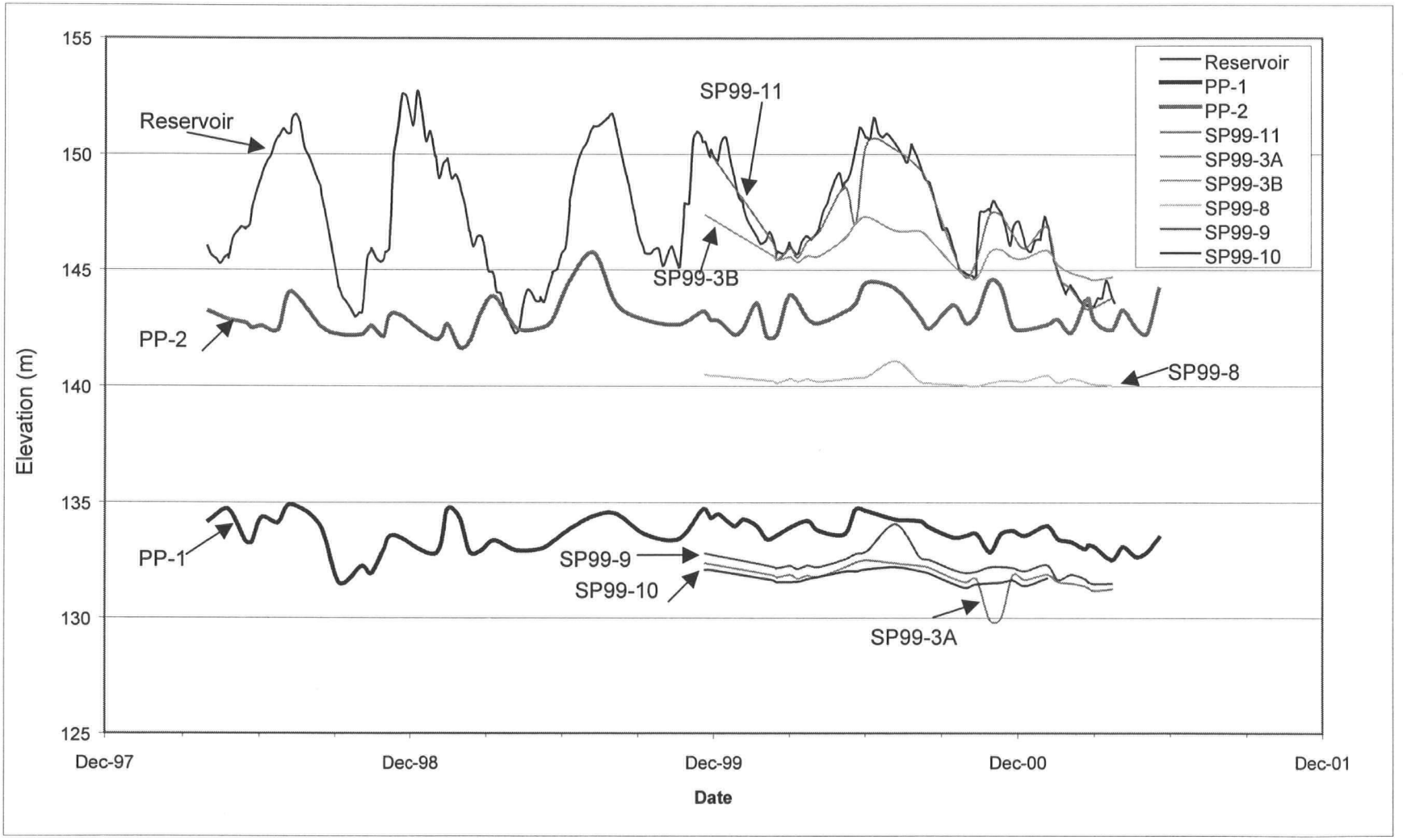

Figure 5.22: Piezometeric Elevations Through Section A-A (data provided by BC Hydro)

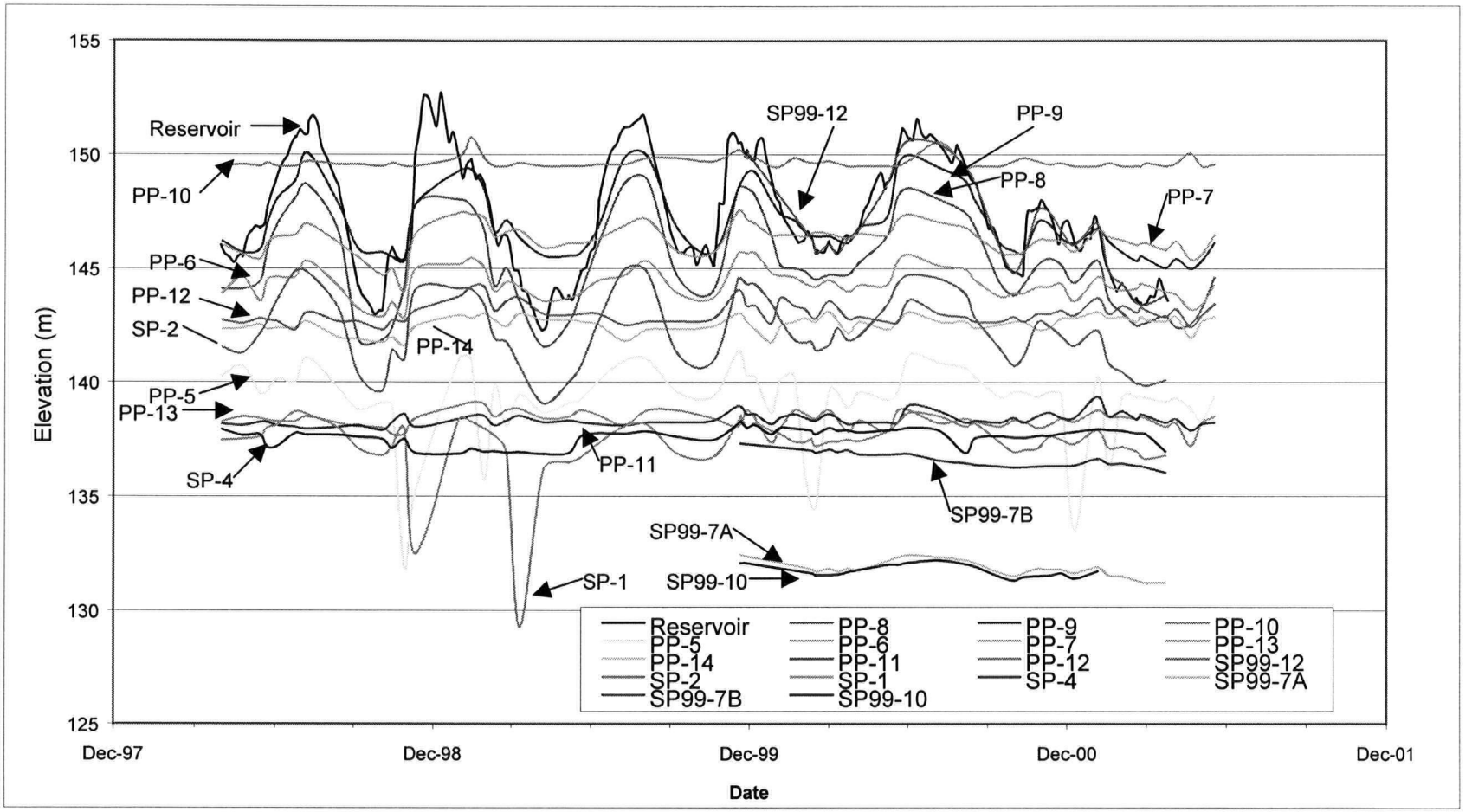

Figure 5.23: Piezometeric Elevations Through Section B-B (data provided by BC Hydro)

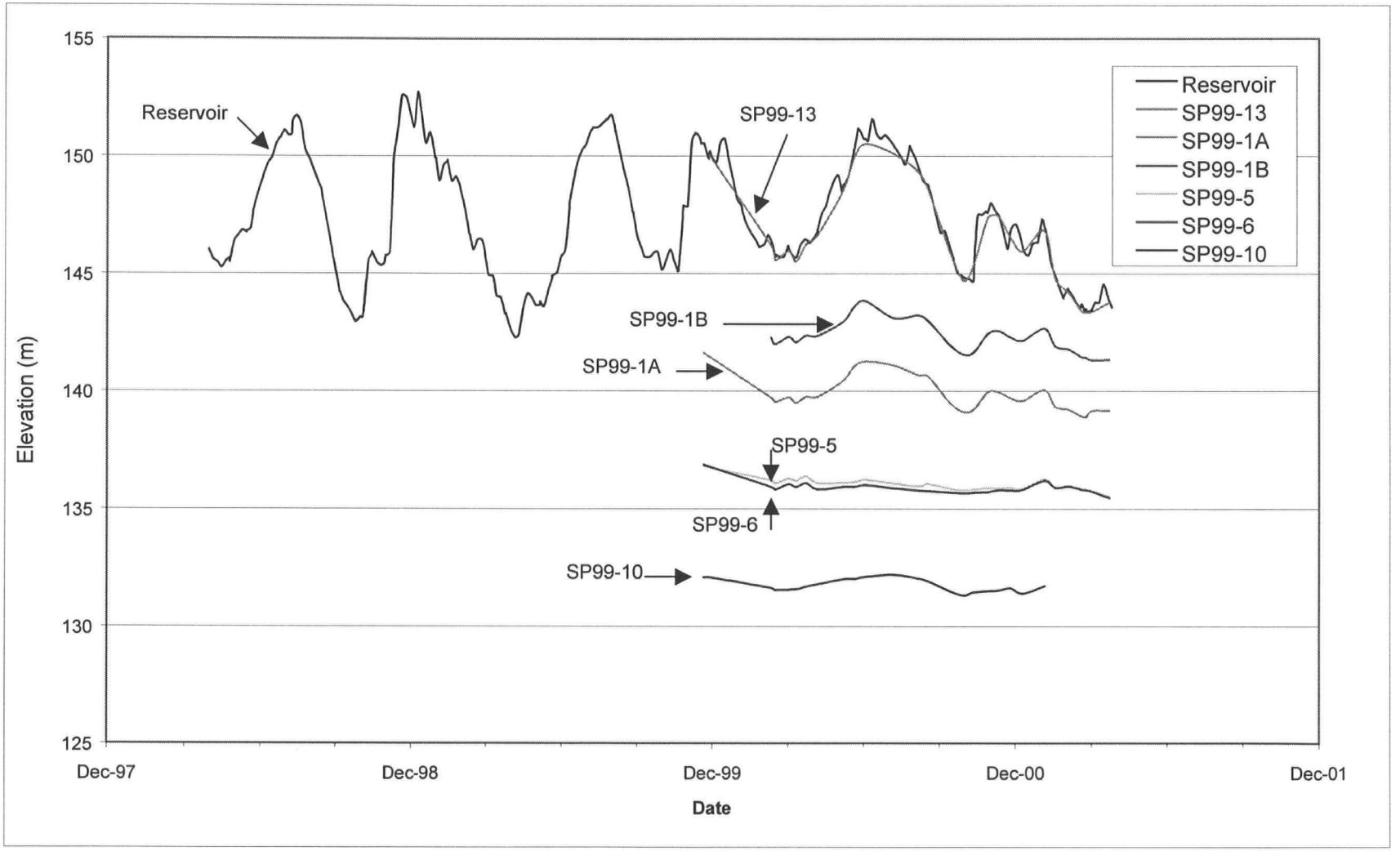

Figure 5.24: Piezometeric Elevations Through Section C-C (data provided by BC Hydro)

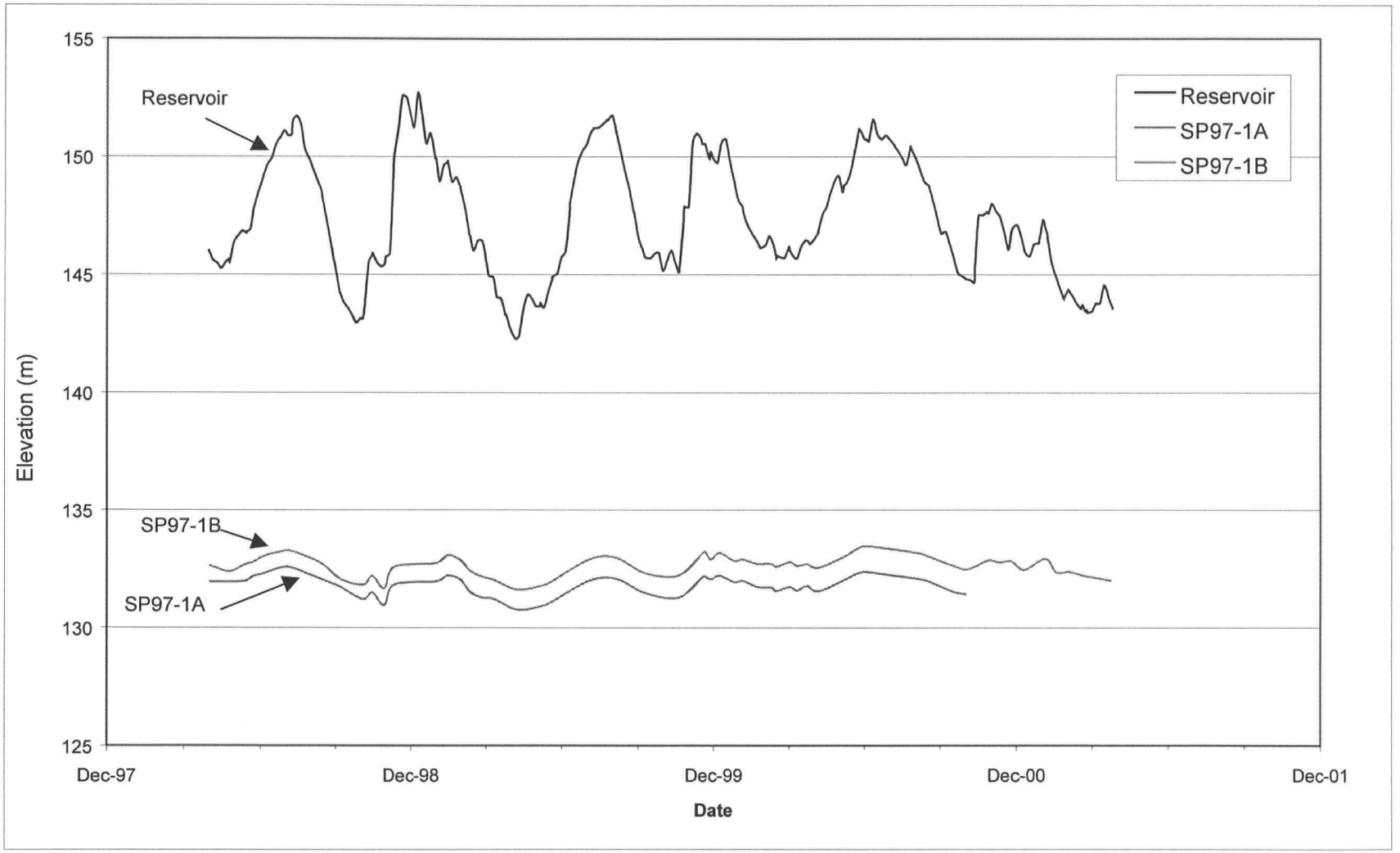

Figure 5.25: Piezometeric Elevations on the West Abutment (data provided by BC Hydro)

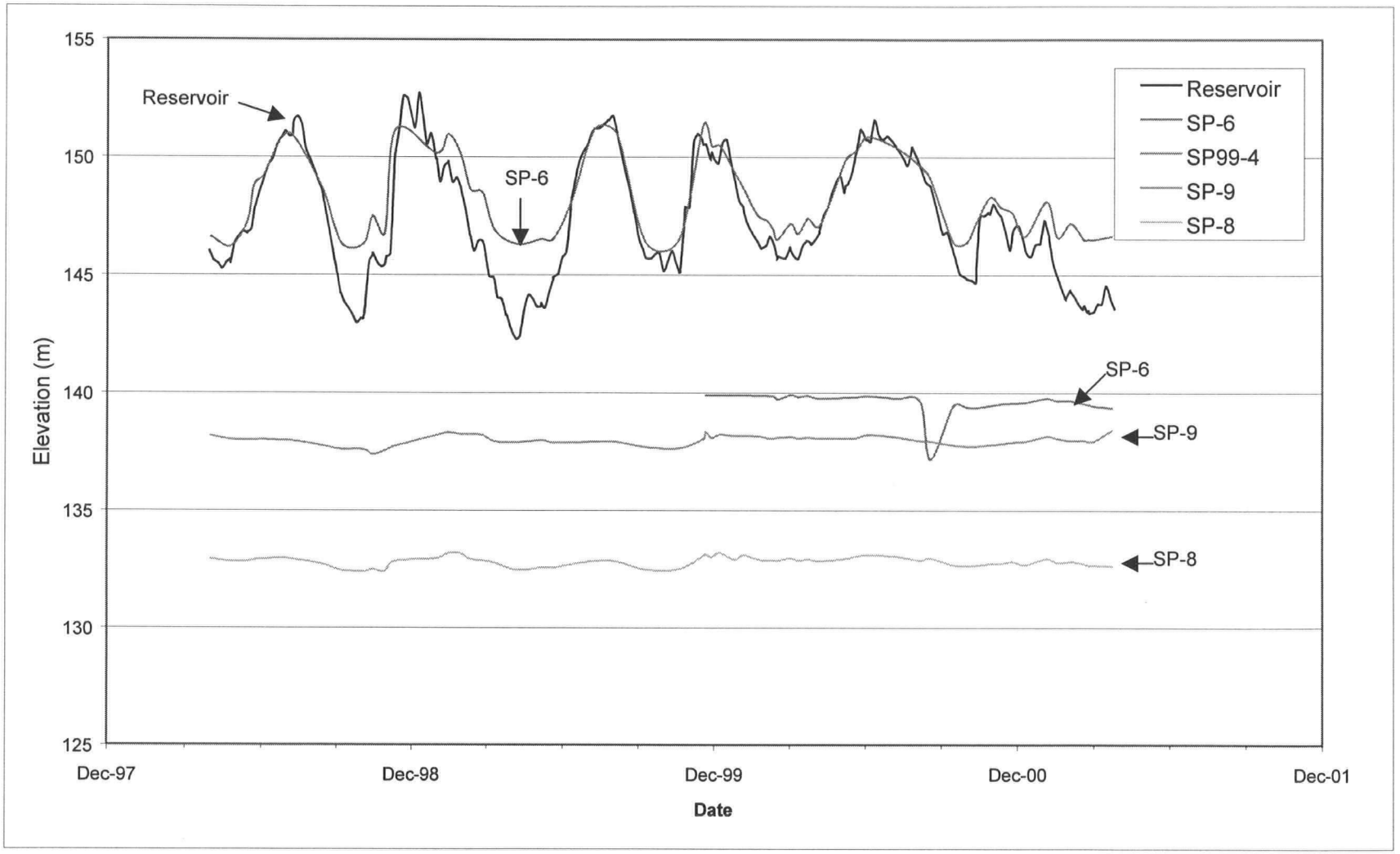

Figure 5.26: Piezometeric Elevations on the East Abutment (data provided by BC Hydro)

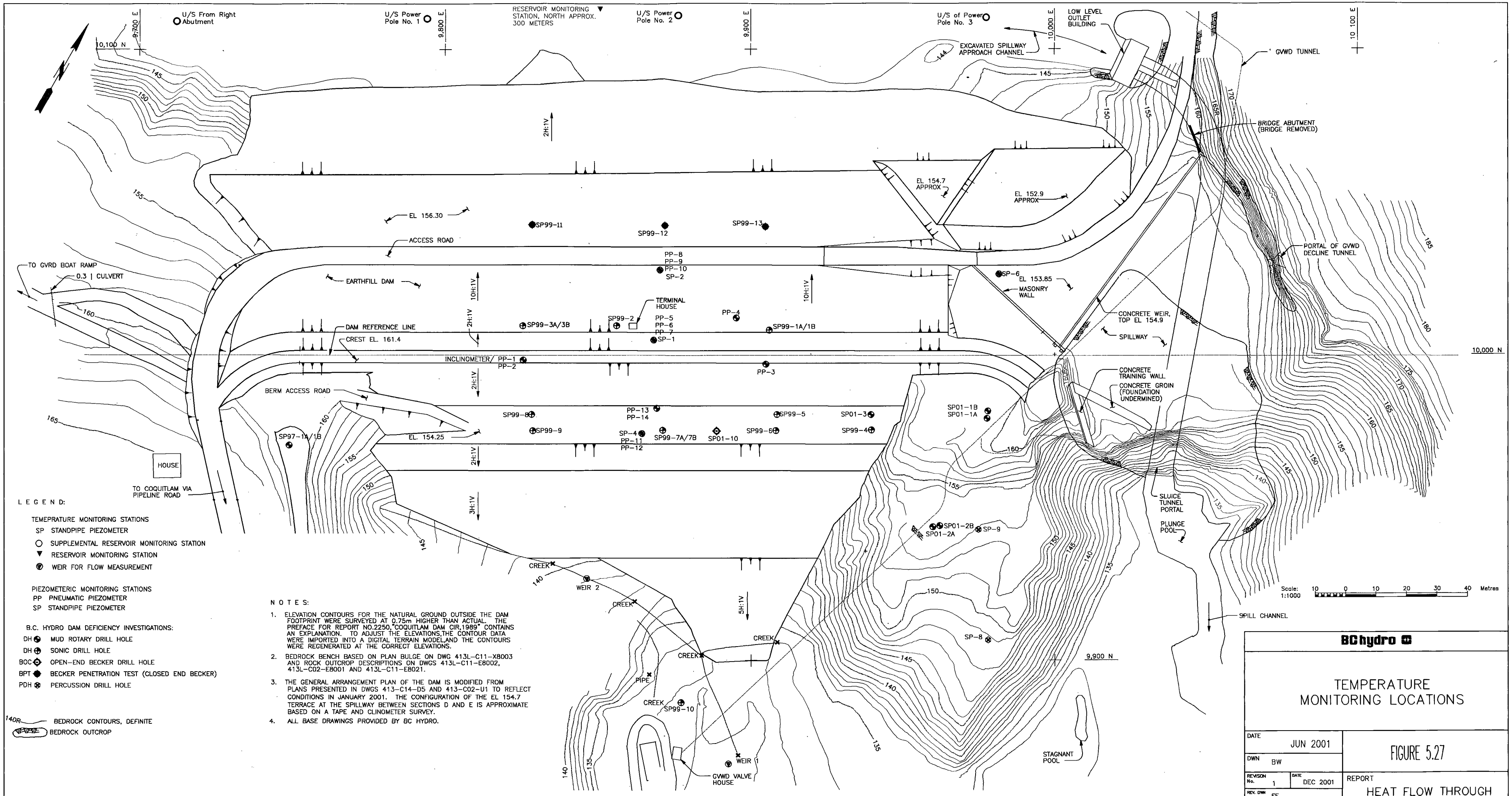

L E G E N D:

TEMEPRATURE MONITORING STATIONS
- SP STANDPIPE PIEZOMETER
- SUPPLEMENTAL RESERVOIR MONITORING STATION
- RESERVOIR MONITORING STATION
- WEIR FOR FLOW MEASUREMENT

PIEZOMETERIC MONITORING STATIONS
- PP PNEUMATIC PIEZOMETER
- SP STANDPIPE PIEZOMETER

B.C. HYDRO DAM DEFICIENCY INVESTIGATIONS:
- DH MUD ROTARY DRILL HOLE
- DH SONIC DRILL HOLE
- BOC OPEN-END BECKER DRILL HOLE
- BPT BECKER PENETRATION TEST (CLOSED END BECKER)
- PDH PERCUSSION DRILL HOLE

140R BEDROCK CONTOURS, DEFINITE

BEDROCK OUTCROP

N O T E S:

1. ELEVATION CONTOURS FOR THE NATURAL GROUND OUTSIDE THE DAM FOOTPRINT WERE SURVEYED AT 0.75m HIGHER THAN ACTUAL. THE PREFACE FOR REPORT NO.2250,"COQUITLAM DAM CIR,1989" CONTAINS AN EXPLANATION. TO ADJUST THE ELEVATIONS,THE CONTOUR DATA WERE IMPORTED INTO A DIGITAL TERRAIN MODEL,AND THE CONTOURS WERE REGENERATED AT THE CORRECT ELEVATIONS.
2. BEDROCK BENCH BASED ON PLAN BULGE ON DWG 413L-C11-X8003 AND ROCK OUTCROP DESCRIPTIONS ON DWGS 413L-C11-E8002, 413L-C02-E8001 AND 413L-C11-E8021.
3. THE GENERAL ARRANGEMENT PLAN OF THE DAM IS MODIFIED FROM PLANS PRESENTED IN DWGS 413-C14-D5 AND 413-C02-U1 TO REFLECT CONDITIONS IN JANUARY 2001. THE CONFIGURATION OF THE EL 154.7 TERRACE AT THE SPILLWAY BETWEEN SECTIONS D AND E IS APPROXIMATE BASED ON A TAPE AND CLINOMETER SURVEY.
4. ALL BASE DRAWINGS PROVIDED BY BC HYDRO.

BC hydro

TEMPERATURE MONITORING LOCATIONS

DATE	JUN 2001	FIGURE 5.27	
DWN	BW		
REVISION No.	1	DATE	DEC 2001
REV. DWN	FE	REPORT	HEAT FLOW THROUGH EARTH DAMS 113
REVISION No.		DATE	

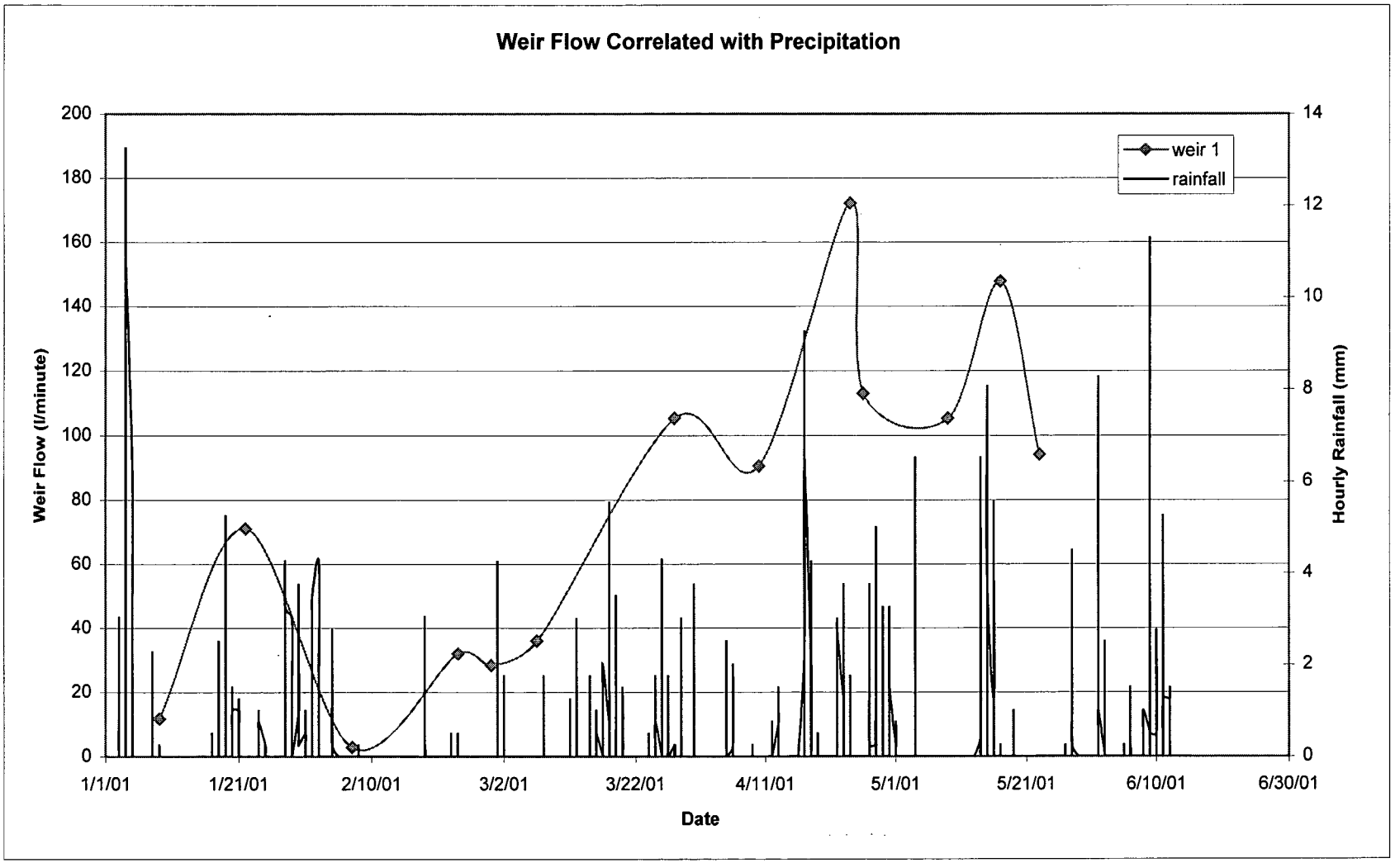

Figure 5.28: Weir Flow Measurements Correlated with Precipitation at Coquitlam Dam (data provided by BC Hydro)

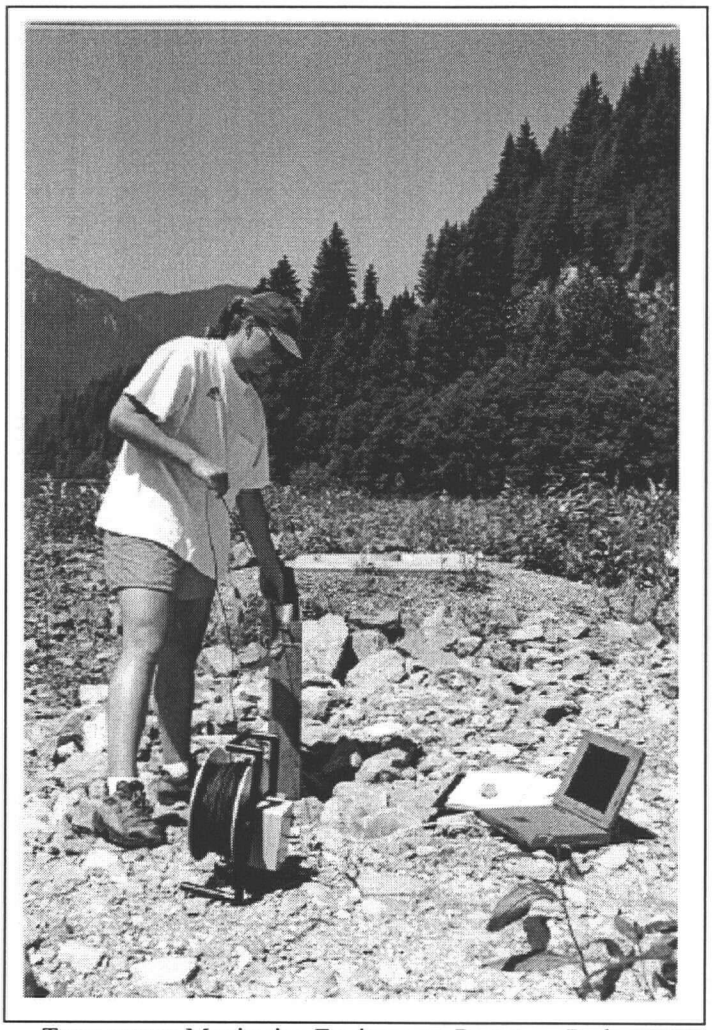

Figure 5.29: Temperature Monitoring Equipment - Prototype Probe

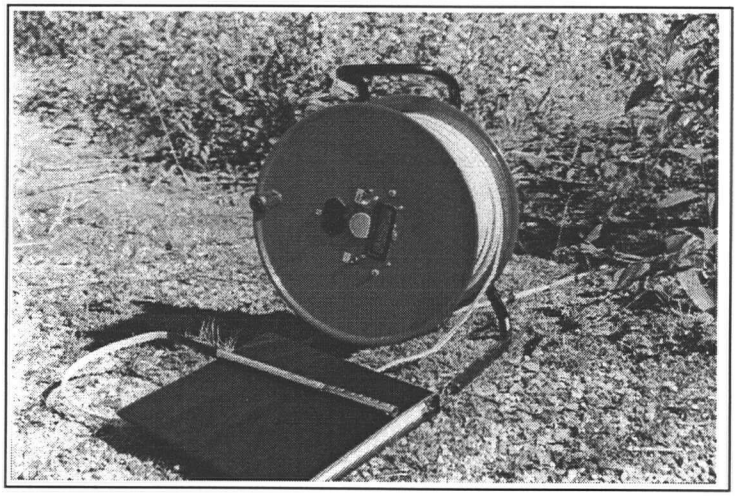

Figure 5.30: Temperature Monitoring Equipment - BC Hydro Probe

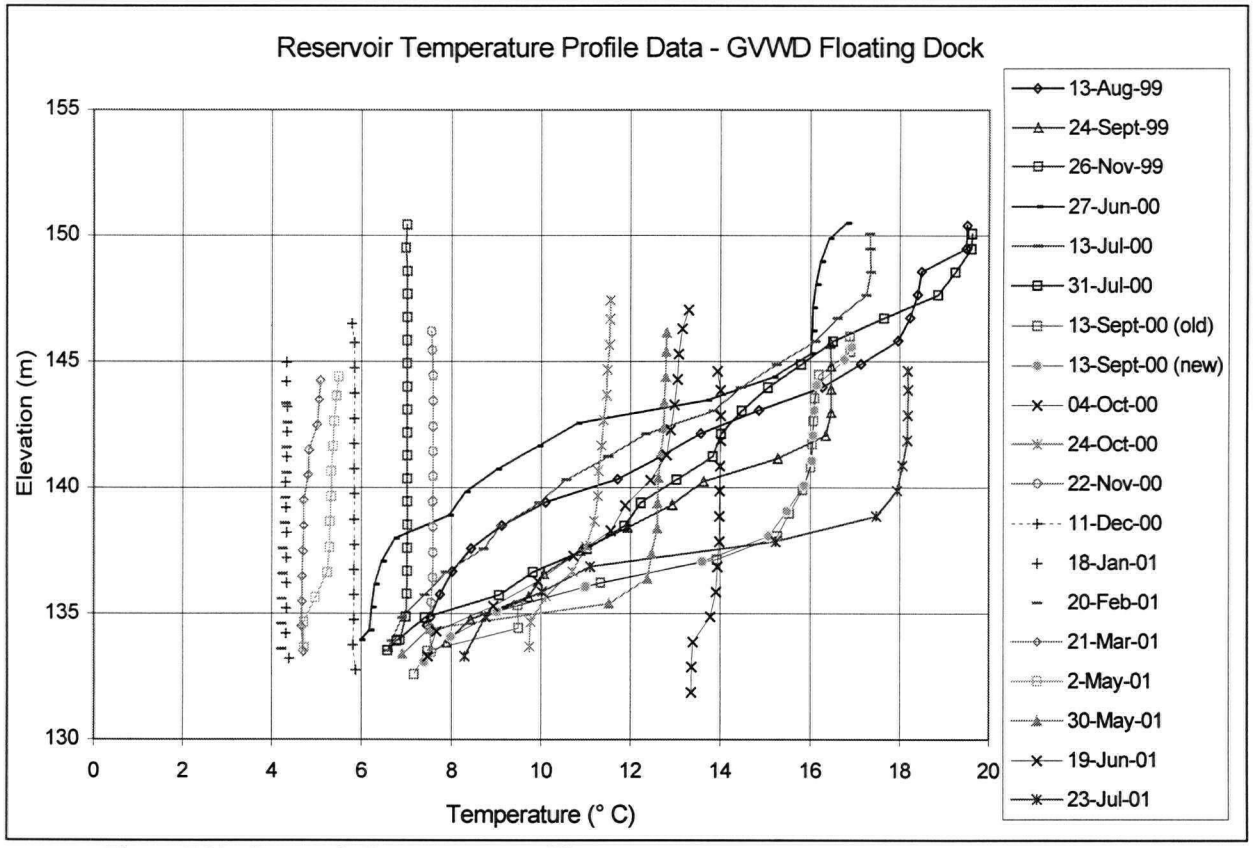

Figure 5.31: Reservoir Temperature Profiling

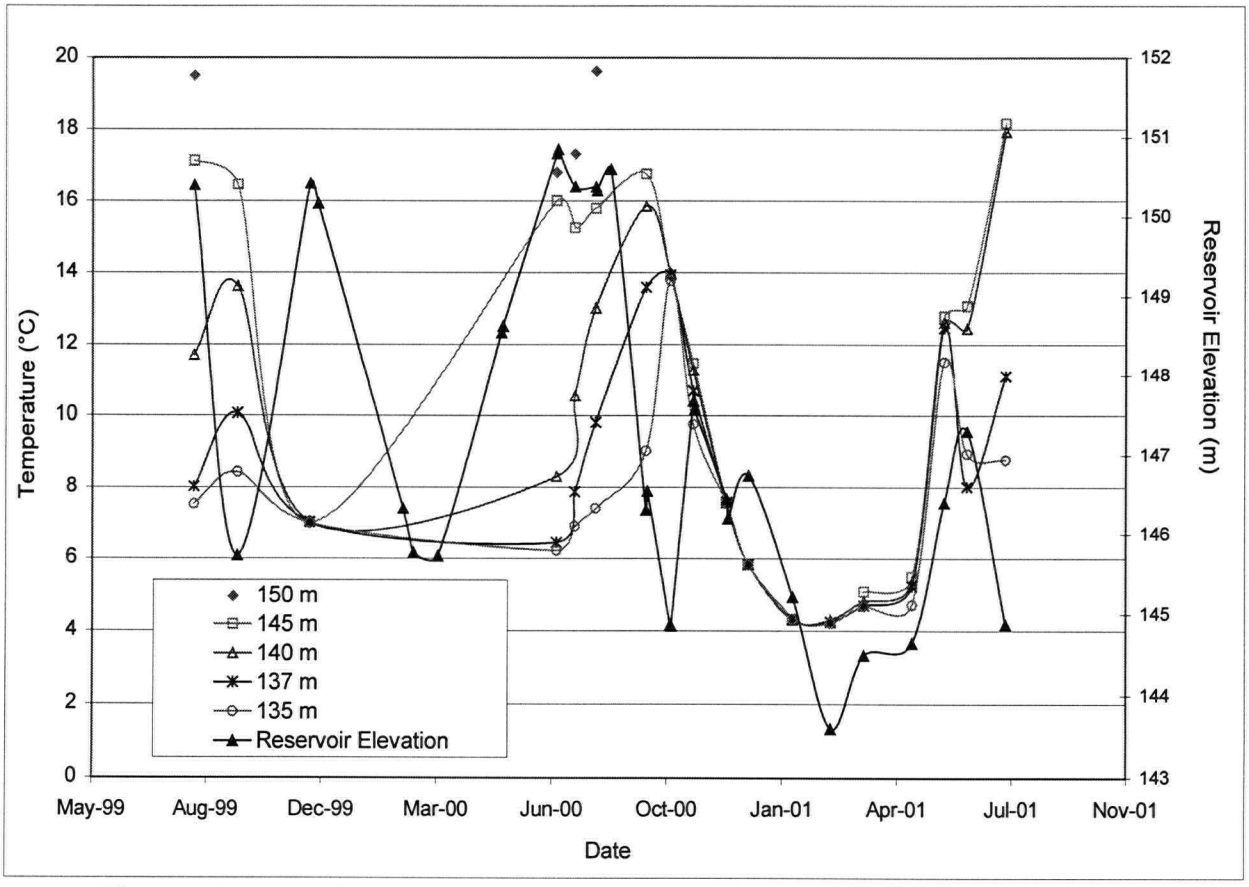

Figure 5.32: Reservoir Annual Temperature Monitoring at Selected Elevations

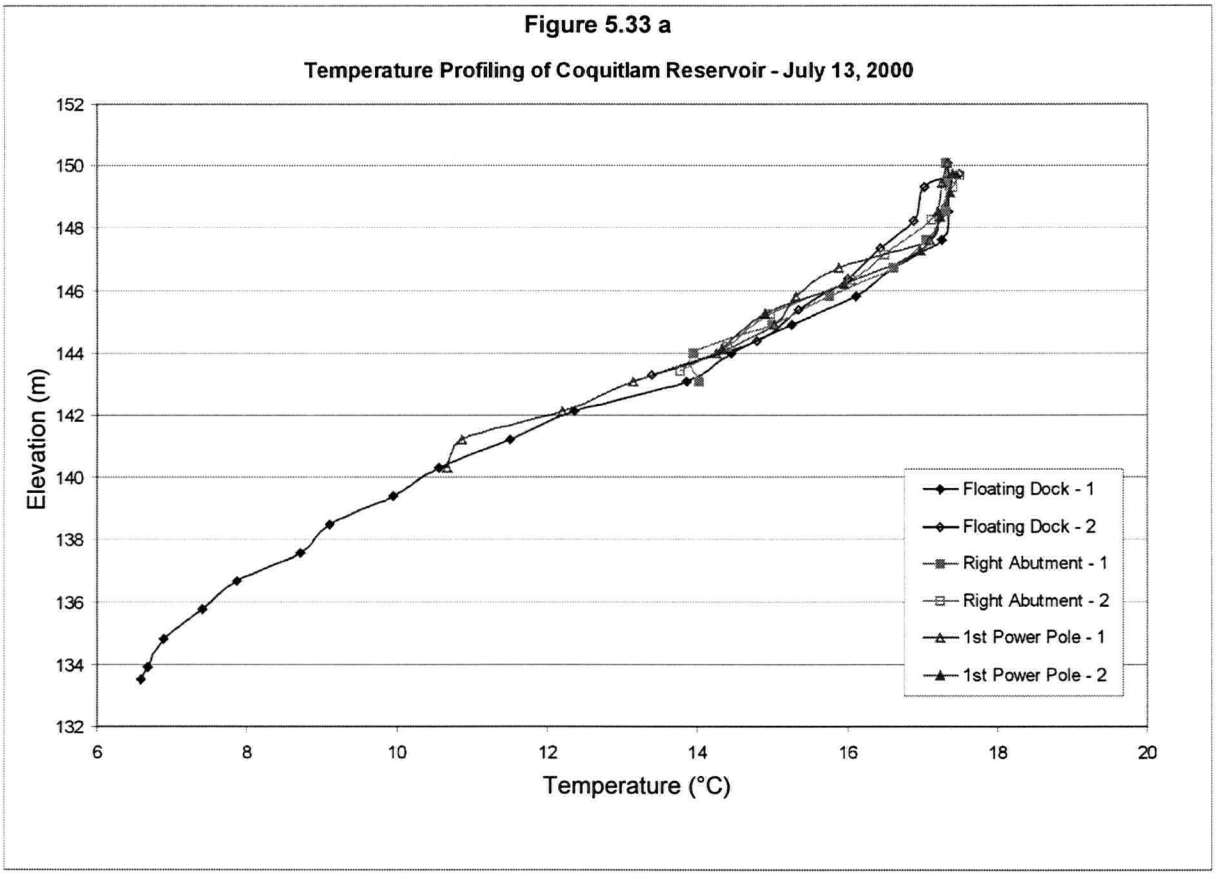

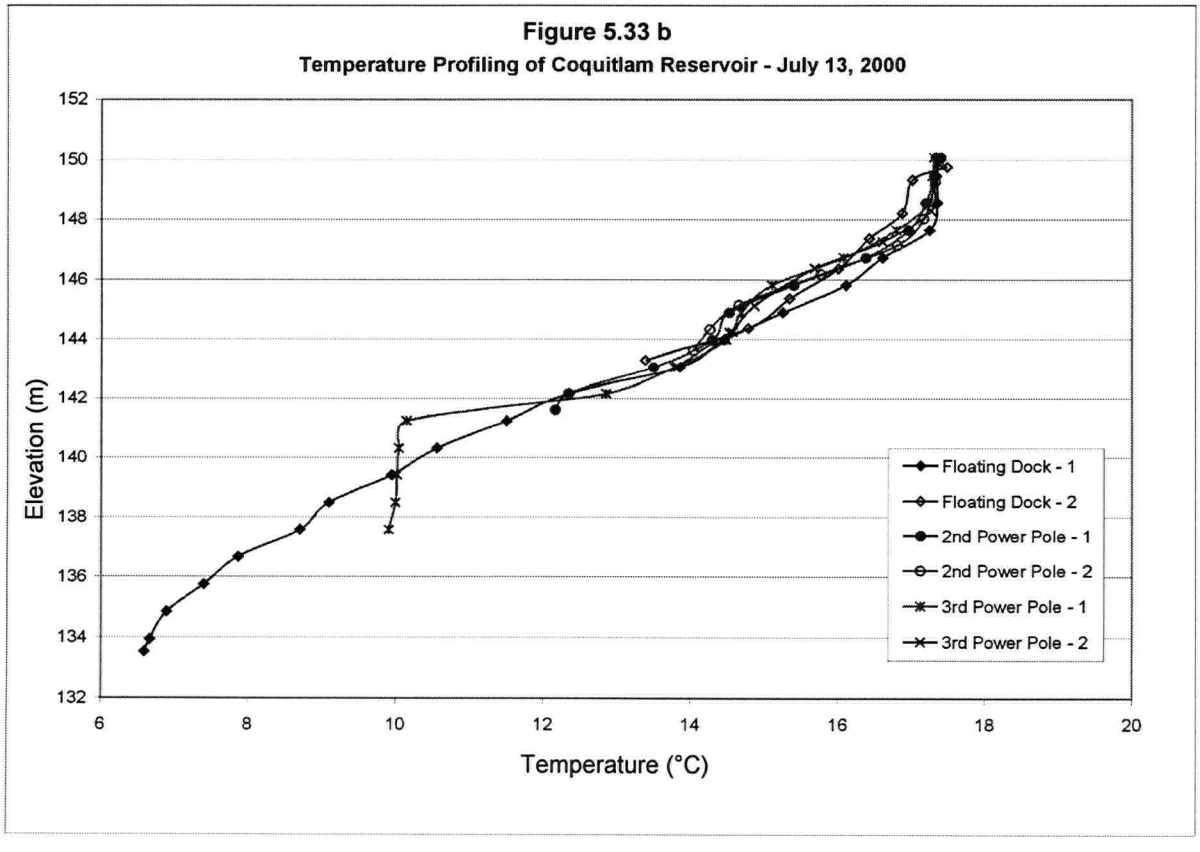

Figure 5.33: Supplemental Reservoir Temperature Profiling

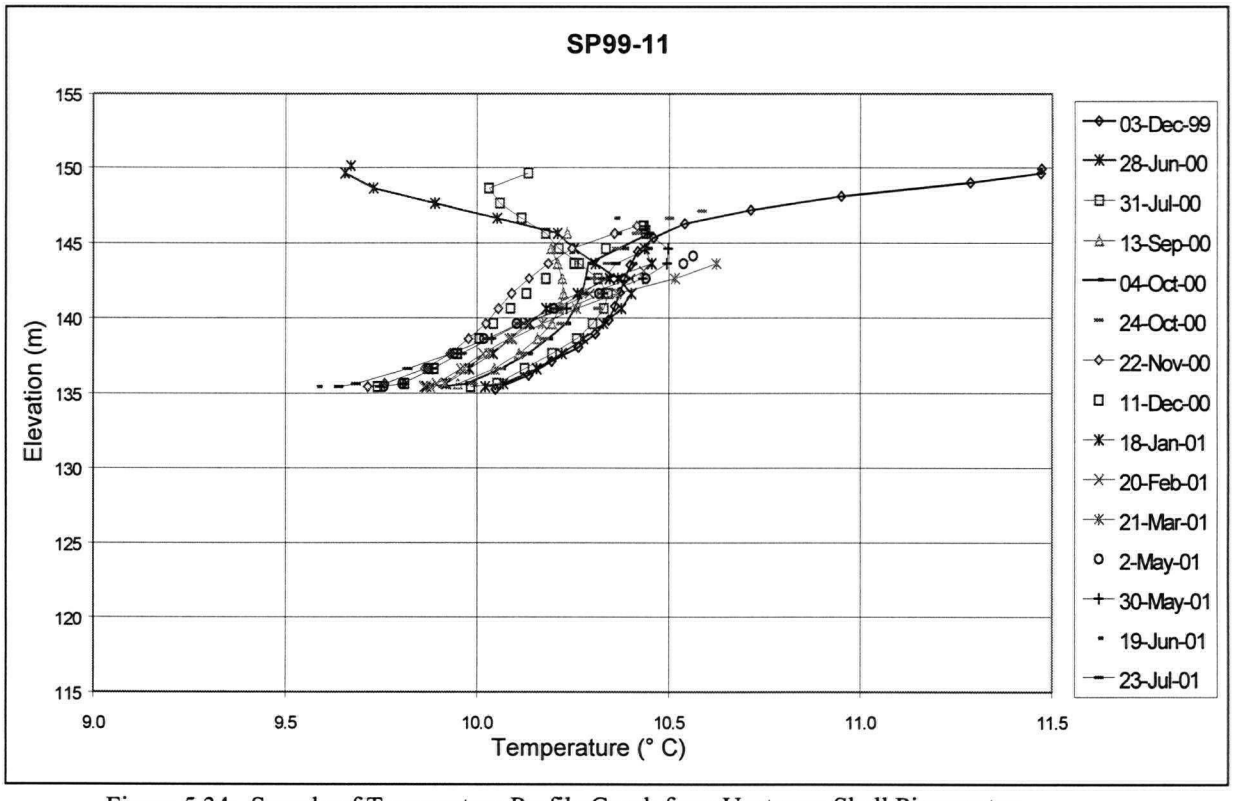

Figure 5.34: Sample of Temperature Profile Graph from Upstream Shell Piezometer

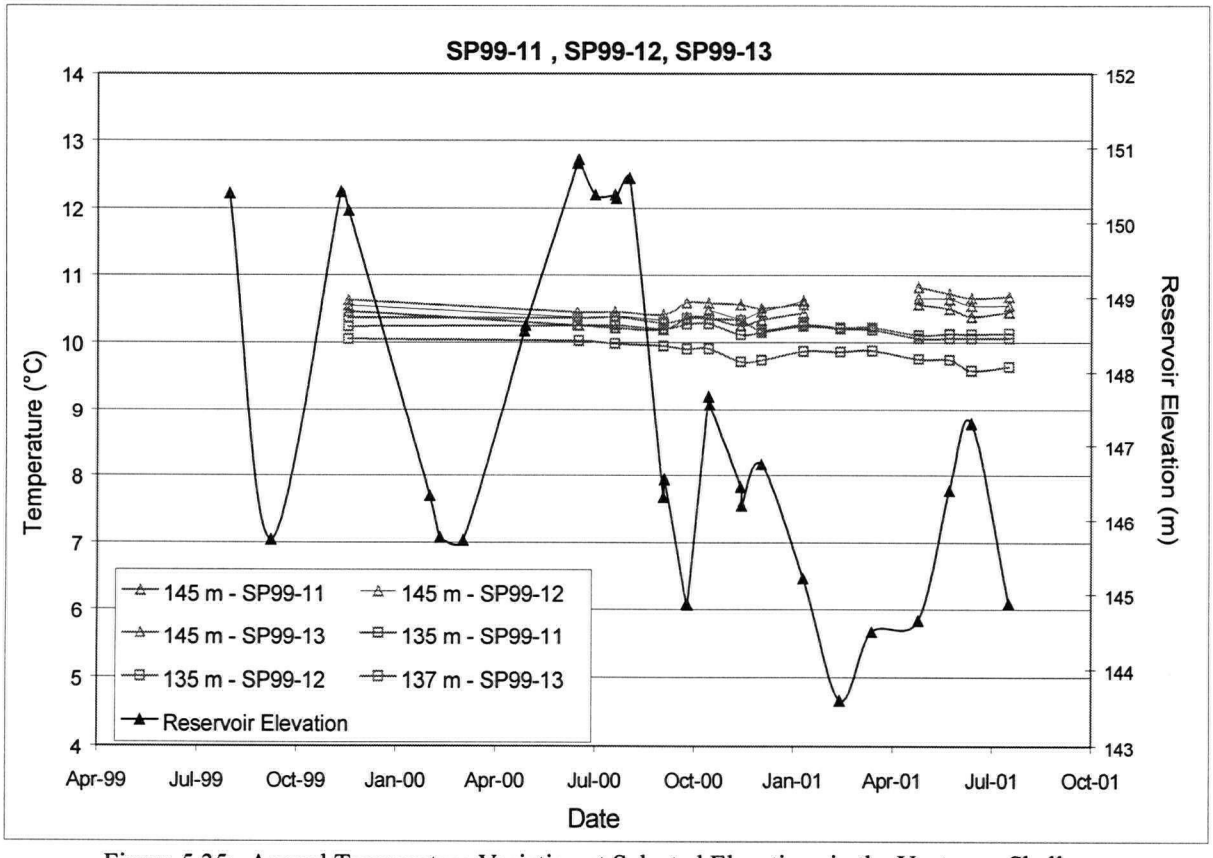

Figure 5.35: Annual Temperature Variation at Selected Elevations in the Upstream Shell

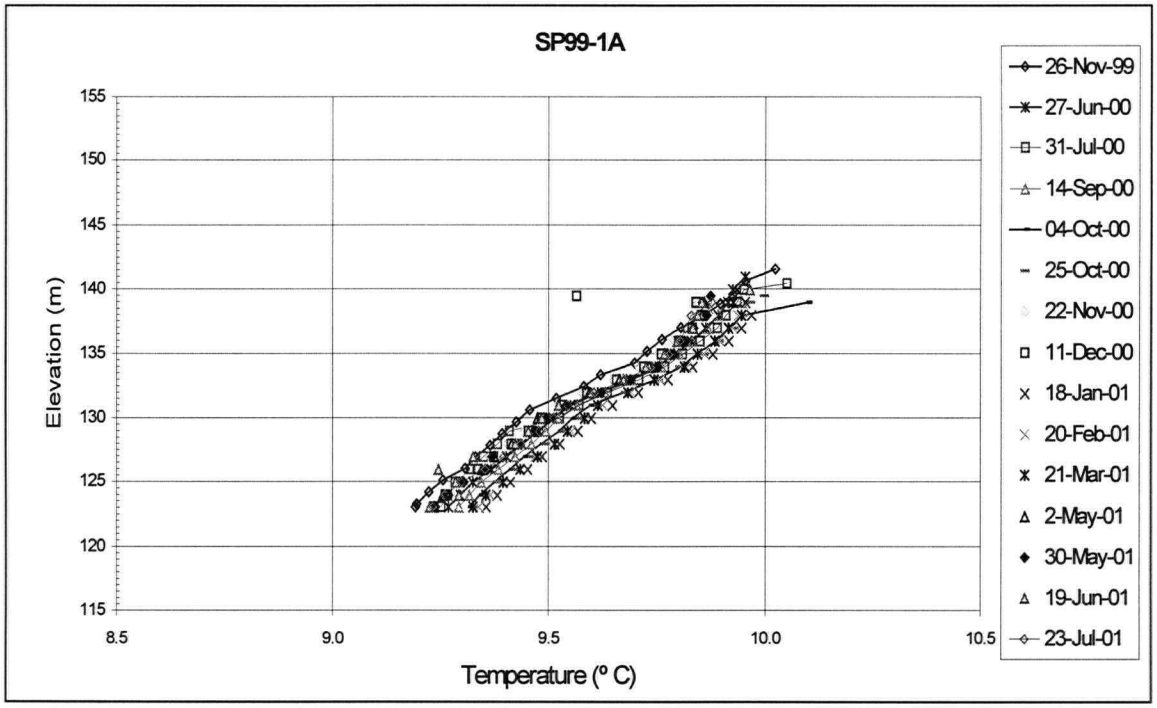

Figure 5.36: Sample of Temperature Profile Graph from Upstream Core Piezometers

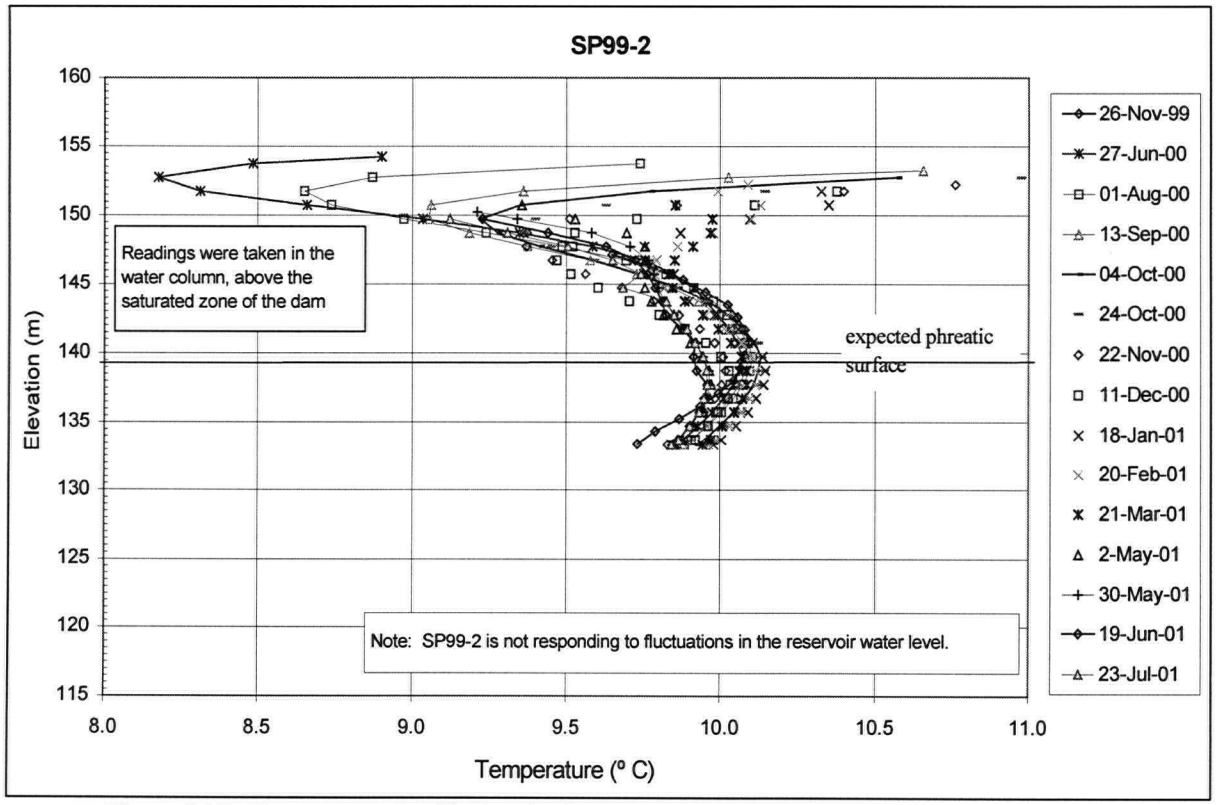

Figure 5.37: Temperature Profile Graph of SP99-2

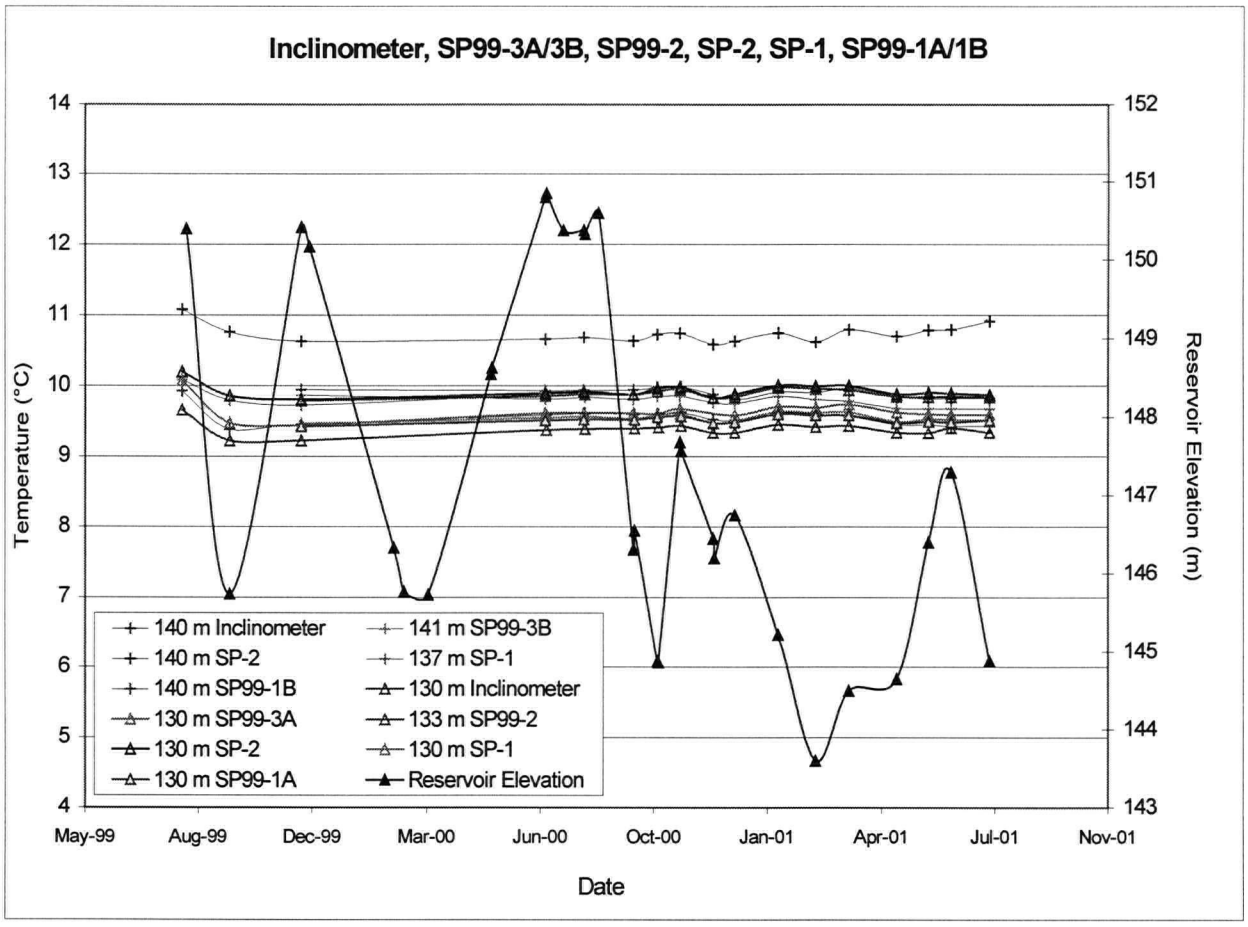

Figure 5.38: Annual Temperature Readings in Upstream Core Piezometers at Selected Elevations

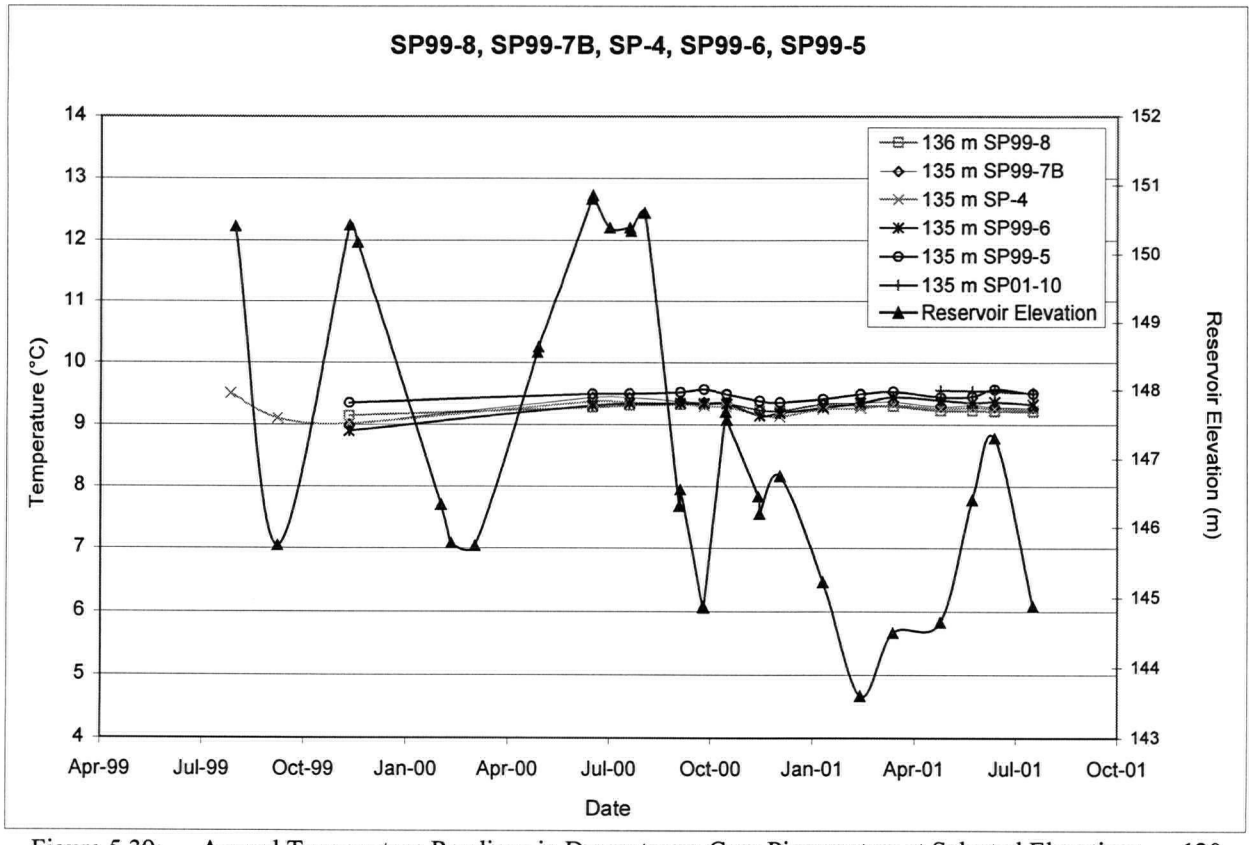

Figure 5.39: Annual Temperature Readings in Downstream Core Piezometers at Selected Elevations

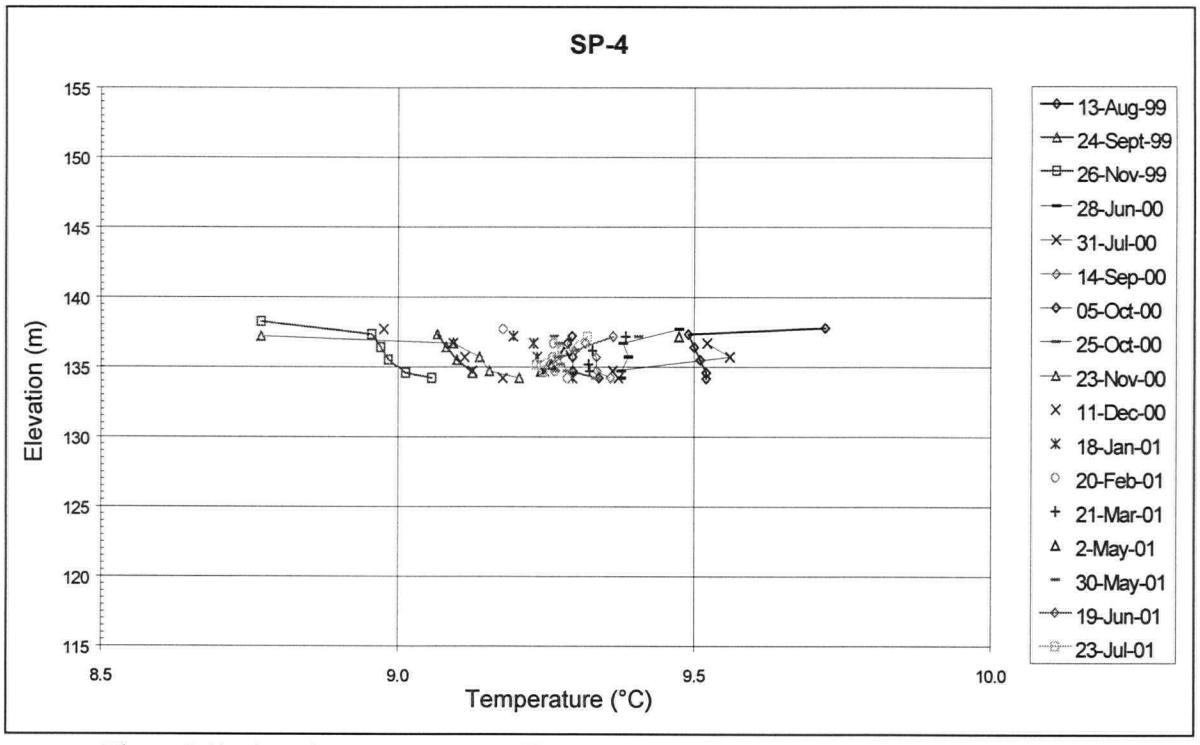

Figure 5.40: Sample Temperature Profile Graph from Downstream Core Piezometers

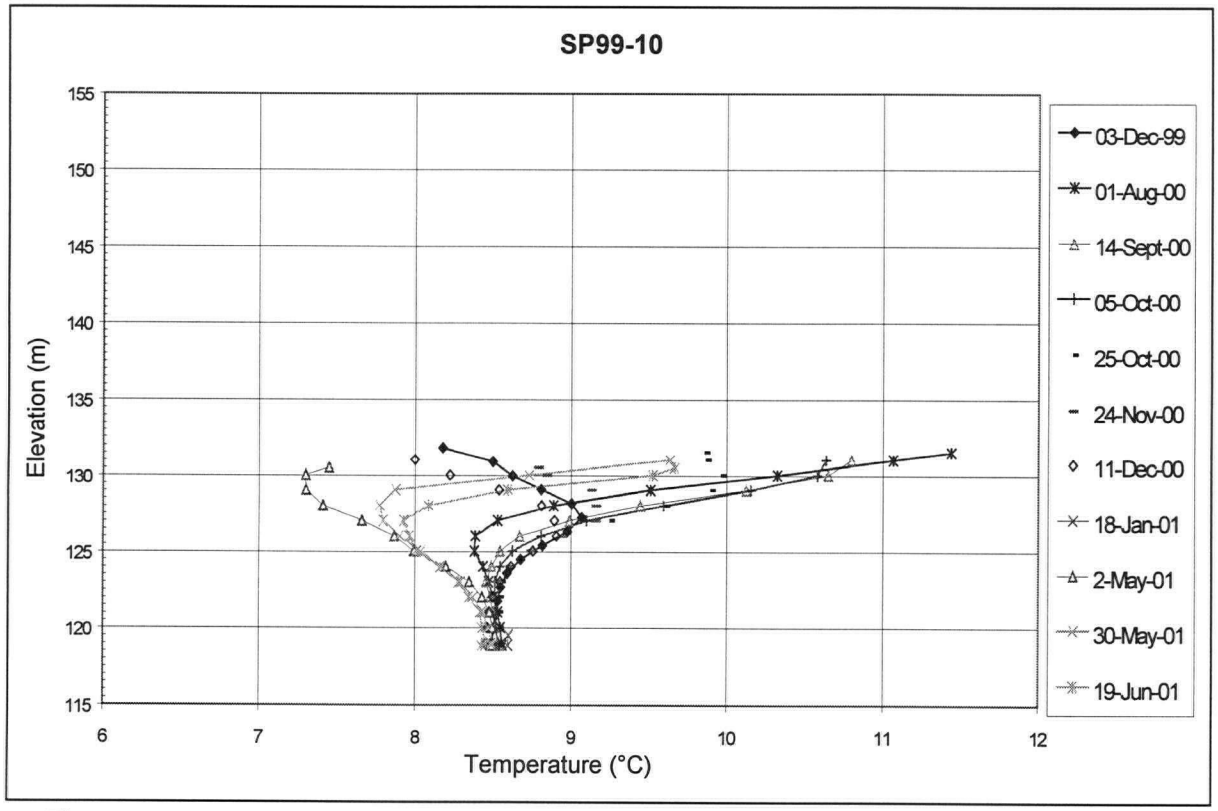

Figure 5.41: Temperature Profile Graph from SP99-10

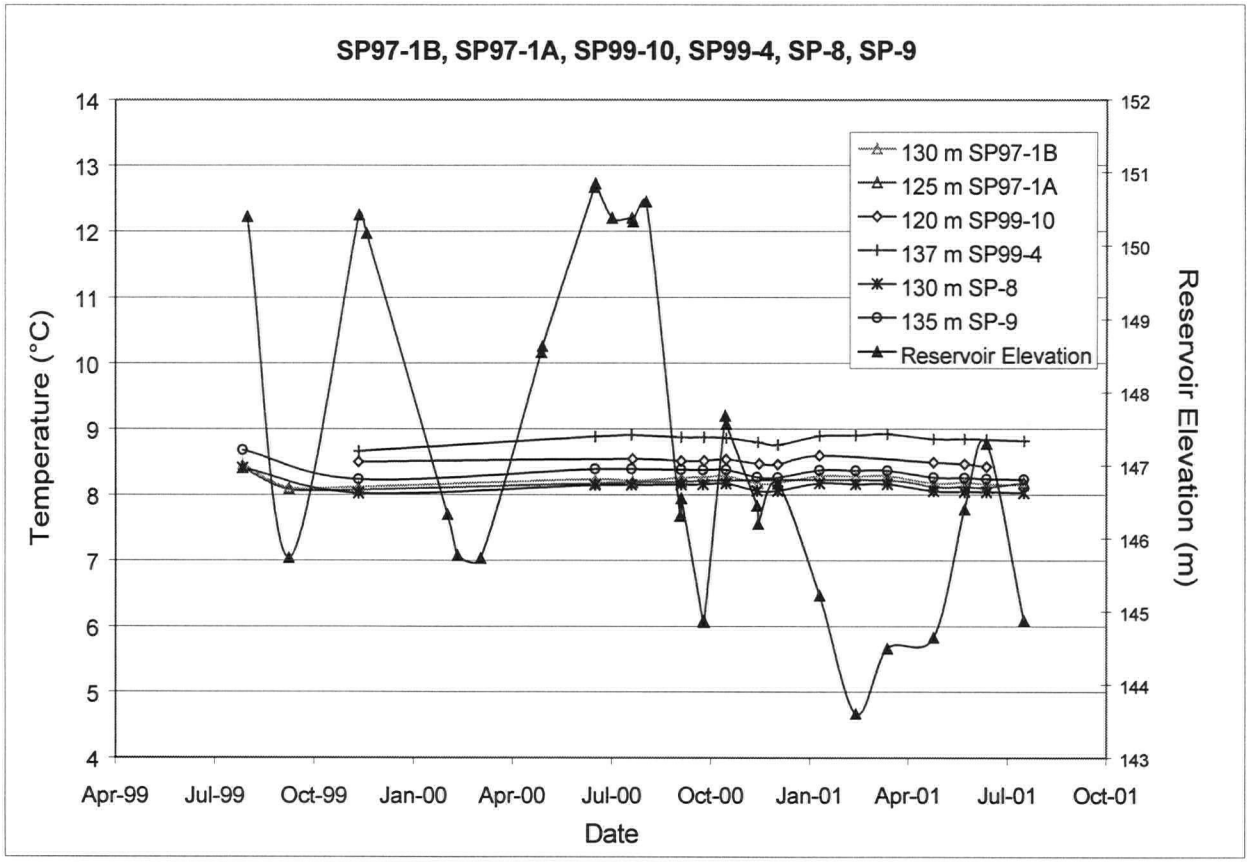

Figure 5.42: Annual Temperature Readings in Abutment and Downstream Toe Piezometers at Selected Elevation

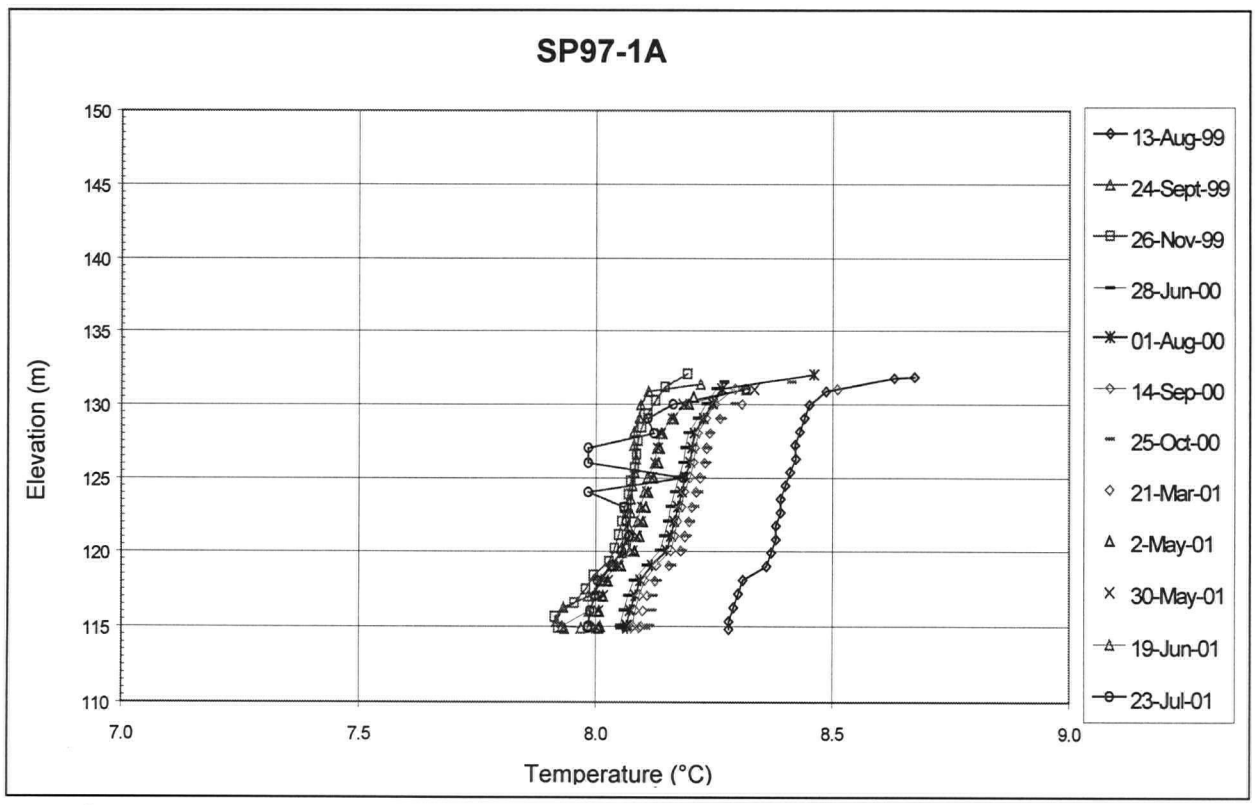

Figure 5.43: Sample Temperature Profile Graph from Abutment Piezometers

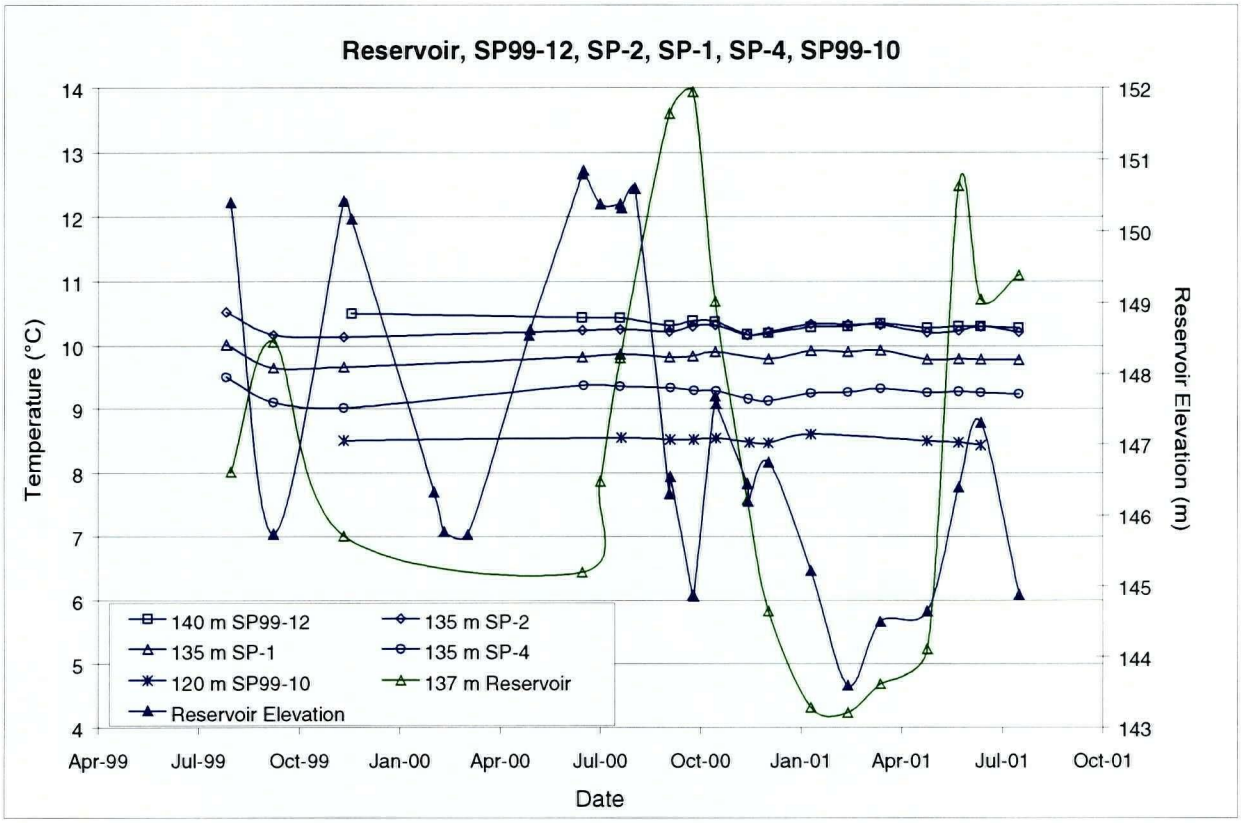

a: Comparison of Upper Elevation Temperatures

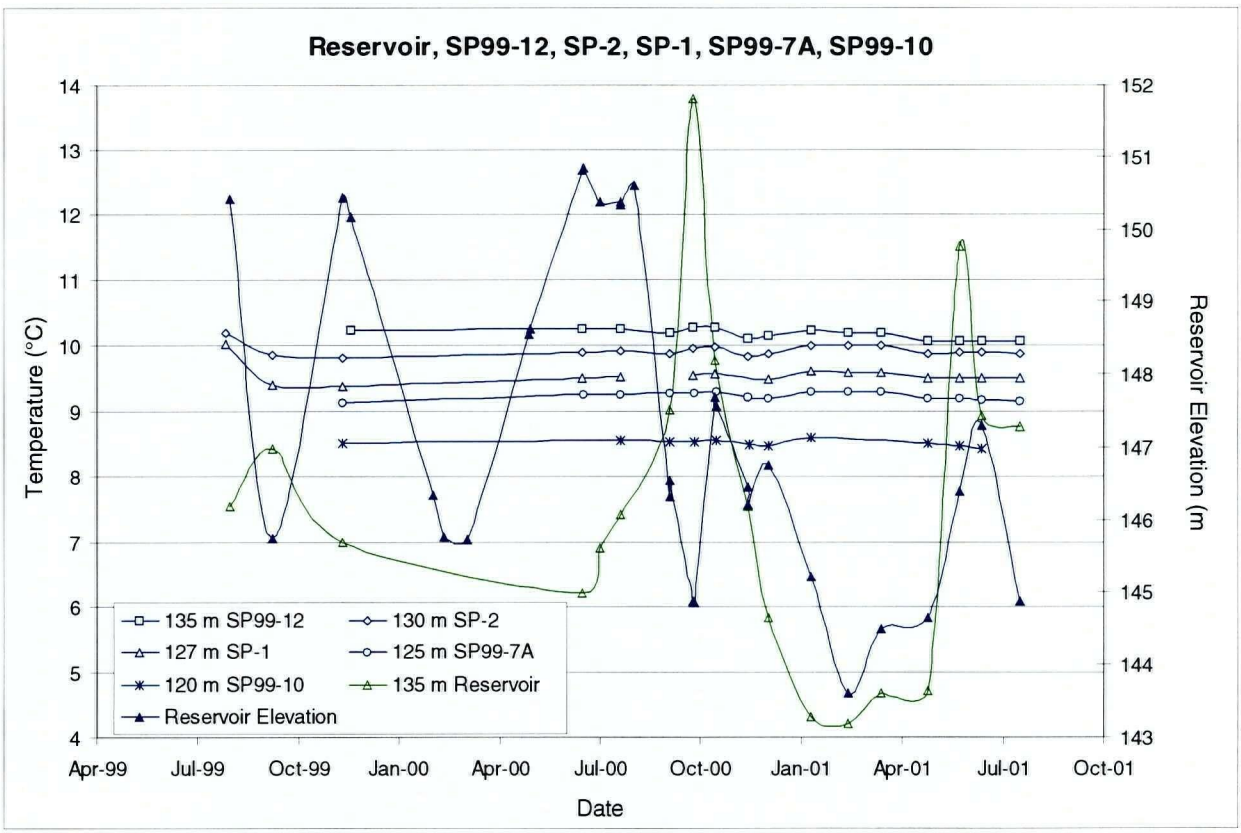

b: Comparison of Lower Elevation Temperatures

Figure 5.44: Annual Temperature Readings at Selected Elevations Along Section B-B

CHAPTER 6: NUMERICAL MODELLING OF COQUITLAM DAM

6.1 INTRODUCTION

The numerical models described, used, and verified in Chapter 3 have been applied to model seepage and heat transport through BC Hydro's Coquitlam Dam. The stratigraphic units of the dam described in Chapter 5 will be used to create the numerical model. The temperature monitoring program, initiated by BC Hydro at Coquitlam Dam was described and the data was also presented in Chapter 5. This data will be used to compare and evaluate the results obtained from the numerical modelling. Section 6.2 describes the seepage model setup for Coquitlam Dam. Section 6.3 presents the results of the seepage analysis. Section 6.4 discusses the problems encountered during the seepage modelling. Section 6.5 describes the model used to simulate heat propagation through the dam, with CTRAN/W. Section 6.6 presents the results of the model. Section 6.7 discusses problems encountered during the heat transport modelling of Coquitlam Dam. Section 6.8 summarizes the model results and presents conclusions.

6.2 SEEP/W MODELLING OF COQUITLAM DAM

BC Hydro staff had previously created a SEEP/W model of Coquitlam Dam to analyse the steady state seepage of the dam (Figure 6.1). This model was used as the starting point for the transient seepage analysis required for this thesis. The cross section presented in Figure 6.1 is taken approximately through the centre of the dam, through standpipe piezometers (from upstream to downstream); SP99-12, SP-2, SP-1, SP99-2, SP-7A/7B, SP-4, and SP99-10.

6.2.1 Grid and Stratigraphic Units

The transient seepage analysis was first conducted with the stratigraphic units, and hydraulic conductivity values presented in Figure 6.1. Then units 6A and 6B, (described in subsection 5.4.2) were added. Unit 1 was subdivided into unit 1A and 1B (also described in subsection 5.4.2), and the infinite elements on the upstream and downstream sides were removed. The elements were removed, as the grid for the SEEP/W and CTRAN/W analysis must be identical, and CTRAN/W can have problems with the use of infinite elements. Figure 6.2 presents the grid and cross section showing the stratigraphic units used for the SEEP/W analysis.

6.2.2 Properties of Stratigraphic Units

SEEP/W requires the user to specify the following information about each stratigraphic unit used in the model:

- hydraulic conductivity as a function of pressure;
- volumetric water content as a function of pressure; and
- hydraulic conductivity ratio (k_y/k_x).

Table 5.2 listed the dam fill materials and hydraulic properties. Table 6.1 lists the range of properties used in the seepage modelling of Coquitlam Dam.

6.2.3 *Hydraulic Boundary Conditions*

The upstream boundary, along the dam face was assigned a time function of total head values based on reservoir elevation data recorded between April 1998 and April 2001 using BC Hydro's advanced data acquisition system (ADAS). Figure 6.3 graphically shows the variation of reservoir elevation recorded by ADAS with respect to time, in comparison to the head versus time data entered into SEEP/W.

A constant head of 131 to 132 metres was used at the downstream toe of the dam, to simulate the constant water level in the fish pond at the downstream toe area of Coquitlam Dam.

Coquitlam Dam was built in the present day valley of the Coquitlam River. However, a buried valley exists below the dam, and as a result, there is some recharge of water into the larger valley (on a regional scale). The concept of regional aquifer recharge in the area of Coquitlam Dam, from the reservoir, is supported by the more or less constant piezometric levels measured in Units 1A and 1B (GVWD's nested pair of wells upstream of the dam (GVWD, 1997), and from water level data collected from SP97-1A). This means that water from the reservoir not only flows through the dam, but also flows into the lower aquifer. To try and simulate this loss of water into the lower aquifer, in the SEEP/W model, a constant flux of water (i.e. removal of water from the model) was specified along the base of the model to simulate water flowing out of the base. A constant flux of -5E-7 to -1E-9 cubic metres per second was applied along the base of the model. Several model simulations were conducted with a variable flux out of the base. One variable case assigned a larger flux out of the system in the middle of the dam, where units 6A and 6B exist (the former river bed sediments) and a smaller flux out of the base along the remaining portion of the cells. A second variable case involved a larger flux out of the system from the middle portion of the dam (6A/6B) to the downstream boundary, and a smaller flux out of the base on the upstream side.

Along the downstream face of the dam a boundary water flux out of the model was applied and the "review" option based on water elevation was selected (see section 3.2 and 3.3 for additional details). This permits the program to calculate a variable flux out of the boundary based on changes in reservoir elevation (pressure/hydraulic gradient).

6.2.4 *Time Steps*

The time step of 10 days was selected for the analysis, to adequately account for the fluctuating reservoir levels, and seasonal temperature variations. The same time step was used for both the SEEP/W and CTRAN/W analyses. The analysis was run for 438 steps, which is equivalent to 12 years. The seepage analysis period was extended to 12 years, to allow sufficient time for the temperature within the dam to reach quasi steady state conditions, by ensuring that the effects of any arbitrarily assigned initial conditions for the heat transport analysis were eliminated

6.2.5 *Initial Conditions*

Prior to running the transient seepage analysis, a steady state model run was conducted with a fixed reservoir elevation of 146 metres. The total head values at each node, obtained from the steady state analysis, were then used as the initial conditions for the transient analysis. This reduced the total number of time steps required for the dam to reach quasi steady state conditions for the transient analysis.

6.3 SEEP/W RESULTS

Numerous model simulations were conducted in an effort to achieve the best overall hydraulic match to the measured data from Coquitlam Dam. This included comparing measured versus predicted piezometric surfaces in each stratigraphic unit, at both high and low reservoir elevations, through cross section B (Figure 5.11). Measured piezometric data from Coquitlam Dam, used for the comparisons, is presented on Figure 6.4. Table 6.2 lists for each model run the hydraulic properties, and any other notes that differentiate one model simulation from the other. Piezometric elevation data from selected model runs and time increments, that correspond to high and low reservoir elevations, and to monitoring elevations within the dam, were plotted and compared to measured data. Representative samples of the comparison graphs are presented on Figure 6.5 through Figure 6.10.

Figure 6.5, Figure 6.7, and Figure 6.9 compare the measured and predicted piezometric elevations for Coquitlam Dam during a high reservoir stage, 151 metres. Similarly, Figure 6.6 and Figure 6.8, and Figure 6.10 present and compare data from a low reservoir stage, 144 metres. From these figures, it is apparent that none of the model simulations accurately predicts all the piezometric elevations recorded at Coquitlam Dam. In general, the computer models most accurately predicted the measured piezometric elevations in the lower core, as shown in Figure 6.5c through Figure 6.10c, during both high and low reservoir stages. At the same time, the piezometric elevation in the middle and upper portion of the core were under predicted (i.e. lower than the measured elevation), as is apparent in Figure 6.5a and Figure 6.5b, through Figure 6.10a and Figure 6.10b. Meanwhile, the piezometric elevations in the foundation units were over predicted (i.e. higher than the measured elevation), as shown in Figure 6.5d through Figure 6.10d.

In an effort to achieve a better hydraulic model for Coquitlam Dam, the input parameters were changed. A better match to the measured values within the core of the dam was achieved as shown by XB-tr.sep (Figure 6.7 and Figure 6.8) by increasing the porosity of the core. However, the improved match within the core came at the cost of an inferior match within the foundation units. Similarly, a better match to the piezometric elevation in the foundation units was achieved in model run XB-tr3.sep (Figure 6.9 and Figure 6.10). This was accomplished by increasing the seepage out of the base of the model (i.e. into the buried valley). However, the predicted piezometric elevations within the core of the dam were further from the measured values.

Although the results from many of the model runs are very similar, the two best overall matches appear to be the simulations identified as XB-mix2 and XB-tr2-25. The piezometric data from model run XB-mix2 are presented on Figure 6.5 and Figure 6.6. The data is also presented on Figure 6.7 and Figure 6.8 for comparison. The piezometric data from model run XB-mix2 tends to be within two metres of the measured data from the core of Coquitlam Dam. However, the predicted piezometric elevation in the foundation unit is still significantly higher (5 to 7 metres) than the measured values. The piezometric data for model run XB-tr2-25 is presented on Figure 6.7 and Figure 6.8. The piezometric data from this model run is approximately within three to four metres of the measured data from the core and the foundation units of Coquitlam Dam.

6.4 PROBLEMS WITH THE SEEPAGE MODELLING

The results presented and discussed in Section 6.3 exemplify the difficulty in achieving an accurate hydraulic model of Coquitlam Dam, using the two dimensional seepage modelling program, SEEP/W.

In an attempt to achieve a better hydraulic match by accounting for the more regional hydraulic conditions that exist at Coquitlam Dam, several model runs were conducted using specified hydraulic head values in the portions of Unit 1B. Although this procedure of including specified head values within a model is not usually done, it has been used to explore potential solutions to the modelling difficulties encountered previously. The hydraulic parameters and distinct boundary conditions used for each of these modelling simulations are presented in Table 6.3. Piezometric elevation data from these model simulations have been plotted and compared to measured elevations in Figure 6.11 and Figure 6.12, for high and low reservoir levels, respectively.

In general, for the high reservoir condition these model simulations provide an improved hydraulic approximation to the measured data within the foundation units of Coquitlam Dam. Some of the simulations provide a reasonable match to the measured data within the lower core. However, in all cases these simulations provide a poor match to the measured data within the downstream portions of the upper and middle core. Simulations labelled, XB-tr2-PB-2h.sep and XB-tr2-PB-2hc.sep provide the best hydraulic match in the foundation units.

The predicted versus measured hydraulic data for the low reservoir condition, are plotted in Figure 6.12. An improved match to the measured data was achieved for the foundation units by using the constant head values in Unit 1B. However, the results provide an inferior match to the measured hydraulic data within the dam core.

Based on the seepage model results presented and described in this section and the previous section (6.3) the two dimensional flow models are unable to provide an accurate simulation of the hydraulic conditions measured at the dam. This is due to the complex geology and flow conditions at Coquitlam Dam. Based on current data from Coquitlam Dam it appears that seepage flow is three dimensional in nature for the following reasons:

- In the vicinity of the dam there appears to be recharge from the reservoir into the lower, regional aquifer. This reduces the flow of water from the reservoir through the dam. The recharge of water from the reservoir does not appear to be constant along the length of the dam, this is due in part to the variation in stratigraphic units along the length of the dam and the variation in each unit's hydraulic conductivity capabilities. An attempt to simulate this potential flow of water out of the base of the section in the SEEP/W simulation by applying a water flux boundary at the base of the model. However, the computer simulation was still not able to account for the variability in the measured piezometric surfaces within the dam.
- There is variation in the stratigraphic units encountered at different sections through Coquitlam Dam, with varying hydraulic conductivities. As a result it appears that flow may occur in and/or out of the sections (i.e. from the sides). The two dimensional SEEP/W program is not capable of accounting for this type of flow situation. A two dimensional model presupposes that there is no flow in or out of the sides of the section.

6.5 CTRAN/W MODELLING OF COQUITLAM DAM

6.5.1 Grid and Stratigraphic Units

The heat transport analysis was conducted using CTRAN/W, and the modified volumetric water content function in SEEP/W. The same grid and stratigraphic units used for the seepage analysis, were again used for the CTRAN/W analysis, as presented on Figure 6.2.

6.5.2 Properties of Stratigraphic Units

The following information about each model stratigraphic unit was specified in the CTRAN/W analysis:

- longitudinal and transverse thermal dispersivity terms; and
- coefficient of diffusion.

Table 6.4 lists the values of material properties used in the thermal modelling of Coquitlam Dam.

6.5.3 Thermal Boundary Conditions

The upstream boundary, along the dam face was assigned a variable temperature function with respect to time, for four reservoir elevations (145, 140, 137, and 135 metres). Data is based on the measured reservoir temperature data recorded between August 1999 and April 2001 using BC Hydro's temperature probe. The data was then cycled over the 12 year analysis period. Figure 6.13 graphically presents the reservoir temperature data.

The boundary cells along the top, downstream face of the dam and ground surface, which represent the soil air interface, were assigned a boundary temperature function. The values for the temperature function were obtained from the air temperature data recorded by BC Hydro as part of their Plant Information System. The air temperature data recorded between May 1999 and June 2001 were used for the CTRAN/W input. From the data, the weekly average air temperature was calculated and then entered into CTRAN/W. The daily average air temperature and weekly average air temperature data is plotted and compared on Figure 6.14. The average weekly temperature data was then cycled over the 12 year analysis period.

Along the base and sides of the model, a zero heat flux was specified (i.e. no heat flow in or out of the model).

6.5.4 Time Steps

The time step of 10 days was selected for the analysis, to adequately account for the fluctuating reservoir levels, and seasonal temperature variations. The same time step was used for both the SEEP/W and CTRAN/W analyses. The analysis was run for 438 steps, which is equivalent to 12 years. The seepage analysis period was extended to 12 years to allow sufficient time for the temperature within the dam to reach quasi steady state conditions. This would eliminate the effects of any arbitrarily assigned temperatures, selected for the models initial condition setup, on the predicted temperatures by the twelfth year.

6.5.5 Initial Conditions

An initial temperature of 8.3°C was assigned to all nodes at the start of the heat transport analysis. A value of 8.3°C was selected, as it is the minimum temperature recorded within the dam's piezometers when air temperature effects are eliminated.

6.6 CTRAN/W RESULTS

Although an accurate hydraulic match to the measured piezometric data was not achieved, CTRAN/W model simulations were still conducted. Several simulations were conducted using the various hydraulic models discussed in Section 6.3 and Section 6.4. The CTRAN/W results can be plotted as a contour map. Figure 6.15 and Figure 6.16 present contour plots for the model simulation "XB-mix2" for June, September, December, and February. Figure 6.17 compares the contour plots of the measured and predicted data for August 1, 2000. The measured temperature data was contoured using Surfer 7.0 krigging function. It is apparent from Figure 6.17 that the measured data and the predicted temperature distribution are not identical. This is not surprising, since the advective component of the heat transport solution relies on the velocity determined from the hydraulic analysis. However, a comparison using this method is difficult. The temperature data used to create the surfer contour plot is concentrated in relatively localized areas. As a result, different contouring functions can create significantly different contour pictures. As a result, the remaining comparisons of the measured and predicted data will be done using plots at particular locations along the flow path (i.e. at monitoring points).

Figure 6.18 through Figure 6.23 present plots comparing the measured and the predicted temperatures within the monitoring piezometers through section B-B of the dam. The thermal properties selected for each of the models are listed in Table 6.4. From these plots it is evident that none of the models successfully predict the measured temperature distribution in the dam. However, by looking at each of the plots and simulations, we can learn something about the seepage regime of the dam. When comparing the measured and predicted data presented in these plots, there are three aspects of each plot worth considering; actual temperature, annual temperature variation, and the temperature variation with depth.

Figure 6.18 compares the results of simulation XB-mix2, to the measured data. From the comparison plot of SP99-12, it is apparent that the seepage velocity of the upstream shell in the model is slightly higher than in the dam itself, as the annual temperature variation is greater in the model than is measured at the dam. The measured temperature profile shows a slight decrease in temperature with depth below the 145 metre elevation, whereas in the model, the temperature is almost constant with depth, below 142 metres. The next two piezometers, SP-2 and SP-1, are both located below the upstream core. The comparison plot for SP-2 shows that the model's seepage velocity in this region is lower than that in the dam. This is evident from the lower annual temperature variation at this location than is measured within the dam. In comparison, the predicted annual temperature variation at SP-1 is much closer to the measured variation. The measured and predicted temperature profile curves, for SP-2 and SP-1, display a decrease in temperature with depth. The temperature decrease is greater in the measured data than in the model simulation. Piezometers SP99-7A/7B and SP-4 are located in the downstream core. The model predicts a constant temperature at these locations, whereas there is approximately 0.2°C to 0.5 °C temperature variation in the measured data. The measured and predicted temperature variation with depth, at SP99-7A/7B, shows a small decrease. The model also predicts a decrease

in temperature with depth at SP-4; however, the measured data is constant with depth. The last piezometer in this section is SP99-10, installed in the downstream toe of the dam. Both the measured and the predicted temperature profile at this location are typical of natural temperature variation near the ground surface caused by annual climatic variations. The seepage water from the reservoir does not influence the temperature profile at this location. The measured groundwater temperature below 123 metres is constant with depth. In comparison, the model predicts a constant temperature below 121 metres. The constant temperature predicted by the model is about 0.5°C warmer than measured at the dam. For this simulation an initial temperature of 9°C was specified. Based on the results presented in Figure 6.19 and Figure 6.20, an initial temperature of 8°C, produces a match closer to that measured at the dam.

The particular results from model simulations presented in Figure 6.19 through 6.23 could also be discussed in the same level of detail as the results presented in Figure 6.18. However, based on the seepage model results, it is apparent that achieving an adequate, two-dimensional, thermal model of the dam is unlikely. Based on this observation, it does not appear prudent, at this point, to analyse the results in such detail. If a better hydraulic model was achieved, this analysis process could be very beneficial in modifying hydraulic and thermal properties to achieve an improved overall heat transport model for a particular dam.

In place of a detailed analysis of each model simulation presented in Figure 6.19 through Figure 6.23, the following paragraph will discuss general observations about the Coquitlam Dam model simulations. In general, the model results are 0.5°C cooler than the temperatures recorded at Coquitlam Dam. The models more successfully predict the temperatures recorded in the piezometers further from the reservoir. The measured results are most accurately predicted for piezometer SP99-10 and least effectively predicted for SP99-12. The actual temperature, annual temperature variation, and temperature profile can be relatively well predicted for SP99-10, whereas the results for SP99-12 tend to have a greater annual variation, and the shape of the temperature distribution does not reflect the pattern of the measured data. Results for the piezometers in the upstream core (SP-2, SP-1 and SP99-2) vary for each simulation. The annual temperature variation was too low, as shown in Figure 6.18, and too high in Figure 6.20. The temperature variation with depth is well predicted, as shown in Figure 6.19. In contrast, the results presented in Figure 6.21 do not resemble the measured temperatures. Temperatures in the downstream core are recorded in SP-4 and SP99-7A/7B. The model results for these piezometers are more similar to the measured data, than the values predicted in the upstream core. The annual temperature range in these piezometers was too large in Figure 6.22, too small in Figure 6.18, and most similar in Figure 6.20. Model simulations more accurately predict the temperature profile at SP-4 and were less similar at SP99-7A/7B.

Although none of the model simulations match all of the measured temperature data, it appears that the simulation identified as XB-tr-mix (Figure 6.19) provides the best overall match to the measured data.

6.7 PROBLEMS WITH THE HEAT TRANSPORT MODELLING

The solution of the heat transport equation is not independent from the solution of the groundwater flow equation, the problems discussed in Section 6.5 are carried over into this solution. Since the convective component of the heat transport equation in CTRAN/W is calculated utilizing the transient seepage velocities obtained from SEEP/W, the inability to obtain an adequate seepage model significantly impacts the results of the thermal analysis. The convection component of the heat transfer equation is significant in the overall transport of heat

through Coquitlam Dam. Modelling the heat transfer through Coquitlam Dam is complex due to the interdependency of heat transfer with seepage through the dam, and due to the changes from year to year.

In general, the predicted temperatures were all cooler than the temperatures measured in the dam. One possible explanation is that warmer surface water in the reservoir is preferentially seeping through the dam. Additional monitoring data will help to verify the annual temperature fluctuations in the reservoir, and within the dam itself. Once a seepage model is better able to predict the hydraulic regime in the dam, then an improved heat transport model of Coquitlam dam should be achievable.

Two of the additional seepage model simulations discussed in Section 6.5 were also analysed for heat transport. The results from these simulations have been plotted and compared to the measured temperature data on Figure 6.24 and Figure 6.25. For both of these simulations, the annual temperature variation throughout the dam is significantly greater than measured within the dam. This signifies that the seepage velocities in these models are too high. It is important to note the sharp change in temperature observed at SP-1 and SP-2, at elevation 131 metres. This change occurs at the boundary between the core and lower sand and gravel (Unit 6A/6B). In particular, the change is evident due to the higher seepage velocity in the lower sand and gravel unit in comparison to the core. It is interesting to note that although the models predicted temperatures are highly variable in comparison to the measured temperatures, the temperatures fluctuate around the measured values.

6.8 SUMMARY AND CONCLUSIONS

Chapter 6 describes the two dimensional, transient seepage and heat transport analysis conducted of Coquitlam Dam. The seepage model results were plotted and compared to the measured piezometric data. Unfortunately, the model was not able to account for all of the natural variations present at Coquitlam Dam. Based on this modelling experience, a three dimensional transient seepage model may be necessary to account for the stratigraphic and hydraulic variations (including recharge) at the dam site.

Although an adequate seepage model was not achieved, CTRAN/W was utilized to conduct the heat transport analysis. The results of the heat transport analysis were plotted and compared to the measured temperature data collected from Coquitlam Dam. Based on these results, it is apparent that a satisfactory seepage analysis is a prerequisite to achieving a more accurate heat transport analysis.

The uncoupled solution of the heat transport analysis, as it applies to solving heat flow through an embankment dam, using SEEP/W and CTRAN/W, appears viable for simple stratigraphic and hydraulic configurations. Regrettably, the stratigraphic and hydraulic conditions at Coquitlam Dam are complex. As a result of the model simplifications, the two dimensional seepage analysis is unable to predict the hydraulic conditions measured at the dam. This in turn negatively affected the accuracy of the heat transport analysis.

Table 6.1: Range of Hydraulic Conductivity Values Used in SEEP/W Simulations

Material	Saturated Hydraulic Conductivity (m/s)		
Rockfill	1E-3	-	5E-2
Coarse Sand and Gravel Shell	8E-5	-	1E-4
Fine Sand and Gravel Shell	2E-6	-	8E-4
Hydraulic Fill Core	2E-6	-	1E-5
Unit 6A	9E-6	-	1E-3
Unit 6B	2.4E-6	-	5E-4
Unit 2A	5E-8	-	5E-6
Unit 1B	2E-6	-	1E-4
Unit 1A	2E-5	-	1E-3
Unit 1A and 1B combined	2E-6	-	5E-5

TABLE 6.2: Material Parameters for Computer Simulations

Model	Material	Saturated Hydrualic Conductivity (m/s)	Saturated Water Content	Hydraulic Conductivity Ratio	Flux out of base (m/s)	Notes
XB-tr.sep	Unit 1A/1B	2.0E-06	0.35	1	-1E-09	
	Stiff Silt	1.0E-06	0.2	1		
	Core	2.2E-06	0.6	0.2		
	Fine Sand/Gravel Shell	4.1E-06	0.29	1		
	Coarse Sand/Gravel Shell	1.0E-04	0.4	1		
	Rockfill	1.0E-03	0.5	1		
	Unit 6A	1.0E-05	0.35	1		
	Unit 6B	2.1E-05	0.3	1		
XB-tr1.sep	Unit 1A/1B	6.0E-06	0.35	1	-1E-09	
	Stiff Silt	4.0E-06	0.2	1		
	Core	2.2E-06	0.6	0.2		
	Fine Sand/Gravel Shell	3.0E-06	0.29	1		
	Coarse Sand/Gravel Shell	1.0E-04	0.4	1		
	Rockfill	1.0E-03	0.5	1		
	Unit 6A	9.0E-06	0.35	1		
	Unit 6B	2.4E-06	0.3	1		
XB-tr2.sep	Unit 1A/1B	6.0E-06	0.35	1	-1E-8 and -1E-7	convergence 0.1, steps 100
	Stiff Silt	4.0E-06	0.2	1		
	Core	2.0E-06	0.5	0.2		
	Fine Sand/Gravel Shell	4.1E-06	0.29	1		
	Coarse Sand/Gravel Shell	1.0E-04	0.4	1		
	Rockfill	1.0E-03	0.5	1		
	Unit 6A	9.0E-06	0.35	1		
	Unit 6B	2.4E-06	0.3	1		
XB-tr2.sep plotted as XB-tr2-7	Unit 1A/1B	6.0E-06	0.35	1	-1E-7	convergence 0.1, steps 100
	Stiff Silt	4.0E-06	0.2	1		
	Core	2.0E-06	0.5	0.2		
	Fine Sand/Gravel Shell	4.1E-06	0.29	1		
	Coarse Sand/Gravel Shell	1.0E-04	0.4	1		
	Rockfill	1.0E-03	0.5	1		
	Unit 6A	9.0E-06	0.35	1		
	Unit 6B	2.4E-06	0.3	1		
XB-tr2.sep plotted as XB-tr2-25	Unit 1A/1B	6.0E-06	0.35	1	-2.5E-07	convergence 0.1, steps 100
	Stiff Silt	4.0E-06	0.2	1		
	Core	2.0E-06	0.5	0.2		
	Fine Sand/Gravel Shell	4.1E-06	0.29	1		
	Coarse Sand/Gravel Shell	1.0E-04	0.4	1		
	Rockfill	1.0E-03	0.5	1		
	Unit 6A	9.0E-06	0.35	1		
	Unit 6B	2.4E-06	0.3	1		
XB-tr22.sep plotted as XB-mix2	Unit 1A/1B	6.0E-06	0.35	1	-1E-8 and -1E-7	convergence 0.05, steps 200
	Stiff Silt	4.0E-06	0.2	1		
	Core	2.0E-06	0.5	0.2		
	Fine Sand/Gravel Shell	4.1E-06	0.29	1		
	Coarse Sand/Gravel Shell	1.0E-04	0.4	1		
	Rockfill	1.0E-03	0.5	1		
	Unit 6A	9.0E-06	0.35	1		
	Unit 6B	2.4E-06	0.3	1		
XB-tr3.sep	Unit 1A/1B	2.0E-06	0.35	1	-2.5E-07	
	Stiff Silt	1.0E-06	0.2	1		
	Core	2.5E-06	0.5	0.2		
	Fine Sand/Gravel Shell	4.1E-06	0.29	1		
	Coarse Sand/Gravel Shell	1.0E-04	0.4	1		
	Rockfill	1.0E-03	0.5	1		
	Unit 6A	9.0E-06	0.35	1		
	Unit 6B	2.4E-06	0.3	1		
XB-tr4.sep	Unit 1A/1B	6.0E-06	0.35	1	-1E-8 and -1E-7	
	Stiff Silt	4.0E-06	0.2	1		
	Core	6.0E-06	0.5	0.2		
	Fine Sand/Gravel Shell	4.1E-06	0.29	1		
	Coarse Sand/Gravel Shell	1.0E-04	0.4	1		
	Rockfill	1.0E-03	0.5	1		
	Unit 6A	9.0E-06	0.35	1		
	Unit 6B	2.4E-06	0.3	1		
XB-tr5.sep	Unit 1A/1B	6.0E-06	0.35	1	-1E-8 and -1E-7	
	Stiff Silt	4.0E-06	0.2	1		
	Core	1.0E-05	0.5	0.1		
	Fine Sand/Gravel Shell	4.1E-06	0.29	1		
	Coarse Sand/Gravel Shell	1.0E-04	0.4	1		
	Rockfill	1.0E-03	0.5	1		
	Unit 6A	9.0E-06	0.35	1		
	Unit 6B	2.4E-06	0.3	1		
XB-tr5.sep plotted as tr5-01	Unit 1A/1B	6.0E-06	0.35	1	-1E-8 and -1E-7	
	Stiff Silt	4.0E-06	0.2	1		
	Core	1.0E-05	0.5	0.01		
	Fine Sand/Gravel Shell	4.1E-06	0.29	1		
	Coarse Sand/Gravel Shell	1.0E-04	0.4	1		
	Rockfill	1.0E-03	0.5	1		
	Unit 6A	9.0E-06	0.35	1		
	Unit 6B	2.4E-06	0.3	1		
XB-tr6.sep plotted as tr6-01	Unit 1A/1B	6.0E-06	0.35	1	-1E-8 and -1E-7	
	Stiff Silt	4.0E-06	0.2	1		
	Core	1.0E-04	0.5	0.01		
	Fine Sand/Gravel Shell	4.1E-06	0.29	1		
	Coarse Sand/Gravel Shell	1.0E-04	0.4	1		
	Rockfill	1.0E-03	0.5	1		
	Unit 6A	9.0E-06	0.35	1		
	Unit 6B	2.4E-04	0.3	1		
XB-trans-alt.sep	Unit 1A/1B	7.0E-06	0.35	1	-1E-09	
	Stiff Silt	4.0E-06	0.2	1		
	Core	2.4E-06	0.6	0.2		
	Fine Sand/Gravel Shell	2.0E-06	0.29	1		
	Coarse Sand/Gravel Shell	1.0E-04	0.4	1		
	Rockfill	1.0E-03	0.5	1		
	Unit 6A	1.0E-05	0.35	1		
	Unit 6B	2.1E-05	0.3	1		

TABLE 6.2: Material Parameters for Computer Simulations

Model	Material	Saturated Hydraulic Conductivity (m/s)	Saturated Water Content	Hydraulic Conductivity Ratio	Flux out of base (m/s)	Notes
XB-tr-alt.sep	Unit 1A/1B	7.0E-06	0.35	1	-1E-09	
	Stiff Silt	4.0E-06	0.2	1		
	Core	2.4E-06	0.6	0.2		
	Fine Sand/Gravel Shell	2.0E-06	0.29	1		
	Coarse Sand/Gravel Shell	1.0E-04	0.4	1		
	Rockfill	1.0E-03	0.5	1		
	Unit 6A	2.0E-05	0.35	1		
	Unit 6B	2.4E-06	0.3	1		
nXB-tr-mix.sep	Unit 1A	2.0E-05	0.4	1	-1E-9 and -1E-8	
	Unit 1B	7.0E-06	0.17	1		
	Stiff Silt (Unit 2A)	1.0E-06	0.38	1		
	Core	2.2E-06	0.6	0.01		
	Fine Sand/Gravel Shell	4.1E-06	0.29	1		
	Coarse Sand/Gravel Shell	1.0E-04	0.3	1		
	Rockfill	1.0E-03	0.5	1		
	Unit 6A	2.0E-05	0.17	1		
	Unit 6B	2.4E-06	0.25	1		
XB-tr6-mix.sep	Unit 1A	2.0E-05	0.4	1	-1E-8 to -1E-7	Unit 1A/1B added, otherwise same values as XB-tr-mix.sep
	Unit 1B	5.0E-06	0.17	1		
	Stiff Silt (Unit 2A)	2.0E-06	0.38	1		
	Core	6.0E-06	0.6	0.01		
	Fine Sand/Gravel Shell	4.1E-06	0.29	1		
	Coarse Sand/Gravel Shell	1.0E-04	0.3	1		
	Rockfill	1.0E-02	0.5	1		
	Unit 6A	2.0E-05	0.17	1		
	Unit 6B	5.0E-06	0.25	1		
XB-tr-mix	Unit 1A/1B	2.0E-06	0.35	1	-1E-9 to -1E-8	
	Stiff Silt	1.0E-06	0.2	1		
	Core	2.2E-06	0.6	0.2		
	Fine Sand/Gravel Shell	4.1E-06	0.29	1		
	Coarse Sand/Gravel Shell	1.0E-04	0.4	1		
	Rockfill	1.0E-03	0.5	1		
	Unit 6A	2.1E-05	0.35	1		
	Unit 6B	2.4E-06	0.3	1		
XB-tr4-leak.sep	Unit 1A/1B	6.0E-06	0.35	1	-1E-8 to -1E-7	with a leakage zone in core
	Stiff Silt	4.0E-06	0.2	1		
	Core	6.0E-06	0.5	0.2		
	Fine Sand/Gravel Shell	4.1E-06	0.29	1		
	Coarse Sand/Gravel Shell	1.0E-04	0.4	1		
	Rockfill	1.0E-03	0.5	1		
	Unit 6A	9.0E-06	0.35	1		
	Unit 6B	2.4E-06	0.3	1		
	linear leakage zone in core	1.0E-05	0.6	0.1		
XB-tr2-PB-2h.sep	Unit 1A	1.0E-03	0.4	1	-1E-8 to -1E-7	constant head value = 132 meters in the downstream portion of Unit 1B
	Unit 1B	1.0E-04	0.17	1		
	Stiff Silt (Unit 2A)	5.0E-06	0.38	1		
	Core	6.0E-06	0.5	0.1		
	Fine Sand/Gravel Shell	8.0E-04	0.29	1		
	Coarse Sand/Gravel Shell	8.0E-05	0.25	1		
	Rockfill	5.0E-02	0.5	1		
	Unit 6A	1.0E-03	0.15	1		
	Unit 6B	5.0E-04	0.25	1		
XB-tr2-PB-2hc.sep	Unit 1A	1.0E-03	0.4	1	-1E-8 to -1E-7	constant head value = 132 meters in the downstream portion of Unit 1B
	Unit 1B	1.0E-04	0.17	1		
	Stiff Silt (Unit 2A)	5.0E-06	0.38	1		
	Core	1.0E-05	0.5	0.1		
	Fine Sand/Gravel Shell	8.0E-04	0.29	1		
	Coarse Sand/Gravel Shell	8.0E-05	0.25	1		
	Rockfill	5.0E-02	0.5	1		
	Unit 6A	1.0E-03	0.15	1		
	Unit 6B	5.0E-04	0.25	1		
XB-tr2-PB-5h.sep	Unit 1A	1.0E-04	0.4	1	-1E-8 to -1E-7	constant head value = 132 meters in the downstream portion of Unit 1B, 4 nodes removed from the upstream side of the node block
	Unit 1B	1.0E-04	0.17	1		
	Stiff Silt (Unit 2A)	5.0E-07	0.38	1		
	Core	6.0E-06	0.5	0.1		
	Fine Sand/Gravel Shell	1.0E-05	0.29	1		
	Coarse Sand/Gravel Shell	1.0E-04	0.25	1		
	Rockfill	5.0E-03	0.5	1		
	Unit 6A	1.0E-03	0.15	1		
	Unit 6B	5.0E-04	0.25	1		
XB-tr2-mix-PBh.sep	Unit 1A	1.0E-04	0.35	1	-1E-8 to -1E-7	
	Unit 1B	2.0E-06	0.17	1		
	Stiff Silt (Unit 2A)	1.0E-06	0.2	1		
	Core	2.2E-06	0.5	0.1		
	Fine Sand/Gravel Shell	4.1E-06	0.29	1		
	Coarse Sand/Gravel Shell	1.0E-04	0.5	1		
	Rockfill	1.0E-03	0.5	1		
	Unit 6A	2.0E-05	0.15	1		
	Unit 6B	2.4E-06	0.25	1		
XB-tr2-PB-ss2h.sep	Unit 1A	1.0E-03	0.4	1	-1E-8 to -1E-7	
	Unit 1B	1.0E-04	0.17	1		
	Stiff Silt (Unit 2A)	5.0E-06	0.38	1		
	Core	6.0E-06	0.5	0.1		
	Fine Sand/Gravel Shell	8.0E-04	0.29	1		
	Coarse Sand/Gravel Shell	8.0E-05	0.25	1		
	Rockfill	5.0E-02	0.5	1		
	Unit 6A	1.0E-03	0.15	1		
	Unit 6B	5.0E-04	0.25	1		
XB-tr2-M.sep	Unit 1A/1B	5.0E-05	0.3	1	-1E-6, -1.15E-6, -4E-7	
	Stiff Silt (Unit 2A)	5.0E-08	0.2	1		
	Core	1.0E-05	0.5	0.1		
	Fine Sand/Gravel Shell	1.0E-05	0.29	1		
	Coarse Sand/Gravel Shell	1.0E-04	0.4	1		
	Rockfill	1.0E-02	0.5	1		
	Unit 6A	9.0E-06	0.3	1		
	Unit 6B	5.0E-06	0.3	1		

TABLE 6.3: Material Parameters for Computer Simulations (for Figures 6.11 and 6.12)

Model	Material	Saturated Hydraulic Conductivity (m/s)	Saturated Water Content	Hydraulic Conductivity Ratio	Flux out of base (m/s)	Notes
XB-tr22.sep plotted as XB-mix2	Unit 1A/1B	6.0E-06	0.35	1	-1E-8 and -1E-7	convergence 0.05, steps 200
	Stiff Silt	4.0E-06	0.2	1		
	Core	2.0E-06	0.5	0.2		
	Fine Sand/Gravel Shell	4.1E-06	0.29	1		
	Coarse Sand/Gravel Shell	1.0E-04	0.4	1		
	Rockfill	1.0E-03	0.5	1		
	Unit 6A	9.0E-06	0.35	1		
	Unit 6B	2.4E-06	0.3	1		
XB-tr2-PB-2h.sep	Unit 1A	1.0E-03	0.4	1	-1E-8 to -1E-7	constant head value = 132 meters in the downstream portion of Unit 1B
	Unit 1B	1.0E-04	0.17	1		
	Stiff Silt (Unit 2A)	5.0E-06	0.38	1		
	Core	6.0E-06	0.5	0.1		
	Fine Sand/Gravel Shell	8.0E-04	0.29	1		
	Coarse Sand/Gravel Shell	8.0E-05	0.25	1		
	Rockfill	5.0E-02	0.5	1		
	Unit 6A	1.0E-03	0.15	1		
	Unit 6B	5.0E-04	0.25	1		
XB-tr2-PB-2hc.sep	Unit 1A	1.0E-03	0.4	1	-1E-8 to -1E-7	constant head value = 132 meters in the downstream portion of Unit 1B
	Unit 1B	1.0E-04	0.17	1		
	Stiff Silt (Unit 2A)	5.0E-06	0.38	1		
	Core	1.0E-05	0.5	0.1		
	Fine Sand/Gravel Shell	8.0E-04	0.29	1		
	Coarse Sand/Gravel Shell	8.0E-05	0.25	1		
	Rockfill	5.0E-02	0.5	1		
	Unit 6A	1.0E-03	0.15	1		
	Unit 6B	5.0E-04	0.25	1		
XB-tr2-PB-5h.sep	Unit 1A	1.0E-04	0.4	1	-1E-8 to -1E-7	constant head value = 132 meters in the downstream portion of Unit 1B, 4 nodes removed from the upstream side of the node block
	Unit 1B	1.0E-04	0.17	1		
	Stiff Silt (Unit 2A)	5.0E-07	0.38	1		
	Core	6.0E-06	0.5	0.1		
	Fine Sand/Gravel Shell	1.0E-05	0.29	1		
	Coarse Sand/Gravel Shell	1.0E-04	0.25	1		
	Rockfill	5.0E-03	0.5	1		
	Unit 6A	1.0E-03	0.15	1		
	Unit 6B	5.0E-04	0.25	1		
XB-tr2-mix-PBh.sep	Unit 1A	1.0E-04	0.35	1	-1E-8 to -1E-7	
	Unit 1B	2.0E-06	0.17	1		
	Stiff Silt (Unit 2A)	1.0E-06	0.2	1		
	Core	2.2E-06	0.5	0.1		
	Fine Sand/Gravel Shell	4.1E-06	0.29	1		
	Coarse Sand/Gravel Shell	1.0E-04	0.5	1		
	Rockfill	1.0E-03	0.5	1		
	Unit 6A	2.0E-05	0.15	1		
	Unit 6B	2.4E-06	0.25	1		
XB-tr2-PB-ss2h.sep	Unit 1A	1.0E-03	0.4	1	-1E-8 to -1E-7	
	Unit 1B	1.0E-04	0.17	1		
	Stiff Silt (Unit 2A)	5.0E-06	0.38	1		
	Core	6.0E-06	0.5	0.1		
	Fine Sand/Gravel Shell	8.0E-04	0.29	1		
	Coarse Sand/Gravel Shell	8.0E-05	0.25	1		
	Rockfill	5.0E-02	0.5	1		
	Unit 6A	1.0E-03	0.15	1		
	Unit 6B	5.0E-04	0.25	1		
XB-tr2-MKL.sep	Unit 1A/1B	5.0E-05	0.3	1	-1E-6, -1.15E-6, -4E-7	
	Stiff Silt (Unit 2A)	5.0E-08	0.2	1		
	Core	1.0E-05	0.5	0.1		
	Fine Sand/Gravel Shell	1.0E-05	0.29	1		
	Coarse Sand/Gravel Shell	1.0E-04	0.4	1		
	Rockfill	1.0E-02	0.5	1		
	Unit 6A	9.0E-06	0.3	1		
	Unit 6B	5.0E-06	0.3	1		

TABLE 6.4: Material Thermal Properties Used in the Modelling of Coquitlam Dam

Model	Material	Saturated Hydrualic Conductivity (m/s)	Saturated Water Content	Substituted Saturated Water Content	Hydraulic Conductivity Ratio	α_{long}	α_{trans}	E*
XB-tr2	Unit 1A/1B	6.0E-06	0.35	0.57	1	6	0.6	9.2E-07
	Stiff Silt (2A)	4.0E-06	0.2	0.55	1	5.5	0.55	8.7E-07
	Core	2.0E-06	0.5	0.69	0.2	7	0.7	6.3E-07
	Fine Sand/Gravel Shell	4.1E-06	0.29	0.6	1	6	0.6	9.6E-07
	Coarse Sand/Gravel Shell	1.0E-04	0.4	0.65	1	6.5	0.65	5.8E-07
	Rockfill	1.0E-03	0.5	0.74	1	10	1	6.4E-07
	Unit 6A	9.0E-06	0.35	0.62	1	6	0.6	8.8E-07
	Unit 6B	2.4E-06	0.3	0.65	1	6.5	0.65	9.6E-07
XB-tr-mix	Unit 1A/1B	2.0E-06	0.35	0.57	1	6.1	0.61	9.2E-07
	Stiff Silt (2A)	1.0E-06	0.2	0.55	1	3.6	0.36	8.7E-07
	Core	2.2E-06	0.6	0.69	0.2	8.8	0.87	6.3E-07
	Fine Sand/Gravel Shell	4.1E-06	0.29	0.6	1	4.9	0.48	9.6E-07
	Coarse Sand/Gravel Shell	1.0E-04	0.4	0.65	1	6.2	0.62	8.5E-07
	Rockfill	1.0E-03	0.5	0.74	1	6.7	0.67	6.4E-07
	Unit 6A	2.1E-05	0.35	0.62	1	5.6	0.56	8.8E-07
	Unit 6B	2.4E-06	0.3	0.65	1	4.7	0.47	9.6E-07
XB-tr6-mix	Unit 1A	2.0E-05	0.4	0.57	1	7	0.7	9.2E-07
	Unit 1B	5.0E-06	0.17	0.57	1	3	0.3	9.2E-07
	Stiff Silt (Unit 2A)	2.0E-06	0.38	0.55	1	6.9	0.7	8.7E-07
	Core	6.0E-06	0.6	0.69	0.01	8.8	0.9	6.3E-07
	Fine Sand/Gravel Shell	4.1E-06	0.29	0.6	1	4.8	0.5	9.6E-07
	Coarse Sand/Gravel Shell	1.0E-04	0.3	0.65	1	4.6	0.5	8.5E-07
	Rockfill	1.0E-02	0.5	0.74	1	6.7	0.7	6.4E-07
	Unit 6A	2.0E-05	0.17	0.62	1	2.7	0.3	8.8E-07
	Unit 6B	5.0E-06	0.25	0.65	1	3.9	0.4	9.6E-07
nXB-tr-mix	Unit 1A	2.0E-05	0.4	0.57	1	7	0.7	9.2E-07
	Unit 1B	7.0E-06	0.17	0.57	1	3	0.3	9.2E-07
	Stiff Silt (Unit 2A)	1.0E-06	0.38	0.55	1	6.9	0.7	8.7E-07
	Core	2.2E-06	0.6	0.69	0.01	8.8	0.9	6.3E-07
	Fine Sand/Gravel Shell	4.1E-06	0.29	0.6	1	4.8	0.5	9.6E-07
	Coarse Sand/Gravel Shell	1.0E-04	0.3	0.65	1	4.6	0.5	8.5E-07
	Rockfill	1.0E-03	0.5	0.74	1	6.7	0.7	6.4E-07
	Unit 6A	2.0E-05	0.17	0.62	1	2.7	0.3	8.8E-07
	Unit 6B	2.4E-06	0.25	0.65	1	3.9	0.4	9.6E-07

TABLE 6.4: Material Thermal Properties Used in the Modelling of Coquitlam Dam

Model	Material	Saturated Hydrualic Conductivity (m/s)	Saturated Water Content	Substituted Saturated Water Content	Hydraulic Conductivity Ratio	α_{long}	α_{trans}	E*
XB-tr2-PB-2h	Unit 1A	1.0E-03	0.4	0.6	1	6	0.6	9.6E-07
	Unit 1B	1.0E-04	0.17	0.58	1	5.8	0.58	9.1E-07
	Stiff Silt (Unit 2A)	5.0E-06	0.38	0.55	1	5.5	0.55	8.7E-07
	Core	6.0E-06	0.5	0.7	0.1	6.9	0.7	6.3E-07
	Fine Sand/Gravel Shell	8.0E-04	0.29	0.6	1	6	0.6	9.6E-07
	Coarse Sand/Gravel Shell	8.0E-05	0.25	0.65	1	6.5	0.65	8.5E-07
	Rockfill	5.0E-02	0.5	0.74	1	10	1	6.4E-07
	Unit 6A	1.0E-03	0.15	0.62	1	6.2	0.62	8.8E-07
	Unit 6B	5.0E-04	0.25	0.65	1	6.5	0.65	9.6E-07
XB-tr2-PB-5h	Unit 1A	1.0E-03	0.4	0.6	1	6	0.6	9.6E-07
	Unit 1B	1.0E-04	0.17	0.58	1	5.8	0.58	9.1E-07
	Stiff Silt (Unit 2A)	5.0E-06	0.38	0.55	1	5.5	0.55	8.7E-07
	Core	1.0E-05	0.5	0.69	0.1	6.9	0.7	6.3E-07
	Fine Sand/Gravel Shell	8.0E-04	0.29	0.6	1	6	0.6	9.6E-07
	Coarse Sand/Gravel Shell	8.0E-05	0.25	0.65	1	6.5	0.65	8.5E-07
	Rockfill	5.0E-02	0.5	0.74	1	10	1	6.4E-07
	Unit 6A	1.0E-03	0.15	0.62	1	6.2	0.62	8.8E-07
	Unit 6B	5.0E-04	0.25	0.65	1	6.5	0.65	9.6E-07

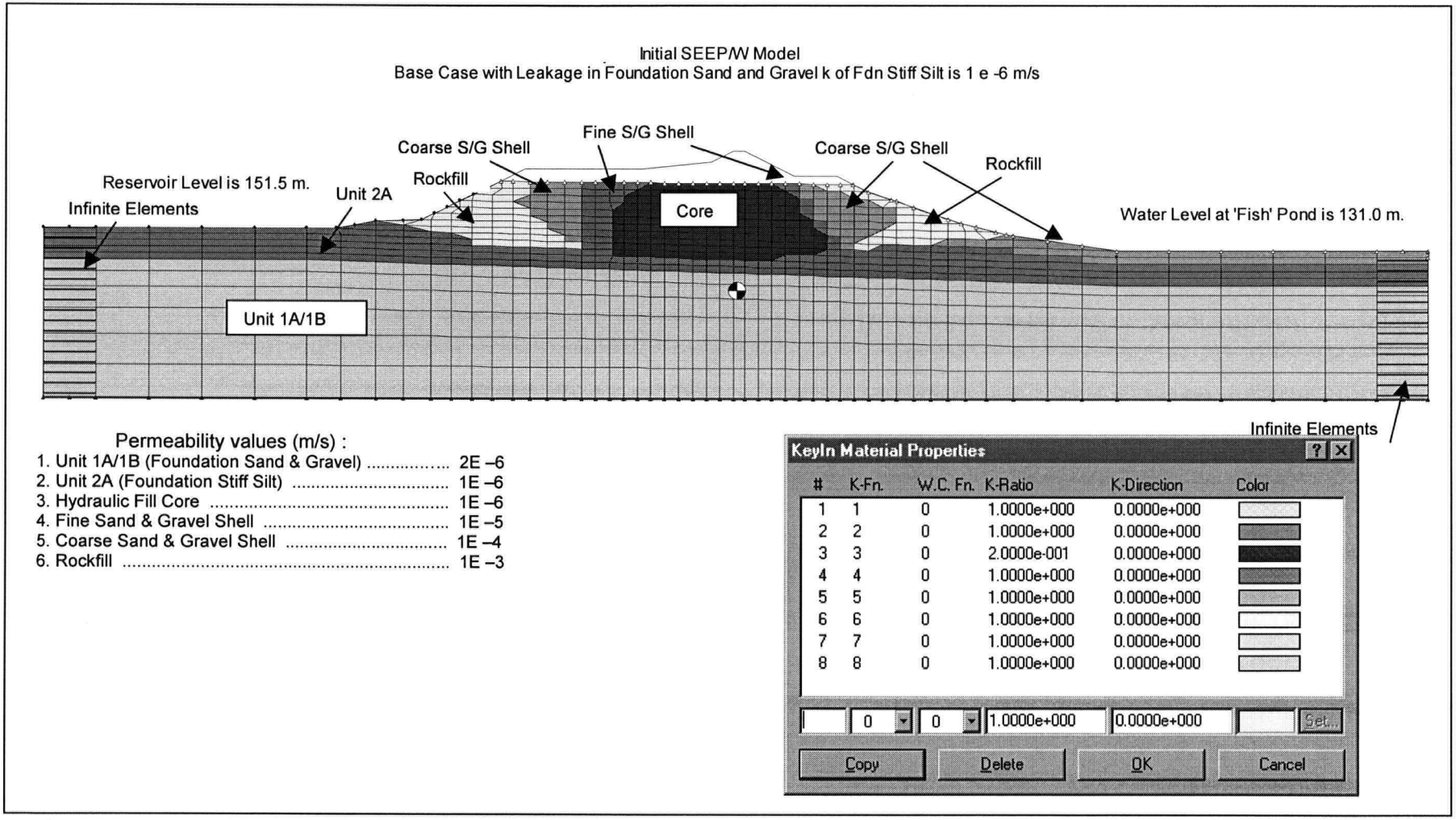

Figure 6.1: Initial SEEP/W Model of Coquitlam Dam (provided by BC Hydro)

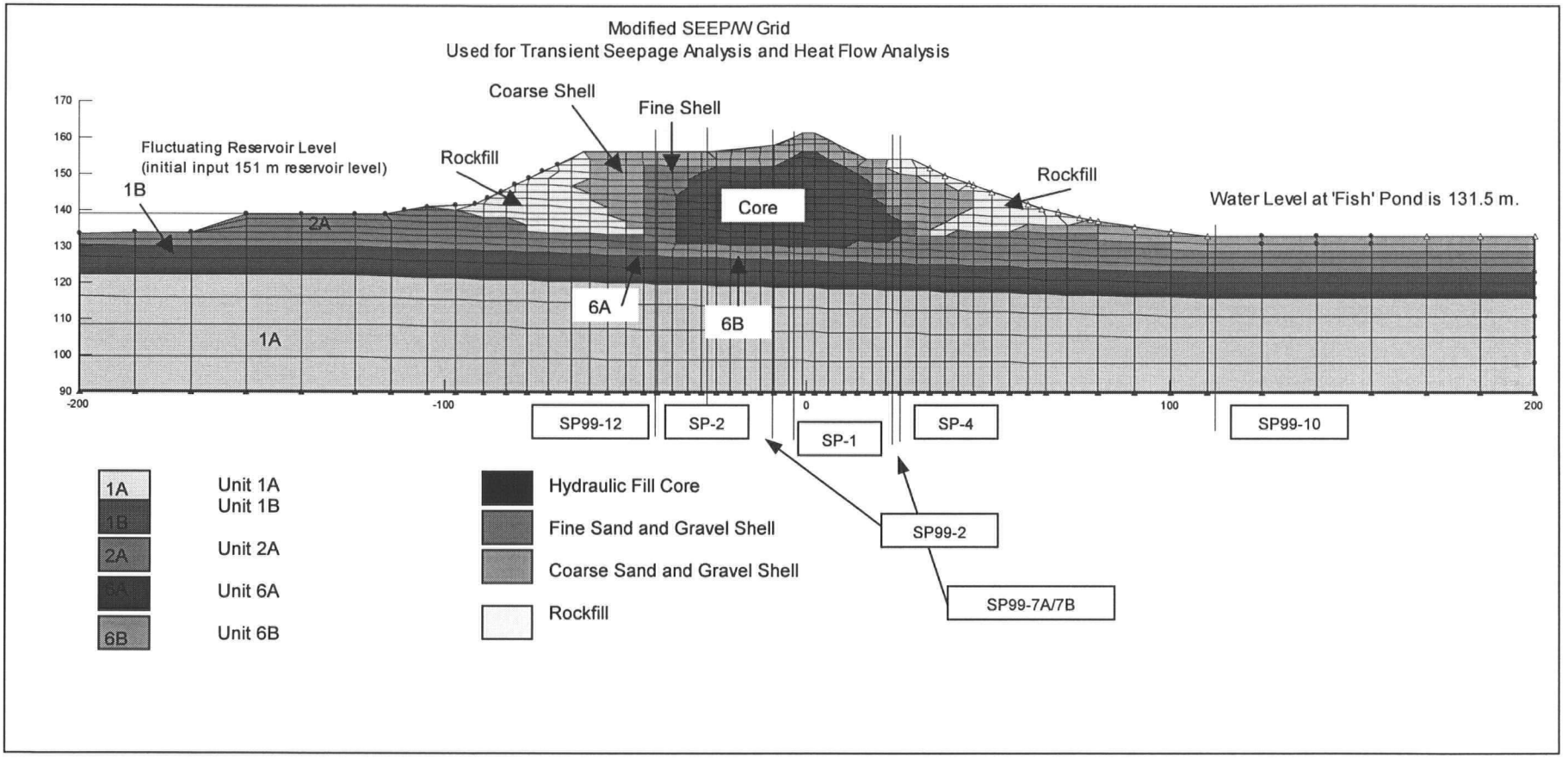

Figure 6.2: Modified SEEP/W Grid of Coquitlam Dam

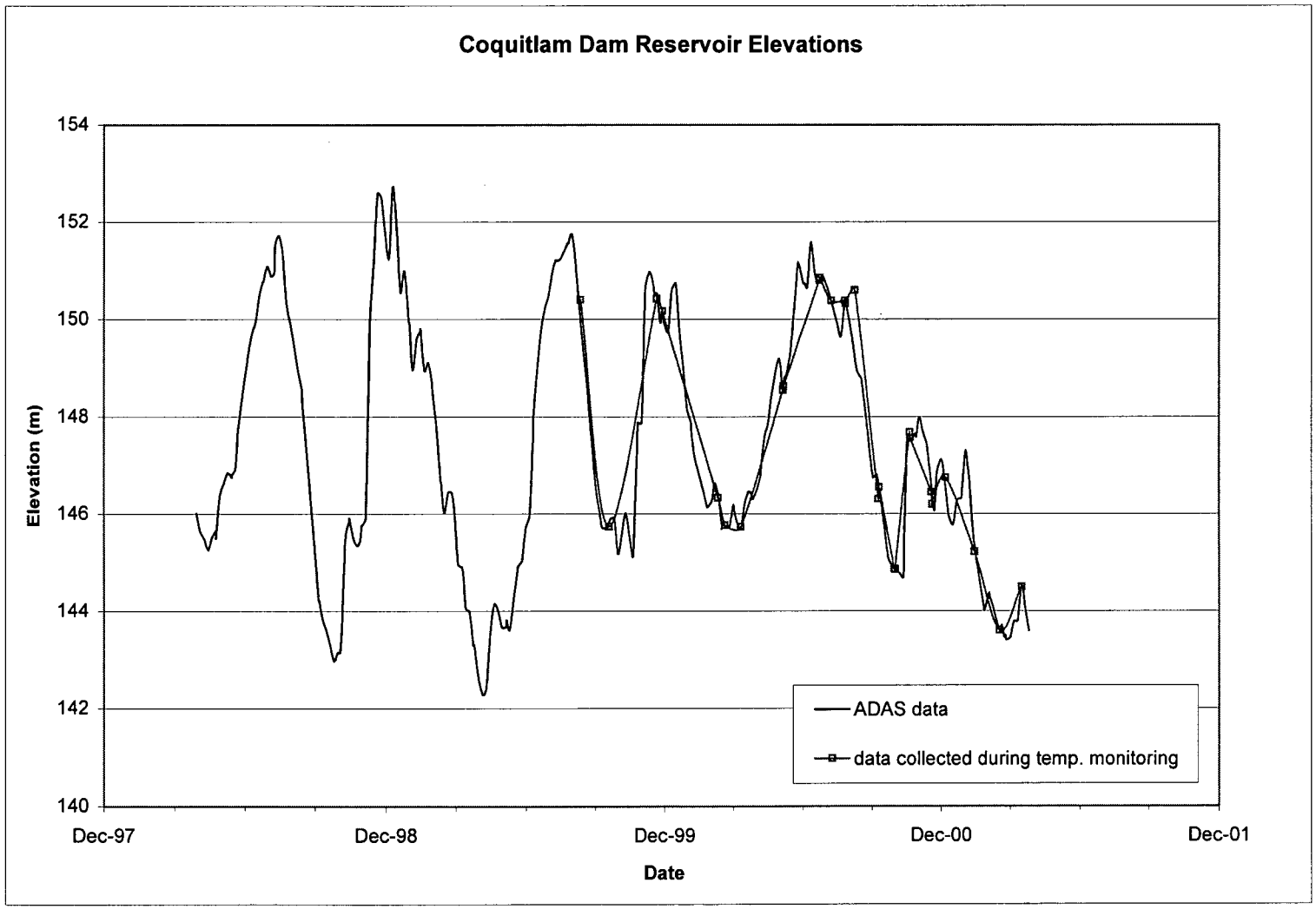

Figure 6.3: Measured Reservoir Elevations from Coquitlam Dam (data provided by BC Hydro)

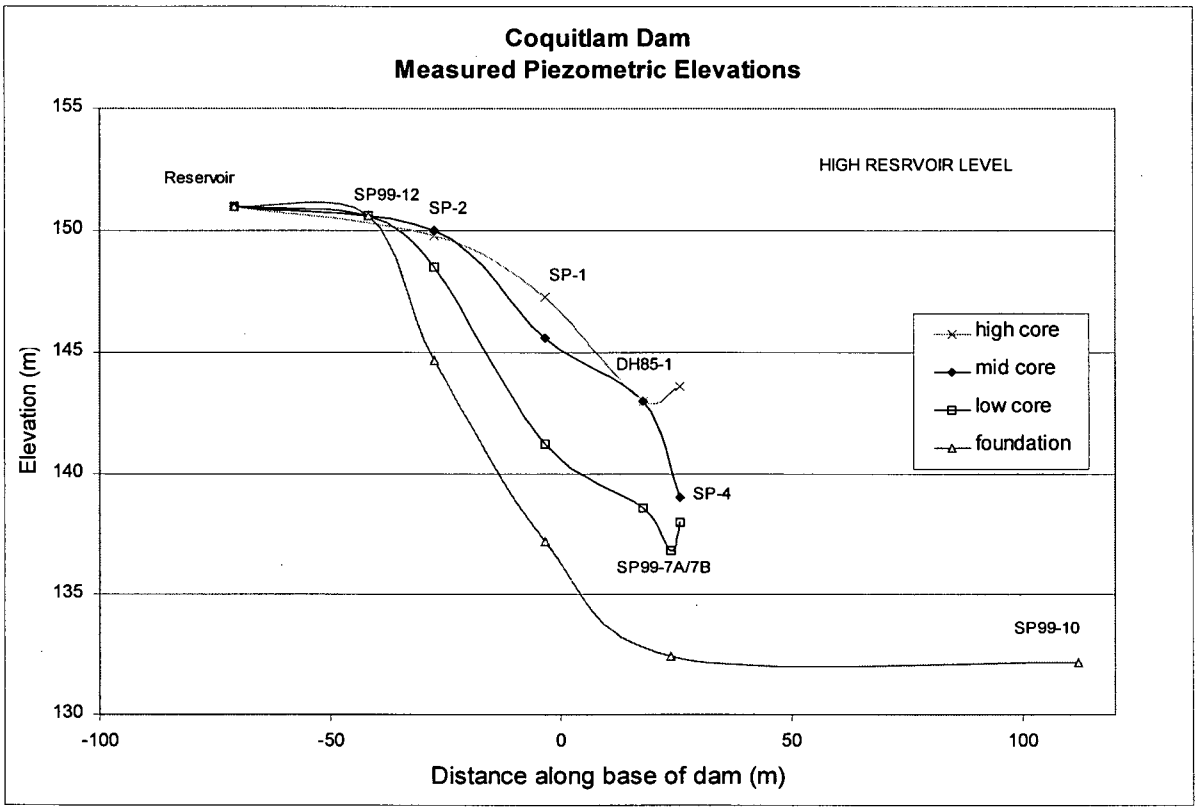

a. High Reservoir Level

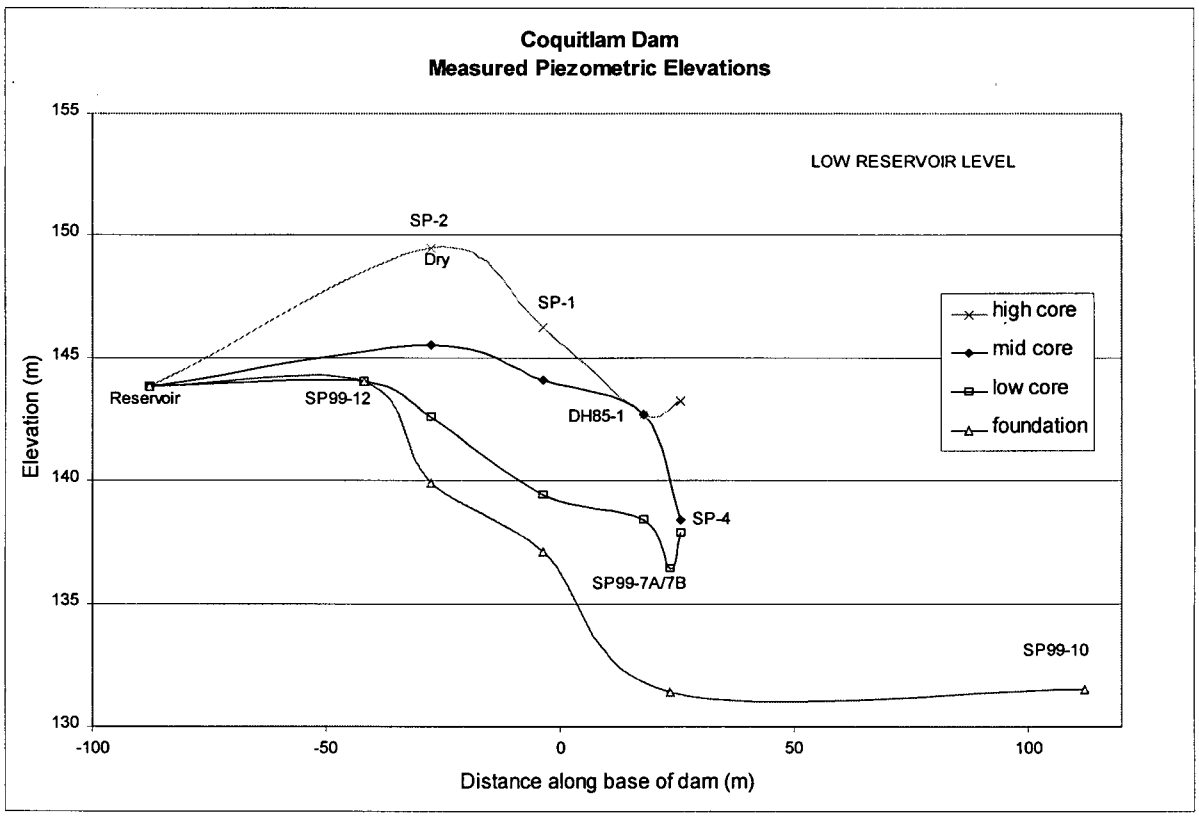

b. Low Reservoir Level

Figure 6.4: Measured Piezometric Elevations from Coquitlam Dam

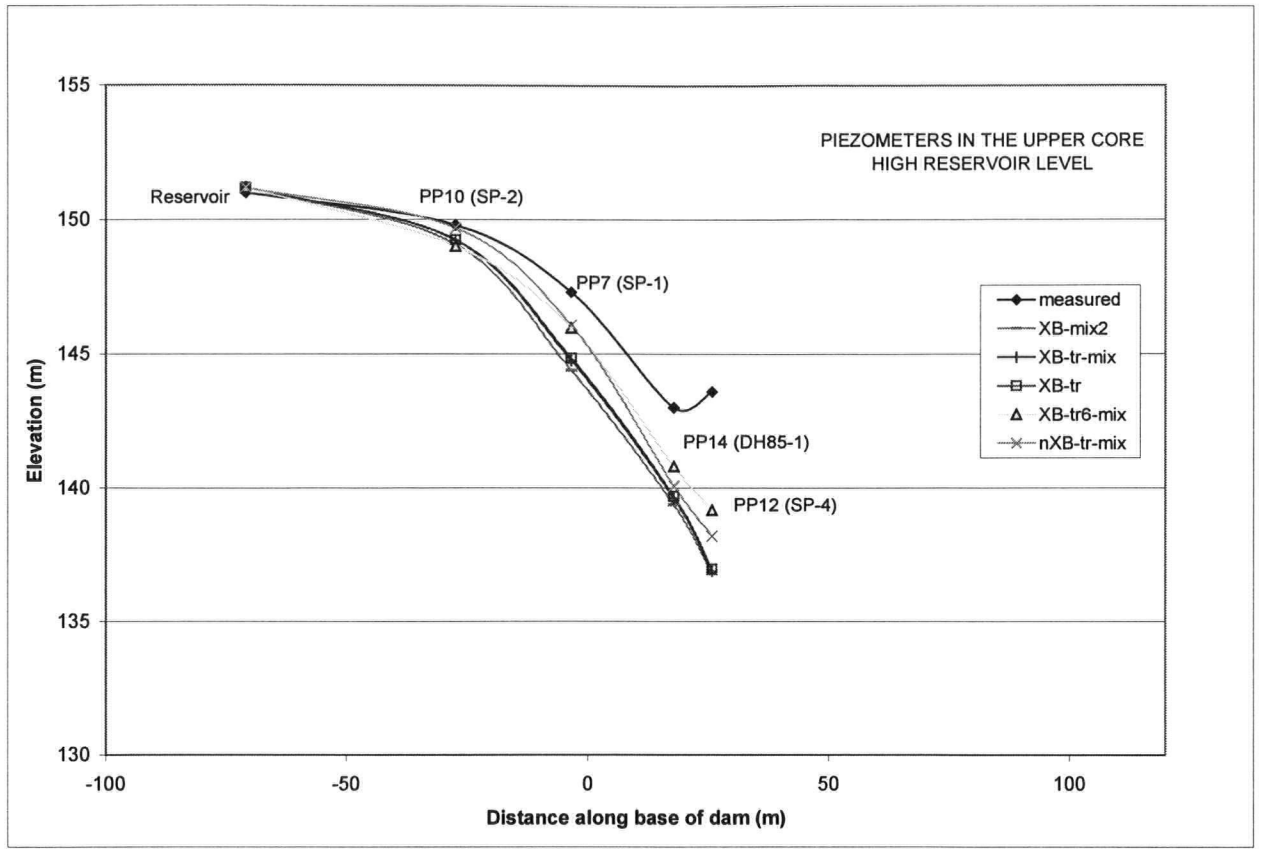

a. Data Comparison with Piezometers in the Upper Core

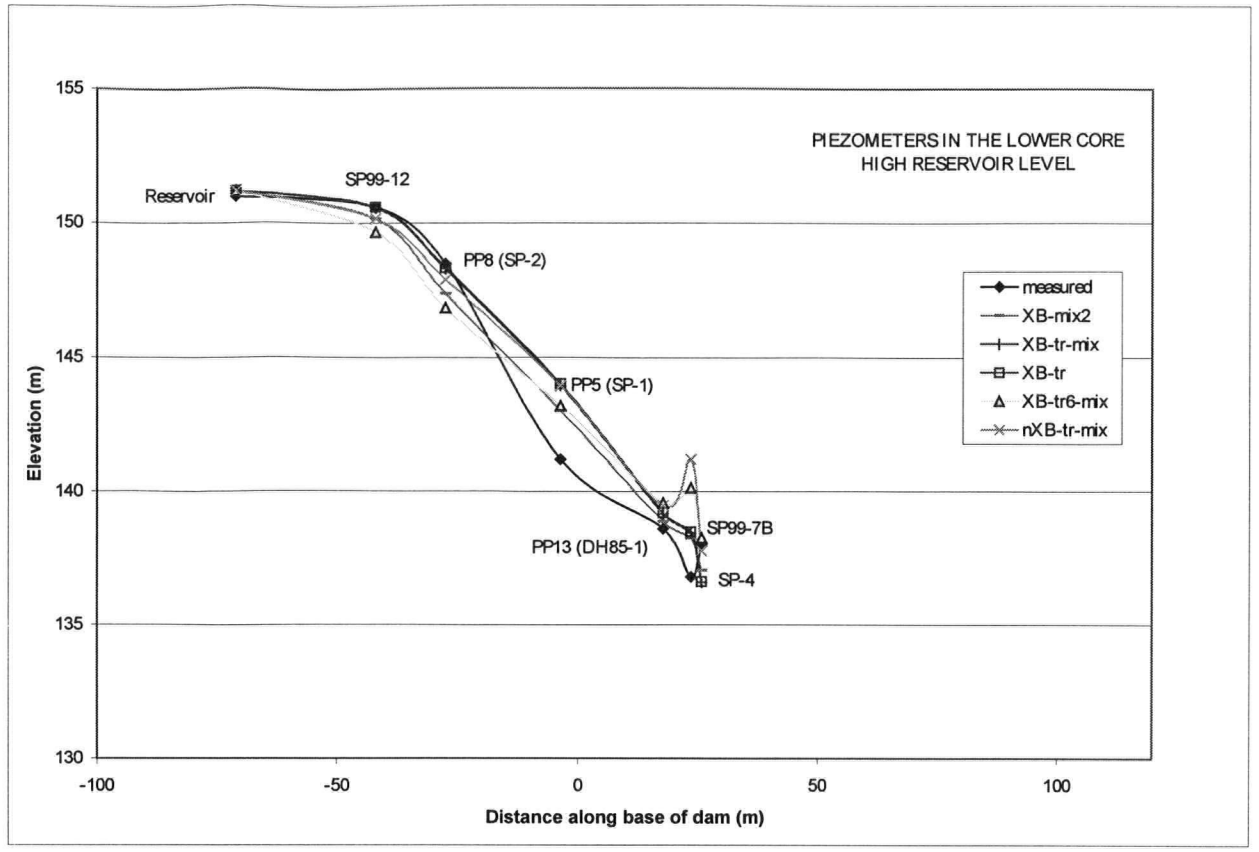

c. Data Comparison with Piezometers in the Lower Core

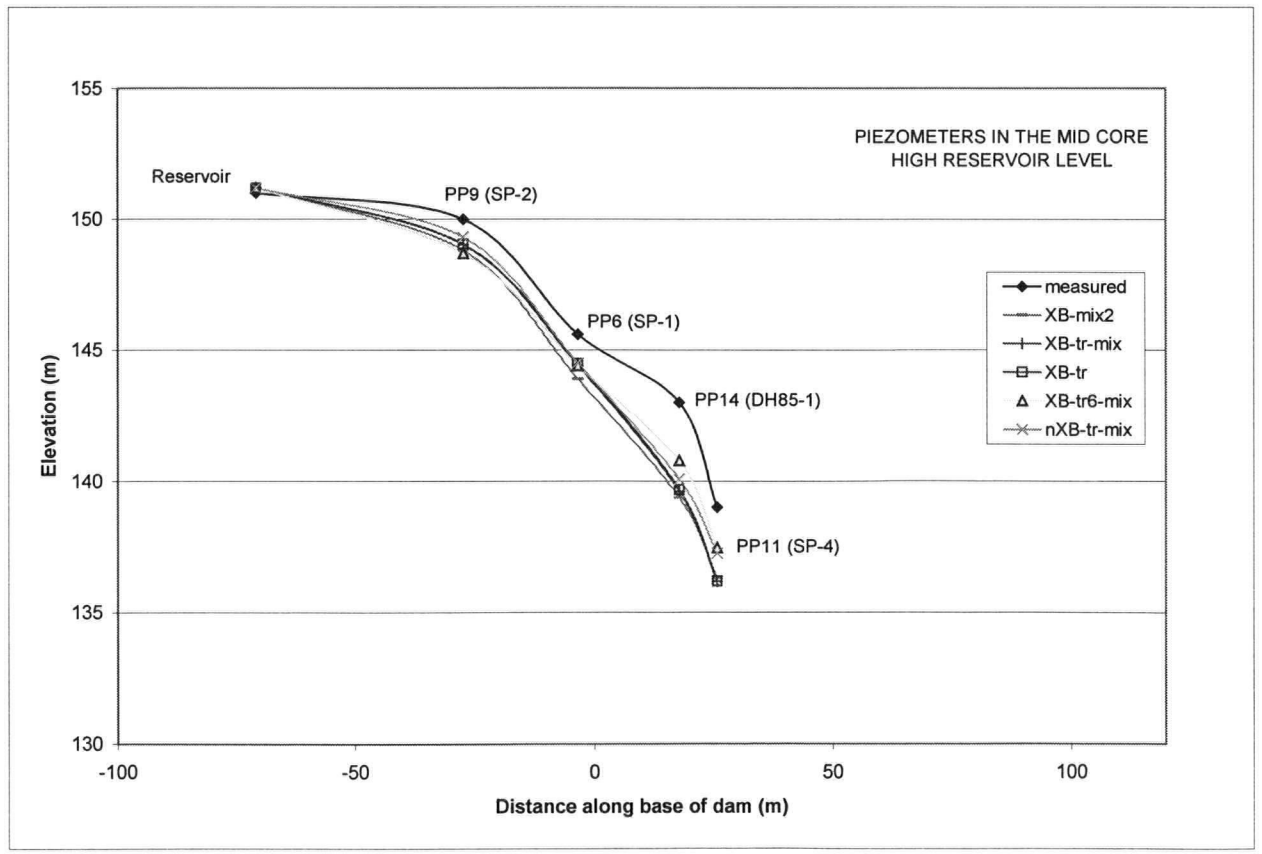

b. Data Comparison with Piezometers in the Mid Core

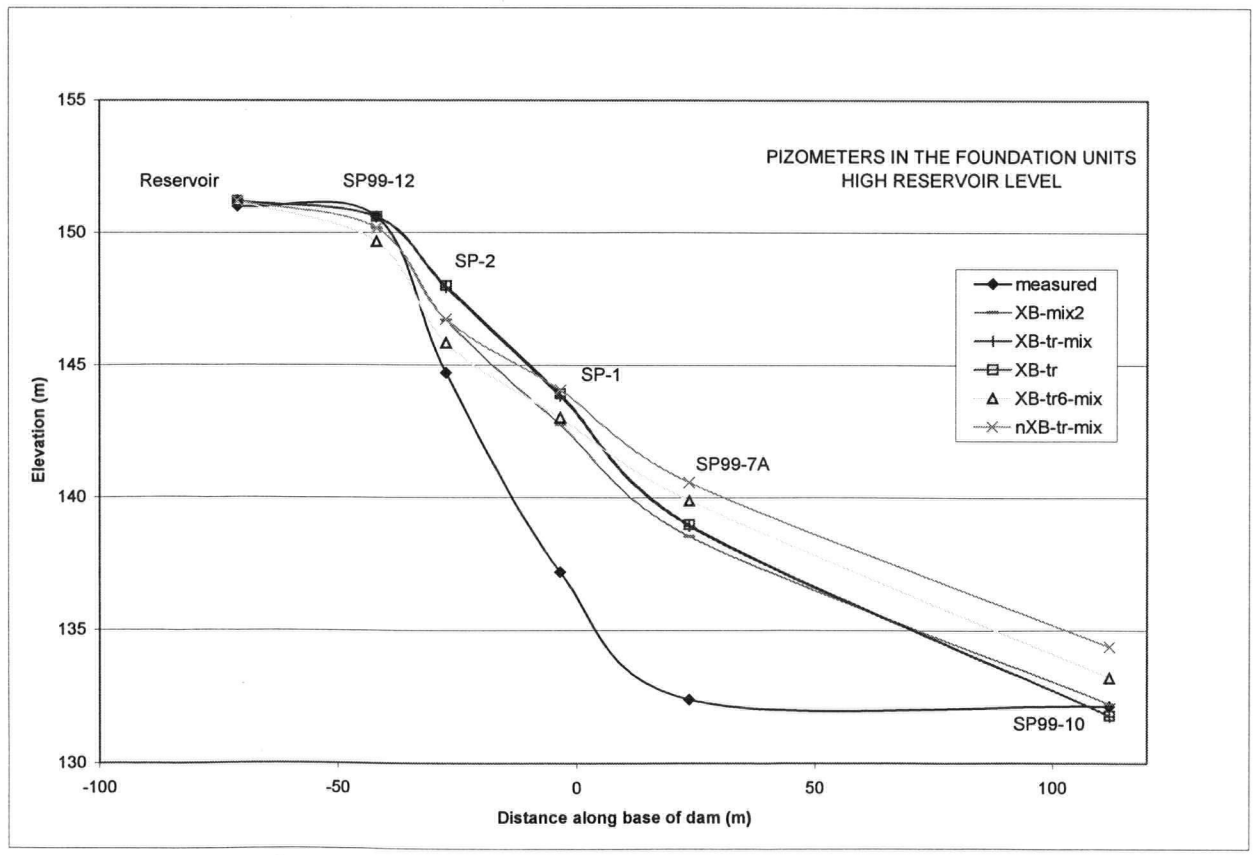

d. Data Comparison with Piezometers in the Foundation Units

Figure 6.5: Comparison of Predicted versus Measured Piezometeric Elevations from Coquitlam Dam, with a High Reservoir Level

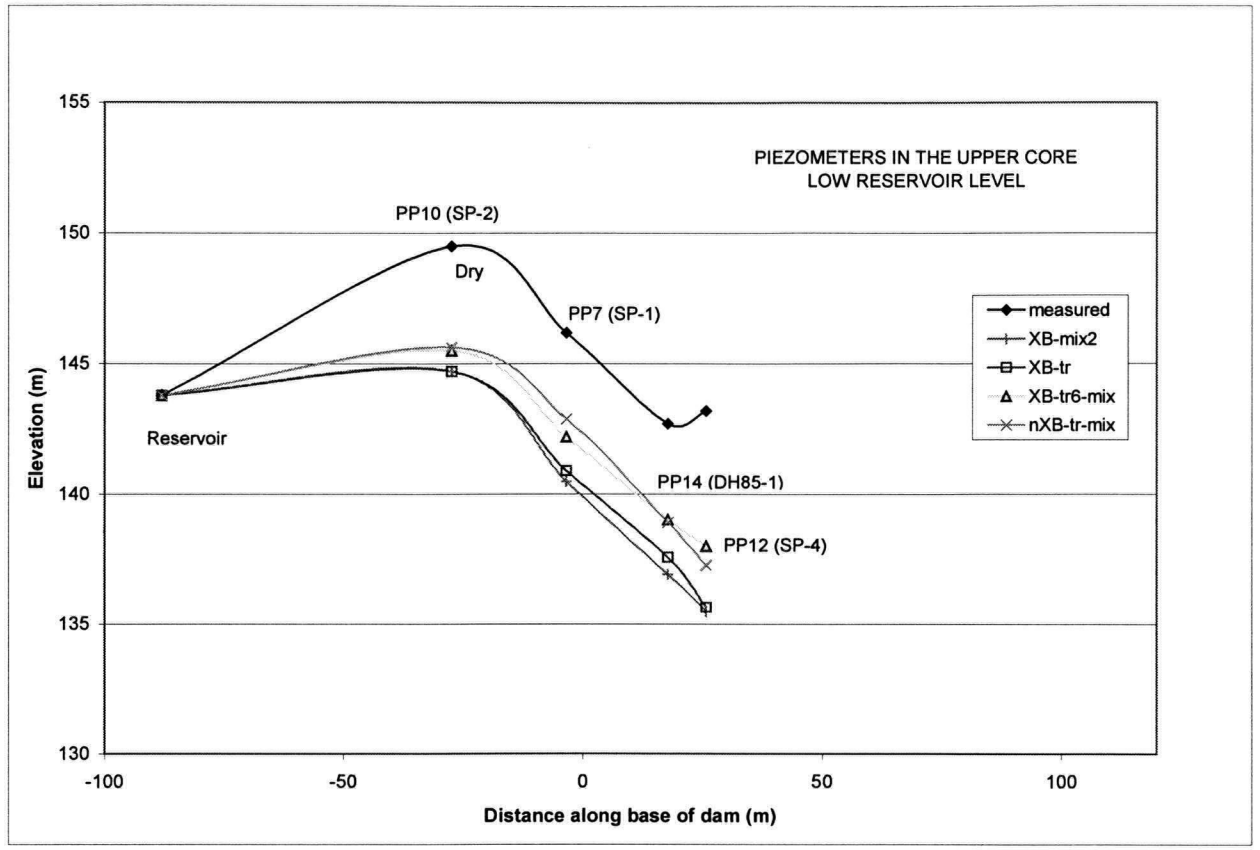

a. Data Comparison with Piezometers in the Upper Core

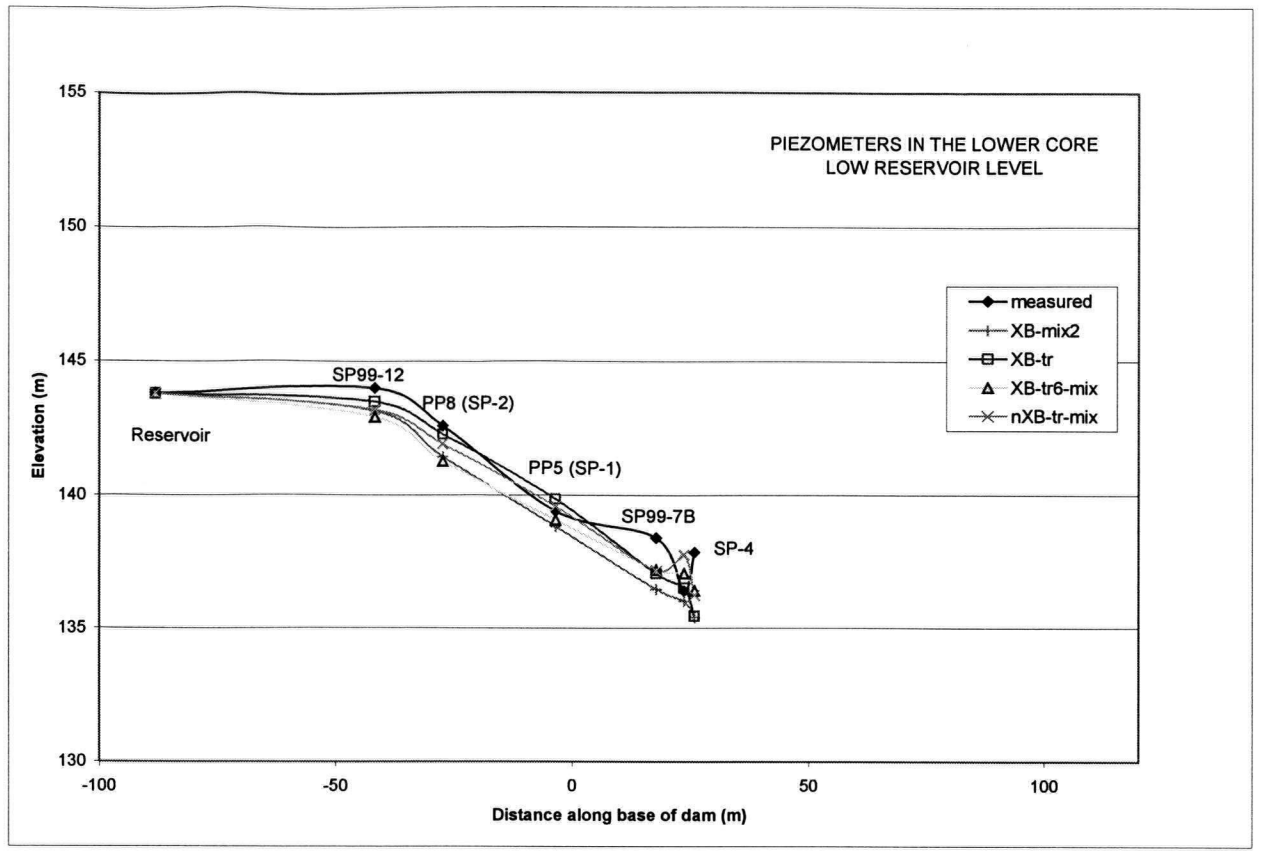

c. Data Comparison with Piezometers in the Lower Core

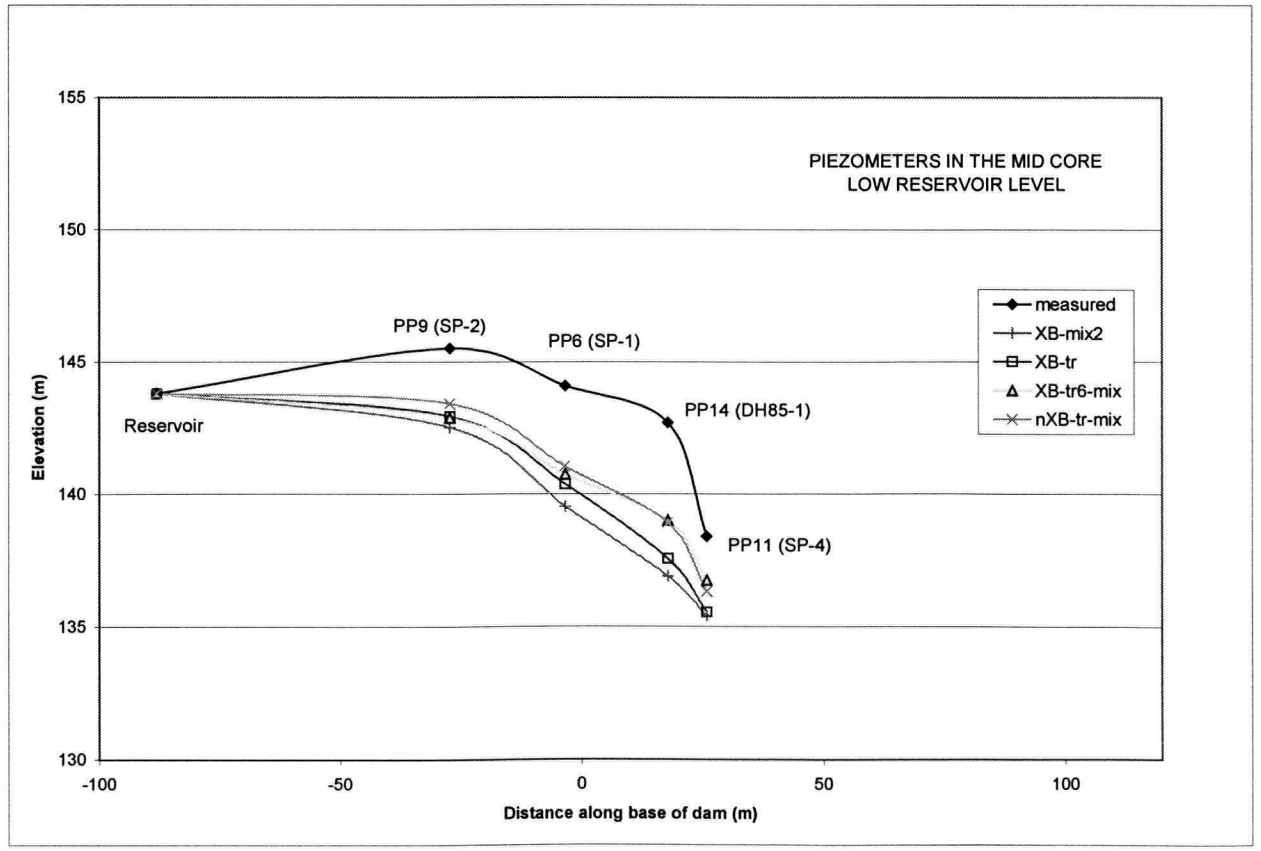

b. Data Comparison with Piezometers in the Mid Core

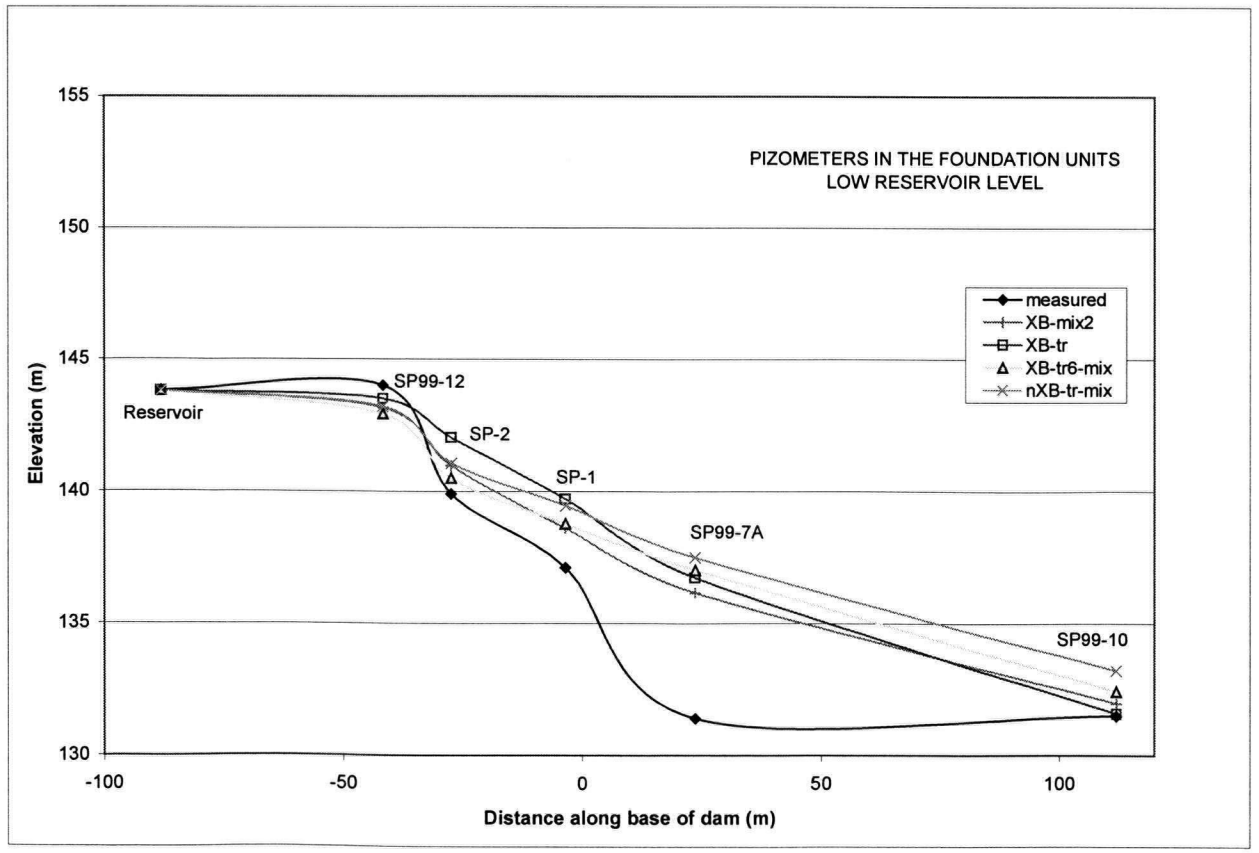

d. Data Comparison with Piezometers in the Foundation Units

Figure 6.6: Comparison of Predicted versus Measured Piezometeric Elevations from Coquitlam Dam, with a Low Reservoir Level

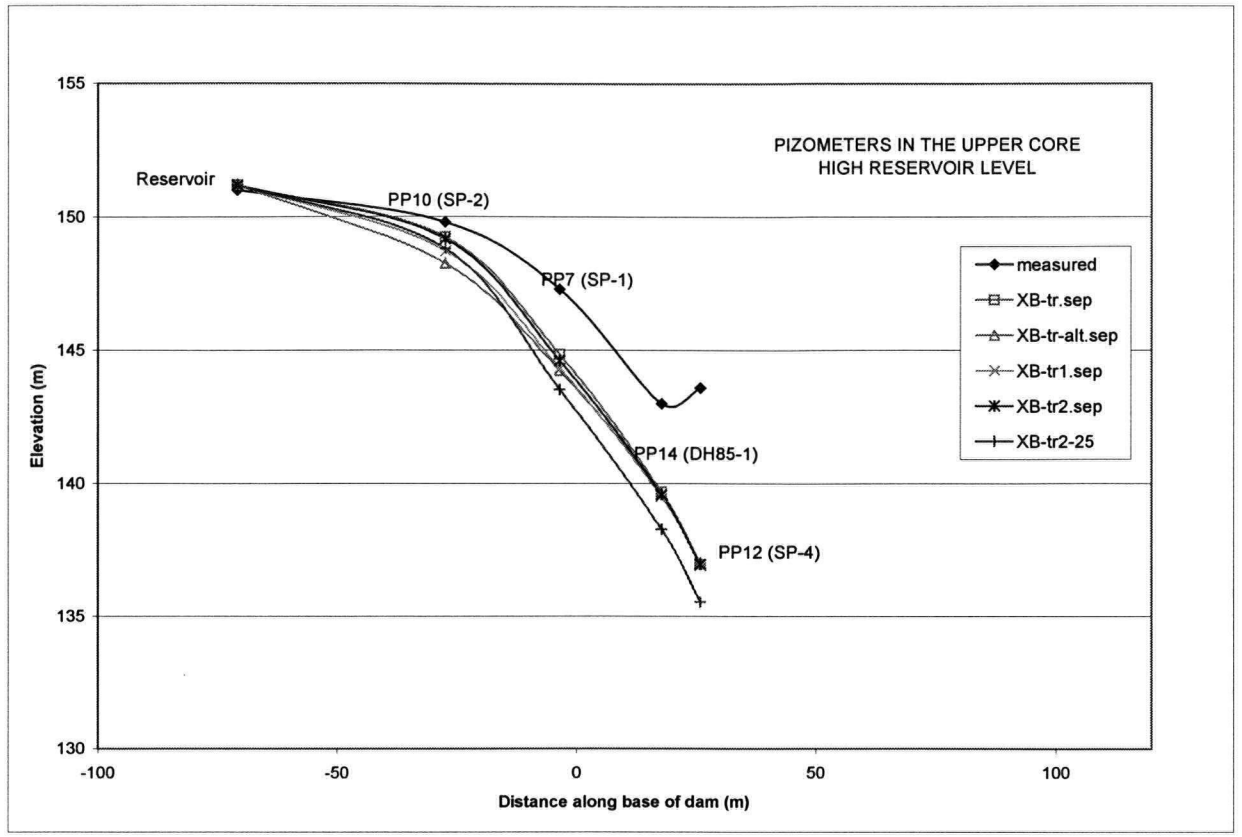

a. Data Comparison with Piezometers in the Upper Core

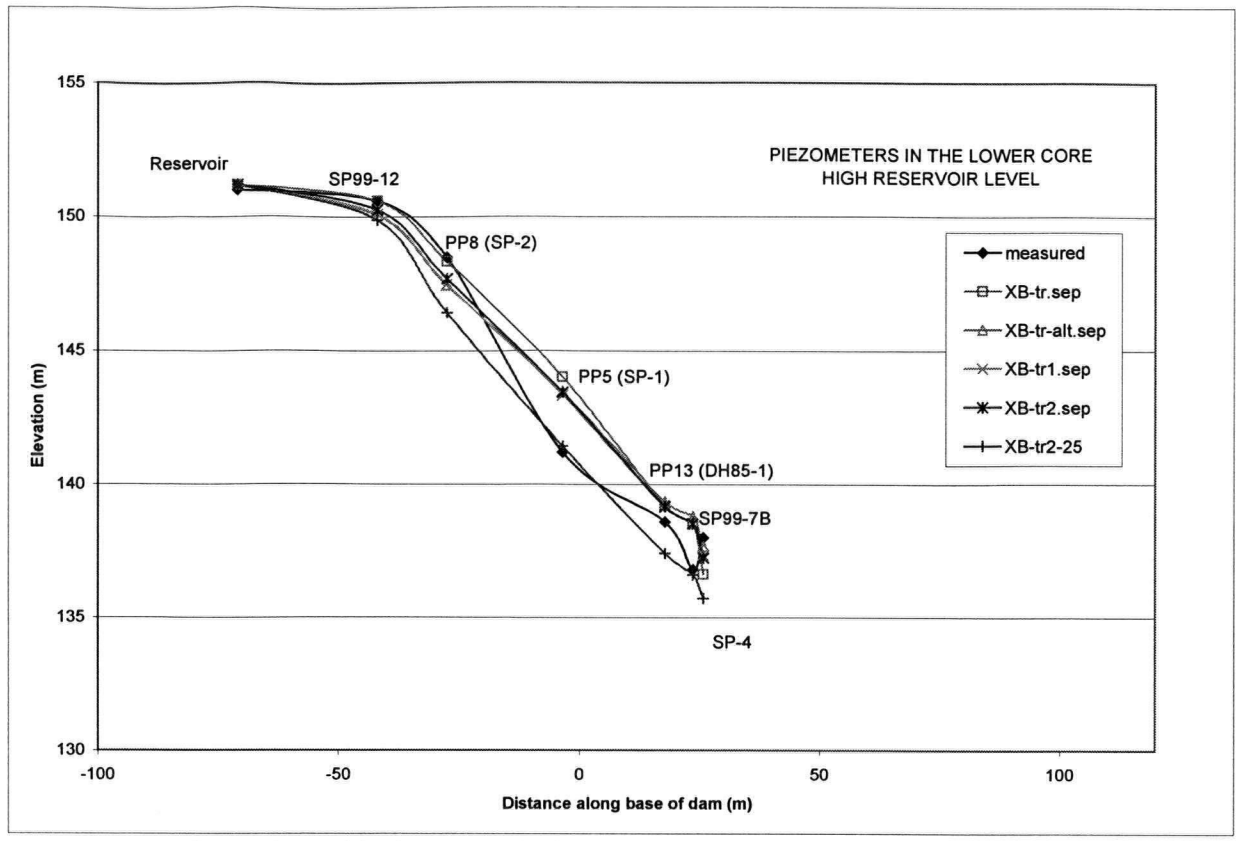

c. Data Comparison with Piezometers in the Lower Core

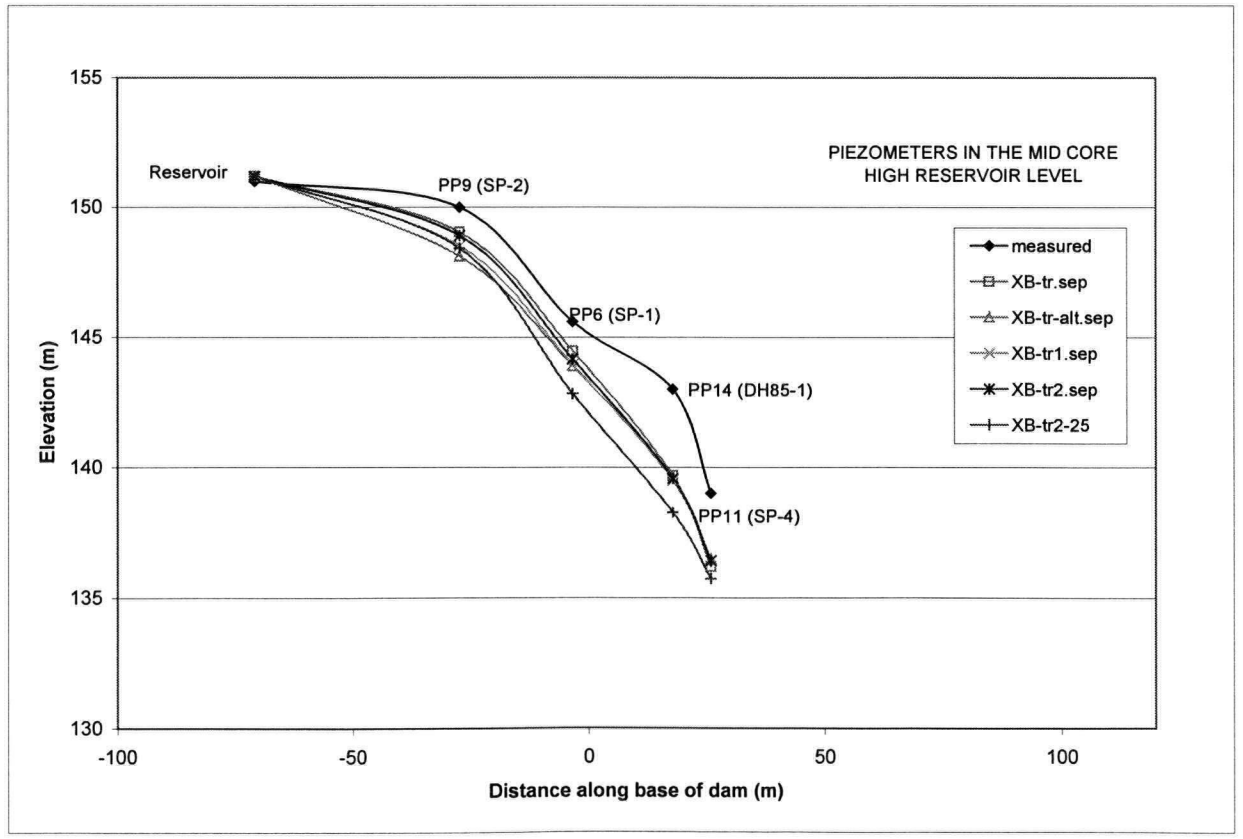

b. Data Comparison with Piezometers in the Mid Core

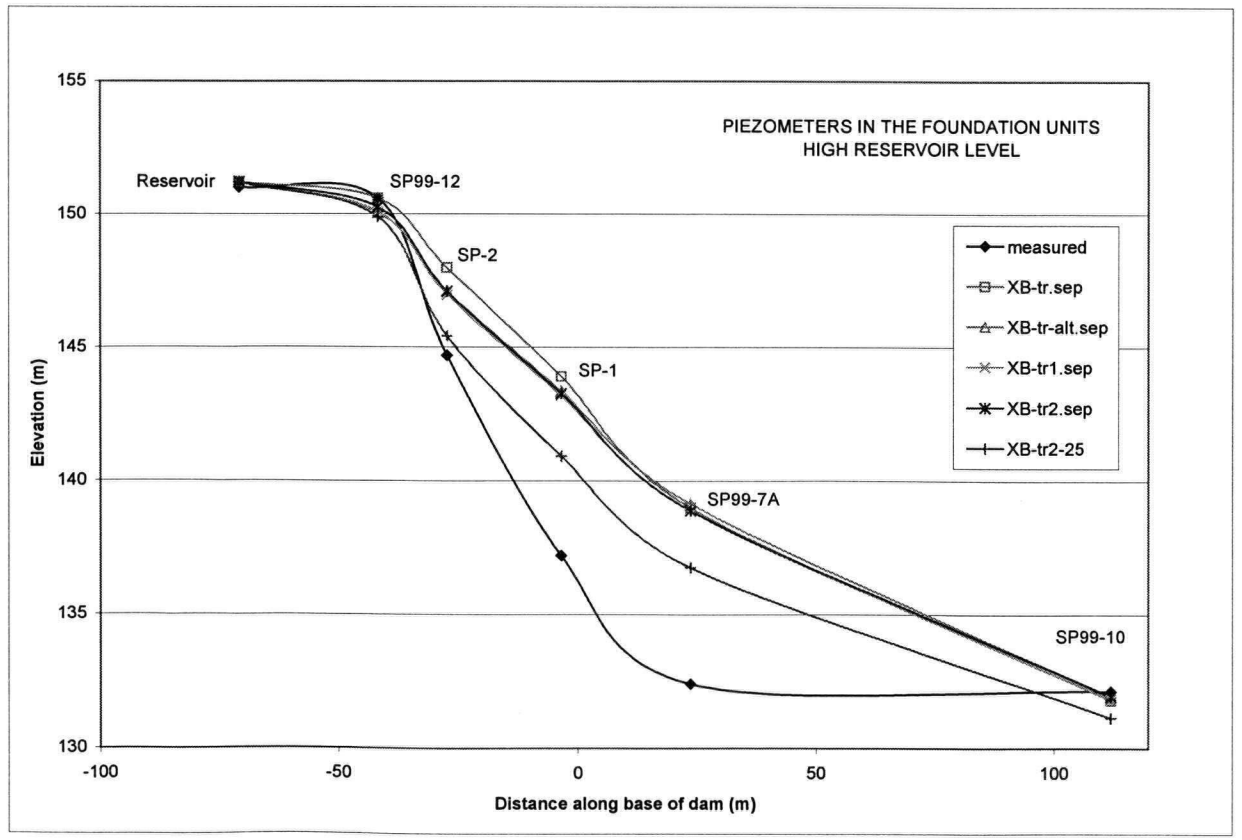

d. Data Comparison with Piezometers in the Foundation Units

Figure 6.7: Comparison of Predicted versus Measured Piezometeric Elevations from Coquitlam Dam, with a High Reservoir Level

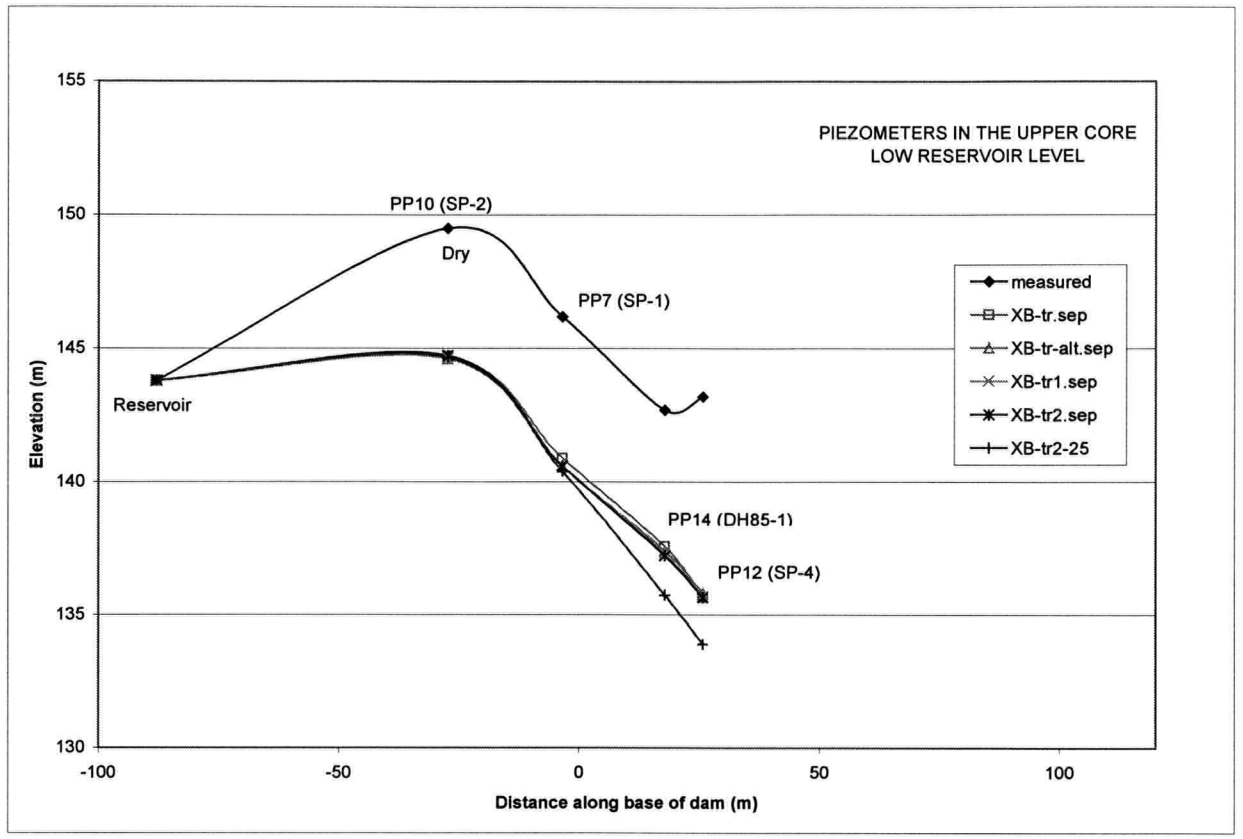

a. Data Comparison with Piezometers in the Upper Core

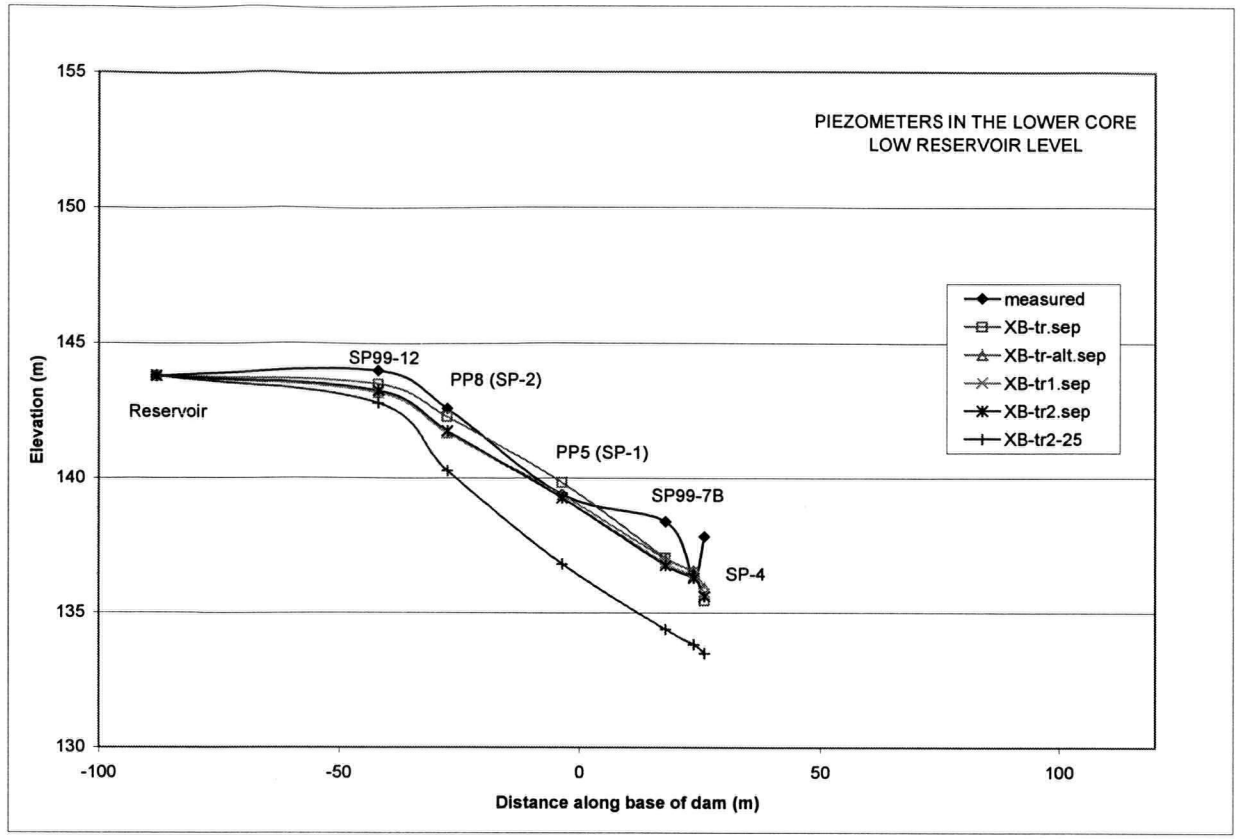

c. Data Comparison with Piezometers in the Lower Core

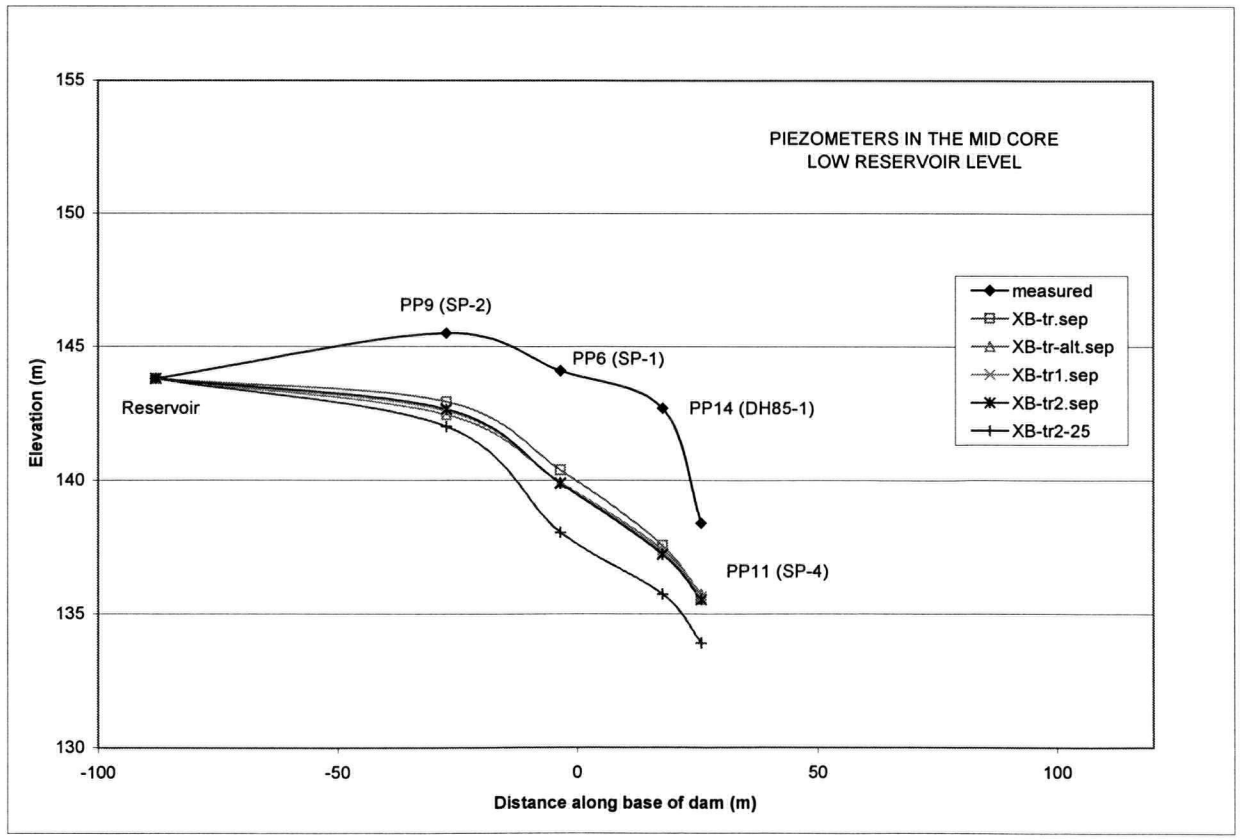

b. Data Comparison with Piezometers in the Mid Core

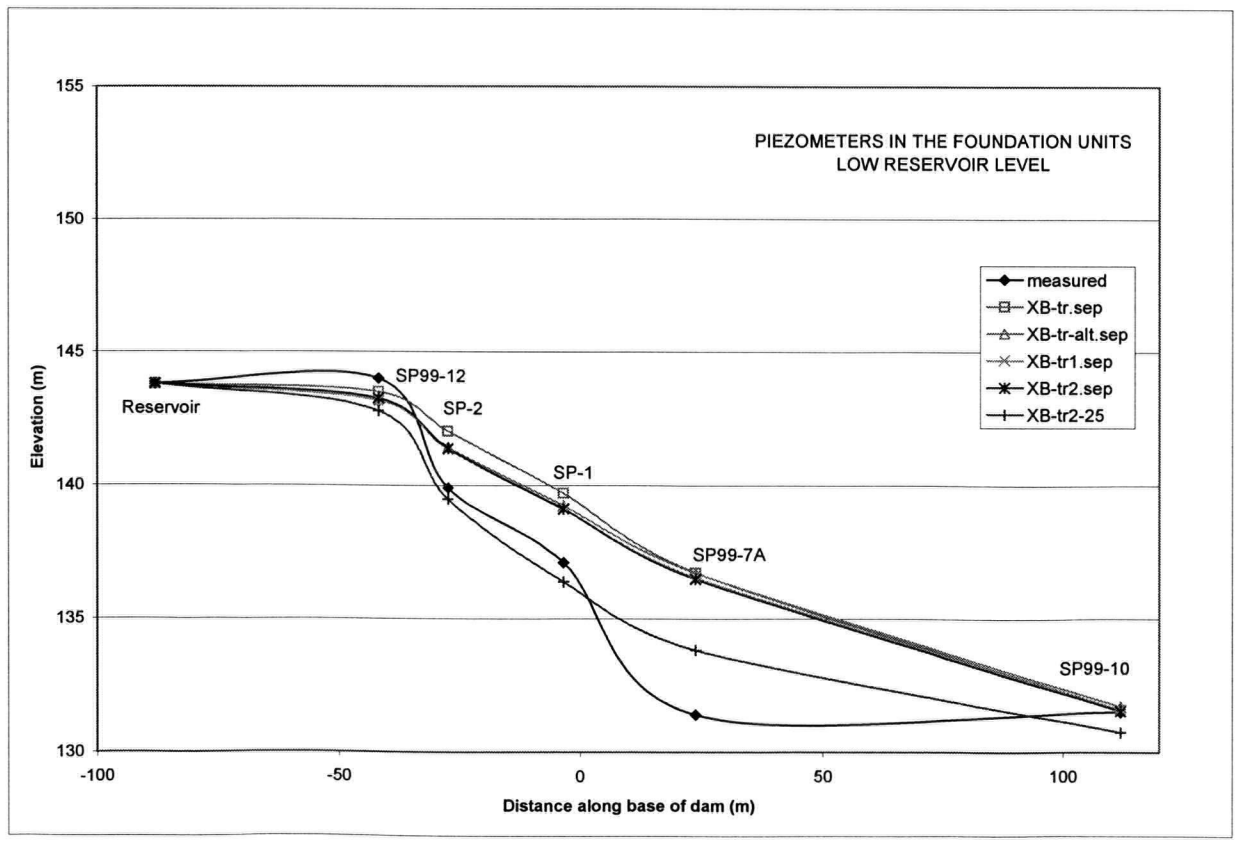

d. Data Comparison with Piezometers in the Foundation Units

Figure 6.8: Comparison of Predicted versus Measured Piezometeric Elevations from Coquitlam Dam, with a Low Reservoir Level

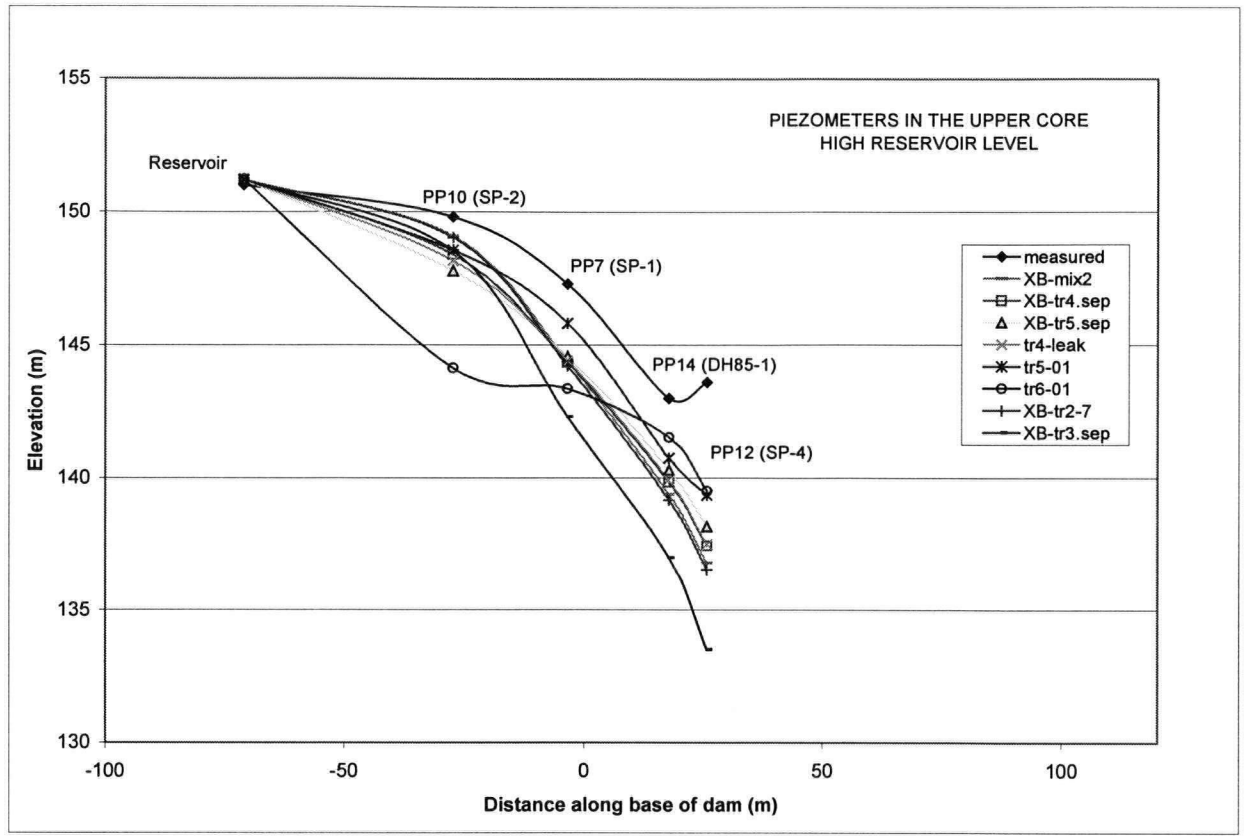

a. Data Comparison with Piezometers in the Upper Core

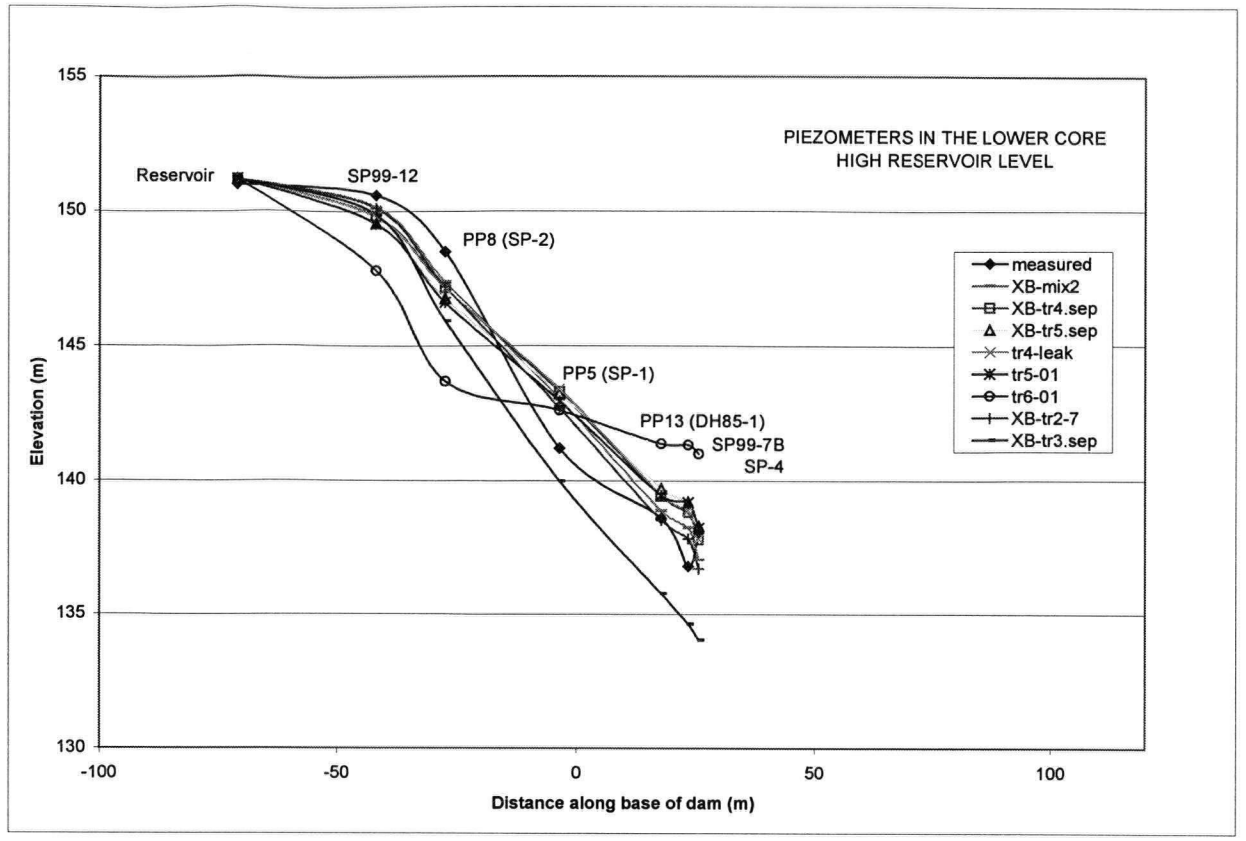

c. Data Comparison with Piezometers in the Lower Core

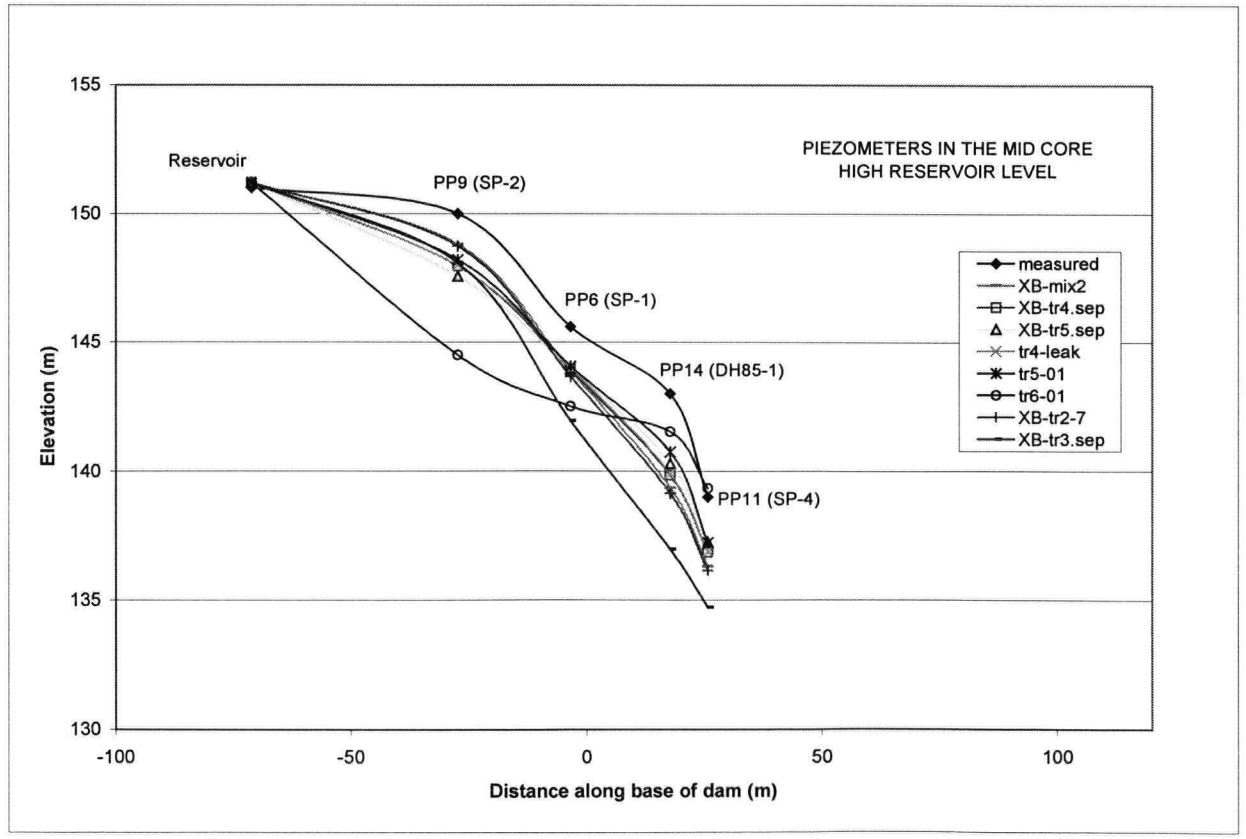

b. Data Comparison with Piezometers in the Mid Core

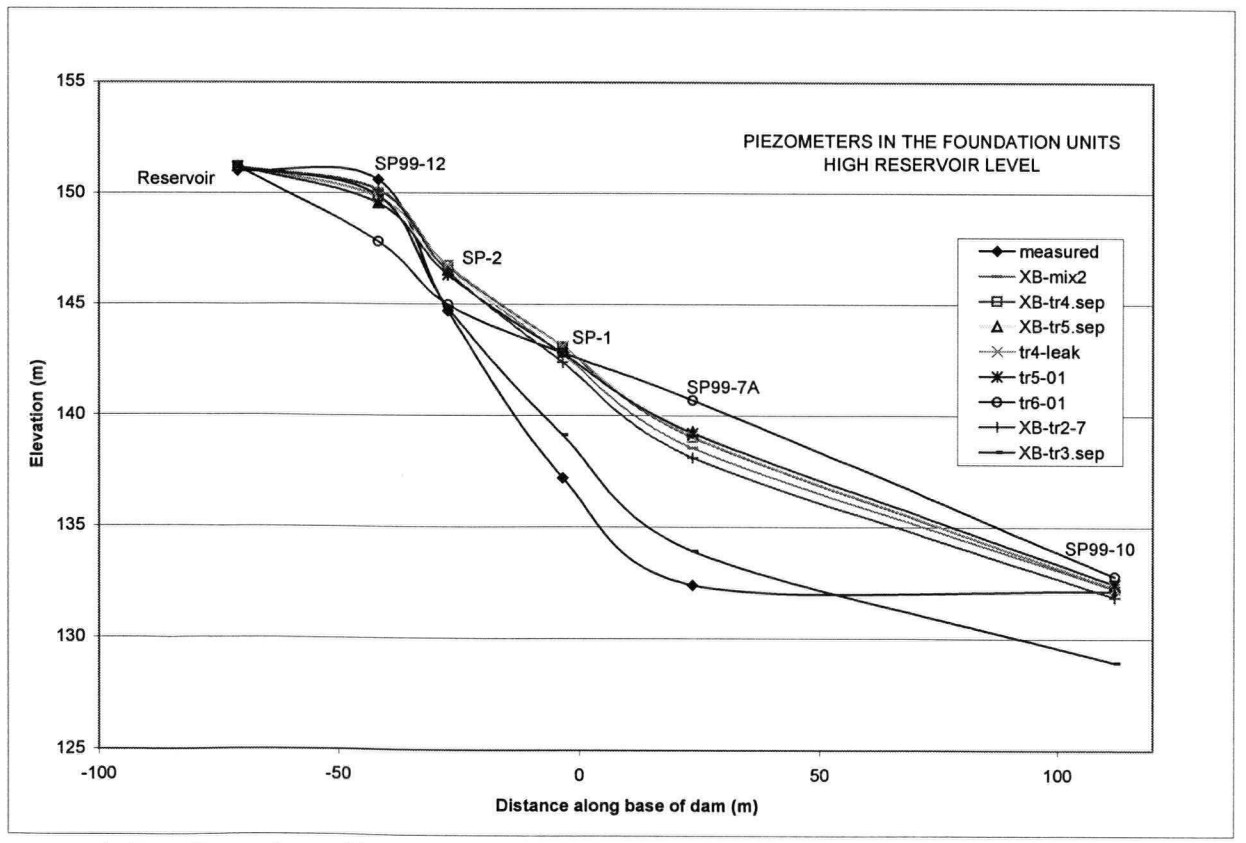

d. Data Comparison with Piezometers in the Foundation Units

Figure 6.9: Comparison of Predicted versus Measured Piezometeric Elevations from Coquitlam Dam, with a High Reservoir Level

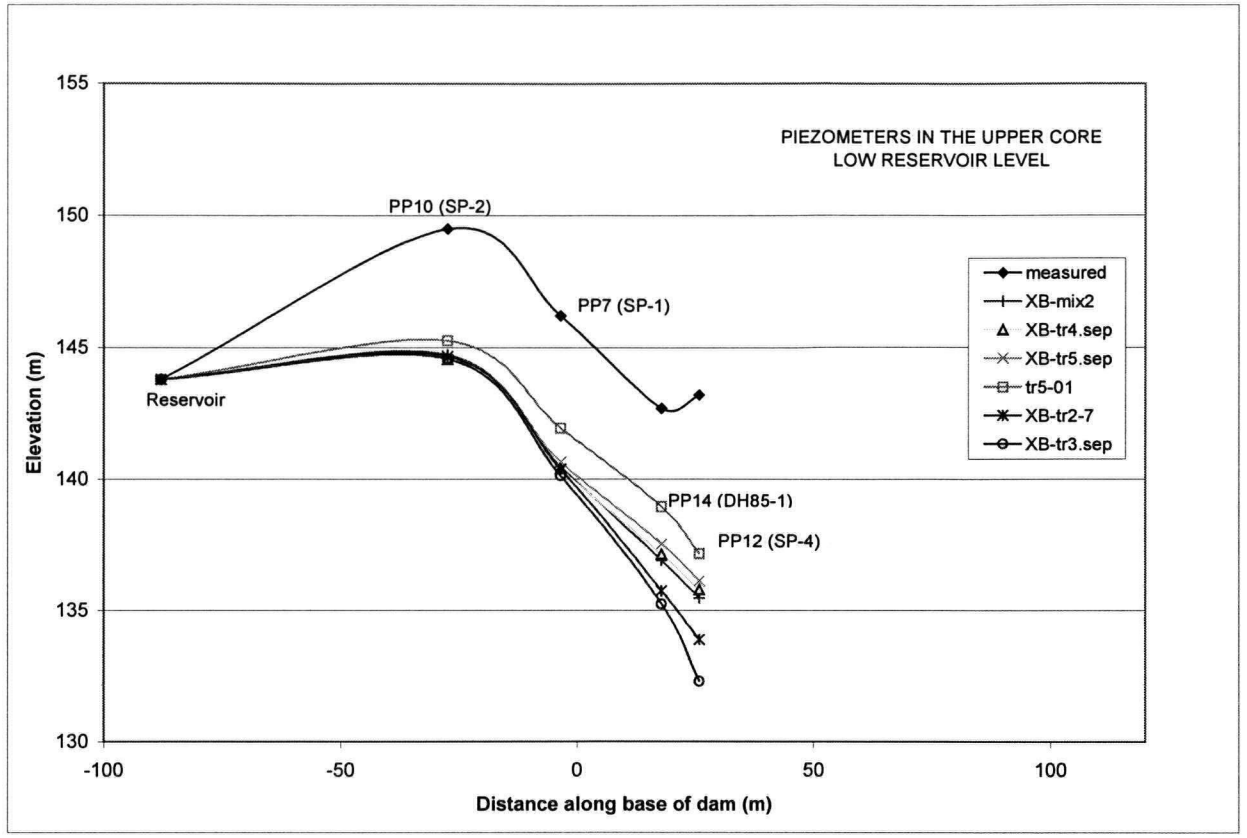

a. Data Comparison with Piezometers in the Upper Core

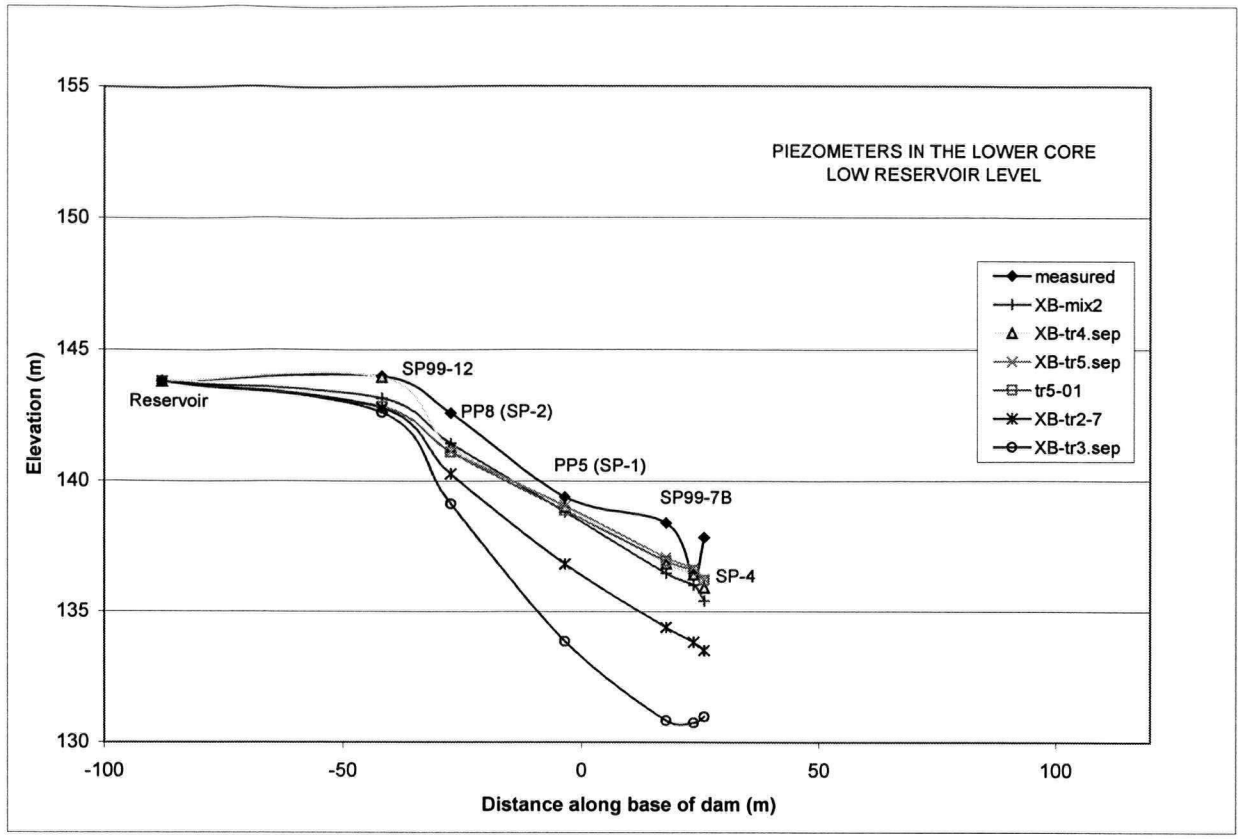

c. Data Comparison with Piezometers in the Lower Core

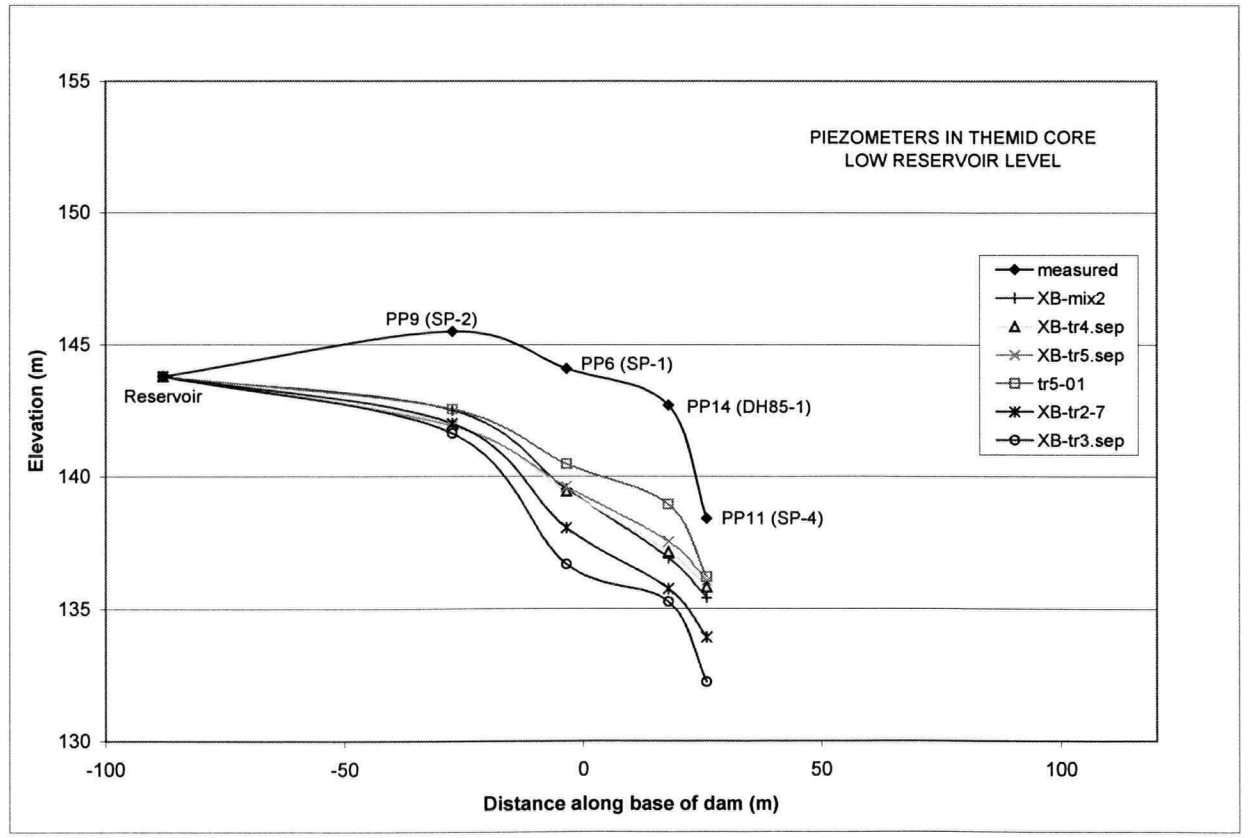

b. Data Comparison with Piezometers in the Mid Core

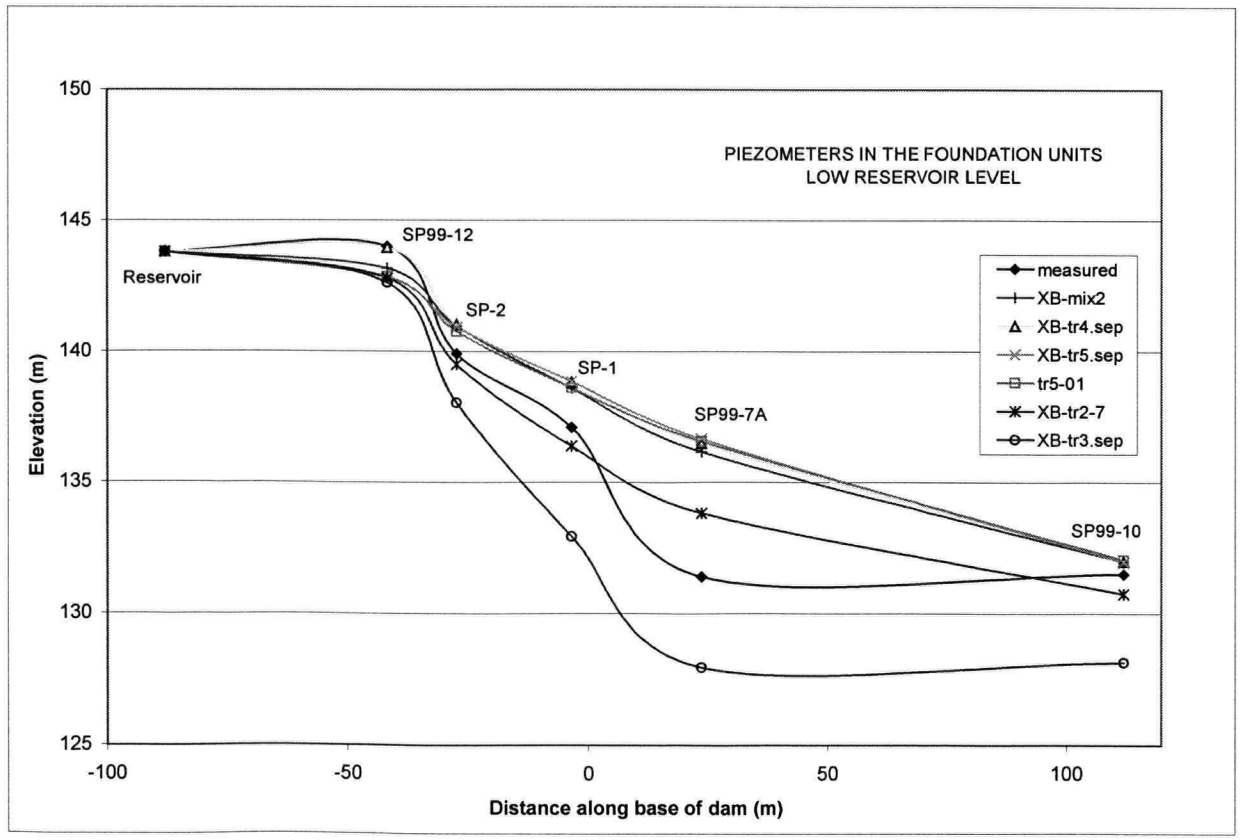

d. Data Comparison with Piezometers in the Foundation Units

Figure 6.10: Comparison of Predicted versus Measured Piezometeric Elevations from Coquitlam Dam, with a Low Reservoir Level

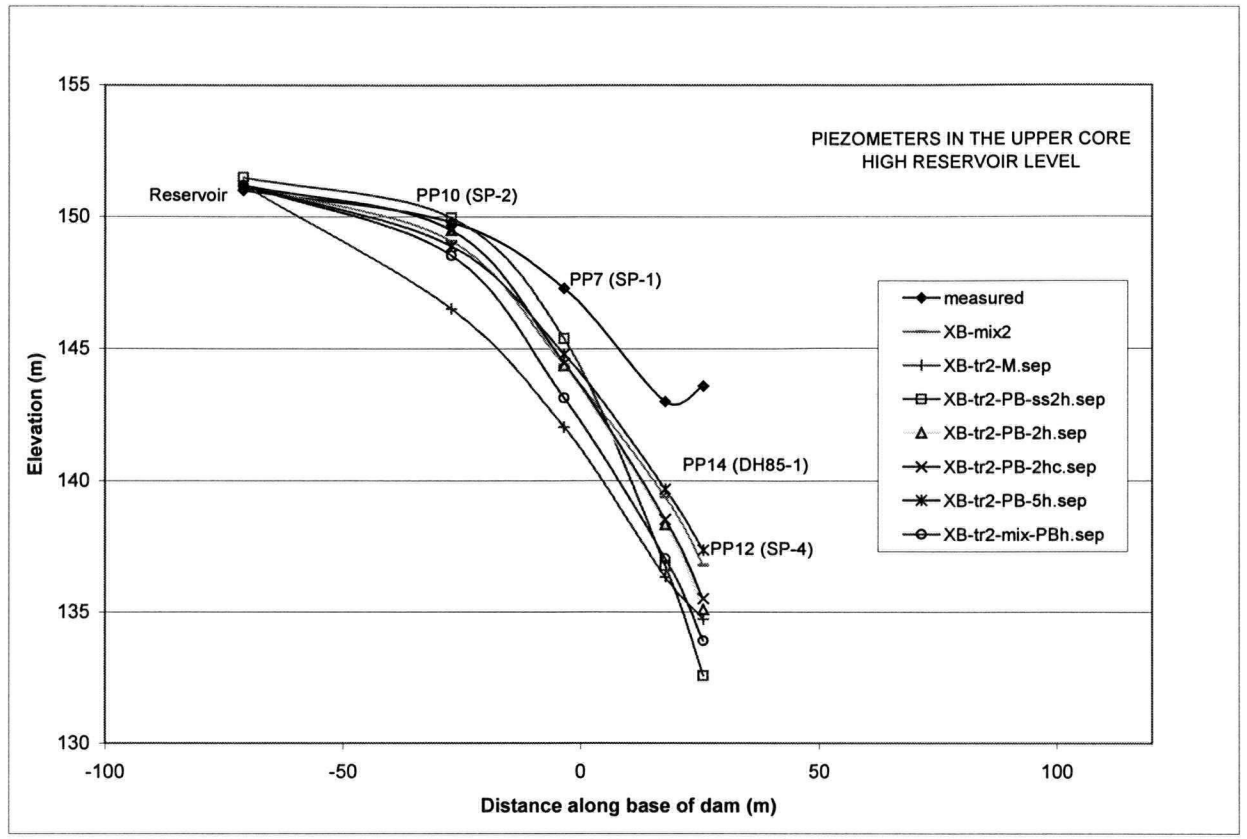

a. Data Comparison with Piezometers in the Upper Core

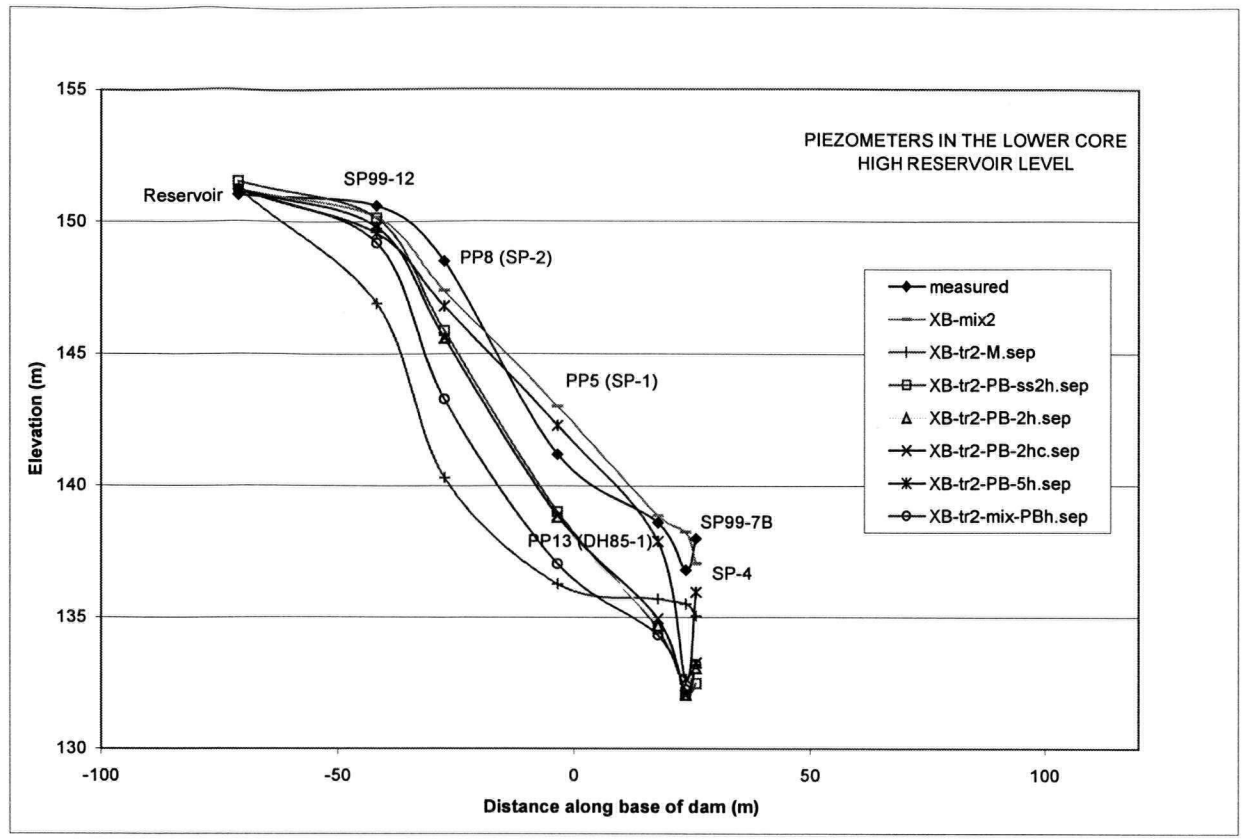

c. Data Comparison with Piezometers in the Lower Core

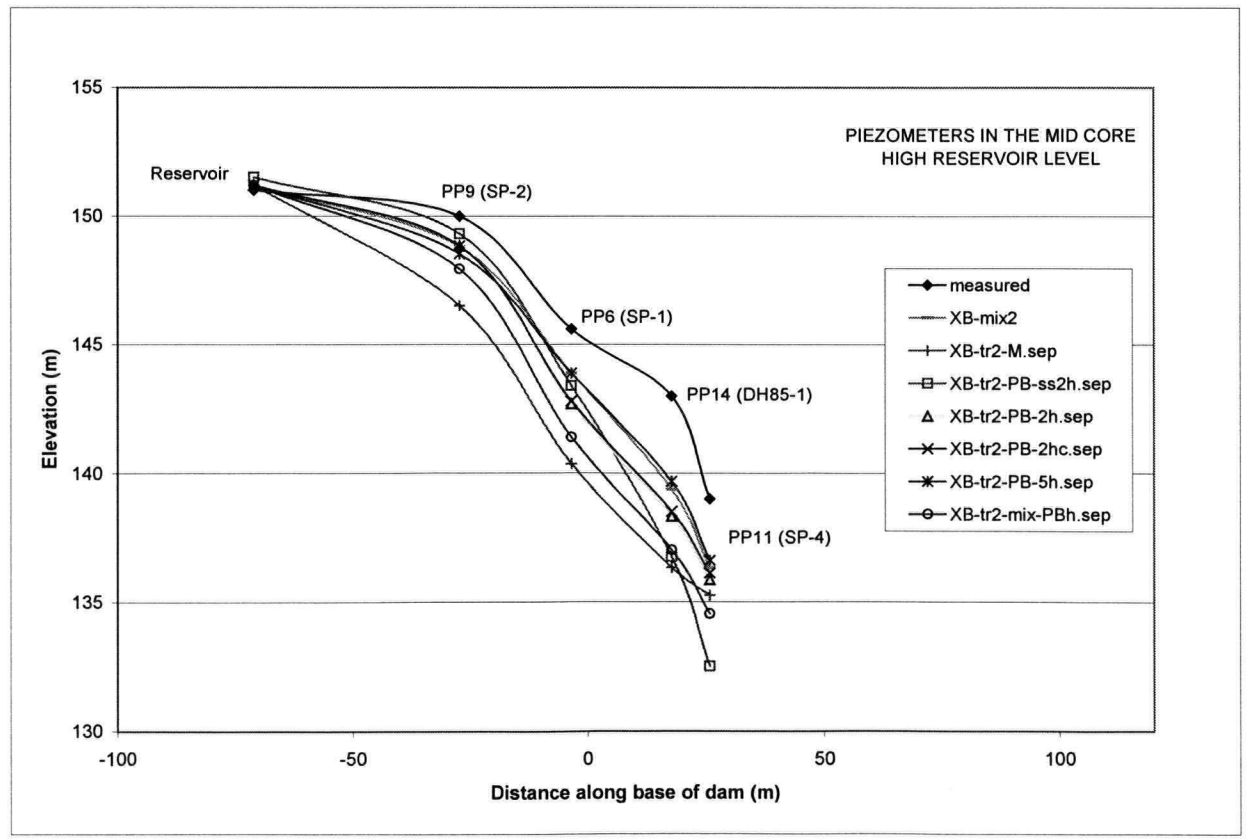

b. Data Comparison with Piezometers in the Mid Core

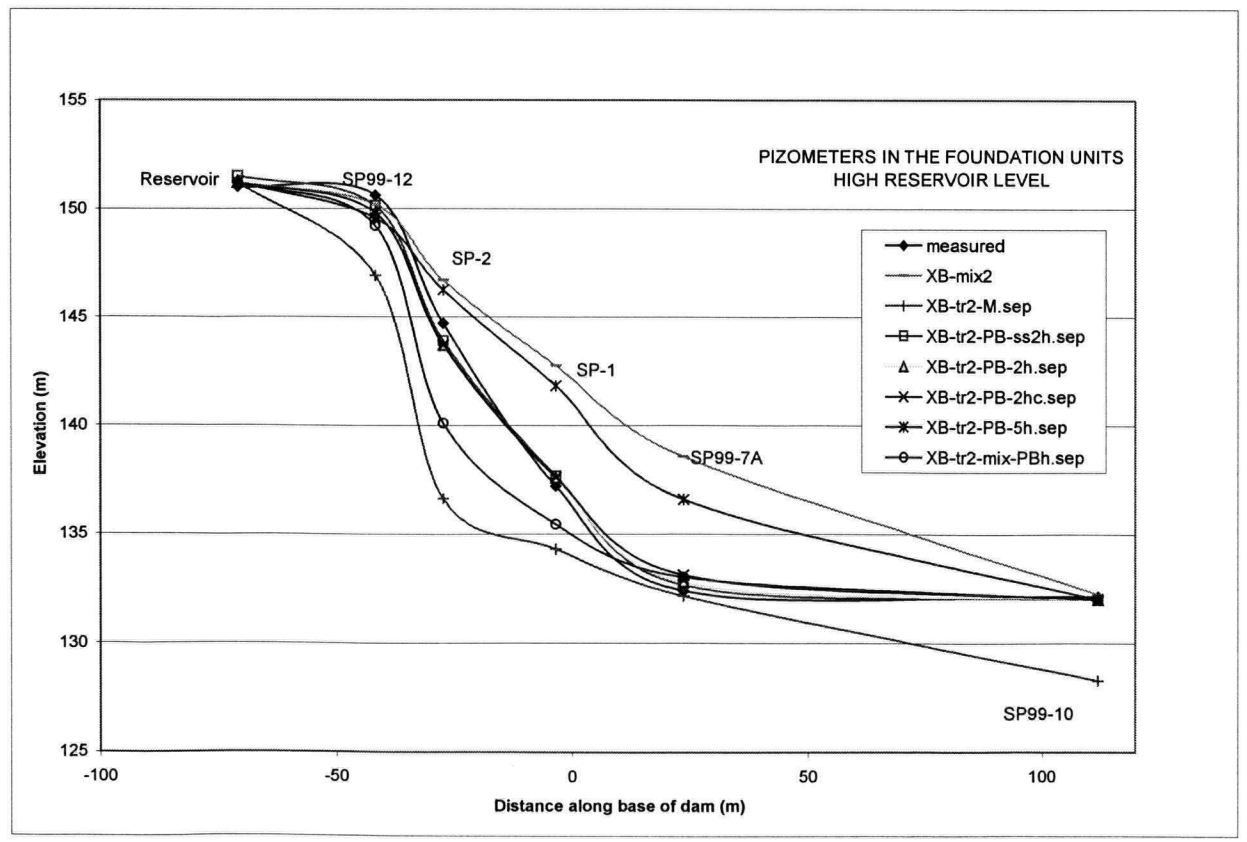

d. Data Comparison with Piezometers in the Foundation Units

Figure 6.11: Predicted versus Measured Piezometeric Elevations from Coquitlam Dam Using Constant Head Values - High Reservoir Level

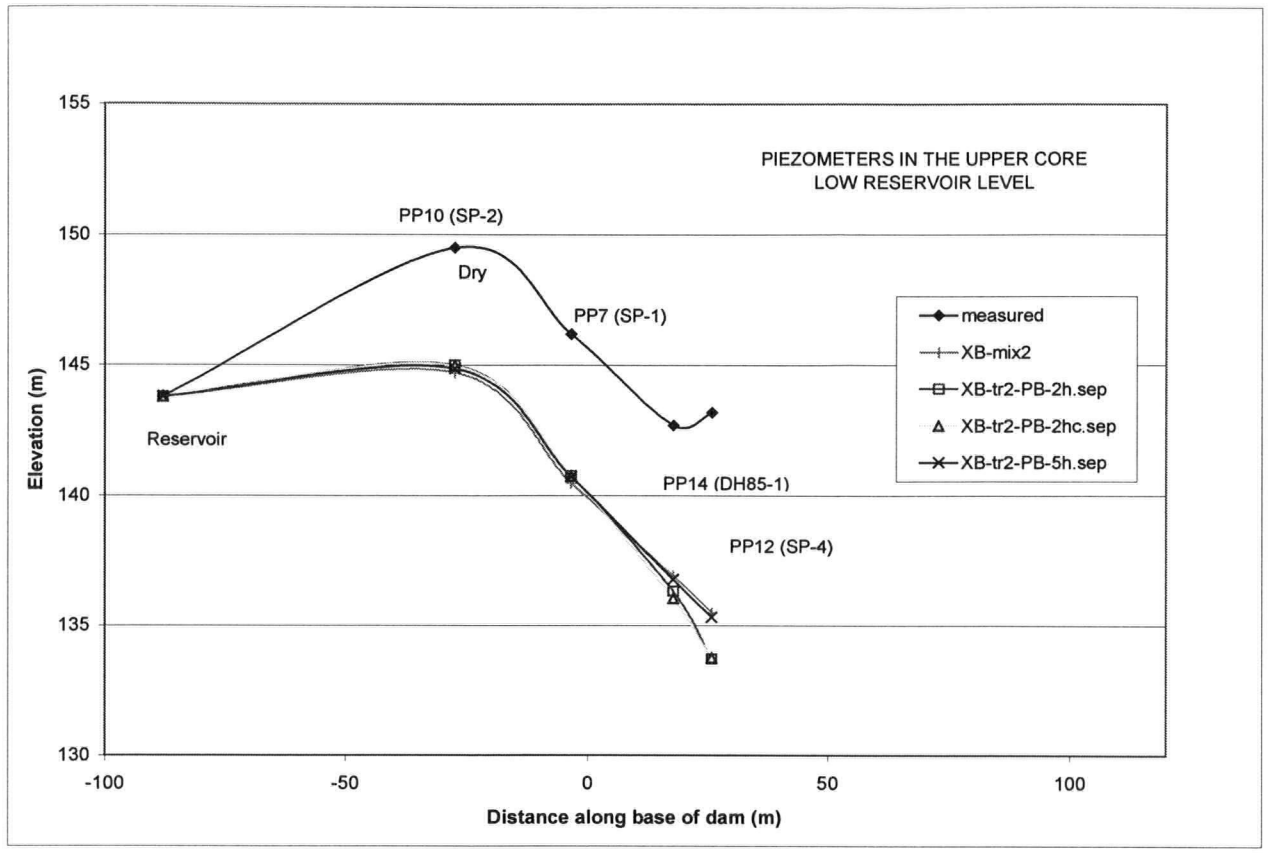

a. Data Comparison with Piezometers in the Upper Core

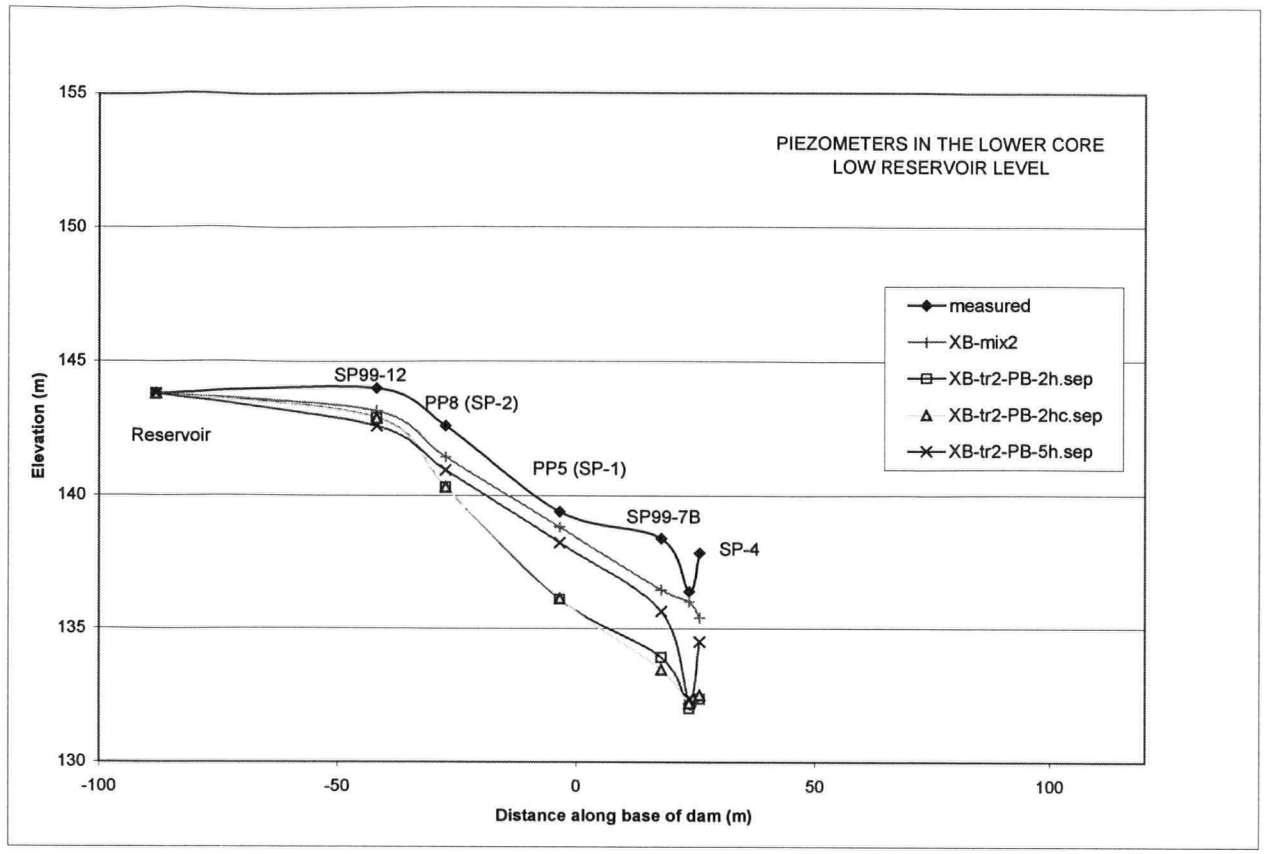

c. Data Comparison with Piezometers in the Lower Core

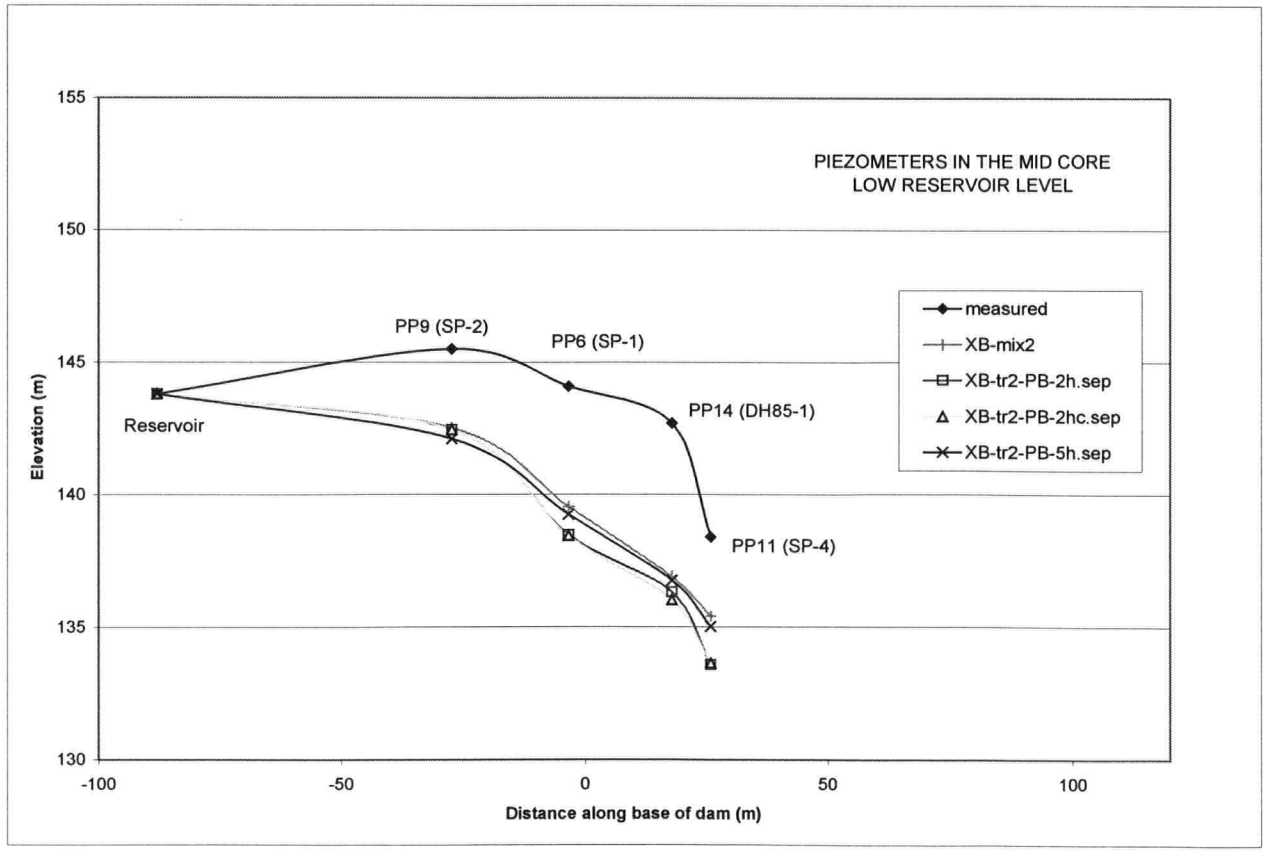

b. Data Comparison with Piezometers in the Mid Core

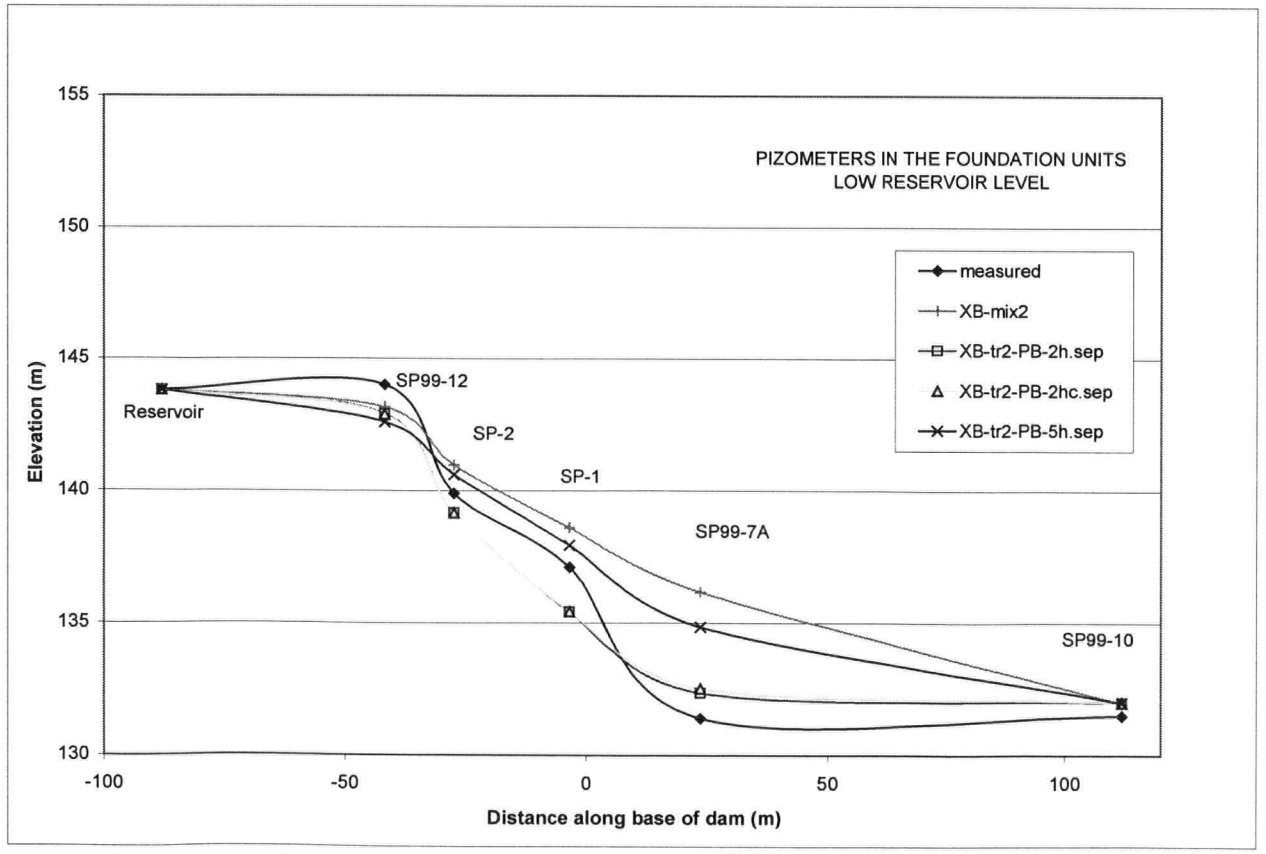

d. Data Comparison with Piezometers in the Foundation Units

Figure 6.12: Predicted versus Measured Piezometeric Elevations from Coquitlam Dam Using Constant Head Values - Low Reservoir Level

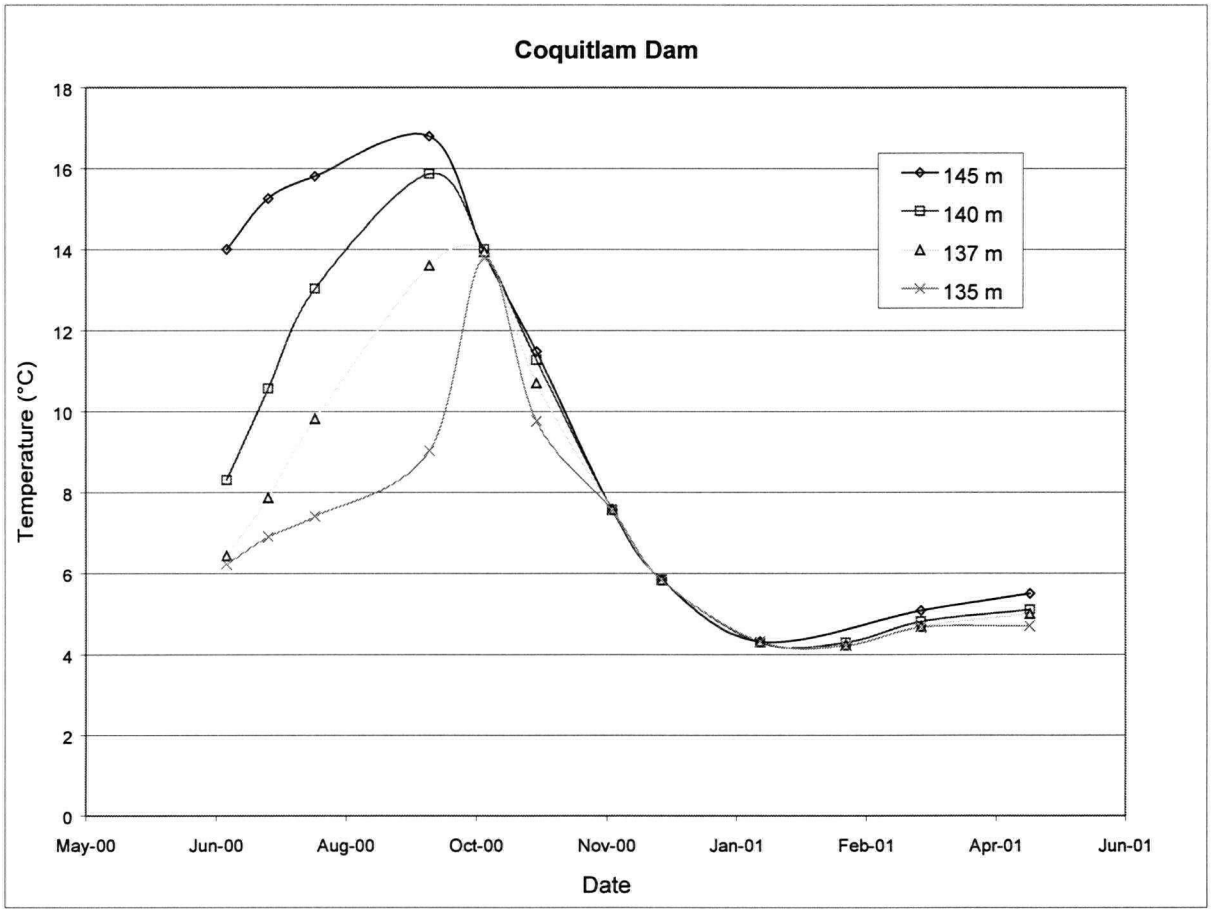

Figure 6.13: Reservoir Temperature Data Inputted Into CTRAN/W

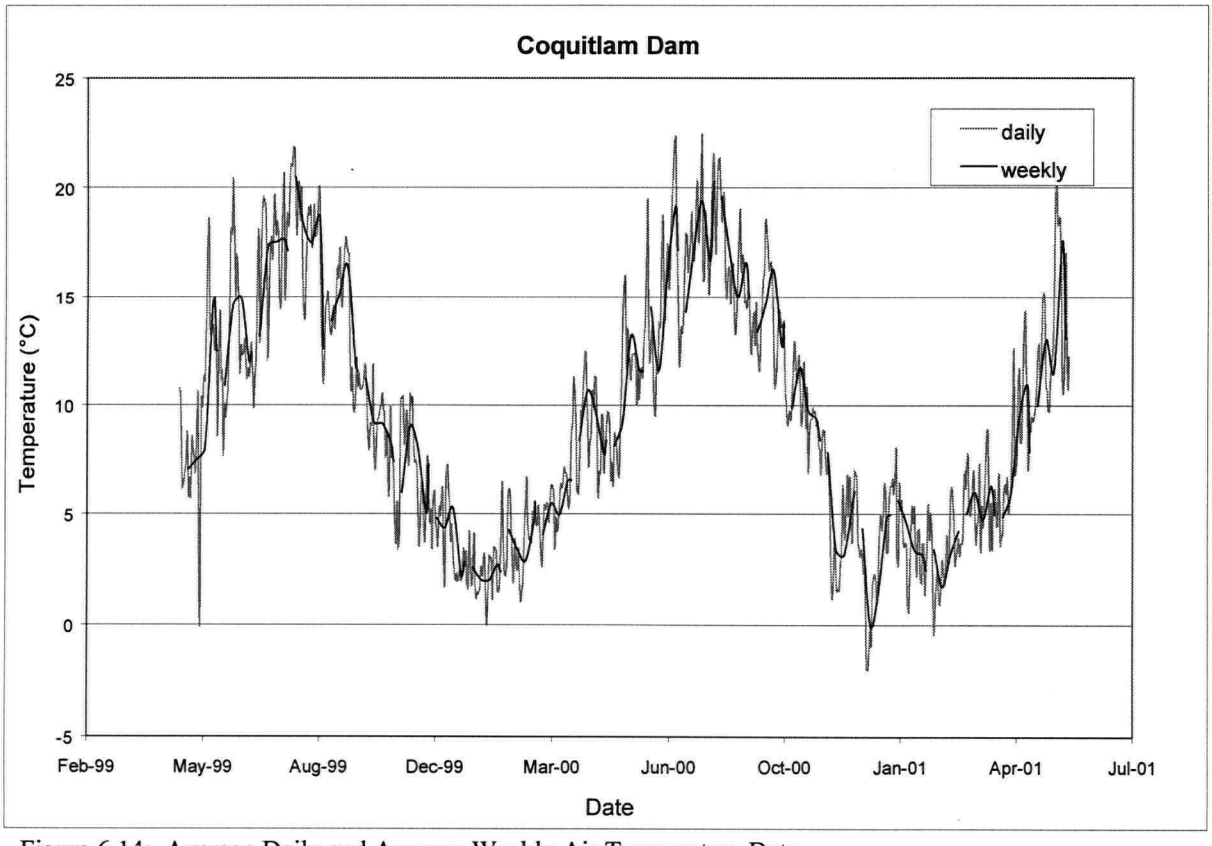

Figure 6.14: Average Daily and Average Weekly Air Temperature Data

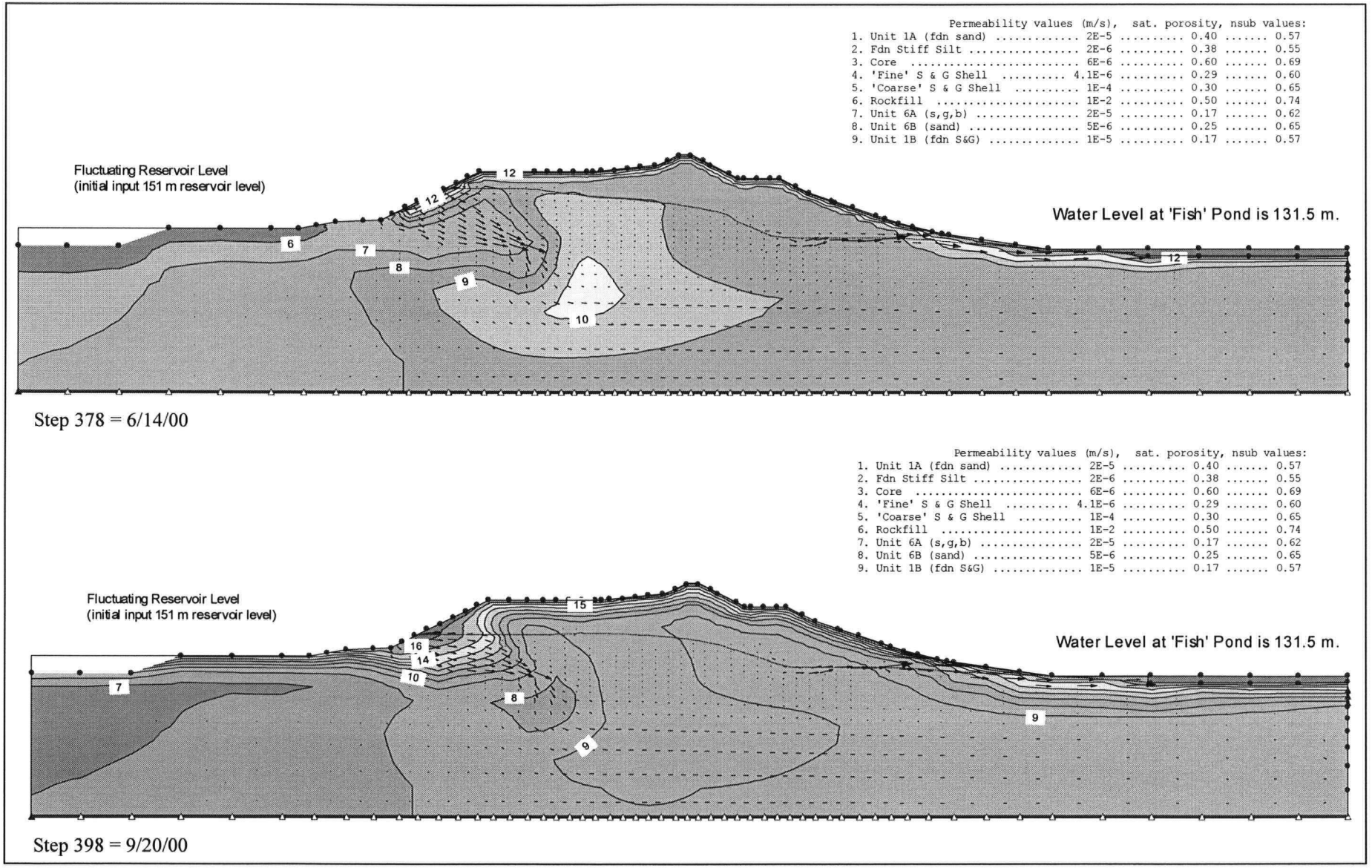

Figure 6.15: Predicted Temperature Distribution within Coquitlam Dam, Model Simulation XB-mix2

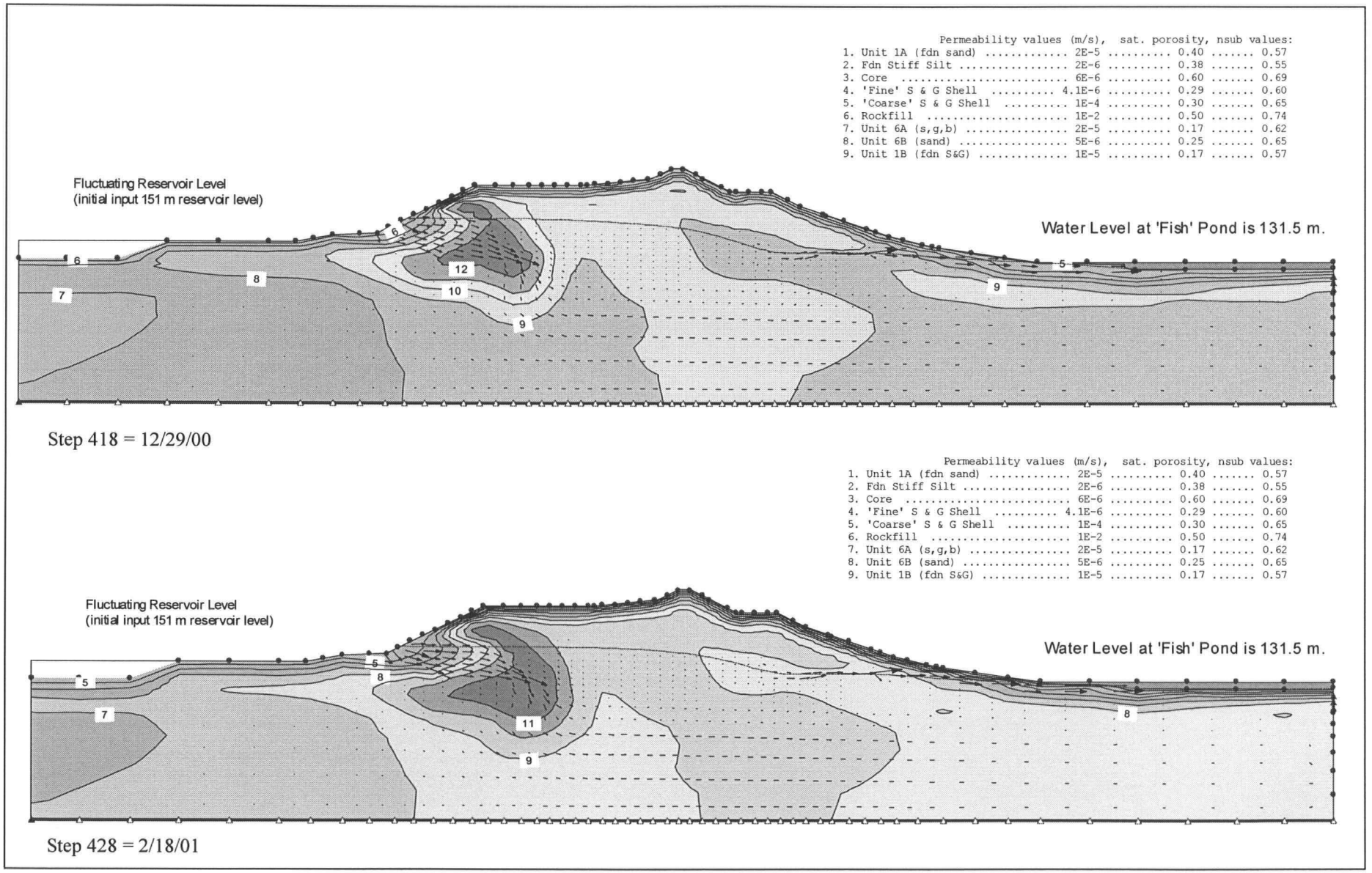

Figure 6.16: Predicted Temperature Distribution within Coquitlam Dam, Model Simulation XB-mix2

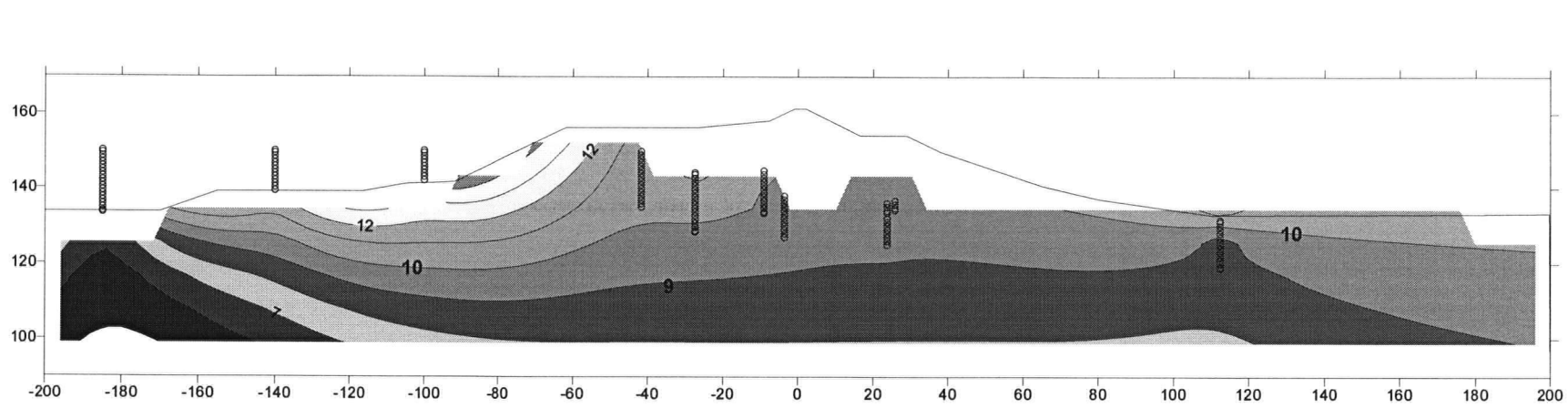

Surfer Krigging Contour Plot of the Temperature Data Collected on July 31, 2000 – Coquitlam Dam

	Permeability values (m/s),	sat. porosity,	nsub values:
1. Unit 1A (fdn sand)	2E-5	0.40	0.57
2. Fdn Stiff Silt	2E-6	0.38	0.55
3. Core	6E-6	0.60	0.69
4. 'Fine' S & G Shell	4.1E-6	0.29	0.60
5. 'Coarse' S & G Shell	1E-4	0.30	0.65
6. Rockfill	1E-2	0.50	0.74
7. Unit 6A (s,g,b)	2E-5	0.17	0.62
8. Unit 6B (sand)	5E-6	0.25	0.65
9. Unit 1B (fdn S&G)	1E-5	0.17	0.57

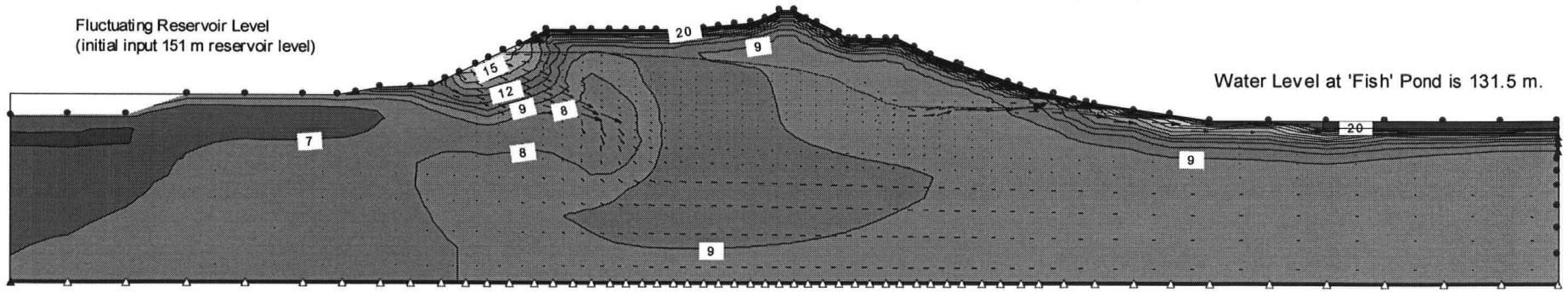

CTRAN/W Contour Plot of the Predicted Temperature Distribution within Coquitlam Dam on August 1, 2000 – Simulation "XB-mix2"

Figure 6.17: Comparison of Measured versus Predicted Temperature Distribution within Coquitlam Dam

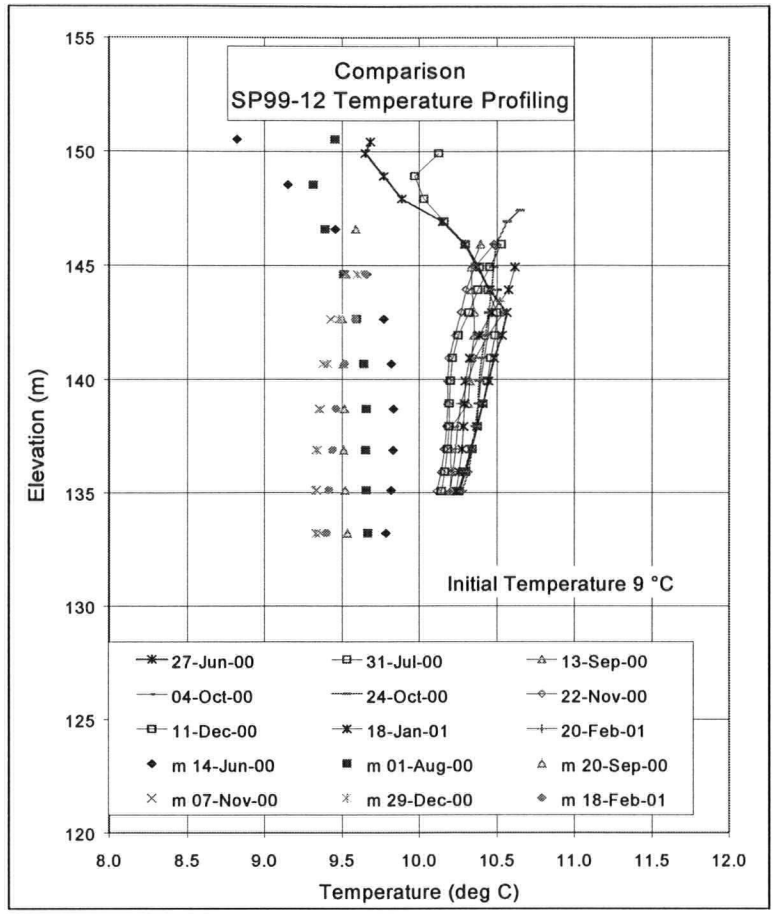

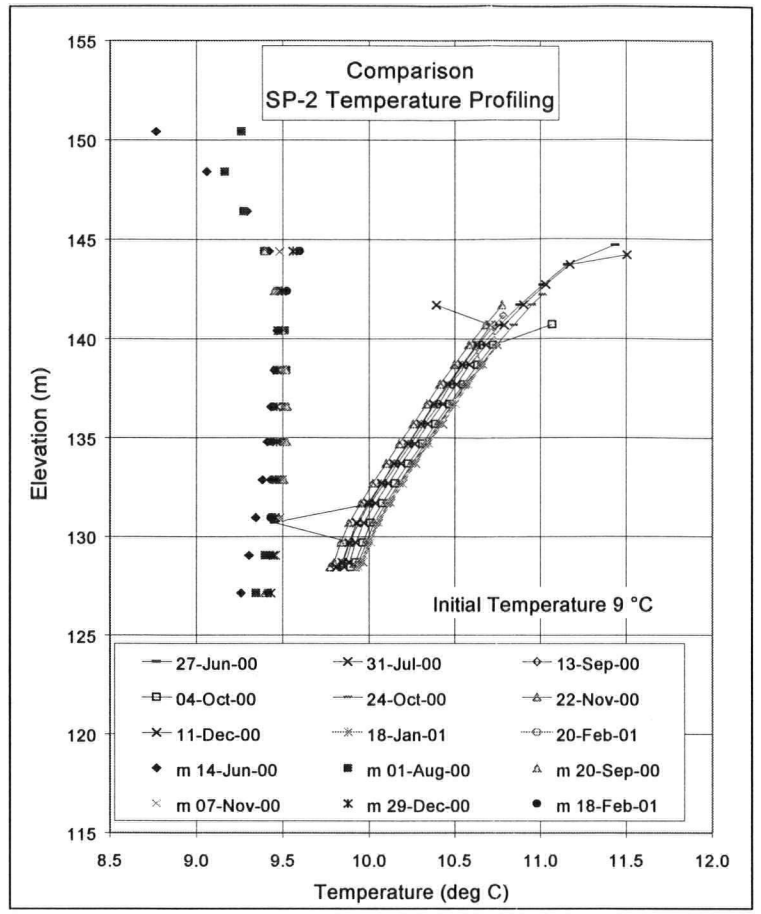

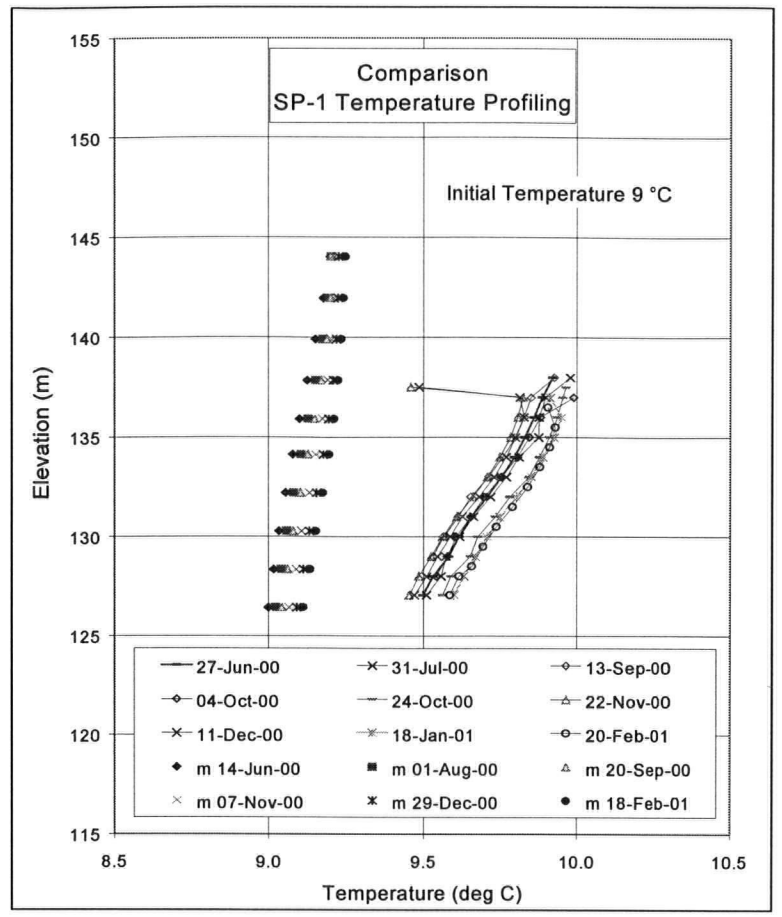

Note:

Data points identified by an m followed by a date are from computer simulations. This data has been plotted as points only.

Data plotted as points and a line represent measured temperatures.

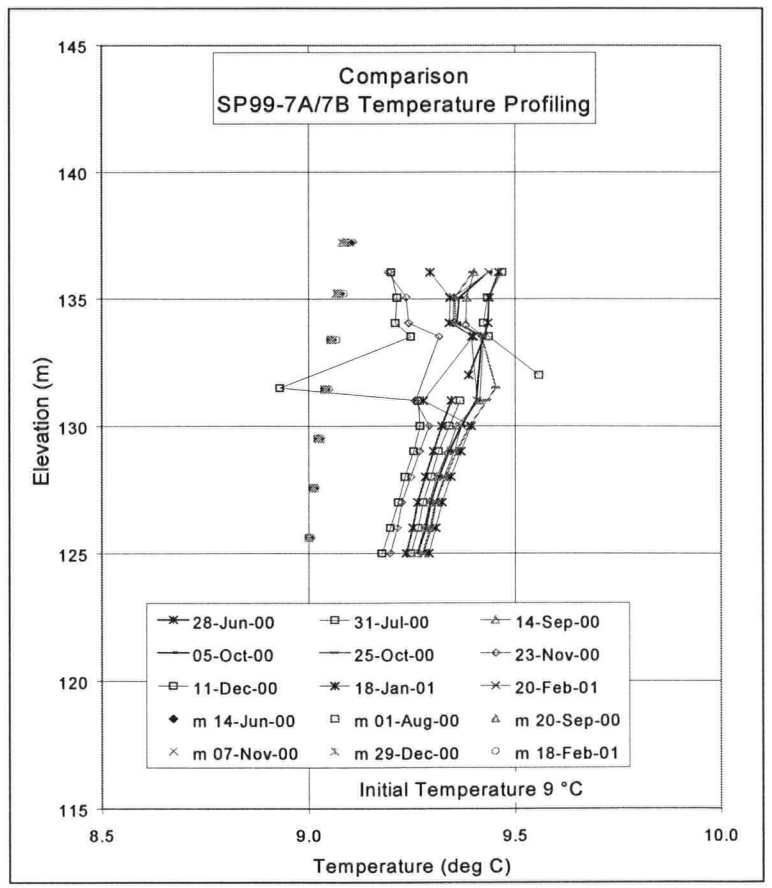

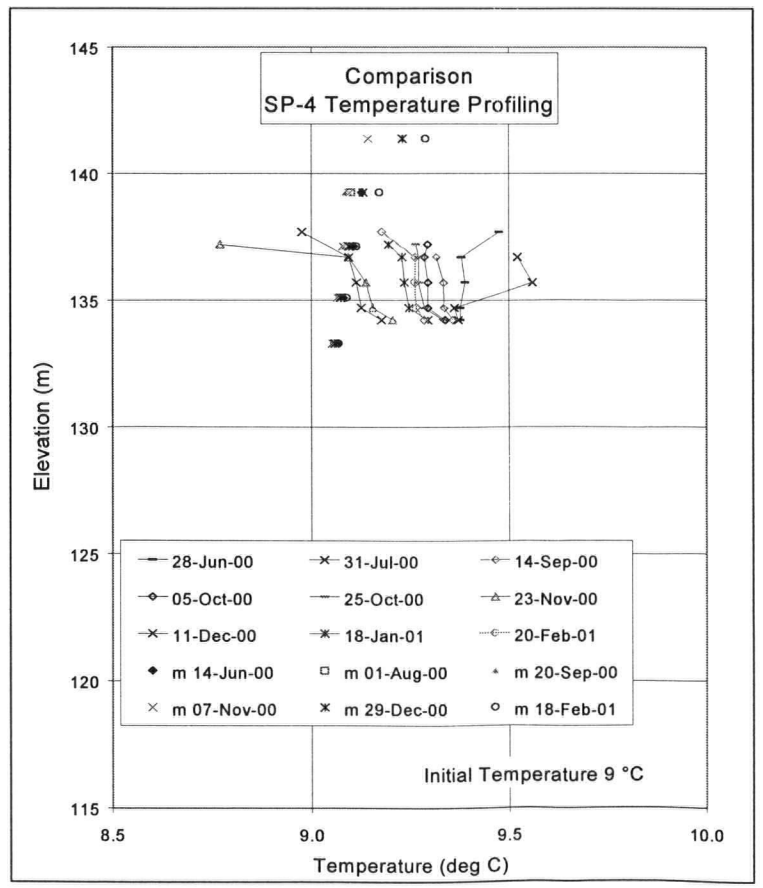

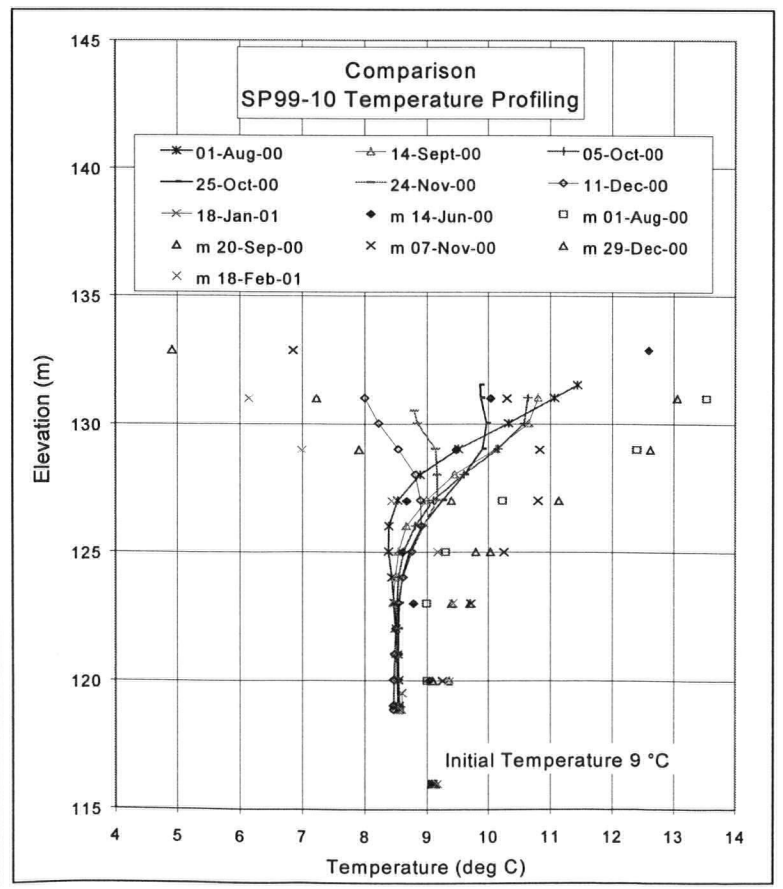

Figure 6.18: Coquitlam Dam Heat Transport Model Results For Model Simulation "XB-mix2"

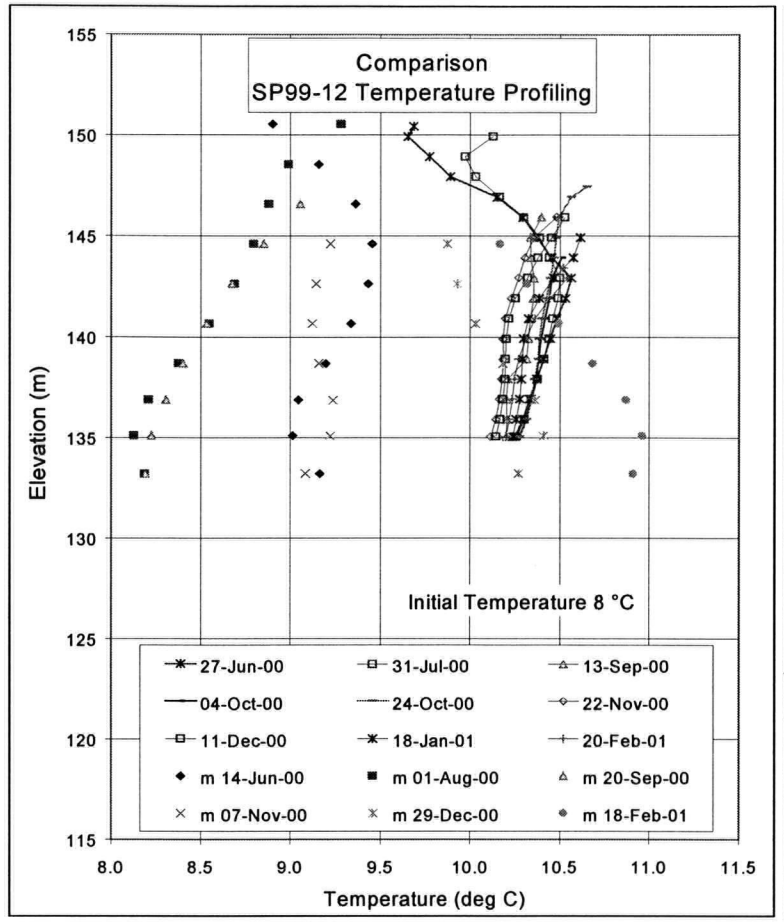

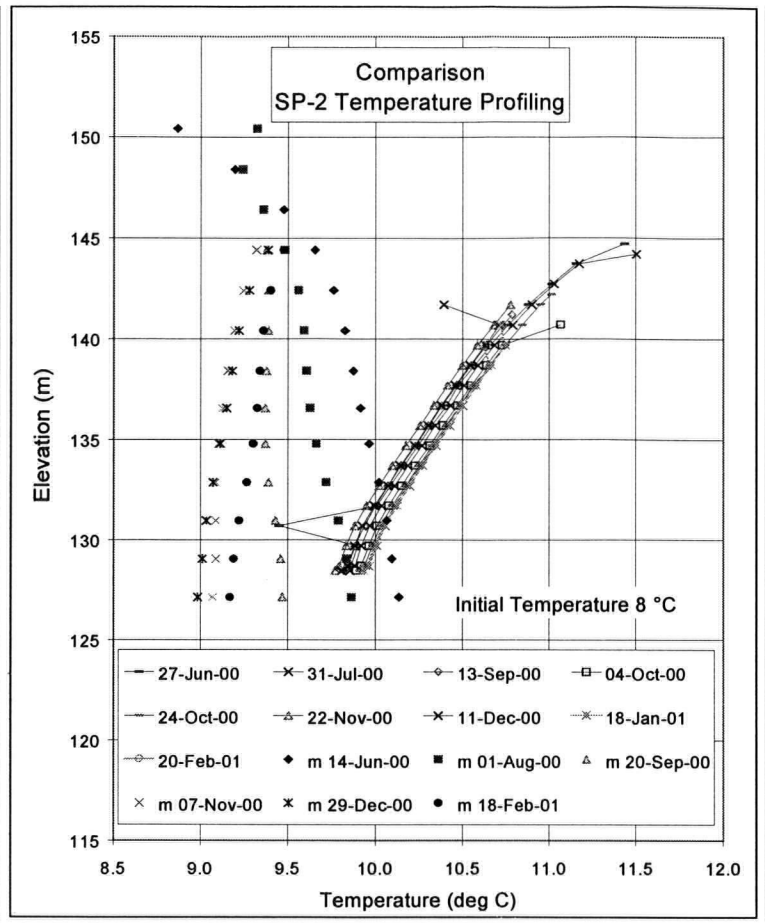

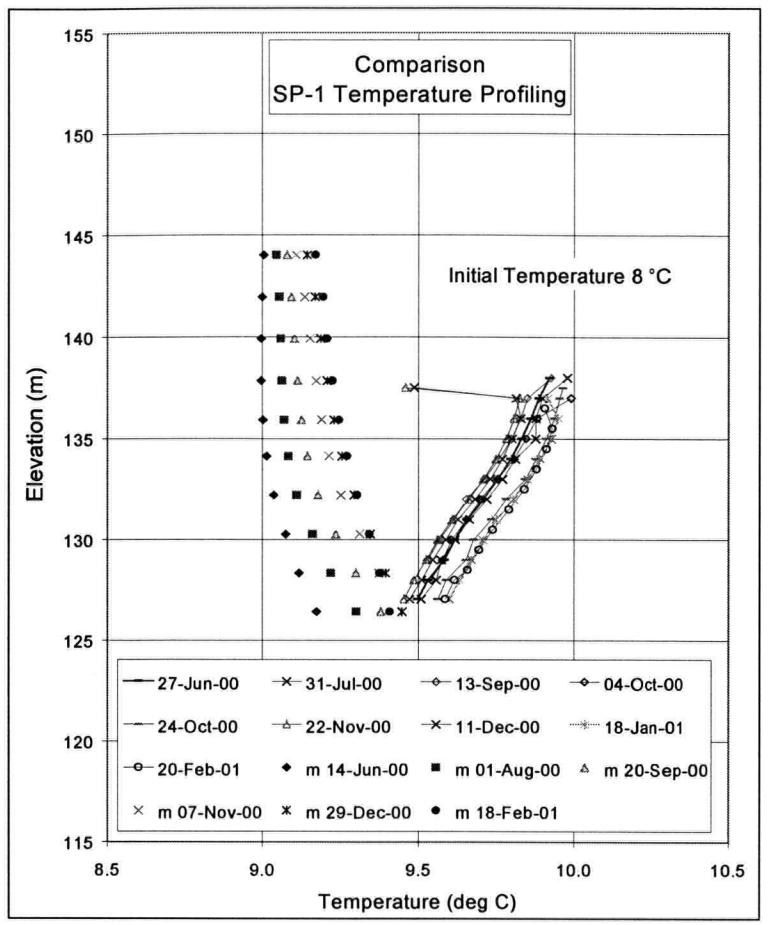

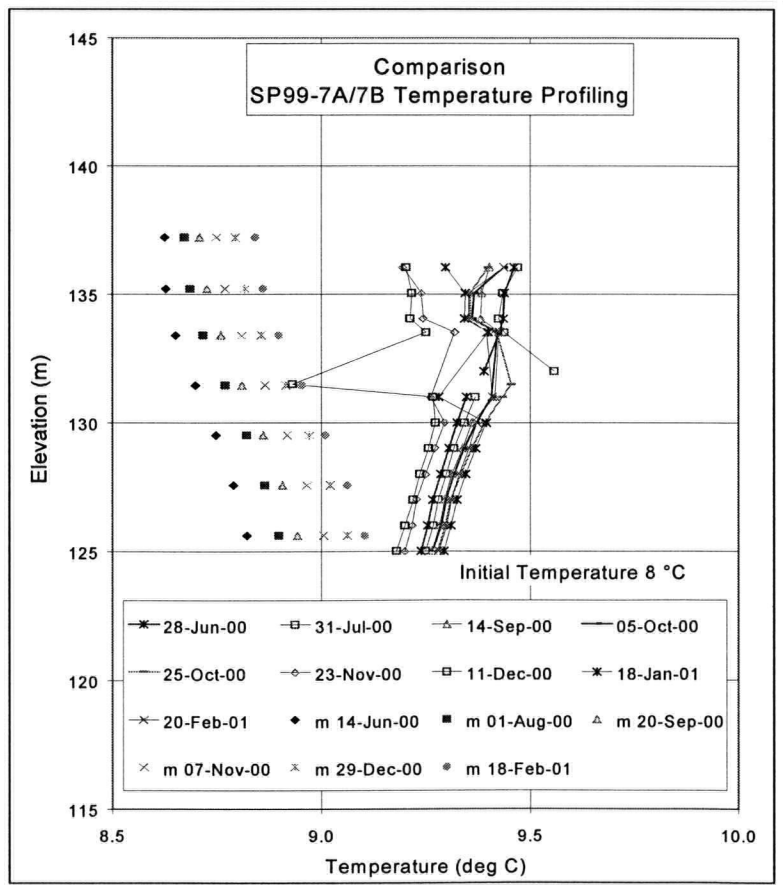

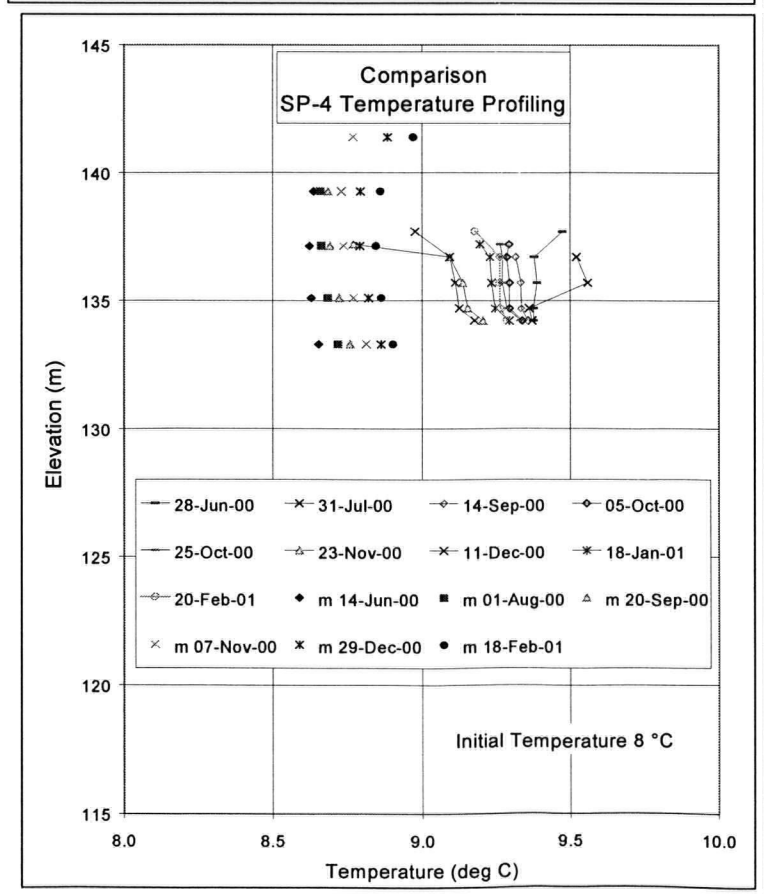

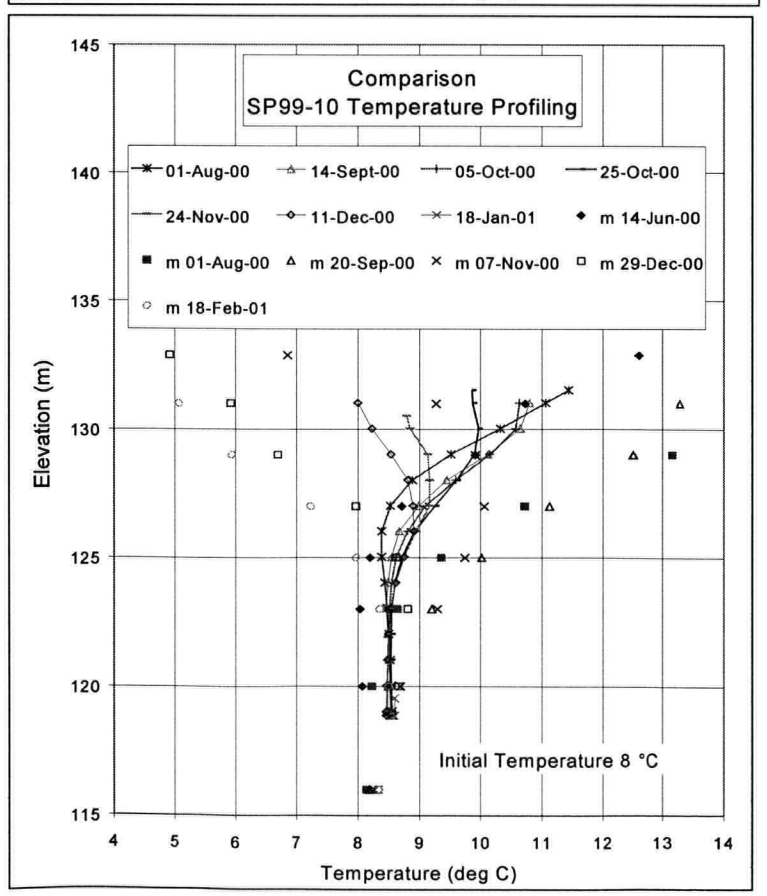

Note:

Data points identified by an m followed by a date are from computer simulations. This data has been plotted as points only.

Data plotted as points and a line represent measured temperatures.

Figure 6.19: Coquitlam Dam Heat Transport Model Results For Model Simulation "XB-tr2"

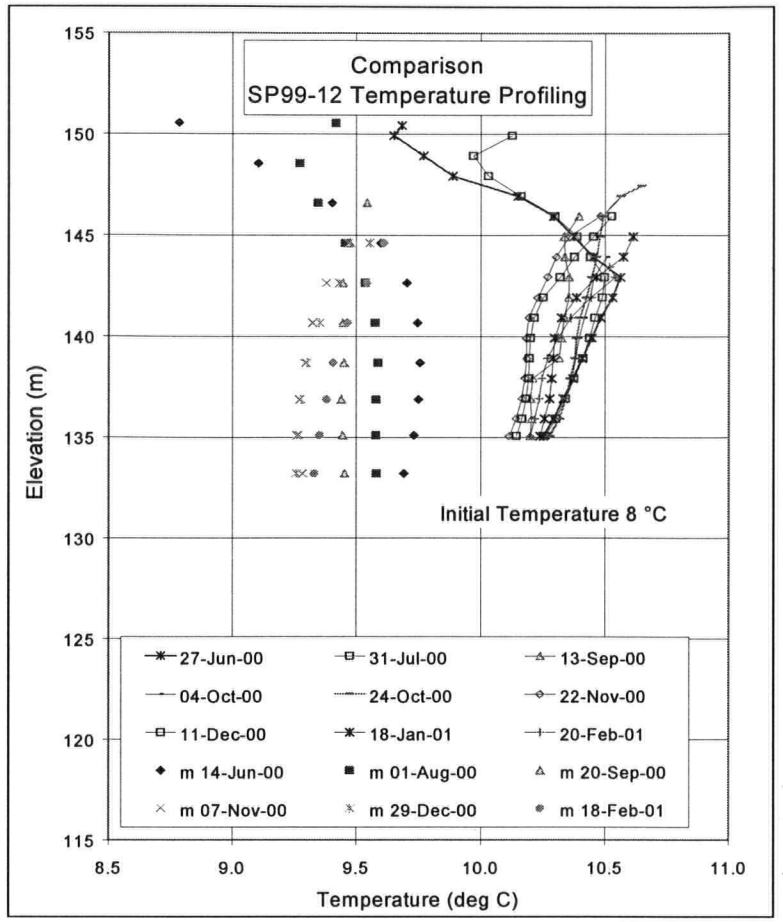

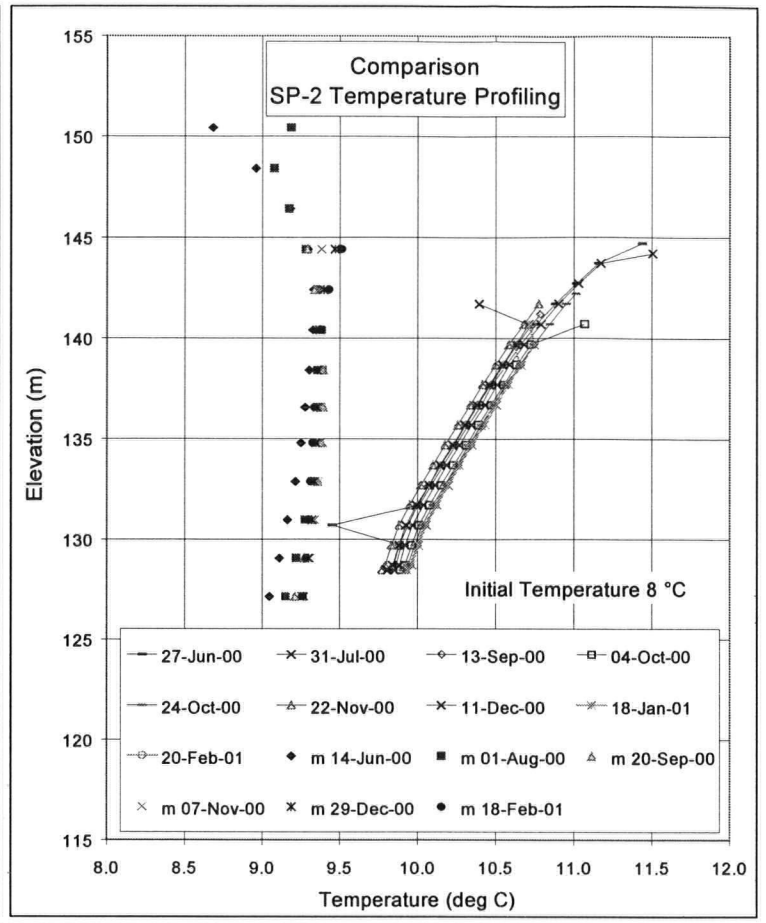

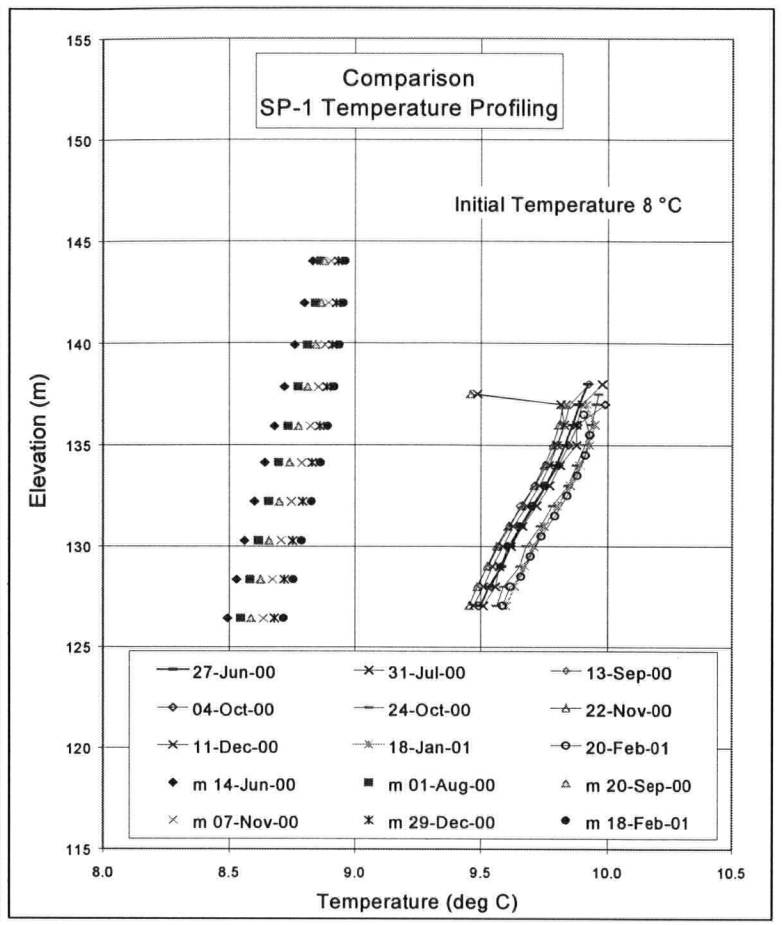

Note:

Data points identified by an m followed by a date are from computer simulations. This data has been plotted as points only.

Data plotted as points and a line represent measured temperatures.

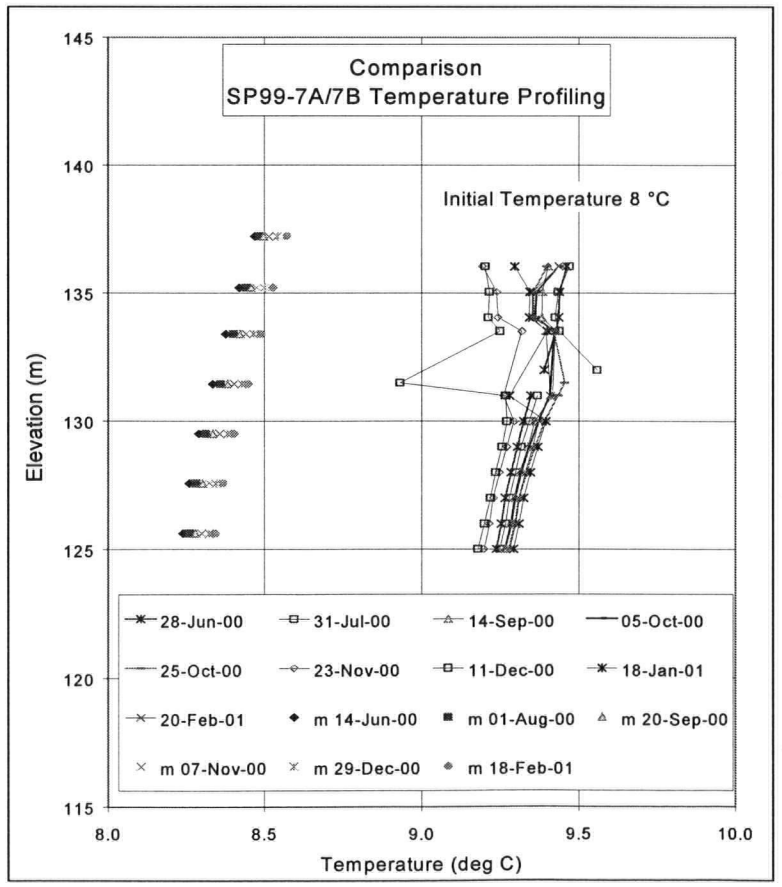

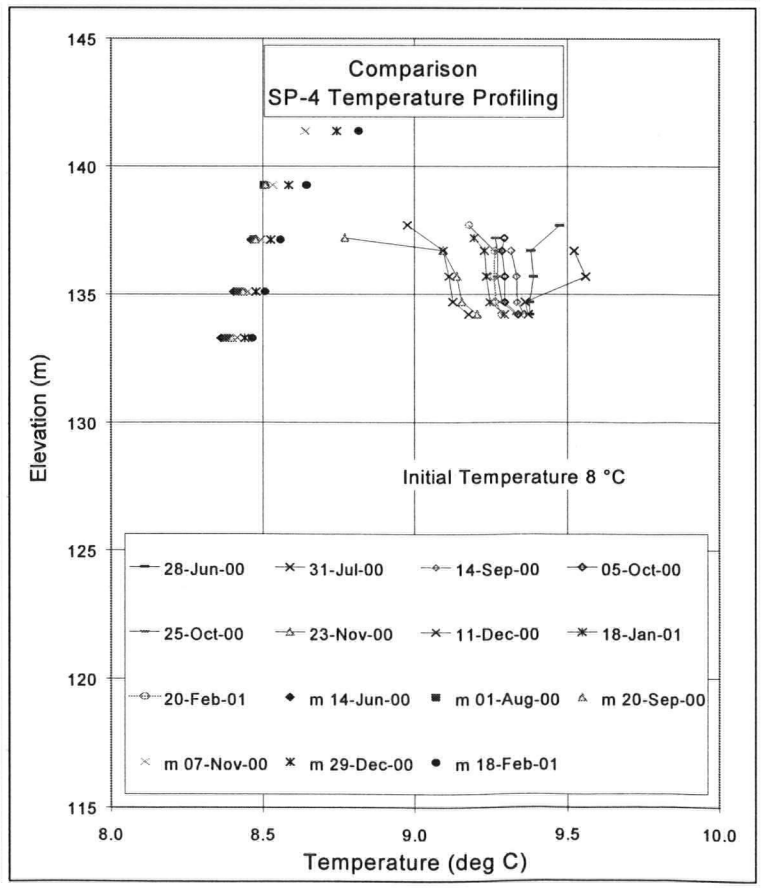

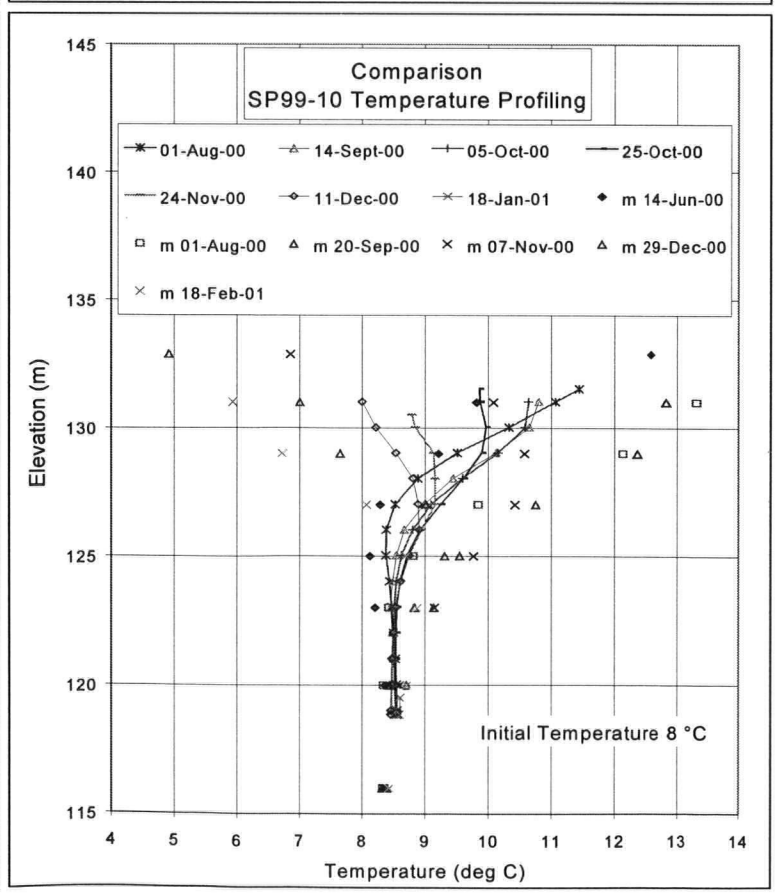

Figure 6.20: Coquitlam Dam Heat Transport Model Results For Model Simulation "XB-tr-mix"

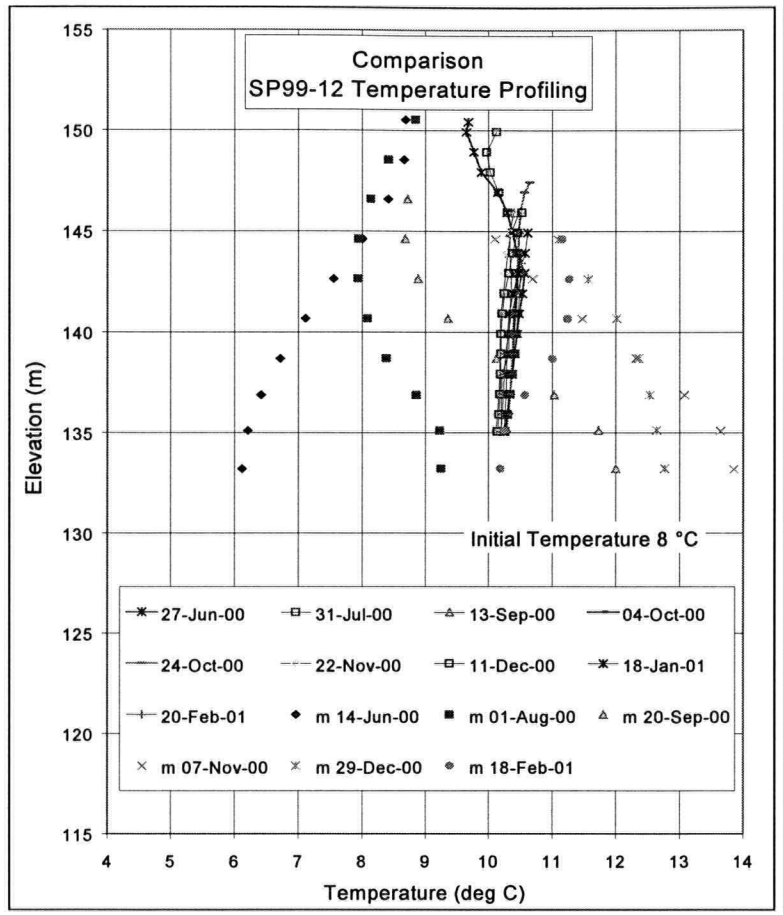

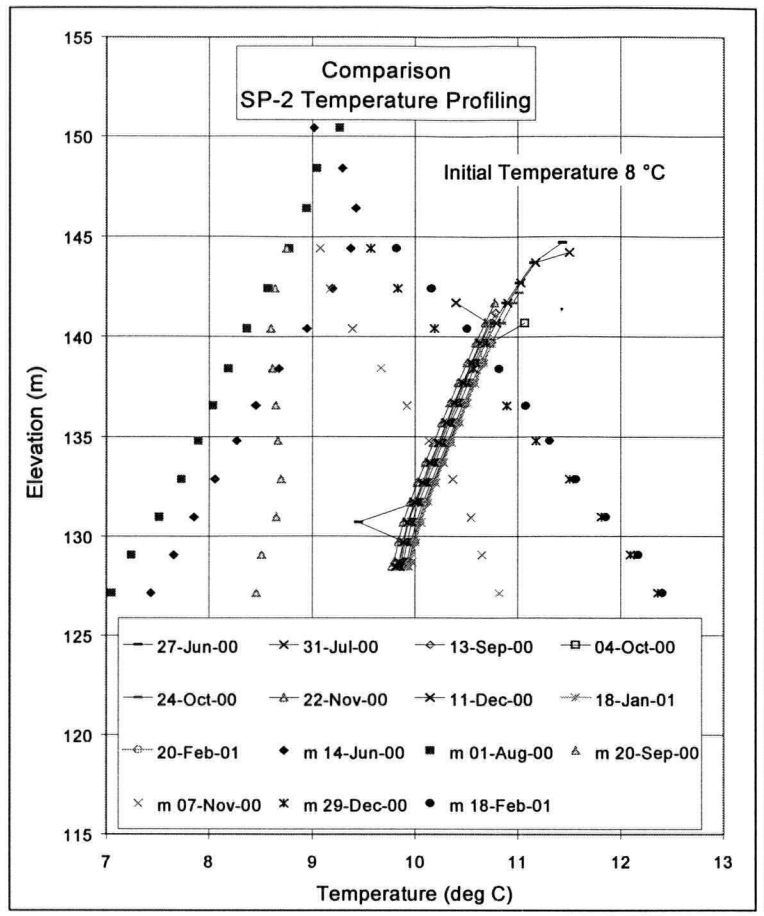

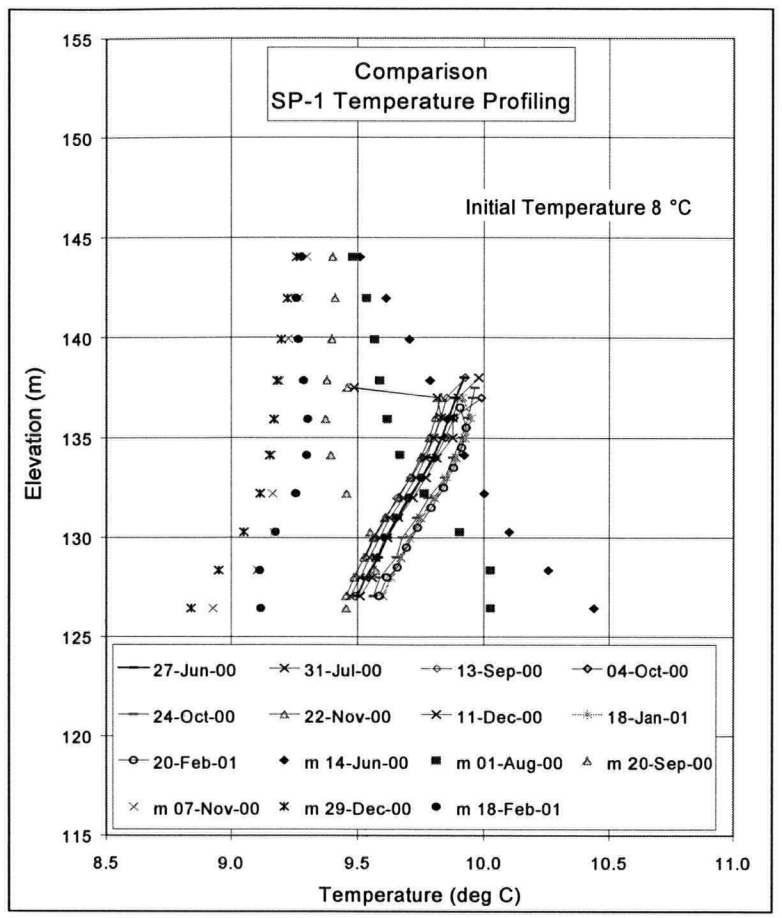

Note:

Data points identified by an m followed by a date are from computer simulations. This data has been plotted as points only.

Data plotted as points and a line represent measured temperatures.

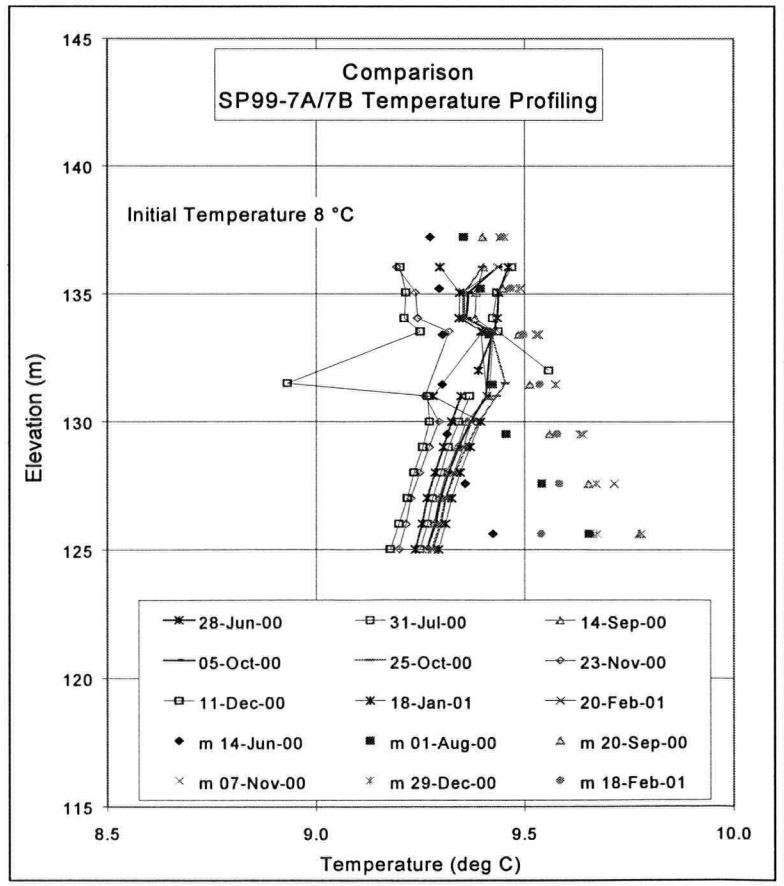

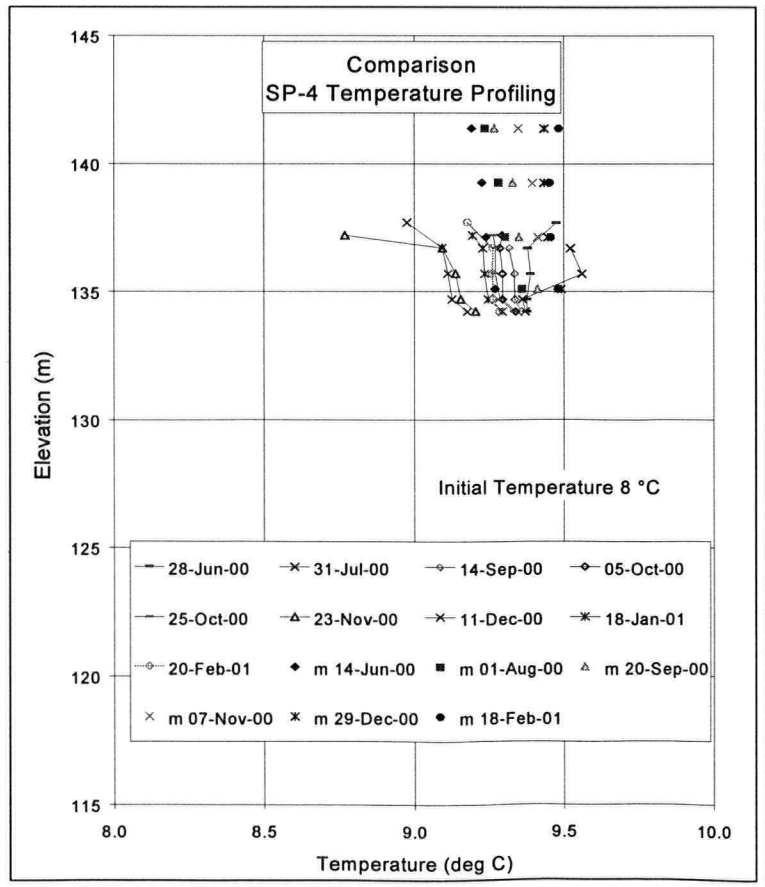

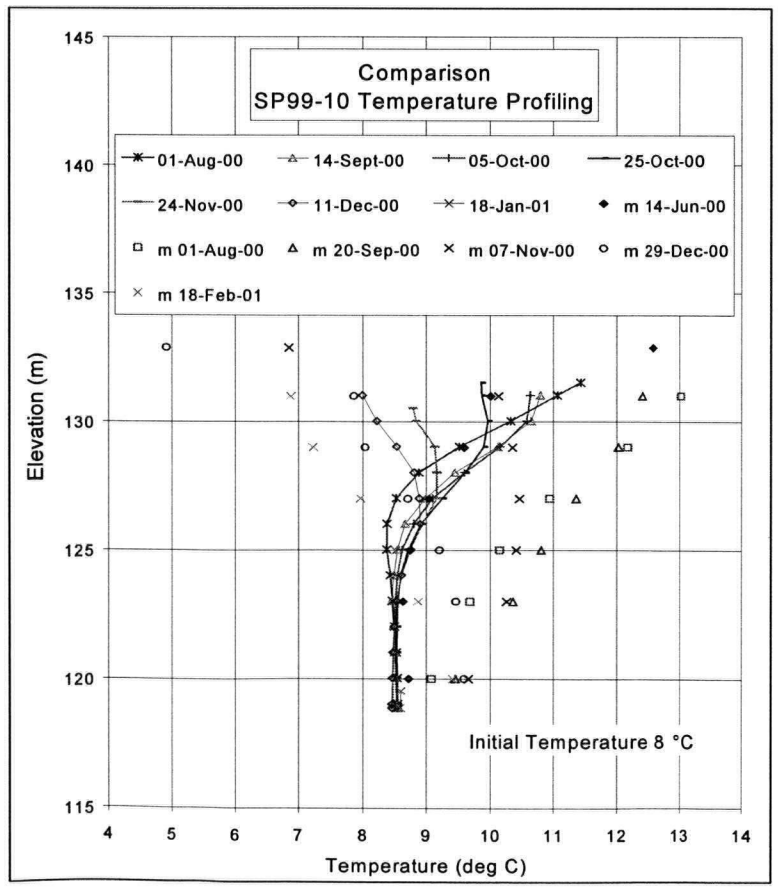

Figure 6.21: Coquitlam Dam Heat Transport Model Results For Model Simulation "XB-tr6-mix"

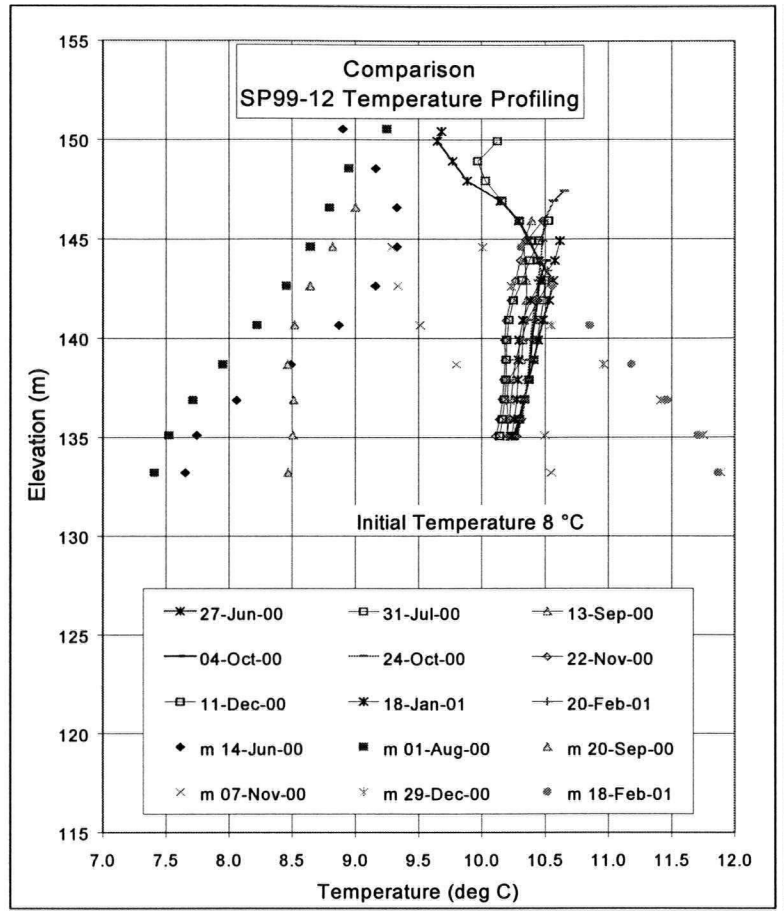

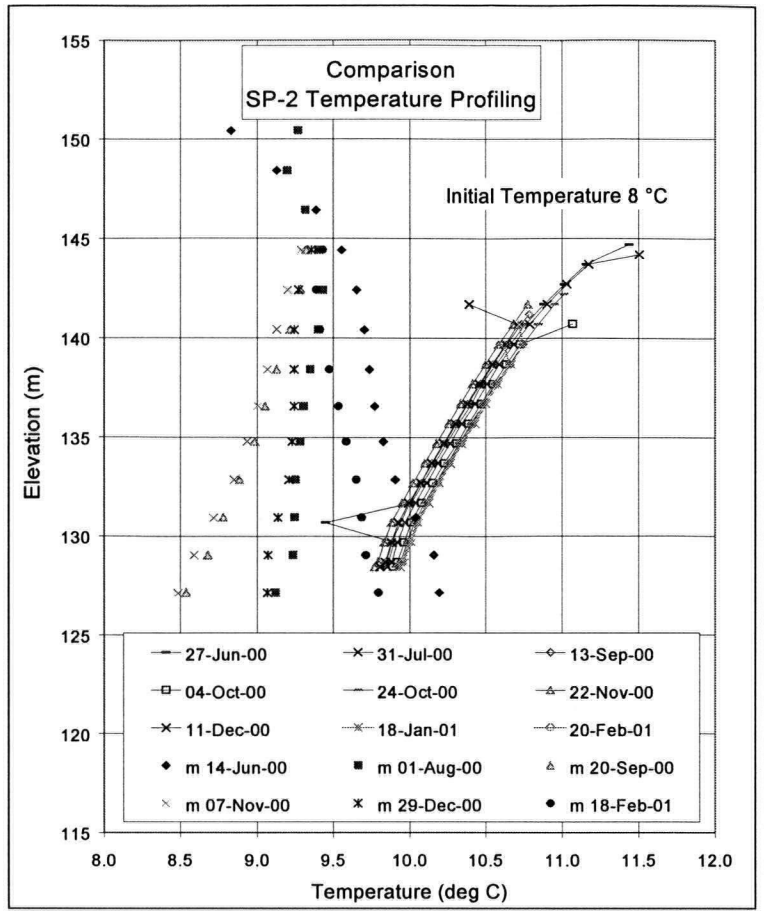

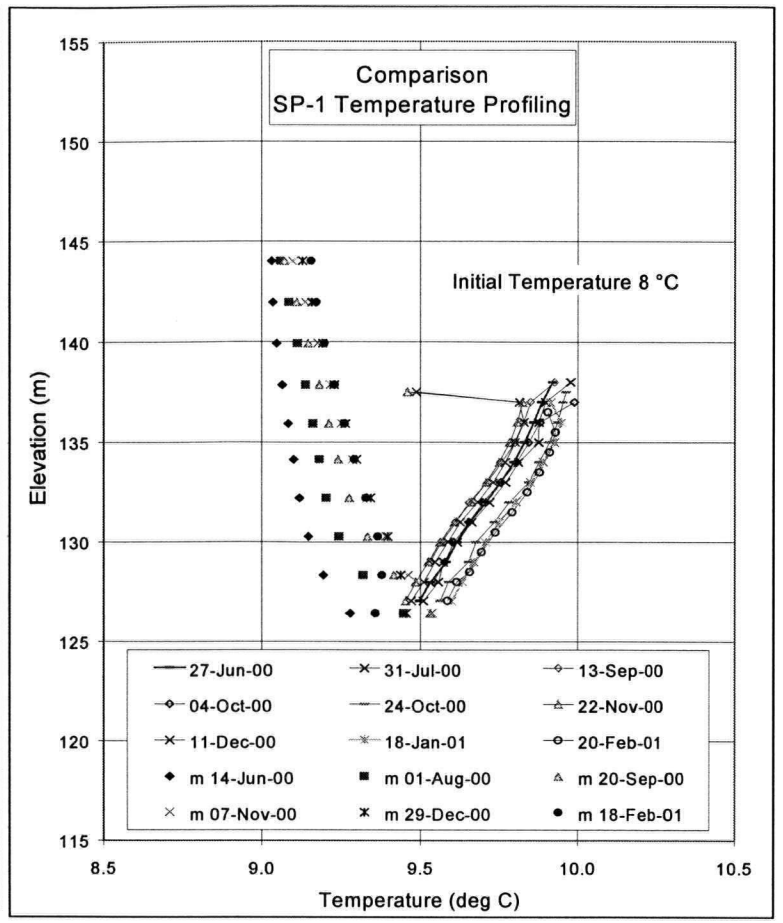

Note:

Data points identified by an m followed by a date are from computer simulations. This data has been plotted as points only.

Data plotted as points and a line represent measured temperatures.

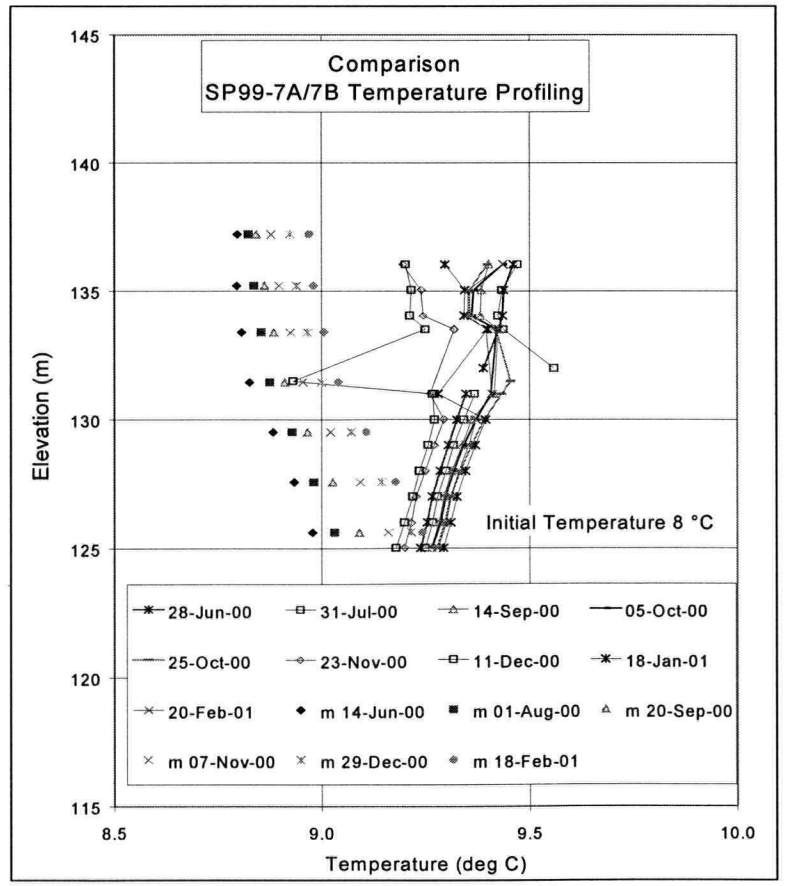

Figure 6.22: Coquitlam Dam Heat Transport Model Results For Model Simulation "nXB-tr-mix"

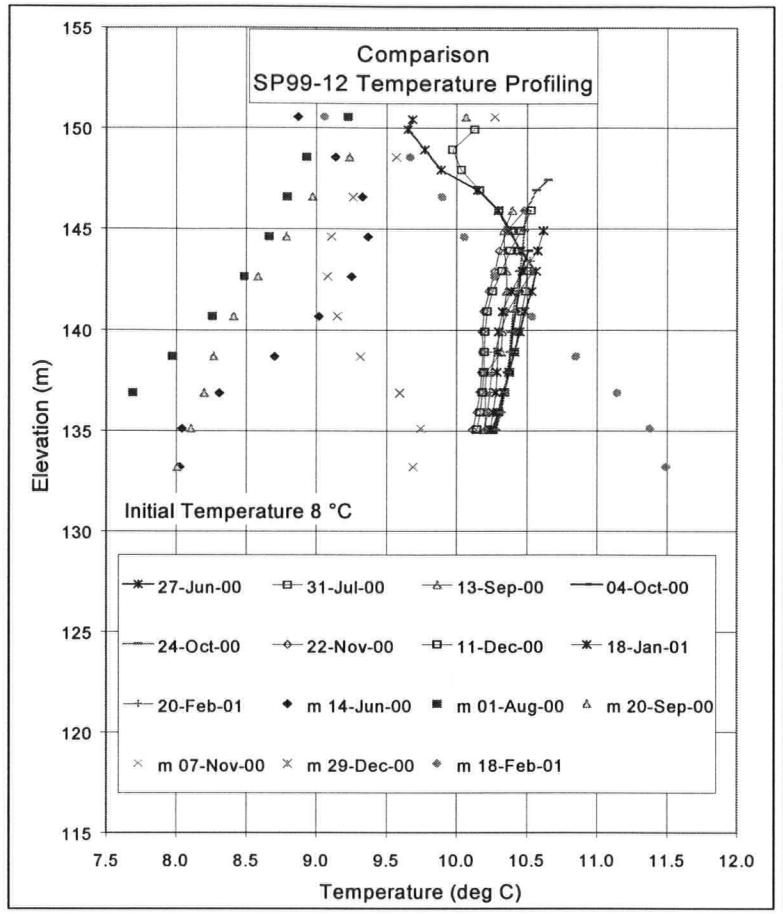

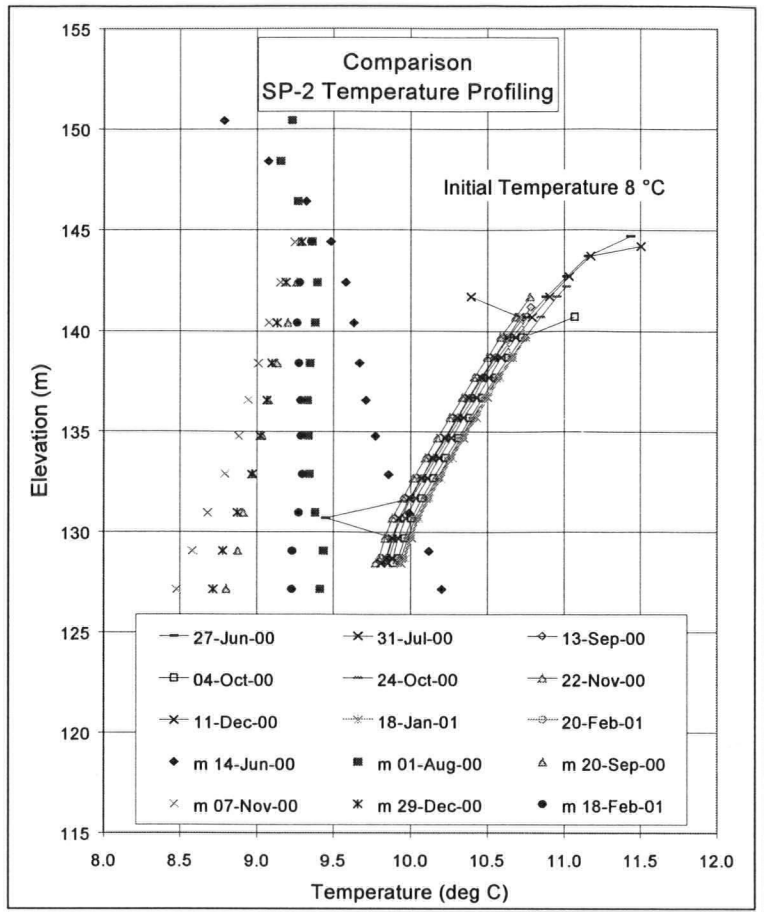

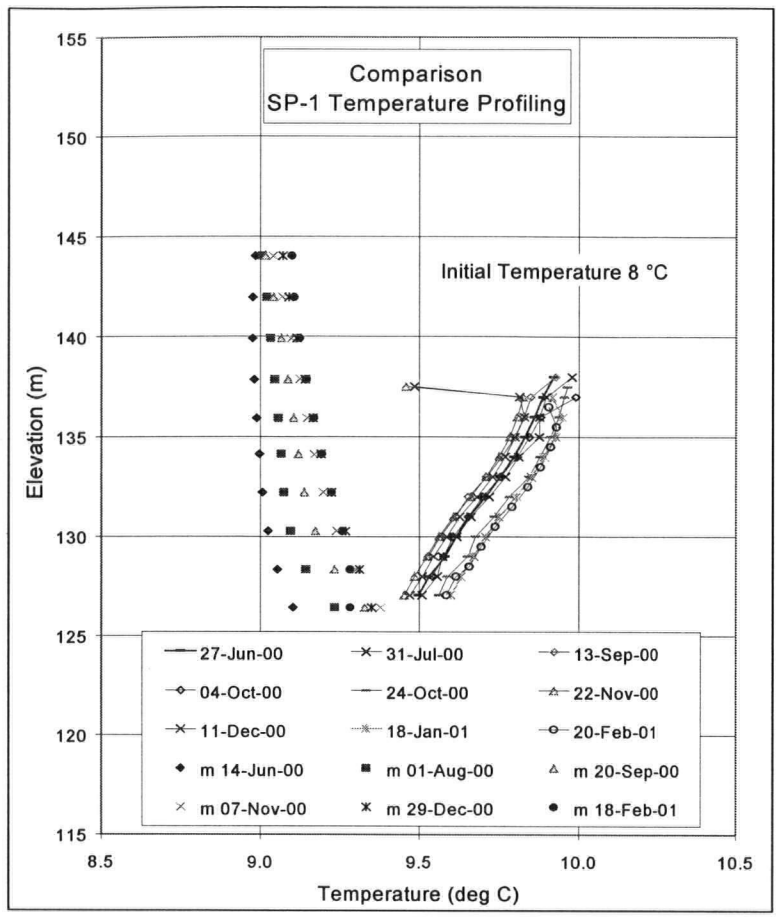

Note:

Data points identified by an m followed by a date are from computer simulations. This data has been plotted as points only.

Data plotted as points and a line represent measured temperatures.

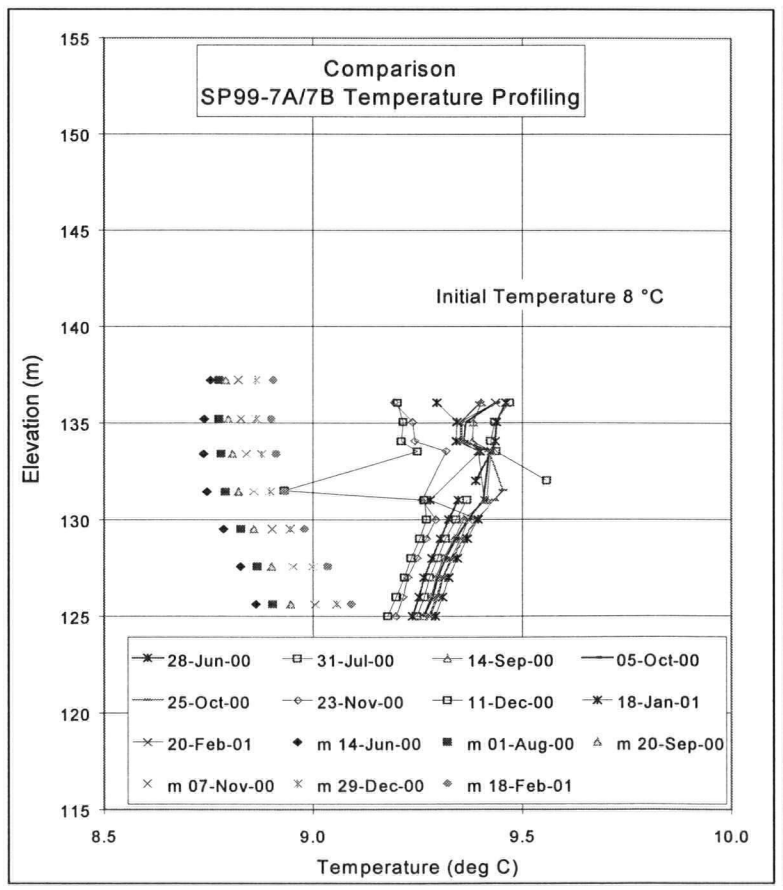

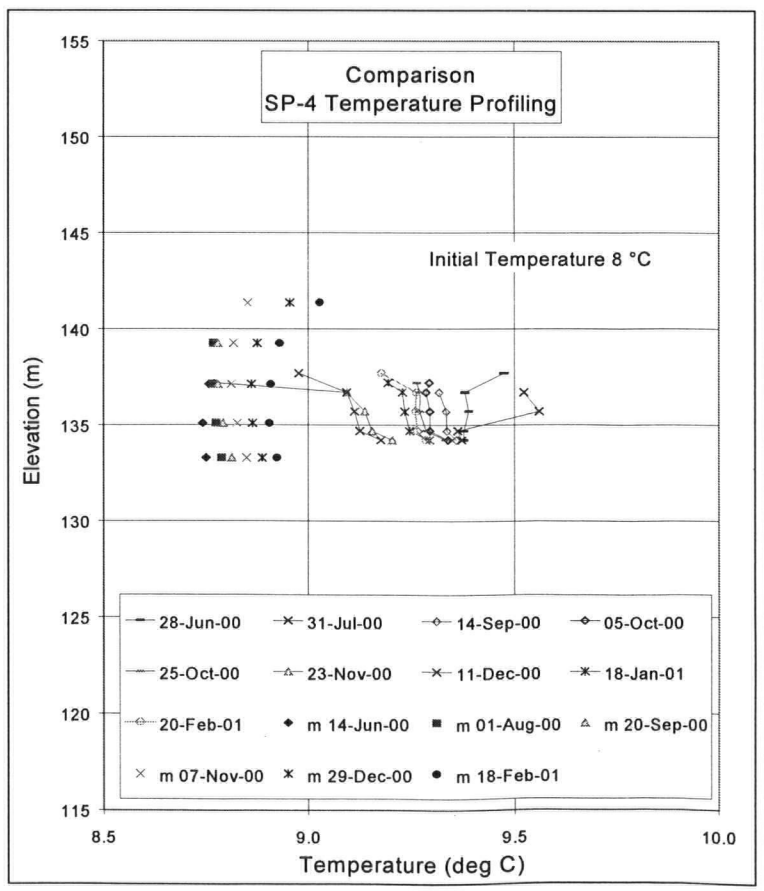

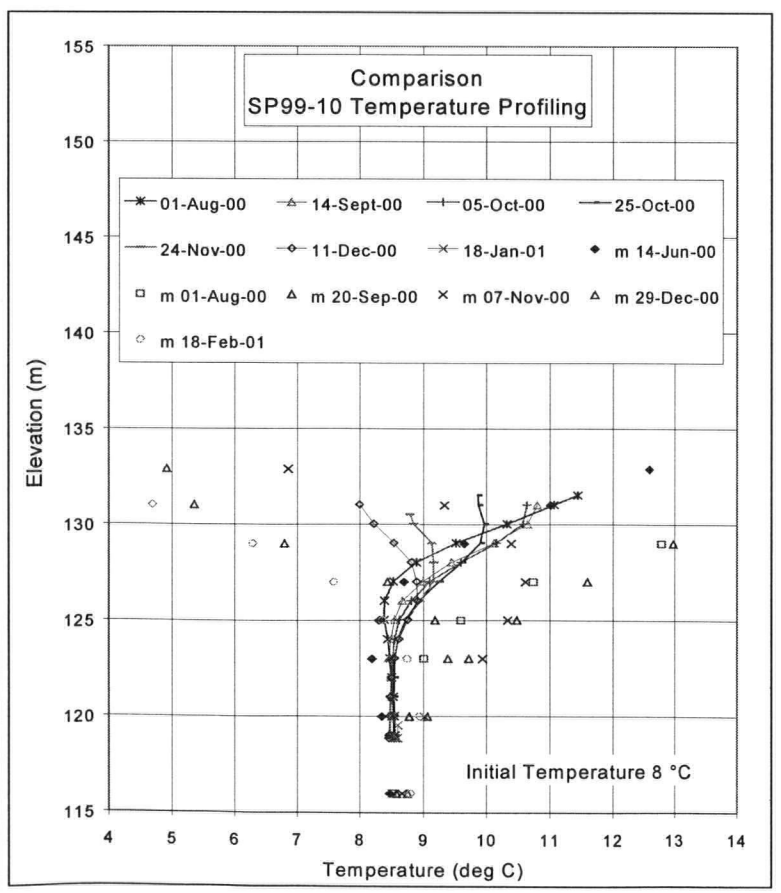

Figure 6.23: Coquitlam Dam Heat Transport Model Results For Model Simulation "re-XB-tr-mix"

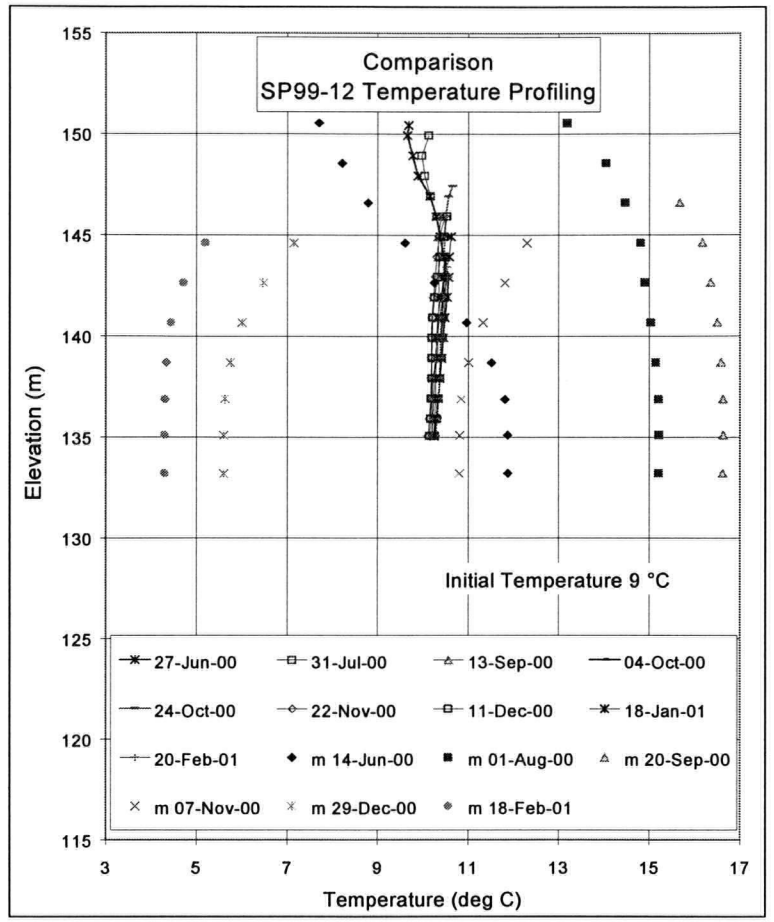

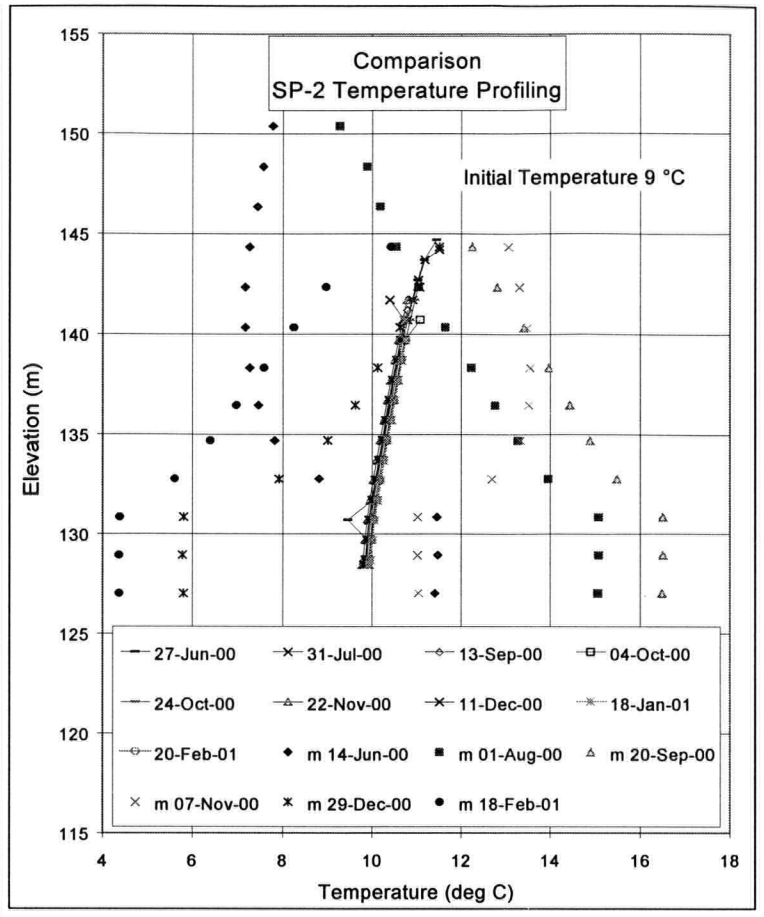

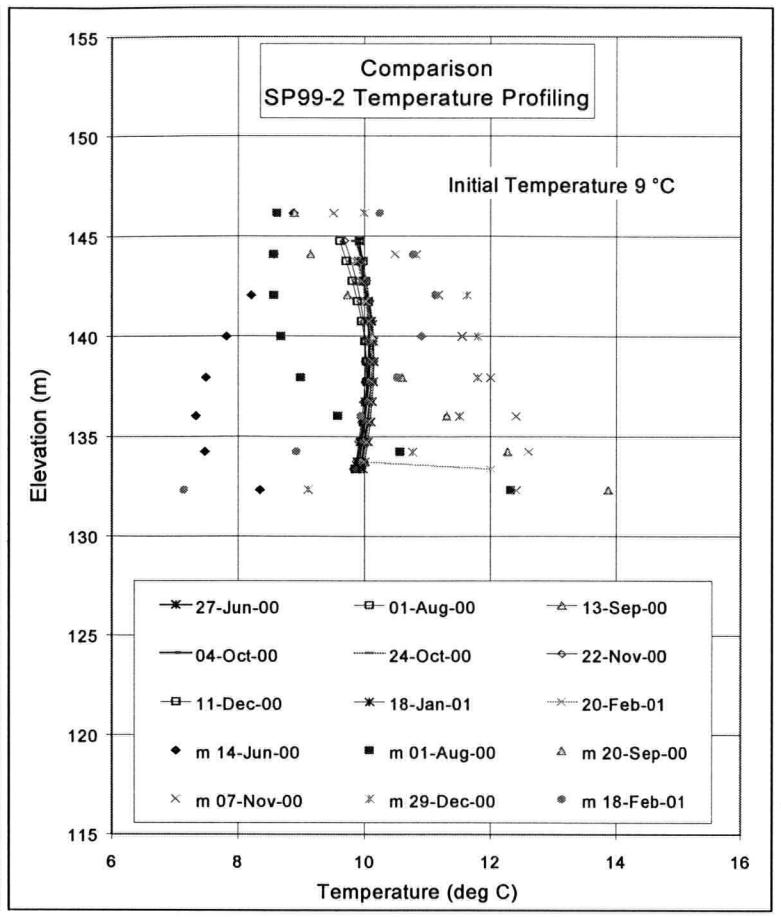

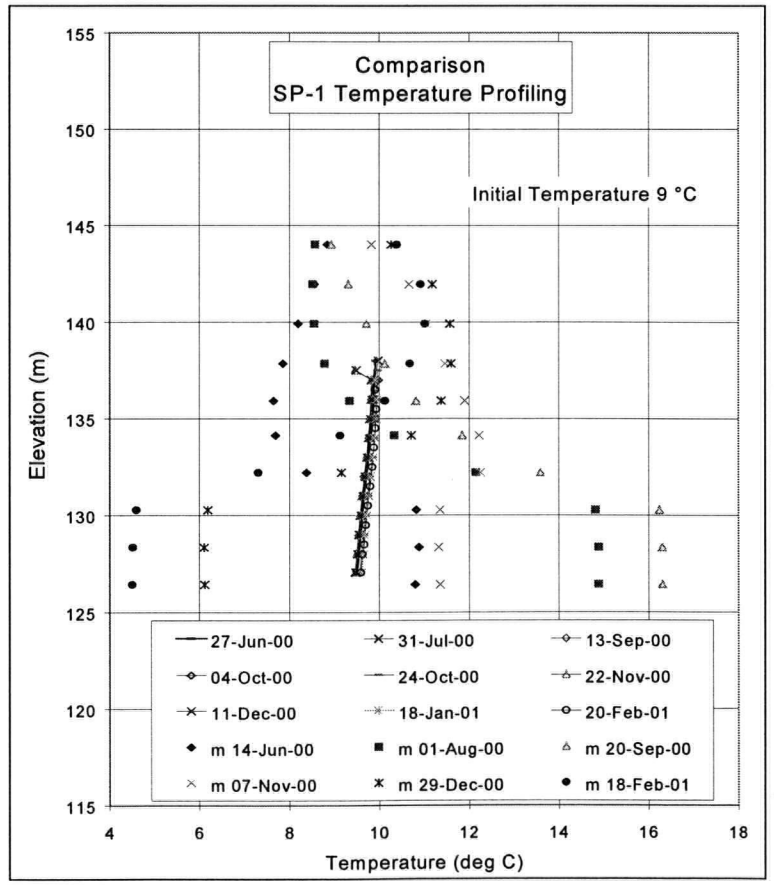

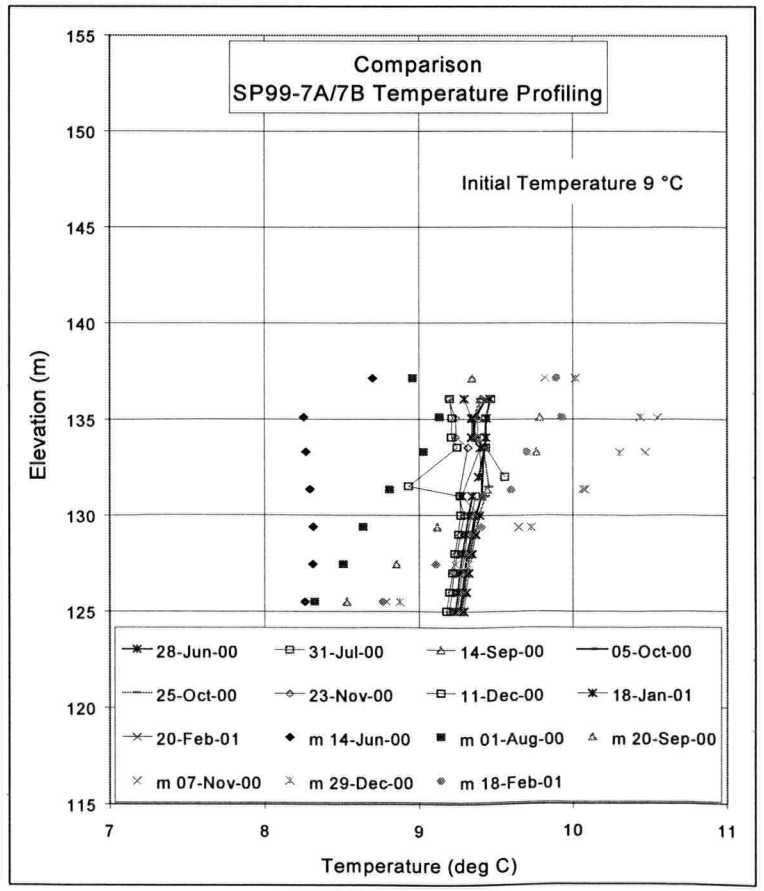

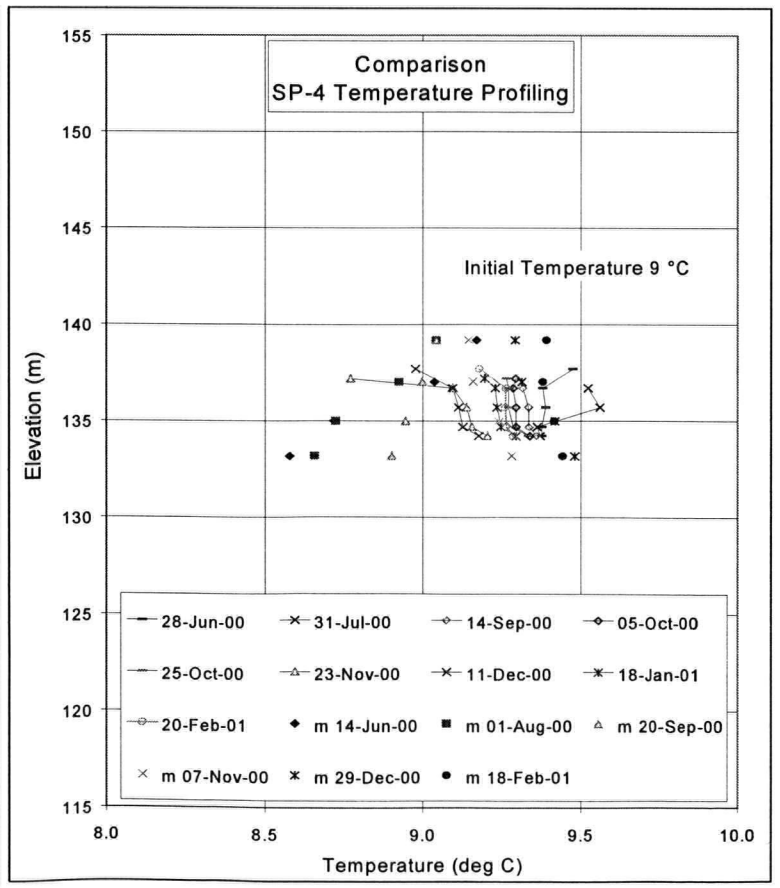

Note:

Data points identified by an m followed by a date are from computer simulations. This data has been plotted as points only.

Data plotted as points and a line represent measured temperatures.

Figure 6.24: Coquitlam Dam Heat Transport Model Results For Model Simulation "XB-tr2-PB-2h"

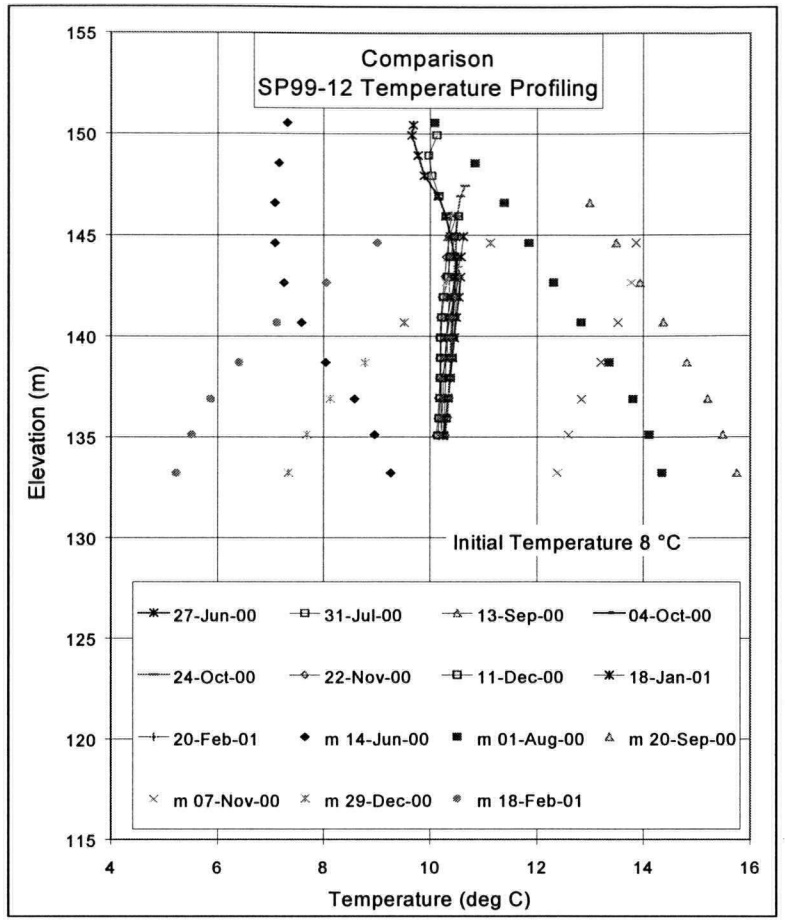

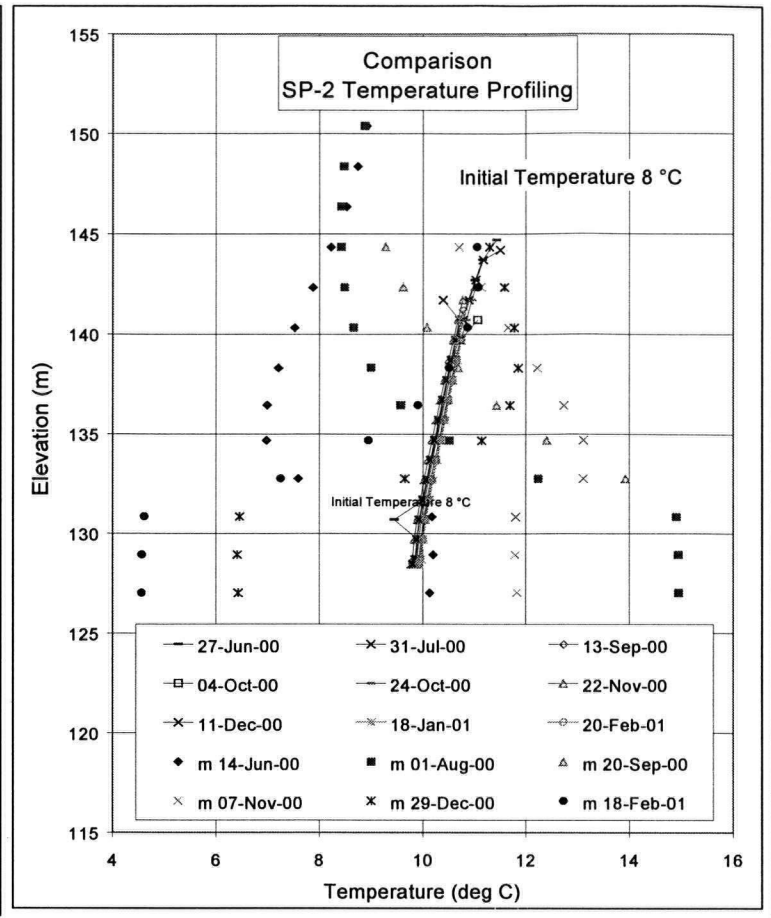

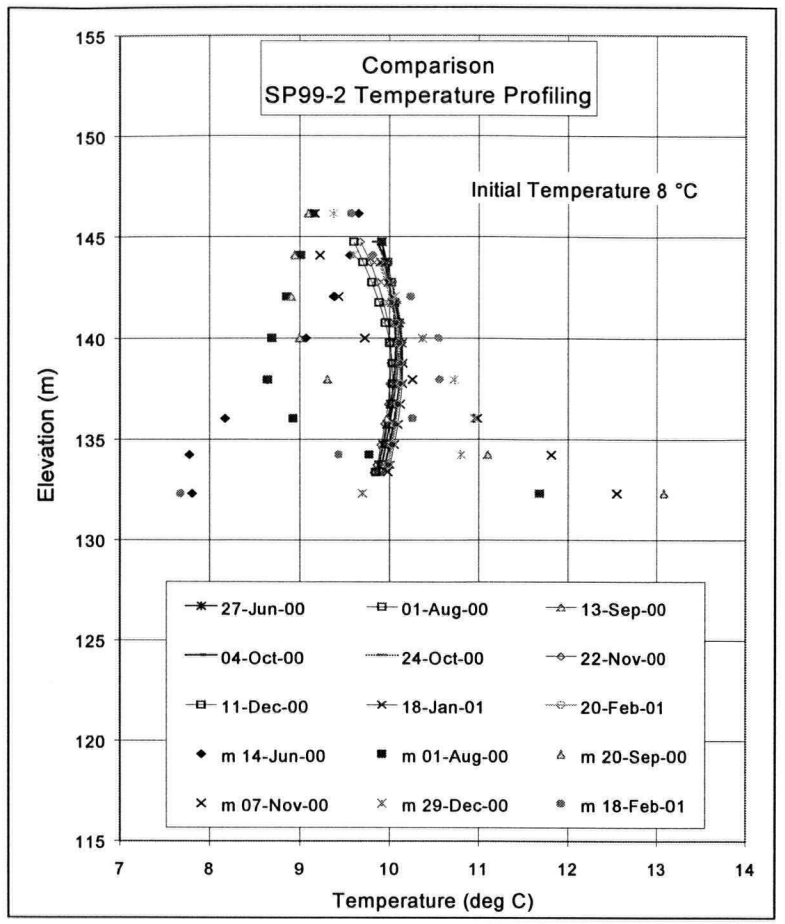

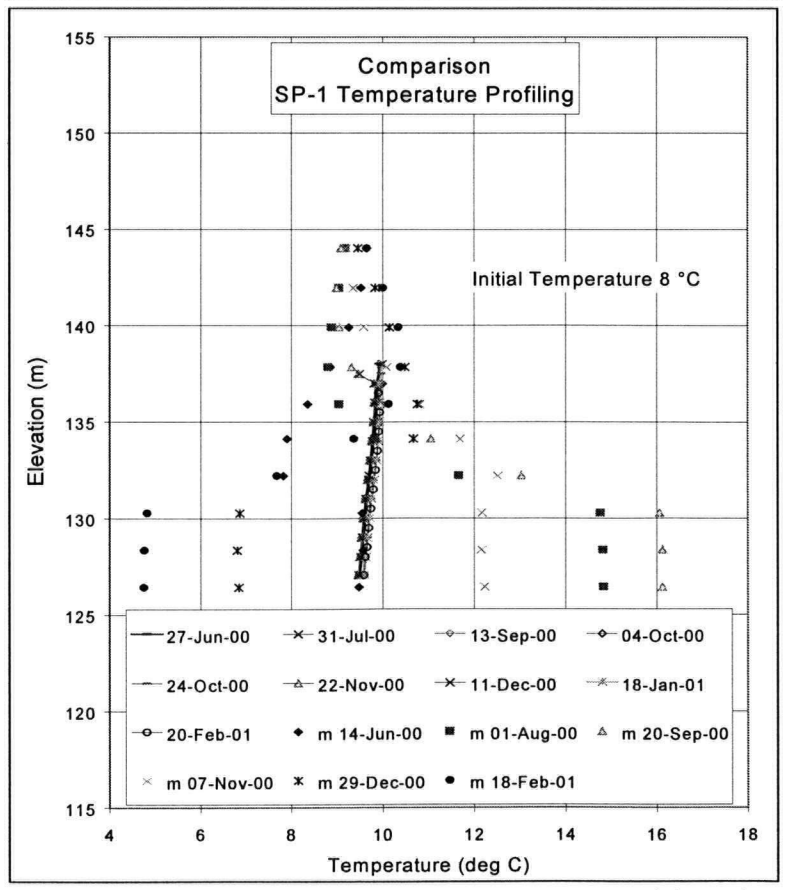

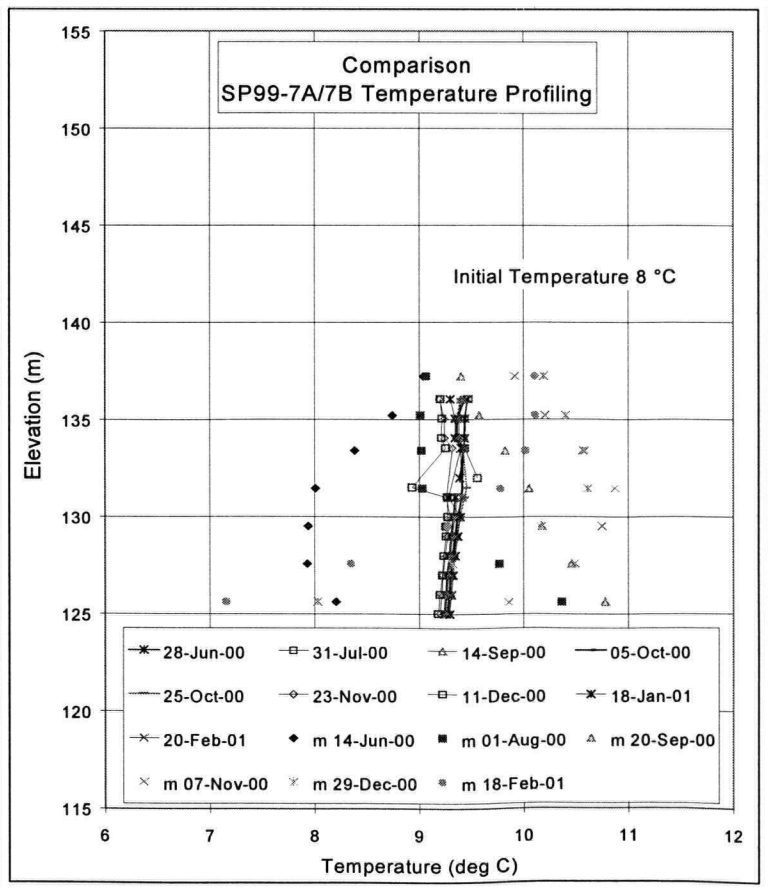

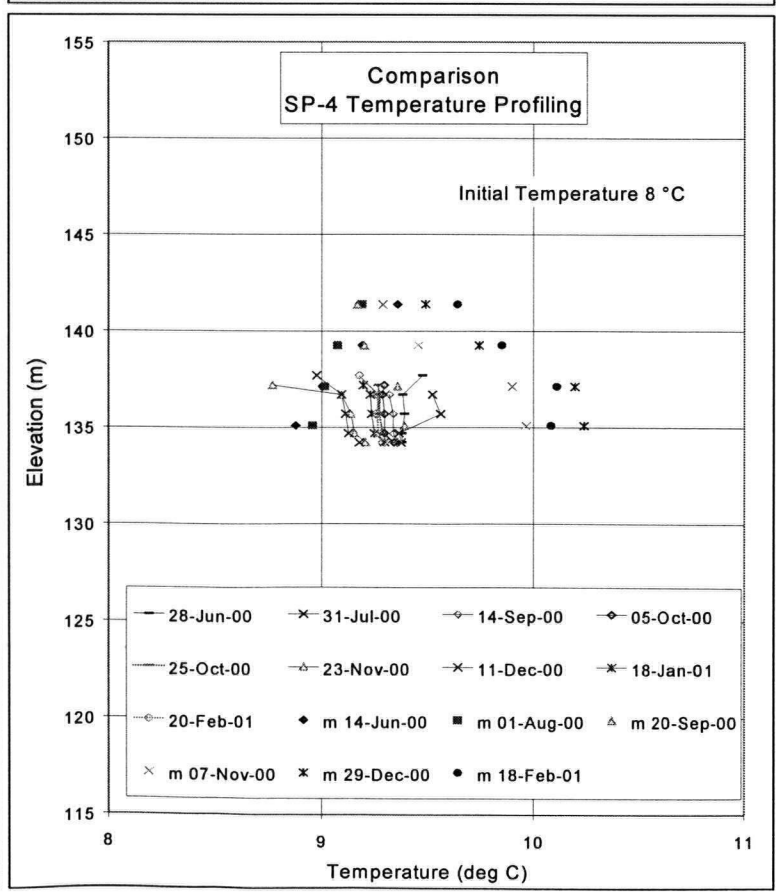

Note:

Data points identified by an m followed by a date are from computer simulations. This data has been plotted as points only.

Data plotted as points and a line represent measured temperatures.

Figure 6.25: Coquitlam Dam Heat Transport Model Results For Model Simulation "XB-tr2-PB-5h"

CHAPTER 7: CONCLUSIONS AND RECOMMENDATIONS

7.1 CONCLUSIONS

The main purpose of this thesis was to evaluate the use of temperature data to infer seepage velocities through dams and to monitor and detect changes in seepage through dams. This thesis began with the following inter-related objectives:

1. Develop an understanding for seepage and heat flow through porous media. Develop and apply a numerical modelling procedure to simulate heat and seepage flow in one dimension through porous media. Compare simulated results to results obtained from a closed form solution.
2. Utilize a two dimensional, numerical model to characterize the temperature distribution and seepage regime measured within the homogeneous, field scale model dam constructed in Karlsruhe, Germany.
3. Collect temperature measurements from Coquitlam Dam and reservoir. Evaluate and monitor the performance of Coquitlam Dam by qualitatively analysing heat flow through the dam.
4. Apply the numerical model and procedure used to evaluate seepage and heat flow through the field scale model dam built in Karlsruhe to Coquitlam Dam.
5. Use piezometric and temperature data to assess and monitor the seepage regime within an embankment dam. Assess if temperature data would be a useful tool for dam performance monitoring.

The objectives have all been met, although the numerical modelling of Coquitlam Dam was not successful.

Important Theoretical Concepts Behind Using Heat Flow as an Indicator of Seepage Velocity in Embankment Dams

Collection and analysis of temperature data from reservoirs and within the saturated zone of embankment dams is a relatively new technique that is gradually being applied at more dams to provide additional information about dams' seepage regimes.

This monitoring technique uses the annual temperature fluctuation in the reservoir water to establish an expected pattern of temperature variation within the dam. An assessment of the hydraulic condition (seepage regime) of the dam can be made based on the expected pattern of temperature variations or on the deviations from the expected pattern. The temperature measured within the dam at any given time, or location is influenced by:

- Initial seepage water temperature;
- Annual variation in seepage water's source temperature
- Reservoir depth;
- Seepage path;
- Monitoring location's distance from seepage water source;
- Monitoring depth;
- Hydraulic flow rate through the dam; and
- Other thermal influences (i.e. groundwater, geothermal, air temperature).

The fluid transport and heat transport equations may be solved concurrently (coupled) or sequentially (uncoupled). The use of uncoupled equations is valid for many embankment dam applications providing the pressure gradient is the dominant force governing flow of seepage water in comparison to the density gradient.

Regardless of whether the heat transport equation is not in a coupled or uncoupled manner, the flow of heat is not independent of the flow of seepage water. The convective component of the heat transport equation is linked to the flow of water by the velocity term. As a result, collection and analysis of temperature data from dams does not replace piezometric monitoring, but provides a supplement to the piezometric measurements and analysis. The analysis of temperature measurements within a dam can provide a greater array of points so that the seepage velocity can be determined and/or monitored at more locations within the dam, thereby improving the overall knowledge and assessment capabilities of dam operators to monitor the dam's performance.

Implementation of a Temperature Monitoring Program

A temperature monitoring program may be implemented in a new dam or in an existing dam. Temperature data needs to be collected from the reservoir and from the saturated zone of the dam. Data can be collected manually or using an automated systems. The instrument used to measure and record temperature values must be sensitive, accurate (0.1 C minimum), and readings must be repeatable, in order to detect and monitor small changes in temperature that may indicate changes in seepage velocity. If temperature measurements are collected through existing standpipe piezometers, there should be no/minimal mixing of water within the standpipe (leaky piezometers or piezometers with diameters larger than 7 centimetres should not be used). Temperature readings need to be taken at regular intervals to accurately capture temperature variations within the reservoir and in the dam. Since groundwater temperature and air temperature may influence the temperature of seepage water, collection of air temperature data and groundwater temperatures (i.e. background) can assist in the analysis. In addition to temperature readings, piezometric data, weir flow rates and volumes (if available), and reservoir elevation fluctuations also need to be recorded.

Numerical Modelling Programs and Procedures

The combined use of SEEP/W and CTRAN/W (using the modified volumetric water content function) effectively modelled fluid and heat transport through porous media, as was evident when the numerical models solutions were compared to the one dimensional, closed form solutions. The programs are user friendly and provide flexibility for the user in terms of program operation and data output.

These programs were also effective in modelling simplified flow conditions when a two dimensional analysis satisfactorily captured the seepage regime in the Karlsruhe field scale model dam. As a result, heat flow modelling results from this dam more closely matched the measured temperatures at the dam.

However, when more complex problems are modelled, and an iterative and process is needed between the two physical processes (i.e. seepage flow and heat flow), as was done in this thesis, the analysis is cumbersome. The complete numerical modelling is actually a three step process SEEP/W, SEEP/W with modified volumetric water content function, followed by CTRAN/W analysis. To model more complex problems (i.e. Coquitlam Dam) an integrated program that is capable of solving both fluid transport and heat transport problems, would be beneficial.

The results from the solution of the heat transport equation are significantly influenced by the results of the fluid transport model, as was apparent in the modeling results from Coquitlam Dam. As a result, a reasonable transient hydraulic model (i.e. transient solution) is required for many dams with reservoirs that elevation fluctuates significantly throughout the year. Hydraulic modelling of seepage flow through the dam should be conducted first, and calibrated if possible, using weir flow rates, prior to initiating the heat transport modelling.

Results from Numerical Modelling – Karlsruhe, Germany

A good agreement was achieved between the transient hydraulic model (using SEEP/W) and the measured piezometric levels within the model dam. A reasonable model for the heat and fluid transport was achieved using SEEP/W and CTRAN/W.

Results from Numerical Modelling of Coquitlam Dam

Numerous transient hydraulic simulations were run using SEEP/W with different hydraulic conductivity combinations for the various stratigraphic layers at Coquitlam Dam. Hydraulic conductivity values were selected based on the range of values obtained from soil samples collected during various field investigation programs, and based on the soil description types. In addition, a variety of boundary conditions were used to try and account for the regional groundwater flow conditions at the dam. However, an accurate transient hydraulic model for Coquitlam Dam was not obtained during the course of this thesis. Based on these results and the complex nature of the dam, it appears that a two dimensional hydraulic model may not be sufficient to model the flow conditions at the dam.

Although an accurate transient hydraulic model was not obtained for the site, several heat transport simulations were run using various hydraulic models. Although there are some similarities between the predicted and measured temperature data from Coquitlam Dam, an accurate heat transport model for Coquitlam Dam was not obtained. This is not surprising, given the reliance of the heat transport solution on an accurate hydraulic model. However, important trends and average values are encouraging.

The collection and qualitative analysis of the temperature monitoring data (Section 5.7) did not reveal any zones of concentrated seepage flow through the dam.

7.2 RECOMMENDATIONS

On the basis of the above conclusions, temperature measurements from dams and their associated reservoirs do provide beneficial information regarding the seepage regime within dams. In addition, temperature measurements could also be used to evaluate and monitor the success of remedial measures conducted to correct seepage problems.

In order to develop a more accurate heat transport model for Coquitlam Dam, a three dimensional hydraulic and heat transport model appears necessary. Three dimensional heat and seepage flow programs that may be considered for modelling Coquitam Dam include NAMMU (produced by AEA Technology), FEFLOW (produced by WASY Software), and HYDROTHERM (produced by the USGS).

It is recognized that temperature monitoring based solely on the temperature profile measured within monitoring piezometers or drill holes is usedful as a surveillance tool for embankment dams. Qualitative and approximate assessment of the performance of the dam can be made based on the measured data. Numerical modelling of the seepage/heat flow through the embankment dam, as described in this thesis, provides a tool for quantitative assessment of the performance. Based on the work performed, the following recommendations for future research is needed to enhance the numerical modelling:

1. Identification of procedures to develop a baseline thermal model.
2. Establish minimum requirements for successful hydraulic and heat flow simulations.
3. Research the influence of geothermal/atmospheric heat balance on the accuracy of heat flow simulations.
4. Determine the sensitivity of input parameters on the predicted thermal distribution.

REFERENCES

Abadjiev, Christo B. 2000. Optimization of Rockfill and Earthfill Dams Monitoring Systems, Q.78 R.16. *In* Vingtième Congrès Internationale des Grands Barrages, Beijing. pp. 233 – 247.

Adivarahan, P., Kunii, D., and Smith, J.M. 1962. Heat Transfer in Porous Rocks Through Which Single-Phase Fluids Are Flowing. *In* Society of Petroleum Engineers Journal, **2** (3) pp. 290 – 296.

Akai, K., Ohnishi, Y, and Nishigaki, M. 1979. Finite Element Analysis of Three-Dimensional Flows in Saturated-Unsaturated Soils. *In* Third International Conference on Numerical Methods in Geomechanics, Aachen, Rotterdam. *Edited by* W. Wittke. pp. 227 – 239.

Amiri, A., and Vafai, K. 1994. Analysis of Dispersion Effects and Non-Thermal Equilibrium, Non-Darcian, Variable Porosity Incompressible Flow Through Porous Media. *In* International Journal of Heat and Mass Transfer, **37** (6): pp. 939 – 954.

Artéus, Martin, and Johansson, Thomas. 1998. Thermohydraulic Processes in Embankment Dams. Master of Science Thesis No. 399. Department of Civil and Environmental Engineering, Royal Institute of Technology, KTH, Stockholm.

Armbruster, H., Brauns, J., Mazur, W., and Merkler, G.P. 1989. Effect of Leaks in Dams and Trials to Detect Leakage by Geophysikal Means. *In* Lecture Notes in Earth Sciences, Vol. 27. *Edited by* G.P. Merkler et. al. Detection of Subsurface Flow Phenomena. Springer-Verlag, Berlin. pp. 3 – 17.

Armbruster, H., Blinde, A., Brauns, J., Hötzl, H., Döscher, H.D., and Merkler, G.P. 1989a. The Application of Geoelectrical and Thermal Measurements to Locate Dam Leakages. *In* Lecture Notes in Earth Sciences, Vol. 27. *Edited by* G.P. Merkler et. al. Detection of Subsurface Flow Phenomena. Springer-Verlag, Berlin. pp. 31 – 47.

Armbruster, H. 1987. The Distribution of Temperature in Water Percolated Earth Dams of a River Barrage. *In* Ninth European Conference of Soil Mechanics and Foundation Engineering, Dublin. pp. 367 – 371.

Armbruster-Veneti, H. ----. Fibre Optic Temperature Measurements in Geotechnical Engineering.

Armstrong, J.E. 1994. Environmental Engineering Applications of he Surficial Geology of the Fraser Lowland, British Columbia. Geological Survey of Canada Paper 83-23.

Aufleger, Markus, Strobl, Theodor, and Dornstädter, Jürgen. 2000. Fibre Optic Temperature Measurements in Dam Monitoring – Four Years of Experience, Q.78 R.1. *In* Vingtième Congrès Internationale des Grands Barrages, Beijing. pp. 1 – 21.

Bachu, Stefan. 1988. Analysis of Heat Transfer Processes and Geothermal Pattern in the Alberta Basin, Canada. *In* Journal of Geophysical Research, **93** (B7): 7767 – 7781.

Bartholomew, Charles L, Murray, Bruce C., and Goins, Dan L. 1987. Embankment Dam Instrumentation Manual. United States Department of the Interior, Bureau of Reclamation.pp. 89 – 99.

Batycky, R.P., Edwards, D.A., and Brenner, H. 1993. Thermal Taylor Dispersion in an Insulated Circular Cylinder II. Applications. In International Journal of Heat and Mass Transfer, **36** (18): pp. 4327 – 4333.

Bauer, Michael S., and Chapman, David S. 1986. Thermal Regime at the Upper Stillwater Dam Site, Uinta Mountains, Utah: Implications for Terrain, Microclimate and StructuralCorretions in Heat Flow Studies. *In* Technophysics, **128** (1986) 1 – 20. Elsevier Science Publishers B.B., Amsterdam. pp. 1 – 20.

Bear, Jacob. 1988. Dynamics of Fluids in Porous Media. Dover Publications Inc., New York, N.Y.

Bell, F.G. ed. 1987. Ground Engineer's Reference Book. Butterworths, Toronto. pp. 4/4, 8/1 - 8/24.

Bettzieche, Volker. 2000. Temperature Measurement in a Masonry Dam by Means of Fibreoptical Sensors, Q.78 R.15. *In* Vingtième Congrès Internationale des Grands Barrages, Beijjing. pp. 211 – 231.

Birman, J.H., Esmilla, A. B., and Indreland, J.B. 1971. Thermal Monitoring of Leakage Through Dams. Geological Society of America Bulletin, **82**. pp. 2261 – 2284.

Blackwell, David D., and Steele, John L. 1988. Thermal Conductivity of Sedimentary Rocks: Measurement and Significance. *In* Thermal History of Sedimentary Basins Methods and Case Histories. *Edited by* Nancy N. Naeser, and Thane H. Mculloh, Springer-Verlag, New York, N.Y. pp. 13 – 36.

Blohm, Harry. 2000. Benefits and Concerns About Dams. *In* Dams in the 21st Century: Exploring Important Questions, Issues. HRW, September. pp. 16 – 17.

Bredehoeft, J.D., and Papadopolous, I.S. 1965. Rates of Vertical Groundwater Movements Estimated from the Earth's Thermal Profile. *In* Water Resources Research **1**. pp. 325-328.

BC Hydro, Power Supply Engineering. 2001. Coquitlam Dam Deficiency Investigations Summary of Information for Advisory Board Meeting No. 1 (4 – 6 July, 2001). June 2001.

BC Hydro, Power Supply Engineering. 2000. Coquitlam Dam Temperature Monitoring Report. No. PSE339. October 2000.

BC Hydro, Power Supply Engineering. 2000a. Draft Dam Safety – Coquitlam Dam Deficiency Investigation, Coquitlam Earthfill Dam – 1999 Field and Laboratory Investigations Report No. PSE288. May 2000.

BC Hydro Engineering Projects Division. 1986. Coquitlam Dam Rehabilitation Memorandum on Construction. Report No. EP1. January 1986.

British Columbia Hydro and Power Authority, Hydroelectric Generation Projects Division. 1984. Coquitlam Dam Rehabilitation Memorandum on Design. Report No. H1757. September 1984.

Cantrell, Shawn and Helm, Mark. 2001. Dam Removal Begins on Northwest Salmon Stream: Restoration of Goldsborough Creek Highlights Importance of Dam Removal for Rebuilding Dwindling Northwest Salmon Runs. Press Release, May 25, 2001. Friends of the Earth. www.foe.org/act//525.html.

Cartwright, Keros. 1971. Redistribution of Geothermal Heat by a Shallow Aquifer. *In* Geological Society of America Bulletin, **82**. November 1971. pp. 3197 – 3200.

Cartwright, Keros. 1970. Ground-water discharge in the Illinois basin, as suggested by temperature anomalies. *In* Water Resource Research, **6** no. 3. pp. 912 – 918.

Cherry, John A., and Freeeze, R. Allan. 1979. Groundwater. Prentice-Hall of Canada, Ltd., Toronto.

Conway, G.R.G. 1915. Coquitlam-Buntzen Hydro-Electric Development, British Columbia. Department of the Interior, Dominion Water Branch, Ottawa, Canada, Water Resources Paper No. 13, Ottawa Government Printing Bureau.

Domenico, P.A. and Schwartz, F.W. 1998. Physical and Chemical Hydrogeology, 2nd Edition. Wiley, New York, N.Y. Chapter 9.

Domenico, Patrick A. 1972. Concepts and Models in Groundwater Hydrology, McGraw Hill Book Company, Toronto. pp. 279 – 314.

Dornstädter, J. 1997. Detection of Internal Erosion in Embankment Dams, Q.73 R.7. Nineteenth Congress on Large Dams, Florence, Italy. pp. 87 – 101.

Energy, Mines and Resources Canada, Surveys and Mapping Branch. 1986. Vancouver (92G) Edition 2, National Topographic Survey Map Scale 1:250 000.

Flynn, T.J., Silliman, S.E., and Simpson, E.S. 1985. Water Temperature as a Groundwater Tracer in Fractured Rock. AGU Front Range Conference. April, 1985. pp. 33 – 42.

Forster, Craig, and Smith, Leslie. 1989. The Influence of Groundwater Flow on Thermal Regimes in Mountainous Terrain: A Model Study. *In* Journal of Geophysical Research, **94** (B7): pp. 9439 – 9451.

Fredlund, Delwyn G., and Rahardjo, Harianto. 1993. An Overview of Unsaturated Soil Behaviour. *In* Unsaturated Soils. Geotechnical Special Publication No. 39. *Edited by* Sandra L. Houston, and Warren K. Wray. American Society of Civil Engineers, New York, NY.

Frind, Emil O. 1988. Solution of the Advection-Dispersion Equation with Free Exit Boundary. *In* Numerical Methods for Partial Differential Equations, 4. John Wiley & Sons, Inc. pp. 301 – 313.

Fredlund, D.G. 1997. An Introduction to Unsaturated Soil Mechanics. *In* Unsaturated Soil Engineering Practice, Geotechnical Special Publication No. 68. *Edited by* Sandra L. Houston, and Delwyn G. Fredlund. American Society of Civil Engineers, New York, N.Y. pp. 1- 37.

Fredlund, D.G., Xing, Anqing, and Huang, Shangyan. 1994. Predicting the Permeability Function for Unsaturated Soils Using the Soil-Water Characteristic Curve. *In* Canadian Geotechnical Journal, **31**: pp. 533 - 546.

Fredlund, D.G., and Xing, Anqing. 1994. Equations for the Soil-Water Characteristic Curve. *In* Canadian Geotechnical Journal, **31**: pp. 521 - 532.

Fredlund, D.G., and Rahardjo, H. 1993. An Overview of Unsaturated Soil Behaviour. *In* Unsaturated Soils. *Edited by* S.L. Houston, and W.K. Wray. American Society of Civil Engineers Geotechnical Special Publication No. 39, New York, NY. pp. 1 – 31.

Fredlund, Murray D., Wilson, G. Ward, and Fredlund, Delwyn G. 2000. Use of Grain-Size Functions in Unsaturated Soil Mechanics. *In* Advances in Unsaturated Geotechnics, Geotechnical Special Publication No. 99, Proceedings of Geo-Denver. Edited by Charles D. Shackelford, Sandra L. Houston, and Nien-Yin Chang. American Society of Civil Engineers, Reston, Virginia. pp. 69 – 124.

Gens, A., Alonso, E.E., and Delage, P. 1997. Computer Modeling and Application to Unsaturated Soils. *In* Unsaturated Soil Engineering Practice, Geotechnical Special Publication No. 68. *Edited by* Sandra L. Houston, and Delwyn G. Fredlund. American Society of Civil Engineers, New York, N.Y. pp. 299- 330.

Geological Survey of Canada. 1965. Geology – Pitt Lake (Vancouver, East Half), Map 1151A. Scale 1:253,440.

GEO-SLOPE International Inc. 1998. User's Guide SEEP/W for Finite Element Seepage Analysis Version 4. Calgary, Alberta.

GEO-SLOPE International Inc. 1998a. User's Guide CTRAN/W for Finite Element Contaminant Transport Analysis Version 4. Calgary, Alberta.

Golder Associates (UK) Ltd. 2000. Coupled Seepage/Temperature Models for Analysis of Earth Dams. Prepared for BC Hydro. Nottingham, England.

Greater Vancouver Water District (GVWD). 1997. Chapter IV, 1997 Drilling Investigation.

Gupta, S.K., Cole, C.R., Kincaid, C.T., and Monti, A.M. 1987. Coupled Fluid, Energy, and Solute Transport (CFEST) Model: Formulation and User's Manual BMI/ONWI-660.

Gvirtzman, Haim, Garven, Grant, and Gvirtzman, Gdaliahu. 1997. Thermal Anomalies Associated with Forced and Free Ground-Water Convection in the Dead Sea Rift Valley. GSA Bulletin, **109** (9): pp. 1167 – 1176.

Hayba, D.O., and Ingebritsen, S.E. 1994. The Computer Model HYDROTHERM, a Three-Dimensional Finite-Difference Model to Simulate Ground-Water Flow and Heat Transport in the Temperature Range of 0 to 1,200 Degrees Celsius: U.S. Geological Survey Water-Resources Investigations. Report 94-4045.

Hess, Alfred, E., and Paillet, Frederick L. 1990. Characterizing Flow Path and Permeability Distribution in Fractured-Rock Aquifers Using a Sensitive, Thermal Borehole Flowmeter. *In* Conference Proceedings on New Field Techniques for Quantifying the Physical and Chemical Properties of Heterogeneous Aquifers: National Water Well Association. *Edited by* F.J. Molz et. al., Dublin, Ohio. pp. 445 – 461.

Ho, P.G. 1979. The Prediction of Hydraulic Conductivity from Soil Moisture Suction Relationship. B.Sc. Thesis, University of Saskatchewan, Saskatoon, Canada.

Hsu, C.T., and Cheng, P. 1990. Thermal Dispersion in a Porous Medium. *In* International Journal of Heat and Mass Transfer, **33** (8): 1587 – 1597.

Ingerbritsen, Steven E., and Sanford, Ward E. 1998. Groundwater in Geologic Processes. Cambridge University Press, New York, N.Y.

Ingerbritsen, S.E., Scholl, M.A., and Sherrod, D.R. 1993. Heat Flow From Four New Research Drill Holes in the Western Cascades, Oregon, U.S.A. *In* Goethermics, **22** (3): 151 – 163.

Ingebristen, S.E., Sherrod, D.R., and Mariner, R.H. 1992. Rates and Patterns of Groundwater Flow in Cascade Range Volcanic Arc, and the Effect on Subsurface Temperatures. *In* Journal of Geophysical Research, **97** (B4): pp. 4599 – 4627.

Ingebritsen, S.E., and Paulson, K.M. 1990. Numerical Simulation of Hydrothermal Circulation in the Cascade Range, North-Central Oregon. Geothermal Resources Council Transactions, **14** (Part 1): pp. 691 – 698.

International Commission on Large Dams (ICOLD). 1995. Dam Failures Statistical Analysis, Bulletin 99.

International Commission on Large Dams (ICOLD). 1992. Improvement of Existing Dam Monitoring, Recommendations and Case Histories, Bulletin 87.

International Commission on Large Dams (ICOLD). 1989. Monitoring of Dams and Their Foundations, State of the Art, Bulletin 68.

International Commission on Large Dams (ICOLD). 1988. Dam Monitoring General Considerations, Bulletin 60.

INTEVEP, S.A. 1993. Permeability Measurement Through Temperature Logging. SPWLA 34th Annual Logging Symposium. pp. 1 – 10.

Jakosky, J.J. 1957. Exploration Geophysics 2nd Edition. Trija Publishing Company, Times-Mirror Press, California, U.S.A. Chapter IX, pp. 969 – 986.

Jansen, Robert B. 2000. A Review of Sinkholes and Related Instrumentation at Embankment Dams. Q. 78 R. 43. *In* Vingtième Congrès Internationale des Grand Barrages, Beijing. pp. 663 – 684.

Johansson, Benny, Johansson, Sam, and Nilsson, Roy. 1996. Investigations and Repair of the Embankment Dam at Porjus Powerstation. *In* Proceedings from Repair and Upgrading of Dams, KTH, Stockhom. pp. 218 – 227.

Johansson, Sam, Farhadiroushan, Mahmoud, and Parker, Tom. 2000. Application of Fibre-Optiics Systems in Embankment Dams for Temperature, Strain and Pressure Measurements – Some Comparisons and Experiences. *In* Vingtième Congrès Internationale des Grands Barrages, Beijing. pp. 1125 – 1146.

Johansson, Sam and Hellström, Göran. 2001. Software Package for Evaluation of Temperature Field in Embankment Dams, DamTemp Ver. 1.0. HydroResearch and NeoEnergy.

Johansson, Sam. 1997a. Seepage Monitoring in Embankment Dams. Doctoral Thesis, Royal Institute of Technology, Stockholm, Sweden.

Johansson, S. 1997b. Internal Erosion Detection and Seepage Monitoring in Embankment Dams by Temperature and Resistivity Measurements, Q.73 R.11. *In* Nineteenth International Congress on Large Dams, Florence, Italy. pp. 281 – 285.

Johansson, Sam, Claesson, Johan, and Hellström, Göran. 1996. Temperature Analyses for Evaluation of Water Flow in Aquifers and Embankment Dams. *In* Water Resources Research.

Johansson, Sam. 1996. Seepage Monitoring in Embankment Dams by Temperature and Resistivity Measurements. *In* Proceedings from Repair and Upgrading of Dams, KTH, Stockhom. pp. 288 – 297.

Johansson, S. 1994. Monitoring During Ongoing Internal Erosion and After Restoration of the Embankment Dam at Porjus Powerstation, Sweeden, Q.68 R.5. *In* Eighteenth International Congress on Large Dams, Durban, South Africa. pp. 94 – 96.

Johansson, Sam. 1991. Localization and Quantification of Water Leakage in Ageing Embankment Dams by Regular Temperature Measurements, Q.65 R.54. ICOLD 17th Congress in Vienna. pp. 991 – 1005.

Jumikis, A.R. 1977. Thermal Geotechnics. Rutgers University Press, New Jersey.

Kazda, I. 1979. Numerical Modeling of Seepage in Earth and Rockfill Dams. *In* Third International Conference on Numerical Methods in Geomechanics, Aachen, Rotterdam. *Edited by* W. Wittke. pp. 257 – 261.

Keys, W.S., and Brown, R.F. 1978. The Use of Temperature Logs to Trace the Movement of Injected Water. *In* Groundwater, **16** (1): pp. 32 - 48.

Keys, W. Scott and MacCary, L.M. 1971. Chapter E1, Application of Borehole Geophysics to Water-Resources Investigations. *In* Techniques of Water-Resources Investigations of the United States Geological Survey, Book 2, Collection of Environmental Data. U.S. Department of the Interior. United States Government Printing Office, Washington.

Konrad, J.M., Alicescu, V., and Shen, M. 2000. Thermal analysis of an Earth Dam Considering Seepage Related Heat Transport. *In* Montréal 2000: 53rd Annual Conference of the Canadian Geotechnical Society. pp. 211 – 217.

Kreith, Frank, and Bohn, Mark S. 1993. Principles of Heat Transfer, Fifth Edition. West Publishing Company, New York.

Kunii, Daizo, and Smith J.M. 1961. Heat Transfer Characteristics of Porous Rocks: II. Thermal Conductivities of Unconsolidated Particles with Flowing Fluids. *In* American Institute of Chemical Engineering Journal, **7** (1): pp. 29 – 34.

Kutateladze, S.S., and Borishanskii, V.M. 1966. A Concise Encyclopedia of Heat Transfer. Pergamon Press, New York, N.Y.

Kuwahara, F., Nakayama, A., and Koyama, H. 1996. A Numerical Study of Thermal Dispersion in Porous Media. *In* Transactions of the American Society of Mechanical Engineers (ASME), Journal of Heat Transfer, **188**: pp. 756 – 761.

Kuznetsov, A.V. 2001. Influence of Thermal Dispersion on Forced Convection in a Composite Parallel-Plate Channel. *In* Zeitschrift für angewandte Mathematik und Physik ZAMP, **52:** pp. 135 –150.

Laphan, Wayne W. 1987. Use of Temperature Profiles Beneath Streams to Determine Rates of Vertical Ground-Water Flow and Vertical Hydraulic Conductivity. *In* United States Geological Survey Water Supply Paper 2337, Washington. pp. 1 –34.

LeBihan, Jean-Pierre, and Leroueil, Serge. 1999. Transient Water Flow Through Unsaturated Soils – Implications for Earth Dams. Proceedings of the 52nd Canadian Geotechnical Conference, Regina. pp. 559 – 566.

Legget, Robert F. (ed.). 1976. Glacial Till An Inter-Disciplinary Study, The Royal Society of Canada Special Publications, No. 12. Royal Society of Canada.

Levec, J., and Carbonell, R.G. 1985. Longitudinal and Lateral Thermal Dispersion in Packed Beds, Part I: Theory. *In* AIChE Journal, **31** (4): 581 – 590.

Levec, J., and Carbonell, R.G. 1985a. Longitudinal and Lateral Thermal Dispersion in Packed Beds, Part II: Comparison between Theory and Experiment. *In* AIChE Journal, **31** (4): 591 – 602.

López, Dina L., Smith, Leslie, and Sorey, Michael L. 1994. Modeling Fluid Flow and Heat Transfer at Basin and Range Faults: Preliminary Results for Leach Hot Springs, Nevada. Geothermal Resources Council Transactions, **18** (October): pp. 11 – 16.

McClure, Robert. 2000. Oregon Governor Endorses Dam Removal. Seattle Post-Intelligencer, February 19, 2000.

Merkler, G.P., Blinde, A., Armbruster, H., and Döscher, H.D. 1985. Field Investigations for the Assessment of Permeability and Identification of Leakages in Dams and Dam Foundations, Q.58 R.7. *In* Quinzième Congres Internationale des Grands Barrages, Lausanne. pp. 125 – 141.

Moyne, C., Didierjean, S., Amaral Souto, H.P., and da Silveira, O.T. 2000. Thermal Dispersion in Porous Media: One-Equation Model. *In* International Journal of Heat and Mass Transfer, **43**: pp. 3853 – 3867.

Murthy, P.V.S.N. 1998. Thermal Dispersion and Viscous Dissipation Effects on Non-Darcy Mixed Convection in a Fluid Saturated Porous Medium. *In* Heat and Mass Transfer, **33**: pp. 295 - 300.

Myers, Barry. 2000. Optimization of Dam Monitoring Systems: Review of the Available Technology and Case Studies. Q. 78, R. 42. *In* Vingtième Congrès Internationale des Grand Barrages, Beijing. pp. 641 – 660.

Ngo, Nam D., and Tamma, K.K. 2001. Non-Isothermal '2-D Flow/2-D Thermal' Developments Encompassing Process Modelling of Composites: Flow/Thermal/Cure Formulations and Validations. *In* International Journal for Numerical Methods in Engineering, **50**: pp. 1559 – 1585.

Nitao, John J., and Bear, Jacob. 1996. Potentials and Their Role in Transport in Porous Media. *In* Water Resources Research, **32** (2): pp. 225 – 250.

Ogata, Akio. 1970. Theory of Dispersion in a Granular Medium. *In* Fluid Movement in Earth Materials. Geological Survey Professional Paper 411-I. United States Government Printing Office, Washington.

Ogata, Akio, and Banks, R.B. 1961. A Solution of the Differential Equation of Longitudinal Dispersion in Porous Media. *In* Fluid Movement in Earth Materials. Geological Survey Professional Paper 411-A. United States Government Printing Office, Washington. pp. A-1 to A-7.

Paulson, Michael. 1999. Clinton Urged to Weigh NW Dam Removal. Seattle Post-Intelligencer. August 5, 1999.

Rahardjo, H., and Leong, E.C. 1997. Soil-Water Characteristic Curves and Flux Boundary Problems. *In* Unsaturated Soil Engineering Practice, Geotechnical Special Publication No. 68. *Edited by* Sandra L. Houston, and Delwyn G. Fredlund. American Society of Civil Engineers, New York, N.Y. pp. 88 – 112.

Sammel, Edward A. 1968. Convective Flow and It's Effect on Temperature Logging in Small-Diameter Wells. *In* Geophysics, **33** (6): pp. 1004 – 1012.

Schimschal, U. 1981. The Relationship of Geophysical Measurements to Hydraulic Conductivity at the Brantley Damsite, New Mexico. *In* Geoexploration, **19**: pp. 115 - 125.

Silva, A.J., and Morin, R.H. 1986. The Sensitivity of Sediment Physical Properties to Changes in Temperature, Pressure, and Porosity. *In* Thermal Modeling in Sedimentary Basins – Proceedings of the 1st IFP Exploration Research Conference, June 3-7, 1985: Paris, France. Edited by J. Burrus. Institut Francais du Petrole. pp. 289 – 309.

Smith, Leslie, Forster, Craig, and Woodbury, Allan. 1989. Numerical Simulation Techniques for Modeling Advectively-Disturbed Thermal Regimes. *In* International Union of Geodesy and Geophysics and American Geophysical Union. pp. 1 – 6.

Smith, M., and Konrad, J.M. ----. Influence of Seepage on the Temperature Distribution in a Zoned Earth Dam.

Sorey, Michael L. 1971. Measurement of Vertical Groundwater Velocity from Temperature Profiles in Wells. *In* Water Resources Research, **7** (4): pp. 963 – 970.

Stallman, R.W. 1965. Steady One-Dimensional Fluid Flow in a Semi-Infinite Porous Medium with Sinusoidal Surface Temperature. *In* Journal of Geophysical Reserach, **70** (12): pp. 2821 – 2827.

Stallman, R.W. 1967. Flow in the zone of aeration. *In* Hydroscience, **4**. *Edited by* Ven Te Chow, Academic Press, New York. pp. 151 – 195.

Stevens, Herbert H. Jr., Ficke, John F., and Smoot, George F. 1975. Chapter D1, Water Temperature - Influential Factors, Field Measurement, and Data Presentation. *In* Techniques of Water-Resources Investigations of the United States Geological Survey. Book 1, Collection of Water Data by Direct Measurement. United States Government Printing Office, Washington. (Stock No. 024-011-02711-9).

Taylor, Sterling A. and Cary, John W. 1960. Analysis of the Simultaneous Flow of Water and Heat or Electricity with the Thermodynamics of Irreversible Processes. Seventh Interim Congress of Soil Science, Madison, Wisconsin. pp. 80 – 90.

Terzaghi, K., and Peck, R.B. 1948. Soil Mechanics in Engineering Practice. John Wiley & Sons, Inc. New York, N.Y. pp. 386 - 393.

Van de Griend, A.A., Camillo, P.J., and Gurney, R.J. 1985. Discrimination of Soil Physical Parameters, Thermal Inertia, and Soil Moisture from Diurnal Surface Temperature Fluctuations. *In* Water Resources Research, **21** (7): pp. 997 – 1009.

Venetis, C. 1989. Temperature Distribution in a Dam Due to Leakage. *In* Lecture Notes in Earth Sciences, Vol. 27. *Edited by* G.P. Merkler et. al. Detection of Subsurface Flow Phenomena. Springer-Verlag, Berlin. pp. 339 – 347.

Voss, C.L. 1984. A Finite-Element Simulation Model for Saturated-Unsaturated, Fluid-Density-Dependent Ground-Water Flow with Energy Transport or Chemically-Reactive Single-Species Solute Transport: U.S. Geological Survey Water-Resources Investigations Report 84-4369.

Wang, Bu-Xuan, and Du, Jian-Hua. 1993. Forced Convective Heat Transfer in a Vertical Annulus Filled with Porous Media. *In* International Journal of Heat and Mass Transfer, **36** (17): pp. 4207 – 4213.

Wang, Kelin, Shen, Po-Yu, and Beck, Alan E. 1989. A Solution to the Inverse Problem of Coupled Hydrological and Thermal Regimes. *In* International Union of Geodesy and Geophysics and American Geophysical Union. pp. 7 – 21.

Willhite, G.P., Kunii, Daizo, and Smith, J.M. 1962. Heat Transfer in Beds of Fine Particles (Heat Transfer Perpendicular to Flow). *In* American Institute of Chemical Engineers Journal, **8** (3): pp. 340 – 345.

Williams, Adrian. 2000. The Use of Risk Analysis To Support Dam Safety Decision, Management. *In* Dams in the 21st Century: Exploring Important Questions, Issues. HRW, September. pp. 14 – 15.

Woodbury, Allan D., Narod, B., Chandra, B., and Bennest, J.R. 1991. Temperature Measurements in Geotechnical Studies Using Low-Noise, High Resolution Digital Techniques. *In* Canadian Geotechnical Journal, **28**. pp. 639 – 649.

Woodside, W., and Messmer, J.H. 1961. Thermal Conductivity of Porous Media. I. Unconsolidated Sands. *In* Journal of Applied Physics, **32** (9): pp. 1688 – 1699.

Woodside, W., and Messmer, J.H. 1961. Thermal Conductivity of Prous Media. II. Consolidated Rocks. *In* Journal of Applied Physics, **32** (9): pp. 1699 – 1706.

Yanagisawa, Eiji, and Tanaka, Motoaki. 1979. Finite Element Analysis of Heat and Moisture Transfer in Unsaturated Soils. *In* Third International Conference on Numerical Methods in Geomechanics, Aachen, Rotterdam. *Edited by* W. Wittke. pp. 275 – 280.

Yong, Jiao. 2000. Dam Monitoring: More Safety, Less Risk, Better Performance. *In* Dams in the 21st Century: Exploring Important Questions, Issues. HRW, September. pp. 18.

Yuan, Zeng-Guang, Somerton, W.H., and Udell, K.S. 1991. Thermal Dispersion in Thick-Walled Tubes as a Model of Porous Media. *In* International Journal of Heat and Mass Transfer, **34** (11): pp. 2715 – 2725.

APPENDIX A MODEL VERIFICATION USING CLOSED FORM SOLUTIONS

- **APPENDIX A-1** CLOSED FORM SOLUTIONS – VISUAL BASIC FUNCTIONS AND SPREADSHEETS
- **APPENDIX A-2** CALCULATIONS FOR MODEL VERIFICATION INPUT PARAMETERS

APPENDIX A-1 CLOSED FORM SOLUTIONS – VISUAL BASIC FUNCTIONS AND SPREADSHEETS

Visual Basic Functions Used In Closed Form Solution Spreadsheet

```
Public Function ADE_fixed(x, t, v, D, Tmax, Tmin)
' provide solution for the advection diffusion equation
' under step changed boundary conditions (ogata & banks)
' ____________________________________________________________
' metric units assumed, although any self-consistent set
' will work, with variables...
' x = distance [m]
' v = seepage velocity [m/s]
' D = diffusivity [m2/s]
' t = time [input as yrs, shifted to s]
' Tmax = max temperature after step change
' Tmin = temperature before step change
Const sec_per_yr = 31557600
Const pi = 3.14159

t = t * sec_per_yr

dT = Tmax - Tmin

a1 = Erfc((x - v * t) / (Sqr(4 * D * t)))
a2 = Exp(x * v / D)
a3 = Erfc((x + v * t) / (Sqr(4 * D * t)))

ADE_fixed = 0.5 * dT * (a1 + a2 * a3) + Tmin
End Function
```

Visual Basic Functions Used In Closed Form Solution Spreadsheet

```
Public Function ADE_sin(x, t, v, D, Tmax, Tmin, omega, lag)
' provide solution for the advection diffusion equation
' under sinusoidal varying boundary conditions
'
' solution from C&J, p389 eqn(14) and is for the steady
' state after decay of transients form initial conditions
'
' ---------------------------------------------------------
' metric units assumed, although any self-consistent set
' will work, with variables...
' x = distance [m]
' L = domain length [m]
' v = seepage velocity [m/s]
' D = diffusivity [m2/s]
' t = time [input as yrs, shifted to s]
' omega = period [input as yrs]
' Tmax = max temperature after step change
' Tmin = temperature before step change
Const sec_per_yr = 31557600

t = t * sec_per_yr
lag = lag / omega * 2 * pi
omega = omega * 2 * pi / sec_per_yr

dT = (Tmax - Tmin) / 2

a = Sqr((v * v / (4 * D * D)) ^ 2 + (omega / D) ^ 2)
root_a = Sqr(a)
phi = atan((omega / D) / (v * v / (4 * D * D)))

Term1 = Exp(v * x / (2 * D) - x * root_a * Cos(phi / 2))
Term2 = Cos(omega * t - x * root_a * Sin(phi / 2) + lag)
ADE_sin = dT * Term1 * Term2 + (dT + Tmin)

End Function
```

Closed Form Solution Heat Transport Using the Advective Dispersion Equation For A 1-D Rod
With a step change in the boundary conditions And Sinusoidal Temperature Variation
(Spreadsheet Created by Golders Associates, 2000)

geometry and boundary conditions

length	100	m
initial temp	3	deg
final temp	12	deg
period	1	year
lag	0.5	year

best-estimate properties

D =	3.00E-06	m2/s	includes some hydraulic dispersion
k * I =	1.00E-07	m/s	
n =	3.00E-01		
v_bar =	3.33E-07	m/sec	
water density	1.00E+03	kg/m3	
core density	2.32E+03	kg/m3	
water specific heat	4.18E+03	J/kg/degK	
core specific heat	8.65E+02	J/kg/degK	
so, transformed v_bar	2.08E-07	m/sec	

step change boundary conditions.....

time for full migration 9.5 years

Time [yrs]:		1	3	6	8
x [m]	T				
0		12	12	12	12
1		11.72308	11.910469	11.96702963	11.98047201
2		11.42887	11.814905	11.9317903	11.95959244
3		11.1189	11.713307	11.89422727	11.93732011
4		10.79489	11.605696	11.85428887	11.91361461
5		10.45876	11.49212	11.81192668	11.8884363
6		10.11256	11.372655	11.76709582	11.86174653
7		9.758477	11.247399	11.7197552	11.83350771
8		9.398966	11.11648	11.66986777	11.80368344
9		9.03637	10.98005	11.61740071	11.77223864
10		8.673003	10.838287	11.56232569	11.73913966
11		8.31116	10.691393	11.50461908	11.70435442
12		7.95308	10.539595	11.44426211	11.66785252
13		7.600901	10.383142	11.3812411	11.62960534
14		7.256628	10.222304	11.31554759	11.5895862
15		6.922104	10.057372	11.24717852	11.54777045

sinusoidal temperature variation on boundary

time of interest...

0.5	0 years
T	T
12	3
11.31364283	3.686357167
10.62432161	4.375678392
9.965326752	5.034673248
9.359933388	5.640066612
8.822885647	6.177114353
8.361900773	6.638099227
7.979116947	7.020883053
7.672431021	7.327568979
7.436691438	7.563308562
7.264727376	7.735272624
7.148207803	7.851792197
7.078333755	7.921666245
7.046374183	7.953625817
7.044060423	7.955939577
7.063857126	7.936142874

Closed Form Solution Heat Transport Using the Advective Dispersion Equation For A 1-D Rod
With a step change in the boundary conditions And Sinusoidal Temperature Variation
(Spreadsheet Created by Golders Associates, 2000)

16	6.598984	9.8886541	11.17613633	11.50413556	7.099128723	7.900871277
17	6.288714	9.7164745	11.10242908	11.45866126	7.144220513	7.855779487
18	5.99252	9.5411722	11.02607059	11.41132965	7.194472554	7.805527446
19	5.711398	9.3630976	10.94708043	11.36212527	7.246183036	7.753816964
20	5.446111	9.1826149	10.86548403	11.31103521	7.296535887	7.703464113
21	5.197194	9.0001647	10.78131268	11.25804921	7.343505254	7.656494746
22	4.964959	8.8161501	10.69460355	11.20315971	7.385747324	7.614252676
23	4.749507	8.6309551	10.60539966	11.14636196	7.422487867	7.577512133
24	4.550744	8.444969	10.51374981	11.0876541	7.453411887	7.546588113
25	4.368399	8.2585837	10.41970856	11.02703717	7.478560073	7.521439927
26	4.202043	8.0721911	10.32333609	10.96451521	7.498235158	7.501764842
27	4.051113	7.8861806	10.22469809	10.90009532	7.512920063	7.487079937
28	3.914932	7.7009369	10.12386564	10.83378765	7.523208648	7.476791352
29	3.792733	7.5168375	10.02091499	10.76560546	7.529749082	7.470250918
30	3.683679	7.3342502	9.915927422	10.69556513	7.533199255	7.466800745
31	3.586888	7.1535317	9.808988976	10.62368621	7.53419323	7.46580677
32	3.501447	6.975025	9.700190243	10.54999138	7.533317465	7.466682535
33	3.426434	6.7990582	9.589626086	10.47450643	7.531095418	7.468904582
34	3.360935	6.6259422	9.477395349	10.39726032	7.527979093	7.472020907
35	3.30405	6.45597	9.363600551	10.31828507	7.524346137	7.475653863
36	3.254914	6.289415	9.248347555	10.23761576	7.520501191	7.479498809
37	3.212699	6.1265302	9.131745217	10.15529049	7.516680348	7.483319652
38	3.176626	5.9675469	9.013905018	10.07135032	7.513057681	7.486942319
39	3.145966	5.8126746	8.894940682	9.985839179	7.509753025	7.490246975
40	3.120047	5.6621	8.774975948	9.898803822	7.506840311	7.493159689
41	3.098253	5.5159872	8.654166933	9.810293717	7.50435591	7.49564409
42	3.080026	5.3744771	8.532638266	9.720360959	7.502306605	7.497693395
43	3.064864	5.2376876	8.410511667	9.629060161	7.500676899	7.499323101
44	3.052318	5.1057141	8.287910538	9.536448338	7.499435492	7.500564508
45	3.041992	4.9786297	8.164959524	9.442584779	7.498540833	7.501459167
46	3.033539	4.8564854	8.041784097	9.347530913	7.497945725	7.502054275
47	3.026657	4.7393115	7.918510131	9.251350166	7.497601005	7.502398995
48	3.021082	4.6271177	7.795263488	9.15410781	7.497458373	7.502541627
49	3.016591	4.5198944	7.672169611	9.055870797	7.497472449	7.502527551
50	3.012992	4.4176136	7.549353124	8.956707599	7.49760216	7.50239784
51	3.010123	4.32023	7.426937443	8.856688026	7.497811567	7.502188433
52	3.007849	4.2276821	7.305044401	8.755883047	7.498070238	7.501929762
53	3.006055	4.1398935	7.183793885	8.65436795	7.498353266	7.501646734
54	3.004648	4.056774	7.06330348	8.552244526	7.498641013	7.501358987
55	3.00355	3.9782212	6.943688146	8.449593536	7.498918686	7.501081314

Closed Form Solution Heat Transport Using the Advective Dispersion Equation For A 1-D Rod
With a step change in the boundary conditions And Sinusoidal Temperature Variation
(Spreadsheet Created by Golders Associates, 2000)

56	3.002698	3.9041215	6.825059888	8.3464903	7.499175781	7.500824219
57	3.00204	3.8343513	6.707527466	8.243011172	7.499405472	7.500594528
58	3.001535	3.7687787	6.591196109	8.139233344	7.499603987	7.500396013
59	3.001149	3.7072644	6.476167255	8.035234639	7.49977	7.50023
60	3.000856	3.6496632	6.362538307	7.931093318	7.499904056	7.500095944
61	3.000634	3.595825	6.250402416	7.82688788	7.500008072	7.499991928
62	3.000468	3.5455961	6.139848276	7.722696867	7.500084885	7.499915115
63	3.000343	3.4988199	6.030959951	7.618598669	7.500137886	7.499862114
64	3.000251	3.4553387	5.923816715	7.51467134	7.500170713	7.499829287
65	3.000182	3.414994	5.818492918	7.410992409	7.500187021	7.499812979
66	3.000131	3.3776276	5.715057877	7.307638701	7.500190298	7.499809702
67	3.000095	3.3430825	5.613575783	7.204686161	7.500183751	7.499816249
68	3.000068	3.3112038	5.514105631	7.10220968	7.500170222	7.499829778
69	3.000048	3.2818388	5.416701179	7.000282938	7.50015215	7.49984785
70	3.000034	3.2548384	5.321410914	6.898978237	7.500131558	7.499868442
71	3.000024	3.230057	5.228278054	6.798366355	7.500110068	7.499889932
72	3.000017	3.2073535	5.137340559	6.698516396	7.500088927	7.499911073
73	3.000012	3.1865911	5.048631168	6.599495659	7.50006904	7.49993096
74	3.000008	3.1676381	4.962177448	6.501369501	7.500051024	7.499948976
75	3.000006	3.150368	4.878001869	6.40420122	7.500035246	7.499964754
76	3.000004	3.1346597	4.796121887	6.308051938	7.500021874	7.499978126
77	3.000003	3.1203977	4.716550052	6.212980499	7.500010917	7.499989083
78	3.000002	3.1074721	4.639294124	6.119043368	7.500002271	7.499997729
79	3.000001	3.0957788	4.564357207	6.026294544	7.499995747	7.500004253
80	3.000001	3.0852192	4.491737892	5.934785485	7.499991106	7.500008894
81	3.000001	3.0757005	4.421430416	5.844565031	7.499988082	7.500011918
82	3	3.0671356	4.353424828	5.755679346	7.499986399	7.500013601
83	3	3.0594426	4.287707168	5.668171866	7.499985793	7.500014207
84	3	3.0525452	4.22425965	5.582083254	7.499986013	7.500013987
85	3	3.0463722	4.163060856	5.497451367	7.499986836	7.500013164
86	3	3.0408573	4.104085933	5.414311229	7.499988068	7.500011932
87	3	3.0359392	4.047306797	5.332695011	7.499989546	7.500010454
88	3	3.0315613	3.992692339	5.25263203	7.499991135	7.500008865
89	3	3.027671	3.940208637	5.174148741	7.499992734	7.500007266
90	3	3.0242203	3.889819161	5.097268747	7.499994262	7.500005738
91	3	3.021165	3.841484992	5.022012819	7.499995668	7.500004332
92	3	3.0184645	3.795165028	4.948398912	7.499996915	7.500003085
93	3	3.016082	3.750816195	4.8764422	7.499997987	7.500002013
94	3	3.0139837	3.708393654	4.806155116	7.499998877	7.500001123
95	3	3.0121391	3.667851009	4.737547389	7.49999959	7.50000041

Closed Form Solution Heat Transport Using the Advective Dispersion Equation For A 1-D Rod With a step change in the boundary conditions And Sinusoidal Temperature Variation (Spreadsheet Created by Golders Associates, 2000)

96	3	3.0105203	3.629140502	4.670626103	7.500000139	7.499999861
97	3	3.0091022	3.592213211	4.605395747	7.50000054	7.49999946
98	3	3.0078622	3.557019244	4.541858281	7.500000812	7.499999188
99	3	3.0067798	3.523507919	4.480013204	7.500000975	7.499999025
100	3	3.0058367	3.491627945	4.419857624	7.500001051	7.499998949

APPENDIX A-2 CALCULATIONS FOR MODEL VERIFICATION INPUT PARAMETERS

APPENDIX A-2

DETAILED CALCULATIONS FOR MODEL VERIFICATION

1D Closed Form Solution

Input Values

$k = 1E\text{-}7$ m/s

$i = 1$

$v = ki/n = 3.33E\text{-}7$ m/s

$n = 0.3$

$\alpha_L = 10$ m

$\alpha_L = 1$ m

$\rho_{core} = 2320$ kg/m^3

$\rho_{water} = 1000$ kg/m^3

$c_{water} = 4180$ J/kg °K

$c_{core} = 2500$ J/kg °K (typical for saturated silt, sand, clay per Johansson and Hellström, 2001)

$\lambda_{core} = 4$ J/ms°K ($\lambda_{limestone} = 2.1$ and $\lambda_{quartz} = 8.4$)

$\lambda_{water} = 0.46$ J/ms°K

Calculated Values

$E^* = \lambda/(\rho c)$
$= 4/(2320*2500) = 6.9E\text{-}7$ m^2/s

$E_{long} = \alpha_L (n\rho_w c_w)/(\rho c)*v$
$= 7.2E\text{-}7$ m^2/s

$E_{trans} = \alpha_T (n\rho_w c_w)/(\rho c)*v$
$= 7.2E\text{-}8$ m^2/s

$E = E^* + E_{long}$
$= 1.4E\text{-}6$ m^2/s

$E = E^* + E_{trans}$
$= 7.6E\text{-}7$ m^2/s

$E_{avg} = 1.1E\text{-}6$ m^2/s

SEEP/W and CTRAN/W Input Parameters and Calculations

$k = 1E\text{-}7$ m/s

$i = (110 - 10)/100 = 1$

$N = 0.3 = \Theta_{sat} = 0.3$

$v = ki/n = 3.33E\text{-}7$ m/s

$E^* = 6.9E\text{-}7$ m/s

$\alpha_L = D_{avg}/(ki/\Theta) = 5.699$

$\alpha_T = (1/10)*\alpha_L = 0.5699$

APPENDIX B CALCULATIONS FOR KARLSRUHE, GERMANY FIELD DAM

- **APPENDIX B-1** CALCULATIONS FOR MODEL THERMAL INPUT PARAMETERS SECTION 4.4
- **APPENDIX B-2** CALCULATIONS FOR MODEL THERMAL INPUT PARAMETERS SECTION 4.5

APPENDIX B-1 CALCULATIONS FOR MODEL THERMAL INPUT PARAMETERS SECTION 4.4

APPENDIX B-1

DETAILED CALCULATIONS FOR THERMAL PROPERTIES – DESCRIBED IN SECTION 4.4 (Summarized on Table 4.4)

Section 4.4 – Thermal Properties for Conduction

The following presents calculations for typical material properties. Based on these calculations values were selected for input into CTRAN/W to represent low, average, and high for these values, as summarized on Table 4.4.

Range of Values For Saturated Sand

λ_{core} = 1.73 to 5.02 J/ms °K (Johansson and Hellström, 2001)

c_{core} = 720 to 1680 J/kg °K (Johansson and Hellström, 2001)

ρ = 2080 kg/m^3 (assumed) (Bell, 1987)

$E^* = \lambda/(\rho c)$ = 1.6E-6 to 7E-7 m^2/s

Range of Values For Sand

λ_{core} = 1.25 to 1.11 J/ms °K (Johansson and Hellström, 2001)

c_{core} = 730 to 995 J/kg °K (Johansson and Hellström, 2001)

ρ = 1600 to 1800 kg/m^3 (Bell, 1987)

$E^* = \lambda/(\rho c)$ = 1.07E-6 to 6.2E-7 m^2/s

Range of Values Moist to Wet Clay

λ_{core} = 0.9 to 2.22 J/ms °K (Johansson and Hellström, 2001)

c_{core} = 730 to 1790 J/kg °K (Johansson and Hellström, 2001)

ρ = 1900 to 2200 kg/m^3 (Bell, 1987)

$E^* = \lambda/(\rho c)$ = 1.6E-6 to 2.3E-7 m^2/s

Water (for comparison)

λ_{water} = 0.6 J/ms °K (Johansson and Hellström, 2001)

c_{water} = 4180 J/kg °K (Johansson and Hellström, 2001)

ρ = 1000 kg/m^3 (Bell, 1987)

$E^* = \lambda/(\rho c)$ = 1.4E-7 m^2/s

APPENDIX B-2 CALCULATIONS FOR MODEL THERMAL INPUT PARAMETERS SECTION 3.9

APPENDIX B-2

DETAILED CALCULATIONS FOR THERMAL PROPERTIES – DESCRIBED IN SECTION 4.5 (Summarized on Table 4.7)

Section 4.5 – Thermal Properties for Conduction and Convection

The following presents calculations for typical material properties. Based on these calculations values were selected for input into CTRAN/W to represent low, average, and high for these values, as summarized on Table 4.7.

Range of Values For Saturated Sand

λ_{core} = 1.73 to 5.02 J/ms °K (Johansson and Hellström, 2001)

c_{core} = 720 to 1680 J/kg °K (Johansson and Hellström, 2001)

ρ = 2080 kg/m^3 (assumed) (Bell, 1987)

$E^* = \lambda/(\rho c)$ = 1.6E-6 to 7E-7 m^2/s

Range of Values For Sand

λ_{core} = 1.25 to 1.11 J/ms °K (Johansson and Hellström, 2001)

c_{core} = 730 to 995 J/kg °K (Johansson and Hellström, 2001)

ρ = 1600 to 1800 kg/m^3 (Bell, 1987)

$E^* = \lambda/(\rho c)$ = 1.07E-6 to 6.2E-7 m^2/s

Range of Values Moist to Wet Clay

λ_{core} = 0.9 to 2.22 J/ms °K (Johansson and Hellström, 2001)

c_{core} = 730 to 1790 J/kg °K (Johansson and Hellström, 2001)

ρ = 1900 to 2200 kg/m^3 (Bell, 1987)

$E^* = \lambda/(\rho c)$ = 1.6E-6 to 2.3E-7 m^2/s

Water (for comparison)

λ_{water} = 0.6 J/ms °K (Johansson and Hellström, 2001)

c_{water} = 4180 J/kg °K (Johansson and Hellström, 2001)

ρ = 1000 kg/m^3 (Bell, 1987)

$E^* = \lambda/(\rho c)$ = 1.4E-7 m^2/s

Values for α_L an α_T vary depending on the soil, α_T is typically less than α_L.

APPENDIX C INDIVIDUAL TEMPERATURE PLOTS FOR EACH MONITORING LOCATION AT COQUITLAM DAM

APPENDIX C – TABLE OF CONTENTS

Reservoir 195
Inclinometer 197
SP-1 199
SP-2 201
SP-4 203
SP-6 205
SP-8 207
SP-9 209
SP97-1A 211
SP97-1B 213
SP99-1A 215
SP99-1B 217
SP99-2 219
SP99-3A 221
SP99-3B 223
SP99-4 225
SP99-5 227
SP99-6 229
SP99-7A 231
SP99-7B 233
SP99-8 235
SP99-9 237
SP99-10 239
SP99-11 241
SP99-12 243
SP99-13 245
SP01-1A 247
SP01-1B 249
SP01-2A 251
SP01-2B 253
SP01-3 255
SP01-10 257

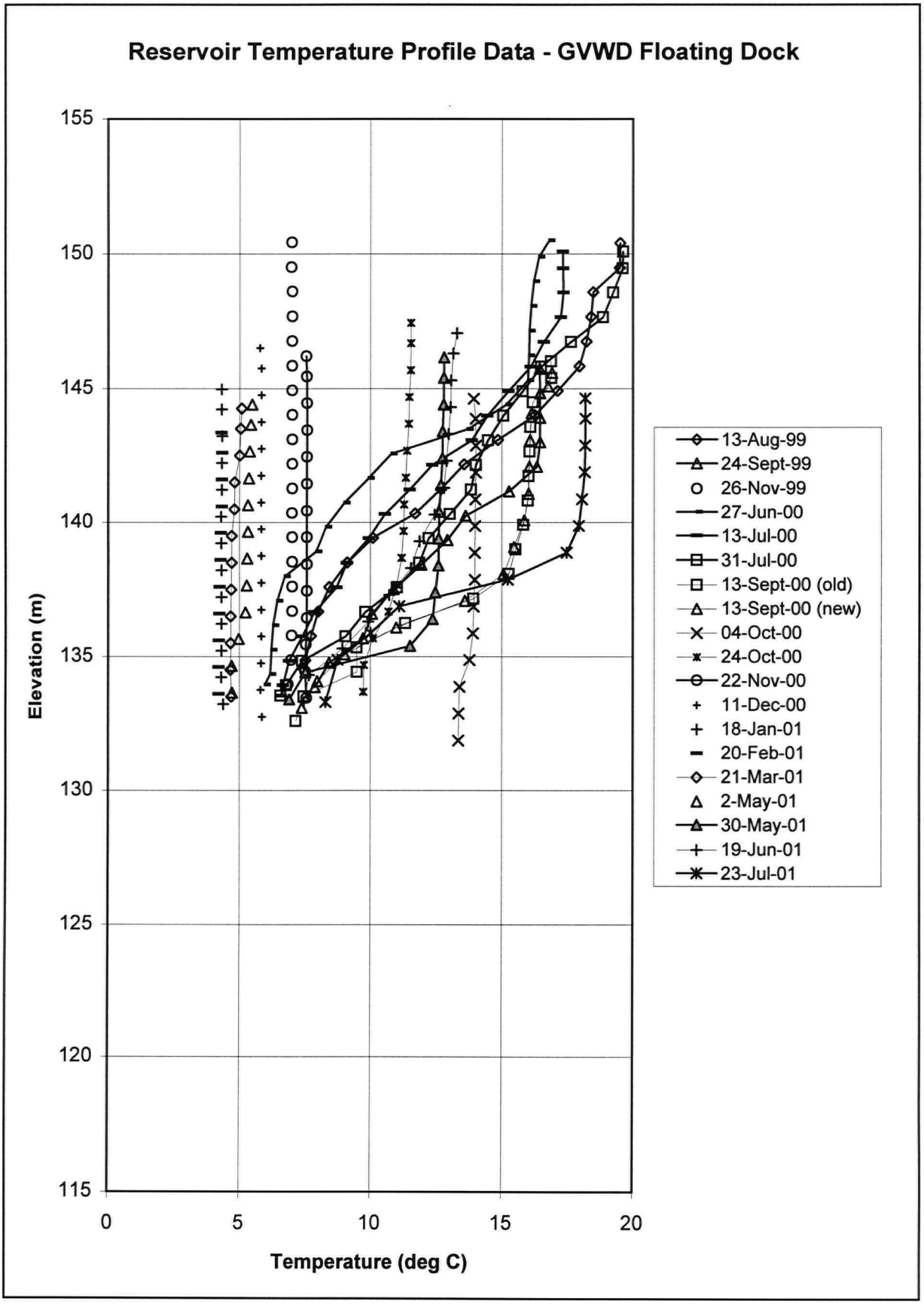
Reservoir Temperature Profile Data - GVWD Floating Dock
155
150
145
140
135
130
125
120
115
Elevation (m)
0
5
10
15
20
Temperature (deg C)
13-Aug-99
24-Sept-99
26-Nov-99
27-Jun-00
13-Jul-00
31-Jul-00
13-Sept-00 (old)
13-Sept-00 (new)
04-Oct-00
24-Oct-00
22-Nov-00
11-Dec-00
18-Jan-01
20-Feb-01
21-Mar-01
2-May-01
30-May-01
19-Jun-01
23-Jul-01

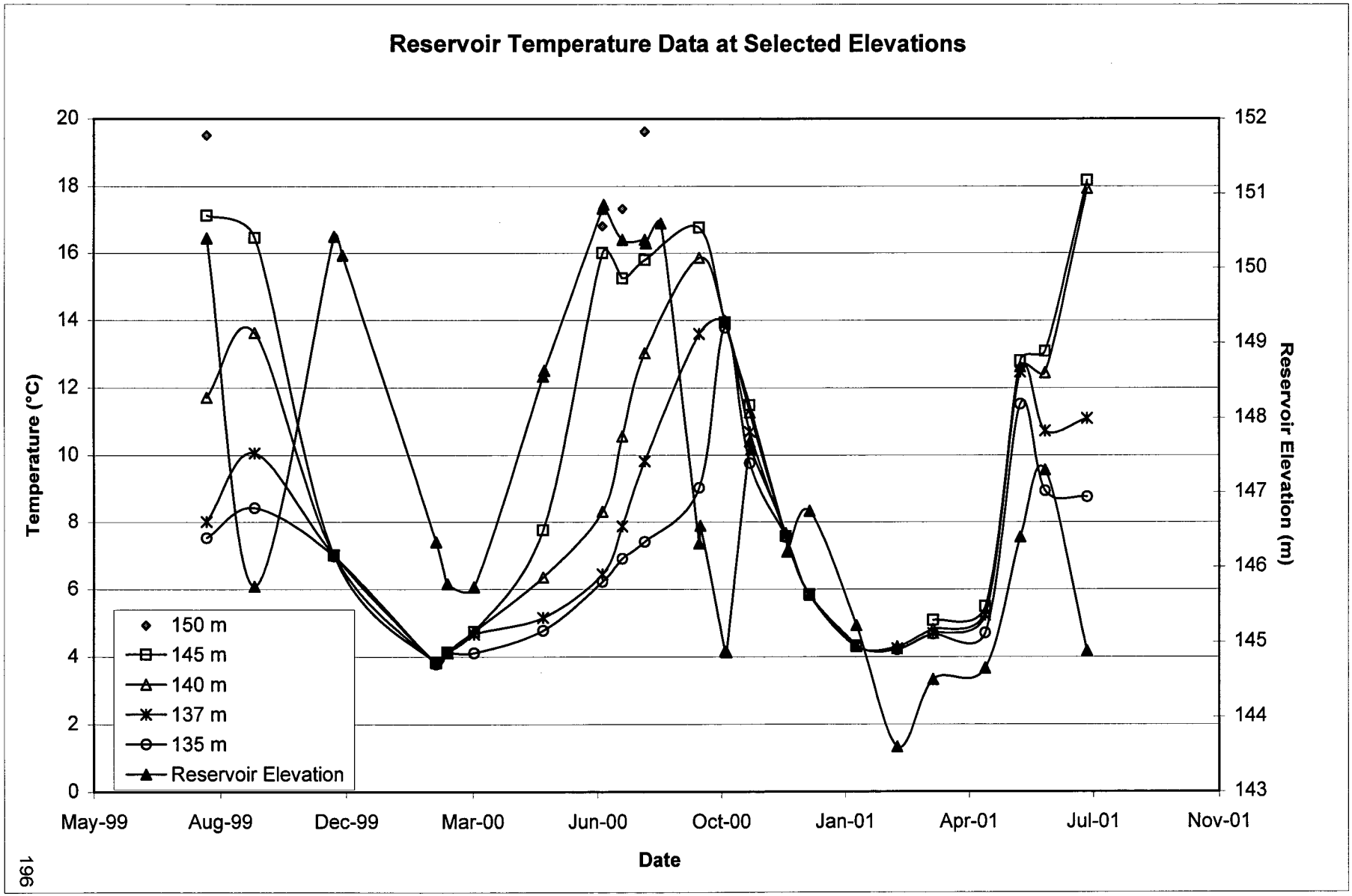
Reservoir Temperature Data at Selected Elevations
Temperature (°C)
Reservoir Elevation (m)
Date
May-99
Aug-99
Dec-99
Mar-00
Jun-00
Oct-00
Jan-01
Apr-01
Jul-01
Nov-01
0
2
4
6
8
10
12
14
16
18
20
143
144
145
146
147
148
149
150
151
152
150 m
145 m
140 m
137 m
135 m
Reservoir Elevation

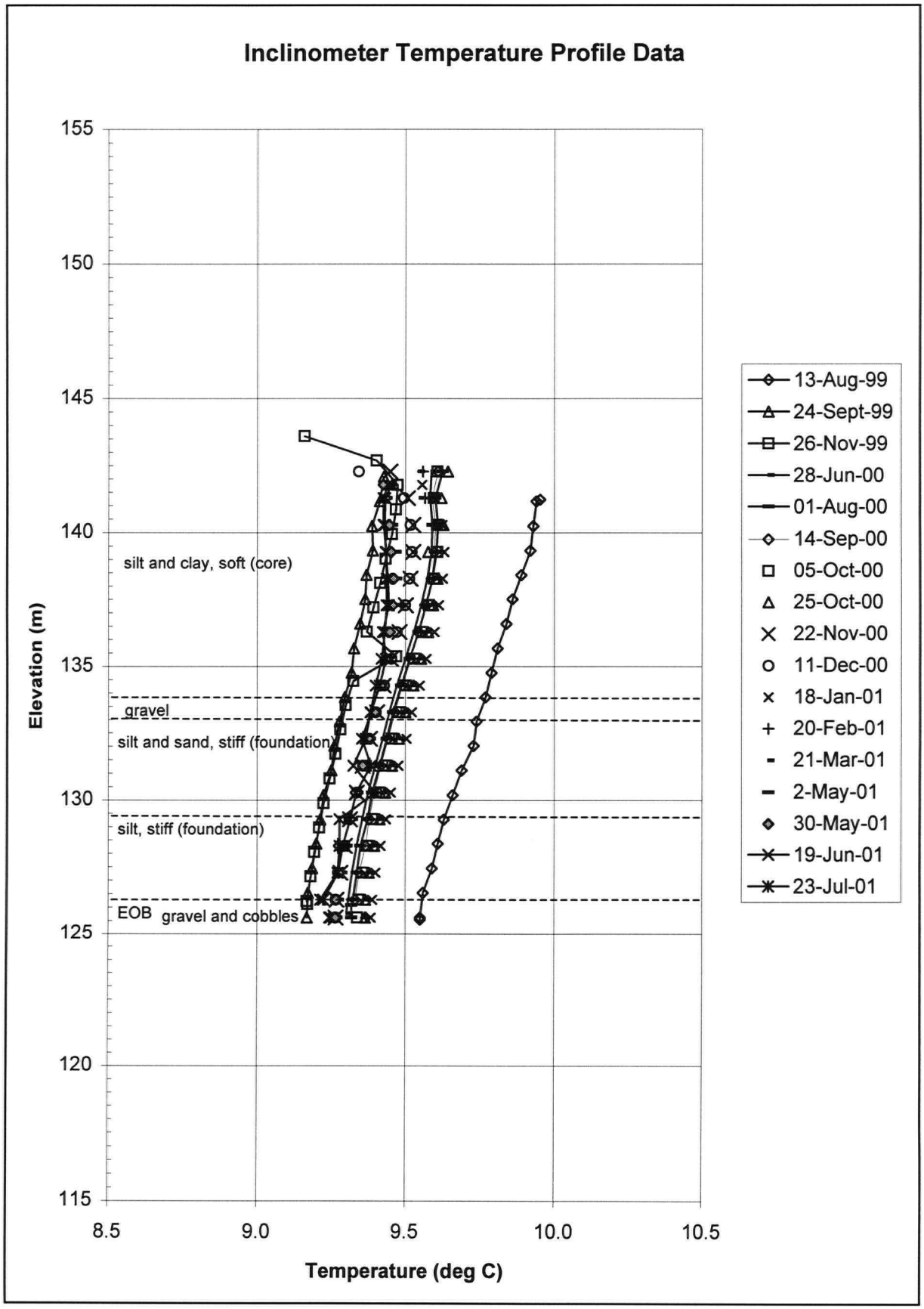
Inclinometer Temperature Profile Data
155
150
145
140
135
130
125
120
115
Elevation (m)
silt and clay, soft (core)
gravel
silt and sand, stiff (foundation)
silt, stiff (foundation)
EOB gravel and cobbles
8.5
9.0
9.5
10.0
10.5
Temperature (deg C)
13-Aug-99
24-Sept-99
26-Nov-99
28-Jun-00
01-Aug-00
14-Sep-00
05-Oct-00
25-Oct-00
22-Nov-00
11-Dec-00
18-Jan-01
20-Feb-01
21-Mar-01
2-May-01
30-May-01
19-Jun-01
23-Jul-01

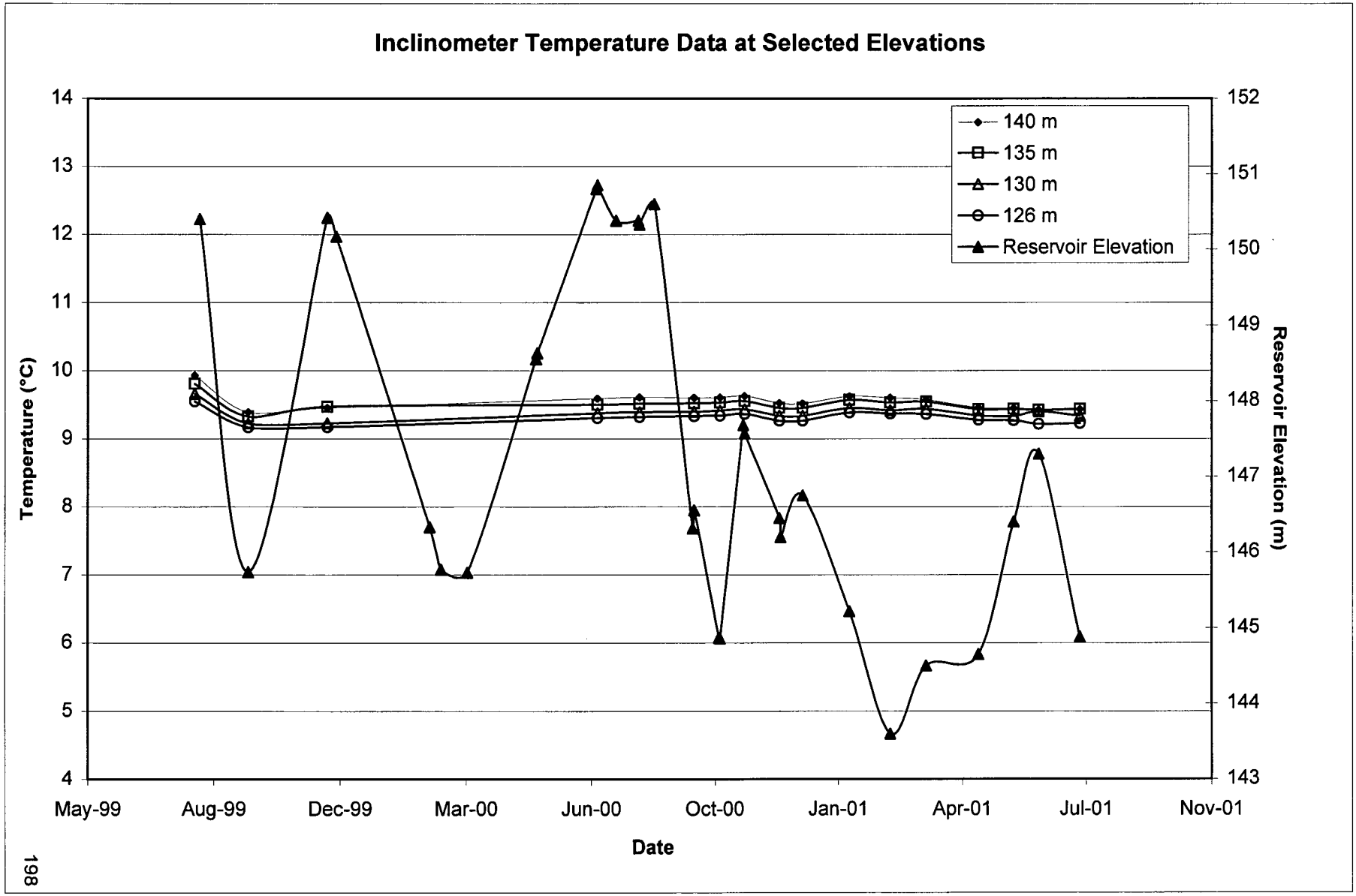
Inclinometer Temperature Data at Selected Elevations
Temperature (°C)
Reservoir Elevation (m)
Date
140 m
135 m
130 m
126 m
Reservoir Elevation
14
13
12
11
10
9
8
7
6
5
4
152
151
150
149
148
147
146
145
144
143
May-99
Aug-99
Dec-99
Mar-00
Jun-00
Oct-00
Jan-01
Apr-01
Jul-01
Nov-01

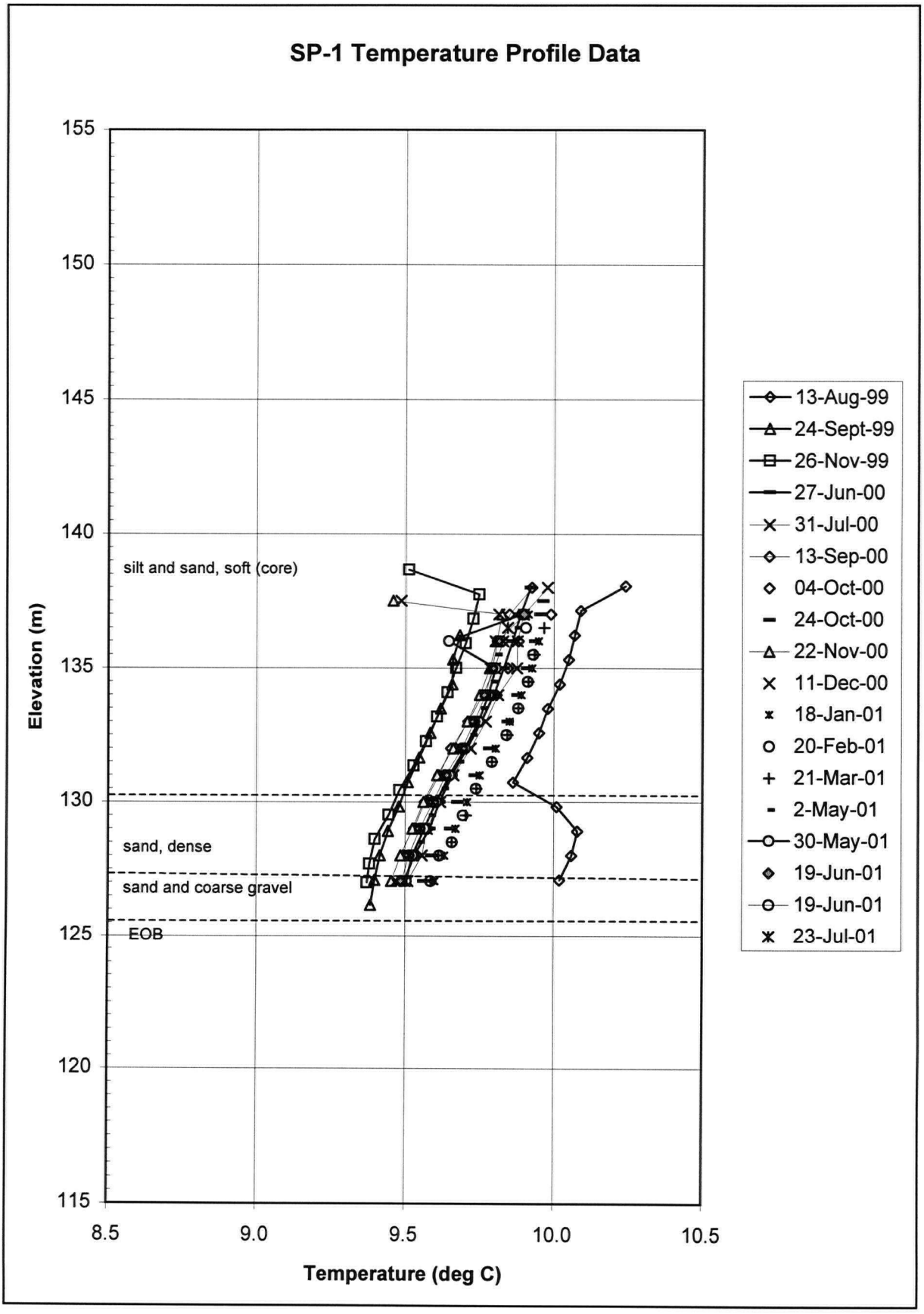
SP-1 Temperature Profile Data
155
150
145
140
135
130
125
120
115
Elevation (m)
silt and sand, soft (core)
sand, dense
sand and coarse gravel
EOB
8.5
9.0
9.5
10.0
10.5
Temperature (deg C)
13-Aug-99
24-Sept-99
26-Nov-99
27-Jun-00
31-Jul-00
13-Sep-00
04-Oct-00
24-Oct-00
22-Nov-00
11-Dec-00
18-Jan-01
20-Feb-01
21-Mar-01
2-May-01
30-May-01
19-Jun-01
19-Jun-01
23-Jul-01

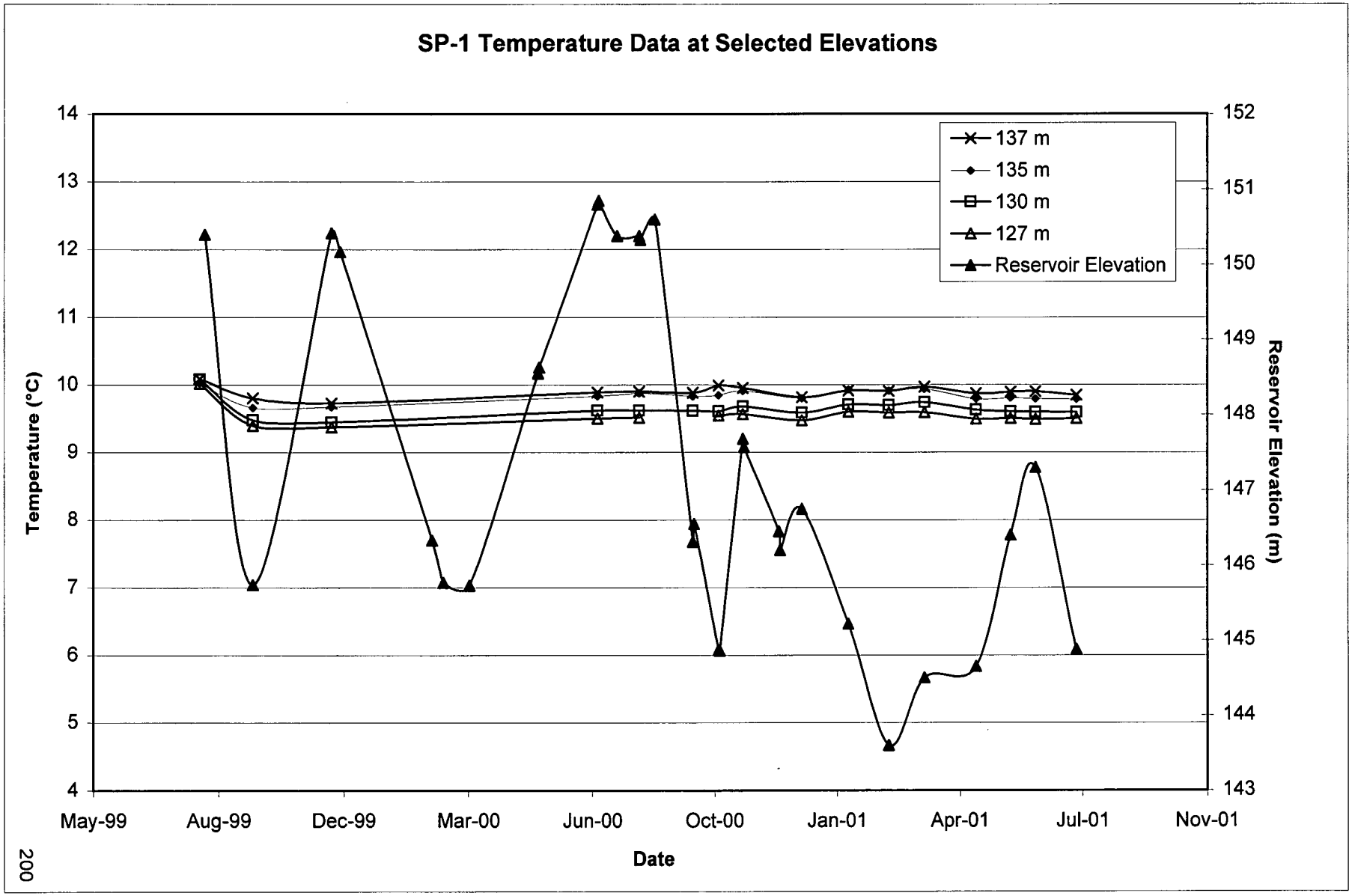
SP-1 Temperature Data at Selected Elevations
Temperature (°C)
Reservoir Elevation (m)
Date
137 m
135 m
130 m
127 m
Reservoir Elevation
14
13
12
11
10
9
8
7
6
5
4
152
151
150
149
148
147
146
145
144
143
May-99
Aug-99
Dec-99
Mar-00
Jun-00
Oct-00
Jan-01
Apr-01
Jul-01
Nov-01

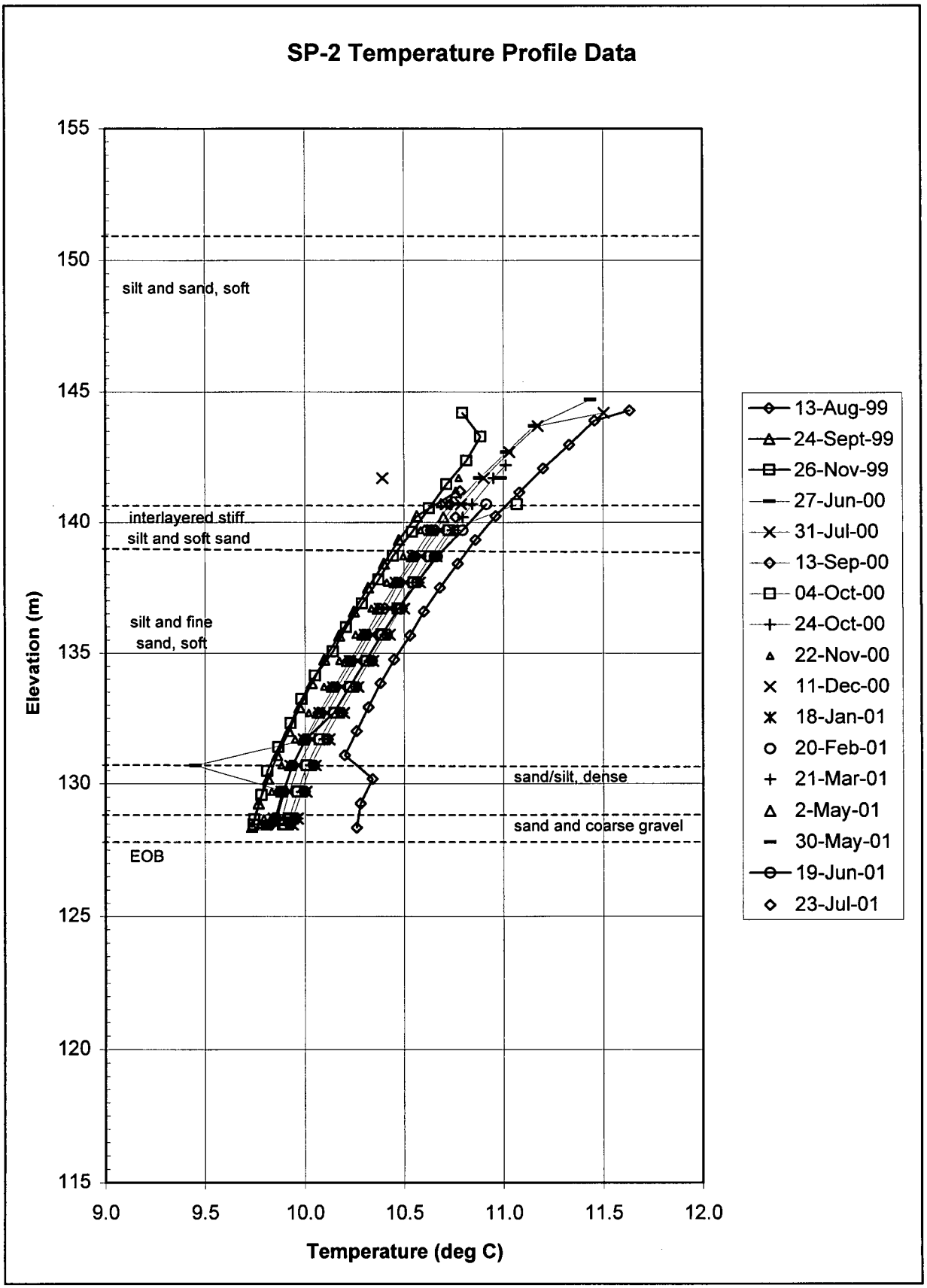
SP-2 Temperature Profile Data
155
150
145
140
135
130
125
120
115
Elevation (m)
silt and sand, soft
interlayered stiff
silt and soft sand
silt and fine
sand, soft
sand/silt, dense
sand and coarse gravel
EOB
9.0
9.5
10.0
10.5
11.0
11.5
12.0
Temperature (deg C)
13-Aug-99
24-Sept-99
26-Nov-99
27-Jun-00
31-Jul-00
13-Sep-00
04-Oct-00
24-Oct-00
22-Nov-00
11-Dec-00
18-Jan-01
20-Feb-01
21-Mar-01
2-May-01
30-May-01
19-Jun-01
23-Jul-01

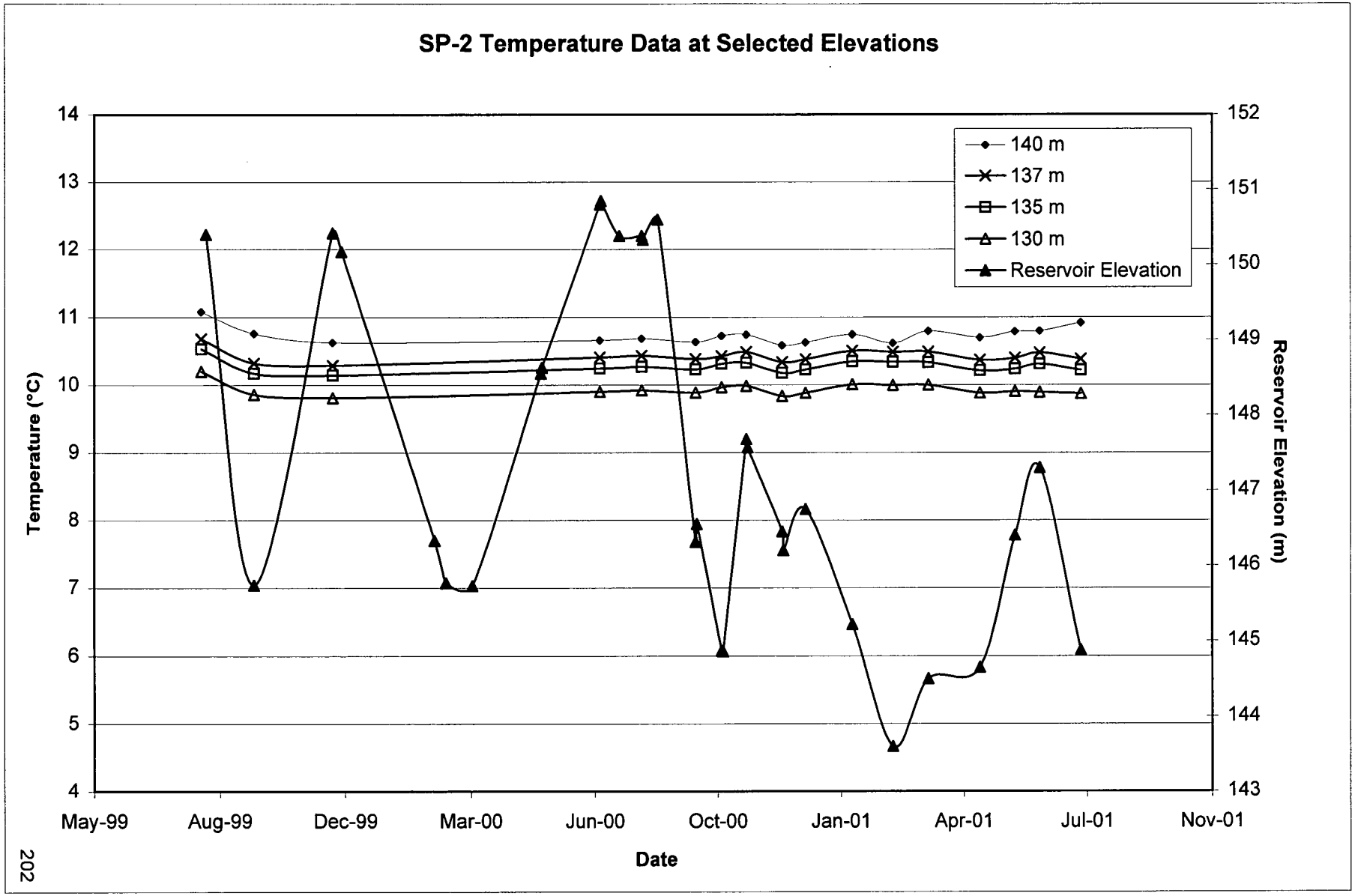
SP-2 Temperature Data at Selected Elevations
140 m
137 m
135 m
130 m
Reservoir Elevation
Temperature (°C)
Reservoir Elevation (m)
Date
14
13
12
11
10
9
8
7
6
5
4
152
151
150
149
148
147
146
145
144
143
May-99
Aug-99
Dec-99
Mar-00
Jun-00
Oct-00
Jan-01
Apr-01
Jul-01
Nov-01

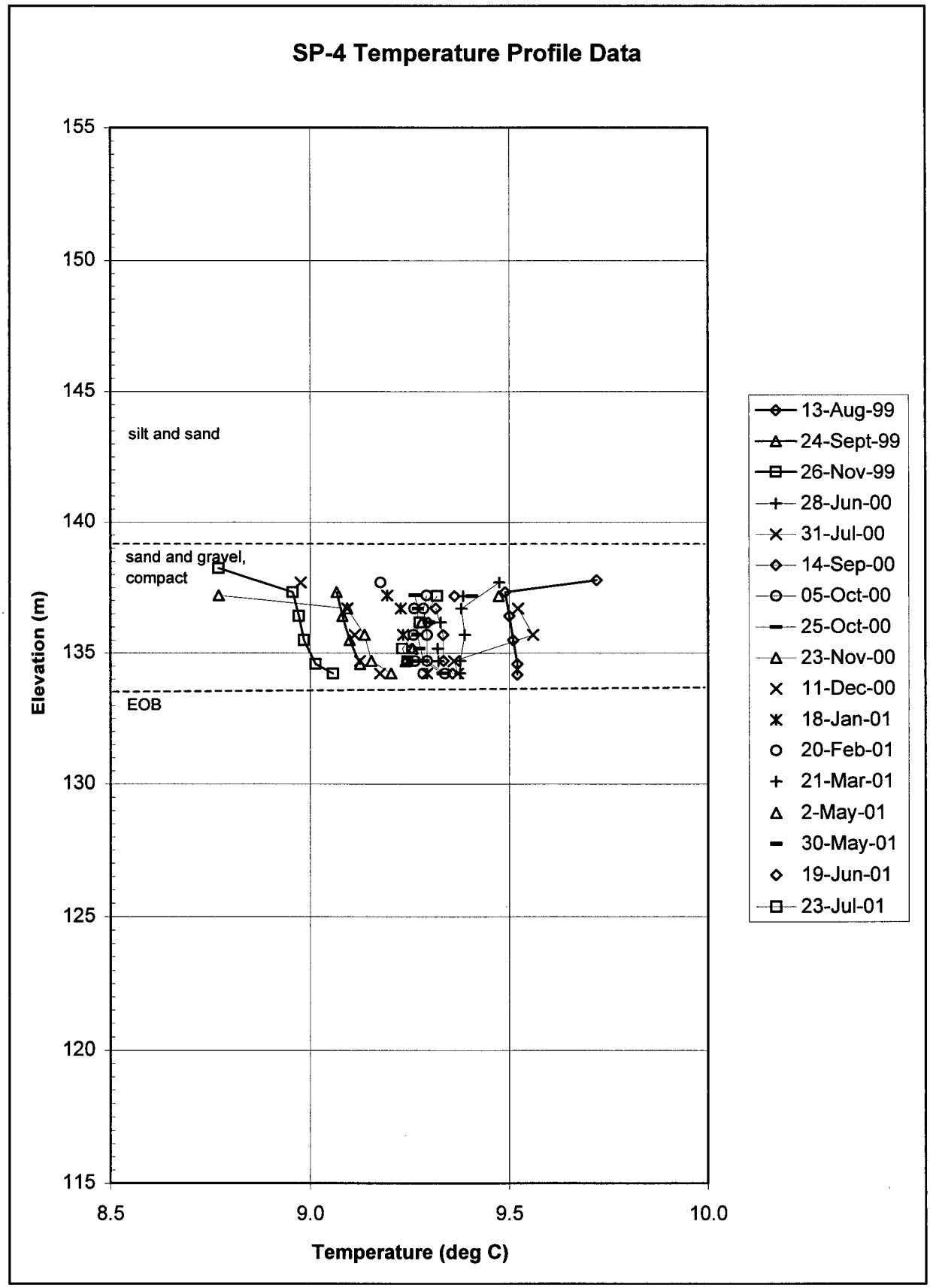
SP-4 Temperature Profile Data
155
150
145
140
135
130
125
120
115
Elevation (m)
silt and sand
sand and gravel, compact
EOB
8.5
9.0
9.5
10.0
Temperature (deg C)
13-Aug-99
24-Sept-99
26-Nov-99
28-Jun-00
31-Jul-00
14-Sep-00
05-Oct-00
25-Oct-00
23-Nov-00
11-Dec-00
18-Jan-01
20-Feb-01
21-Mar-01
2-May-01
30-May-01
19-Jun-01
23-Jul-01

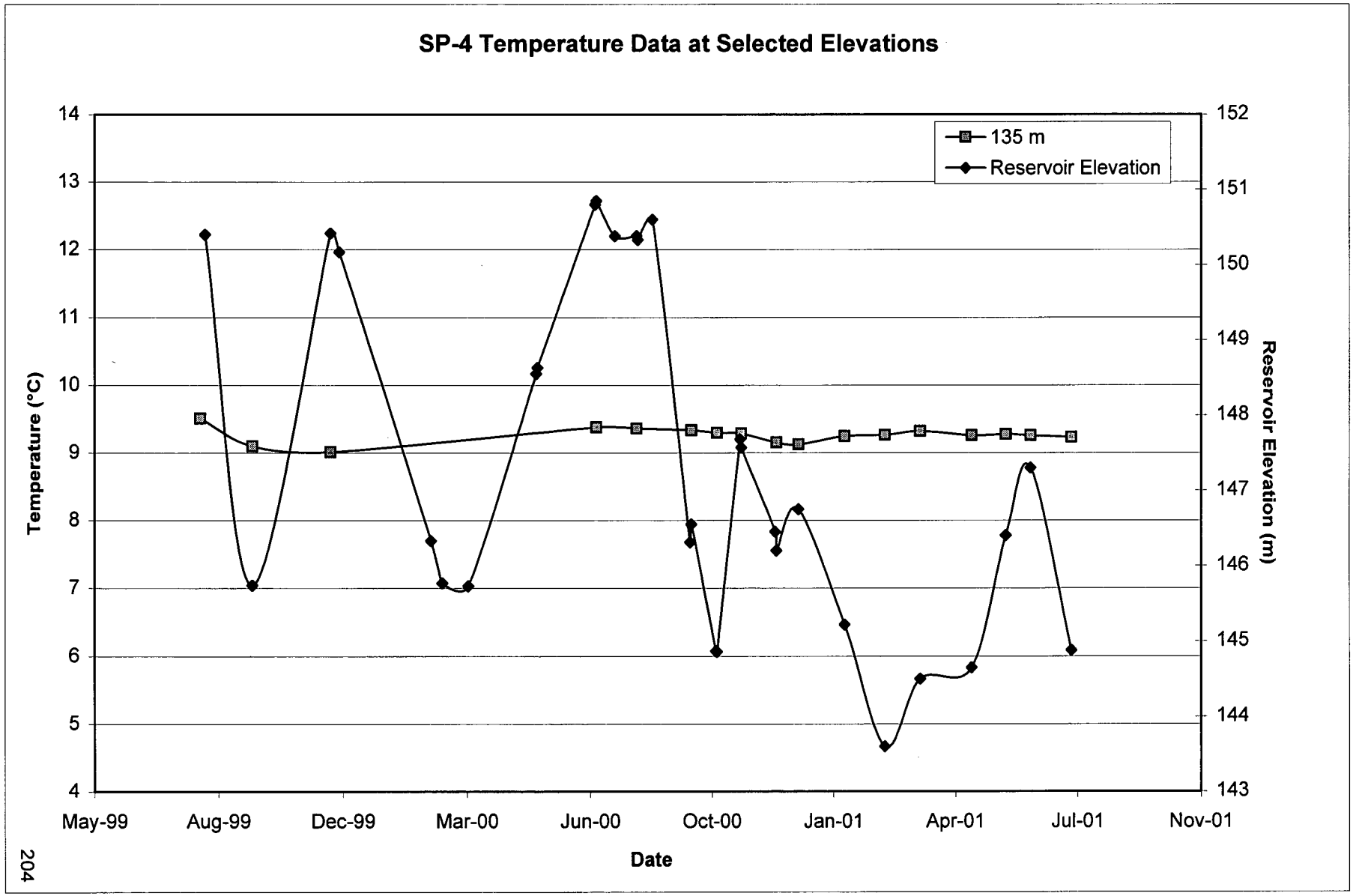
SP-4 Temperature Data at Selected Elevations
135 m
Reservoir Elevation
Temperature (°C)
Reservoir Elevation (m)
Date
14
13
12
11
10
9
8
7
6
5
4
152
151
150
149
148
147
146
145
144
143
May-99
Aug-99
Dec-99
Mar-00
Jun-00
Oct-00
Jan-01
Apr-01
Jul-01
Nov-01

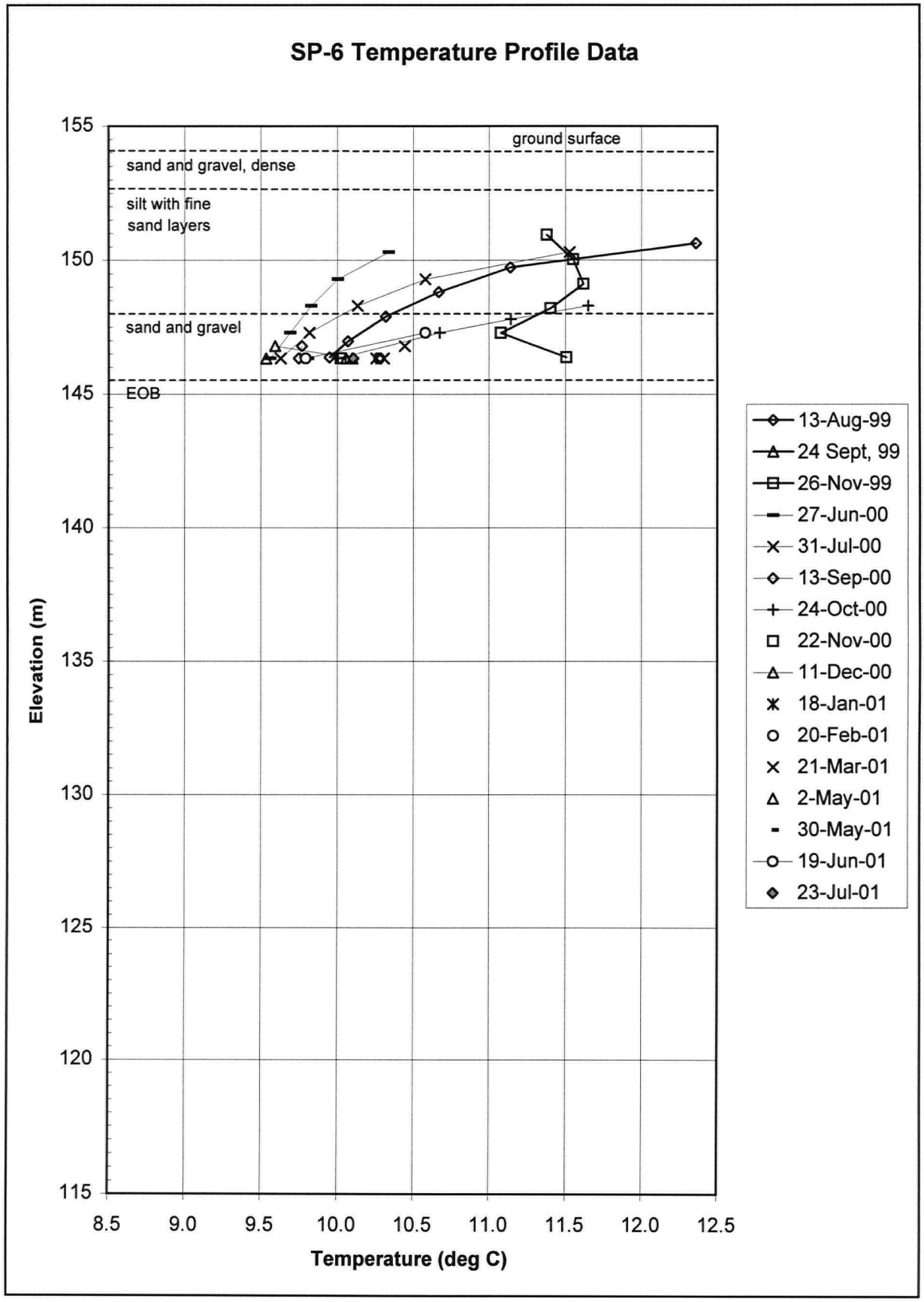
SP-6 Temperature Profile Data
ground surface
sand and gravel, dense
silt with fine
sand layers
sand and gravel
EOB
155
150
145
140
135
130
125
120
115
Elevation (m)
8.5
9.0
9.5
10.0
10.5
11.0
11.5
12.0
12.5
Temperature (deg C)
13-Aug-99
24 Sept, 99
26-Nov-99
27-Jun-00
31-Jul-00
13-Sep-00
24-Oct-00
22-Nov-00
11-Dec-00
18-Jan-01
20-Feb-01
21-Mar-01
2-May-01
30-May-01
19-Jun-01
23-Jul-01

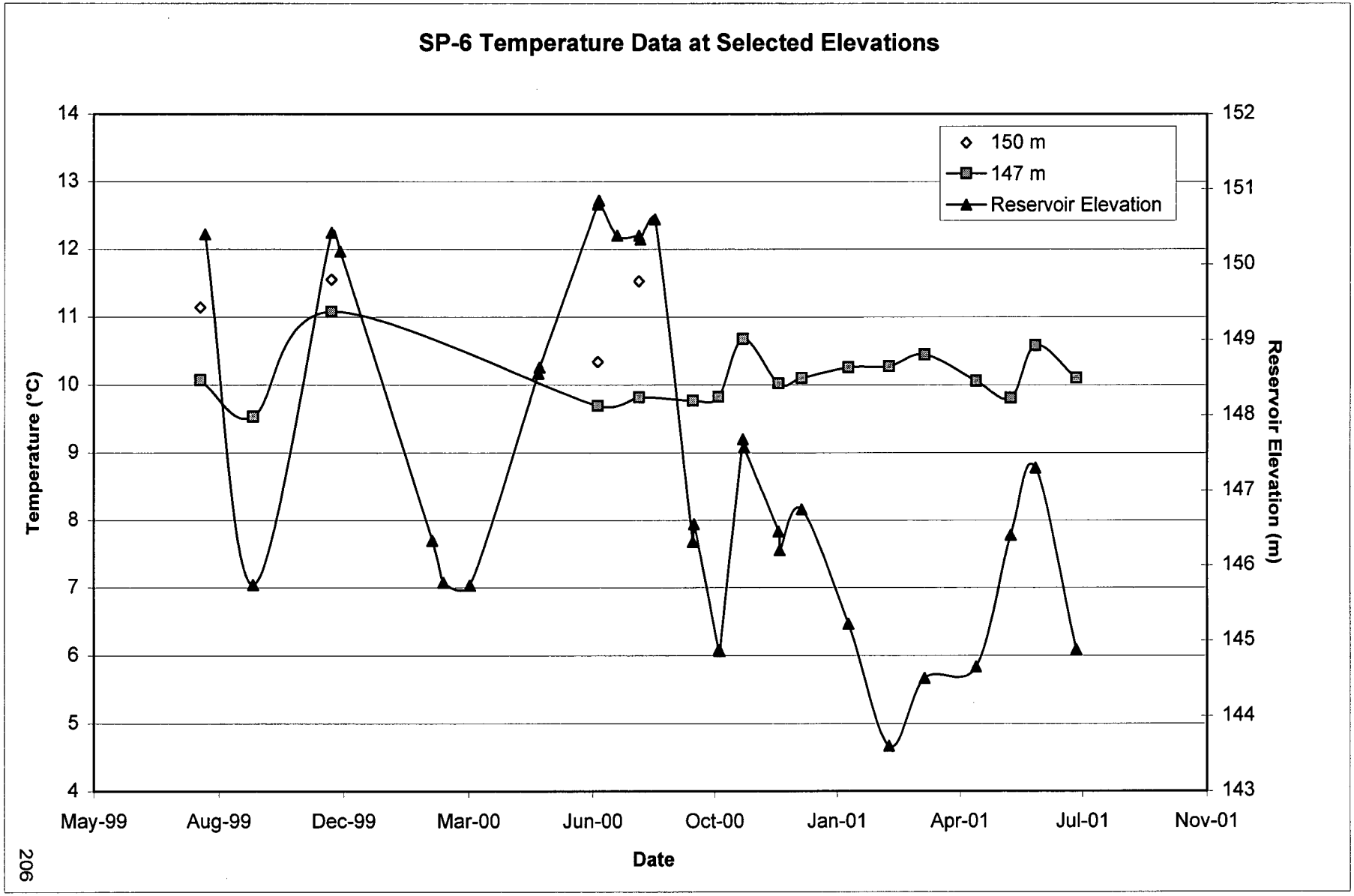
SP-6 Temperature Data at Selected Elevations
150 m
147 m
Reservoir Elevation
Temperature (°C)
Reservoir Elevation (m)
Date
14
13
12
11
10
9
8
7
6
5
4
152
151
150
149
148
147
146
145
144
143
May-99
Aug-99
Dec-99
Mar-00
Jun-00
Oct-00
Jan-01
Apr-01
Jul-01
Nov-01

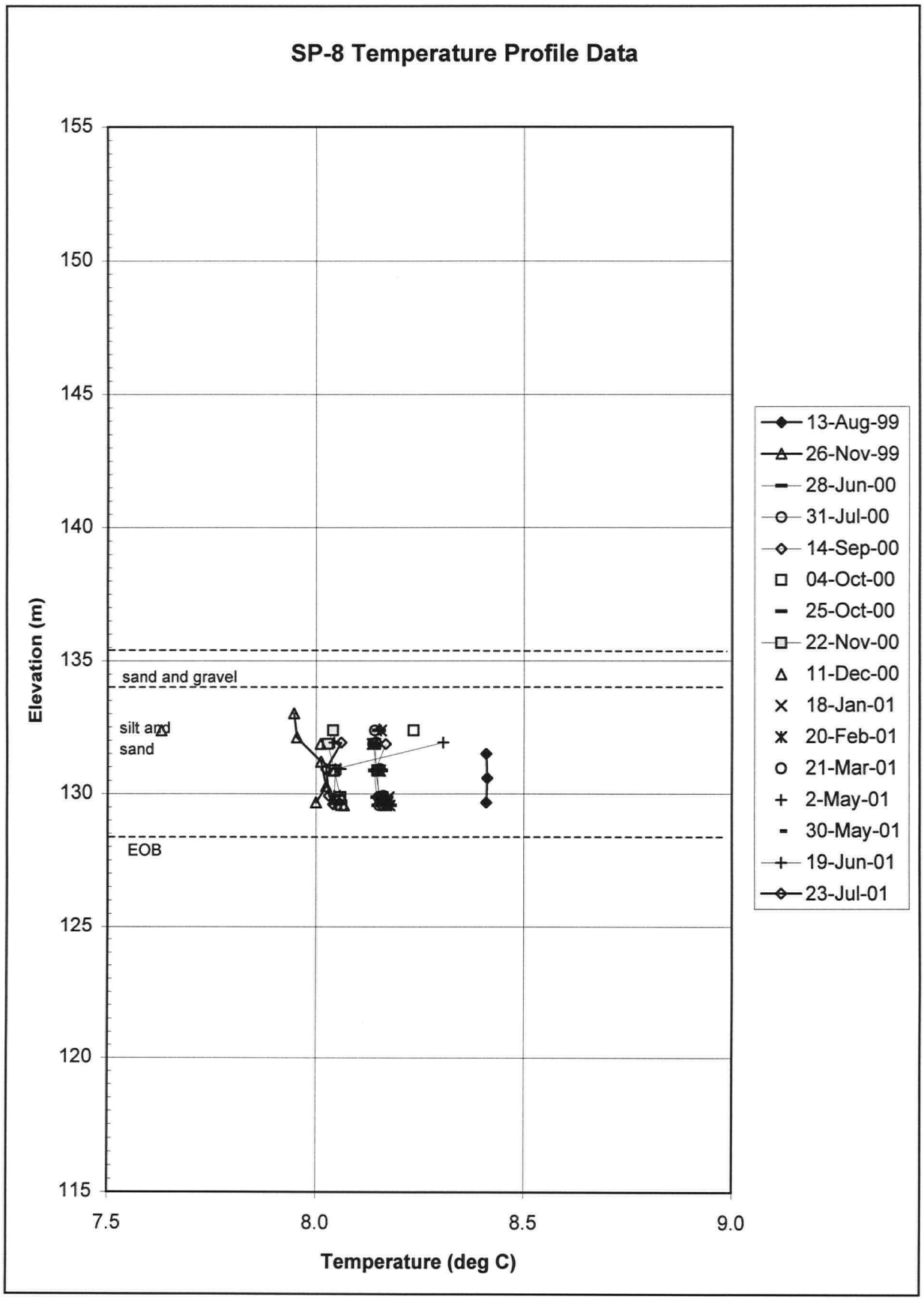
SP-8 Temperature Profile Data
155
150
145
140
135
130
125
120
115
Elevation (m)
sand and gravel
silt and sand
EOB
7.5
8.0
8.5
9.0
Temperature (deg C)
13-Aug-99
26-Nov-99
28-Jun-00
31-Jul-00
14-Sep-00
04-Oct-00
25-Oct-00
22-Nov-00
11-Dec-00
18-Jan-01
20-Feb-01
21-Mar-01
2-May-01
30-May-01
19-Jun-01
23-Jul-01

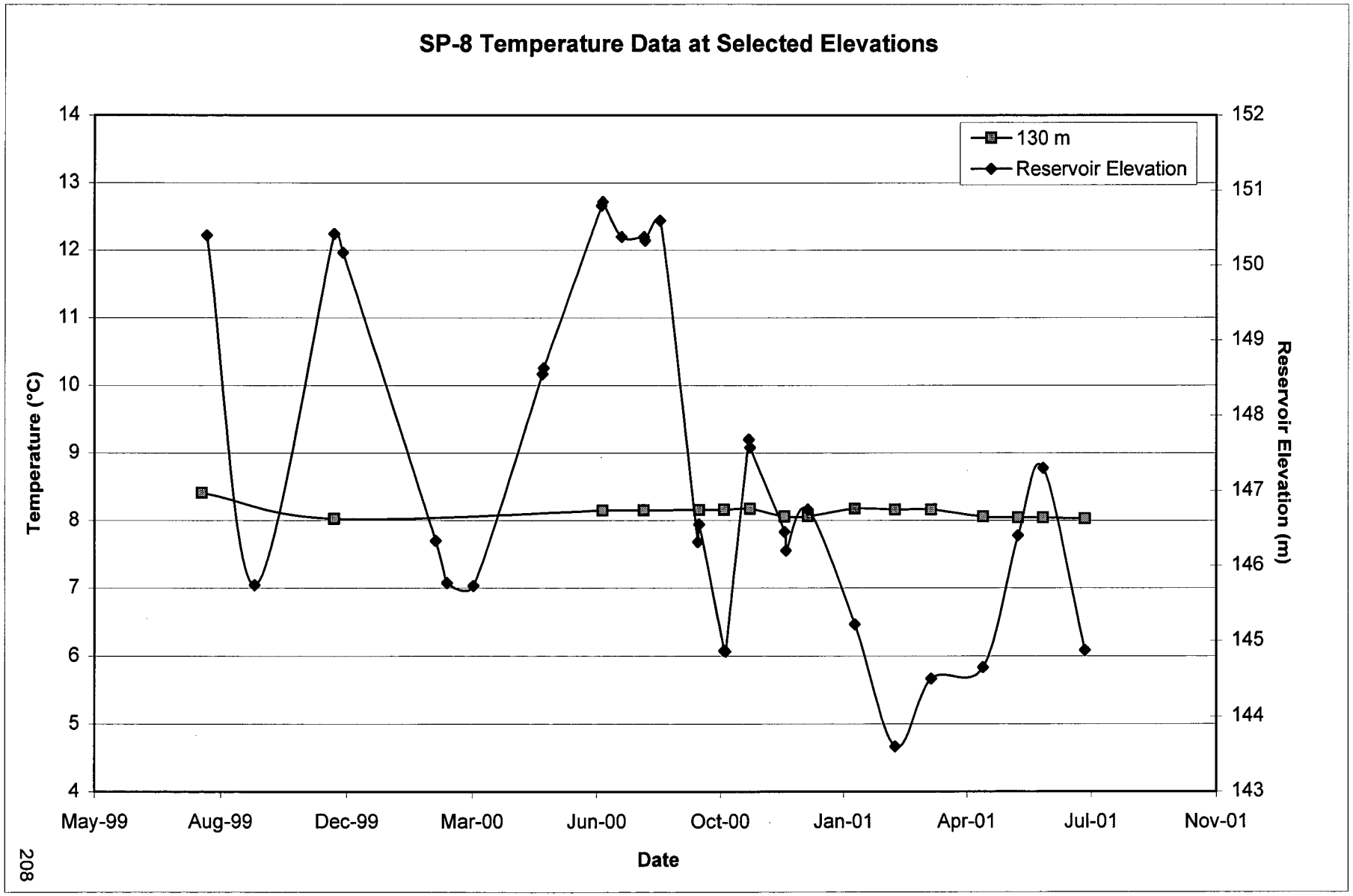
SP-8 Temperature Data at Selected Elevations
130 m
Reservoir Elevation
Temperature (°C)
Reservoir Elevation (m)
Date
14
13
12
11
10
9
8
7
6
5
4
152
151
150
149
148
147
146
145
144
143
May-99
Aug-99
Dec-99
Mar-00
Jun-00
Oct-00
Jan-01
Apr-01
Jul-01
Nov-01

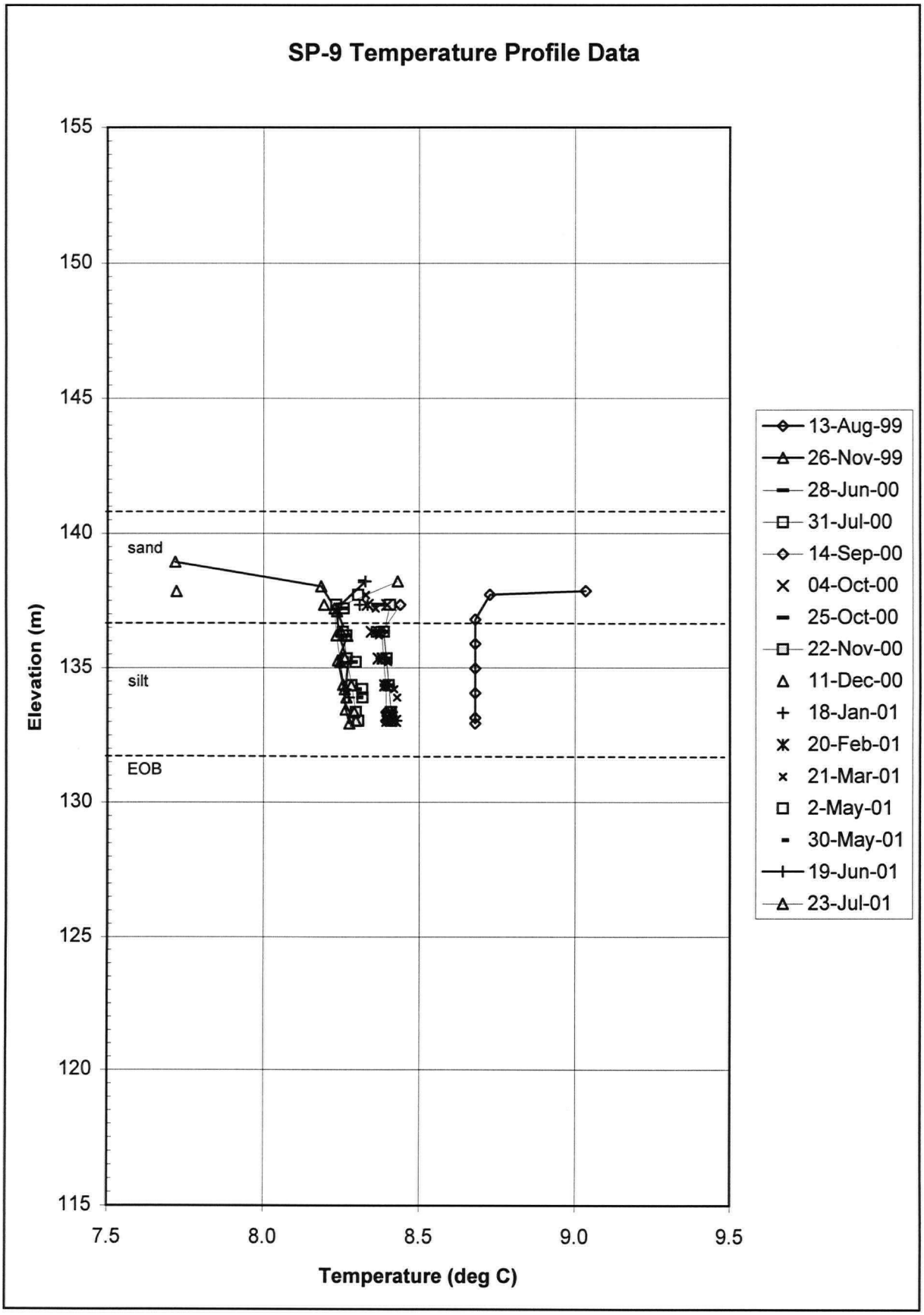
SP-9 Temperature Profile Data
155
150
145
140
135
130
125
120
115
Elevation (m)
sand
silt
EOB
7.5
8.0
8.5
9.0
9.5
Temperature (deg C)
13-Aug-99
26-Nov-99
28-Jun-00
31-Jul-00
14-Sep-00
04-Oct-00
25-Oct-00
22-Nov-00
11-Dec-00
18-Jan-01
20-Feb-01
21-Mar-01
2-May-01
30-May-01
19-Jun-01
23-Jul-01

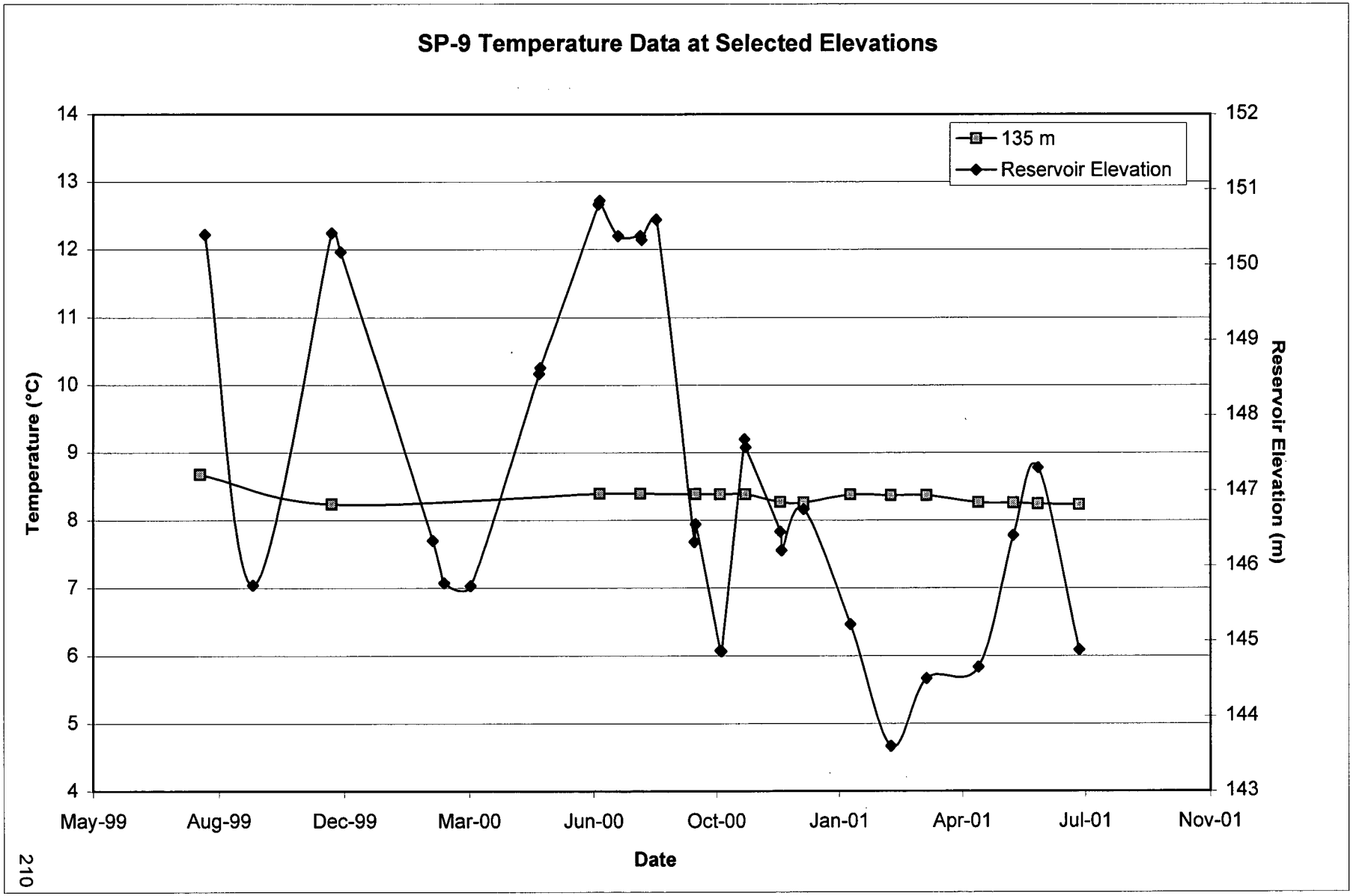
SP-9 Temperature Data at Selected Elevations
135 m
Reservoir Elevation
Temperature (°C)
Reservoir Elevation (m)
Date
14
13
12
11
10
9
8
7
6
5
4
152
151
150
149
148
147
146
145
144
143
May-99
Aug-99
Dec-99
Mar-00
Jun-00
Oct-00
Jan-01
Apr-01
Jul-01
Nov-01

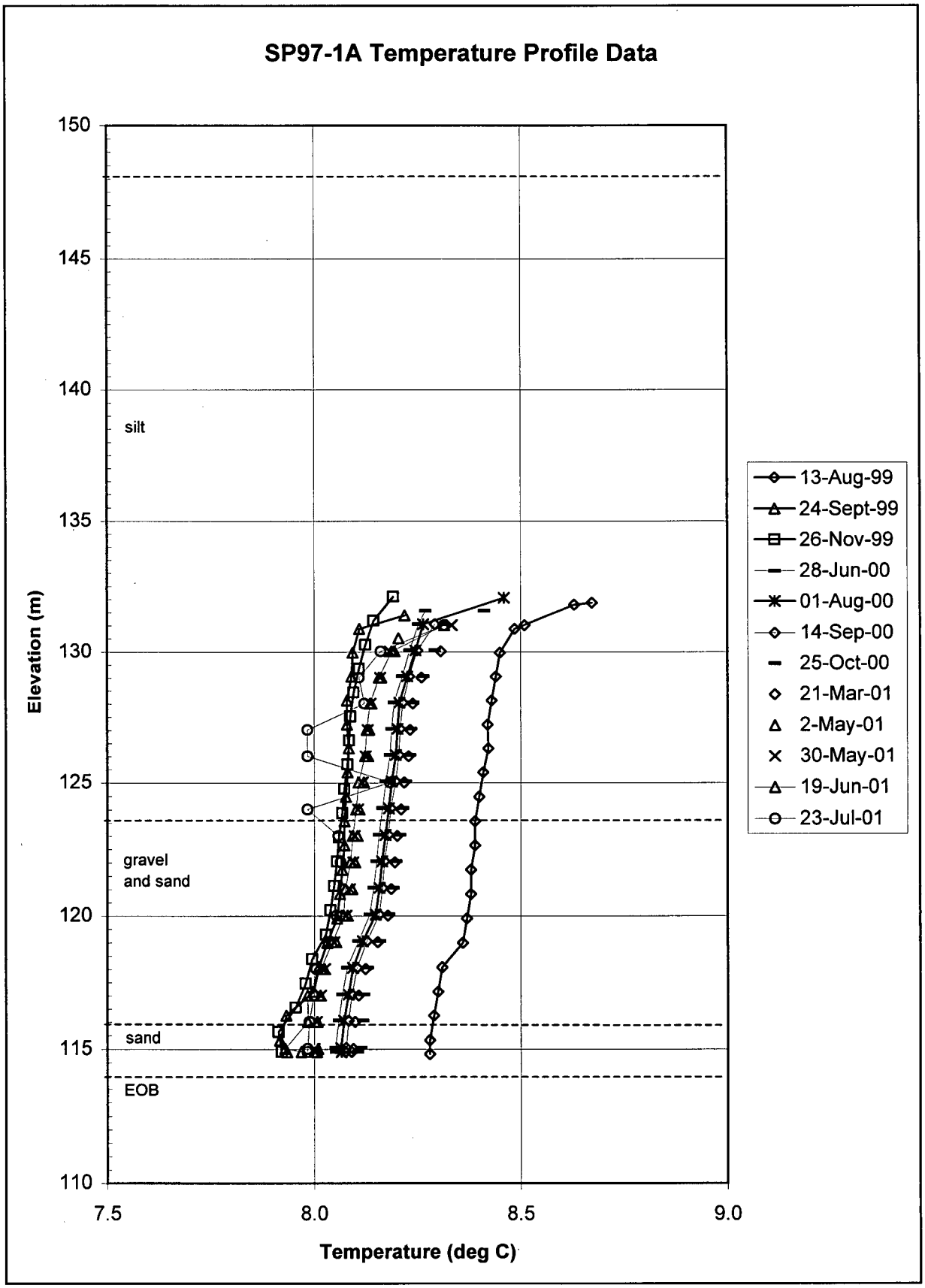
SP97-1A Temperature Profile Data
150
145
140
135
130
125
120
115
110
silt
gravel
and sand
sand
EOB
Elevation (m)
7.5
8.0
8.5
9.0
Temperature (deg C)
13-Aug-99
24-Sept-99
26-Nov-99
28-Jun-00
01-Aug-00
14-Sep-00
25-Oct-00
21-Mar-01
2-May-01
30-May-01
19-Jun-01
23-Jul-01

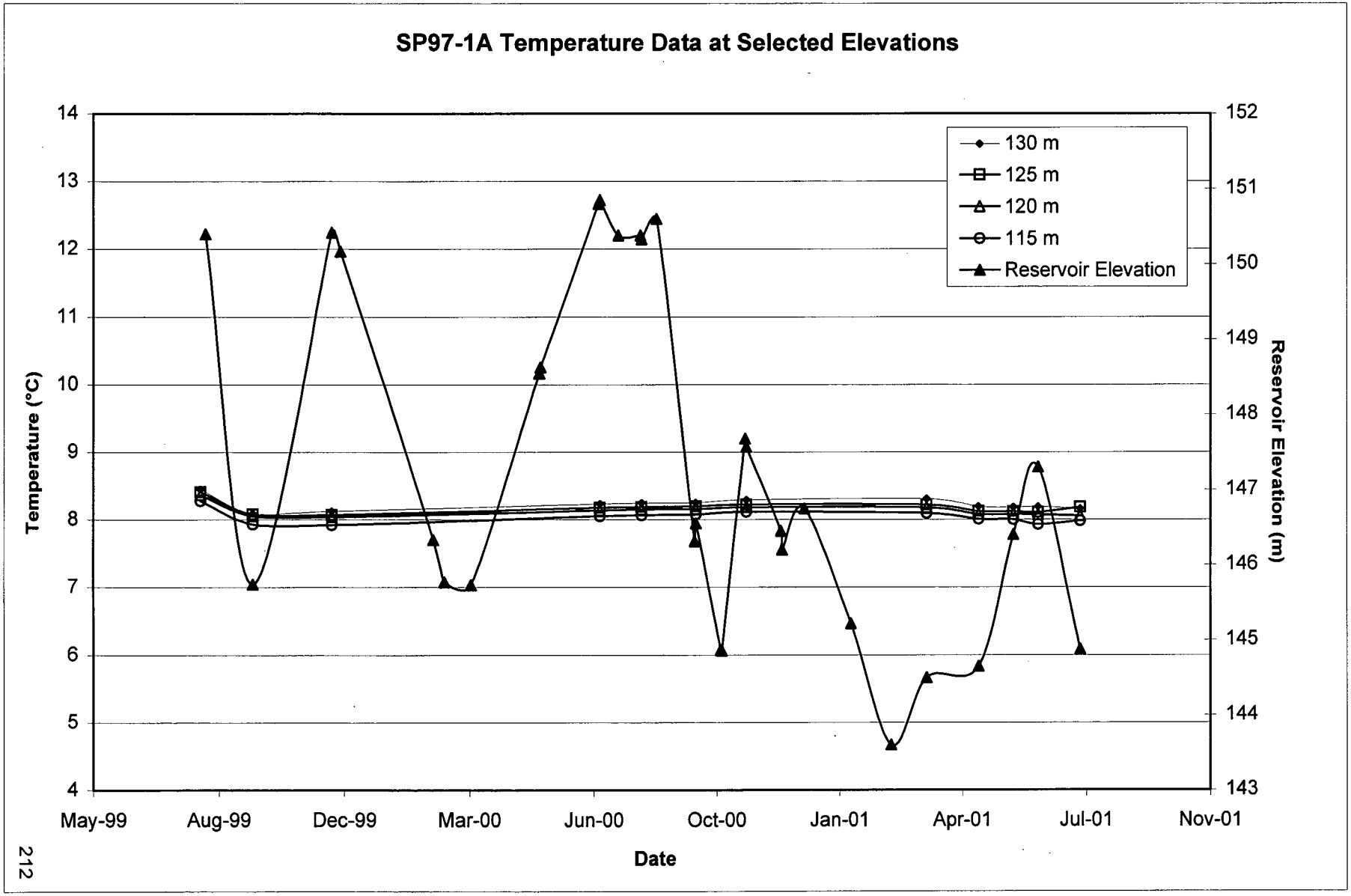
SP97-1A Temperature Data at Selected Elevations
Temperature (°C)
Reservoir Elevation (m)
Date
130 m
125 m
120 m
115 m
Reservoir Elevation
14
13
12
11
10
9
8
7
6
5
4
152
151
150
149
148
147
146
145
144
143
May-99
Aug-99
Dec-99
Mar-00
Jun-00
Oct-00
Jan-01
Apr-01
Jul-01
Nov-01

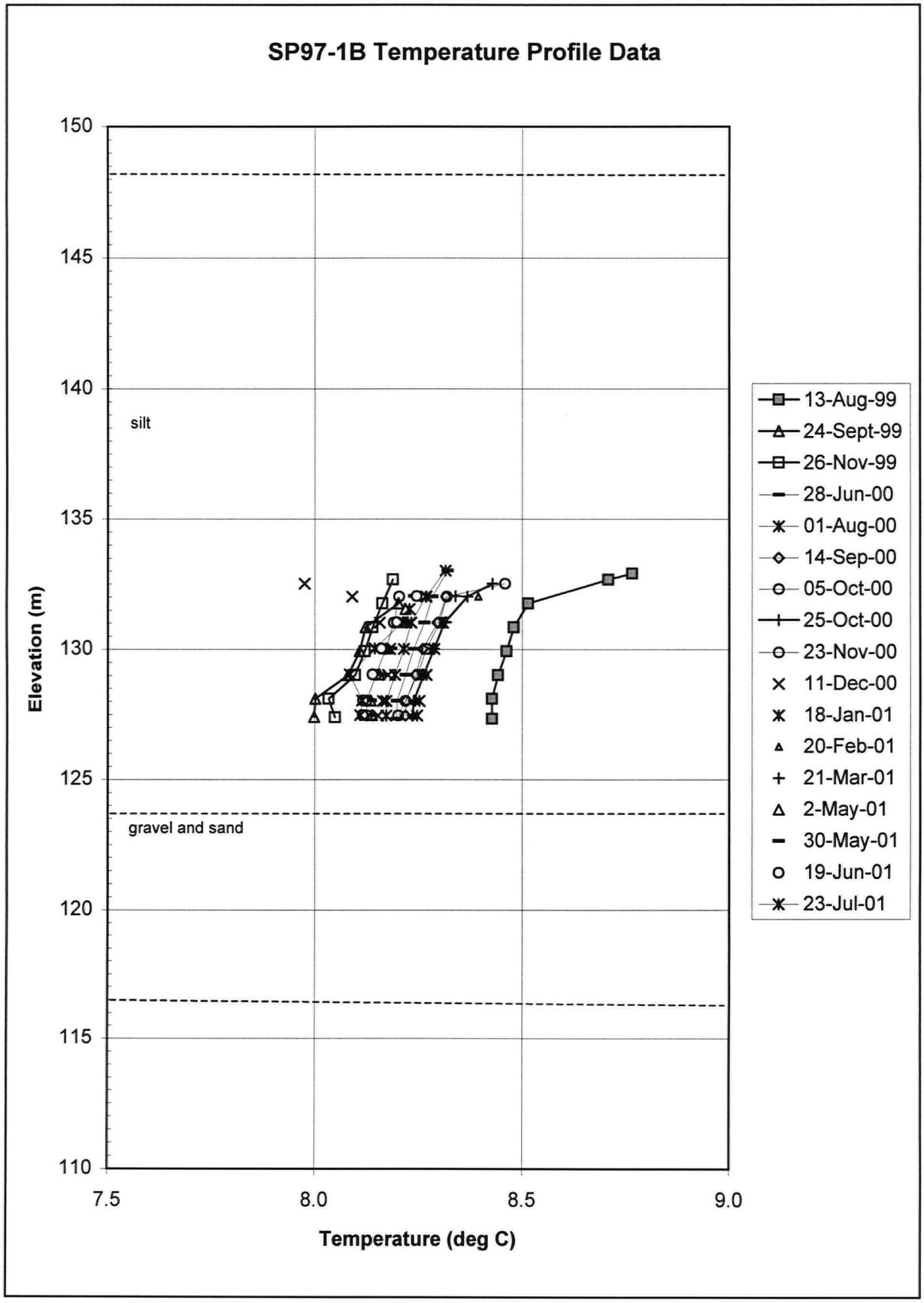
SP97-1B Temperature Profile Data
150
145
140
135
130
125
120
115
110
Elevation (m)
silt
gravel and sand
7.5
8.0
8.5
9.0
Temperature (deg C)
13-Aug-99
24-Sept-99
26-Nov-99
28-Jun-00
01-Aug-00
14-Sep-00
05-Oct-00
25-Oct-00
23-Nov-00
11-Dec-00
18-Jan-01
20-Feb-01
21-Mar-01
2-May-01
30-May-01
19-Jun-01
23-Jul-01

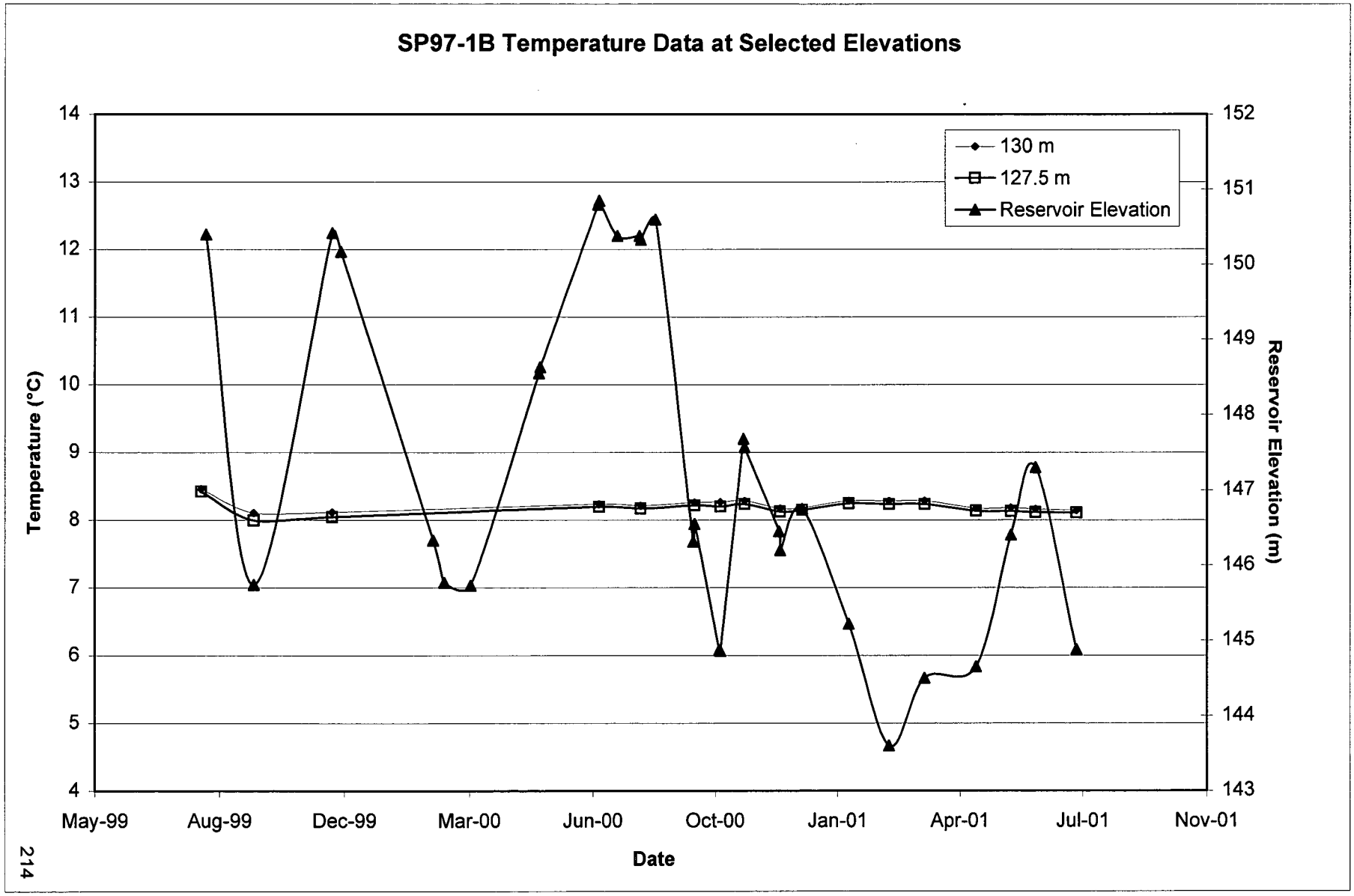
SP97-1B Temperature Data at Selected Elevations
130 m
127.5 m
Reservoir Elevation
Temperature (C°)
Reservoir Elevation (m)
Date
14
13
12
11
10
9
8
7
6
5
4
152
151
150
149
148
147
146
145
144
143
May-99
Aug-99
Dec-99
Mar-00
Jun-00
Oct-00
Jan-01
Apr-01
Jul-01
Nov-01

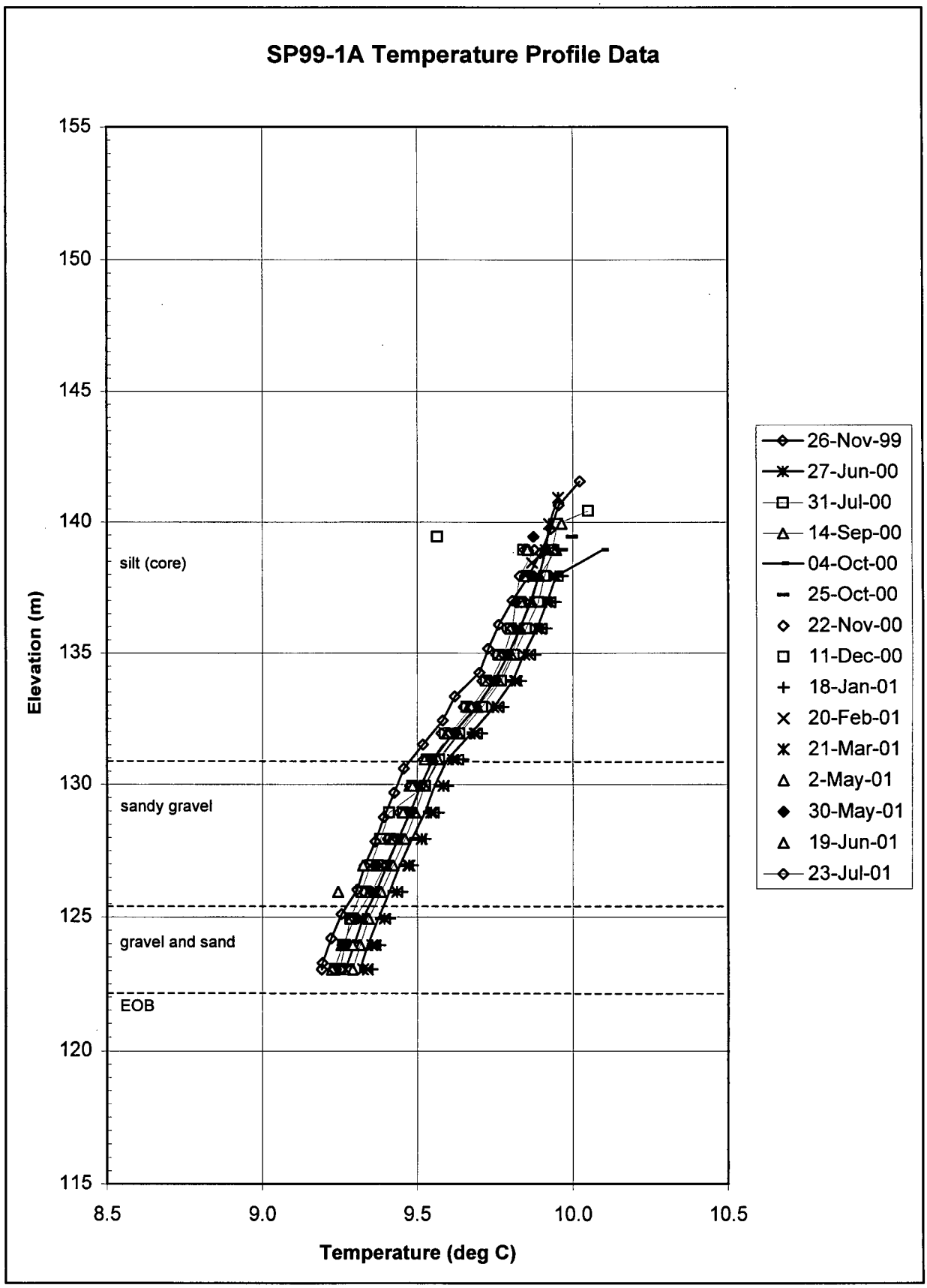
SP99-1A Temperature Profile Data
155
150
145
140
135
130
125
120
115
Elevation (m)
silt (core)
sandy gravel
gravel and sand
EOB
8.5
9.0
9.5
10.0
10.5
Temperature (deg C)
26-Nov-99
27-Jun-00
31-Jul-00
14-Sep-00
04-Oct-00
25-Oct-00
22-Nov-00
11-Dec-00
18-Jan-01
20-Feb-01
21-Mar-01
2-May-01
30-May-01
19-Jun-01
23-Jul-01

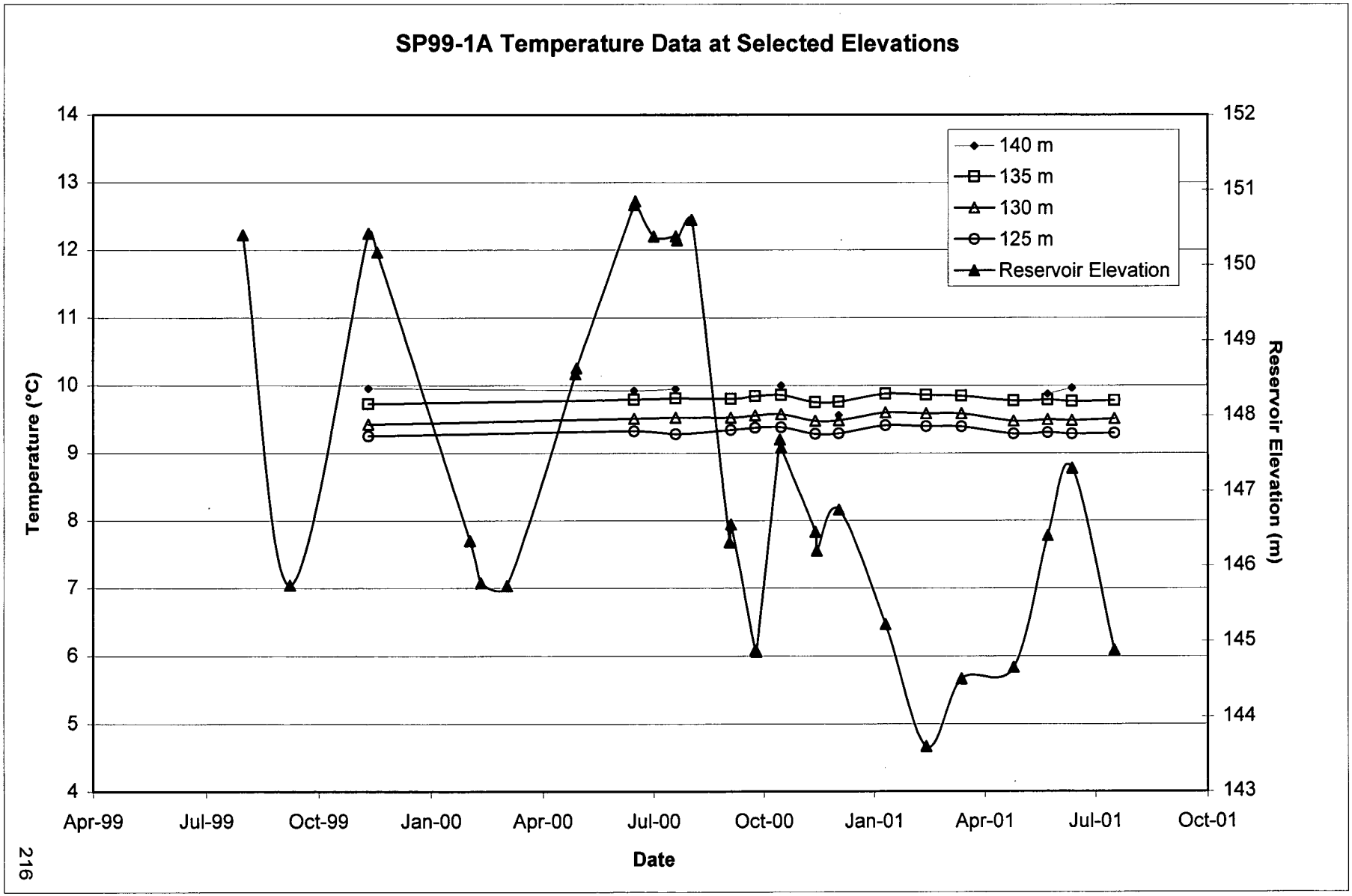
SP99-1A Temperature Data at Selected Elevations
140 m
135 m
130 m
125 m
Reservoir Elevation
Temperature (°C)
Reservoir Elevation (m)
Date
14
13
12
11
10
9
8
7
6
5
4
152
151
150
149
148
147
146
145
144
143
Apr-99
Jul-99
Oct-99
Jan-00
Apr-00
Jul-00
Oct-00
Jan-01
Apr-01
Jul-01
Oct-01

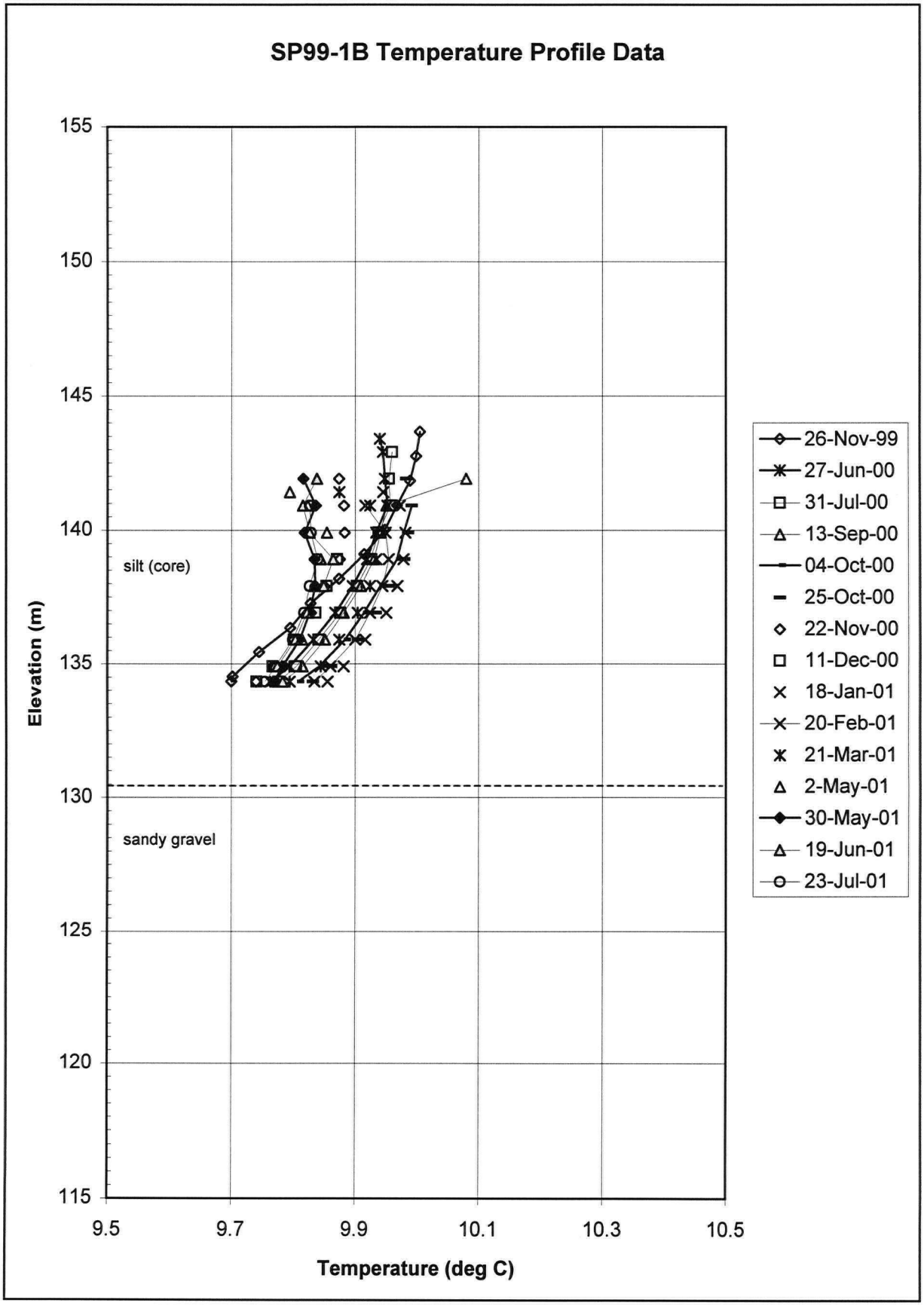
SP99-1B Temperature Profile Data
155
150
145
140
135
130
125
120
115
Elevation (m)
silt (core)
sandy gravel
9.5
9.7
9.9
10.1
10.3
10.5
Temperature (deg C)
26-Nov-99
27-Jun-00
31-Jul-00
13-Sep-00
04-Oct-00
25-Oct-00
22-Nov-00
11-Dec-00
18-Jan-01
20-Feb-01
21-Mar-01
2-May-01
30-May-01
19-Jun-01
23-Jul-01

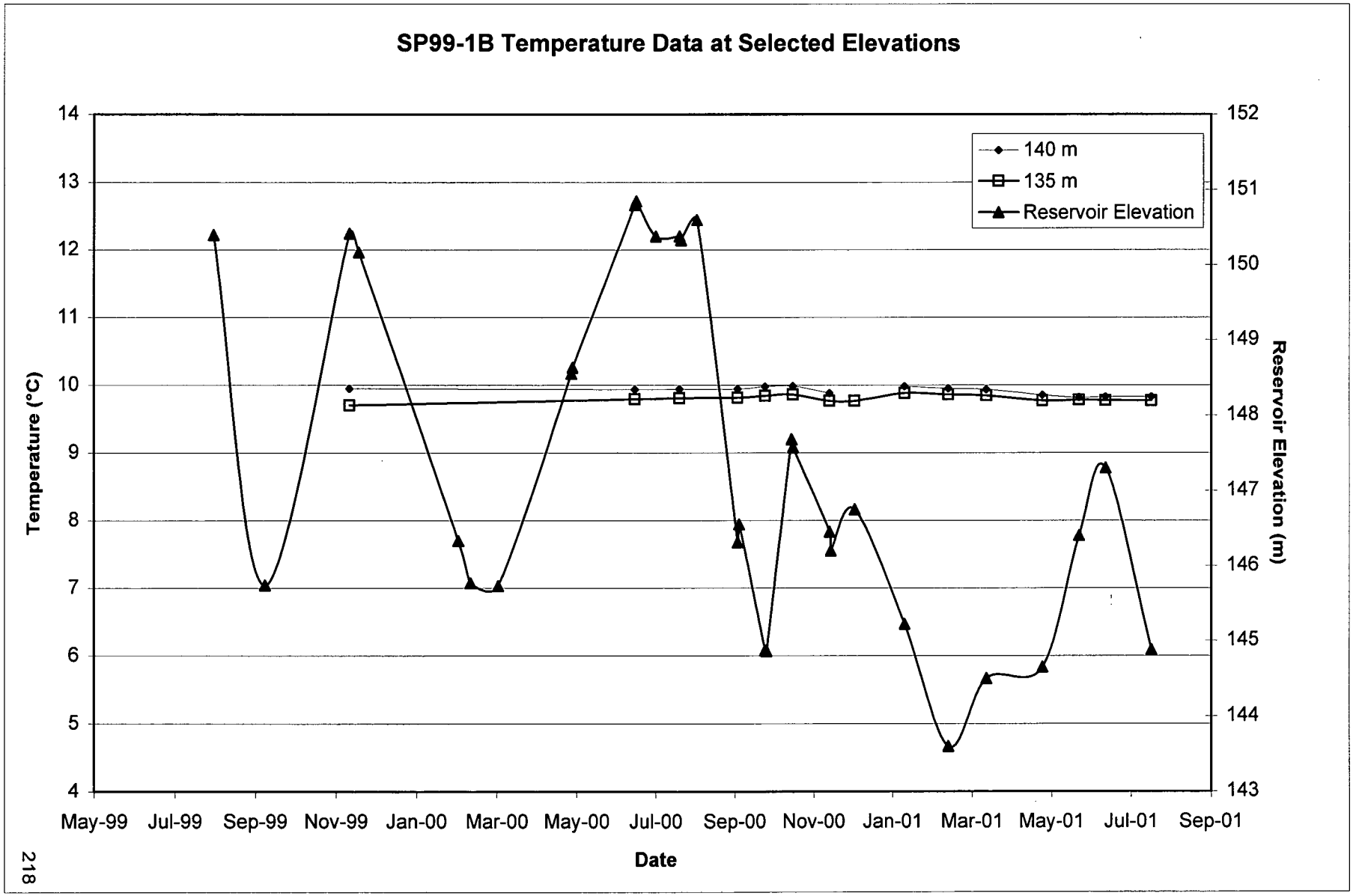
SP99-1B Temperature Data at Selected Elevations
140 m
135 m
Reservoir Elevation
Temperature (°C)
Reservoir Elevation (m)
Date
14
13
12
11
10
9
8
7
6
5
4
152
151
150
149
148
147
146
145
144
143
May-99
Jul-99
Sep-99
Nov-99
Jan-00
Mar-00
May-00
Jul-00
Sep-00
Nov-00
Jan-01
Mar-01
May-01
Jul-01
Sep-01

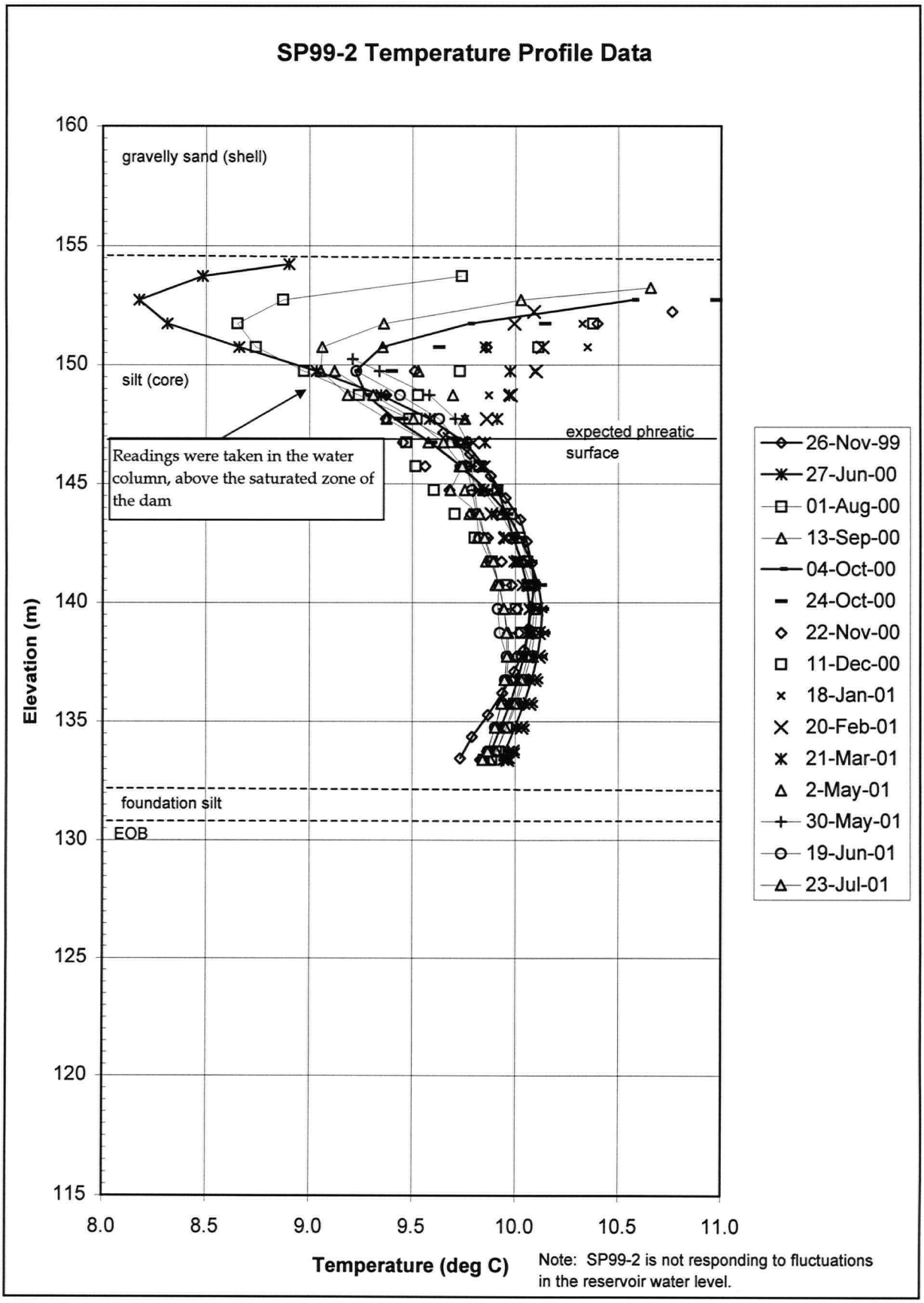
SP99-2 Temperature Profile Data
gravelly sand (shell)
silt (core)
expected phreatic surface
Readings were taken in the water column, above the saturated zone of the dam
foundation silt
EOB
Elevation (m)
160
155
150
145
140
135
130
125
120
115
8.0
8.5
9.0
9.5
10.0
10.5
11.0
Temperature (deg C)
26-Nov-99
27-Jun-00
01-Aug-00
13-Sep-00
04-Oct-00
24-Oct-00
22-Nov-00
11-Dec-00
18-Jan-01
20-Feb-01
21-Mar-01
2-May-01
30-May-01
19-Jun-01
23-Jul-01
Note: SP99-2 is not responding to fluctuations in the reservoir water level.

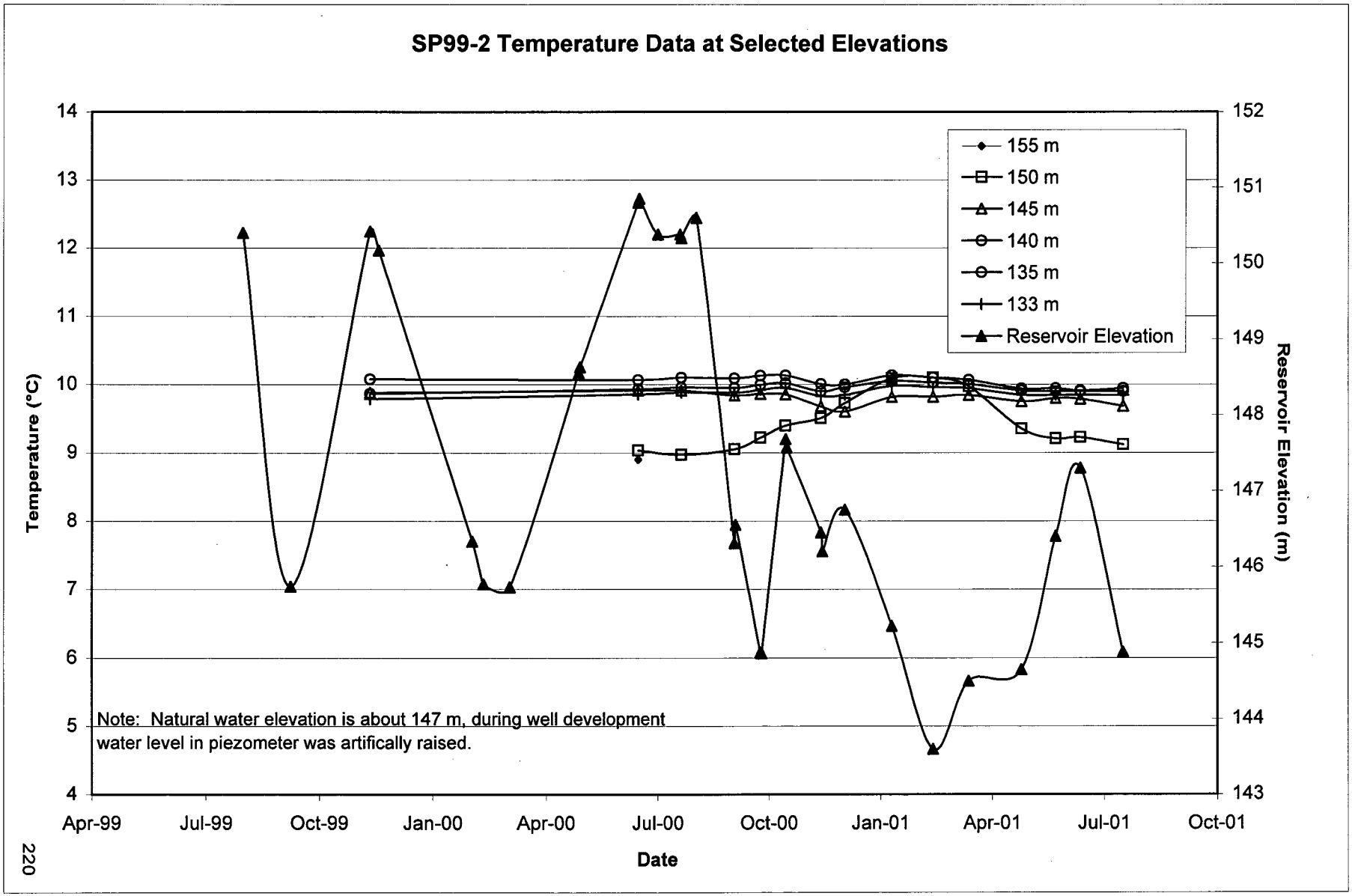
SP99-2 Temperature Data at Selected Elevations
Temperature (°C)
Reservoir Elevation (m)
Date
155 m
150 m
145 m
140 m
135 m
133 m
Reservoir Elevation
Note: Natural water elevation is about 147 m, during well development water level in piezometer was artifically raised.
14
13
12
11
10
9
8
7
6
5
4
152
151
150
149
148
147
146
145
144
143
Apr-99
Jul-99
Oct-99
Jan-00
Apr-00
Jul-00
Oct-00
Jan-01
Apr-01
Jul-01
Oct-01

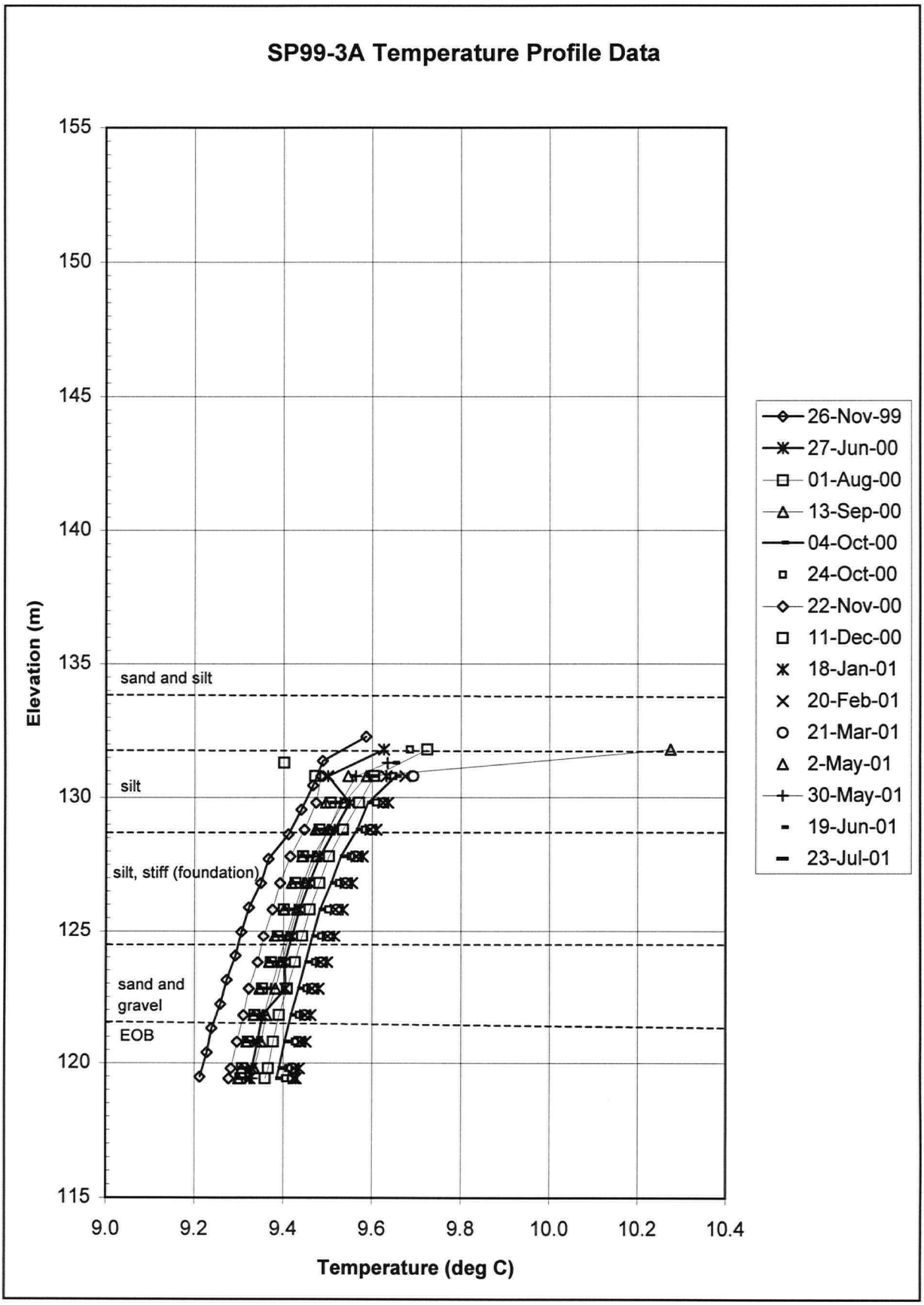
SP99-3A Temperature Profile Data
155
150
145
140
135
130
125
120
115
Elevation (m)
sand and silt
silt
silt, stiff (foundation)
sand and gravel
EOB
9.0
9.2
9.4
9.6
9.8
10.0
10.2
10.4
Temperature (deg C)
26-Nov-99
27-Jun-00
01-Aug-00
13-Sep-00
04-Oct-00
24-Oct-00
22-Nov-00
11-Dec-00
18-Jan-01
20-Feb-01
21-Mar-01
2-May-01
30-May-01
19-Jun-01
23-Jul-01

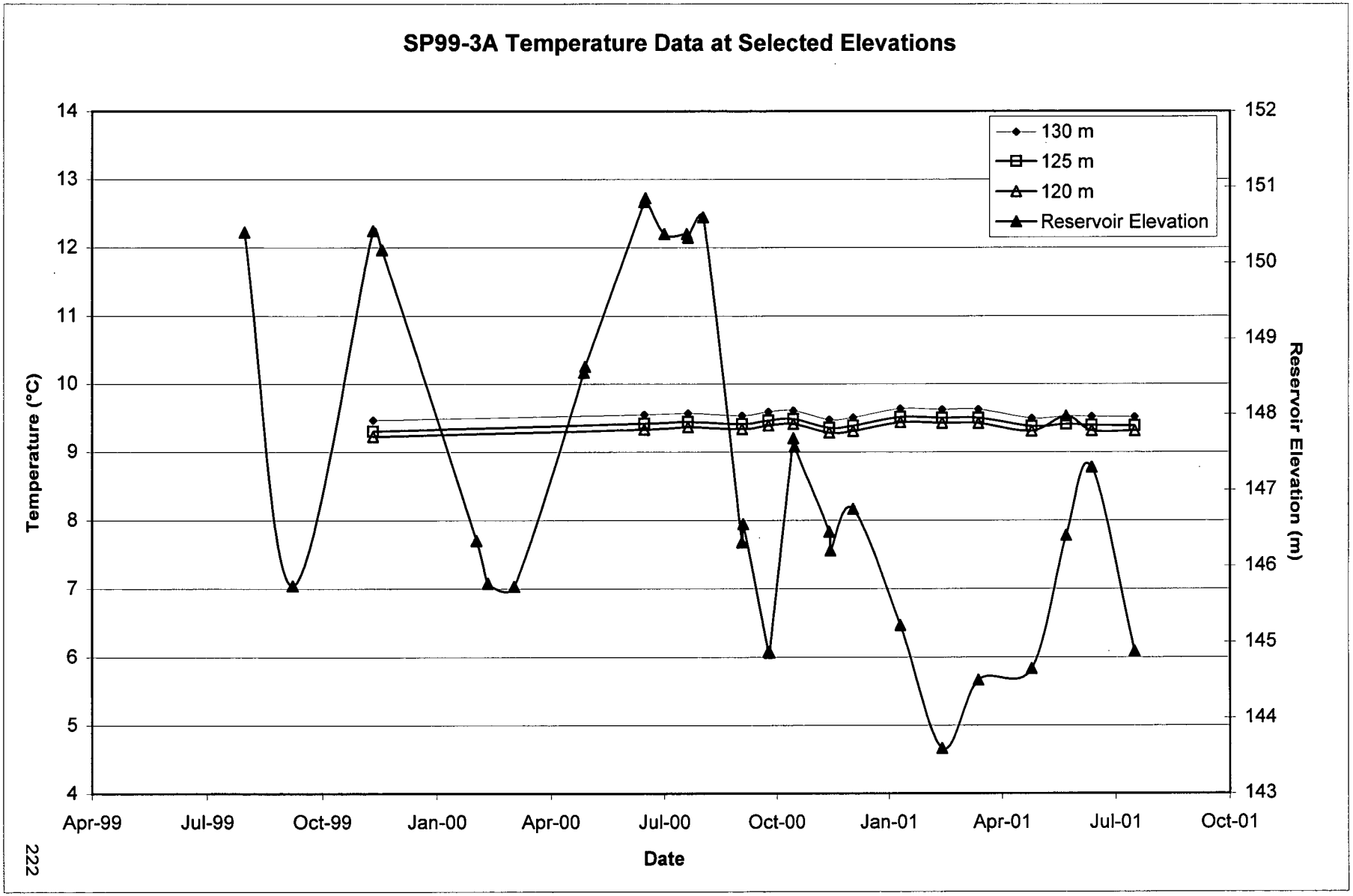
SP99-3A Temperature Data at Selected Elevations
130 m
125 m
120 m
Reservoir Elevation
Temperature (°C)
Reservoir Elevation (m)
Date
14
13
12
11
10
9
8
7
6
5
4
152
151
150
149
148
147
146
145
144
143
Apr-99
Jul-99
Oct-99
Jan-00
Apr-00
Jul-00
Oct-00
Jan-01
Apr-01
Jul-01
Oct-01

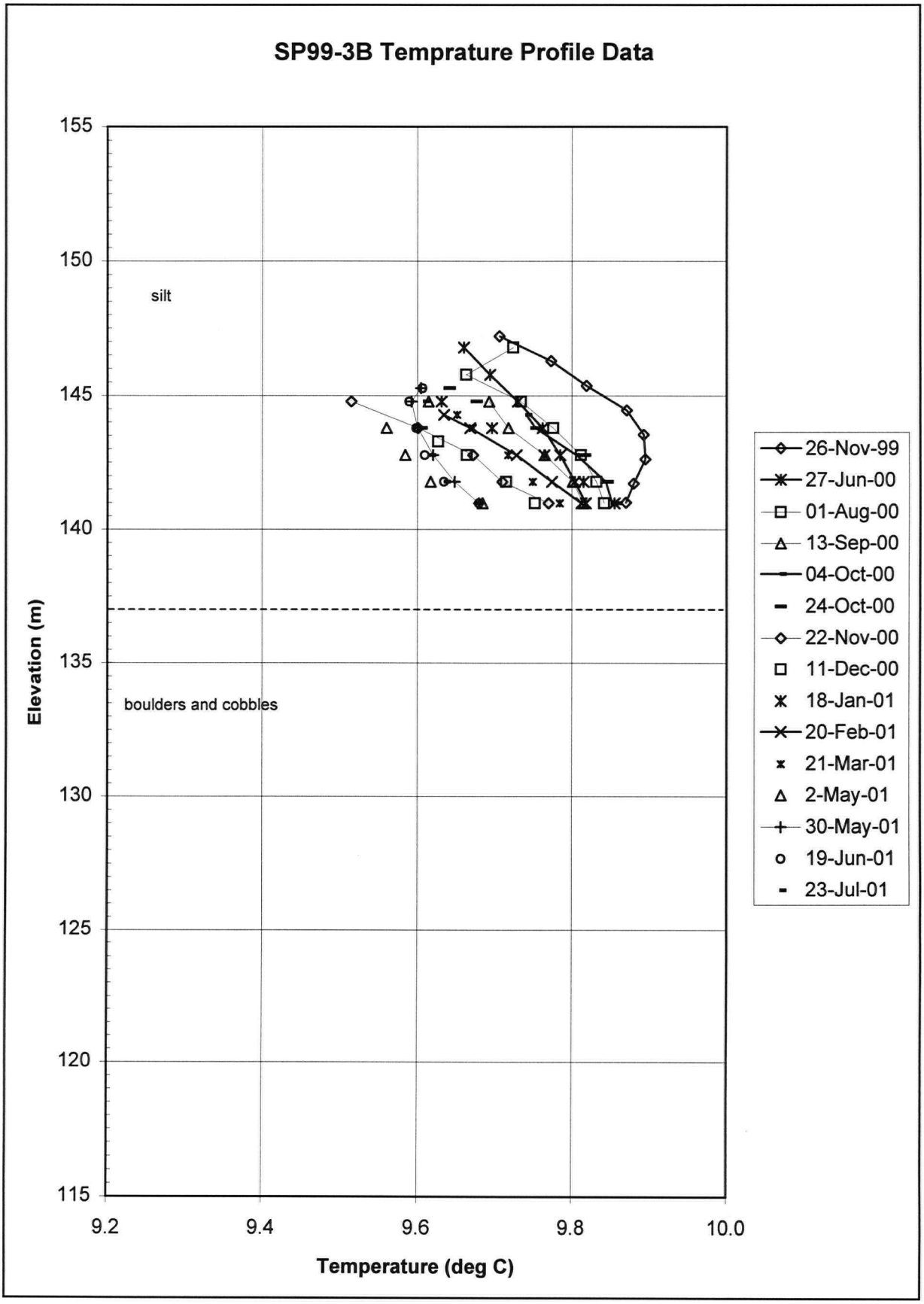
SP99-3B Temprature Profile Data
155
150
145
140
135
130
125
120
115
silt
boulders and cobbles
Elevation (m)
9.2
9.4
9.6
9.8
10.0
Temperature (deg C)
26-Nov-99
27-Jun-00
01-Aug-00
13-Sep-00
04-Oct-00
24-Oct-00
22-Nov-00
11-Dec-00
18-Jan-01
20-Feb-01
21-Mar-01
2-May-01
30-May-01
19-Jun-01
23-Jul-01

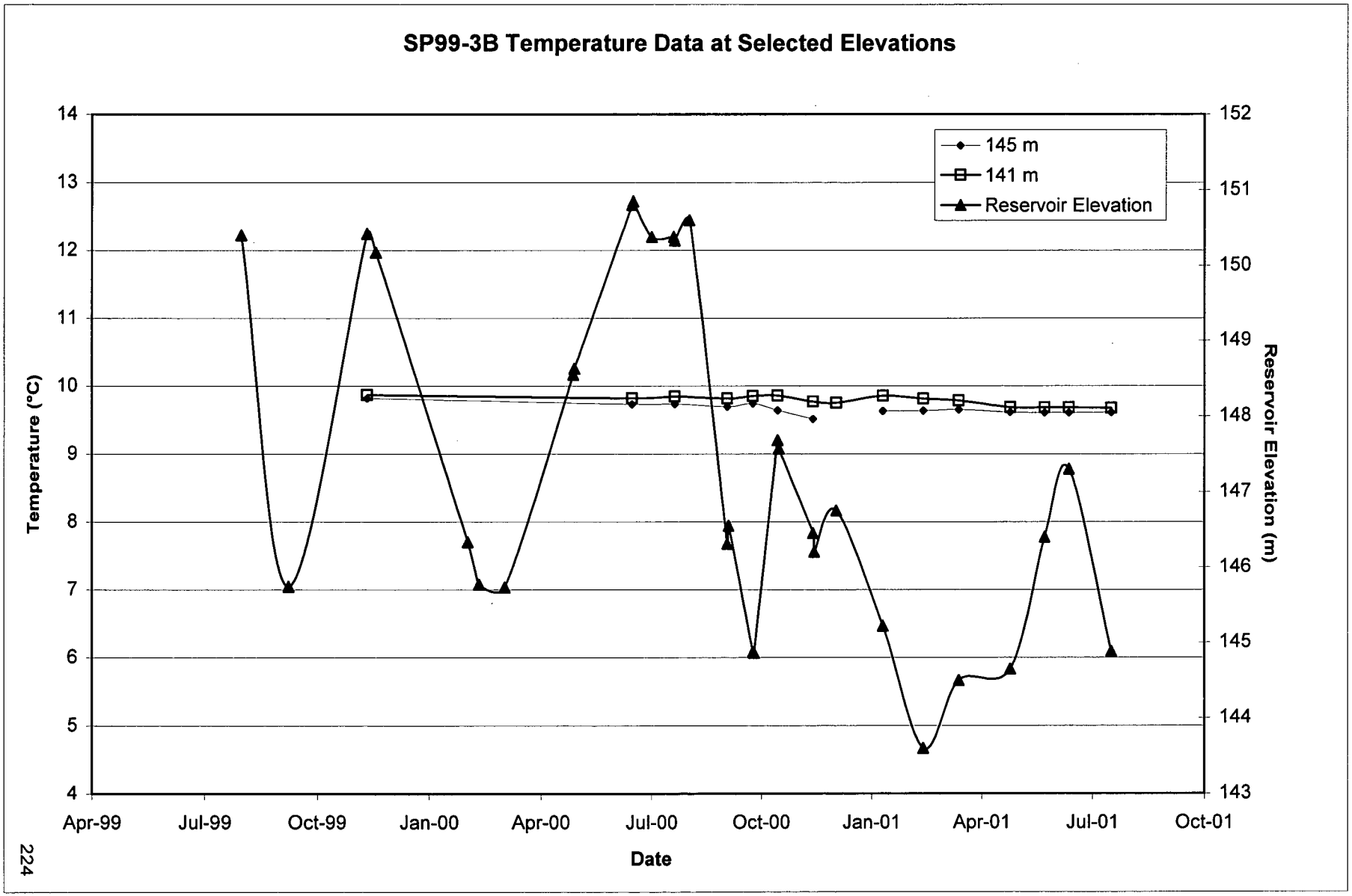
SP99-3B Temperature Data at Selected Elevations
145 m
141 m
Reservoir Elevation
Temperature (°C)
Reservoir Elevation (m)
Date
14
13
12
11
10
9
8
7
6
5
4
152
151
150
149
148
147
146
145
144
143
Apr-99
Jul-99
Oct-99
Jan-00
Apr-00
Jul-00
Oct-00
Jan-01
Apr-01
Jul-01
Oct-01

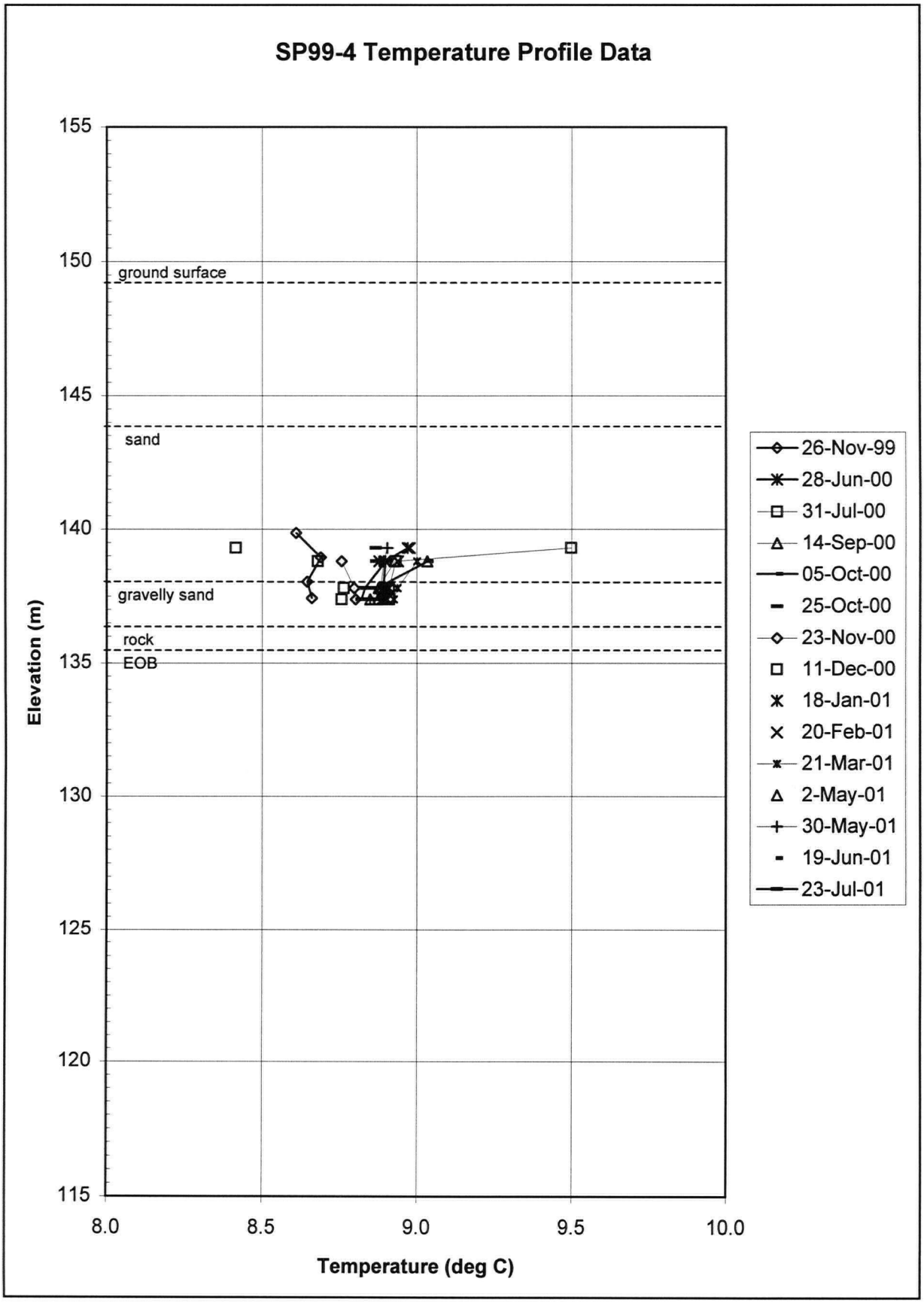
SP99-4 Temperature Profile Data
155
150
145
140
135
130
125
120
115
ground surface
sand
gravelly sand
rock
EOB
Elevation (m)
8.0
8.5
9.0
9.5
10.0
Temperature (deg C)
26-Nov-99
28-Jun-00
31-Jul-00
14-Sep-00
05-Oct-00
25-Oct-00
23-Nov-00
11-Dec-00
18-Jan-01
20-Feb-01
21-Mar-01
2-May-01
30-May-01
19-Jun-01
23-Jul-01

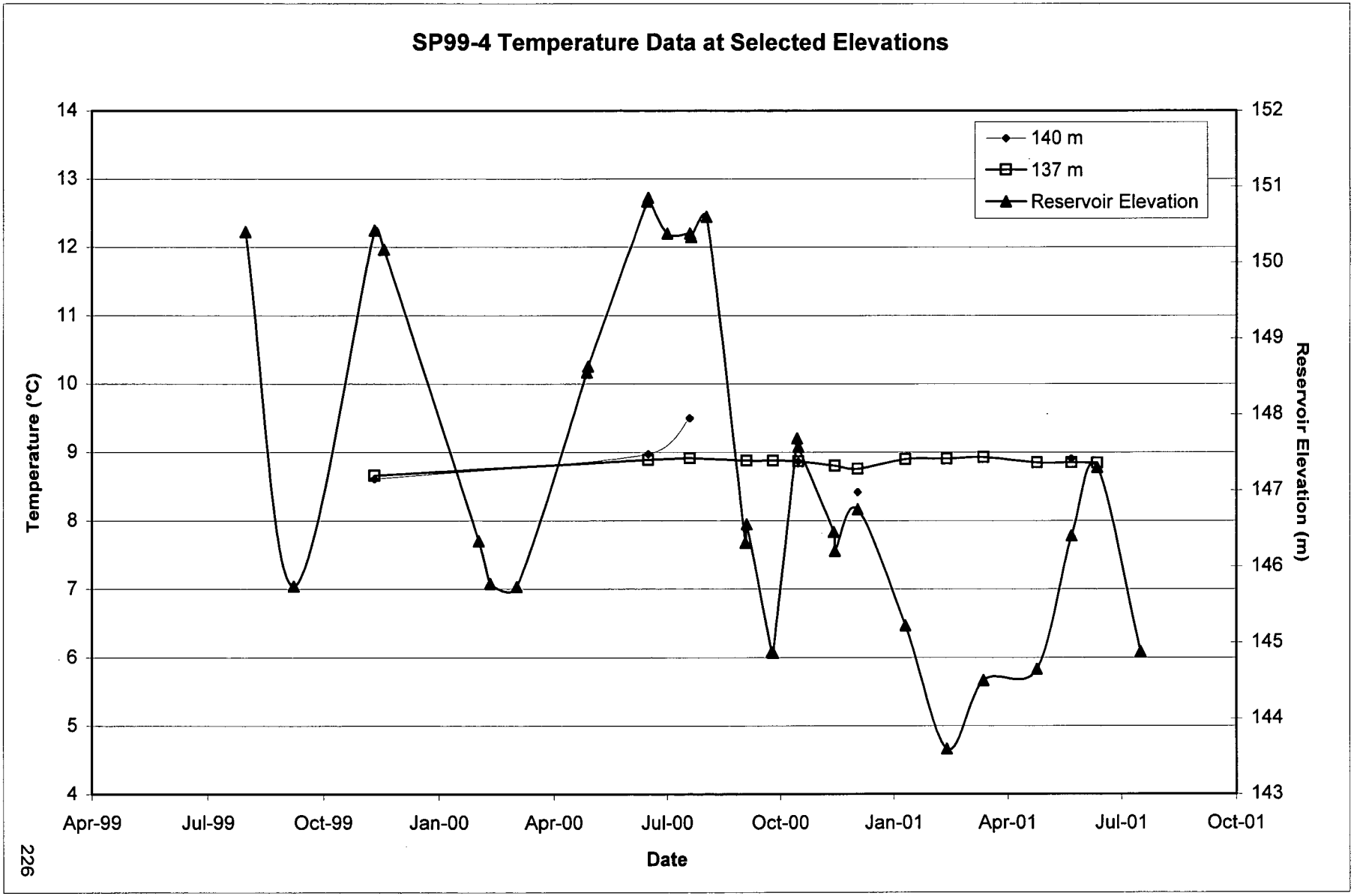
SP99-4 Temperature Data at Selected Elevations
140 m
137 m
Reservoir Elevation
Temperature (°C)
Reservoir Elevation (m)
Date
14
13
12
11
10
9
8
7
6
5
4
152
151
150
149
148
147
146
145
144
143
Apr-99
Jul-99
Oct-99
Jan-00
Apr-00
Jul-00
Oct-00
Jan-01
Apr-01
Jul-01
Oct-01

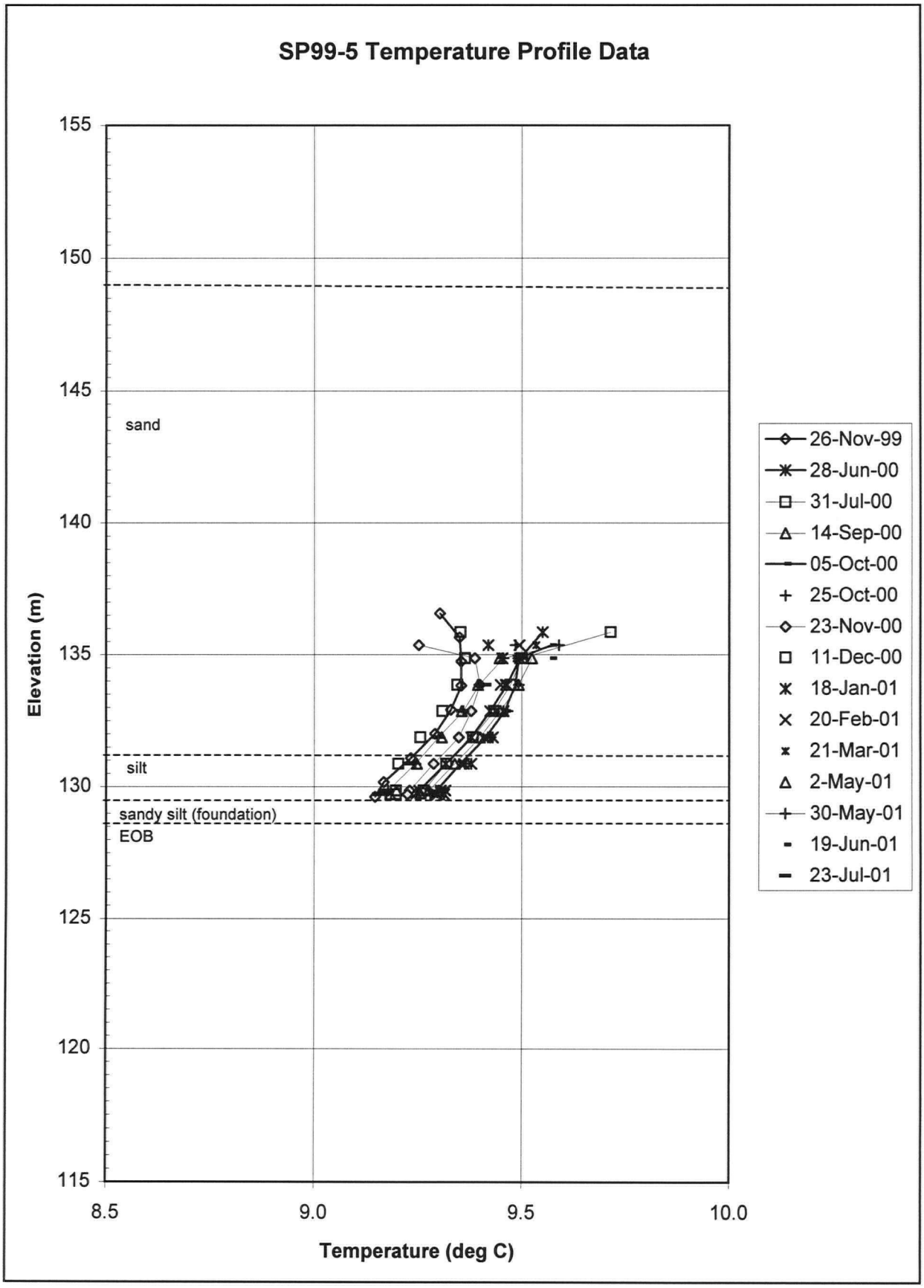
SP99-5 Temperature Profile Data
155
150
145
140
135
130
125
120
115
Elevation (m)
sand
silt
sandy silt (foundation)
EOB
8.5
9.0
9.5
10.0
Temperature (deg C)
26-Nov-99
28-Jun-00
31-Jul-00
14-Sep-00
05-Oct-00
25-Oct-00
23-Nov-00
11-Dec-00
18-Jan-01
20-Feb-01
21-Mar-01
2-May-01
30-May-01
19-Jun-01
23-Jul-01

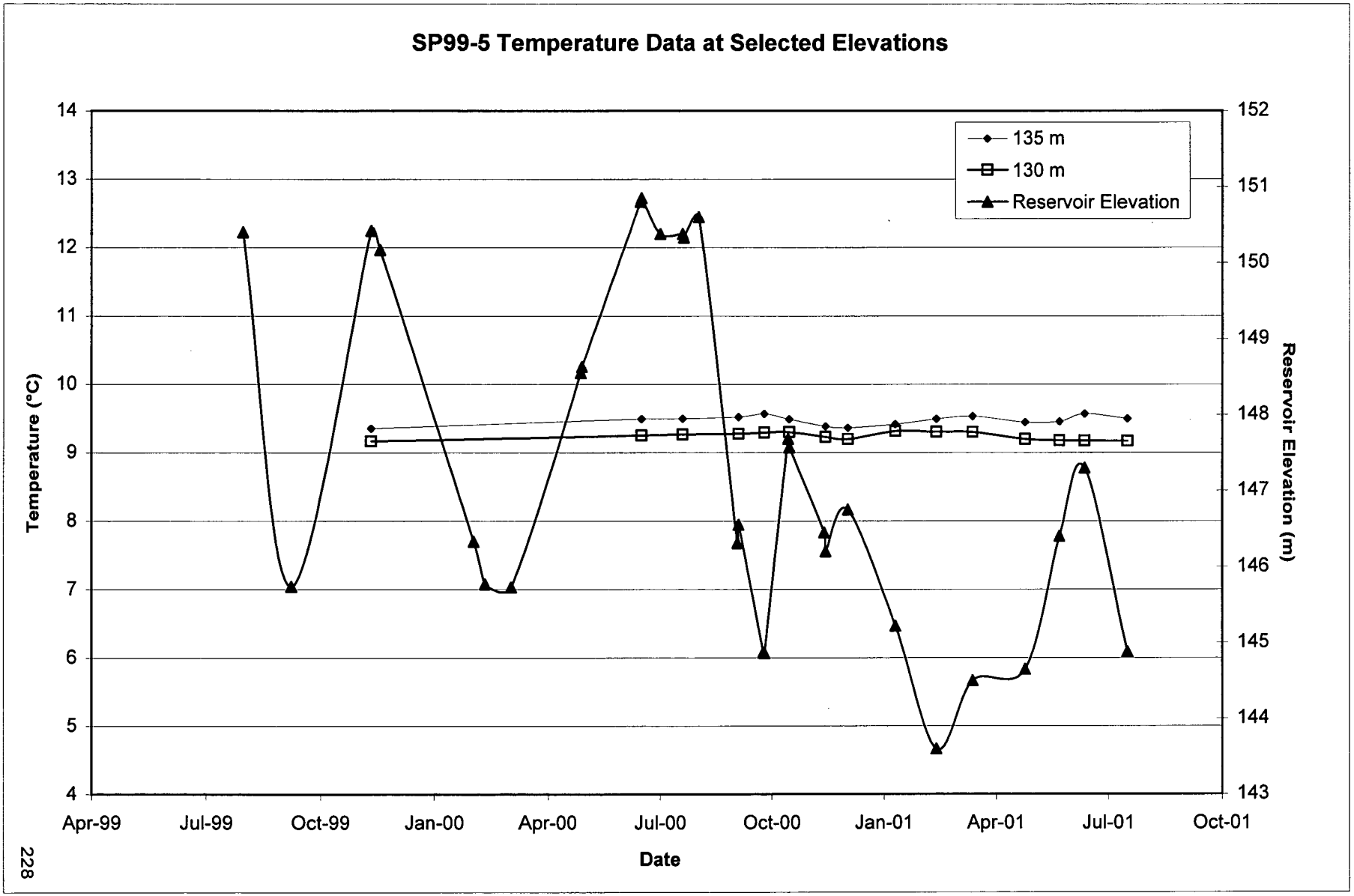
SP99-5 Temperature Data at Selected Elevations
135 m
130 m
Reservoir Elevation
Temperature (°C)
Reservoir Elevation (m)
Date
14
13
12
11
10
9
8
7
6
5
4
152
151
150
149
148
147
146
145
144
143
Apr-99
Jul-99
Oct-99
Jan-00
Apr-00
Jul-00
Oct-00
Jan-01
Apr-01
Jul-01
Oct-01

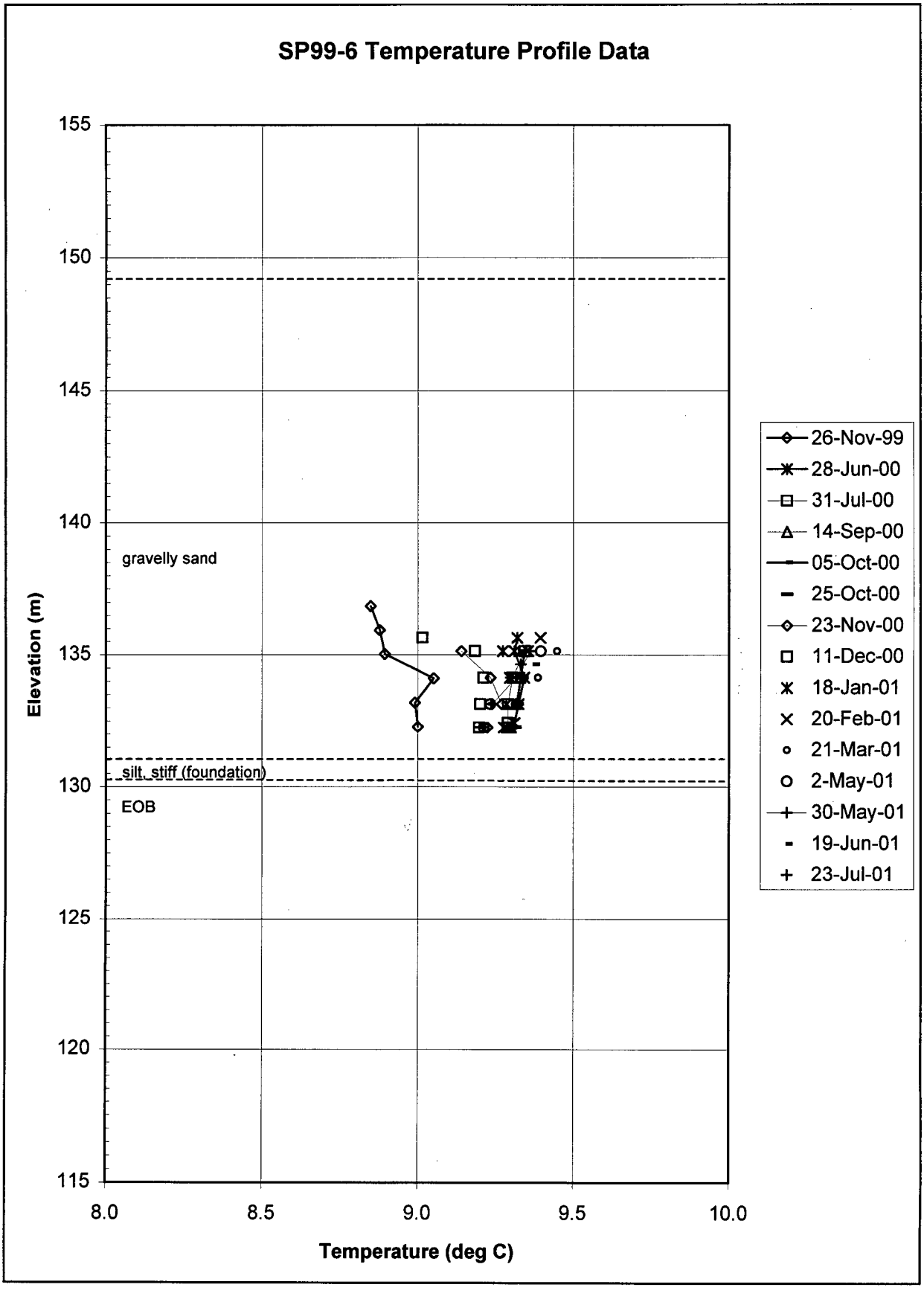
SP99-6 Temperature Profile Data
155
150
145
140
135
130
125
120
115
Elevation (m)
gravelly sand
silt, stiff (foundation)
EOB
8.0
8.5
9.0
9.5
10.0
Temperature (deg C)
26-Nov-99
28-Jun-00
31-Jul-00
14-Sep-00
05-Oct-00
25-Oct-00
23-Nov-00
11-Dec-00
18-Jan-01
20-Feb-01
21-Mar-01
2-May-01
30-May-01
19-Jun-01
23-Jul-01

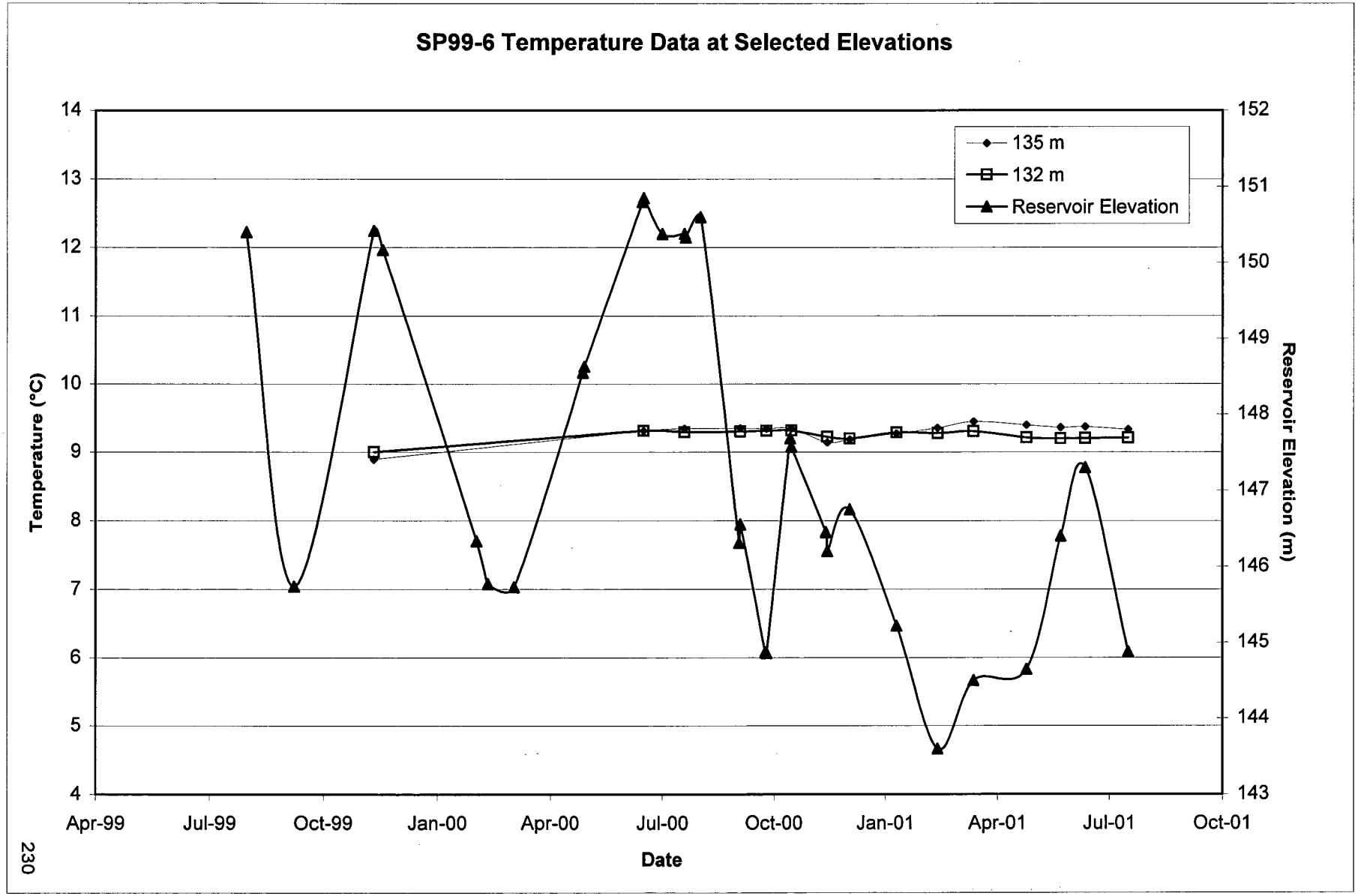
SP99-6 Temperature Data at Selected Elevations
135 m
132 m
Reservoir Elevation
Temperature (°C)
Reservoir Elevation (m)
Date
14
13
12
11
10
9
8
7
6
5
4
152
151
150
149
148
147
146
145
144
143
Apr-99
Jul-99
Oct-99
Jan-00
Apr-00
Jul-00
Oct-00
Jan-01
Apr-01
Jul-01
Oct-01

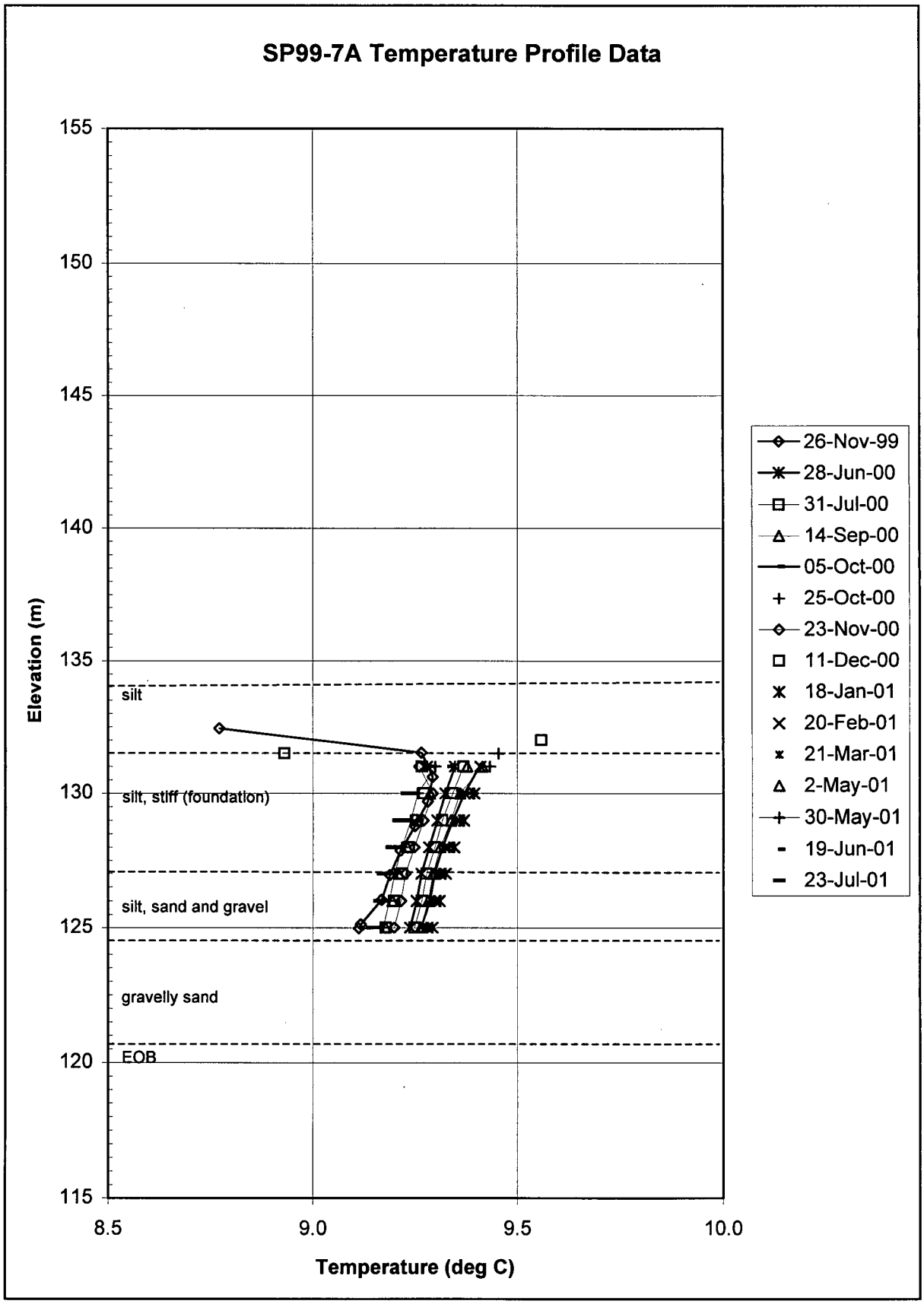
SP99-7A Temperature Profile Data
155
150
145
140
135
130
125
120
115
Elevation (m)
silt
silt, stiff (foundation)
silt, sand and gravel
gravelly sand
EOB
8.5
9.0
9.5
10.0
Temperature (deg C)
26-Nov-99
28-Jun-00
31-Jul-00
14-Sep-00
05-Oct-00
25-Oct-00
23-Nov-00
11-Dec-00
18-Jan-01
20-Feb-01
21-Mar-01
2-May-01
30-May-01
19-Jun-01
23-Jul-01

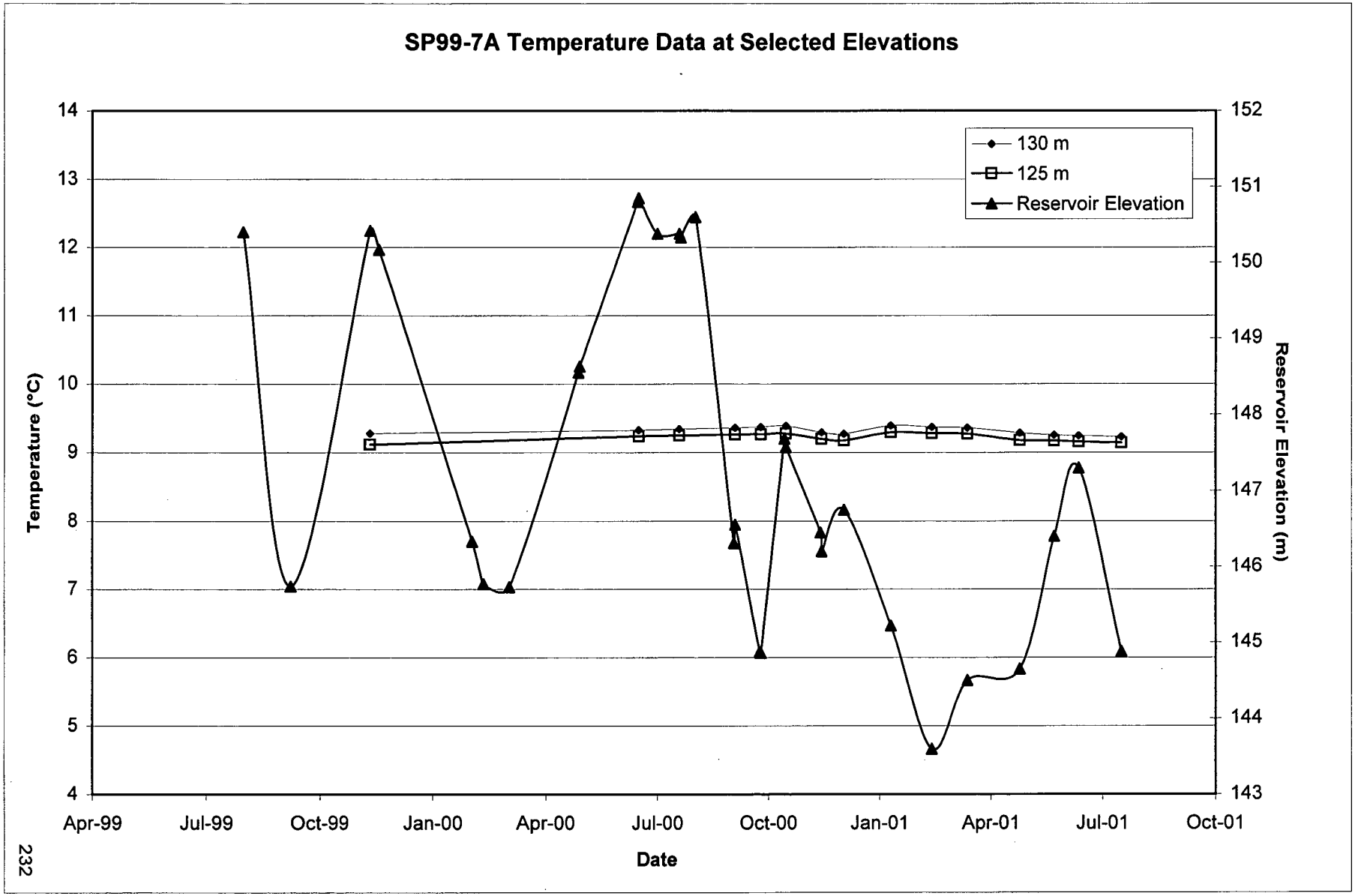
SP99-7A Temperature Data at Selected Elevations
130 m
125 m
Reservoir Elevation
Temperature (°C)
Reservoir Elevation (m)
Date
14
13
12
11
10
9
8
7
6
5
4
152
151
150
149
148
147
146
145
144
143
Apr-99
Jul-99
Oct-99
Jan-00
Apr-00
Jul-00
Oct-00
Jan-01
Apr-01
Jul-01
Oct-01

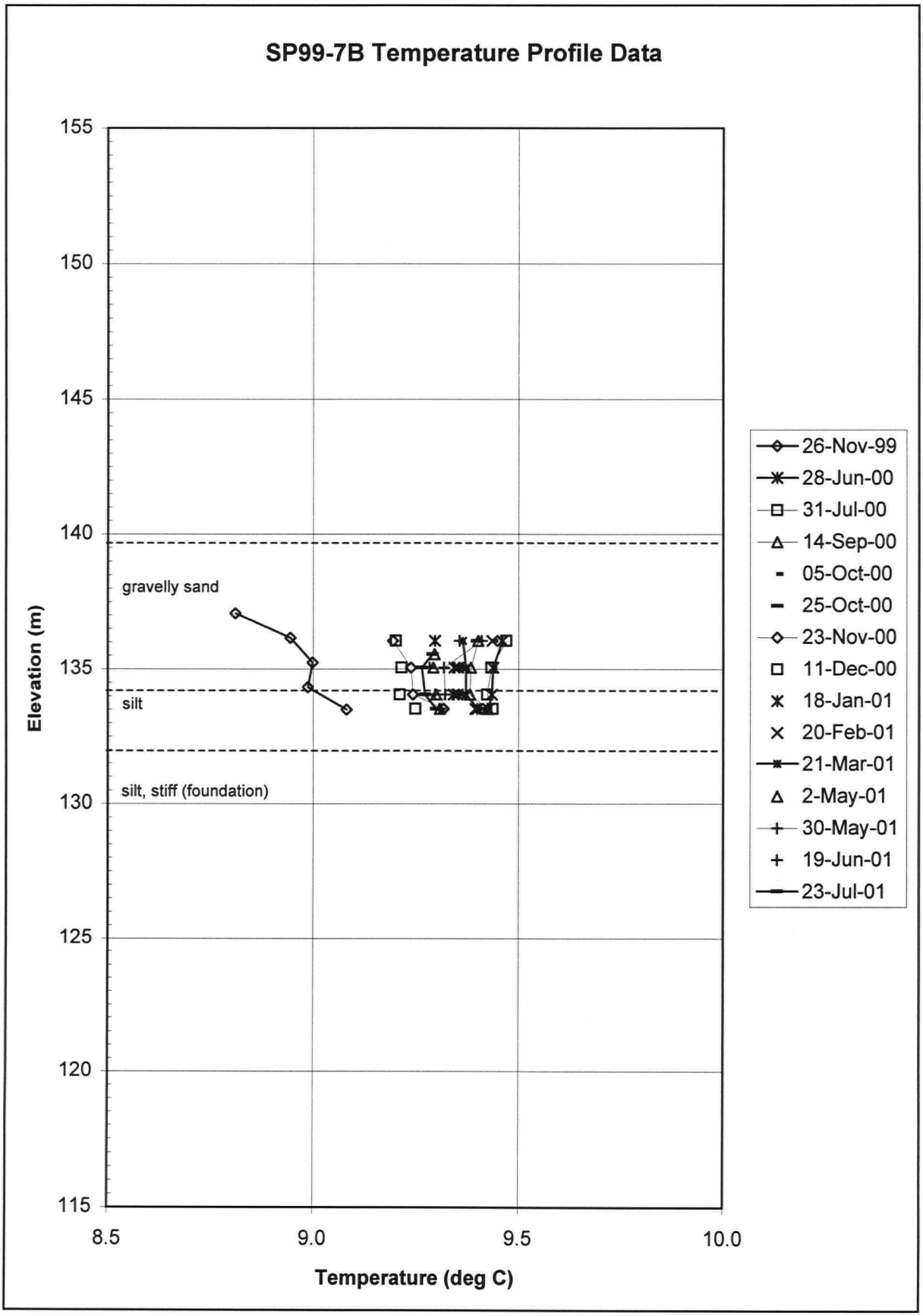
SP99-7B Temperature Profile Data
155
150
145
140
135
130
125
120
115
Elevation (m)
gravelly sand
silt
silt, stiff (foundation)
8.5
9.0
9.5
10.0
Temperature (deg C)
26-Nov-99
28-Jun-00
31-Jul-00
14-Sep-00
05-Oct-00
25-Oct-00
23-Nov-00
11-Dec-00
18-Jan-01
20-Feb-01
21-Mar-01
2-May-01
30-May-01
19-Jun-01
23-Jul-01

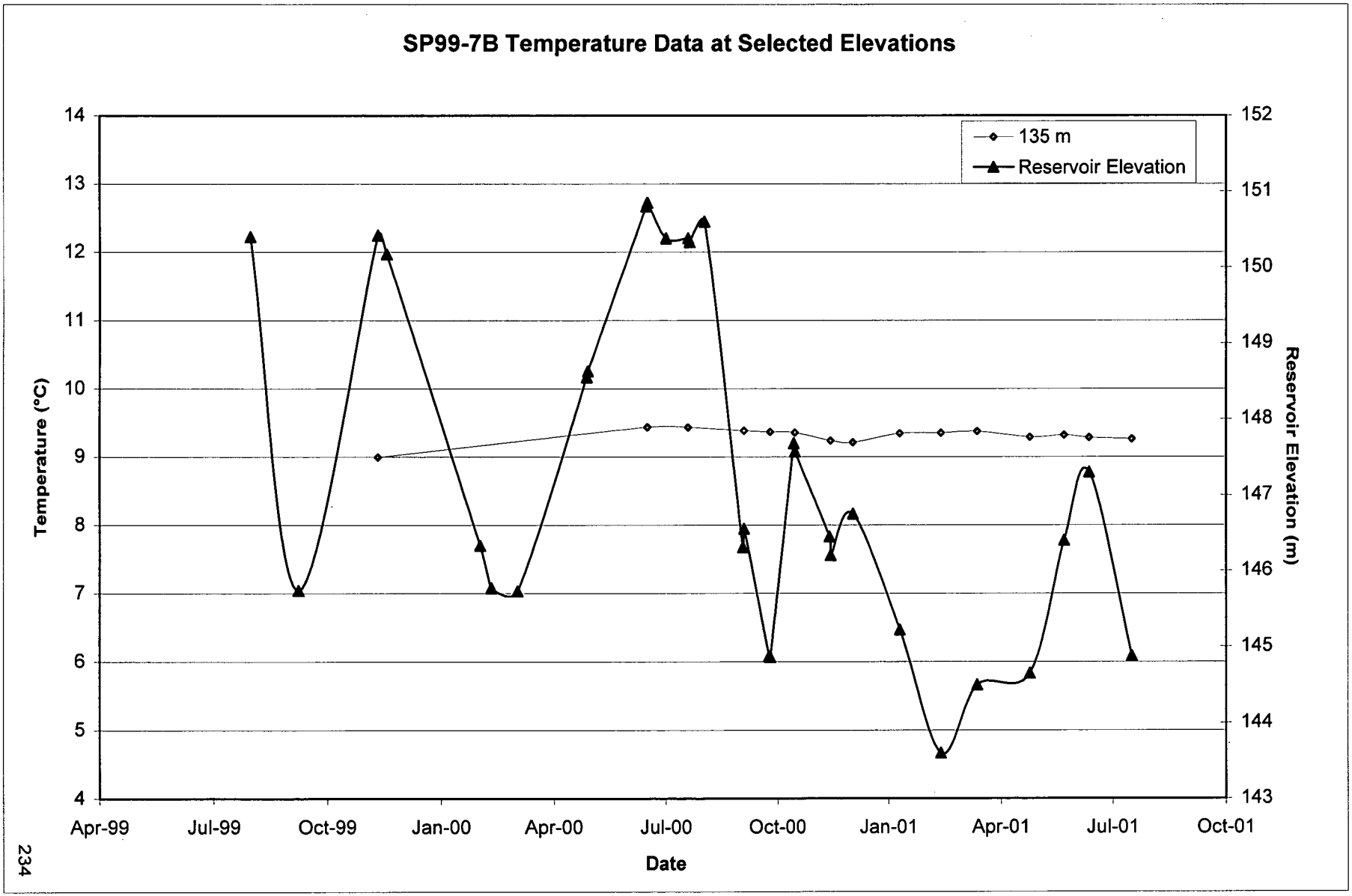
SP99-7B Temperature Data at Selected Elevations
135 m
Reservoir Elevation
Temperature (°C)
Reservoir Elevation (m)
Date
14
13
12
11
10
9
8
7
6
5
4
152
151
150
149
148
147
146
145
144
143
Apr-99
Jul-99
Oct-99
Jan-00
Apr-00
Jul-00
Oct-00
Jan-01
Apr-01
Jul-01
Oct-01

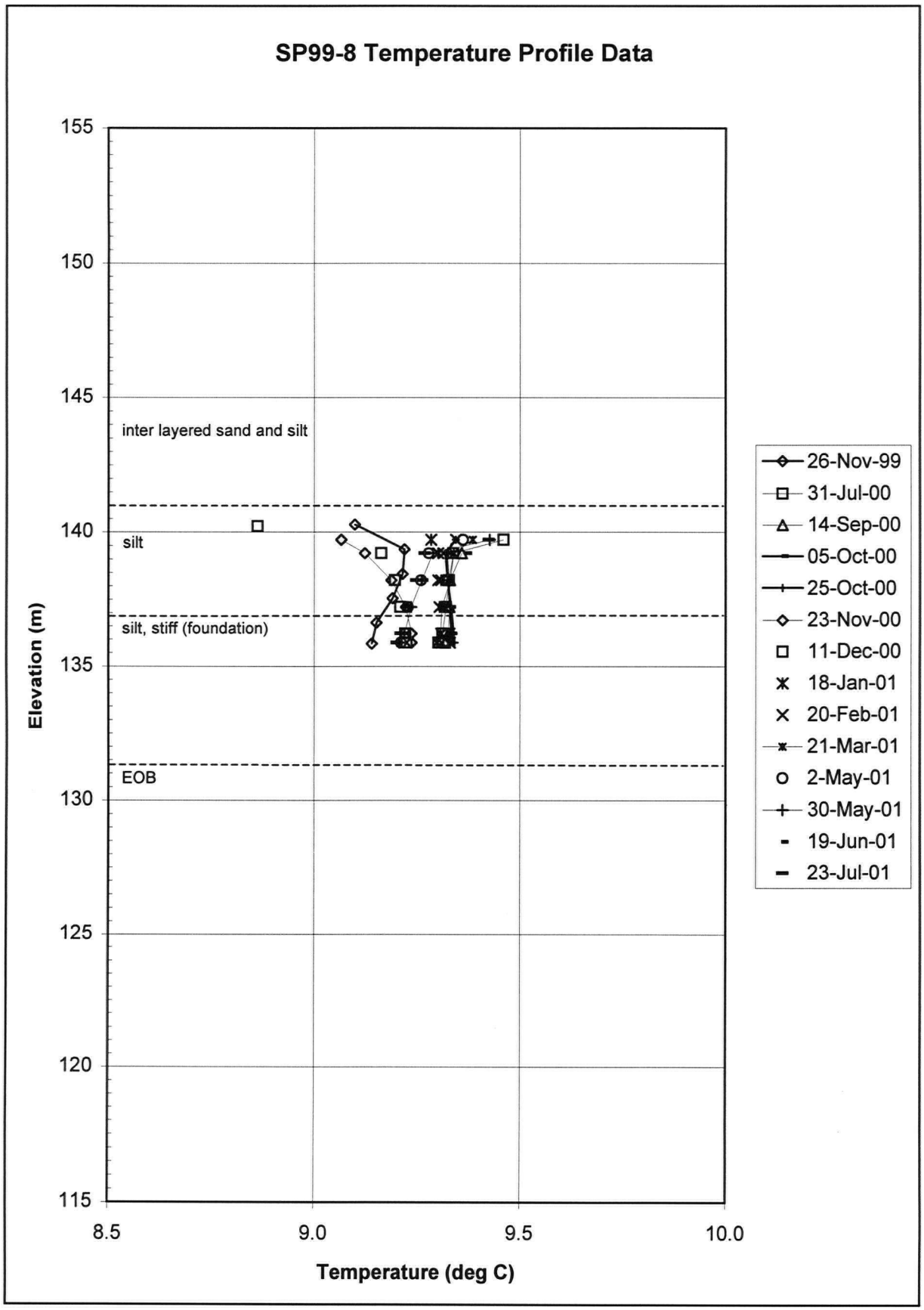
SP99-8 Temperature Profile Data
155
150
145
140
135
130
125
120
115
inter layered sand and silt
silt
silt, stiff (foundation)
EOB
Elevation (m)
8.5
9.0
9.5
10.0
Temperature (deg C)
26-Nov-99
31-Jul-00
14-Sep-00
05-Oct-00
25-Oct-00
23-Nov-00
11-Dec-00
18-Jan-01
20-Feb-01
21-Mar-01
2-May-01
30-May-01
19-Jun-01
23-Jul-01

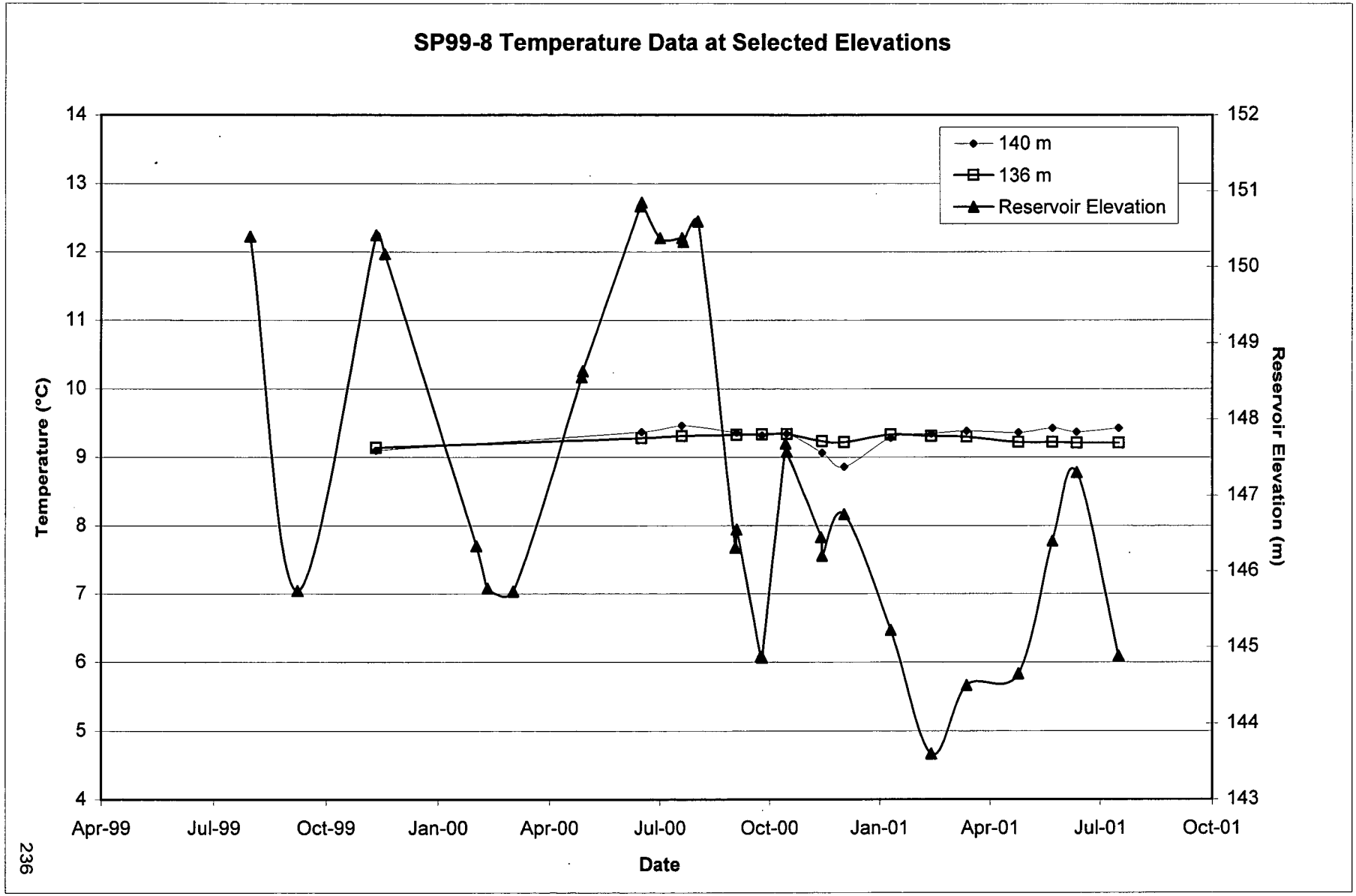
SP99-8 Temperature Data at Selected Elevations
140 m
136 m
Reservoir Elevation
Temperature (°C)
Reservoir Elevation (m)
Date
14
13
12
11
10
9
8
7
6
5
4
152
151
150
149
148
147
146
145
144
143
Apr-99
Jul-99
Oct-99
Jan-00
Apr-00
Jul-00
Oct-00
Jan-01
Apr-01
Jul-01
Oct-01

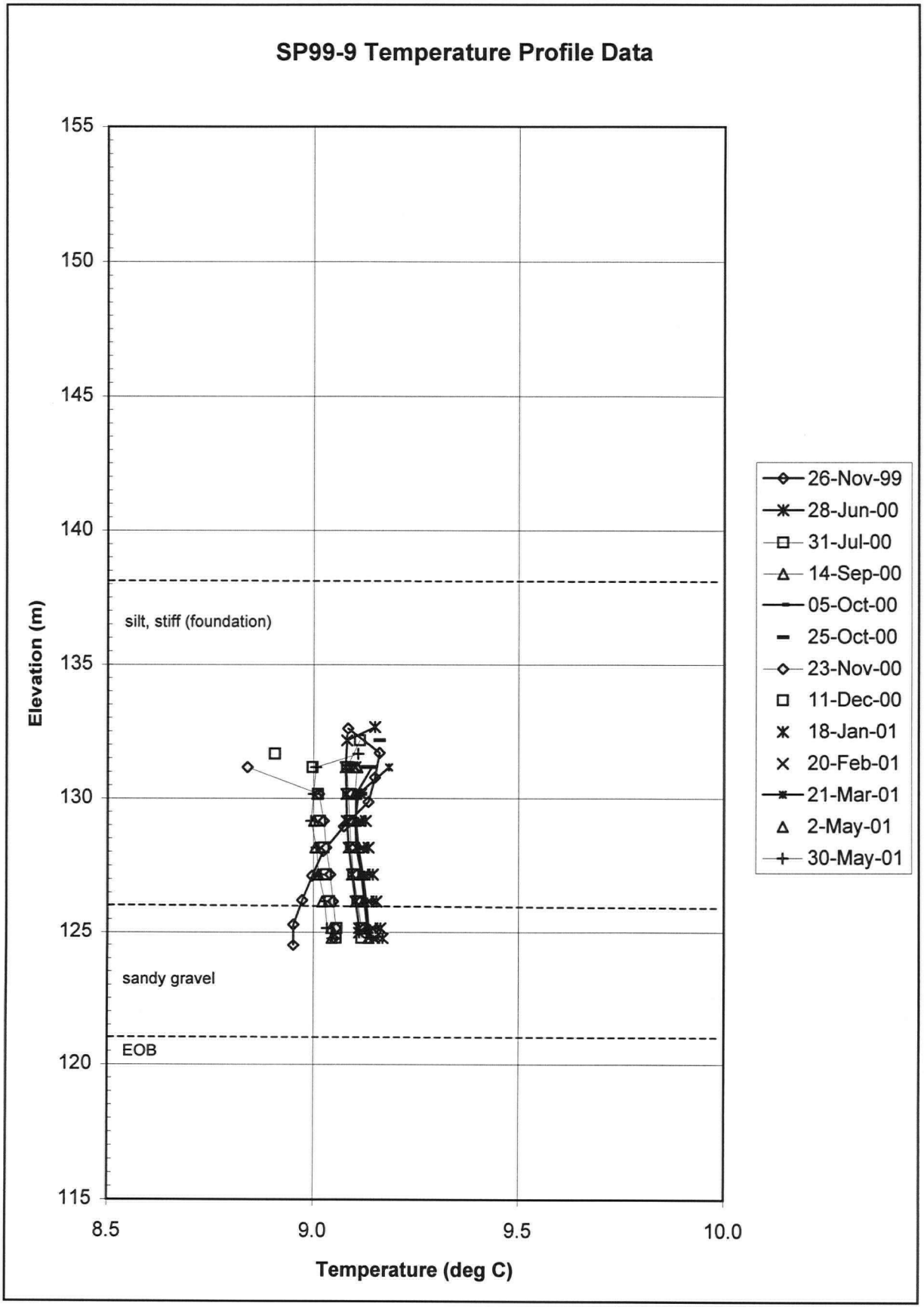
SP99-9 Temperature Profile Data
155
150
145
140
135
130
125
120
115
Elevation (m)
silt, stiff (foundation)
sandy gravel
EOB
8.5
9.0
9.5
10.0
Temperature (deg C)
26-Nov-99
28-Jun-00
31-Jul-00
14-Sep-00
05-Oct-00
25-Oct-00
23-Nov-00
11-Dec-00
18-Jan-01
20-Feb-01
21-Mar-01
2-May-01
30-May-01

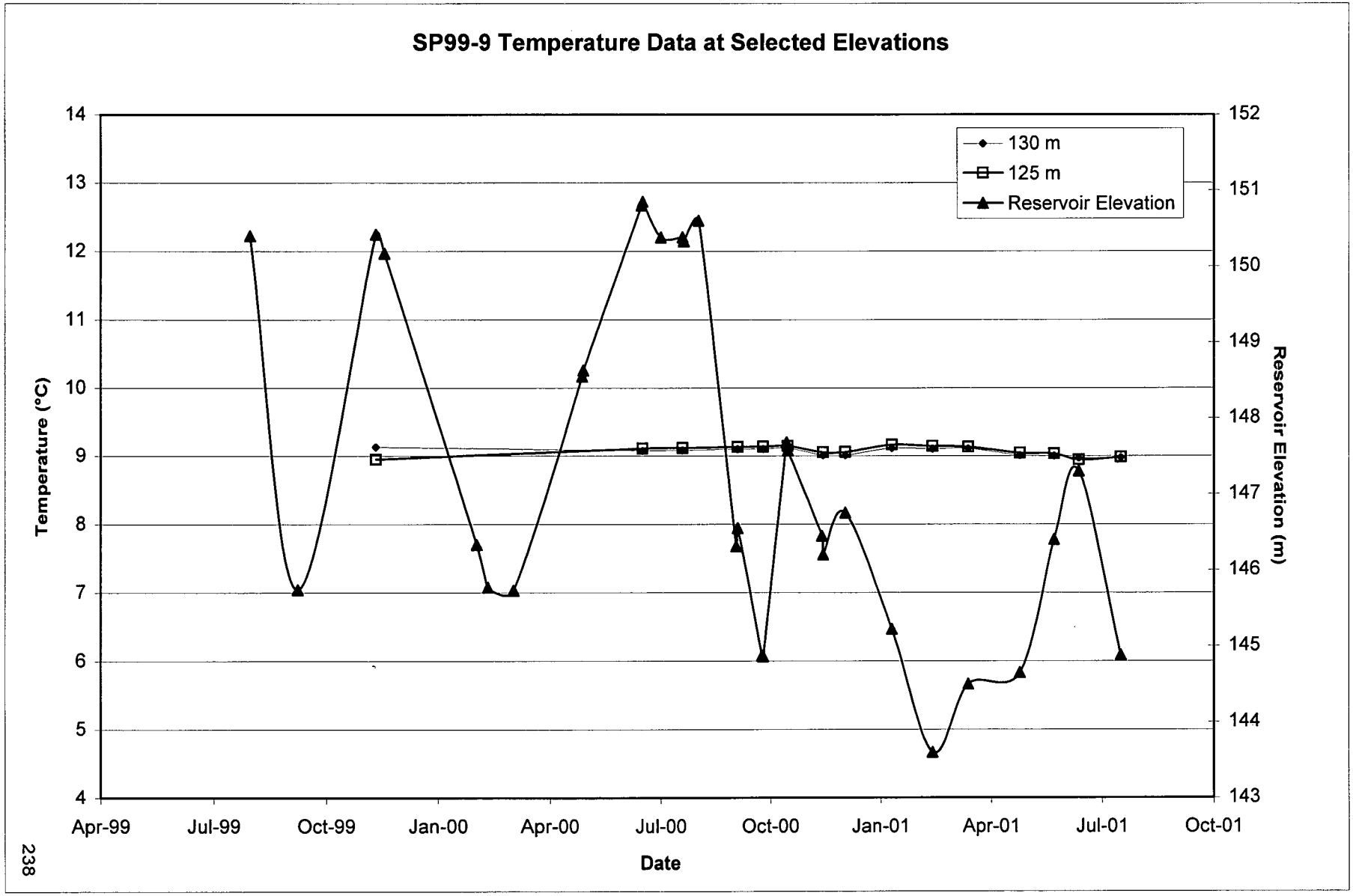
SP99-9 Temperature Data at Selected Elevations
130 m
125 m
Reservoir Elevation
Temperature (°C)
Reservoir Elevation (m)
Date
14
13
12
11
10
9
8
7
6
5
4
152
151
150
149
148
147
146
145
144
143
Apr-99
Jul-99
Oct-99
Jan-00
Apr-00
Jul-00
Oct-00
Jan-01
Apr-01
Jul-01
Oct-01

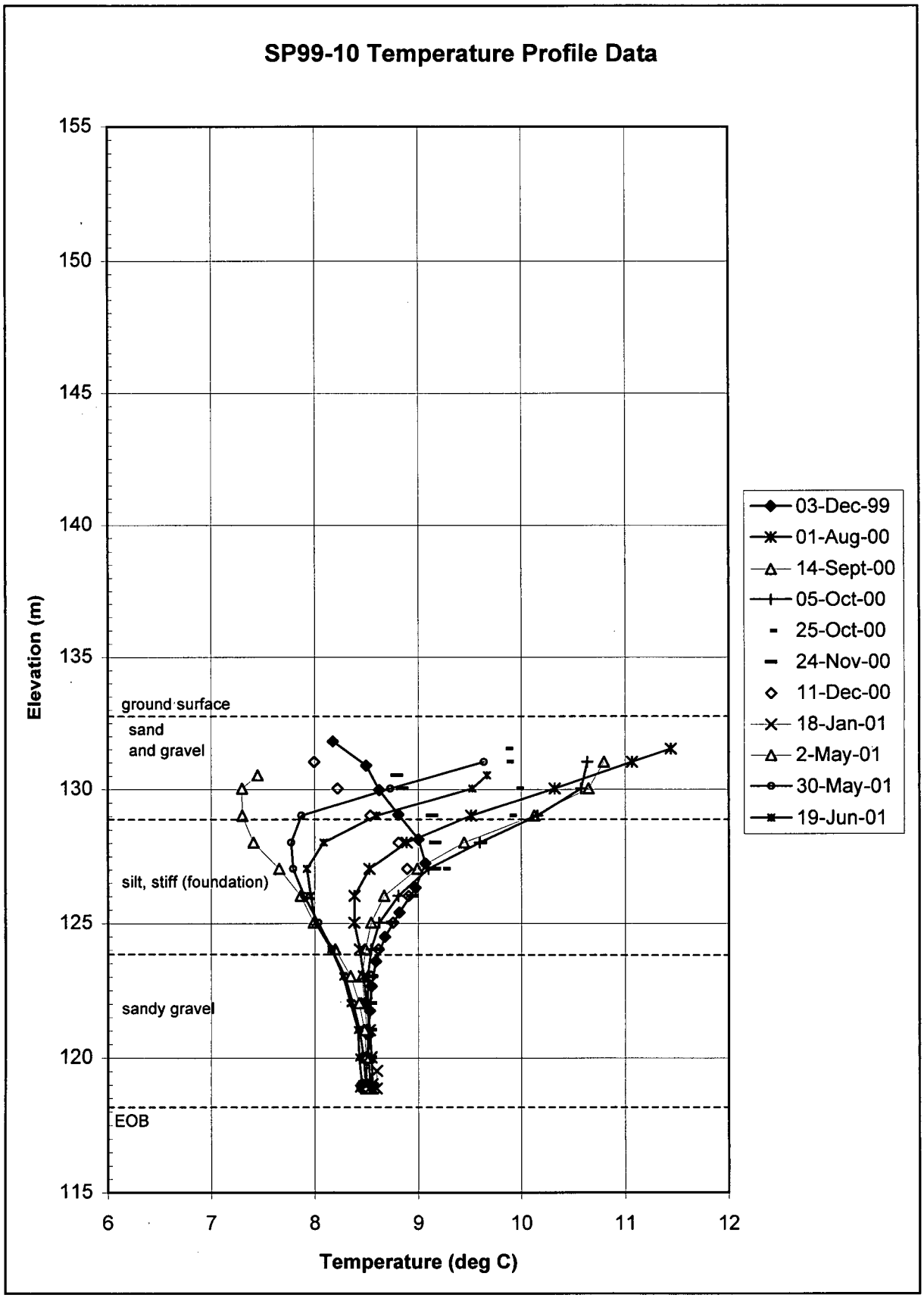
SP99-10 Temperature Profile Data
155
150
145
140
135
130
125
120
115
Elevation (m)
ground surface
sand
and gravel
silt, stiff (foundation)
sandy gravel
EOB
6
7
8
9
10
11
12
Temperature (deg C)
03-Dec-99
01-Aug-00
14-Sept-00
05-Oct-00
25-Oct-00
24-Nov-00
11-Dec-00
18-Jan-01
2-May-01
30-May-01
19-Jun-01

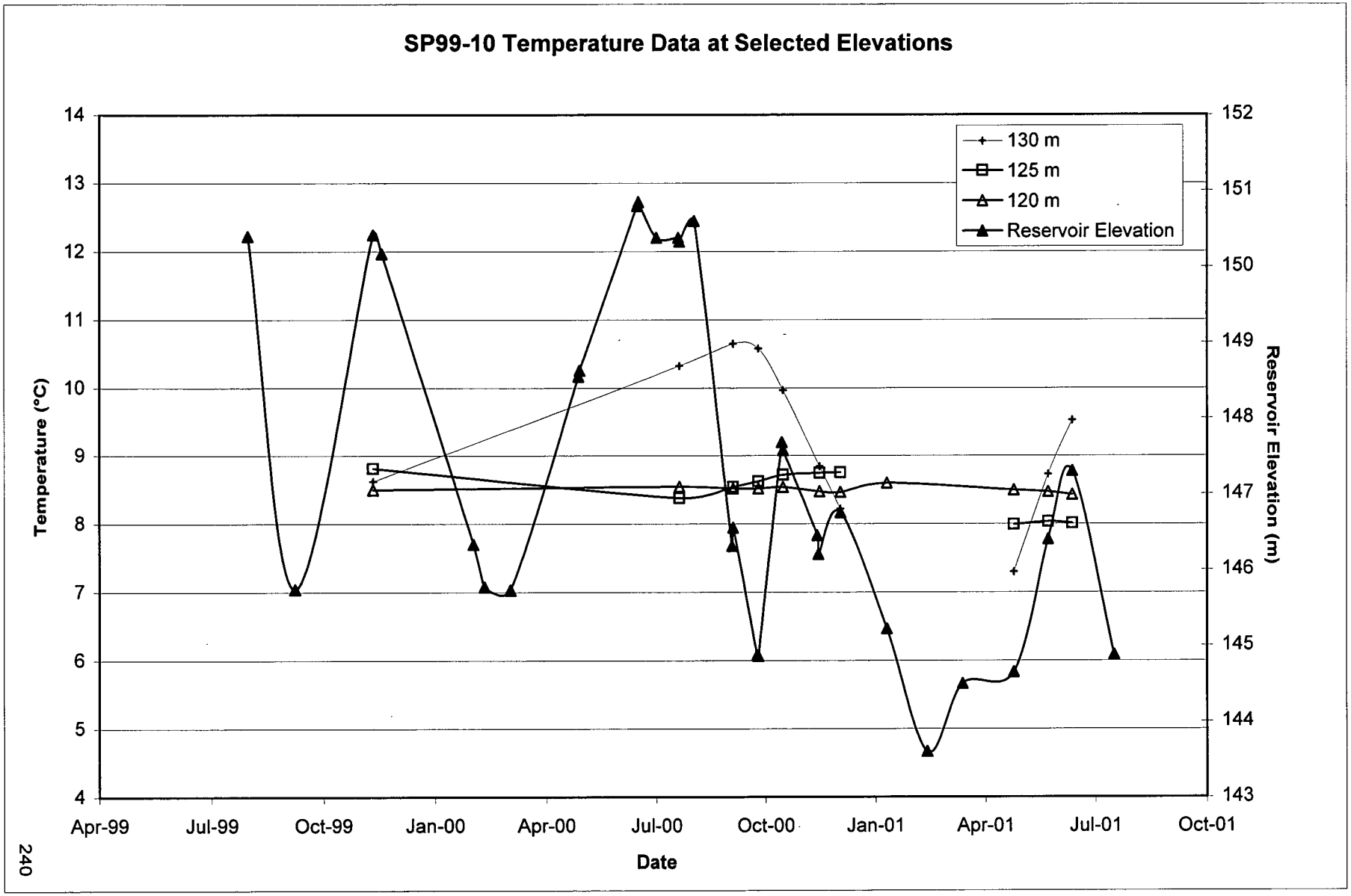
SP99-10 Temperature Data at Selected Elevations
Temperature (°C)
Reservoir Elevation (m)
Date
130 m
125 m
120 m
Reservoir Elevation
14
13
12
11
10
9
8
7
6
5
4
152
151
150
149
148
147
146
145
144
143
Apr-99
Jul-99
Oct-99
Jan-00
Apr-00
Jul-00
Oct-00
Jan-01
Apr-01
Jul-01
Oct-01

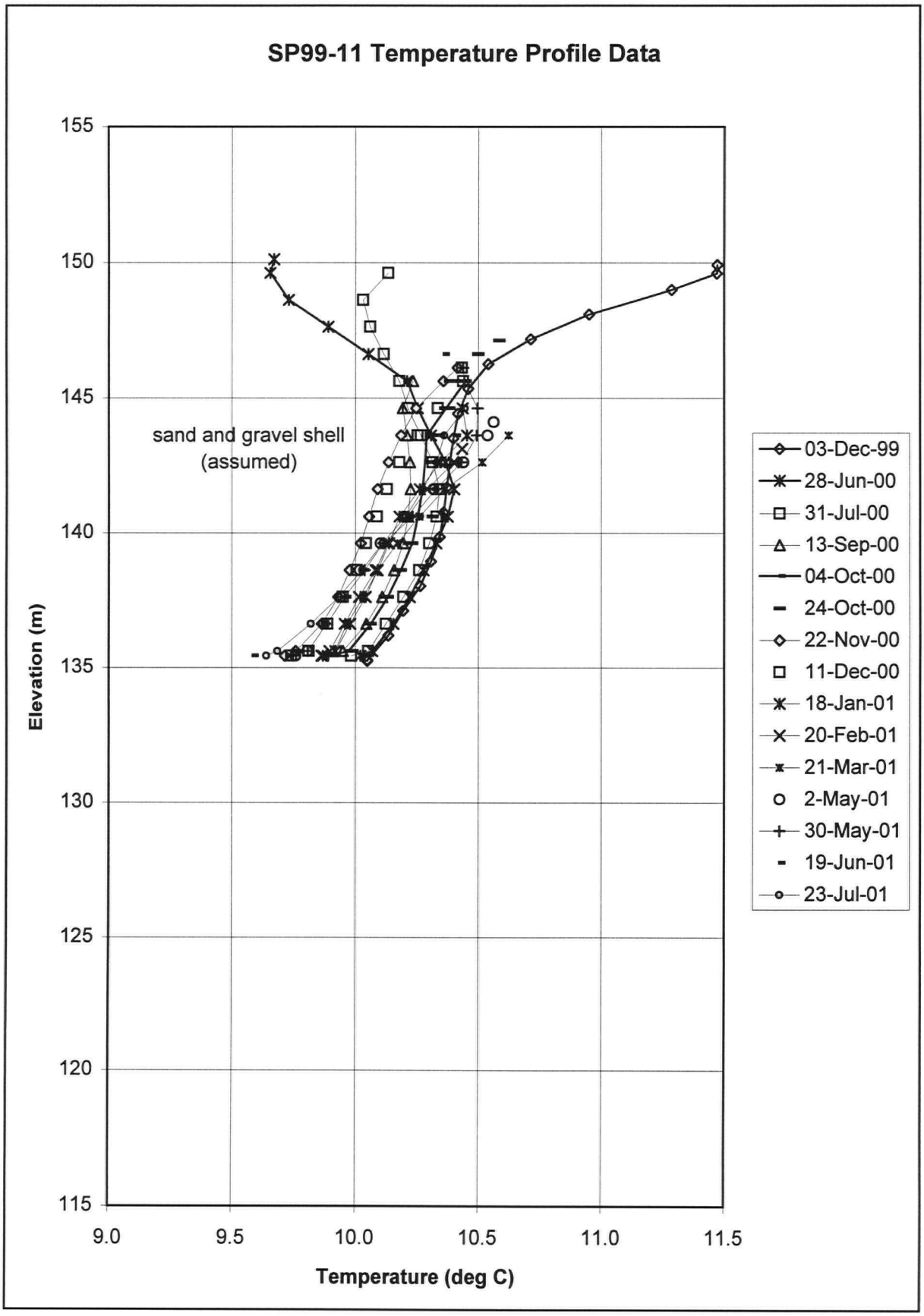
SP99-11 Temperature Profile Data
155
150
145
140
135
130
125
120
115
Elevation (m)
sand and gravel shell
(assumed)
9.0
9.5
10.0
10.5
11.0
11.5
Temperature (deg C)
03-Dec-99
28-Jun-00
31-Jul-00
13-Sep-00
04-Oct-00
24-Oct-00
22-Nov-00
11-Dec-00
18-Jan-01
20-Feb-01
21-Mar-01
2-May-01
30-May-01
19-Jun-01
23-Jul-01

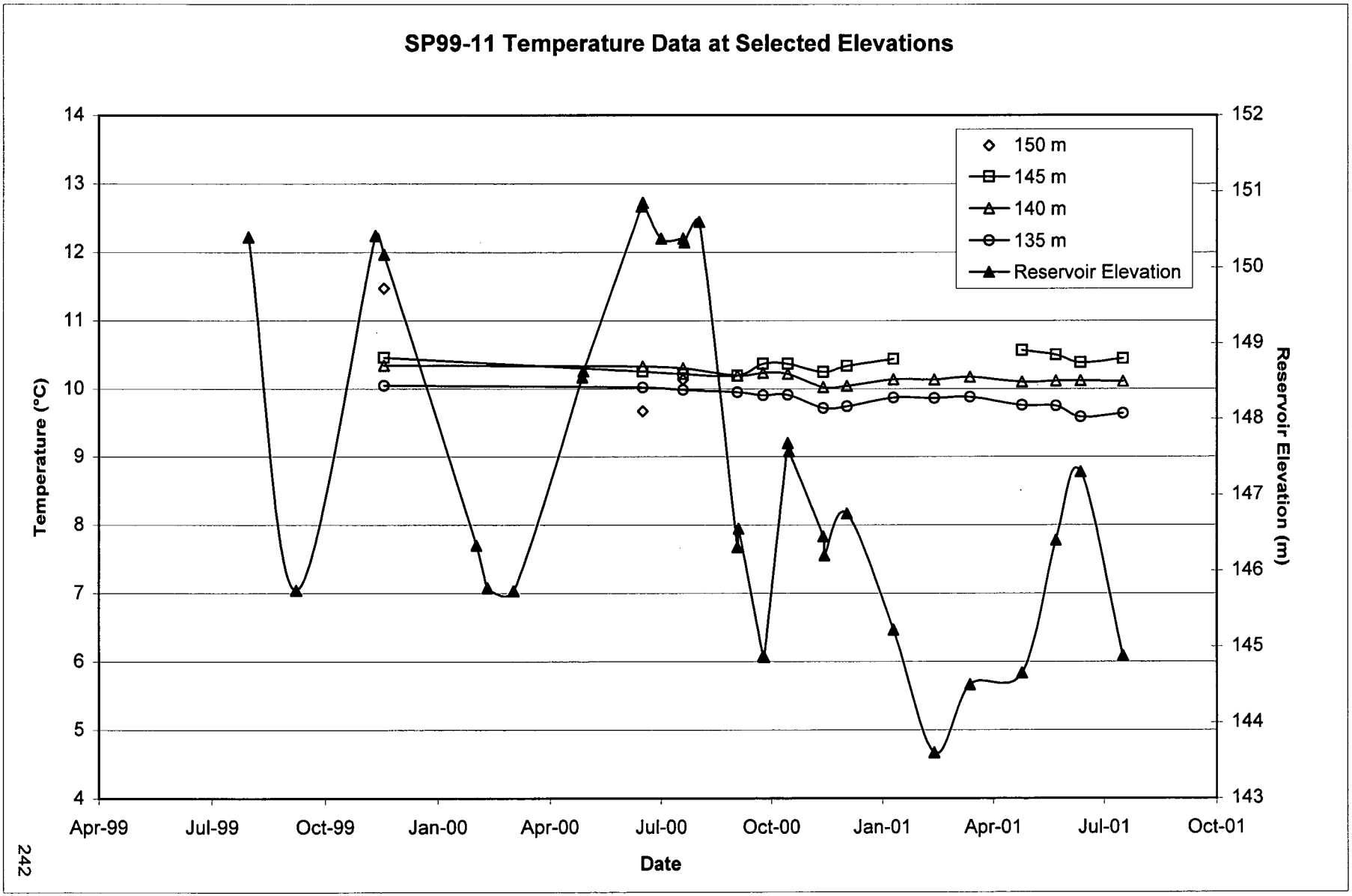
SP99-11 Temperature Data at Selected Elevations
Temperature (°C)
Reservoir Elevation (m)
Date
150 m
145 m
140 m
135 m
Reservoir Elevation
14
13
12
11
10
9
8
7
6
5
4
152
151
150
149
148
147
146
145
144
143
Apr-99
Jul-99
Oct-99
Jan-00
Apr-00
Jul-00
Oct-00
Jan-01
Apr-01
Jul-01
Oct-01

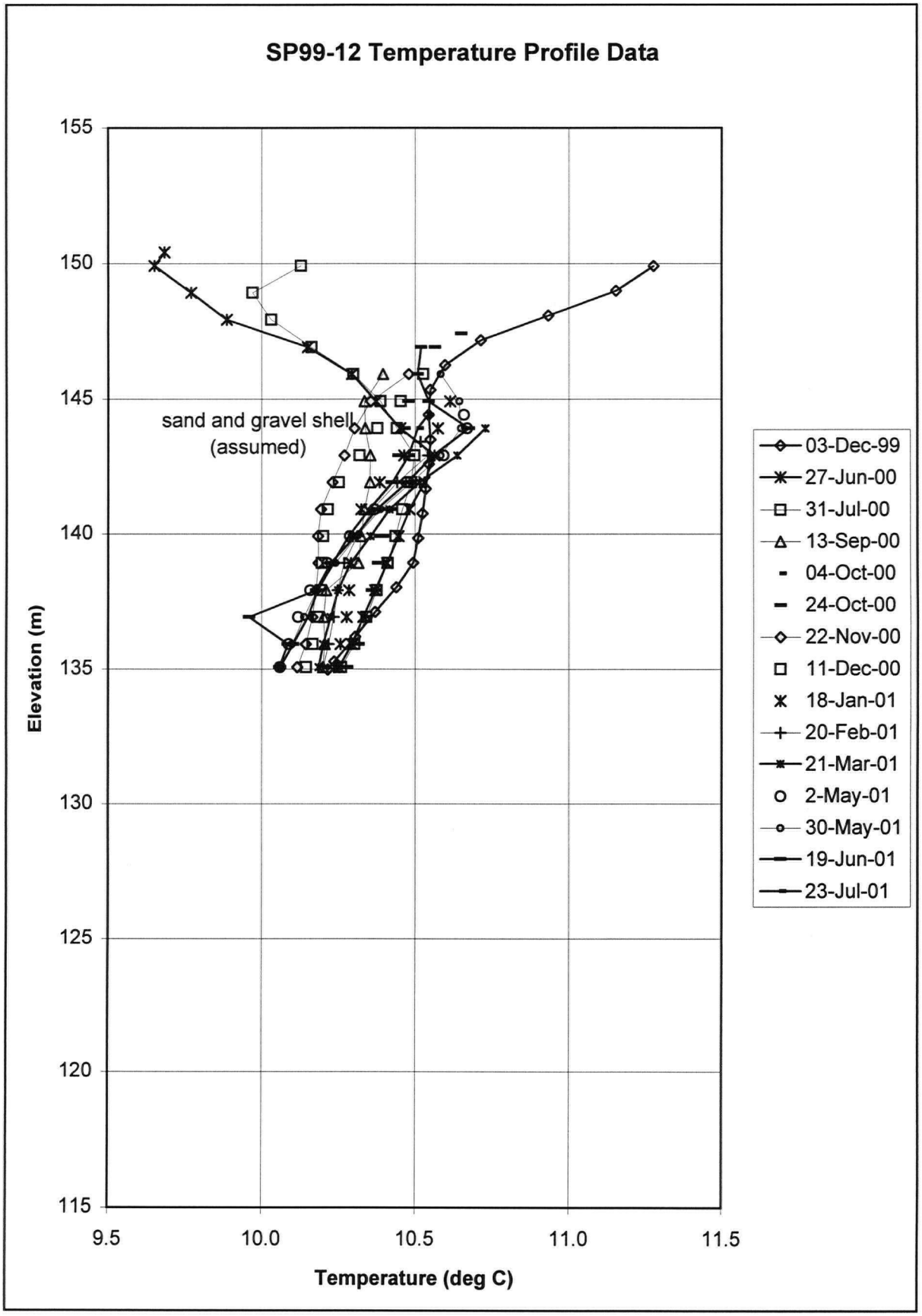
SP99-12 Temperature Profile Data
155
150
145
140
135
130
125
120
115
Elevation (m)
sand and gravel shell
(assumed)
9.5
10.0
10.5
11.0
11.5
Temperature (deg C)
03-Dec-99
27-Jun-00
31-Jul-00
13-Sep-00
04-Oct-00
24-Oct-00
22-Nov-00
11-Dec-00
18-Jan-01
20-Feb-01
21-Mar-01
2-May-01
30-May-01
19-Jun-01
23-Jul-01

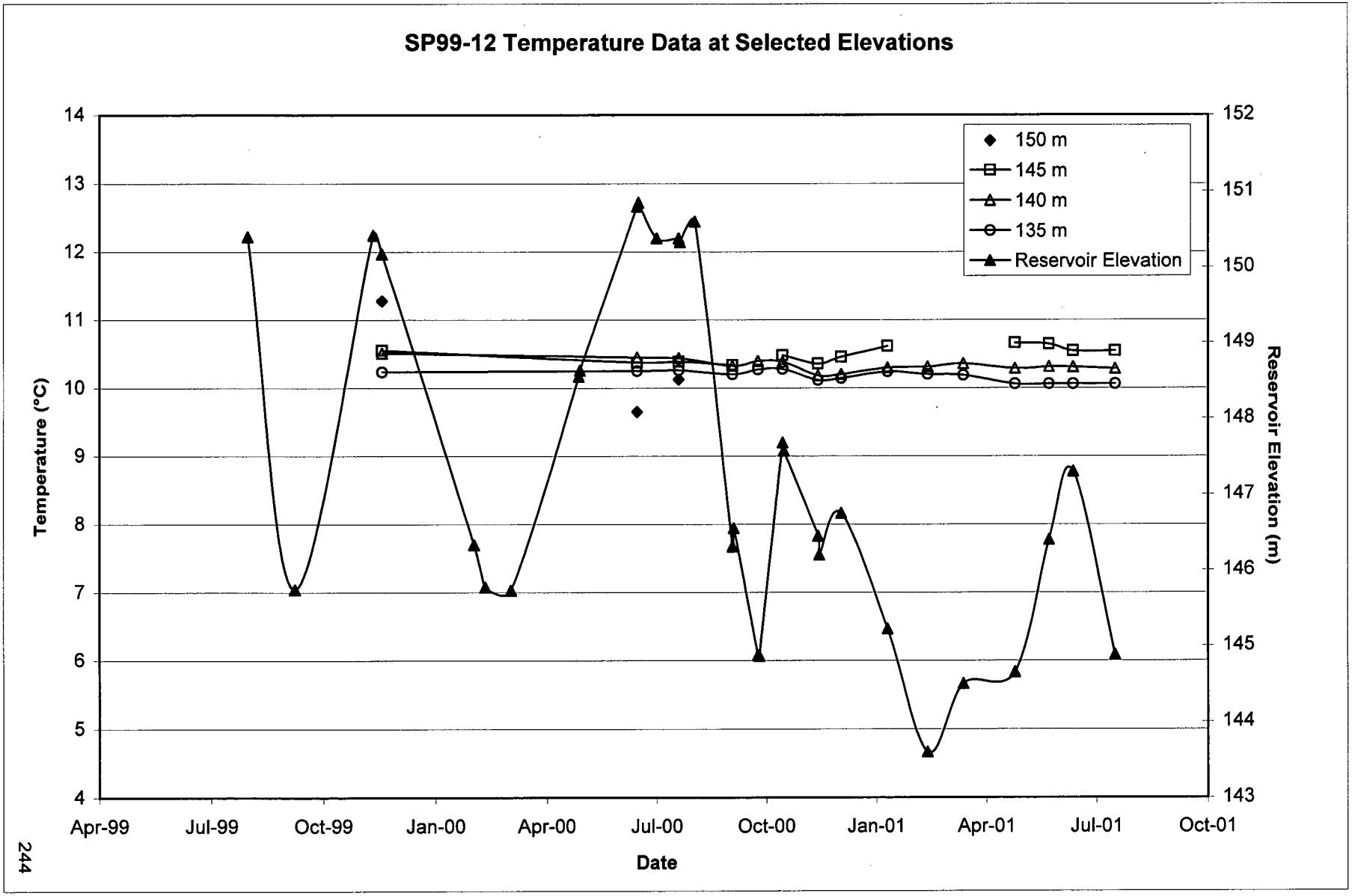
SP99-12 Temperature Data at Selected Elevations
Temperature (°C)
Reservoir Elevation (m)
Date
150 m
145 m
140 m
135 m
Reservoir Elevation
14
13
12
11
10
9
8
7
6
5
4
152
151
150
149
148
147
146
145
144
143
Apr-99
Jul-99
Oct-99
Jan-00
Apr-00
Jul-00
Oct-00
Jan-01
Apr-01
Jul-01
Oct-01

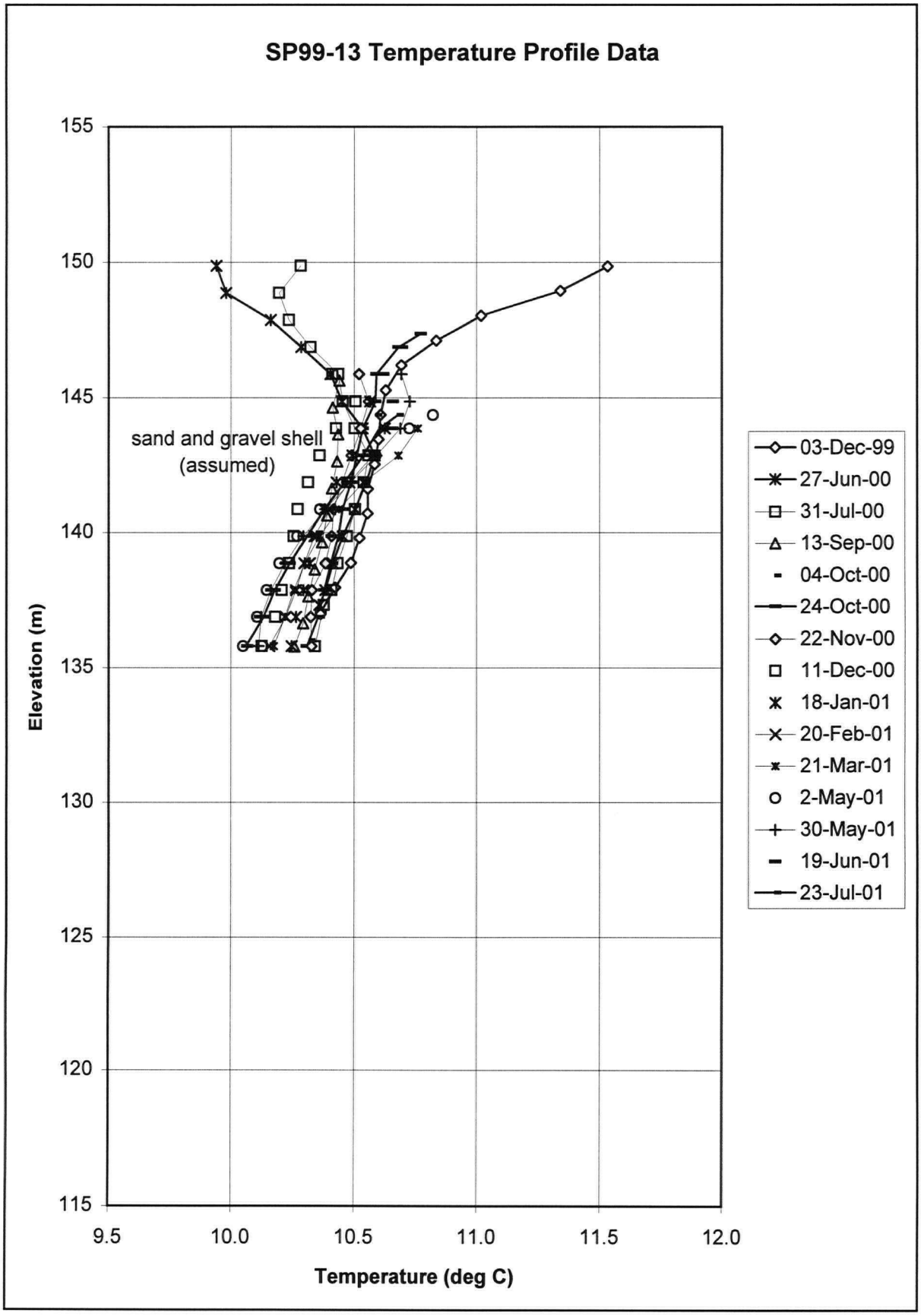
SP99-13 Temperature Profile Data
155
150
145
140
135
130
125
120
115
Elevation (m)
sand and gravel shell
(assumed)
9.5
10.0
10.5
11.0
11.5
12.0
Temperature (deg C)
03-Dec-99
27-Jun-00
31-Jul-00
13-Sep-00
04-Oct-00
24-Oct-00
22-Nov-00
11-Dec-00
18-Jan-01
20-Feb-01
21-Mar-01
2-May-01
30-May-01
19-Jun-01
23-Jul-01

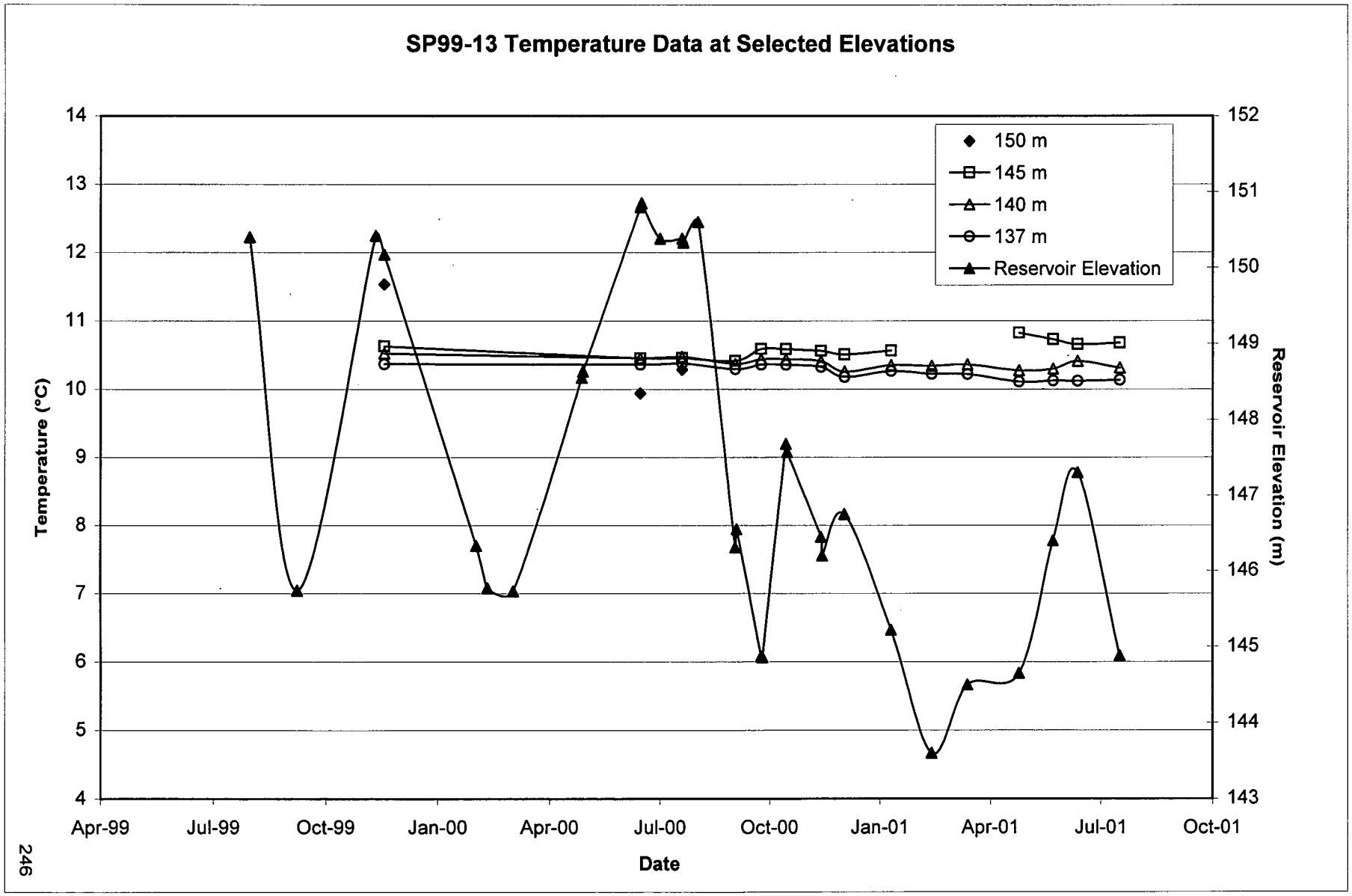
SP99-13 Temperature Data at Selected Elevations
Temperature (°C)
Reservoir Elevation (m)
Date
150 m
145 m
140 m
137 m
Reservoir Elevation
14
13
12
11
10
9
8
7
6
5
4
152
151
150
149
148
147
146
145
144
143
Apr-99
Jul-99
Oct-99
Jan-00
Apr-00
Jul-00
Oct-00
Jan-01
Apr-01
Jul-01
Oct-01

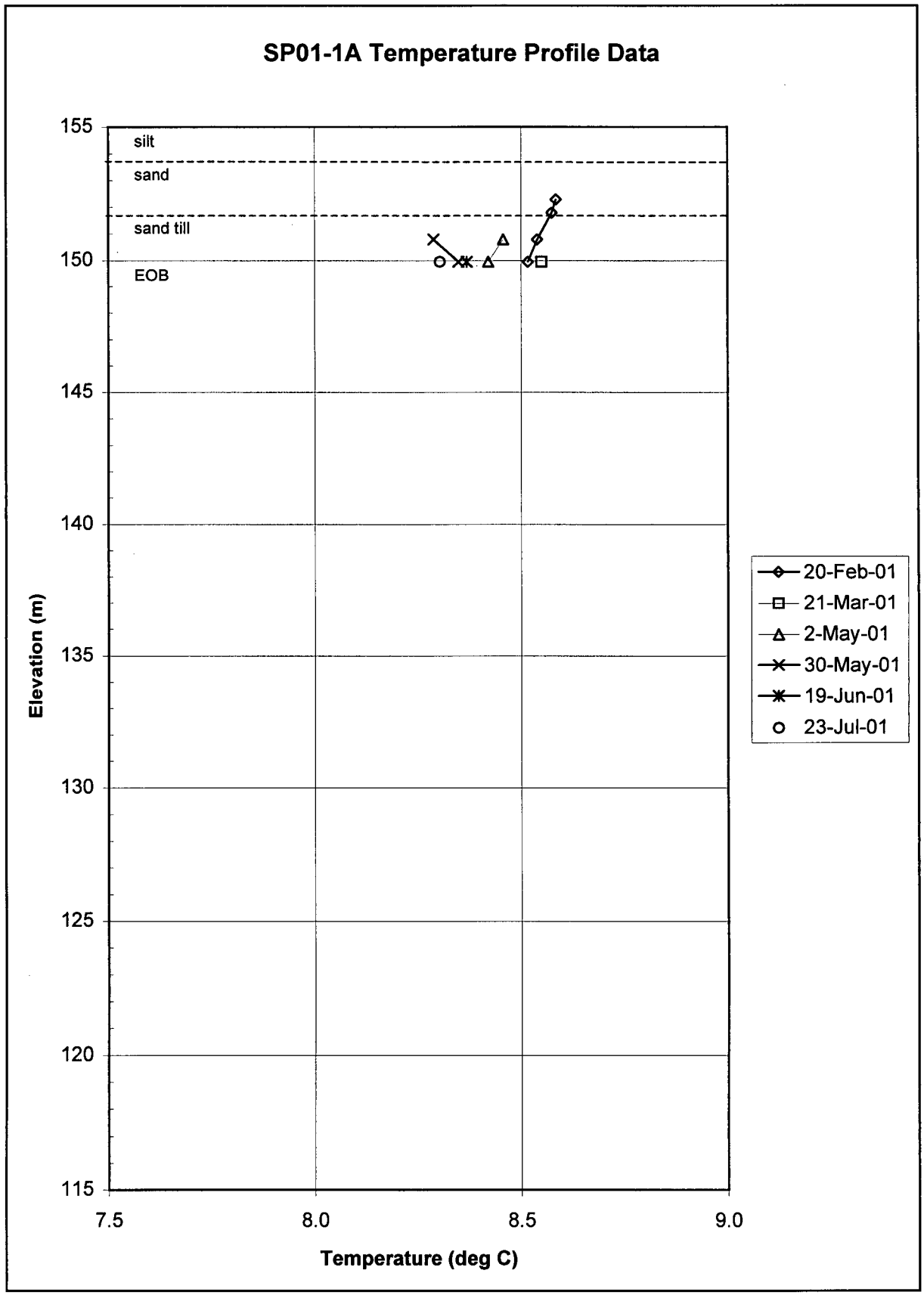
SP01-1A Temperature Profile Data
155
150
145
140
135
130
125
120
115
silt
sand
sand till
EOB
Elevation (m)
7.5
8.0
8.5
9.0
Temperature (deg C)
20-Feb-01
21-Mar-01
2-May-01
30-May-01
19-Jun-01
23-Jul-01

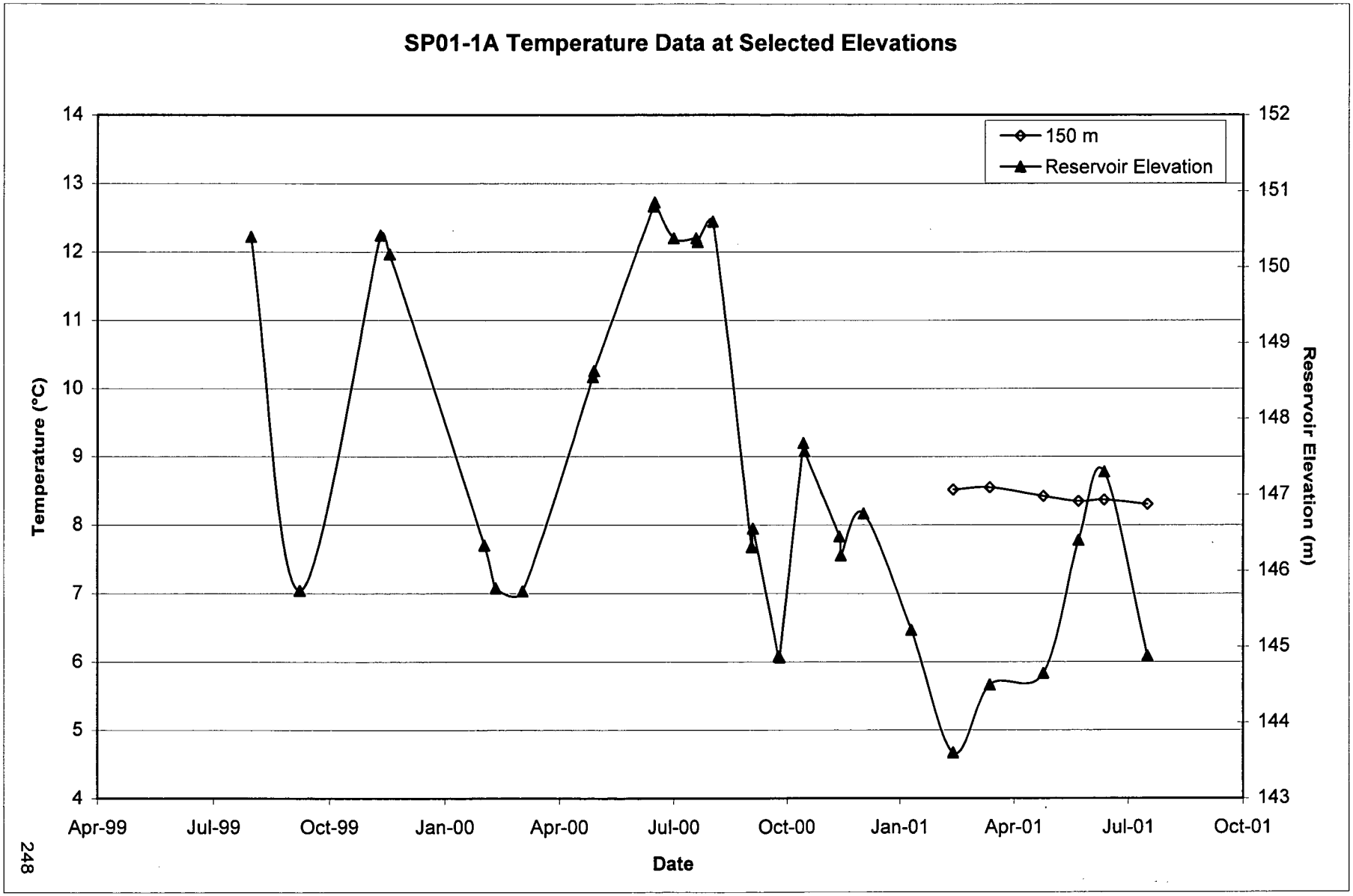
SP01-1A Temperature Data at Selected Elevations
150 m
Reservoir Elevation
Temperature (°C)
Reservoir Elevation (m)
Date
14
13
12
11
10
9
8
7
6
5
4
152
151
150
149
148
147
146
145
144
143
Apr-99
Jul-99
Oct-99
Jan-00
Apr-00
Jul-00
Oct-00
Jan-01
Apr-01
Jul-01
Oct-01

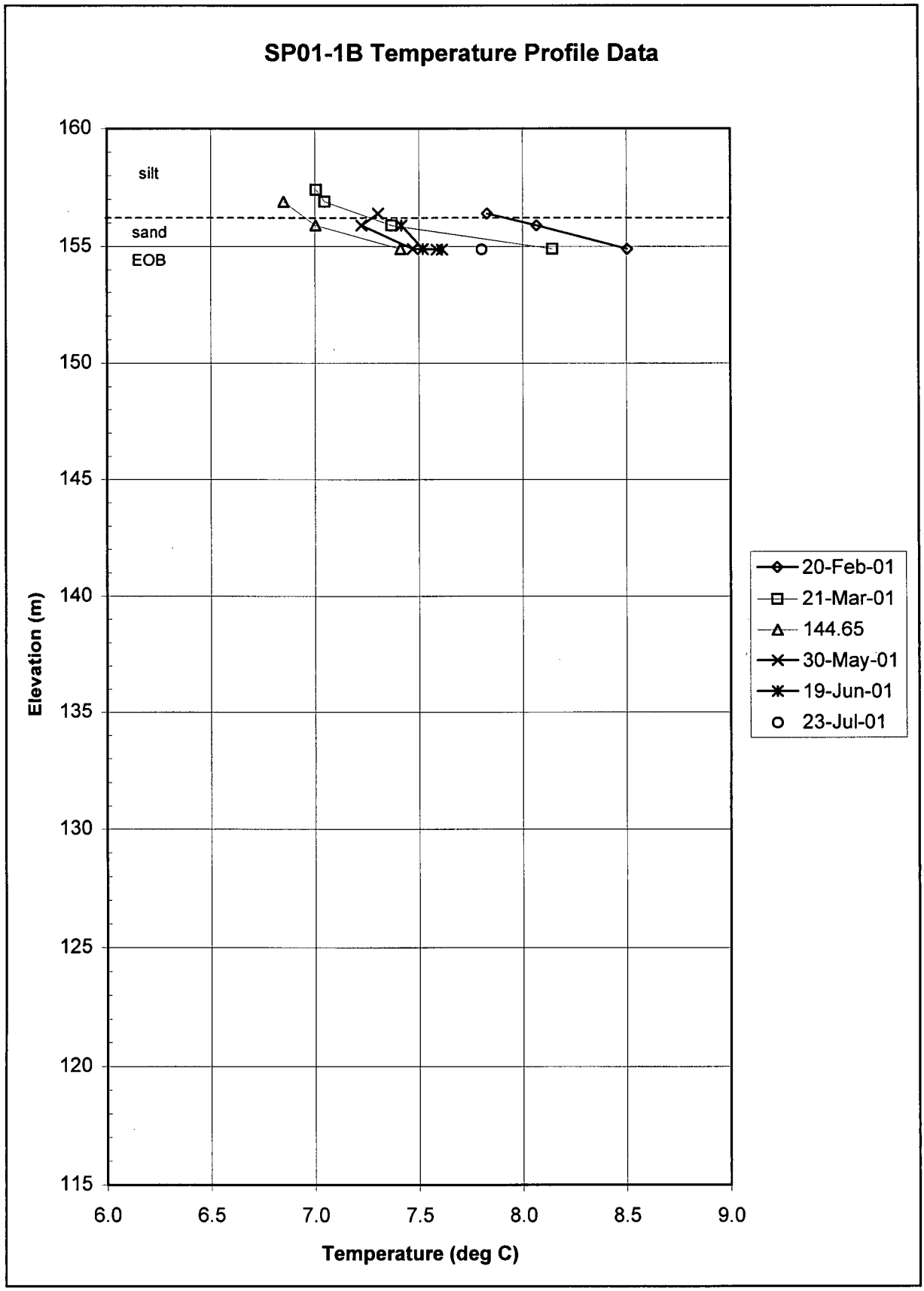
SP01-1B Temperature Profile Data
160
155
150
145
140
135
130
125
120
115
silt
sand
EOB
Elevation (m)
6.0
6.5
7.0
7.5
8.0
8.5
9.0
Temperature (deg C)
20-Feb-01
21-Mar-01
144.65
30-May-01
19-Jun-01
23-Jul-01

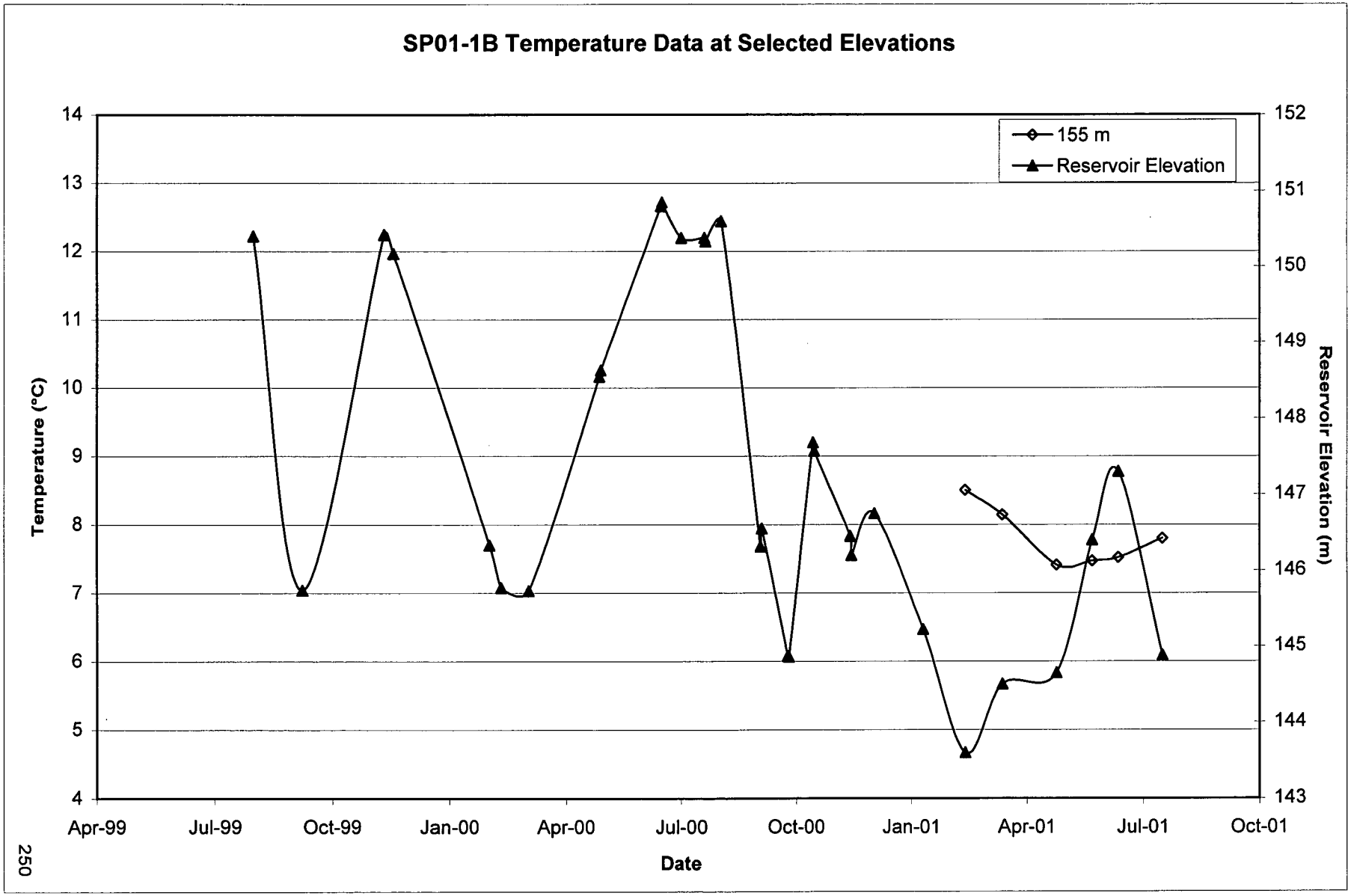
SP01-1B Temperature Data at Selected Elevations
155 m
Reservoir Elevation
Temperature (°C)
Reservoir Elevation (m)
Date
14
13
12
11
10
9
8
7
6
5
4
152
151
150
149
148
147
146
145
144
143
Apr-99
Jul-99
Oct-99
Jan-00
Apr-00
Jul-00
Oct-00
Jan-01
Apr-01
Jul-01
Oct-01

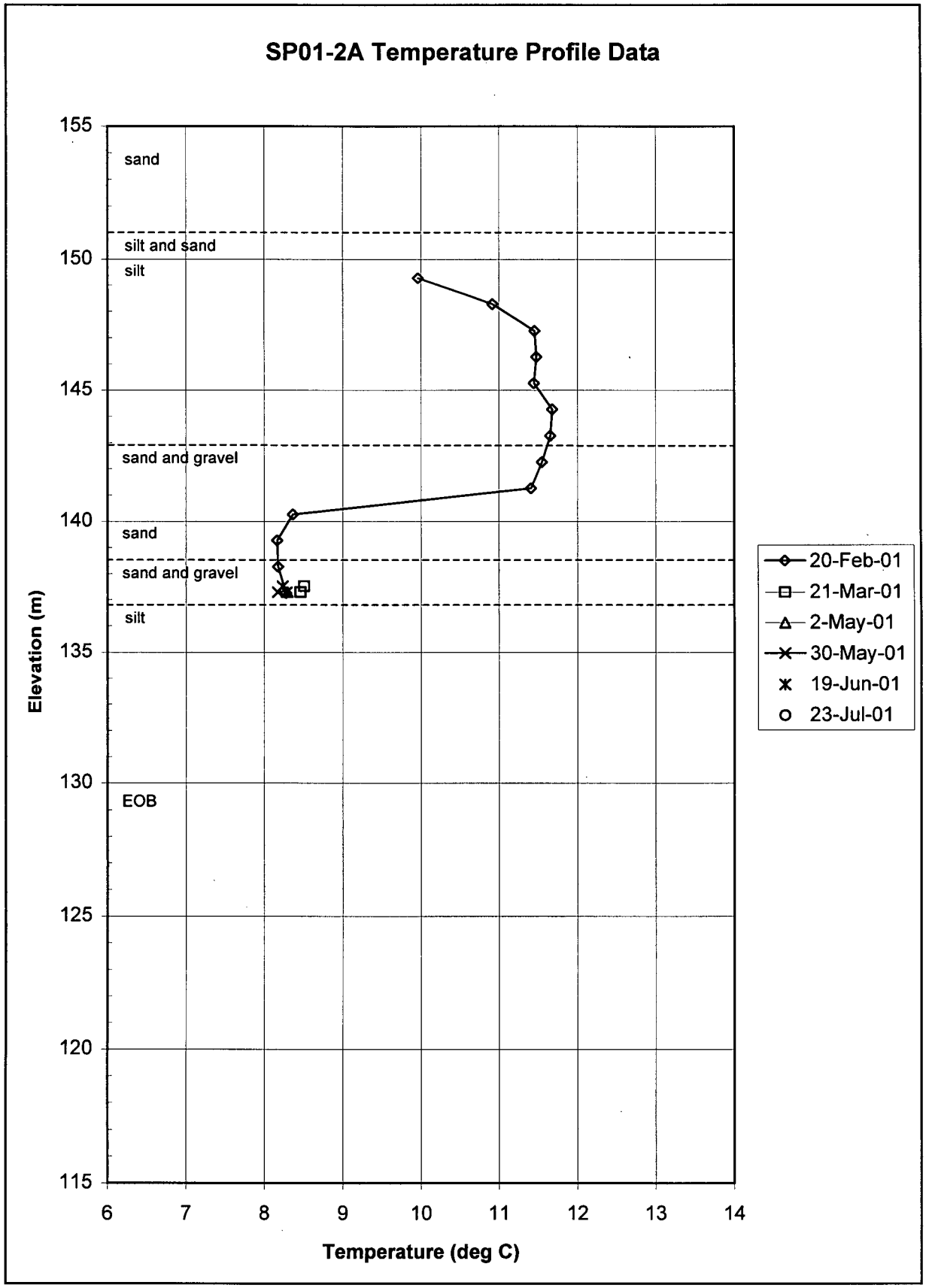
SP01-2A Temperature Profile Data
155
150
145
140
135
130
125
120
115
sand
silt and sand
silt
sand and gravel
sand
sand and gravel
silt
EOB
Elevation (m)
6
7
8
9
10
11
12
13
14
Temperature (deg C)
20-Feb-01
21-Mar-01
2-May-01
30-May-01
19-Jun-01
23-Jul-01

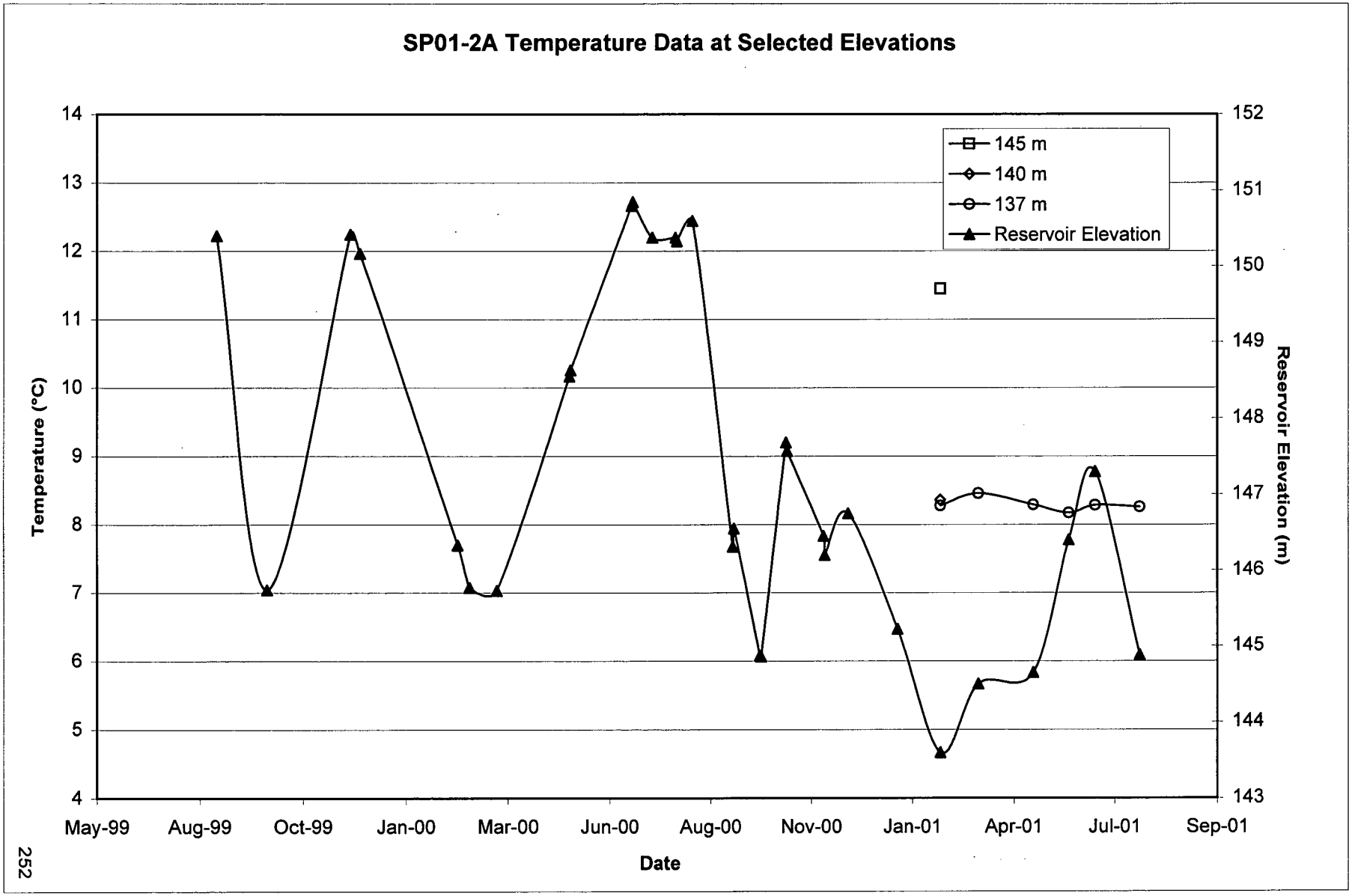
SP01-2A Temperature Data at Selected Elevations
Temperature (°C)
Reservoir Elevation (m)
Date
145 m
140 m
137 m
Reservoir Elevation
14
13
12
11
10
9
8
7
6
5
4
152
151
150
149
148
147
146
145
144
143
May-99
Aug-99
Oct-99
Jan-00
Mar-00
Jun-00
Aug-00
Nov-00
Jan-01
Apr-01
Jul-01
Sep-01

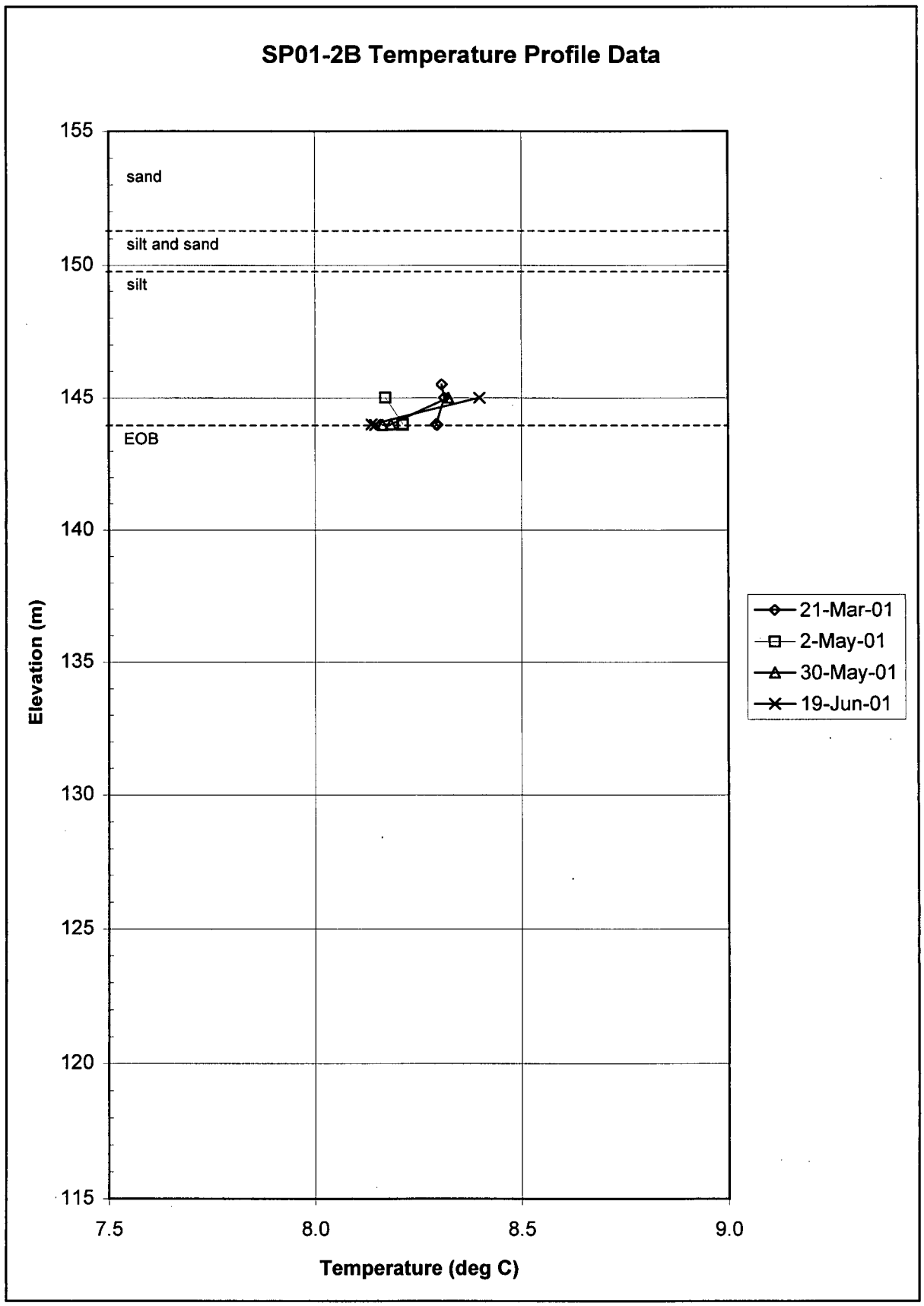
SP01-2B Temperature Profile Data
155
150
145
140
135
130
125
120
115
sand
silt and sand
silt
EOB
Elevation (m)
7.5
8.0
8.5
9.0
Temperature (deg C)
21-Mar-01
2-May-01
30-May-01
19-Jun-01

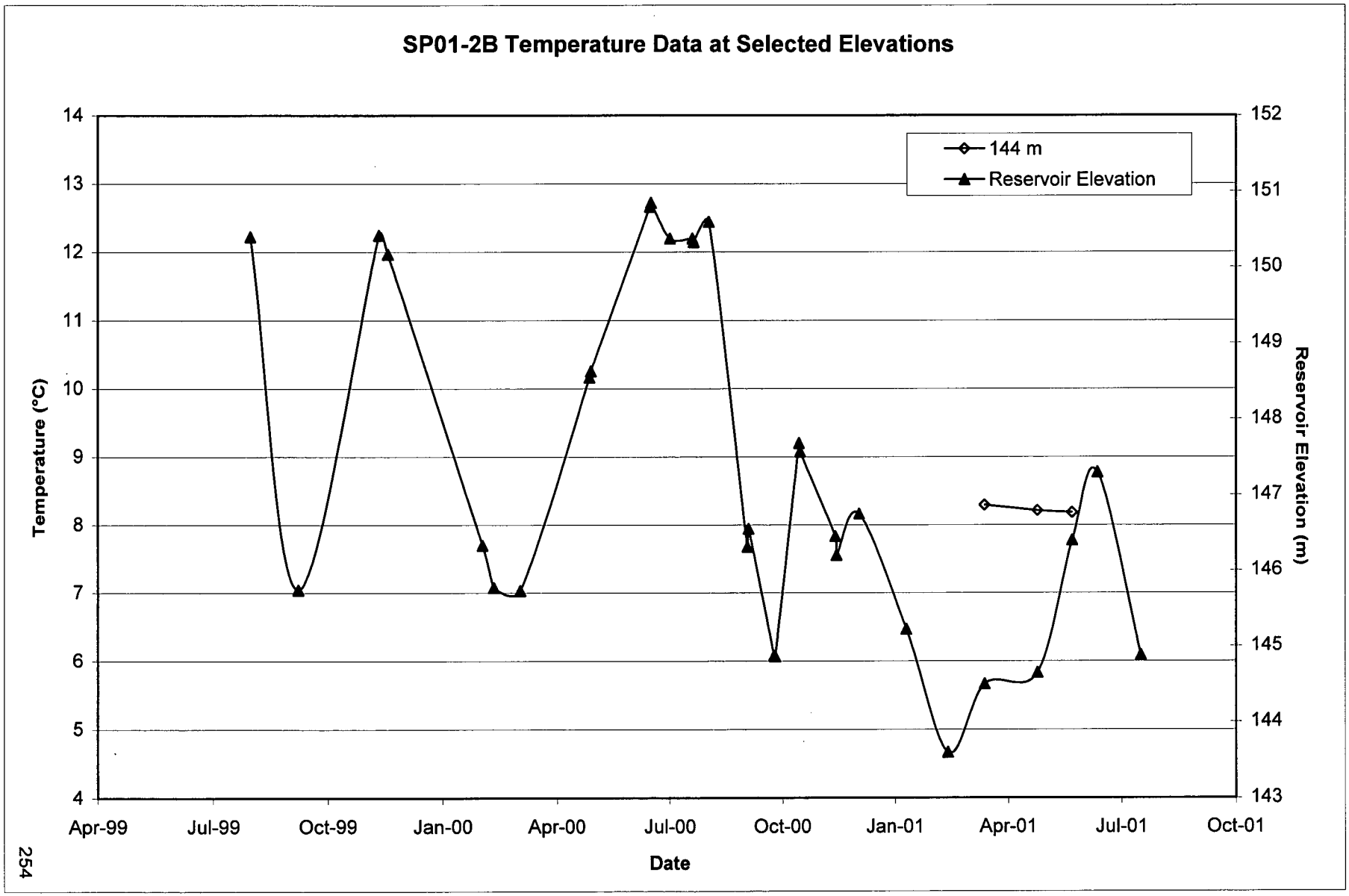
SP01-2B Temperature Data at Selected Elevations
144 m
Reservoir Elevation
Temperature (°C)
Reservoir Elevation (m)
Date
14
13
12
11
10
9
8
7
6
5
4
152
151
150
149
148
147
146
145
144
143
Apr-99
Jul-99
Oct-99
Jan-00
Apr-00
Jul-00
Oct-00
Jan-01
Apr-01
Jul-01
Oct-01

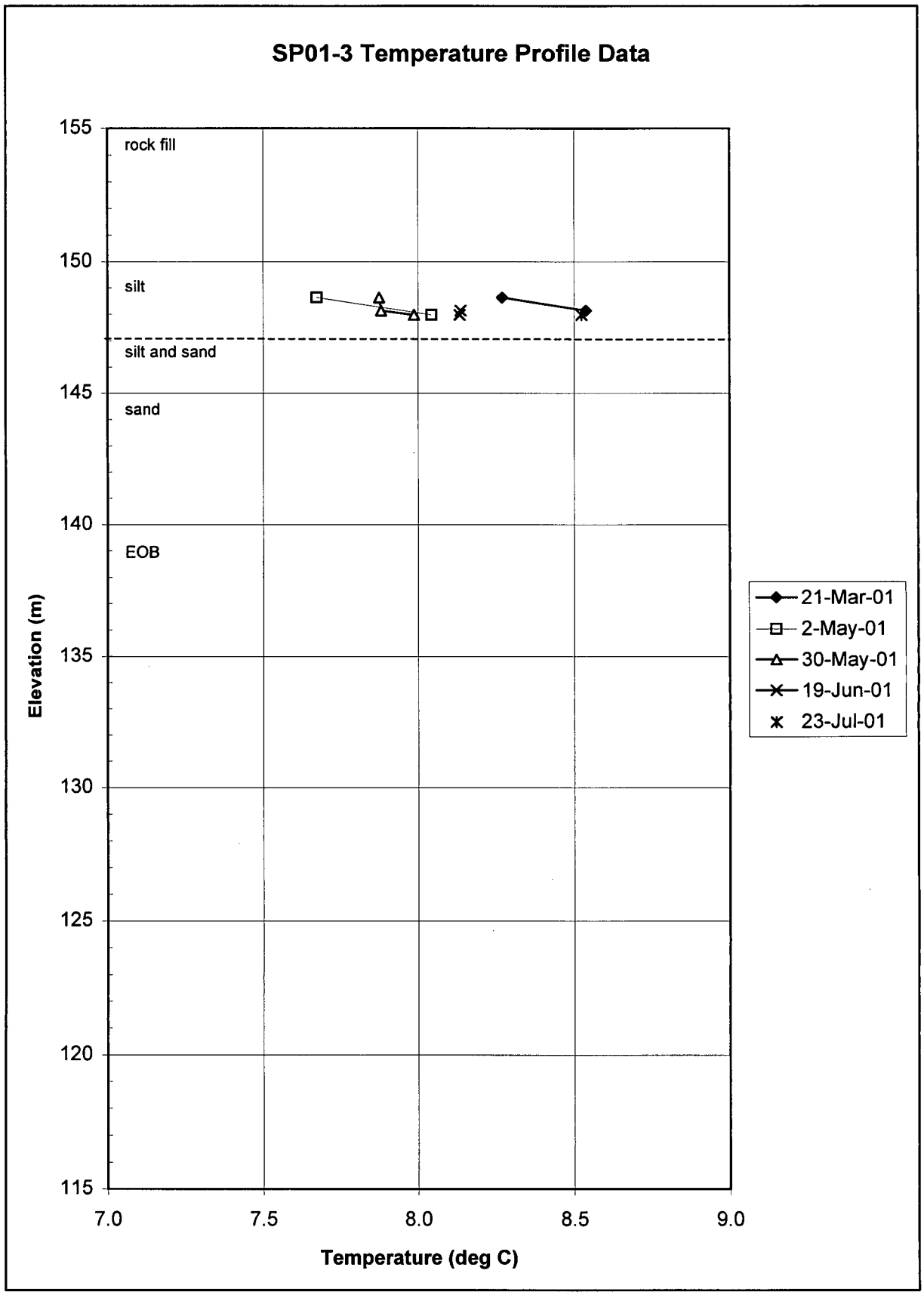
SP01-3 Temperature Profile Data
155
150
145
140
135
130
125
120
115
rock fill
silt
silt and sand
sand
EOB
Elevation (m)
7.0
7.5
8.0
8.5
9.0
Temperature (deg C)
21-Mar-01
2-May-01
30-May-01
19-Jun-01
23-Jul-01

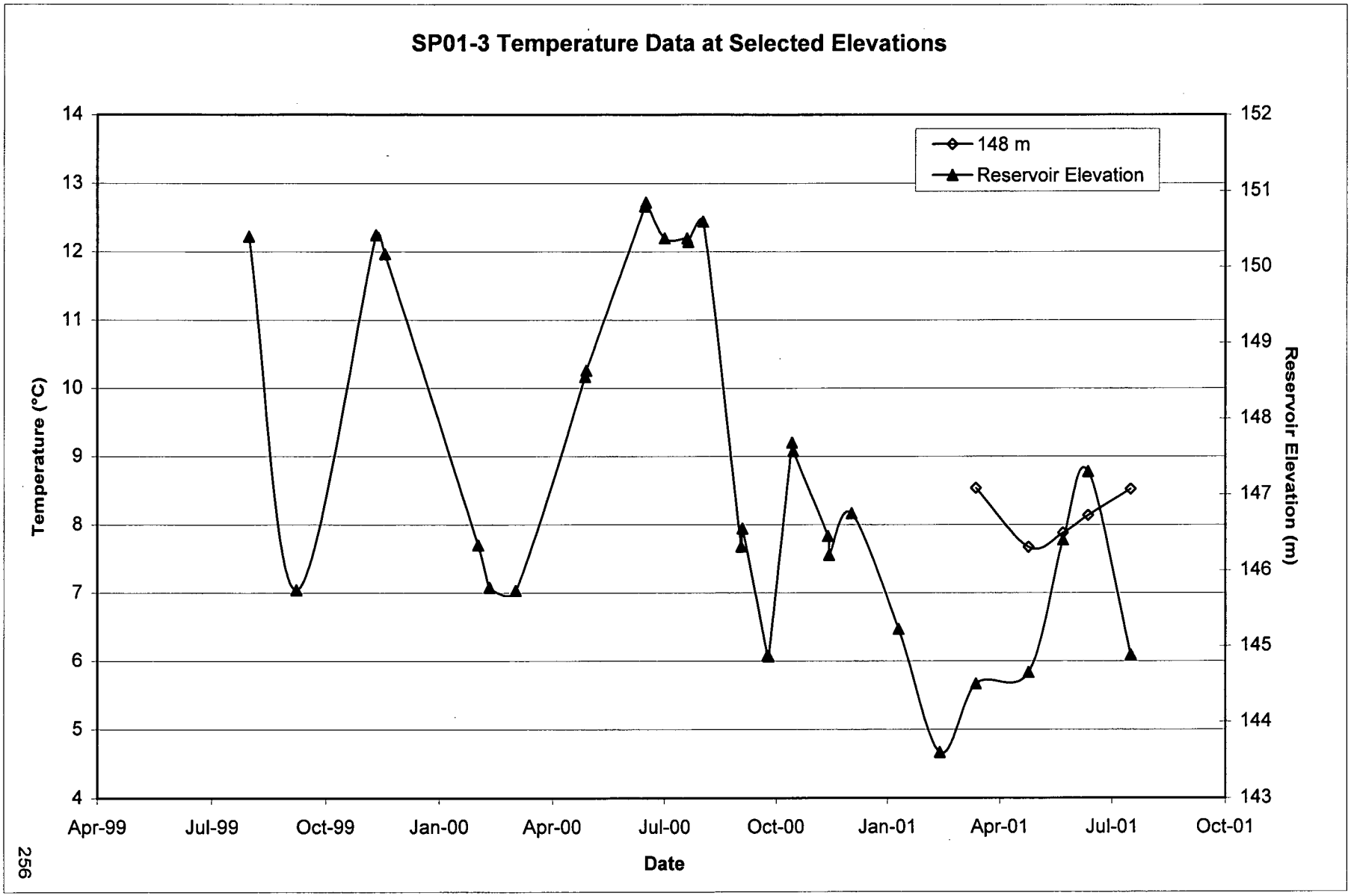
SP01-3 Temperature Data at Selected Elevations
148 m
Reservoir Elevation
Temperature (°C)
Reservoir Elevation (m)
Date
14
13
12
11
10
9
8
7
6
5
4
152
151
150
149
148
147
146
145
144
143
Apr-99
Jul-99
Oct-99
Jan-00
Apr-00
Jul-00
Oct-00
Jan-01
Apr-01
Jul-01
Oct-01

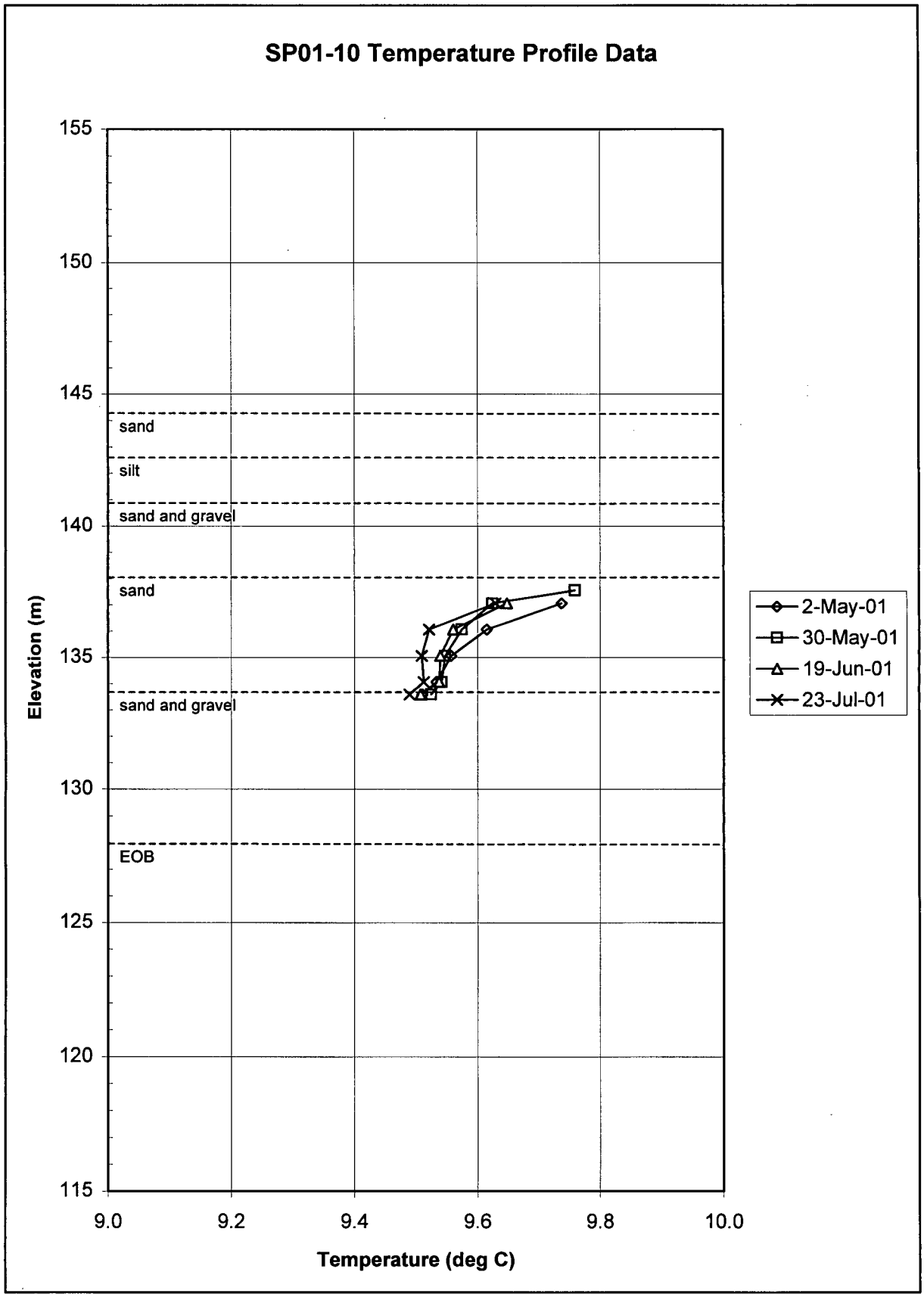
SP01-10 Temperature Profile Data
155
150
145
140
135
130
125
120
115
sand
silt
sand and gravel
sand
sand and gravel
EOB
Elevation (m)
9.0
9.2
9.4
9.6
9.8
10.0
Temperature (deg C)
2-May-01
30-May-01
19-Jun-01
23-Jul-01

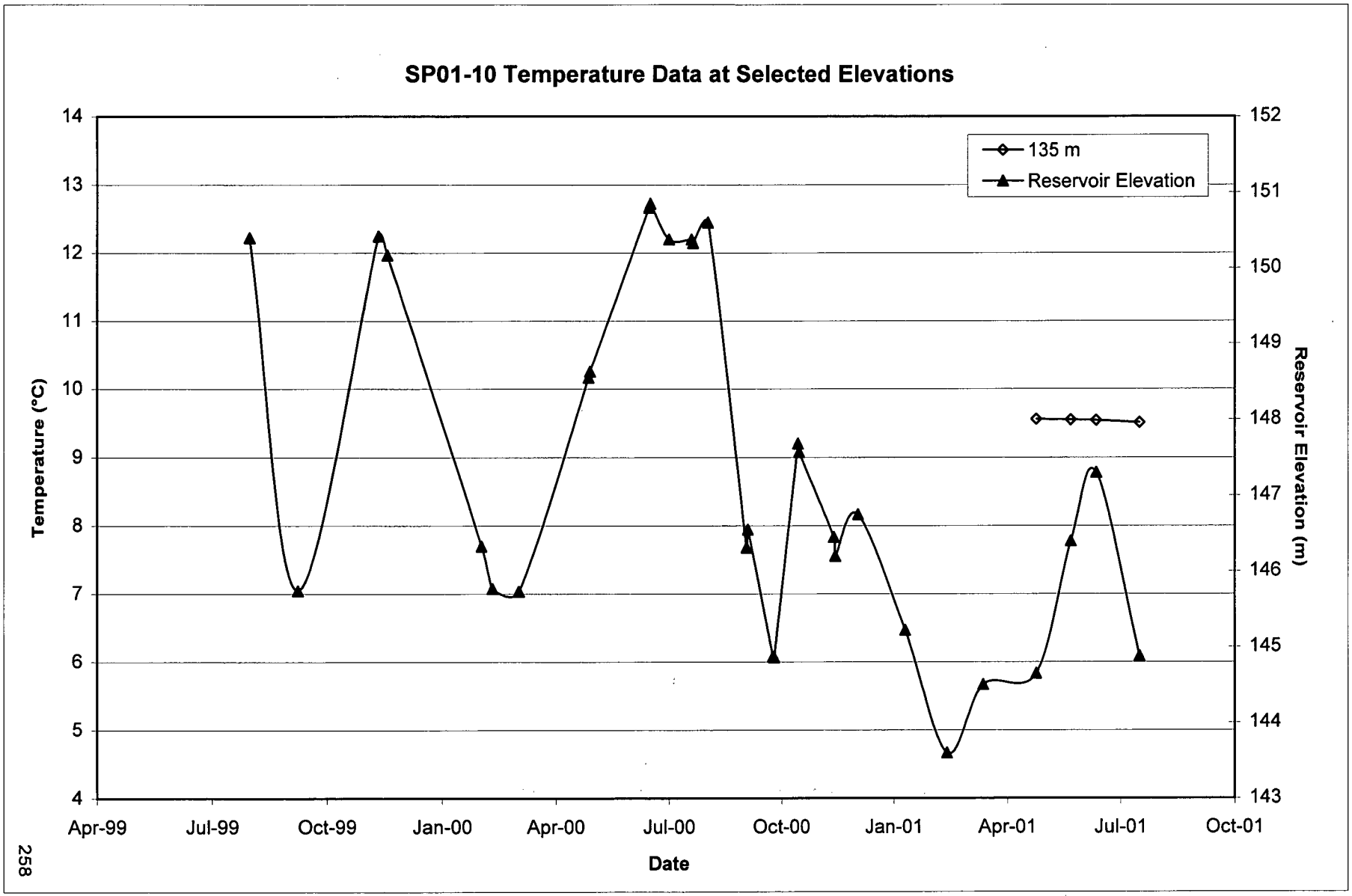
SP01-10 Temperature Data at Selected Elevations
135 m
Reservoir Elevation
Temperature (°C)
Reservoir Elevation (m)
Date
14
13
12
11
10
9
8
7
6
5
4
152
151
150
149
148
147
146
145
144
143
Apr-99
Jul-99
Oct-99
Jan-00
Apr-00
Jul-00
Oct-00
Jan-01
Apr-01
Jul-01
Oct-01